REPORT SERIES IN AEROSOL SCIENCE
No. 300 (2025)

Abstract Book of

THE 22nd INTERNATIONAL CONFERENCE ON NUCLEATION AND ATMOSPHERIC AEROSOLS

August 24-29, 2025
Vienna, Austria

Editors: Paul Winkler, Aenne Jacobshagen, Markku Kulmala, Katrianne Lehtipalo and Aino Ovaska

Aerosolitutkimusseura r.y.
Helsinki 2025

ISBN 978-952-7507-75-9 (print)
ISBN 978-952-7507-76-6 (pdf)
ISSN 0784-3496 (print)
ISSN 2814-4236 (pdf)

www.FAAR.fi

Contents

Main Topic 1: Nucleation Theory & Experiment 1

Alfoldy, B., Gregorič, A., Ivančič, M., Ježek Brecelj, I., Rodenas, M., Borras, E., Soler, R.,Vera, T., Munoz, A., Yubero, E., Crespo, J., and Rigler, M.
PARTICLE NUCLEATION IN WOOD COMBUSTION EMISSION 2

Alvarez-Galera, E., Martí, J., and Batet, L.
MOLECULAR DYNAMICS SIMULATIONS OF HELIUM NUCLEATION IN LIQUID LEAD-LITHIUM ALLOYS 5

Broad, A., and Ford, I.J.
NUCLEATION DRIVEN BY NON-MARKOVIAN NOISE 9

Dinu, D.F., Liedl, K.R., Grothe, H., Loerting, T., and Stolzenburg, D.
FREEZING ATMOSPHERIC ORGANIC NUCLEATION: QUANTUM CHEMICAL CALCULATIONS AND MATRIX ISOLATION FTIR EXPERIMENTS OF FORMIC ACID 11

Elm, J.
QUANTUM CHEMICAL MODELLING OF ATMOSPHERIC CLUSTER FORMATION: BIGGER, STRONGER, FASTER! 14

Graber, F., Feusi, S., Khatri, J., Li, C., and Signorell, R.
ACCELERATION OF LOW TEMPERATURE WATER NUCLEATION IN THE PRESENCE OF CO2 18

Halonen, R.
ATOMISTIC INSIGHTS INTO ARGON CLUSTERS AND NUCLEATION 20

Jiang, Y.R., Yan, C., Nie, W., Chen, Z.H., Zha, Q.Z., Zhou, C., Qi, X.M., and Ding, A.J.
CHARACTERISTICS OF PARTICLE EMISSION FROM DIFFERENT HOUSEHOLD COOKING ACTIVITIES 23

Kroll, R., and Tsori, Y.
ION-INDUCED NUCLEATION IN FLUIDS CONTAINING SALT 24

Lian, Y., Bai, X., Yuan, R., and Jiang, S.
DEVELOPING THE UNIVERSAL NEURAL NETWORK FORCE FIELD FOR ATMOSPHERIC AEROSOL NUCLEATION 27

Liu, L., Roldin, P., Simon, M., Yang, L., Yan, C., Nie, W., Dada, L., Kirkby, J., Donahue, N.M., CLOUD collaboration, and El Haddad, I.
TEMPERATURE DEPENDENCE OF AUTOXIDATION AND DIMERIZATION IN α-PINENE OZONOLYSIS FROM 223 TO 298K 35

Lukianov, M., Lukianova, T., and Hrubý, J.
EXPERIMENTAL STUDIES OF THE INFLUENCE OF CARRIER GASES ON THE WATER HOMOGENEOUS NUCLEATION IN MIXTURES 39

McGraw, R.L.
ADVANCES AND KEY PLAYERS IN NUCLEATION THEORY 43

Montero de Hijes, P., and Dellago, C.
TOWARDS UNDERSTANDING ICE NUCLEATION ON MICROCLINE FELDSPAR BY MEANS OF MACHINE LEARNING AB INITIO SIMULATIONS 48

Reguera, D., Llamas, A., and Latella, I.
EVALUATING THE PROPERTIES OF THE CRITICAL NUCLEUS BY SIMULATIONS IN A SMALL SYSTEM 50

Reischl, B., Tikkanen, V., Yang, H., and Vehkamäki, H.
GAS-PHASE COLLISION RATE ENHANCEMENT FACTORS FOR ACID-BASE CLUSTERS UP TO 2 nm IN DIAMETER FROM ATOMISTIC SIMULATION AND THE INTERACTING HARD SPHERE MODEL 52

Salminen, T., Niskanen, M., Mönkkönen, P., Seppänen, A., Lehtinen, K.
FINITE ELEMENT-BASED EXTENDED KALMAN FILTER AND SMOOTHER FOR RETRIEVAL OF AEROSOL SIZE DISTRIBUTIONS AND PROCESS RATES 55

Shen, J., Russell, D.M., DeVivo, J., Kunkler, F., Baalbaki, R., Mentler, B., CLOUD collaboration, Harder, H., Hansel, A., Donahue, N.M., Worsnop, D.R., Kulmala, M., Kirkby, J., Curtuzs, J., and He, X.C.
NEW PARTICLE FORMATION FROM ISOPRENE IN THE FREE TROPOSPHERE 58

Signorell, R.
WATCHING AT THE MOLECULAR LEVEL HOW GASES NUCLEATE AT LOW TEMPERATURE 61

Smith, J.N., Miller, C.E., Perraud, V., and Myllys, N.
CHEMICALLY RESOLVING THE GROWTH OF GAS PHASE CLUSTERS INTO NANOPARTICLES 63

Sommer, E., Almeida, J., Simon, M., Caudillo-Plath, L., Yu, W., Junninen, H., Zheng, Z., Judmaier, B., Xenofontos, C., Pozzer, A., Kirkby, J., and the CLOUD collaboration
NEW PARTICLE FORMATION FROM ALPHA PINENE AND TRACE SULFURIC ACID 66

Špalová, A., Holubová Šmejkalová, A., Roztočil, P., Ondráček, J., Zíková, N., and Ždímal, V.
NEW PARTICLE FORMATION MEASUREMENTS - NAIS, nanoSMPS, AND PSM COMPARISON 68

Tsona Tchinda, N., and Du, L.
THE EFFECT OF CHEMICAL SUBSTITUTION ON THE TRANSFORMATION OF ORGANOSULFATES 70

Tuovinen, S., Liu, C., Sarnela, N., Liu, Y., Kerminen, V-M., and Kulmala, M.
ON THE MEAN DIAMETER OF SMALL IONS: INSIGHT INTO ION CLUSTER COMPOSITION AND GROWTH 74

Vehkamäki, H., Kähärä, J., Franzon, L., Ingram, S., and Kurtén, T.
EVAPORATION RATES OF COMPLEX ORGANIC CLUSTERS DEPEND STRONGLY ON MOLECULAR FLEXIBILITY 77

Wagner, P. E.
INTERNATIONAL CONFERENCES ON NUCLEATION AND ATMOSPHERIC AEROSOLS (ICNAA) A BRIEF HISTORY 79

Yu, W., Baalbaki, R., DeVivo, J., Shen, J., Caudillo, L., Sommer, E., He, X-C., Lehtipalo, K., and the CLOUD collaboration
IMPACT OF HUMIDITY ON THE AEROSOL GROWTH BY METHANESULFONIC ACID 89

Main Topic 2: Tropospheric & Stratospheric Aerosols 94

Artaxo, P., Rizzo, L.V., Machado, L.A., Meller, B.B., Valiati, R., Franco, M.A., and Pohlker, C.
AEROSOLS IN AMAZONIA: PRIMARY PARTICLES, NEW PARTICLE FORMATION, CHEMICAL PRODUCTION, AND THE COMPLEX MIXTURE OF ALL THESE COMPONENTS 95

Brauner, P., Appel, O., Eppers, O., Köllner, F., Clemen, H.-C., Kaiser, K., Schneider, J., Lachnitt, H.-C., Dragoneas, A., Hünig, A., Molleker, S., Schlager, H., Voigt, C., Cheng, Y., Anderson, B.E., and Borrmann, S.

AEROSOL CHEMICAL COMPOSITION MEASURED IN THE UTLS OVER GERMANY IN WINTER 2018 98

Clusius, P., Baykara, M., Xavier, C., Zhou, P., Tyree, J., Foreback, B., Äijälä, M., Graeffe, F., Petäjä, T., Kulmala, M., Paasonen, P., Palmer, P.I., and Boy, M.

MODELLING THE IMPACT OF ANTHROPOGENIC AEROSOLS ON CCN CONCENTRATIONS OVER A RURAL BOREAL FOREST ENVIRONMENT 101

Cooke, M.E., and Smith, J.N.

DEEP CONVECTION LEADS TO ULTRAFINE PARTICLE FORMATION AND GROWTH AT CONTINENTAL MID-LATITUDES 104

Curtius, J., Heinrizi, M., Beck, L., Pöhlker, M.L., Tripathi, N., Krumm, B.E., Holzbeck, P., Nussbaumer, C.M., Hernández Pardo, L., Klimach, T., Barmpounis, K., Albrecht, R.I., Andreae, M.O., Artaxo, P., Crowley, J.N., Fischer, H., Harder, H., Herdies, D.L., Hewson, M., Machado, L.A.T., Pöhlker, C., Pöschl, U., Possner, A., Schneider, J., Williams, J., Lelieveld, J., and the CAFE-Team

ISOPRENE DRIVES NEW PARTICLE FORMATION IN THE TROPICAL UPPER TROPOSPHERE 108

DeVivo, J., Alton, M., Canagaratna, M., and Donahue, N.M.

REACTIVE CONDENSATION PROCESSES MEASURED USING FIGAERO BIPOLAR SWITCHING TIME-OF-FLIGHT MASS SPECTROMETRY 112

Giannakaki, E., and Karageorgopoulou, A.

TYPE-RESOLVED RETRIEVAL OF CLOUD CONDENSATION NUCLEI AND ICE-NUCLEATING PARTICLE NUMBER CONCENTRATIONS FROM CALIPSO AEROSOL TYPING AND AERONET INVERSION DATA 115

Glasius, M., Björgvinsdóttir, Þ.N., Åbom, K.O.M., Thomsen, D., Iversen, E.M., Elm, J., and Bilde, M.

TRACING LOW-VOLATILITY OXIDATION PRODUCTS OF MONOTERPENES IN ATMOSPHERIC AEROSOLS 118

Hao, L., Kommula, S., Kokkola, T., Somero, M., Kartikainen, A., Ihalainen, M., Köster, K., Yli-Pirila, P., Miettinen, P., Peltokorpi, S., Buchholz, A., Shahzaib, M., Mukherjee, A., Schobersberger, S., Sippula, O., and Virtanen, A.

PRIMARY EMISSIONS AND SECONDARY FORMATION OF ORGANIC AEROSOL IN OPEN BOREAL FOREST FIRE 120

Joppe, P., Schneider, J., Kaiser, K., Wilsch, J., Bozem, H., Breuninger, A., Curtius, J., Ebert, M., Emig, N., Fischer, H., Hoor, P., Ismayil, S., Kandler, K., Kunkel, D., Kohl, M., Kurth, I., Lachnitt, H.-C., Li, Y., Marsing, A., Miltenberger, A., Pozzer, A., Richter, S., Röder, L., Rolf, C., Schlager, H., Schneider, L., Schwenk, C., Spelten, N., Tomsche, L., Voigt, C., Vogel, A.L., Zahn, A., Borrmann, S., and Cheng, Y.

THE INFLUENCE OF SMALL-SCALE PROCESSES ON THE CHEMICAL COMPOSITION OF AEROSOL PARTICLES IN THE EXTRATROPICAL UTLS 122

Kanawade, V.P., Bhandari, R., Sarangi, C., Sebastian, M., Hooda, R.K., Hyvärinen, A.-P., Asmi, E., Vakkari, V., Pandithurai, G., Singh, S.N., Soni, V.K., Nieminen, T., Van Zyl, P.G., Jaars, K., Laakso, L., Beddows, D.C.S., Harrison, R.M., Beukes, J.P., Kalivitis, N., Mihalopoulos, N., Salma, I., Vörösmarty, M., Young, L.-H., Watson, Z., Lee, S.-H., Pikridas, M., Sciare, J., and Jokinen, T

IDENTIFICATION OF NEW PARTICLE FORMATION EVENTS USING DEEP LEARNING ALGORITHM 126

Klebach, H., Beck, L., Heinritzi, M., Richter, S., Kaiser, K., Zauner-Wiecorek, M., Granzin, M., Keber, T., Russell, D., Caudillo-Plath, L., Schneider, J., and Curtius, J.

SULFURIC ACID AND METHANESULFONIC ACID MEASUREMENTS IN THE TROPICAL TROPOSPHERE 129

Köllner, F., Kohl, M., Ekinci, F., Eppers, O., Schneider, J., Dragoneas, A., Molleker, S., Johansson, S., Ungermann, J., Kretschmer, E., Höpfner, M., Lauther, V., Volk, C.M., Appel, O., Brauner, P., Kunkel, D., Lachnitt, H.-C., Bozem, H., Weyland, F., Emig, N., Ort, L., Zahn, A., Tomsche, L., Pozzer, A., Lelieveld J., Cheng, Y., Riese, M., Hoor, P., and Borrmann, S.

LONG-RANGE TRANSPORT AND MIXING OF AEROSOL FROM THE ASIAN TROPOPAUSE AEROSOL LAYER (ATAL) INTO THE NORTHERN LATITUDE LOWER STRATOSPHERE 132

Koutounidis, I., and Giannakaki, E.

DERIVATION OF CLOUD CONDENSATION NUCLEI VERTICAL DISTRIBUTIONS FROM CALIOP LIDAR DATA IN THE CAPO VERDE REGION 135

Kulmala, M., Du, W., Zhang, X., Zhang, T., Xia, M., Wang, Y., Zou, Z., Zheng, F., Zhang, Y., Zha, Q., Yan, C., Yuan, Q., Qi, L., Petäjä, T., Sarnela, N., Ylivinkka, I., Aliaga, D., Cai, R., Agro', M., Ahonen, L., Schiestl-Aalto, P., Tuovinen, S., Cai, J., Kujansuu, J., Ciarelli, G., Cheng, Y., Ding, A., Dällenbach, K., Dada, L., Worsnop, D., Bianchi, F., Jiang, J., Liu, Y., Kerminen, V.-M., and Kokkonen, T.

INSIGHTS FROM THE COMPARISON BETWEEN HYYTIÄLÄ AND BEIJING 139

Lampilahti, J., Tuovinen, S., Lehtipalo, K., Paasonen, P., Kerminen, V.-M., and Kulmala, M.
AUTOMATIC ESTIMATION OF PARTICLE GROWTH RATES USING CROSS CORRELATION TECHNIQUE 142

Lei, L., Xu, W., Lin, C., Chen, B., Fossum, K.N., Ceburnis, D., O'Dowd, C., and Ovadnevaite, J.
ADVANCED SOURCE APPORTIONMENT OF CARBONACEOUS AEROSOLS: INTEGRATING PMF AND MACHINE LEARNING FOR OA AND BC ATTRIBUTION 144

McMurry, P.H.
RESEARCH ON NEW PARTICLE FORMATION (NPF) IN THE EARTH'S TROPOSPHERE: A HISTORICAL AND PERSONAL PERSPECTIVE 148

Miljevic, B., Mallet, M., Alroe, J., Saraswathy, A., Osuagwu, C.G., Ristovski, Z., Humphries, R., Selleck, P., Keywood, M., and Taylor, S.
ANTARCTIC CONTINENTAL OUTFLOW OF BIOGENICALLY DOMINATED AEROSOLS 153

Nieminen, T., Joutsensaari, J., Yli-Juuti, T., Leinonen, V., Miettinen, P., Virtanen, A., Mikkonen, S., Laaksonen, A., Decesari, S., and Facchini, M.C.
LONG-TERM TRENDS OF PARTICLE NUMBER-SIZE DISTRIBUTIONS AND NEW PARTICLE FORMATION AT SAN PIETRO CAPOFIUME, ITALY 155

Peltokorpi, S., Buchholz, A., Hao, L., Kommula, S., Miettinen, P., Pullinen, I., Kokkola, T., Ihalainen, M., Vakkari, V., Asmi, E., Sippula, O., and Virtanen, A.
CHARACTERIZATION OF PRESCRIBED FIRE EMISSIONS IN A FINNISH BOREAL FOREST 157

Pullinen, I., Buchholz, A., Korrensalo, A., Skaldina, O., Männistö, E., and Virtanen, A.
CHANGING PEATLANDS: EFFECTS ON AEROSOL FORMATION POTENTIAL 160

Radecka, M.W., Kang, H.G., Zhang, Z., Pöschl, U., and Berkemeier, T.
A KINETIC MODEL OF MULTIPHASE CHEMISTRY INTEGRATING NEW PARTICLE FORMATION AND SIZE DISTRIBUTION DYNAMICS IN SECONDARY ORGANIC AEROSOL FORMATION (KM3C-NPF) 163

Schwarz, J., Vodička, P., Lhotka, R., Zíková, N., Mbengue, S., and Ždímal, V.
VERTICAL DIFFERENCES IN NR-PM1 ATMOSPHERIC AEROSOL COMPOSITION 165

Skønager, J.T., Teng, Z., Salter, M., Bilde, M., Massling, A., Skov, H., and Rosati, B.
AEROSOL-RADIATION INTERACTIONS OF COASTAL AEROSOLS IN SCANDINAVIA 167

Steiner, G., Kunath, C., Merker, E., Keck, L., Krause, C., and Götz, M.
TRACEABLE CALIBRATION OF ULTRAFINE PARTICLE COUNTERS 169

Thomas, S.J., Campbell, J., Congrong, W., Bianchi, F., and Mao, J.
FORMATION AND CHARACTERISTICS OF ATMOSPHERIC AEROSOLS IN AN ALASKAN BOREAL FOREST 171

Vartiainen, A., Roldin, P., Irfan, M., Thomasson, A., Kokkola, H., and Yli-Juuti, T.
TOWARDS A MORE DETAILED REPRESENTATION OF MONOTERPENE OXIDATION IN CLIMATE MODELS – BIAS CORRECTION OF VBS WITH NEURAL NETWORKS 173

Vignesh, P., Fossum, K.N., Lei, L., Moschos, V., Lin, C., Korhale, N., Coleman, L., Petit, J.-E., Acharja, P., Rinaldi, M., Vasilescu, J. ,Dandocsi, A.V., Petrionoli, K., Bougiatioti, A., Mihalopoulos, N., and Ovadnevaite, J.
SOURCE APPORTIONMENT OF ORGANIC AEROSOLS IN FIVE EUROPEAN LOCATIONS 176

Winkler, P.M:, Steiner, G., Morawiec, A., Vrtala, A.E., and Winklmayr, W.
ON THE QUEST FOR THE FIRST EVER MEASURED "BANANA" IN THE ATMOSPHERE 179

Wlasits, P.J., Kunze, D., Konrat, R., Jacobshagen, A. and Winkler, P.M.
CHARACTERISATION OF A THERMODENUDER-TYPE INLET USING NANOPLASTIC AEROSOL 183

Xia, M., Jiang, Y., Xue, L., Wang, X., Zhong, X., Liu, Y., Kulmala, M., Ma, T., Wang, J., Wang, Y., Gao, J., and Wang, T.
QUANTIFYING HONO PRODUCTION FROM NITRATE PHOTOLYSIS IN A POLLUTED ATMOSPHERE 185

Zhao, J.-Y., Tseng, Y.-L., and Yuan, C.-S.
CHEMICAL FINGERPRINTS AND SOURCE APPORTIONMENT OF PM2.5 AT OFFSHORE AND REMOTE ISLANDS IN TAIWAN AND JAPAN TRANSPORTED THROUGH EAST AND WEST CHANNELS 186

Main Topic 3: Cloud Drop and Ice Nucleation 190

Aleff, C., and Koop, T.
ON THE ICE NUCLEATION ACTIVITY OF MOLECULAR ICE NUCLEATORS 191

Andan, C.S., Moravec, P., Zíková, N., Lhotka, R., Mbengue, S., Ondráček, J., Schwarz, J., Vodička, P., and Ždímal, V.
HYGROSCOPICITY AND CLOUD CONDENSATION NUCLEI ACTIVATION OF ATMOSPHERIC AEROSOLS AT A CENTRAL EUROPEAN RURAL SITE 193

Bieber, P., and Borduas-Dedekind, N.
THE ROLE OF CONTACT LINE ICE-NUCLEATION FOR FREEZING OF WATER ON PLASTIC INTERFACES 197

Bogert, P., Lacher, L., Höhler, K., Ludewig, E., Maier, C., Schrod, J., Curtius, J., and Möhler, O.
FREE-TROPOSPHERIC ICE-NUCLEATING PARTICLE MEASUREMENTS AT CIRRUS FORMATION TEMPERATURES 201

Brooks, S.D., Thornton, D.C.O., and Sofa, R.
WHAT DRIVES BIOGENIC ICE NUCLEATION? 204

Gratzl, J., Böhmländer, A., Möhler, O., Asmi, E., Pätsi, S., Saarto, A., Pogner, C.-E., Gorfer, M., Brus, D., Doulgeris, K.M., Stolzenburg, D., Wieland, F., and Grothe, H.
SUB-ARCTIC FUNGAL SPORES AS ATMOSPHERIC ICE-NUCLEATING PARTICLES 206

Kaniyodical Sebastian, M., Wagner, R., Kiselev, A., Saathoff, H., Li, Y., Hoehler, K., Umo, N.S., and Moehler, O.
ROLE OF ISOPRENE-DERIVED SECONDARY ORGANIC AEROSOLS IN THE GLACIATION OF DEEP CONVECTIVE CLOUDS 208

Kiselev, A.A., Seidel, J.S., and Hartmann, S.
COMPETITION BETWEEN DYNAMIC WETTING AND FREEZING OF SUPERCOOLED WATER DROPLETS UPON CONTACT WITH ICE OR ICE-NUCLEATING SURFACE 211

Krautwig, T., and Marcolli, C.
THE ROLE OF ORGANIC MATTER FOR ICE NUCLEATION ON MINERAL AND SOIL DUSTS 215

Laaksonen, A., Roudsari, G., A Piedehierro, A., and Welti, A.
DEPOSITION ICE NUCLEATION VIA FREEZING OF ADSORBED WATER 219

Molinero, V.
THE MOST POTENT SNOW MAKERS 220

Naik, M., Vispute, A., Shinde, C., Wagh, S., and Ghude, S.D.
AEROSOL'S CCN ACTIVITY AND AEROSOL CHEMICAL COMPOSITION DURING FOG AND HAZE EVENTS IN NEW DELHI, INDIA 221

Perkins, R., Zhou, R., Juergensen, D., Ayars, K., Dutton, O., DeMott, P., and Kreidenweis, S.
COMPREHENSIVE CHARACTERIZATION OF THE SEASONAL CYCLES OF ICE NUCLEATING PARTICLES IN COMPLEX MOUNTAINOUS TERRAIN 224

Righi, C., Elomaa, T., Chan, T., Graeffe, F., Quéléver, L.L.J., Petäjä, T., Berthier, A., Ganeau, L., Ortega, I.K., Vandestoc, A., Arsicaud, L., Badhe, A.S., Renard, C., May-Carle, J.B., Sarnela, N., and Duplissy, J.
COMPARISON OF THE MEASURED CHEMICAL COMPOSITION OF LOW VOLATILITY ORGANIC COMPOUNDS FROM DIFFERENT AIRCRAFT FUELS LEADING TO NEW PARTICLE AND ICE NUCLEI FORMATION 225

Schlagin, J., Tonauer, C., Liedl, K.R., and Loerting, T.
ON THE IDENTIFICATION OF ICE PHASES AND PHASE TRANSITIONS USING NIR AND MIR SPECTROSCOPY 228

Seidel, J.S., Kiselev, A.A., Krause, B., Kamiński, M., Heuser, D.A., Abart, R., and Petrishcheva, E.
IN SITU X-RAY DIFFRACTION STUDY OF ICE CRYSTALS GROWING ON NATURAL ALKALI FELDSPAR 229

Seifried, T.M., Uppal, G., Nikkho, S., Morales Murillo, A., Andrew, L.J., Varcoe, C., Grant, E.R., and Bertram, A.K.
EMERGING CONTAMINANTS IN THE AIR: IMPACT OF MICROPLASTICS ON CLOUD FORMATION THROUGH ICE NUCLEATION 233

Vadgama, D.D., Srivastava, R., and Shinde, S.M.
STUDY OF MULTICOMPONENT AEROSOL-WATER INTERACTIONS USING MOLECULAR DYNAMIC SIMULATION: IMPLICATIONS FOR CLOUD DROPLET FORMATION 236

Welti, A., Viisanen, Y., Piedehierro, A.A., and Laaksonen, A.
PHASE TRANSITION IN THIN LAYERS OF ADSORBED WATER ON PbI2 240

Wieland, F. and, Grothe, H.
EXPLORING THE ROLE OF AGGREGATION IN BIOLOGICAL ICE-NUCLEATING MACROMOLECULES 242

Zhang, C., Shen, X., Jacquot, J.L., Lacher, L., Brem, B.T., Modini, R.L., Selvakumar, V., Sprenger, M., Steinbacher, M., Henne, S., Coen, M.C., Conen, F., Höhler, K., Möhler, O., Gysel-Beer, M., Cziczo, D.J., and Kanji, Z.A.
SINGLE-PARTICLE ICE-NUCLEATING PARTICLE (INP) CHARACTERIZATION AT MIXED-PHASE AND ICE CLOUD CONDITIONS AT THE HIGH ALTITUDE STATION JUNGFRAUJOCH (3580 M A.S.L.), SWITZERLAND 245

Main Topic 4: Aerosol-Climate Interactions **249**

Castin, L., Coopman, Q., Dziduch, A., Jourdan, O., and Riedi, J.
INFLUENCE OF AIR PARCEL HISTORY ON THE THERMODYNAMIC PHASE OF LOW-LEVEL ARCTIC CLOUDS 250

Cho, H., Kang, H., Yoon, Y., and Park, K.
DEVELOPMENT OF MACHINE LEARNING MODEL TO PREDICT CCN NUMBER CONCENTRATION IN THE ARCTIC 253

Fattahi Masrour, P., and Coopman, Q.
THE INFLUENCE OF VARIOUS AEROSOL TYPES ON CLOUD MICROPHYSICAL PROCESSES: AN EXAMINATION OF ARCTIC AEROSOL-CLOUD INTERACTIONS IN RELATION TO WRF-CHEM PARAMETERIZATION SENSITIVITY. 256

Junkermann, W., Hacker, J.M., and McGrath, A.
SHORTCOMINGS IN ULTRAFINE PARTICLE MEASUREMENT AND SOURCE ATTRIBUTION, MAJOR SOURCES AND ENVIRONMENTAL IMPACT 260

Kulmala, M., Petäjä, T., Lintunen, A., Laakso, A., Ehn, M., Lehtipalo, K., and Kerminen, V.-M.
HOW ATMOSPHERIC NEW PARTICLE FORMATION AFFECTS INTERLINKED ENVIRONMENTAL GRAND CHALLENGES? 261

Paasonen, P., Li, X., Basyal, S., Okuljar, M., Ding, D., Clusius, P., Foreback, B., Ovaska, A., Li, X., Portin, H., Niemi, J., Paunu, V.-V., Karvosenoja, N., Jalkanen, J.-P., Klimont, Z., Kerminen, V.-M., Kulmala, M., Petäjä, T., and Lehtipalo, K.
EMITTED NUCLEATION MODE PARTICLES – HOW TO DISTINGUISH FROM NEW PARTICLE FORMATION AND TO INLCUDE IN MODELS? 265

Shinde, C.D., Wagh, S., Vispute, A., Deshmukh, S., and Ghude, S.
INFLUENCE OF AEROSOL MIXING STATE ON HYGROSCOPIC GROWTH AND FOG FORMATION IN NEW DELHI: INSIGHTS FROM HTDMA MEASUREMENTS 269

Xenofontos, C., Kohl, M., Ruhl, S., Pozzer, A., Lelieveld, J., and Christoudias, T.
IMPACT OF ANTHROPOGENIC AMMONIA ON UPPER TROPOSPHERIC AEROSOL COMPOSITION AND CLIMATIC IMPLICATIONS 272

Special Session 1: Global observations of aerosols, clouds and trace gases: longterm monitoring networks and research infrastructure **275**

Ahn, C., Seo, P., Yum, S.S., and Moore, R.H.
NEW PARTICLE FORMATION EVENTS OBSERVED DURING THE AIRCRAFT MEASUREMENT OF THE ASIA-AQ CAMPAIGN 276

Cao, M., Yan, C., Liu, Y., Yin, J., Ge, D., Li, Y., Han, B., Wang, Z., Nie, W., and Ding, A.
NEW INSIGHTS INTO THE MOLECULAR CHEMICAL CHARACTERISTICS AND SOURCES OF ATMOSPHERIC ORGANIC AEROSOLS IN EAST CHINA 280

Hartl, H.G., Kulmala, M., Vanhanen, J., and Lehtipalo, K.
INSIGHTS OF LONG-TERM AEROSOL PARTICLE SIZE DISTRIBUTION MEASUREMENTS DOWN TO 1 nm WITH THE NEW AIRMODUS A12 IN HYYTIÄLÄ, FINLAND 282

Höhler, K., Bachleitner, T., Büttner, N., Fösig, R., Karrais, A., Käfer, U., Lacher, L., Ludewig, E., Maier, C., Möhler, O., Van Pinxteren, D., and Schwarzenböck, A.
OBSERVING CLOUDS IN A WARMING WORLD: THE ACTRIS TOPICAL CENTRE FOR CLOUD IN SITU MEASUREMENTS 284

Jiang, J., Wu, J., Li, Y., Wu, H., Zhang, Q., Liao, H., and Wang, Y.
CHARACTERIZING AIRBORNE ULTRAFINE PARTICLES IN CHINA BASED ON A BIPOLAR SMPS NETWORK 286

Kivekäs, N., Juurola, E., Saponaro, G., Paramonov, M., Petäjä, T., Cornacchia, C., Petracca Altieri, R., Wiedensohler, A., Tillmann, R., Höhler, K., Haeffelin, M., De Maziere, M., Nicolae, D., and Lund Myhre, C.
ACTRIS – HIGH QUALITY ATMOSPHERIC DATA TO ALL USERS 289

Lehtipalo, K., Lampilahti, J., Hartl, H., Petäjä, T., and Häme, S.
ACTRIS CLUSTER CALIBRATION CENTER: TOWARDS STANDARDIZING THE MEASUREMENTS OF SUB-10 NM AEROSOL PARTICLES 292

Lhotka, R., Pokorná, P., Vodička, P., Zíková, N., Chen, G.I., Prévôt, A.S.H., Mbengue, S., Schwarz, J., and Ždímal, V.
THE INFLUENCE OF ATMOSPHERIC TRANSPORT AND MIXING ON INTERPRETATION OF PM1 AND ORGANIC AEROSOL SOURCE APPORTIONMENT AT A RURAL BACKGROUND SITE IN CENTRAL EUROPE 294

Liu, C., Perakyla, O., Kolhinen, V.S., Ahonen, L., Ehn, M., and Sarnela, N.
MULTI-YEAR MEASUREMENT OF LOW-VOLATILITY VAPORS AND THEIR IMPLICATIONS IN BOREAL ENVIRONMENT 296

Moschos, V., Chevassus, E., Fossum, K.N., Lei, L., Prabhu, V., Martin, D., Ceburnis, D., O'Dowd, C., and Ovadnevaite, J.
DECADAL TRENDS AND SOURCE ATTRIBUTION OF ATMOSPHERIC AEROSOLS AT MACE HEAD 299

Pernov, J.B., Alroe, J., Sulo, J., Li, Z., Ristovski, Z., and Miljevic, B.
CAPE-K CHEM: NEW PARTICLE FORMATION AND PRECURSORS VAPORS AT CAPE GRIM 301

Sarnela, N., Mettke, P., Simon, M., Vera, T., Soler, R., and the intercomparison collaboration
THE FIRST ACTRIS CHEMICAL IONIZATION MASS SPECTROMETRY INTERCOMPARISON WORKSHOP PROVIDED CRUCIAL INFORMATION ON THE DETECTION OF CONDENSABLE VAPOURS 304

Toanca, F., Dandocsi, A.V., Ilie, A., Vasilescu, J.G., Nicolae, D., and Nemuc, A.
INVESTIGATION OF LOW-VISIBILITY ATMOSPHERIC EVENTS AT RADO-BUCHAREST ACTRIS FACILITY, ROMANIA 308

Virtanen, A., Joutsensaari, J., Kokkala, H., Partrige, D.G., Blichner, S., Seland, Ø., Holopainen, E., Tovazzi, E., Lipponen, A., Mikkonen, S., Leskinen, A., Hyvärinen, A.-P., Zieger, P., Krejci, R., Ekman, A.M.L., Riipinen, I., Quaas, J., and Romakkaniemi, S.
LONG TERM IN-SITU OBSERVATIONS REVEAL HIGH SENSITIVITY OF CLOUD FORMATION TO AEROSOL CHANGES 312

Wang, Z., Nie, W., Liu, Y., Yang, L., Liu, C., Zhang, Y., Yan, C., Zha, Q., Ge, D., Qi, X., Zhou, C., Chen, L., Zhou, X., Wang, L., Huang, D.D., Chi, X., and Ding, A.
GASEOUS SULFURIC ACID CONTRIBUTIONS TO SULFATE FORMATION IN URBAN ATMOSPHERE 314

Wiedensohler, A., Weinhold, K., Merkel, M., Pfeifer, S., Düsing, S., Müller, T., and Pöhlker, M.
ACTRIS QUALITY ASSURANCE OF THE NEW AEROSOL MEASUREMENTS IN THE EUROPEAN AIR QUALITY DIRECTIVE: PARTICLE NUMBER CONCENTRATION, PARTICLE NUMBER SIZE DISTRIBUTION, AND EQUIVALENT BLACK CARBON 316

Yang, T., Li, H., Song, Y., Tian, Y., Tan, Y., Sun, Y., and Wang, Z.
ADVANCING VERTICAL PROFILING OF PM2.5 CHEMICAL COMPONENTS: INTEGRATING REMOTE SENSING RETRIEVAL WITH DATA ASSIMILATION SYSTEMS 319

Zhang, C. Lam, Y.H., Welti, A., David, R.O., Schrod, J., Ickes, L., Thomson, E.S., and Kanji, Z.A.
GLOBAL ICE-NUCLEATING PARTICLE NUMBER CONCENTRATION DATABASE: AMBIENT MEASUREMENTS FROM 1948 TO 2025 322

Zou, Z., Du, W., Yuan, Q., Liu, Y., Ciarelli, G., and Kokkonen, T.V.
FIVE-YEAR COMPARATIVE SECONDARY INORGANIC AEROSOL STUDY: EMMISSION SOURCES AND TRANSPORT PATTERNS IN FINLAND'S BOREAL FOREST AND BEIJING MEGACITY 325

Special Session 2: Solar radiation management by aerosols 328

Chapman, J., and Hunt, H.
PRELIMINARY AEROSOL CHARACTERIZATION OF SALINE RAYLEIGH JETS FOR THE PURPOSE OF MARINE CLOUD BRIGHTENING 329

Chapman, J., McGrath, D., and Hunt, H.
ELECTROSPRAYING HIGHLY CONDUCTIVE SALINE SOLUTIONS FOR THE PURPOSE OF MARINE CLOUD BRIGHTENING 332

Li, Z., Alroe, J., Harrison, L., Scoble, H., Harrison, D., and Ristovski, Z.
ESTIMATING SHADING FROM ARTIFICIAL SEAWATER DROPLET PLUME ON THE GREAT BARRIER REEF 335

McGrath, D., and Hunt, H.
EXPERIMENTAL INSIGHTS INTO THE DRYING OF SEAWATER DROPLETS FOR MARINE CLOUD BRIGHTENING 337

Raj, Y., and Hunt, H.
BUBBLE-BURSTING ATOMISATION FOR MARINE CLOUD BRIGHTENING 339

Reardon, E.
ADVANCES IN SUB MICRON AEROSOL GENERATION BY SUPERHEATED ATOMISATION FOR MARINE CLOUD BRIGHTENING 341

Rug, L., Ascher, B., Kainz, J., Lim, J.-S., and Hoffmann, F.
MARINE CLOUD BRIGHTENING: CONSTRAINING SMALL-SCALE UNCERTAINTY 344

Sulo, J., Okuljar, M., Alroe, J., Li, Z., Horchler, E., Cravigan, L., Trounce, H., Harrison, L., Harrison, D., and Ristovski, Z.
DIRECT OBSERVATIONS OF CORAL REEF INFLUENCE ON AEROSOL LOADING OVER THE GREAT BARRIER REEF 346

Special Session 3: Young principal investigators: shaping the research of the future **349**

Duft, D., Leisner, T., and Jones, S.H.
USING SINGLE PARTICLE LEVITATION TO PROBE TRANSFORMATIONS OF ATMOSPHERIC AEROSOL IN THE LABORATORY 350

Gani, S.
AEROSOLS IN MEGACITIES IN THE 21ST CENTURY: ROLE OF SCIENCE AND SCIENTISTS 353

Heikkinen, L., Faivre, L., Behr, N., Blichner, S., Talvinen, S., Wu, C., Partridge, D.G., Zieger, P., Riipinen, I., Krejci, R., and Mohr, C.
INVESTIGATING AEROSOL–CLOUD INTERACTIONS: THE ROLE OF BVOC-DERIVED SOA AND CLOUD WATER CHEMISTRY IN A CHANGING ATMOSPHERE 354

Mahrt, F., Nikkho, S., Testa, B., Uppal, G., Zaks, J., Lam, A., Peng, L., Kanji, Z.A., Ammann, M., and Bertram, A.K.
UNEXPECTED CRYSTALLINE SOLID PHASE STATE OF SECONDARY ORGANIC AEROSOL 358

Rosati, B., and Stolzenburg, D.
FROM OCEANS TO CITIES AND FROM CLUSTERS TO CLOUDS: INTRODUCING FUTURE PERSPECTIVES 359

Yan, Y., Fárníková, K., Li, K., Pysanenko, A., Pluhařová, E., Fárník, M., and Lengyel, J.
UPTAKE OF INDIVIDUAL MOLECULES BY BINARY WATER-NITRIC ACID CLUSTERS: NUCLEATION AT THE SUBNANOMETER SCALE 362

Zíková, N., Julaha, K., Sedlák, P., Ždímal, V., and Brus, D.
CLOUD DROPLET SPECTRA MEASUREMENTS: COMPARISON IN LOW STRATIFORM CLOUDS 364

Special Session 4: Urban new particle formation 366

Agro', M., Bettineschi, M., Melina, S., Sulo, J., Lehtipalo, K., Petäjä, T., Grigioni, I., Ciarelli, G., Lampilahti, J., Colombi, C., Biffi, B., Marinoni, A., Bigi, A., Oliewo, C., Kulmala, M., and Bianchi, F.
ATMOSPHERIC MIXING AND LOW POLLUTION ENHANCE NEW PARTICLE FORMATION IN MILAN, ITALY 367

Cai, R., Li, X., Li, Y., Blichner, S., Stolzenburg, D., Wang, L., Worsnop, D., Jiang, J., Kulmala, M., and Kangasluoma, J.
RAPID INITIAL GROWTH OF NEW ATMOSPHERIC PARTICLES BY LARGE NANOPARTICLE CONCENTRATION GRADIENT 370

Das, B., Bhattacharjee, U., Pathak, B., Borgohain, A., Kundu, S.S., and Bhuyan, P.K.
CLOUD CONDENSATION NUCLEI ENHANCEMENT BY NEW PARTICLE FORMATION EVENTS OVER A LOCATION IN THE EASTERN HIMALAYAN FOOTHILLS 374

Du, W., Sun, Y.L., Zhao, J., Dada, L., Wang, Y.Y., Chen, X.S., Li, Z.Q., Zhang, Y.J., Hu, F., Kokkonen, T.V., Kerminen, V.M., and Kulmala, M.
UNDERSTANDING THE INFLUENCE OF PARTICLE GROWTH ON AIR QUALITY AND LOCAL CLIMATE IN MEGACITY 378

Fossum, K.N., Lin, C., O'Sullivan, N., Lei, L., Hellebust, S., Ceburnis, D., Afzal, A., Tremper, A., Green, D., Jain, S., Byčenkienė, S., O'Dowd, C., Wenger, J., and Ovadnevaite, J.
SHIP EMISSION PROFILES FROM AMBIENT MEASUREMENTS IN DUBLIN PORT AND WHAT WE ARE MISSING 380

Li, Z., Han, S., Lau, Y., Xiao, Y., Miljevic, B., Horchler, J., Hu, W-P., Wang, H., Wang, B., and Ristovski, Z.
SECONDARY ORGANIC AEROSOL FORMATION FROM ISOPRENE AND TOLUENE MIXTURE 383

Meda, B.N.M., Sarangi, C., Kanawade, V.P., Sebastian, M., Chakraborty, O., Hooda, R.K., Hyvärinen, A.-P., Cherian, P., and Jokinen, T.
METEOROLOGY-INDUCED NEW PARTICLE FORMATION DURING WINTER OVER INDIA 385

Oliewo, C.A., Paglione, M., Rinaldi, M., Trentini, A., Ghermandi, G., and Bigi, A.
INVESTIGATING AIR IONS DURING SUMMER NEW PARTICLE FORMATION EVENTS IN BOLOGNA 389

Pichelstorfer, L., Kumar, A., Vinkvist, N., Iyer, S., and Rissanen, M.
SEMI-EMPIRICAL CONSTRAINT ON THE RATE OF P-XYLENE AUTOXIDATION CHEMISTRY FROM A FLOW TUBE SETUP 393

Srivastav, G., Lampilahti, J., Lehtipalo, K., and Gani, S.
AN OPEN TOOLKIT FOR PARTICLE SIZE DISTRIBUTION ANALYSIS 396

Srivastav, G., Wagay, A., Lampilahti, J., Rathore, J., Kunchala, R.K., Ganguly, D., Kulmala, M., Paasonen, P., Thakur, R., and Gani, S.
ATMOSPHERIC IONS AND PARTICLES IN THE INDO-GANGETIC PLAIN 398

Stolzenburg, D., Tischberger, M., Verma, R., and Grothe, H.
NEW PARTICLE FORMATION POTENTIAL OF EMERGING AIR POLLUTANTS PROBED BY MULTI-PRESSURE CHEMICAL IONIZATION MASS SPECTROMETRY 401

Sun, H., Liu, Y., Nie, W., Li, Y., Ge, D., Xu, T., Yin, J., Liu, C., Fu, Z., Qi, X., Liu, T., Zha, Q., Yan, C., Chi, X., and Ding, A.
UNEXPECTED GAS-PHASE FORMATION OF GLYCOLIC ACID SULFATE IN THE ATMOSPHERE 405

Tang, L., Feng, Z., Shang, D., Zeng, L., Wu, Z., Wang, H., Chen, S., Li, X., Zeng, L., Hu, J., and Hu, M.
ONGOING ANTHROPOGENIC EMISSION ABATEMENT PROMOTES NEW PARTICLE GROWTH IN A CHINESE MEGACITY 407

Verma, R., Perrier, S., Rohner, U., Michoud, V., Di Biagio, C., Gratien, A., Hawkins, L., D'Anna, B., Kammer, J., Monod, A., Cantrell, C., George, C., Hilfiker, F.L., Stark, H., and Riva, M.
COMPREHENSIVE SOURCE APPORTIONMENT OF URBAN VOCs: EVIDENCE FOR VCP-DOMINATED EMISSIONS USING HIGH-RESOLUTION MASS SPECTROMETRY AND BINPMF DURING THE ACROSS CAMPAIGN IN PARIS 411

Wei, Y., Chen, X., Liao, Z., Ma, P., and Quan, J.
THE SIGNIFICANT IMPACT OF ORGANIC TRANSPORT ON NEW PARTICLE FORMATION AND ULTRAFINE PARTICLE CONCENTRATION IN BEIJING 415

Yan, C., Nie, W., Kulmala, M., and Ding, A.J.
NEW PARTICLE FORMATION IN CHINA'S MEGACITIES 417

Zhang, T., Du, W., Lampilahti, J., Zhang, X., Zou, Z., Kokkonen, T., Kerminen, V.-M., and Kulmala, M.
NEW INSIGHTS INTO NEW PARTICLE FORMATION FROM A COMPARISON STUDY BETWEEN BIOGENIC AND ANTHROPOGENIC EMISSIONS DOMINATED ENVIRONMENTS 419

Zhang, X., Li, C., Cai, R., Yao, L., and Wang, L.
VOLATILITY PARAMETRIZATION OF ATMOSPHERIC ORGANIC COMPOUNDS BASED ON MOLECULAR FORMULA 421

Zhang, X., Li, Y., Gu, Y., Vettikkat, L., Schobesberger, S., Kulmala, M., and Ehn, M.
DRCREASING SO2 LEVELS FORM COAL POWERPLANTS INFLUENCE ATMOSPHERIC PARTICLE FORMATION 422

Special Session 5: Instruments, chambers, facilities 424

Bauer, P.S., Berger, V., Risby, K.M., Sorani, E., Schulz, H.J., Swanson, J., and Boies, A.
HOMOGENEOUS AND HETEROGENEOUS GENERATION OF NANOPARTICLES BY EVAPORATION-CONDENSATION WITH THE SILVER PARTICLE GENERATOR 425

Casalnuovo, D.A., Cheng, D., Flores-Romero, M., Montesinos-Castellanos, A., and Jen, C.N.
A REACTIVE CONDENSATION PARTICLE COUNTER FOR MEASURING ATMOSPHERICALLY RELEVANT CONCENTRATIONS OF SULFURIC ACID 428

Cheng, D., Kiguru, J., and Jen, C.N.
DETECTION EFFICIENCY OF A WATER CONDENSATION PARTICLE COUNTER USING ELECTRICALLY NEUTRAL SULFURIC ACID AND SULFURIC ACID-DIMETHYLAMINE CLUSTERS 432

Enders, V., Dinu, D.F., Grothe, H., Podewitz, M., Tischberger, M., and Stolzenburg, D.
FREEZING ATMOSPHERIC ORGANIC NUCLEATION: USING MATRIX ISOLATION FTIR AS A NEW METHOD 435

Liu, Y., Han, B., Yan, C., Nie, W., Bianchi, F., Kulmala, M., and Ding, A.
VOLTAGE SCANNING APPLICATION OF NITRATE CHEMICAL IONIZATION MASS SPECTROMETER 439

Milani, Z.R., Nichman, L., and Matida, E.
EXPLORING IN-FLIGHT ATMOSPHERIC AEROSOL SAMPLING CHALLENGES 442

Niskanen, M., Seppänen, A., and Lehtinen, K.E.J.
CHARGER-RELATED UNCERTAINTY IN ELECTRICAL AEROSOL MEASUREMENTS 446

Park, M., Cha, J.W., Park, S., Kim, J., Kim, Y., Belorid, M., Kim, B.-Y., Baek, J., Kim, S., Lee, K., Seo, P., Ahn, C., Lee, J., Yum, S.S., and Um, J.
THE KOREA CLOUD PHYSICS EXPERIMENTAL CHAMBER (K-CPEC): DESIGN, CAPABILITIES, AND PRELIMINARY RESULTS FROM ICE NUCLEATION EXPERIMENTS 448

Rothenfluh, D., Zeder, Y., Graf, E., Schwendimann, A., Burch, P., Abt, R., and Niederberger, E.
DISTUINGISH MINERAL DUST AND BIOLOGICAL AEROSOL PARTICLES AS WELL AS WATER DROPLETS AND ICE CRYSTALS AUTOMATIC AND IN REAL-TIME WITH SWISENS POLENO JUPITER 452

Shah, J.S., Abdul, R., Balint, Tibor, A., and Bozoki, Z.
QUANTITATIVE ABSORPTION SPECTRUM OF HYDROCARBON AEROSOLS USING DUAL-CELL PHOTOACOUSTIC SPECTROSCOPY 455

Shcherbinin, A., Finkenzeller, H., Partovi, F., Vinkvist, N., Mikkilä, J., Kontro, J., Mikkilä, J., Jost, H.-J., Kangasluoma, J., Iyer, S., and Rissanen, M.
ADVANCING GAS PHASE ANALYSIS IN AEROSOL RESEARCH: MPCIMS WITH URONIUM FOR COMPREHENSIVE TRACE GAS DETECTION 456

Shen, J., Zhang, J., Juuti, P., Mikkila, J., Rissanen, M., Shcherbinin, A., Ehn, M., Kangasluoma, J., and He, X-C.
CHARACTERIZATION OF MULTI-SCHEME BROMIDE-BASED CHEMICAL IONISATION (Br-MION2) USING TIME-OF-FLIGHT AND ORBITRAP MASS SPECTROMETERS 458

Tischberger, M., Kaiser, M., Grothe, H., Lair, M., Opacak, M., Schachamayr, D., Verma, R., and Stolzenburg, D.
INSUFFICIENT MASS SPECTROMETRIC DETECTION OF SYNTHESIZED HYDROPEROXY ACIDS FROM LPHA-PINENE OZONOLYSIS 462

Umo, N.S., Connolly, P., Ascher, B., Bi, K., Chen, S., Deng, Z., Etcheto, J., Hoffmann, F., Hu, Y., Kim, N., Riemer, N., Tang, W., Topping, D., Wagner, R., Xu, X., Xue, L., Yum, S.S., Zhu, B., and Möhler, O.

CLOUD CONDENSATION AND ICE NUCLEATION PROCESS STUDIES BY COMBINED CLOUD SIMULATION CHAMBER AND PROCESS MODELLING ACTIVITIES 465

Special Session 6: CLOUD **468**

Junninen, H., Koemets, P., Sommer, E., Konrat, R., Mirme, S., Tamme, K., Winkler, P., Canagaratna, M., Worsnop, D., and the CLOUD collaboration

STABILITY OF CLUSTERS OF HIGHLY OXYGENATED ORGANIC MOLECULES FROM ALPHA-PINENE OZONOLYSIS AND SULPHURIC ACID OXIDATION. 469

Rato, P., Sommer, E., Almeida, J., Koemets, P., Mirme, S., Liu, L., Yang, B., Klebach, H., Kirkby, J., and CLOUD collaboration

COLLISION RATES OF MULTIPLY-CHARGED AEROSOL PARTICLES IN THE CERN CLOUD CHAMBER 471

Russell, D.M., Kunkler, F., Shen, J., Vivo, J.D., CLOUD collaboration, Donahue, N.M., Harder, H., Kirkby, J., He, X.C., and Curtius, J.

ISOPRENE CHEMISTRY PRODUCING NUCLEATOR MOLECULES UNDER UPPER-TROPOSPHERIC CONDITIONS 472

Yang, B., Liu, L., Pignatelli, A., Caudillo-Plath, L., Russel, D.M., Kunkler, F., Judmaier, B., Zheng, Z., Scholz, W., DeVivo, J., Sommer, E., Yu, W., Dada, L., Cloud collaboration, and Haddad, I.E.

RO2 LIFETIME DRIVES BIOGENIC NEW PARTICLE FORMATION AND GROWTH IN THE PLANETARY BOUNDARY LAYER 475

Sponsors **479**

Main Topic 1: Nucleation Theory & Experiment

PARTICLE NUCLEATION IN WOOD COMBUSTION EMISSION

B. ALFOLDY[1], A. GREGORIČ[1,2], M. IVANČIČ[1], I. JEŽEK BRECELJ[1], M. RODENAS[3], E. BORRAS[3], R. SOLER[3], T. VERA[3], A. MUNOZ[3], E. YUBERO[4], J. CRESPO[4] and M. RIGLER[1]

[1]*Aerosol d.o.o., Ljubljana, SI-1000, Slovenia.*

[2]*Center of Atmospheric Research, University of Nova Gorica, Ajdovščina, Slovenia.*

[3]*EUPHORE Labs., CEAM Foundation, Paterna, Valencia, Spain.*

[4]*Atmospheric Pollution Laboratory (LCA-UMH), Miguel Hernandez University, Elche, 03202, Spain*

Keywords: BIOMASS BURNING, DIESEL EMISSION, SECONDARY ORGANIC AEROSOL, CHAMBER EXPERIMENT.

INTRODUCTION

Wood combustion is a significant source of airborne particulate matter, including black carbon (BC), primary organic aerosol (POA), and secondary organic aerosol (SOA), which have profound impacts on climate, air quality, and human health. This study investigates the chemical, physical and optical properties of secondary aerosols formed in wood combustion exhaust by both pathways, photochemical reactions and dark aging. The experiments were carried out int the EUPHORE simulation chamber, a controlled environment designed to replicate atmospheric conditions. Different types of wood (vine, orange, and beech) and combustion modes (flaming and smoldering) were used, with comparisons to Euro 2 diesel emissions to provide a comprehensive understanding of the optical and chemical properties of aerosols from various sources. Following the primary emission, combustion products were exposed to light, or aged under dark conditions in order to reveal the atmospheric transformation of the pollution.

METHODS

The emission were introduced into a hemispherical Teflon (FEP – fluorinated ethylene propylene) tent with a volume of 200 m^3 installed on the rooftop of CEAM Foundation building. FEP foil has excellent transparency in the UV-VIS range allowing the chamber to simulatie atmospheric photochemical processes. The chamber can be covered by a retractable steel housing that significantly reduces the light in the chamber and povide conditions that simulate dark atmospheric aging of the combustion products.
The optical properties of the aerosols were measured using a newly developed 9-wavelength Aethalometer (AE36s, Aerosol Magee Scientific) and a nephelometer (Aurora 3000, Acoem). The Aethalometer provided wavelength resolved absorption information in the 340-950 nm range, allowing for precise characterization of light absorption of BC and BrC.
Total carbon content of the aerosol (TC) was measured by the TCA-08 of Aerosol Magee Scientific whereas the organic carbon (OC) content was determined as the difference between TC and BC (TC-BC method, Rigler et al., 2020).
The dynamics of particle formation and growth were monitored using a Scanning Mobility Particle Sizer (SMPS, TSI), which provided real-time measurements of particle size distributions in the 14-796 nm range.

CONCLUSIONS

Primary emissions from wood combustion were characterized by high concentrations of BC and primary organic carbon (POC), with significant variations depending on the combustion mode. Flaming combustion generally produced more BC and less POC compared to smoldering combustion, which emitted higher amounts of POC with higher brown carbon (BrC) content. The average BC and POC emission factors, and POC/BC ratios of th different emissions are summarized in Table 1. The last column of the table shows the ratio of secondary organic carbon (SOC) to the primary OC after the aging cycle, indicating the aging mode (light exposure – le, or dark aging – da). In one experiment, a massive nucleation burst event was observed resulting in the highest SOC/POC ratio, which is shown separately in the table (N).

The SOC/POC ratio was higher in the experiments where the pollution was exposed to sunlight. More SOC precursor molecules were released by smoldering combustion than by flaming, as it is reflected in a higher SOC/POC ratios. Surprisingly, the aging of diesel emission resulted in higher SOC/POC ratio despite the high temperature and excess of oxygen combustion and catalytic after-treatment system. The highest SOC/POC ratio (3.16) was recorded during the massive nucleation burst event.

Figure 1 shows the nucleation event reflected by the SMPS measurement. Following the emission into the dark chamber at 8:00, the particle number concentration dropped due to deposition, dilution and coagulation of the particles. The latter contributed to the increase in the count median diameter (CMD) of the particles which grew from an initial 78 nm to 150 nm at a growth rate of 24.5 nm/h during the dark period. After the exposure to light (11:00), the nucleation process started which initially caused the CMD decrease to 100 nm due to the contribution of the freshly nucleated low diameter aerosol. The CMD then started to grow again due to coagulation and condensation of volatile compounds on the surface of the particles. The CMD grew up to 238 nm with a growth rate of 45.4 nm/h. The coagulation-corrected average nucleation rate was 8.04 particles/cm^3/s for the whole photochemical cycle.

Emission	BC (g/kg fuel)	POC (g/kg fuel)	POC/BC	SOC/POC
Diesel	0.55	0.34	0.62	1.40 le 0.18 da
Flaming-B, O	0.46	0.59	1.28	0.68 le 3.16 N
Flaming-V	0.73	1.11	1.52	0.39 le 0.19 da
Smoldering-B	0.10	4.62	46.2	1.18 le 0.29 da
Smoldering-O	0.36	19.2	53.3	1.10 le 0.45 da

Table 1. BC and primary OC emission factors of different sources, and the secondary-to-primary OC ratios after different aging (light exposure - le or dark aging - da). N denotes massive nucleation event.

Overall, this work provides a comprehensive understanding of the physical, optical, and chemical properties of wood combustion aerosols, including their primary emissions, secondary formation, and aging processes. The results highlight the importance of considering secondary aerosol formation and aging when assessing the impact of wood combustion on the global radiation budget and air quality. The study also demonstrates the utility of advanced instrumentation, such as the 9-wavelength Aethalometer and real-time carbon speciation system (CASS) in characterizing the complex properties of atmospheric aerosols. The research contributes to ongoing efforts to improve our understanding of aerosol-climate interactions and to develop effective strategies to mitigate the impacts of biomass burning on air quality and climate change.

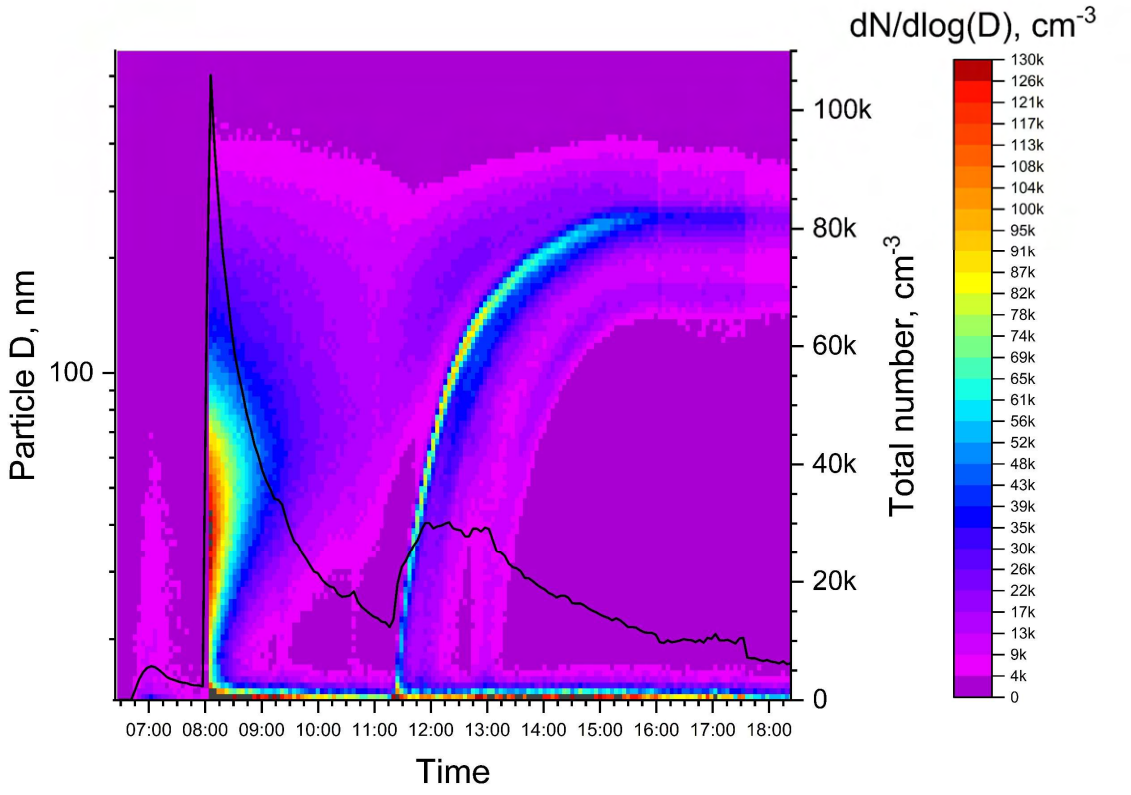


Figure 1. Variation of the particle diameter and particle number concentration during the experiment of the massive nucleation burst event (beech flaming emission and subsequent light exposure).

ACKNOWLEDGEMENTS

This work is part of a project supported by the European Commission under Horizon 2020 - R&I Framework Programme through the ATMO-ACCESS Integrating Activity under grant agreement number 101008004.

REFERENCES

Rigler, M., L. Drinovec, G. Lavrič, A. Vlachou, A.S.H. Prevot, J.L. Jaffrezo, I. Stavroulas, J. Sciare, J. Burger, I. Kranjc, J. Turšič, A.D.A. Hansen, and G. Močnik (2020). The new instrument using a TC–BC (total carbon–black carbon) method for the online measurement of carbonaceous aerosols, *Atmos. Meas. Tech*., **13**, 4333–4351.

MOLECULAR DYNAMICS SIMULATIONS OF HELIUM NUCLEATION IN LIQUID LEAD-LITHIUM ALLOYS

E. ALVAREZ-GALERA[1], J. MARTÍ[2] and L. BATET[3]

[1]*Doctoral degree in Computational and Applied Physics, B4-B5 Campus Nord, Department of Physics, Universitat Politècnica de Catalunya, Barcelona, 08034, Catalonia, Spain.*

[2]*Condensed, Complex and Quantum Matter Group, F.I.B., B4-B5 Campus Nord, Department of Physics, Universitat Politècnica de Catalunya, Barcelona, 08034, Catalonia, Spain.*

[3]*Advanced Nuclear Technologies Research Group, E.T.S.E.I.B., Diagonal 647, Department of Physics, Universitat Politècnica de Catalunya, Barcelona, 08028, Catalonia, Spain.*

Keywords: helium nucleation, liquid lead-lithium alloys, surface tension, solubility, nuclear fusion breeding blankets.

INTRODUCTION

The nucleation of helium in lead-lithium alloys, examined through classical molecular dynamics simulations, presents both theoretical interest and significant technological importance. Due to the extremely low solubility of helium in liquid metals, the noble gas rapidly aggregates into nanobubbles. Understanding this phenomenon is relevant for the development of nuclear fusion technologies. Indeed, fusion reactors' fuel cycle depends on producing tritium from neutron captures by lithium atoms:

$$\mathrm{n} + {}^{6}_{3}\mathrm{Li} \longrightarrow {}^{3}_{1}\mathrm{H} + {}^{4}_{2}\mathrm{He} + 4.78\ \mathrm{MeV} \quad (1)$$

$$\mathrm{n} + {}^{7}_{3}\mathrm{Li} \longrightarrow {}^{3}_{1}\mathrm{H} + {}^{4}_{2}\mathrm{He} + \mathrm{n} - 2.47\ \mathrm{MeV} \quad (2)$$

Helium generated during tritium breeding may spontaneously form bubbles, potentially affecting the performance of the liquid metal (LM) breeder, typically composed of Pb-16Li (Kordač and Košek, 2017). Lead plays a dual role in this alloy, multiplying neutrons and stabilizing the highly reactive lithium.
Figure 1 illustrates the Pb-Li phase diagram, showing the states explored in our simulations, and highlighting the eutectic point, isotherms, and phase regions of pure lithium, Pb16Li, and pure lead.

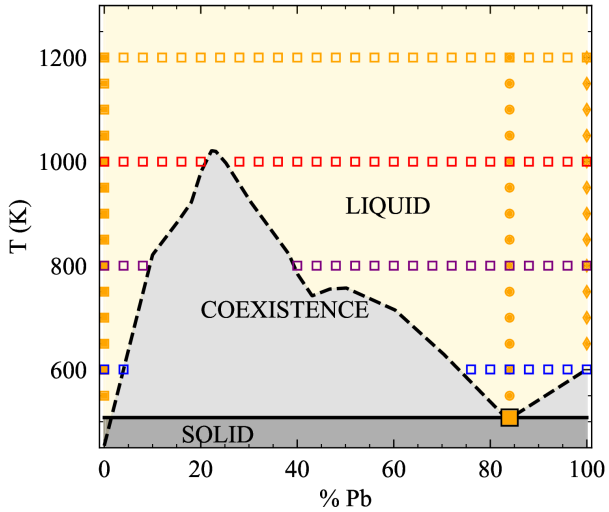


Figure 1. Schematic representation of the lead-lithium phase diagram (Okamoto, 1993), showing thermodynamic states explored in the simulations. Empty squares indicate isotherms at 600 K (blue), 800 K (purple), 1000 K (red),

and 1200 K (yellow). Yellow symbols (squares, circles, diamonds) denote simulation states for pure lithium, Pb16Li, and pure lead, respectively, at different temperatures The eutectic point is marked with a large square, and the liquidus line of the alloy is shown as a dashed black line.

Classical nucleation theory (CNT) identifies two key parameters governing the free energy barrier of nucleation: the solubility (Henry's law constant) and the gas–LM interfacial tension. We have employed mechanical and thermodynamic integration methods in order to evaluate those magnitudes from the analysis of molecular dynamics trajectories.

METHODS

Classical molecular dynamics simulations are conducted to model Pb-Li-He systems and to investigate helium segregation mechanisms across various LM compositions. The interatomic potentials used are based on the models developed by Al-Awad et al. (2023), Belashchenko (2012), Sheng and Tang (2021) and Sladek et al. (2014).

The CNT nucleation barrier comprises two terms: a surface term, derived using the mechanical route by Thompson et al. (1984) and computed from pressure profile integrations, and a volumetric (bulk) term, dependent on the thermodynamic β factor, helium size σ, and the supersaturation ratio.

The supersaturation ratio relates the partial pressure of helium dissolved in the LM to its saturated partial pressure.

We study Henry's law constants for infinite diluted solutions, using a thermodynamic integration method. This method couples the Hamiltonian to an *insertion* parameter accounting for the strength of interactions between helium and the liquid metal. We verified the good performance of the calculations for many alkali metal solutions in (Alvarez-Galera et al. 2024). In a recent paper (Alvarez-Galera et al., 2025), we predicted the Henry's law constants of helium in liquid lead and in liquid lead-lithium alloys, which have not been experimentally measured, to date. Furthermore, the activity coefficient a must be included in the calculation of the real helium partial pressure, which indicates how the system deviates from ideal infinite dilution conditions.

RESULTS

We investigate both interfacial tension and Henry's constant values by varying (a) temperature while holding the solvent composition constant (e.g., pure lithium, pure lead, Pb16Li); and (b) the lead/lithium fraction of the solvent at specific isotherms where any lead-lithium alloy is liquid according to its phase diagram (Okamoto, 1993), as depicted in *Figure 1*.

Simulations examined the influence of temperature and lead/lithium ratio on both interfacial tension and solubility across relevant liquid-state compositions.

Solvent	Melting point temperature (K)	Atomic packing factor	Henry's law constant (Pa)
Lithium	453	0.0603	3.137e+18
Lead	600	0.5486	1.446e+14
Pb16Li	508	0.5752	1.566e+15

Table 1. Simulated values of the atomic packing factor and Henry's law constant at temperatures slightly above the experimental melting points of lithium, lead and eutectic lead-lithium.

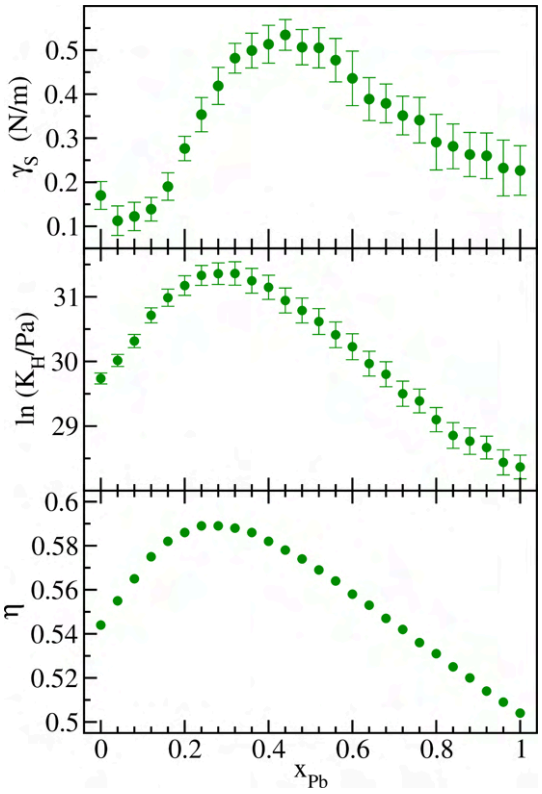


Figure 2. Trends of interfacial tension (top), natural logarithm of Henry's law constants (middle), and atomic packing factor (bottom) as functions of solvent composition. Data correspond to simulations at 1000 K. These plots illustrate how thermophysical properties vary with the lead/lithium atomic ratio, revealing key extrema relevant to helium solubility and segregation.

Table 1 presents some atomic packing factors and Henry's law constants for simulations conducted at temperatures around the melting points of each metal.
Figure 2 illustrates the dependence of bubble interfacial tension, Henry's law constants and atomic packing fraction on the composition of the LM at the isotherm of 1000 K.
The results reveal that: (a) interfacial tension values decrease with increasing temperature, while helium solubility increases exponentially with temperature; (b) there are two distinct lead/lithium ratios for which (1) the interfacial tension exhibits a maximum and (2) the solubility reaches a minimum.

CONCLUSIONS

Key observations include:

- **Interfacial tension** decreases linearly with temperature, while solubility decreases exponentially with the inverse of temperature.
- Two **specific lead/lithium ratios** are notable: one maximizes interfacial tension, while the other minimizes solubility.

Mechanical analysis reveals:

- The interfacial tension peak is explained by the fact that repulsive forces between helium and the solvent are maxima when lithium and lead are present in nearly equal amounts, reflecting competitive helium repulsion by both metals.
- The solubility minimum aligns with atomic packing maximum, which promotes helium exclusion, consistent with hard-sphere interaction models. Lead atoms tend to be the preferred neighbors due to size and density effects.
- These behaviors are attributed to strong non-idealities in intermediate alloy compositions.

ACKNOWLEDGEMENTS

This work was supported by the Spanish Nuclear Safety Council under the ARGOS Chair of Nuclear Safety and Radiation Protection. This communication is part of the EUROfusion project (HORIZON-101052200-EUROfusion), of the I+D+i project PID2021-124297NB-C32 funded by MCIN/AEI/10.13-039/501100011033 and "FEDER: Una manera de hacer Europa" and of the project 2021SGR-01411, funded by AGAUR (Generalitat de Catalunya).

REFERENCES

(Kordač and Košek, 2017) Kordač, M., & Košek, L. (2017). Helium bubble formation in Pb-16Li within the breeding blanket. *Fusion Engineering and Design*, *124*, 700-704.

Al-Awad et al. (2023) Al-Awad, A. S., Batet, L., & Sedano, L. (2023). Parametrization of embedded-atom method potential for liquid lithium and lead-lithium eutectic alloy. *Journal of Nuclear Materials*, *587*, 154735.

Belashchenko (2012) Belashchenko, D. K. (2012). Computer simulation of the properties of liquid metals: Gallium, lead, and bismuth. *Russian Journal of Physical Chemistry A*, *86*, 779-790.

Sheng and Tang (2021) Sheng, X. W., & Tang, K. T. (2021). The development of a full range analytical interatomic potential. *Physical Chemistry Chemical Physics*, *23*(13), 7748-7757.

Sladek et al. (2014) Sladek, V., Bučinský, L., Matuška, J., Ilčin, M., Lukeš, V., & Laurinc, V. (2014). Ab initio X 1 0+ ground state potential curves of Pb··· RG dimers (RG= He, Ne, Ar) including spin–orbit effects. Simulation of diffusion coefficients. *Physical Chemistry Chemical Physics*, *16*(34), 18519-18532.

Thompson et al. (1984) Thompson, S. M., Gubbins, K. E., Walton, J. P. R. B., Chantry, R. A. R., & Rowlinson, J. S. (1984). A molecular dynamics study of liquid drops. *The Journal of chemical physics*, *81*(1), 530-542.

(Alvarez-Galera et al. 2024) Alvarez-Galera, E., Laria, D., Batet, L., & Martí, J. (2024). Henry's constant of helium in liquid alkali metals. *Journal of Molecular Liquids*, *395*, 123853.

(Alvarez-Galera et al., 2025) Alvarez-Galera, E., Laria, D., Mazzanti, F., Batet, L., & Marti, J. (2024). Henry constant of helium in liquid lead-lithium alloys. *arXiv preprint arXiv:2412.14152*.

(Okamoto, 1993) Okamoto, H. (1993). Li-Pb (lithium-lead). *Journal of phase equilibria*, *14*(6), 770-770.

NUCLEATION DRIVEN BY NON-MARKOVIAN NOISE

A. BROAD and I. J. FORD

Department of Physics and Astronomy, University College London, London WC1E 6BT, U.K.

INTRODUCTION

The kinetics of aerosol nucleation are typically characterised as a random walk in a coarse-grained configuration space describing a molecular cluster, starting from a region representing a metastable phase, such as sub-critical nucleus, and ending in a region describing a stable phase such as a large droplet. The walk is usually assumed to be Markovian, meaning that the probabilities for selecting the next configuration depend only on the current configuration and not on previous history. This is an approximation that will break down in certain circumstances, particularly when configurations are described by too few collective variables. We demonstrate this in a simple toy model (Broad 2022) and show that as the collective variables are reduced in number, the effective noise driving the process becomes non-Markovian, such that more coarse-grained random walks proceed with ever deeper memory of the past.

TOY MODEL

We consider a Markovian random walk in a space described by two discrete coordinates. The free energy surface over the space forms a saddle point barrier impeding passage from one side, the metastable state, to the opposite side representing the stable region. We consider barriers with different skew, as illustrated in Figure 1. We deduce probabilities for moves in the 2-d space consistent with these free energy surfaces and conduct stochastic simulations to obtain a rate of barrier crossing starting from an initial point x_0, y_0 on the left hand side.

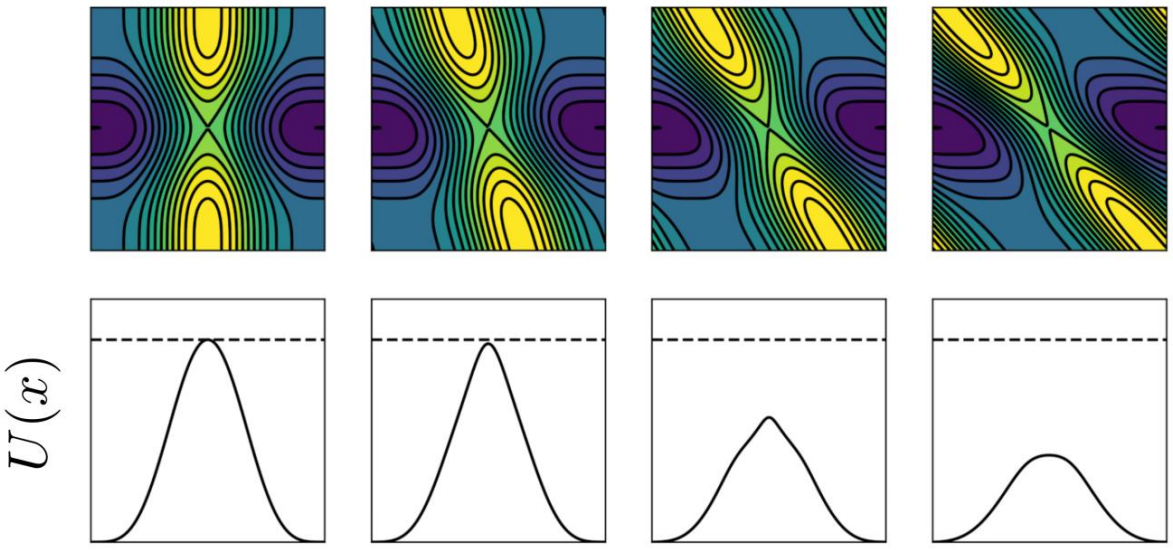


Figure 1. Free energy surfaces with different skewed shapes but the same saddle point height in a 2-d coordinate space spanned by x and y, (yellow is high, blue low). Also the effective barrier in the one dimensional space described by x alone. If the kinetics of the 2-d barrier crossing are Markovian, the crossing of the 1-d barrier has to be non-Markovian to accommodate the apparently lower barrier height.

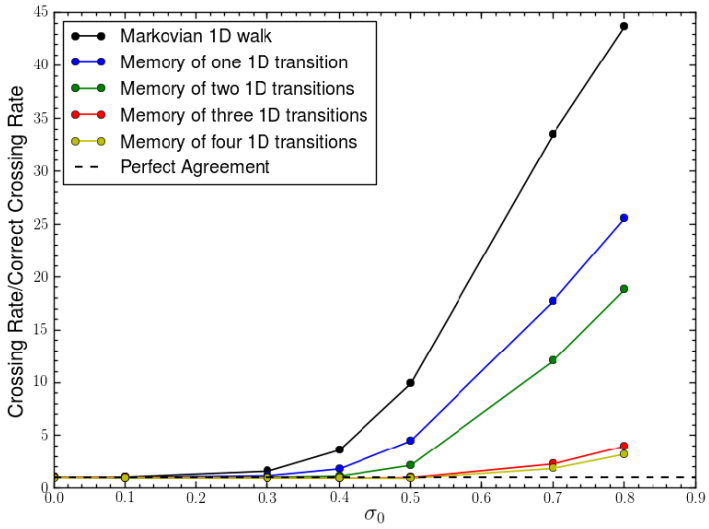


Figure 2. Mean crossing rates of 1-d barriers with an increasing skew (larger σ_0) derived from random walks driven by non-Markovian noise with a memory of past transitions. Deeper memory is needed to obtain agreement with the 2-d Markovian process when the 1-d coordinate crosses the underlying saddle point at a greater angle.

We then consider the same process in a 1-d coordinate space spanned by discrete coordinate x alone. The free energy barriers $U(x)$ consistent with the 2-d surfaces for each case are shown in Figure 1: it should be noted that the barrier height depends on the skew. The rate of crossing is the same in all cases, so we deduce that the noise driving the 1-d process must depend on the skew. Indeed we can show that the dependence takes the form of non-Markovian memory.

This is illustrated in Figure 2. Barriers with greater skew are labelled by a larger value of a parameter σ_0. Mean rates of barrier crossing are shown for 1-d non-Markovian random walk models with memory of up to four previous transitions. Deeper memory allows the crossing rate in the underlying 2-d Markovian system to be reproduced with better accuracy. Introducing non-Markovianity is particularly necessary for the more skewed 2-d barriers.

CONCLUSIONS

Nucleation processes are typically modelled using stochastic kinetics, but an assumption of Markovian noise is not always valid. We have investigated a simple toy model that demonstrates this. Modelling the nucleation of complex molecular clusters in the atmosphere inevitably involves a coarse graining of the description to some extent and we speculate that non-Markovian barrier crossing might be a more accurate model in certain circumstances.

ACKNOWLEDGEMENTS

This work was supported by an Engineering and Physical Sciences Research Council Programme grant (EP/R018820/1). AB acknowledges support of an EPSRC Doctoral Training Partnership studentship (EP/R513143/1).

REFERENCES

A. Broad, UCL PhD thesis (2022).

FREEZING ATMOSPHERIC ORGANIC NUCLEATION: QUANTUM CHEMICAL CALCULATIONS AND MATRIX ISOLATION FTIR EXPERIMENTS OF FORMIC ACID

D.F. DINU[1], K.R. LIEDL[2], H. GROTHE[1], T. LOERTING[3], and D. STOLZENBURG[1]

[1]*Institute of Materials Chemistry, TU Wien, Vienna, Austria.*
[2] *Institute of General, Inorganic and Theoretical Chemistry, University of Innsbruck, Innsbruck, Austria.*
[3]*Institute of Materials Chemistry, University of Innsbruck, Innsbruck, Austria.*

Keywords: Matrix isolation, formic acid, atmospheric nanoparticles, infrared spectroscopy, anharmonic calculations

INTRODUCTION

Understanding the process of atmospheric nucleation, particularly the formation of atmospheric nanoparticles with dimensions below 10 nm, is a significant challenge. (Smith et al., 2021) Especially for nanoparticles including organic molecules, the stage at which they begin contributing to new particle formation remains uncertain (Elm et al., 2020). State-of-the-art mass spectrometry techniques lack the structural insights necessary for a deeper understanding of atmospheric nanoparticle growth (Stolzenburg et al., 2023). In contrast to mass spectrometry, Infrared (IR) spectroscopy, which probes the vibration of molecules, can provide structural insights. In our studies, we utilize matrix-isolation Fourier transform infrared spectroscopy (MI-FTIR) to provide structural insights for single molecules and their clusters. In this context, MI-FTIR has two advantages. First, it avoids the complexity of rotational-vibrational fine structure commonly found in gas-phase IR spectroscopy, thereby yielding pure vibrational transitions. Second, it avoids bulk formation, thus yielding narrower bands than in liquid- or solid-phase IR spectroscopy. Consequently, this paves the way for studying the chemical structure of atmospheric nanoparticles. For assigning the observed vibrational transitions in MI-FTIR, quantum chemical (QC) calculations have proven successful. (Dinu et al., 2020) While the accuracy of quantum chemical (QC) calculations has been extensively tested in the context of atmospheric nucleation, particularly in deriving the free energy of formation (Elm et al., 2020), their application to predicting molecular vibrations has received less attention. Our studies aim to fill this gap by investigating the accuracy of QC calculations in predicting vibrational transitions of small atmospheric nanoclusters, with a specific focus on anharmonic approaches. Here, we present the first results for formic acid, the most abundant organic acid in the atmosphere (Franco et al., 2021), which could serve as a model substance for other small organic acids, potentially participating in organic-mediated NPF (Elm et al., 2017; Fang et al., 2020) (Fang et al., 2020; Elm et al., 2017)

METHODS

Our computational spectroscopy is based on N-mode expansions of the potential energy surfaces (PES) (Rauhut, 2004) relying on the CCSD(T)-F12 approach, i.e., explicitly correlated coupled cluster theory with up to perturbative triples (Adler et al., 2007). For formic acid calculations, we compute a 4-mode PES, with 1- and 2-mode terms using a VTZ-F12 basis set, and 3- and 4-mode terms using a VDZ-F12 basis set. We calculate anharmonic vibrational frequencies using the vibrational configuration interaction (VCI) approach (Mathea & Rauhut, 2021). For MI-FTIR spectroscopy, we prepare a host-guest mixture, where the host is an IR-inert noble gas, such as Argon or Neon, and the guest is formic acid. The host-guest mixture is solidified on a gold-plated mirror in a cryostat maintained at 5 K and a high vacuum of 10^{-6} mbar. The result is a so-called matrix, i.e., a solid nanofilm of the host doped with guest molecules. The matrix is analyzed using a Bruker Vertex 80 V FTIR spectrometer. In previous work, we demonstrated that MI-FTIR spectroscopy is a reliable tool for studying small molecular clusters, such as the monomethyl ester of carbonic acid (Köck et al., 2020) and the CO_2 dimer (Dinu et al., 2022). In the present work, we use commercially available, purified formic acid samples of all four hydrogen-deuterium

isotope combinations. We prepare mixing ratios of 1:250 to 1:1000 in both Argon and Neon matrices, to probe the evolution of vibrational frequencies from the single formic acid molecule and its dimer.

RESULTS

In the context of atmospheric nucleation, the carboxyl group in formic acid can be considered a major contributor to clustering. Table 1 presents the four dominant vibrational features for this organic acid: the hydroxyl stretching, or ν(OH), the carbonyl stretching, or ν(C=O), and additional, more delocalized vibrations along the entire carboxyl group, denoted as ν(C-O) and δ(OH). These vibrational features are also expected in other atmospheric organic acids. For example, the carboxyl group is a common feature of oxidation products of the monoterpene α-pinene, most notably the pinic and pinonic acids. As shown in Table 1, anharmonic VCI calculations agree well with the pure vibrational transitions observed in MI-FTIR spectroscopy.

	MI-FTIR Experiment		Calculation	
	Argon	Neon	Harmonic	Anharmonic (VCI)
δ(OH)	635.6	638.0	637.2	648.3
ν(C-O)	1103.7	1102.8	1141.0	1104.7
ν(C=O)	1768.4	1774.2	1817.5	1782.8
ν(OH)	3550.1	3570.7	3765.1	3579.0

Table 1. The four most IR-intense vibrational transitions of formic acid, as observed in MI-FTIR spectroscopy and predicted theoretically (see Methods section).

CONCLUSIONS

Our spectroscopic study on formic acid, conducted using laboratory MI-FTIR spectroscopy and VCI calculations, demonstrates the potential for gathering structural insights into atmospheric nanoparticles. The preliminary results presented here pertain to the monomer. The effect of cluster formation is observable in the MI-FTIR experiment through frequency shifts in the vibrational modes involved in the clustering, and the corresponding calculations are readily available. Differences in QC calculations (e.g., conformers, level of theory) of the formic acid model system can be probed with experimental evidence, thereby improving our understanding of QC calculations for molecular clusters. In addition, we plan to combine our methodology with future studies, adopting it as a new tool to investigate clustering routes in NPF of more complex systems, which may lead to significant advancements in our understanding of atmospheric nucleation.

ACKNOWLEDGEMENTS

This research was funded in whole or in part by the Austrian Science Fund (FWF) 10.55776/PAT8221324.

REFERENCES

Adler, T. B., Knizia, G., & Werner, H.-J. (2007). A simple and efficient CCSD(T)-F12 approximation. *The Journal of Chemical Physics*, *127*(22), 221106. https://doi.org/10.1063/1.2817618

Dinu, D. F., Bartl, P., Quoika, P. K., Podewitz, M., Liedl, K. R., Grothe, H., & Loerting, T. (2022). Increase of Radiative Forcing through Midinfrared Absorption by Stable CO 2 Dimers? *The Journal of Physical Chemistry A*, *126*(19), 2966–2975. https://doi.org/10.1021/acs.jpca.2c00857

Dinu, D. F., Podewitz, M., Grothe, H., Loerting, T., & Liedl, K. R. (2020). On the synergy of matrix-isolation infrared spectroscopy and vibrational configuration interaction computations. *Theoretical Chemistry Accounts*, *139*(12), 174. https://doi.org/10.1007/s00214-020-02682-0

Elm, J., Kubečka, J., Besel, V., Jääskeläinen, M. J., Halonen, R., Kurtén, T., & Vehkamäki, H. (2020). Modeling the formation and growth of atmospheric molecular clusters: A review. *Journal of Aerosol Science*, *149*, 105621. https://doi.org/10.1016/j.jaerosci.2020.105621

Elm, J., Myllys, N., & Kurtén, T. (2017). What Is Required for Highly Oxidized Molecules To Form Clusters with Sulfuric Acid? *The Journal of Physical Chemistry A*, *121*(23), 4578–4587. https://doi.org/10.1021/acs.jpca.7b03759

Fang, X., Hu, M., Shang, D., Tang, R., Shi, L., Olenius, T., Wang, Y., Wang, H., Zhang, Z., Chen, S., Yu, X., Zhu, W., Lou, S., Ma, Y., Li, X., Zeng, L., Wu, Z., Zheng, J., & Guo, S. (2020). Observational Evidence for the Involvement of Dicarboxylic Acids in Particle Nucleation. *Environmental Science & Technology Letters*, *7*(6), 388–394. https://doi.org/10.1021/acs.estlett.0c00270

Franco, B., Blumenstock, T., Cho, C., Clarisse, L., Clerbaux, C., Coheur, P.-F., De Mazière, M., De Smedt, I., Dorn, H.-P., Emmerichs, T., Fuchs, H., Gkatzelis, G., Griffith, D. W. T., Gromov, S., Hannigan, J. W., Hase, F., Hohaus, T., Jones, N., Kerkweg, A., … Taraborrelli, D. (2021). Ubiquitous atmospheric production of organic acids mediated by cloud droplets. *Nature*, *593*(7858), 233–237. https://doi.org/10.1038/s41586-021-03462-x

Köck, E.-M., Bernard, J., Podewitz, M., Dinu, D. F., Huber, R. G., Liedl, K. R., Grothe, H., Bertel, E., Schlögl, R., & Loerting, T. (2020). Alpha-Carbonic Acid Revisited: Carbonic Acid Monomethyl Ester as a Solid and its Conformational Isomerism in the Gas Phase. *Chemistry – A European Journal*, *26*(1), 285–305. https://doi.org/10.1002/chem.201904142

Mathea, T., & Rauhut, G. (2021). Advances in vibrational configuration interaction theory—Part 1: Efficient calculation of vibrational angular momentum terms. *Journal of Computational Chemistry*, *42*(32), 2321–2333. https://doi.org/10.1002/jcc.26762

Rauhut, G. (2004). Efficient calculation of potential energy surfaces for the generation of vibrational wave functions. *The Journal of Chemical Physics*, *121*(19), 9313–9322. https://doi.org/10.1063/1.1804174

Smith, J. N., Draper, D. C., Chee, S., Dam, M., Glicker, H., Myers, D., Thomas, A. E., Lawler, M. J., & Myllys, N. (2021). Atmospheric clusters to nanoparticles: Recent progress and challenges in closing the gap in chemical composition. *Journal of Aerosol Science*, *153*, 105733. https://doi.org/10.1016/j.jaerosci.2020.105733

Stolzenburg, D., Cai, R., Blichner, S. M., Kontkanen, J., Zhou, P., Makkonen, R., Kerminen, V.-M., Kulmala, M., Riipinen, I., & Kangasluoma, J. (2023). Atmospheric nanoparticle growth. *Reviews of Modern Physics*, *95*(4), 045002. https://doi.org/10.1103/RevModPhys.95.045002

QUANTUM CHEMICAL MODELLING OF ATMOSPHERIC CLUSTER FORMATION: BIGGER, STRONGER, FASTER!

J. ELM

Department of Chemistry, Aarhus University, Aarhus, Denmark.

Keywords: Clusters, Quantum Chemistry, New particle formation.

INTRODUCTION

New particle formation (NPF) gives rise to up to half the number of cloud condensation nuclei in the atmosphere and is thereby a major source of the large uncertainty in global radiative forcing modelling. The formation of non-covalently bonded atmospheric molecular clusters is a crucial step leading to NPF. Sulfuric acid (SA) clustering with atmospheric bases such as ammonia (AM) and alkyl amines (methylamine (MA), dimethylamine (DMA) and trimethylamine (TMA)) are believed to be a prevalent source of NPF in many regions due to the formation of strongly bound clusters. In marine environments iodine species such as iodine oxo-acids and iodine oxides have been shown to rapidly form new particles. Over the oceans, emissions of dimethylsulfide (DMS) reacts with OH radicals leading to the formation of SA and methane sulfonic acid (MSA). MSA has also been speculated to assist in cluster formation process together with atmospheric bases emitted from the ocean. In most regions oxygenated organic molecules (OOMs) are also believed to play a role, but it remains ambiguous exactly which compounds that are involved in the initial cluster formation steps and which that are only involved in the growth of the freshly nucleated particles. Ions are also believed to be involved in the cluster formation, especially in cases where the precursors bind weakly such as in pure organic nucleation. Overall, there is a myriad of relevant atmospheric species that can cluster together in a plethora of combinations. This can be viewed as the ***chemical complexity puzzle*** of atmospheric nucleation.

Quantum chemical (QC) calculations are an exceptionally powerful tool to identify the molecular structure of atmospheric clusters, by constructing the clusters using a bottom-up approach. This allows for direct molecular-level insight into the chemical identity of the vapours participating in NPF. Calculated accurate QC thermochemistry can be applied in cluster dynamics simulations using for instance the Atmospheric Cluster Dynamics Code (ACDC), allowing the simulation of NPF rates. These simulated NPF rates can be directly compared to experimental results. To simulate accurate NPF rates using QC methods, clusters of up to 8-10 molecules are required to ensure adequate ACDC modelling. Hence, to simulate realistic multi-component NPF rates the chemical complexity becomes a challenge. In addition, each combination of molecules, i.e. cluster, can also be assembled in ***numerous different stable configurations***. This implies that millions of cluster configurations must be examined and screened using QC methods to identify the most stable configuration at the given atmospheric conditions. Thorough configurational sampling techniques based on genetic algorithms, coupled to metadynamics simulations exist, making the exploration of the potential energy surface of these complex clusters technically feasible. Configurational sampling is usually performed using a funnelling approach where increasingly accurate QC methods are applied in each step, while filtering out high energy cluster configurations. However, accurate QC calculations are very computationally demanding, severely limiting the number of combinations that can be studied and has been the main obstacle in the past years.

In this presentation I will outline two ongoing and emerging topics in modelling cluster formation using quantum chemical (QC) methods: 1) Introduction of machine learning models for cluster configurational sampling to move towards more complex multi-component clusters, 2) To push the boundaries by modelling significantly larger clusters than previous possible. This will be used to identify the cluster-to-particle transition point, yielding a new definition of freshly nucleated particles (FNPs).

The main obstacle in applying QC methods to study cluster formation is the chemical complexity puzzle and sheer number of configurations that needs to be sampled to identify the cluster structure lowest in free energy. In addition, the steep scaling of QC methods with cluster size also impairs the modelling of large clusters. We devised a holistic approach denoted ***Clusteromics*** (**Elm, 2021**) where we massively screened small cluster systems up to four molecules to get insight into chemical complexity. Performing high-throughput screening of numerous cluster configurations will simultaneously provide the foundation for the thermochemical databases that are required for developing machine learning models. A total of five papers were subsequently published in the ***Clusteromics I-V*** series, each yielding new insight into the chemical complexity. We initially explored the application of the simple machine learning method kernel ridge regression (KRR) for modelling the binding energies of atmospheric molecular clusters (**Kubečka, 2022**). Using sulfuric acid and water clusters we made some very interesting observations:

1) Models within chemical accuracy (below 1 kcal/mol) could be achieved.
2) Delta machine learning (Δ-ML) yielded improved results. I.e. training the model on the difference between a low level and a high-level quantum chemical method could significantly improve the model.
3) Non-equilibrium clusters were important to have in the database if the trained model should be able to predict the binding energies of new clusters. Non-equilibrium clusters can easily be obtained by running a short molecular dynamics simulation on the equilibrium clusters, saving regular snap shots for the database.
4) The trained KRR model could be extrapolated to cluster sizes at least twice the size of the training set. As machine learning models often can yield extremely large errors when applied outside the training data, this is an astonishing and encouraging result.
5) We identified a limitation in the speed of the KRR model, as it became slow when trained on many datapoints.

These observations laid the foundation for using KRR in cluster formation studies. Appending the clusteromics database with out-of-equilibrium clusters let to the ***clusterome*** dataset (**Knattrup, 2023**) comprising 250,000 data points. Using this expansive dataset, we further derived extrapolation rules for KRR in regard to cluster configurations, interactions, molecules and size (see Figure 1).

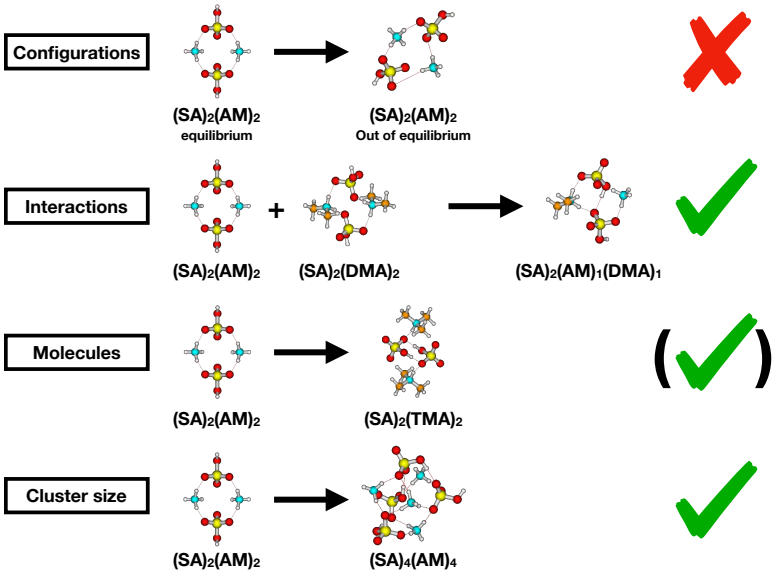


Figure 1. Different tests of kernel ridge regression extrapolations.

Overall, we have identified a solid approach for applying KRR for studying atmospheric cluster binding energies. However, the real potential for ML lies in optimizing the clusters, as this is often the main bottleneck in configurational sampling of the clusters (**Kubečka, 2023**). Hence, we also need a method that can train on the gradients as well as the energies. As we have 3*N* gradient component for each *N* atoms in the cluster this is not a viable approach for KRR. We tested the polarizable atom interaction neural network (PaiNN) architecture for training on forces as well as the energies. We found that the trained PaiNN model could also be extrapolated to larger sizes than those in the training database (**Kubečka, 2024**). This is a very important finding in the field, and we are now working on integrating the methodology in our cluster configurational sampling workflows, massively speeding up the exploration of the configurational space.

MODELLING CLUSTER-TO-PARTICLE TRANSITION

The point at which a given assembly of molecules represents a molecular cluster, or a particle remains ambiguous. Obtaining an understanding of this cluster-to-particle transition point will give us fundamental insight its basic aerosol properties and will help us to constrain how different aerosol particle sizes are handled in aerosol process models. I will give an overview of our recent endeavours in exploring the cluster-to-particle transition concept. By applying state-of-the-art quantum chemical calculations, we studied the thermochemistry of large $(SA)_n(base)_n$ clusters (with n up to 10), with the bases: AM, MA, DMA and TMA. These clusters are significantly larger than what has previous been routinely studied, which complicates the search for the most stable cluster configurations. We will present a newly developed improved configurational sampling technique to handle the vast configurational space of such large systems (**Wu, 2023**). Applying this new methodology, we deduce a property-based criteria for defining the cluster-to-particle transition point, leading to freshly nucleated particles (FNPs). Such FNPs act as a boundary between discrete cluster configurations and large particles. We define the onset of FNPs as being when one or more ions are fully solvated inside the cluster (see **Figure 2**) and when the size-averaged binding free energies resemble bulk properties. This definition easily allows the identification of FNPs and is applicable to particles of arbitrary chemical composition. For the studied $(SA)_n(base)_n$ clusters, the cluster-to-particle transition point occurs around 16–20 monomers (**Wu, 2024**).

We extended the work to SA mixed base $(SA)_n(AM)_x(DMA)_{n-x}$ clusters, with n from 1 to 10, where x runs from 0 to n. We find that the strong base DMA is important in the very first steps in cluster formation, but for larger clusters an increased ammonia content is found. This manifests in a cluster-to-particle transition point for the mixed SA–AM–DMA clusters occurring at a cluster size of 14 monomers, which is notably smaller than the transition points for the pure SA–AM or pure SA–DMA systems. This indicates a strong synergistic effect when both AM and DMA are present, leading to the formation of stable FNPs at smaller cluster sizes (**Hasan, 2025**).

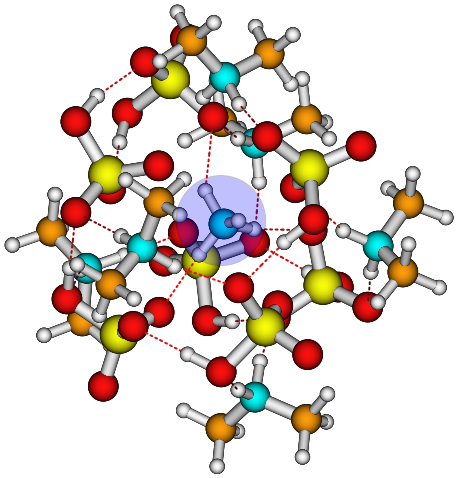


Figure 2. Example of a fully coordinated ammonium (AM) ion inside the $(SA)_7(AM)_1(DMA)_6$ cluster.

Furthermore, we studied the uptake of organic oxidation products from isoprene and α-pinene onto $(SA)_{10}(base)_{10}$ FNPs. Calculating the addition free energy under realistic atmospheric conditions, we find that the FNPs studied are too small (~1.4 nm) to support the growth of the studied monomer oxidation products. However, we find that the accretion product (dimer) pinyl diaterpenylic ester (PDPE, $C_{17}H_{26}O_8$) can overcome the strong Kelvin effect of a 1.4 nm FNP and lead to spontaneous uptake at ambient conditions (**Knattrup, 2025**).

CONCLUSIONS

To conclude, we will present how ML techniques can be integrated in quantum chemical studies of atmospheric molecular clusters. We will outline future avenues in how ML can be used to obtain accurate molecular dynamics of cluster formation directly from precursor vapours. In addition, we will present our recent work on modelling much larger cluster than previously possible. This new data allows us to define deduce a property-based criteria for defining the cluster-to-particle transition point, leading to freshly nucleated particles (FNPs).

ACKNOWLEDGEMENTS

This work was funded by the European Union (ExploreFNP grant no. 101040353). The authors thank the Independent Research Fund Denmark grant number 9064-00001B for financial support. This work was funded by the Danish National Research Foundation (DNRF172) through the Center of Excellence for Chemistry of Clouds

REFERENCES

Elm, J.; *J. Phys. Chem. A*, **2021**, 125, 4, 895–902.

Hasan, G.; Wu, H.; Knattrup, Y.; Elm, J.; *Aerosol Res.*, **2025**, 3, 101–111.

Knattrup, Y.; Kubečka, J.; Ayoubi, D.; and Elm, J.; *ACS Omega*, **2023**, 8, 28, 25155–25164.

Knattrup, Y.; Elm, J.; *Aerosol Res.*, **2025**, 3, 125–137.

Kubečka, J.; Christiansen, A. S.; Rasmussen, F. R.; and Elm, J.; *Environ. Sci. Technol. Lett.*, **2022**, 9, 3,

239–244.

Kubečka, J.; Knattrup, Y.; Engsvang, E.; Jensen, A. B.; Ayoubi, D.; Wu, H.; Christiansen, O.; Elm, J.; *Nat. Comp. Sci.*, **2023**, 3, 495–503.

Kubečka, J.; Ayoubi, D.; Tang, Z.; Knattrup, Y.; Engsvang, E.; Wu, H.; and Elm, J.; *Environ. Sci.: Adv.*, **2024**, 3, 1438–1451.

Wu, H.; Engsvang, M.; Knattrup, Y.; Kubečka, J.; and Elm, J.; *ACS Omega*, **2023**, 8, 45065−4507.

Wu, H.; Knattrup, Y.; Jensen, A. B.; and Elm, J.; *Aerosol Res.*, **2024**, 2, 303–314.

Acceleration of low temperature water nucleation in the presence of CO_2

F. GRABER[1], S. FEUSI[1], J. KHATRI[1,2], C. LI[3] and R. SIGNORELL[1]

[1]*Department of Chemistry and Applied Biosciences, ETH Zürich, CH-8093 Zürich, Switzerland.*
[2]*Department of Chemistry, University of Missouri, Columbia, MO, USA*
[3]*School of Environmental Science and Engineering, Shanghai Jiao Tong University, Shanghai 200240, China*

Keywords: Supersonic expansion, homogeneous gas phase nucleation, binary nucleation, cluster dynamics, condensation, dimerization, supersaturation, reaction rate constants, time of flight mass spectrometry.

INTRODUCTION

In planetary atmospheres like those of Earth and Mars, clouds often form from species present in only small amounts. We have recently shown, that intermolecular interactions with a second gas species may facilitate gas-phase nucleation (Li, 2021; Feusi, 2024). Here, we demonstrate this behavior for the binary CO_2 / H_2O system at temperatures of 57 K and 75 K. The nucleation behavior was measured for different CO_2 / H_2O concentrations in a carrier gas in the uniform post-nozzle flow of a de Laval nozzle. Our results indicate, that the addition of CO_2 significantly increases the nucleation rate of water.

Our setup provides information about the cluster composition and absolute cluster concentrations, allowing us to apply a kinetic model for nucleation and the initial stages of cluster growth. The model suggests that nucleation is accelerated through the formation of short-lived, transient heteromolecular H_2O – CO_2 dimers, which we refer to as a chaperone cluster.

METHODS

In our experiment, a gas mixture containing H_2O, CO_2 and carrier gas was expanded through a Laval nozzle. The pressure in the vacuum chamber was adjusted to match the gas pressure in the uniform post-nozzle flow, ensuring constant temperature, pressure, and supersaturation in the post-nozzle flow. The post-nozzle flow acts as a wall-less flow reactor, allowing us to control the nucleation time by adjusting the nozzle position relative to the detection system. The clusters that form in the post-nozzle flow were softly ionized using single-photon ionization with a photon energy close to the lowest ionization threshold and detected with a homebuilt time-of-flight mass spectrometer.
From the mass spectra, we obtain cluster number concentrations as a function of the nucleation time. The experimental nucleation rate, J_{exp}, can then be calculated from:

$$J_{\mathrm{exp}} = \frac{\mathrm{d}N_{\mathrm{tot}}}{\mathrm{d}t} = \frac{\mathrm{d}\sum_{i=2}^{i_{\mathrm{max}}} N_i}{\mathrm{d}t} \tag{1}$$

Where t is the nucleation time, N_{tot} the total number concentration and N_i is the number concentration of clusters that contain i molecules. This provides a basis for comparing our experimental data with a kinetic model. Under these conditions, dimer formation is the rate determining step (Dingilian, 2021), leading to a simplified model nucleation rate J_{model}:

$$J_{\mathrm{model}} = k_{1,1}\left(C_1^{\mathrm{H_2O}}\right)^2 + \beta C_1^{\mathrm{H_2O}} C_1^{\mathrm{CO_2}} \tag{2}$$

where $C_1^{CO_2}$ and $C_1^{H_2O}$ are the concentrations of carbon dioxide and water. $k_{1,1}$ is the nucleation rate constant for the reaction with only water (unary nucleation) while β is the rate constant for binary processes involving both water and CO_2 (binary nucleation). The modeled nucleation rate J_{model} can then be compared with the experimental nucleation rate J_{exp}, with the resulting fit parameters listed in Table 1.

Table 1: Nucleation rate constants $k_{1,1}$ and β for water nucleation in the presence of CO_2 at 57 K and 75 K. The unary water rate constant $k_{1,1}$ was obtained from unary experiments (without CO_2). The binary rate constant was obtained through fitting equation 2 (Feusi, 2024).

T (K)	$k_{1,1}$ ($s^{-1}cm^{-3}$)	β ($s^{-1}cm^{-3}$)
57	$3\ (1) \times 10^{-13}$	$5\ (3) \times 10^{-14}$
75	$2\ (1) \times 10^{-13}$	$1\ (0.7) \times 10^{-14}$

CONCLUSION

When adding CO_2, we observed a linear increase in the nucleation rate of water J_{exp}. At 57 K and 75 K the pathway via CO_2 is one order of magnitude slower than the unary pathway. However, if the concentration of CO_2 is ten times higher than the H_2O concentration, the presence of CO_2 already results in a doubling in the nucleation rate of water clusters. For even higher concentrations of CO_2, the nucleation is dominated by the chaperone interaction.

At 57 K, CO_2 also influences early cluster growth. This indicates that at 57 K, CO_2 plays a role not only in nucleation but also in the early stages of cluster growth, whereas at 75 K, its impact is limited to the nucleation process itself.

ACKNOWLEDGEMENTS

The financial support was provided by the Swiss National Science Foundation (SNSF: Project No. 200020_200306) and the ETH Zurich.

REFERENCES

S. Feusi, F. Graber, J. Khatri, C. Li, R. Signorell (2024), How CO2 gas accelerates water nucleation at low temperature. *J. Chem. Phys.* 161 (18): 184304.

K. K. Dingilian, M. Lippe, J. Kubečka, J. Krohn, C. Li, R. Halonen, F. Keshavarz, B. Reischl, T. Kurtén, H. Vehkamäki, R. Signorell, and B. E. Wyslouzil (2021), New particle formation from the vapor phase: From barrier-controlled nucleation to the collisional limit. *J. Phys. Chem. Lett.* 12(19), 4593–4599

C. Li, J. Krohn, M. Lippe, R. Signorell (2021), How volatile components catalyze vapor nucleation. *Sci. Adv.* 7, 3

ATOMISTIC INSIGHTS INTO ARGON CLUSTERS AND NUCLEATION

R. HALONEN[1]

[1]*Nanjing-Helsinki Institute in Atmospheric and Earth System Sciences, Nanjing University, Suzhou, China*

Keywords: NUCLEATION, ARGON, STATISTICAL MECHANICS, THERMOCHEMISTRY, ANHARMONICITY.

INTRODUCTION

Nucleation and cluster formation in the gas phase have long presented challenges for theoretical modeling, particularly due to finite-size effects and non-standard thermodynamic behavior. Historically, argon has served as a fundamental system for exploring nucleation dynamics. As a simple fluid with minimal quantum effects, argon is well-suited for classical atomistic modeling, allowing for computationally efficient simulations. Extensive experimental investigations of nucleation of argon vapor have been conducted across a wide range of temperatures, vapor pressures, and nucleation rates, providing a solid foundation for understanding homogeneous nucleation. This study re-examines argon cluster formation using advanced theoretical methodologies, including *ab initio*-based potentials, atomistic simulations, and anharmonic statistical thermochemistry, to bridge the gap between experiment and computation.

METHODS

Our research primarily focuses on assessing the suitability of interaction models and statistical thermochemistry, particularly at higher nucleation temperatures. To accurately model argon-argon interactions, we use an *ab initio*-based two-body potential (Nasrabad et al., 2004), along with a three-body Axilrod–Teller potential (Axilrod and Teller, 1943). We estimate theoretical nucleation rates and critical cluster sizes using the standard kinetic scheme of nucleation while studying the atomistic properties of clusters containing up to 50 argon atoms. Additionally, we incorporate novel anharmonic corrections into the standard statistical cluster model for calculating formation free energies (Halonen, 2024a), which are rigorously benchmarked against molecular dynamics (MD) simulations of supersaturated Axilrod-Teller-Lennard-Jones vapor.

Reference	Instrument type	Temperature range	Nucleation rate
Sinha et al. (2010)	Supersonic nozzle	35-53 K	10^{17} cm^{-3}s^{-1}
Iland et al. (2007)	Nucleation pulse chamber	43-58 K	10^{7} cm^{-3}s^{-1}
Fladerer and Strey (2006)	Nucleation pulse chamber	49-60 K	10^{7} cm^{-3}s^{-1}
Zahoransky et al. (1999)	Hypersonic shock tube	56-70 K	10^{6} cm^{-3}s^{-1}
Zahoransky et al. (1995)	Supersonic shock tube	74-85 K	10^{6} cm^{-3}s^{-1}
Koppenwallner and Dankert (1987)	Free jet expansion	13-34 K	10^{21} cm^{-3}s^{-1}
Steinwandel and Buchholz (1984)	Cryogenic Ludwieg tube	42-62 K	10^{0} cm^{-3}s^{-1}
Matthew and Steinwandel (1983)	Cryogenic shock tube	55-76 K	10^{0} cm^{-3}s^{-1}
Wu et al. (1978)	Supersonic nozzle	29-43 K	10^{15} cm^{-3}s^{-1}
Lewis and Williams (1974, 1976)	Free-jet expansion	13-37 K	10^{21} cm^{-3}s^{-1}
Pierce et al. (1971)	Hypersonic nozzle	55-63 K	10^{17} cm^{-3}s^{-1}

Table 1. Compiled experimental datasets of homogeneous argon nucleation comprising a total of 508 data points.

RESULTS

Firstly, the employed interaction model accurately reproduces the relevant liquid-vapor coexistence properties at the macroscopic limit. By analyzing the nucleation results from our MD simulations, we confirm that the anharmonic statistical thermochemical approach effectively reproduces the nucleation free energy barriers and indicates the correct critical cluster sizes.

Unlike MD nucleation simulations, the statistical approach is not so limited by computational restrictions, which means its domain overlaps with experimental setups. We analyze diverse experimental nucleation data of argon spanning nearly five decades of research (1971–2010), as shown in Table 1. Overall, Figure 1 illustrates that the atomistic model with anharmonic corrections consistently reproduces the nucleation rates across the studied range, with temperatures from $T = 13$ to 85 K and nucleation rates from $J = 1$ to about 10^{21} cm^{-3}s^{-1}. The harmonic approach only captures the experimental results at low temperatures, where the critical cluster sizes are small and barriers shallow. In contrast, classical nucleation theory (CNT) underestimates the nucleation rates by tens of orders of magnitude.

Additionally, the critical cluster sizes derived from the model align well with those obtained from the first nucleation theorem and experimental data. A new nucleation relation has been developed to further reveal the inherent dynamics behind nucleation experiments (Halonen, 2024b). Our atomistic inspection of cluster structures provides all necessary energetic information, and we thus also study the second nucleation theorem, which retrieves excess energies of the critical clusters from the experimental data (Sinha et al., 2010). The good agreement between the experimental cluster energies and the modeled ones suggests that, beyond accurately describing bulk properties, the *ab initio* three-body potential can also provide quantitative descriptions of finite-sized systems. For further details, we refer to the published article on the topic (Halonen, 2024b).

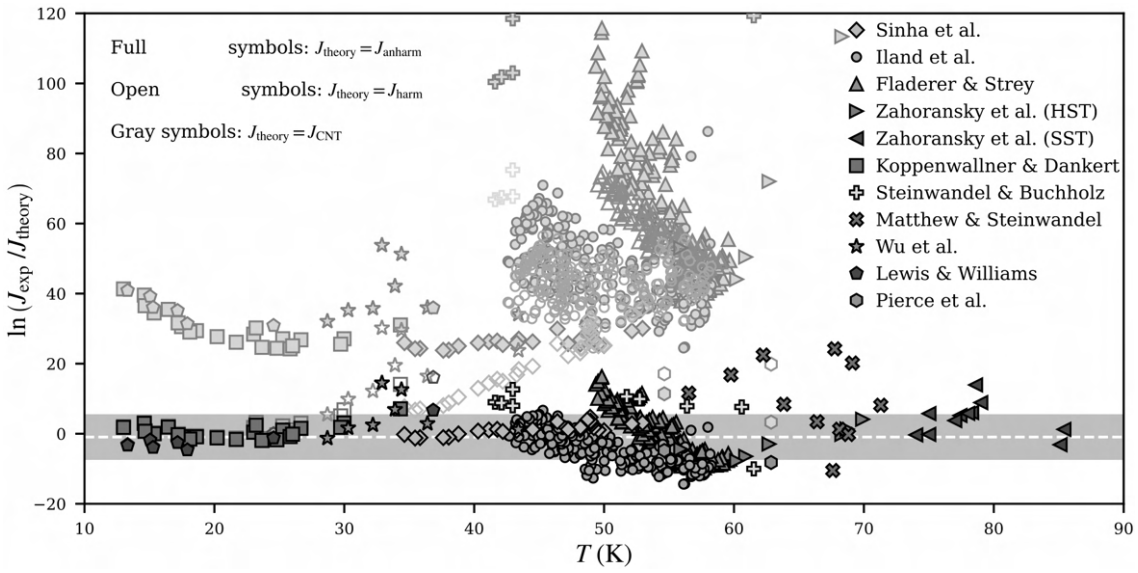


Figure 1. Experimental argon nucleation rates versus the theoretical predictions: classical nucleation theory (gray markers) and atomistic cluster modeling with anharmonicity (full markers) and without (open markers) using the *ab initio* potential. The averaged value for $\ln(J_{exp}/J_{anharm}) = -0.96$ is depicted with a white dashed line, and the standard deviation (about 6.50) is indicated by the shaded area. Note that the data points corresponding to $\ln(J_{exp}/J_{CNT}) > 120$ are omitted from the figure.

CONCLUSIONS

Even in the case of what may be considered the most elementary form of nucleation, involving a chemically simple system nucleating homogeneously, the theoretical description of the phenomenon has not achieved widespread success (Kalikmanov et al., 2008; Sinha et al., 2010). However, in this study, we demonstrate that by accounting for anharmonicities using a recently developed approach (Halonen, 2024a), we can achieve a high level of agreement through statistical thermochemistry based on atomic cluster structures. Our modeling has shown robust qualitative and quantitative success, providing valuable insights into the observed nucleation patterns across various measurements. Despite the apparent scatter in the overall data, previous conclusions regarding severe inconsistencies (Fladerer and Strey, 2006; Sinha et al., 2010) may need reassessment. Based on the results presented here, we assert that the 12 analyzed experiments conducted between 1971 and 2010 successfully probed homogeneous argon nucleation. Although some issues related to the precision of reported values exist, the unprecedented consistency and agreement between theory and experiments in the field of nucleation studies are noteworthy.

REFERENCES

Axilrod, B. and Teller, E. (1943). Interaction of the van der Waals type between three atoms. *J. Chem. Phys*. **11**(6), 299–300.

Fladerer, A. and Strey, R. (2006). Homogeneous nucleation and droplet growth in supersaturated argon vapor: The cryogenic nucleation pulse chamber. *J. Chem. Phys*. **124**(16).

Halonen, R. (2024a). Assessment of anharmonicities in clusters: Developing and validating a minimum-information partition function. *J. Chem. Theo. Comp*. **20**(10), 4099–4114.

Halonen, R. (2024b). Atomistic insights into argon clusters and nucleation dynamics. *J. Aerosol Sci.* **181**, 106406.

Iland, K., Wölk, J., Strey, R. and Kashchiev, D. (2007). Argon nucleation in a cryogenic nucleation pulse chamber. *J. Chem. Phys*. **127**(15).

Kalikmanov, V., Wölk, J. and Kraska, T. (2008). Argon nucleation: Bringing together theory, simulations, and experiment. *J. Chem. Phys*. **128**(12).

Koppenwallner, G. and Dankert, C. (1987). Homogeneous condensation in nitrogen, argon, and water vapor free jets. *J. Chem. Phys*. **91**(10), 2482–2486.

Lewis, J. and Williams, W. (1974). Argon condensation in free-jet expansions: DTIC Paper AEDC-TR-74-32.

Matthew, M. and Steinwandel, J. (1983). An experimental study of argon condensation in cryogenic shock tubes. *J. Aerosol Sci.* **14**(6), 755–763.

Nasrabad, A. E., Laghaei, R. and Deiters, U. (2004). Prediction of the thermophysical properties of pure neon, pure argon, and the binary mixtures neon-argon and argon-krypton by Monte Carlo simulation using ab initio potentials. *J. Chem. Phys*. 121(13), 6423–6434.

Pierce, T., Sherman, P. and McBride, D. (1971). Condensation of argon in a supersonic stream. Astronautica Acta, 16(1).

Sinha, S., Bhabhe, A., Laksmono, H., Wölk, J., Strey, R. and Wyslouzil, B. (2010). Argon nucleation in a cryogenic supersonic nozzle. *J. Chem. Phys*. **132**(6).

Steinwandel, J. and Buchholz, T. (1984). Homogeneous condensation of argon: an experimental study using the nozzle flow of a cryogenic Ludwieg tube. *Aerosol Sci. Tech.* **3**(1), 71–76.

Williams, W. and Lewis, J. (1976). Argon condensation in free-jet expansions: DTIC Paper AEDC-TR-76-67.

Wu, B. J., Wegener, P. P. and Stein, G. D. (1978). Homogeneous nucleation of argon carried in helium in supersonic nozzle flow. *J. Chem. Phys*. **69**(4), 1776–1777.

Zahoransky, R., Höschele, J. and Steinwandel, J. (1995). Formation of argon clusters by homogeneous nucleation in supersonic shock tube flow. *J. Chem. Phys*. **103**(20), 9038–9044.

Zahoransky, R., Höschele, J. and Steinwandel, J. (1999). Homogeneous nucleation of argon in an unsteady hypersonic flow field. *J. Chem. Phys*. **110**(17), 8842–8843.

CHARACTERISTICS OF PARTICLE EMISSION FROM DIFFERENT HOUSEHOLD COOKING ACTIVITIES

Y. R. Jiang[1], C. Yan[1,2], W. Nie[1,2], Z. H. Chen[1], Q. Z. Zha[1], C. Zhou[1], X. M. Qi[1,2], A. J. Ding[1,2]

[1]School of Atmospheric Sciences, Nanjing University, Nanjing, 210046, China
[2] Nanjing-Helsinki Institute in Atmospheric and Earth System Sciences, Nanjing University, Nanjing, 210046, China

Keywords: cooking method, particulate matter, Respiratory deposition, Organic aerosols

Household cooking activities are a major source of indoor particulate matter and may exert significant impacts on human health (Pikmann et al., 2024), especially considering that people spend approximately 90% of their time indoors (Zannoni et al., 2022). Previous studies have shown that particulate matter emissions vary substantially depending on the cooking method (Song et al., 2022; Wang et al., 2023). Understanding the characteristics of particles emitted during different cooking processes is therefore essential for evaluating their effects on indoor air quality and human health.

In this study, we conducted a comprehensive investigation of particulate emissions from three common household cooking methods: pan-frying, air frying, and oven baking. $PM_{2.5}$ mass concentrations were used to quantify emissions, revealing considerable variation among methods. The highest average concentration was observed for pan-frying (1133.4 μg/m³), followed by air frying (238.3 μg/m³), with oven baking showing the lowest level (9.7 μg/m³). Maximum particle diameters also differed by cooking method, reaching 117.6 nm for pan-frying, 57.3 nm for air frying, and 21.7 nm for oven baking. Organic matter dominated the aerosol composition across all cooking methods, accounting for up to 99% of the total particulate mass.

To further assess potential health impacts, the ICRP (International Commission on Radiological Protection) model was applied to estimate particle deposition in the human respiratory tract for particles ranging from 3 nm to 500 nm in the human respiratory tract, considering particle number, surface area, and mass distributions. The effect of hygroscopic growth under respiratory tract humidity conditions was also accounted for to reflect the actual deposition behavior. These findings emphasize the significant influence of cooking methods on indoor aerosol characteristics and their potential implications for human health.

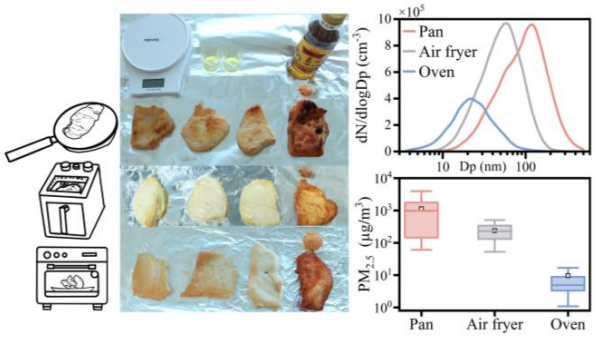


Fig 1. Particle size distribution and $PM_{2.5}$ concentration from three different household cooking activities

ACKNOWLEDGEMENTS

This study is funded by the National Natural Science Foundation of China (NSFC) project 42475118.

REFERENCES

Pikmann J., et al (2024). Particulate emissions from cooking: emission factors, emission dynamics, and mass spectrometric analysis for different cooking methods, Atmos. Chem. Phys. 24: 12295-12321.

Song K., et al (2022). Impact of cooking style and oil on semi-volatile and intermediate volatility organic compound emissions from Chinese domestic cooking, Atmos. Chem. Phys. 22: 9827-9841.

Wang X., et al (2023). Particulate Matter and Volatile Organic Compound Emissions Generated from a Domestic Air Fryer, Environ. Sci. Technol. 57: 17384-17392.

Zannoni N., et al (2022). The human oxidation field, Science. 337: 1071-1077.

ION-INDUCED NUCLEATION IN FLUIDS CONTAINING SALT

R. KROLL and Y. TSORI

Department of Chemical Engineering, Ben-Gurion University of the Negev, Israel.

Keywords: Ion-induced nucleation, electrostatics, Debye-Hückel, Poisson-Boltzmann, Wetting.

INTRODUCTION

The influence of electrostatic forces on nucleation was first studied in the 1890s when Wilson observed nucleation enhancement due to the presence of ions in a supersaturated vapor (Wilson and Thomson, 1897). Since then, experiments in ion-induced nucleation, mostly conducted in cloud chambers, proved that the presence of ions lowers the supersaturation needed to initiate phase transition and significantly increases the nucleation rates compared to homogeneous nucleation (Adachi *et al.*, 1992; Kirkby *et al.*, 2016; Rabeony *et al.*, 1987). Recent works demonstrated the ability to manipulate drop condensation by controlling the electrode's structure and electrowetting properties (Hoek *et al.*, 2021; Damak and Varnassi, 2018). Despite the rapid improvements in the control of liquid condensation, the nucleation mechanism is often poorly understood. The nucleation rates are commonly based on the classical nucleation theory, where the rates depend exponentially on the free energy cost of creating the critical nucleus (Oxtoby, 1998a; Oxtoby, 1998b). For ion-induced nucleation, the Thomson model from 1933 allows the calculation of the nucleation energy of a dense liquid layer from a vapor around a core ion (Thomson, 1933). Both models use the bulk properties for the liquid and vapor phases and assume a sharp interface between them.

METHODS

We present a model to describe ion-induced nucleation in fluids that include dissociated ions (Wilson and Thomson, 1897). Nucleation is induced by a charged molecular aggregate, a large ion, a charged colloid, or an aerosol particle. The ions contribute to nucleation both electrostatically and through the preferential solvation effect (Adachi *et al.*, 1992; Kirkby *et al.*, 2016; Rabeony and Mirabel, 1987). We include the Gibbs transfer energies of ions and solve a modified Poisson-Boltzmann equation for the potential around a charged colloid. The ions' free energy is calculated and added to surface and bulk terms to obtain a generalized Thomson model (Kirkby *et al.*, 2016).

CONCLUSIONS

In the Debye-Hückel limit, we obtain analytical solutions while the nonlinear regime is evaluated numerically. The ions reduce the nucleation energy barrier due to the solvation effect. The ions' free energy has two terms. The first can be short or long range, depending on their density. The second is proportional to the nucleus' volume and shifts the state from undersaturation to supersaturation. The resultant state diagram in the plane of saturation and core charge includes regions with one phase, electro-prewetting, classical nucleation, ion-induced and spontaneous nucleation (Kroll and Tsori, 2022; Kroll and Tsori, 2023). The lines separating these regions depend sensitively on preferential solvation (Kroll and Tsori, 2024).

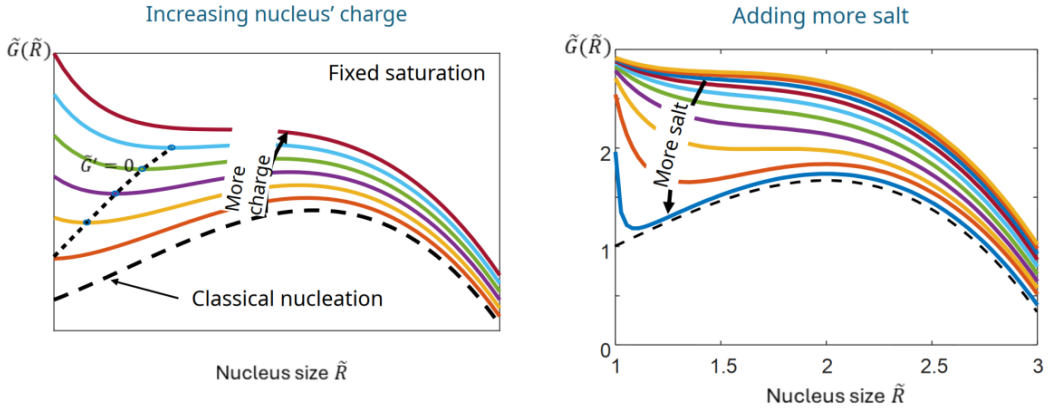


Figure 1. Left: Gibbs energy curves vs dimensionless nucleus size $\tilde{R}$ for increasing nucleus charge. A metastable nucleus exists at finite $\tilde{R}$ (dashed line). It disappears at large nucleus charges. Right: Gibbs energy vs $\tilde{R}$ at a fixed core charge and increasing salt content in the fluid. As salt is added, the energy barrier for nucleation decreases.

ACKNOWLEDGEMENTS

We are grateful for support by the Israel Science Foundation Grant No. 332/24.

REFERENCES

Damak, Maher and Varnassi, Kripa K. (2018). Electrostatically driven fog collection using space charge injection. *Sci. Adv.* **4**, eaao5323.

Hoek, Harmen,Dey, Ranabir and Mugele, Frieder (2021). Electrowetting-Controlled Dropwise Condensation with Patterned Electrodes: Physical Principles, Modeling, and Application Perspectives. *Adv. Mater. Interfaces* **8**, 2001317.

Kirkby, Jasper and Duplissy, J., Sengupta, Kamalika, Frege, Carla, Gordon, Hamish, Williamson, Christina, Heinritzi, Martin, Simon, Mario and Yan, Chao, Almeida, João, Tröstl, Jasmin, Nieminen, Tuomo, Ortega, Ismael, Wagner, Robert, Adamov, Alexey, Amorim, Antonio, Bernhammer, Anne-Kathrin, Bianchi, Federico, Breitenlechner, Martin, Curtius, Joachim (2016). Ion-induced nucleation of pure biogenic particles. *Nature* **533** 521-526.

Kroll, Roni and Tsori, Yoav (2023). Nucleation by a charged particle in fluids containing salt. *J. Coll. Interf. Sci.* **650**, 13--18.

Kroll, Roni and Tsori, Yoav (2024). The effect of ion solvation on ion-induced nucleation -- A modified Thomson model. *Phys. Fluids*. **36**, 127139.

Kroll, Roni and Tsori, Yoav (2022). Phase lines in mean-field models with nonuniform external forces *J. Chem. Phys.* (Communication) **157**, 231103.

Motoaki Adachi, Motoaki, Okuyama, Kikuo and Seinfeld, John H. (1992). Experimental studies of ion-induced nucleation, *J. Aerosol Science* **23**, 327-337.

Oxtoby, David W. (1998a). Homogeneous nucleation: theory and experiment. *J. Phys.: Condens. Matter*, **10**, 897.

Oxtoby, David W. (1998b). Nucleation of First-Order Phase Transitions. *Acc. Chem. Res.* **31**, 91-97.

Rabeony, H. and Mirabel, P. (1987). Experimental study of vapor nucleation on ions. *J. Phys. Chem.* **91**, 1815-1818.

Thomson, J. J. and Thomson, G. T. (1933). Conduction of Electricity through Gases. Cambridge University Press, Cambridge.

Wilson, Charles Thomson Rees and Thomson, Joseph John (1897). Condensation of water vapour in the presence of dust-free air and other gases. Philosophical Transactions of the Royal Society of London **189**, 265-307.

Developing the universal neural network force field for atmospheric aerosol nucleation

Yongjian Lian[1], Xurong Bai[1], Ruoying Yuan[1], Shuai Jiang[1*]

[1]*Tianjin Key Laboratory of Urban Transport Emission Research & State Environmental Protection Key Laboratory of Urban Ambient Air Particulate Matter Pollution Prevention and Control, College of Environmental Science and Engineering, Nankai University, Tianjin 300071, China.*
[*]*E-mail: shuaijiang@nankai.edu.cn.*

Keywords: New Particle Formation, Aerosol Nucleation, Quantum Chemistry, Machine Learning.

INTRODUCTION

Atmospheric aerosols significantly impact Earth's radiative balance and human health (Rose et al., 2018; Wang et al., 2015). Notably, 50%–90% of aerosols are formed through gas-to-particle conversion processes (Spracklen et al., 2006), a phenomenon known as new particle formation (NPF) (Lee et al., 2019). In other words, ubiquitous gaseous molecules in the atmosphere undergo processes such as collision, evaporation, and nucleation to gradually form molecular clusters, which subsequently grow into particulate matter. However, the detailed mechanisms governing NPF remain poorly understood due to the vast complexity of the atmosphere, involving thousands of molecular species and the unique influences of environmental factors like temperature, humidity, and pressure.

The introduction of classical nucleation theory (CNT) provided a robust theoretical foundation for understanding atmospheric nucleation mechanisms (Frenkel et al., 1939), offering a general framework for investigating nucleation thermodynamics and kinetics (Vehkamäki et al., 2012). However, CNT employs the approximation of modeling the smallest clusters as liquid droplets when calculating formation rates within specific size ranges, leading to significant inaccuracies in the predicted rates (Merikanto., 2007). Subsequently, the Atmospheric Cluster Dynamics Code (ACDC) theoretical model overcame the limitations of CNT by coupling master equations with quantum chemical thermodynamics (Mcgrath et al., 2012) and has been widely adopted (Almeida et al., 2013; Liu et al., 2021; Shen et al., 2020; Yao et al., 2018). Within the ACDC framework, the accuracy of the results is directly determined by the quantum chemically calculated thermodynamic data. Therefore, obtaining accurate thermodynamic data necessitates employing high-level quantum chemical methods and basis sets to perform comprehensive searches of the high-dimensional potential energy surfaces of cluster structures to locate global minima, from which their thermodynamic properties can be derived (Elm et al., 2023; Zhang et al., 2022). Nevertheless, this computational process often faces the challenge of prohibitively large computational demands. Furthermore, when addressing the critical transition steps from clusters >1 nm to particles in the real atmosphere, involving hundreds to thousands of potential precursor molecules, existing computational resources and the ACDC framework become completely inadequate. This severely impedes our understanding of the NPF process.

Machine learning (ML) offers a versatile and powerful solution for accelerating time-consuming processes characterized by repetitive patterns (Turing et al., 2009). ML has been successfully applied to various computational chemistry domains, including potential energy surface (PES) modeling, molecular structure prediction, molecular recognition and classification, enhancing molecular dynamics (MD) simulations, predicting kinetics and other properties, and gaining deeper insights into molecular behavior (Unke et al., 2021; Keith et al., 2021; Wang et al., 2024; Chen et al., 2024). Recently, Jonas Elm et al. and Jiang et al. have applied ML neural network techniques to theoretical calculations and simulations in atmospheric nucleation research, demonstrating significant progress (Kubečka et al., 2024; Jiang et al., 2022). However, the transferability and scalability of ML models remain critical technical bottlenecks (Unke et al., 2021). This limitation has hindered the effective application of ML in atmospheric nucleation studies, particularly in handling diverse precursor molecules and cluster systems across varying sizes. The recent development of the Large Atomic Model (LAM), based on a pre-training–fine-tuning–distillation framework and driven by large-scale atomic and molecular datasets, has achieved breakthroughs not only

in accuracy but also in significantly enhancing computational efficiency and reducing costs (Zhang et al., 2024). Currently, LAM has found widespread application in critical areas such as drug design and the development of novel battery materials (Yang et al., 2025, prepint; Wu et al., 2025, prepint). Consequently, LAM holds substantial promise for addressing key challenges in atmospheric nucleation theory, such as the multi-precursor, multi-size system problem and the high time cost associated with acquiring accurate thermodynamic data.

In this study, we propose the first universal neural network force field for atmospheric aerosol nucleation acid-base systems. Utilizing a substantial dataset of atmospheric cluster structures provided by the ACDB database, we uniformly relabeled the dataset under the B973C method. This relabeled dataset was then used to fine-tune the LAM, resulting in the first general-purpose ML model specifically tailored for atmospheric nucleation research. The accuracy of this model approaches that of density functional theory (DFT) calculations. Furthermore, it demonstrates the capability to predict binding energies for clusters across diverse chemical systems and varying sizes. Significantly, this model not only provides thermochemical data for clusters at ab initio accuracy but does so at a fraction of the computational cost. Additionally, it enables molecular dynamics (MD) simulations of the molecule-cluster conversion process, thereby offering deeper insights into the kinetics of cluster formation at the molecular level.

METHODS

The Large Atomic Model employed in this study is the DPA-2 model (Zhang et al., 2024). The dataset was sourced from cluster structures within the ACDB database (Kubečka et al., 2023; Elm et al., 2019). It primarily includes SA-Bases clusters of various sizes and conformations, totaling approximately 60,000 structures. All structures were uniformly labeled for energy and forces using the ORCA program (Neese et al., 2022; Neese et al., 2018) at the B973C level of theory (Brandenburg et al., 2018). The dataset was partitioned into training and validation sets in a 9:1 ratio. The B973C method has been rigorously tested and demonstrates excellent performance on atmospheric cluster datasets, maintaining high accuracy and low computational cost even for large clusters (Wu et al., 2023). Fine-tuning was performed using DeePMD-kit version v3.0.0b3 (Zeng et al., 2025). Molecular dynamics simulations were conducted using the Atomic Simulation Environment (ASE) (Larsen et al., 2017). Semi-empirical binding energies for the clusters were calculated using the GFN2-xTB method (Bannwarth et al., 2021) within the XTB program (Bannwarth et al., 2019).

CONCLUSIONS

Firstly, the model accuracy is benchmarked against 27-head DPA-2 LAM, proving its high accuracy. The trained model exhibited root mean square (RMS) validation and training errors for energy of 0.023 kcal/mol and 7.797×10^{-5} kcal/mol, respectively. Similarly, the RMS validation and training errors for force were 0.7291 kcal/mol/Å and 0.6394 kcal/mol/Å, respectively. Following fine-tuning, the model's accuracy on the validation set achieved parity with the performance of the original 27-head DPA-2 LAM on benchmark databases for pharmaceuticals, alloys, and polymers (reported energy errors: 0.019–0.2553 kcal/mol; force errors: 0.437–2.392 kcal/mol/Å) (Zhang et al., 2024).

Secondly, the accuracy of the model has been compared with that of GFN2-xTB method. As shown in Fig. 1, a clear trend emerges: the prediction accuracy of the fine-tuned model progressively approaches that of the B973C method as cluster size increases. Conversely, the accuracy of the semi-empirical GFN2-xTB method deteriorates with increasing cluster size. Consequently, it is concluded that the fine-tuned model significantly outperforms the semi-empirical method in predicting cluster binding energies, achieving accuracy comparable to the B973C method.

To further quantify the accuracy difference in cluster binding energy predictions between the fine-tuned model and the density functional theory (DFT) method at the B973C level, and to evaluate the model's

transferability across different chemical systems and cluster sizes, we analyzed the mean absolute error (MAE) and root mean square error (RMSE) of the fine-tuned model relative to the B973C reference values. This analysis was performed for clusters of varying sizes within the SA-W, SA-AM, SA-DMA, and SA-AM-DMA systems. As shown in Fig. 2, for all tested systems and cluster sizes that were represented within the training set, the fine-tuned model consistently achieved MAE < 1 kcal/mol and RMSE < 1 kcal/mol. This demonstrates the model's robust transferability across diverse systems and cluster sizes. Furthermore, for systems absent from the fine-tuning training set, such as 2SA6W and 2SA2AM1DMA, the model still maintained MAE < 1 kcal/mol and RMSE < 1 kcal/mol, indicating its strong extrapolation capability. Notably, the model exhibited superior accuracy for the complex ternary system 2SA2AM1DMA compared to binary systems like 2SA6W, 12SA12AM, and 4SA4DMA. Its performance for 2SA2AM1DMA even surpassed that for systems like 4SA4W and 7SA7AM, whose sizes were included in the training data. This suggests the model is particularly effective at predicting binding energies for complex multi-component (≥ ternary) systems beyond those initially present in the dataset. Additionally, for larger clusters absent from the fine-tuning dataset in terms of size (12SA12AM and 4SA4DMA), the prediction error is increasing as expected.

Finally, we applied the model to perform ab initio accuracy molecular dynamics (MD) simulations of nucleation under high concentrations. Using the Packmol program (Martínez et al., 2009), 5 sulfuric acid (SA) molecules and 5 dimethylamine (DMA) molecules were initially placed randomly within a 2.0 nm × 2.0 nm × 2.0 nm simulation box. To mitigate the effects from periodic image interactions, the box dimensions were subsequently increased to 3.5 nm in all three directions, and the molecules were repositioned near the center of the enlarged box. This configuration served as the initial structure for MD simulations, conducted using the Atomic Simulation Environment (ASE) program under NVT ensemble conditions. The simulations employed a timestep of 0.1 fs, a temperature of 300 K, a damping coefficient of 0.01 fs^{-1}, and periodic boundary conditions. Structural snapshots from the 1 ns MD trajectory are presented in Fig. 3. A clear evolution is observed: the system transitions from a dispersed state at 0 ps to an aggregated, and eventually clustered, state by 1.1 ns. Notably, the aggregation process reveals that the 5 SA molecules initially accumulate, forming a relatively stable cage-like cluster structure stabilized by hydrogen bonding. Subsequently, at around 10 ps, a DMA molecule interacts with an SA molecule on the periphery of SA cluster, undergoing proton transfer to form a $DMAH^+$ ammonium salt. Intriguingly, this $DMAH^+$ ion remains associated with the periphery of the SA cluster for the remainder of the simulation. Furthermore, the cage structure of the SA cluster is disrupted around 210 ps, coinciding with another DMA molecule undergoing proton transfer with a peripheral SA molecule to form a second $DMAH^+$ ion. The SA molecules then re-form a cage-like structure, and the newly formed $DMAH^+$ ion also remains on the cluster periphery. No further proton transfer events between SA and DMA were observed during the remaining simulation time. The two remaining free DMA molecules dimerize and move away from the SA cluster. We hypothesize that both the persistent localization of $DMAH^+$ ions on the cluster periphery and the dimerization of free DMA molecules away from the cluster may be attributed to steric effects arising from the two methyl groups of the DMA molecules. Analysis of the potential energy profile in Fig. 3 shows a significant decrease between 0-100 ps, likely corresponding to the first proton transfer event and the formation of the initial SA cage structure. An even more pronounced energy drop occurs between 100-200 ps, presumably resulting from the second proton transfer event. Notably, no significant subsequent energy drops or proton transfer events were observed. This suggests the cluster structure stabilizes after the two transfers. Further proton transfer from peripheral DMA molecules to internal SA sites may require disrupting this stable structure, presenting a significant kinetic barrier. Exploring this possibility would necessitate significantly longer simulation timescales. The pathway observed is influenced by the initial configuration and high precursor concentration. Further investigation employing enhanced sampling techniques, such as Metadynamics, under conditions closer to realistic atmospheric concentrations is required to elucidate the authentic nucleation pathway.

All in all, this study presents the first universal force field for multicomponent aerosol nucleation systems. This yields the first foundation model within the atmospheric new particle formation (NPF) field capable of cross-system and cross-size predictions. The model achieves errors below 1 kcal/mol for binding energy predictions across diverse systems and cluster sizes within the validation sets. Furthermore, the model demonstrates high fidelity in molecular dynamics (MD) simulations of cluster structures. Notably,

the model enabled simulations of the molecule-to-cluster transition under high atmospheric precursor concentrations. In summary, the developed LAM provides ab initio accuracy energy predictions for multi-component, multi-size cluster structures. Critically, it also facilitates MD simulations of cluster formation, yielding unique molecular-level insights into nucleation pathways. Consequently, ab initio-accurate LAMs represent a promising, powerful tool for future atmospheric cluster theory research, offering rapid, precise, and generalizable capabilities.

Figures:

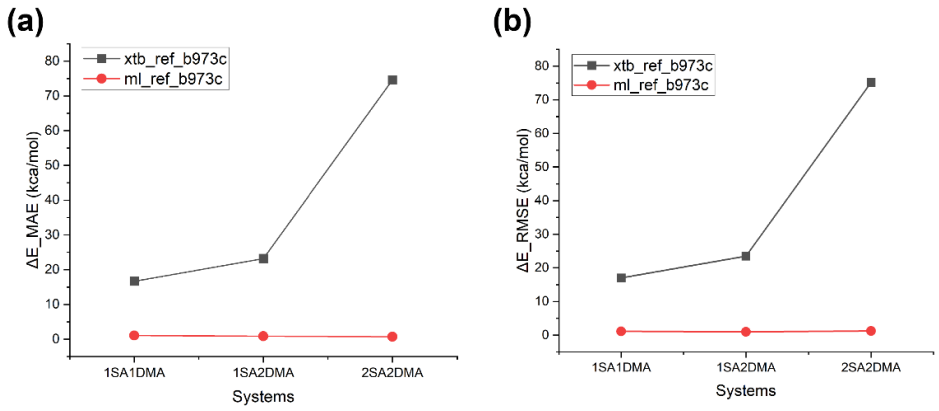


Fig. 1 (a) mean absolute error and (b) root mean square error in the binding energy prediction of sulfuric acid-dimethylamine clusters by the large-atom model and the XTB semiempirical method compared to the density-functional calculation method (B973C)

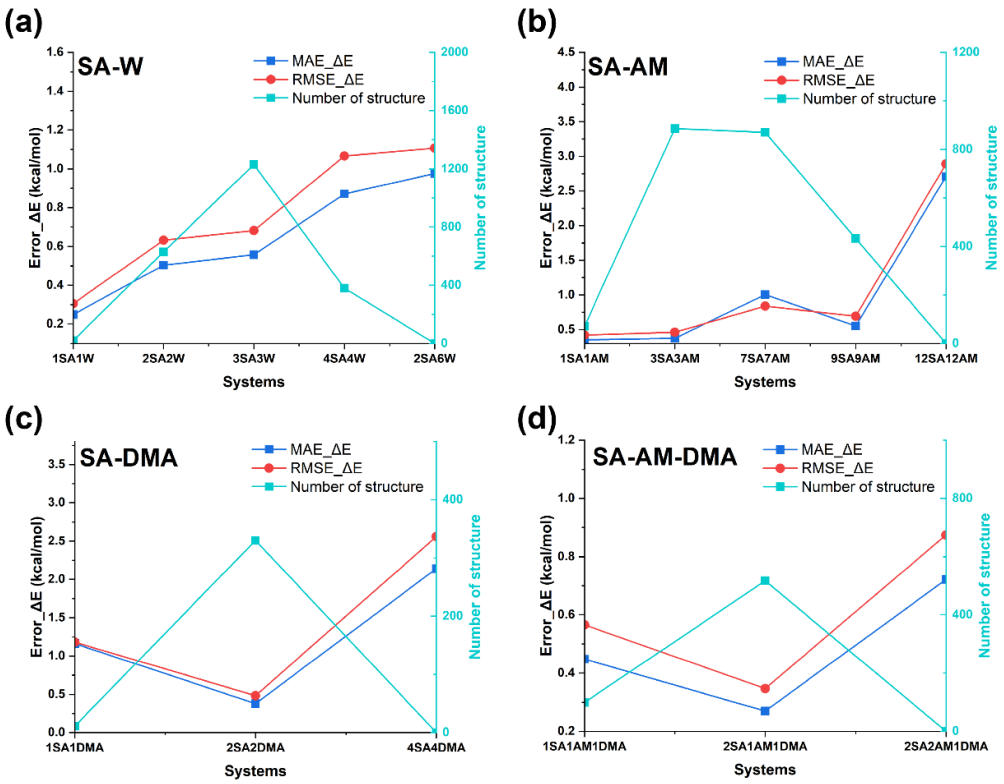


Fig. 2 The Large-atom model validation results for SA-W, SA-AM, SA-DMA, SA-AM-DMA systems. When the number of structures is 0, which indicates that this system is not included in the database, such as 2SA6W, 12SA12AM, 4SA4DMA, 2SA2AM1DMA.

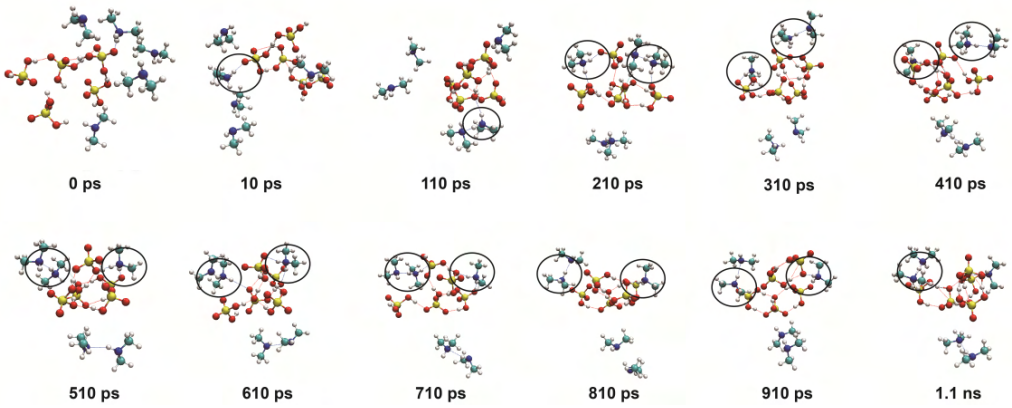


Fig. 3 Snapshot plot of 1ns simulation results. Inside the black circle is $DMAH^{+}$.

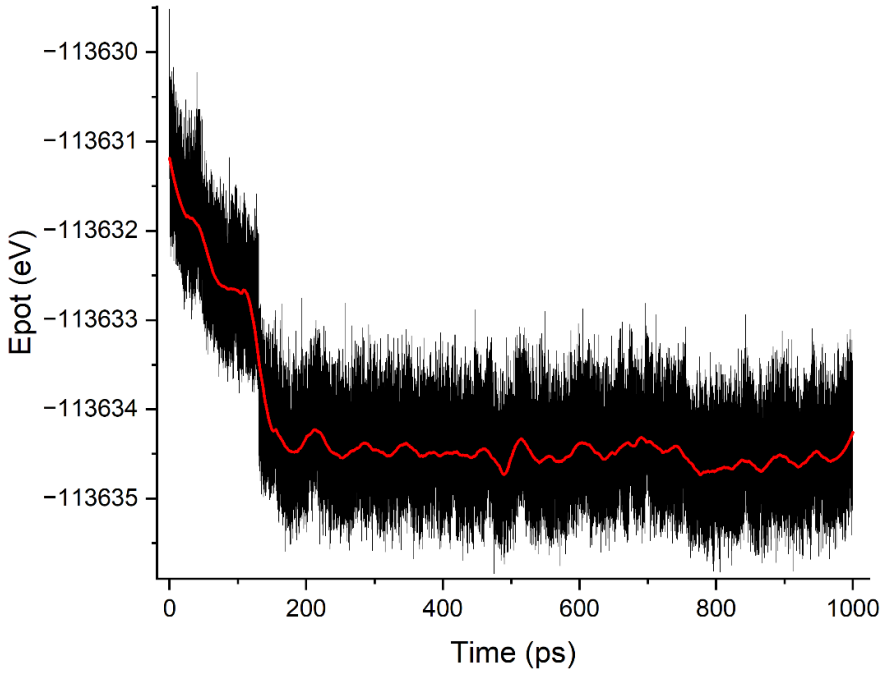


Fig. 4 Variation curves of the potential energy surface for the 1ns simulation. The red folded line is the smoothed curve and the number of windows used for smoothing is 50000.

ACKNOWLEDGEMENTS

This research was funded by National Natural Science Foundation of China (42477111), the Fundamental Research Funds for the Central Universities of China (63243126), Natural Science Foundation of Tianjin Municipality (24JCYBJC01700) and Tianjin Key Research and Development Project (24YFXTHZ00070). The work was carried out at National Supercomputer Center in Tianjin, and the calculations were performed on Tianhe new generation supercomputer.

REFERENCES

Rose C, Zha Q, Dada L, et al. Observations of biogenic ion-induced cluster formation in the atmosphere[J]. Science advances, 2018, 4(4): eaar5218.

Wang Y H, Liu Z R, Zhang J K, et al. Aerosol physicochemical properties and implications for visibility during an intense haze episode during winter in Beijing[J]. Atmos. Chem. Phys., 2015, 15(6): 3205-3215.

Spracklen D V, Carslaw K S, Kulmala M, et al. The contribution of boundary layer nucleation events to total particle concentrations on regional and global scales[J]. Atmos. Chem. Phys., 2006, 6(12): 5631-5648.

Lee S-H, Gordon H, Yu H, et al. New Particle Formation in the Atmosphere: From Molecular Clusters to Global Climate[J]. Journal of Geophysical Research: Atmospheres, 2019, 124(13): 7098-7146.

Frenkel J. Statistical Theory of Condensation Phenomena[J]. The Journal of Chemical Physics, 1939, 7(3): 200-201.

Vehkamäki H, Riipinen I. Thermodynamics and kinetics of atmospheric aerosol particle formation and growth[J]. Chemical Society Reviews, 2012, 41(15): 5160-5173.

Merikanto J, Zapadinsky E, Lauri A, et al. Origin of the Failure of Classical Nucleation Theory: Incorrect Description of the Smallest Clusters[J]. Physical Review Letters, 2007, 98(14): 145702.

Mcgrath M J, Olenius T, Ortega I K, et al. Atmospheric Cluster Dynamics Code: a flexible method for solution of the birth-death equations[J]. Atmos. Chem. Phys., 2012, 12(5): 2345-2355.

Almeida J, Schobesberger S, Kürten A, et al. Molecular understanding of sulphuric acid–amine particle nucleation in the atmosphere[J]. Nature, 2013, 502(7471): 359-363.

Liu L, Yu F, Du L, et al. Rapid sulfuric acid–dimethylamine nucleation enhanced by nitric acid in polluted regions[J]. Proceedings of the National Academy of Sciences, 2021, 118(35): e2108384118.
Shen J, Elm J, Xie H-B, et al. Structural effects of amines in enhancing methanesulfonic acid-driven new particle formation[J]. Environmental Science & Technology, 2020, 54(21): 13498-13508.
Yao L, Garmash O, Bianchi F, et al. Atmospheric new particle formation from sulfuric acid and amines in a Chinese megacity[J]. Science, 2018, 361(6399): 278-281.
Elm J, Ayoubi D, Engsvang M, et al. Quantum chemical modeling of organic enhanced atmospheric nucleation: A critical review[J]. WIREs Computational Molecular Science, 2023, 13(5): e1662.
Zhang X, Tan S, Chen X, et al. Computational chemistry of cluster: Understanding the mechanism of atmospheric new particle formation at the molecular level[J]. Chemosphere, 2022, 308: 136109.
Turing A M: Computing Machinery and Intelligence, Epstein R, Roberts G, Beber G, editor, Parsing the Turing Test: Philosophical and Methodological Issues in the Quest for the Thinking Computer, Dordrecht: Springer Netherlands, 2009: 23-65.
Unke O T, Chmiela S, Sauceda H E, et al. Machine Learning Force Fields[J]. Chemical Reviews, 2021, 121(16): 10142-10186.
Keith J A, Vassilev-Galindo V, Cheng B, et al. Combining Machine Learning and Computational Chemistry for Predictive Insights Into Chemical Systems[J]. Chemical Reviews, 2021, 121(16): 9816-9872.
Wang T, He X, Li M, et al. Ab initio characterization of protein molecular dynamics with AI2BMD[J]. Nature, 2024, 635(8040): 1019-1027.
Chen Y, Pios S V, Gelin M F, et al. Accelerating Molecular Vibrational Spectra Simulations with a Physically Informed Deep Learning Model[J]. Journal of Chemical Theory and Computation, 2024, 20(11): 4703-4710.
Muratov E N, Bajorath J, Sheridan R P, et al. QSAR without borders[J]. Chemical Society Reviews, 2020, 49(11): 3525-3564.
Kubečka J, Ayoubi D, Tang Z, et al. Accurate modeling of the potential energy surface of atmospheric molecular clusters boosted by neural networks[J]. Environmental Science: Advances, 2024.
Jiang S, Liu Y-R, Huang T, et al. Towards fully ab initio simulation of atmospheric aerosol nucleation[J]. Nature Communications, 2022, 13(1): 6067.
Lin-Feng Z, Han W. Simulating the microscopic world: from the Schrödinger equation to the large atomic model[J]. PHYSICS, 2024, 53(7): 431-441.
M Y, D Z. Ab initio Accuracy Neural Network Potential for Drug-like Molecules[J]. ChemRxiv, 2024, 53(7): 431-441.
Z W, L Z. A Machine-Learning-Based Interatomic Potential Universal Model[J]. ChemRxiv, 2024, 53(7): 431-441.
Zhang D, Liu X, Zhang X, et al. DPA-2: a large atomic model as a multi-task learner[J]. npj Computational Materials, 2024, 10(1): 293.
Kubečka J, Besel V, Neefjes I, et al. Computational Tools for Handling Molecular Clusters: Configurational Sampling, Storage, Analysis, and Machine Learning[J]. ACS Omega, 2023, 8(47): 45115-45128.
Elm J. An Atmospheric Cluster Database Consisting of Sulfuric Acid, Bases, Organics, and Water[J]. ACS Omega, 2019, 4(6): 10965-10974.
Neese F. The ORCA program system[J]. Wiley Interdisciplinary Reviews: Computational Molecular Science, 2012, 2(1): 73-78.
Neese F. Software update: the ORCA program system, version 4.0[J]. WIREs Computational Molecular Science, 2018, 8(1): e1327.
Brandenburg J G, Bannwarth C, Hansen A, et al. B97-3c: A revised low-cost variant of the B97-D density functional method[J]. J Chem Phys, 2018, 148(6): 064104.
Wu H, Engsvang M, Knattrup Y, et al. Improved Configurational Sampling Protocol for Large Atmospheric Molecular Clusters[J]. ACS Omega, 2023, 8(47): 45065-45077.
Zeng J, Zhang D, Peng A, et al. DeePMD-kit v3: A Multiple-Backend Framework for Machine Learning Potentials[J]. Journal of Chemical Theory and Computation, 2025.
Larsen A H, Mortensen J J, Blomqvist J, et al. The atomic simulation environment—a Python library for working with atoms[J]. Journal of Physics: Condensed Matter, 2017, 29(27): 273002.

Bannwarth C, Caldeweyher E, Ehlert S, et al. Extended tight-binding quantum chemistry methods[J]. WIREs Computational Molecular Science, 2021, 11(2): e1493.
Bannwarth C, Ehlert S, Grimme S. GFN2-xTB—An Accurate and Broadly Parametrized Self-Consistent Tight-Binding Quantum Chemical Method with Multipole Electrostatics and Density-Dependent Dispersion Contributions[J]. Journal of Chemical Theory and Computation, 2019, 15(3): 1652-1671.
Mart ńez L, Andrade R, Birgin E G, et al. PACKMOL: A package for building initial configurations for molecular dynamics simulations[J]. Journal of Computational Chemistry, 2009, 30(13): 2157-2164.

Temperature Dependence of Autoxidation and Dimerization in α-Pinene Ozonolysis from 223 to 298K

L. Liu[1], P. Roldin[2], M. Simon[3], L. Yang[4], C. Yan[4], W. Nie[4], L. Dada[1], J. Kirkby[5], N.M. Donahue[6], CLOUD collaboration, and I. EI Haddad[1]

[1]*Laboratory of Atmospheric Chemistry, Paul Scherrer Institute, PSI, Villigen, Switzerland*
[2]*Division of Nuclear Physics, Department of Physics, Lund University, Lund, Sweden*
[3]*Institute for Atmospheric and Environmental Sciences, Goethe University Frankfurt, Frankfurt am Main, Germany*
[4]*Joint International Research Laboratory of Atmospheric and Earth System Research, School of Atmospheric Sciences, Nanjing University, Nanjing, China*
[5]*CERN, Geneva, Switzerland.*
[6]*Center for Atmospheric Particle Studies, Carnegie Mellon University, Pittsburgh, PA, USA.*

Keywords: HOMs, autoxidation, temperature dependence, CLOUD chamber, Box model.

INTRODUCTION

Highly oxygenated organic molecules (HOMs) rapidly form from the autoxidation of VOCs, such as monoterpenes, influencing atmospheric aerosols formation and impacting climate and human health (Jimenez et al., 2009). During autoxidation, peroxyl radicals (RO_2) undergo temperature-dependent hydrogen shifts (H-shifts) and subsequent addition of O_2.(Bianchi et al., 2019; Quéléver et al., 2019). Additionally, radical dimerization increases the carbon number of products, further contributing to low-volatility compounds. Despite extensive studies, the complex mechanism of HOMs formation, in particular its temperature dependence, remains incompletely understood.

METHODS

HOMs were formed during α-pinene ozonolysis experiments at four temperatures (223K, 248K, 278K, and 298K) in the Cosmics Leaving OUtdoor Droplets (CLOUD) chamber at CERN (Geneva, Switzerland). The CLOUD chamber is enclosed within a thermal housing that ensures precise temperature control within a range of 203 to 373 K, with an accuracy of ±0.1 K. Gas-phase HOMs in the CLOUD chamber were detected using a nitrate chemical ionization atmospheric-pressure interface time-of-flight mass spectrometer (CI-APi-TOF), while precursors and less oxygenated products were measured by PTR3-TOF-MS to achieve carbon closure (Simon et al., 2020). The box model, ADCHAM (Aerosol Dynamics gas- and particle-phase chemistry model)(Roldin et al., 2019) was employed to simulate HOMs formation in the gas phase during α-pinene ozonolysis at various temperatures and compared with CLOUD-chamber measurements. The gas-phase chemistry module in the ADCHAM model incorporates the Master Chemical Mechanism (MCMv3.3.1) and the peroxyl radical autoxidation mechanism (PRAM) module. PRAM includes approximately 300 species and 2,500 reactions related to HOMs formation (Nie et al., 2023). Together, the ADCHAM consists of 1,881 species and 15,407 reactions for gas-phase chemistry. ADCHAM has demonstrated good predictions of HOM formation in previous chamber comparison studies conducted at room temperature (278–289 K)(Nie et al., 2023; Roldin et al., 2019), but lacks research over a broader temperature range.

CONCLUSIONS

This study optimizes the parameterization of the autoxidation and dimerization reactions in α-pinene ozonolysis by incorporating CLOUD measurements and the latest findings from molecular dynamics studies (Iyer et al., 2021; Yang et al., 2025). After model optimization, the box model not only accurately predicts the overall monomer and dimer yield across the temperature range of 223 to 298 K with a deviation of less than 2 (Figure 1a, 1b), but also effectively captures the oxygenation levels of the individual monomers (Figure 2). A significant improvement in ultra-low volatile organic compound (ULVOC) prediction is also observed across a wide temperature range, where the difference between the measurement result and model prediction decreased from a factor of 11 to less than 80% in the 223K to 298K range (Figure 1d). The precise prediction of ULVOCs provides a solid basis for extending the model to include the particle-phase processes. Additionally, the increased discrepancy in dimer formation at higher temperatures (Figure 1b, represented by yellow line) suggests potential shifts in the branching ratio of RO_2-RO_2 bimolecular reactions, altering the relative proportions of the resulting products: (1) two alkoxy radicals (RO), (2) an alcohol (ROH) and a carbonyl compound (RC=O), or (3) an accretion product (ROOR). To investigate this, a negative temperature dependence was applied to the dimer-formation pathway to simulate the temperature-dependent variability in that branching ratio, and the improved model performance (Figure 1 shown by red line) indicates that this hypothesis is plausible.

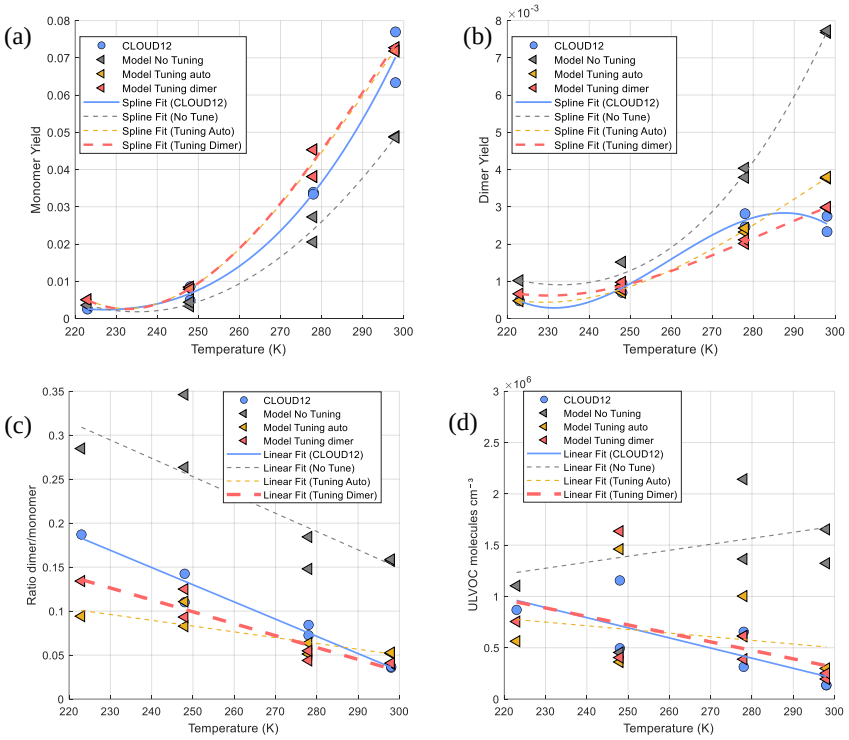


Figure 1: Comparison of the CLOUD measurements and the predictions made by the ADCHAM model for (a) monomer yield, (b) dimer yields, (c) dimer to monomer ratio, and (d) ULVOC concentration in the α-pinene ozonolysis system. Blue markers represent CLOUD measurements, while gray markers indicate default model predictions before optimization. Yellow markers show model results with improved autoxidation parameterization, and red markers depict the final model output, incorporating an additional negative temperature dependence in the dimerization process.

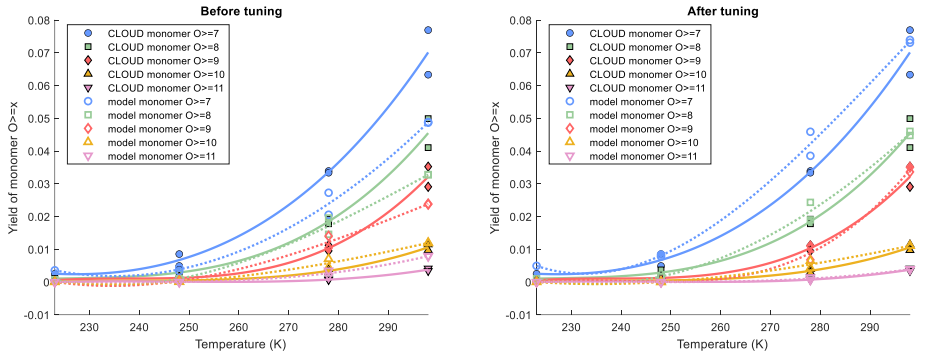


Figure 2: Comparison of monomer yields grouped by oxygen number between the CLOUD measurement and prediction of the model across the temperature range from 223K to 298K, before and after model tuning (from left to right). The measurement of monomer yields from the CLOUD-chamber is represented by solid markers, with variations fitted by solid lines. The monomer yields predicted by the ADCHAM model are shown by hollow markers, with the fitted trends depicted by dashed lines.

ACKNOWLEDGEMENTS

This work was supported by the SNF project 205504022002. We extend our gratitude to the European Commission Seventh Framework Programme and European Union Horizon 2020 program (Marie Skłodowska Curie ITNs no.316662 “CLOUD-TRAIN”, no. 764991 “CLOUD-MOTION”, MSCA-IF no. 656994 “nano-CAVa”, and MC-COFUND grant no. 600377) and all funding that supported the CLOUD12 and CLOUD16 campaigns and to our collaborators for their valuable contributions.

REFERENCES

Bianchi, F., Kurten, T., Riva, M., Mohr, C., Rissanen, M. P., Roldin, P., Berndt, T., Crounse, J. D., Wennberg, P. O., Mentel, T. F., Wildt, J., Junninen, H., Jokinen, T., Kulmala, M., Worsnop, D. R., Thornton, J. A., Donahue, N., Kjaergaard, H. G., & Ehn, M. (2019). Highly Oxygenated Organic Molecules (HOM) from Gas-Phase Autoxidation Involving Peroxy Radicals: A Key Contributor to Atmospheric Aerosol. *Chemical Reviews*, *119*(6), 3472-3509. https://doi.org/10.1021/acs.chemrev.8b00395

Iyer, S., Rissanen, M. P., Valiev, R., Barua, S., Krechmer, J. E., Thornton, J., Ehn, M., & Kurten, T. (2021). Molecular mechanism for rapid autoxidation in alpha-pinene ozonolysis. *Nat Commun*, *12*(1), 878. https://doi.org/10.1038/s41467-021-21172-w

Jimenez, J. L., Canagaratna, M. R., Donahue, N. M., Prevot, A. S., Zhang, Q., Kroll, J. H., DeCarlo, P. F., Allan, J. D., Coe, H., Ng, N. L., Aiken, A. C., Docherty, K. S., Ulbrich, I. M., Grieshop, A. P., Robinson, A. L., Duplissy, J., Smith, J. D., Wilson, K. R., Lanz, V. A., . . . Worsnop, D. R. (2009). Evolution of organic aerosols in the atmosphere. *Science*, *326*(5959), 1525-1529. https://doi.org/10.1126/science.1180353

Nie, W., Yan, C., Yang, L., Roldin, P., Liu, Y., Vogel, A. L., Molteni, U., Stolzenburg, D., Finkenzeller, H., Amorim, A., Bianchi, F., Curtius, J., Dada, L., Draper, D. C., Duplissy, J., Hansel, A., He, X. C., Hofbauer, V., Jokinen, T., . . . Ding, A. (2023). NO at low concentration can enhance the formation of highly oxygenated biogenic molecules in the atmosphere. *Nat Commun*, *14*(1), 3347. https://doi.org/10.1038/s41467-023-39066-4

Quéléver, L. L. J., Kristensen, K., Normann Jensen, L., Rosati, B., Teiwes, R., Daellenbach, K. R., Peräkylä, O., Roldin, P., Bossi, R., Pedersen, H. B., Glasius, M., Bilde, M., & Ehn, M. (2019). Effect of temperature on the formation of highly oxygenated organic molecules (HOMs) from alpha-pinene ozonolysis. *Atmos. Chem. Phys.*, *19*(11), 7609-7625. https://doi.org/10.5194/acp-19-7609-2019

Roldin, P., Ehn, M., Kurten, T., Olenius, T., Rissanen, M. P., Sarnela, N., Elm, J., Rantala, P., Hao, L., Hyttinen, N., Heikkinen, L., Worsnop, D. R., Pichelstorfer, L., Xavier, C., Clusius, P., Ostrom, E., Petaja, T., Kulmala, M., Vehkamaki, H., . . . Boy, M. (2019). The role of highly oxygenated organic molecules in the Boreal aerosol-cloud-climate system. *Nat Commun*, *10*(1), 4370. https://doi.org/10.1038/s41467-019-12338-8

Simon, M., Dada, L., Heinritzi, M., Scholz, W., Stolzenburg, D., Fischer, L., Wagner, A. C., Kürten, A., Rörup, B., He, X. C., Almeida, J., Baalbaki, R., Baccarini, A., Bauer, P. S., Beck, L., Bergen, A., Bianchi, F., Bräkling, S., Brilke, S., . . . Curtius, J. (2020). Molecular understanding of new-particle formation from α-pinene between −50 and +25 °C. *Atmos. Chem. Phys.*, *20*(15), 9183-9207. https://doi.org/10.5194/acp-20-9183-2020

Yang, H., Raucci, U., Iyer, S., Hasan, G., Golin Almeida, T., Barua, S., Savolainen, A., Kangasluoma, J., Rissanen, M., Vehkamäki, H., & Kurtén, T. (2025). Molecular dynamics-guided reaction discovery reveals endoperoxide-to-alkoxy radical isomerization as key branching point in α-pinene ozonolysis. *Nature Communications*, *16*(1), 661. https://doi.org/10.1038/s41467-025-55985-w

EXPERIMENTAL STUDIES OF THE INFLUENCE OF CARRIER GASES ON THE WATER HOMOGENEOUS NUCLEATION IN MIXTURES

M. LUKIANOV[1], T. LUKIANOVA[1] and J. HRUBÝ[1]

[1] *Institute of Thermomechanics of the Czech Academy of Sciences, Prague, Czech Republic*

Keywords: HOMOGENEOUS NUCLEATION, NUCLEATION RATE, REAL GAS CORRECTION, CRITICAL CLUSTER SIZES.

INTRODUCTION

Various devices and methods have been developed to investigate homogeneous nucleation, and also many different temperature and pressure regimes have been studied.(Heist and He, 1994; Wyslouzil and Wölk, 2016) The homogeneous nucleation of water was studied in argon and other monatomic gases(Holten et al., 2005; Viisanen et al., 1993; Wölk and Strey, 2001), as well as in nitrogen and mixtures of carbon dioxide and nitrogen.(Campagna et al., 2021; Lukianov et al., 2023) In recent studies, the correction of experimental data was carried out, taking into account the behavior of real gases. Additionally, the nucleation theorem was used to obtain information about the sizes of critical clusters. The main objective of this study is to investigate the effect of different carrier gases on the nucleation rate. These gases differ in the number of atoms per molecule, which affects the rate of expansion required to reach the target nucleation temperature.

METHODS

The experimental setup for studying the homogeneous nucleation of water was originally developed by Wagner and Strey and it was used for numerous homogeneous nucleation studies by Prof. R. Strey's group at the Max Planck Institute for Biophysical Chemistry, Göttingen (Wagner and Strey, 1981), and later at the University of Cologne. (Wölk and Strey, 2001) After a series of modernizations, including the complete replacement of the oil-free vacuum unit, research using this setup is successfully continuing at the Institute of Thermomechanics of the Czech Academy of Sciences in Prague (Lukianov et al., 2023). The nucleation experiments were performed within a temperature of 220 to 260 K, at pressures from 40 to 73 kPa, and supersaturation from levels 6.5 to 20.

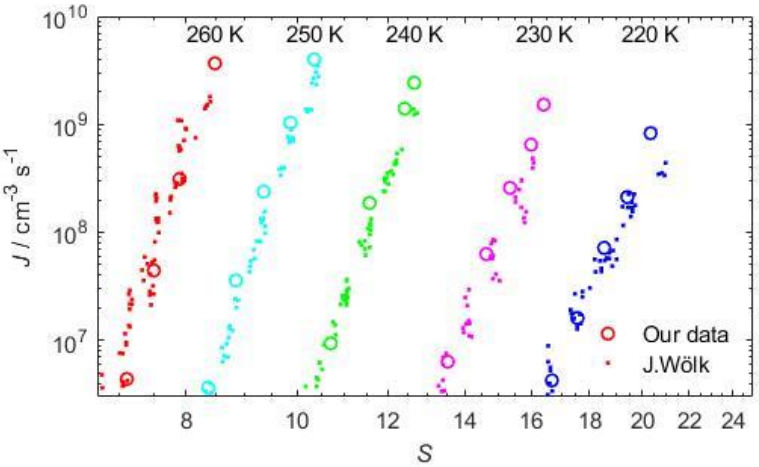


Figure 1. Comparison of our water nucleation rate data at different isotherms with data from J. Wölk and R. Strey (Wölk and Strey, 2001) in the presence of Ar

New experimental data on water nucleation, assuming ideal gas behavior, were compared with the literature experimental data from (Wölk and Strey, 2001) to confirm the reliability of the setup and are presented in Figure 1.

Further experiments demonstrated that different carrier gases have distinct effects on the nucleation rate and the next step involved estimating the mixture composition and nucleation temperature using the virial equation of state truncated after the second virial coefficient (Campagna et al., 2021). This model was found to work well for the studied vapor-gas mixtures and the obtained results were compared with those obtained during the experiments. This process was necessary to ensure that the observed differences represented a physical effect of the carrier gases on water nucleation rather than an artifact of a simplified estimation procedure that neglects real gas effects.

After calculating the molar fractions of the components, temperatures were calculated assuming constant entropy during expansion. Supersaturation correction was performed according to the method described by M.M Campagna. (Campagna et al., 2021), which accounts for the fugacity coefficients of water vapor both in equilibrium and in the presence of carrier gas, as well as the Poynting effect.

CONCLUSIONS

Experimental results for the homogeneous nucleation of water in the presence of Ar, N_2, CO_2, and N_2O as carrier gases are presented.

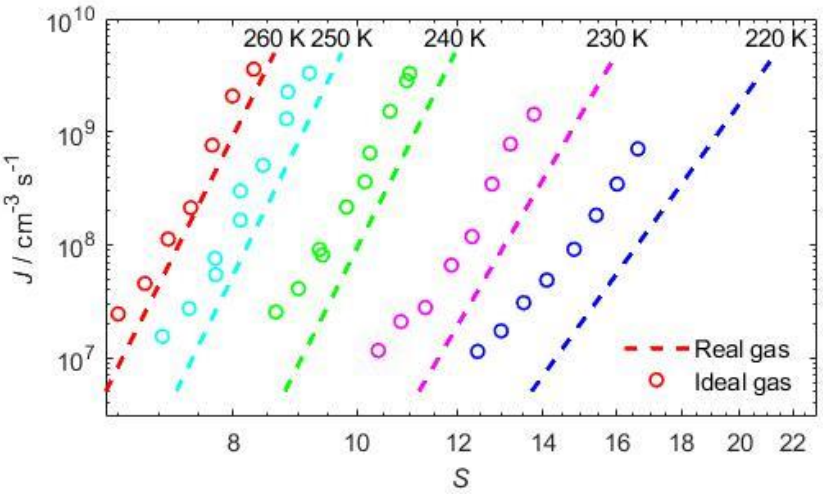


Figure 2. Nucleation rates of water with CO_2. Comparison of real gas and ideal gas calculations.

The results of the real gas correction are shown in all subsequent figures. For example, Figure 2 compares the supersaturation and nucleation temperature calculations for water nucleation in a CO_2 mixture under real and ideal gas assumptions. As evident from the figure, the real gas effect is significant for this system. Nevertheless, as shown in Figure 3, when real gas corrections are applied, the differences among the various carrier gases—except for CO_2—are relatively small and comparable to the experimental uncertainty.(Fransen et al., 2015; Luijten and Van Dongen, 1999)

Figure 4, for example, shows a comparison with M. M. Campagna's data on water nucleation at 0.1 MPa, 240 K for nitrogen and carbon dioxide carrier gas mixes.

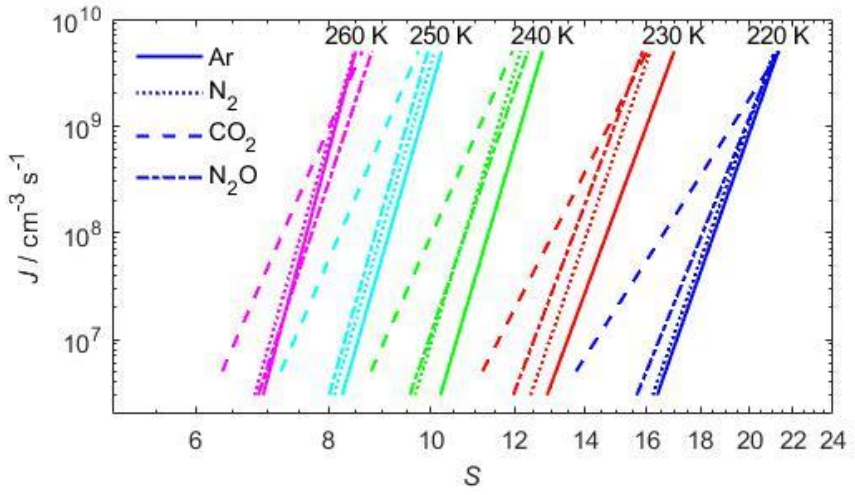


Figure 3. Comparison of real gas corrected Ar, N_2, N_2O and CO_2 mixtures at nominal isotherms.

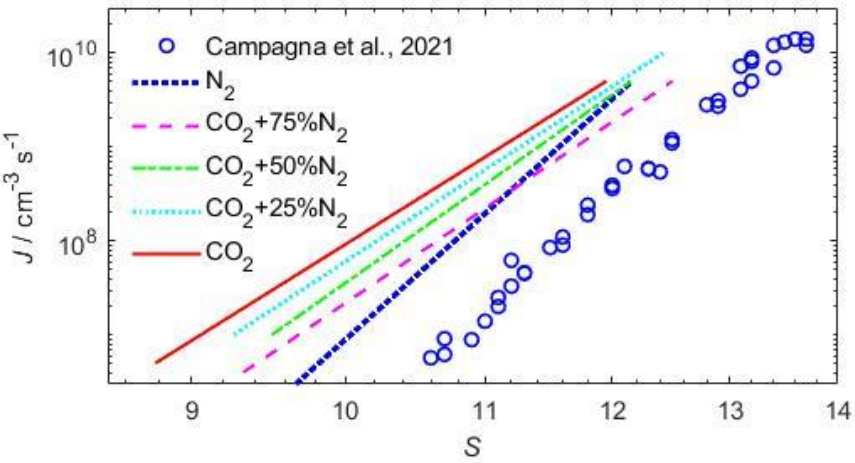


Figure 4. Comparison with M. M. Campagna (Campagna et al., 2021) data of water nucleation at pressure 0.1 MPa, 240 K for nitrogen and carbon dioxide carrier gas.

Using expression from the nucleation theorem (Oxtoby and Kashchiev 1994; Kashchiev 1981) the sizes of critical clusters were calculated from slopes of experimental data with real gas recomputing.

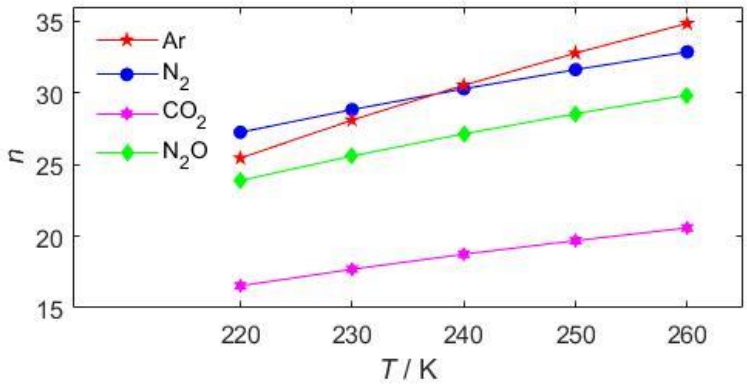


Figure 5. Dependence of critical cluster sizes from nucleation temperature for different carrier gases.

In comparison with literature data (Campagna et al., 2020; Wölk and Strey, 2001) significant differences were observed in the presence of CO_2.

Homogeneous nucleation rates were determined for different temperatures, supersaturations, and carrier gas compositions. In this study, real gas calculations were used to estimate temperatures and supersaturations, in contrast to previous studies conducted with this setup (Wagner and Strey, 1981). The results indicate that the real gas effect has a strong influence on the homogeneous nucleation of water with a CO_2 carrier gas. However, the effect of CO_2 concentration is minor. It is evident that CO_2 promotes nucleation even at low pressures, primarily due to gas adsorption, which reduces surface tension. Additionally, Figure 3 shows that the slope of the isotherms decreases with increasing CO_2 concentration. This behavior suggests a reduction in the number of water molecules forming the critical cluster.

ACKNOWLEDGEMENTS

The research leading to these results has received funding from the Czech Science Foundation under project No. GA22-28869S and from the Czech Academy of Sciences under project No. RVO: 61388998.

REFERENCES

Campagna, M.M., Hrubý, J., Van Dongen, M.E.H., Smeulders, D.M.J. (2021). Homogeneous water nucleation in carbon dioxide-nitrogen mixtures: Experimental study on pressure and carrier gas effects. J. Chem. Phys. 154. https://doi.org/10.1063/5.0044898

Campagna, M.M., van Dongen, M.E.H., Smeulders, D.M.J. (2020). Novel test section for homogeneous nucleation studies in a pulse expansion wave tube: experimental verification and gasdynamic 2D numerical model. Exp. Fluids 61, 108. https://doi.org/10.1007/s00348-020-02945-3

Fransen, M.A.L.J., Hrubý, J., Smeulders, D.M.J., Van Dongen, M.E.H. (2015). On the effect of pressure and carrier gas on homogeneous water nucleation. J. Chem. Phys. 142, 1–8. https://doi.org/10.1063/1.4919249

Heist, R.H., He, H. (1994). Review of Vapor to Liquid Homogeneous Nucleation Experiments from 1968 to 1992. J. Phys. Chem. Ref. Data 23, 781–805. https://doi.org/10.1063/1.555951

Holten, V., Labetski, D.G., Van Dongen, M.E.H. (2005). Homogeneous nucleation of water between 200 and 240 K: New wave tube data and estimation of the Tolman length. J. Chem. Phys. 123. https://doi.org/10.1063/1.2018638

Luijten, C.C.M., Van Dongen, M.E.H. (1999). Nucleation at high pressure. I. Theoretical considerations. J. Chem. Phys. 111, 8524–8534. https://doi.org/10.1063/1.480193

Lukianov, M., Lukianova, T., Hruby, J. (2023). Homogeneous water nucleation in argon, nitrogen and nitrous oxide as carrier gases. J. Chem. Phys. 124301. https://doi.org/10.1063/5.0138794

Viisanen, Y., Strey, R., Reiss, H. (1993). Homogeneous nucleation rates for water. J. Chem. Phys. 99, 4680–4692. https://doi.org/10.1063/1.466066

Wagner, P.E., Strey, R. (1981). Homogeneous nucleation rates of water vapor measured in a two-piston expansion chamber. J. Phys. Chem. 85, 2694–2698. https://doi.org/10.1021/j150618a026

Wölk, J., Strey, R. (2001). Homogeneous Nucleation of H2O and D2O in Comparison: The Isotope Effect. J. Phys. Chem. B 105, 11683–11701. https://doi.org/10.1021/jp0115805

Wyslouzil, B.E., Wölk, J. (2016). Overview: Homogeneous nucleation from the vapor phase—The experimental science. J. Chem. Phys. 145, 211702. https://doi.org/10.1063/1.4962283

ADVANCEMENTS AND KEY PLAYERS IN NUCLEATION THEORY

ROBERT L. MCGRAW

Environmental Sciences and Technologies Department, Brookhaven National Laboratory
Upton, NY 11973

Keywords: Gibbs, Thermodynamics, Kinetics, Classical vs Molecular Theories, Computation, ICNAA-Facilitated Collaboration

INTRODUCTION

As an excursion day talk, this will be more on the informal side, with focus on discussions of a selected few key ideas and the players and collaborations that developed them. The speaker's "institutional memory" of nucleation theory, and of those who made it happen, dates back to August 1977 when he first arrived at UCLA to begin what would turn out to be career-changing postdoctoral research with Howard Reiss. That first day (using only a yellow legal pad) Howard sketched out for me two perfectly equivalent expressions for the thermodynamic work of critical nucleus formation, both due to Gibbs. One mentions only the surface energy, the other only the bulk - so how could they possibly give the same result? Amazing! I quickly found myself fascinated and absorbed into my new field.

CLASSICAL vs. MOLECULAR-BASED NUCLEATION THEORIES

For simplicity, let's take the vapor-to-liquid phase transition as an example. The capillarity approximation of classical nucleation theory (CNT) assumes a sharp interface, surface tension without curvature dependence, and an interior phase having properties identical to bulk. Eq. 1 gives the thermodynamic relations of (Gibbs, 1878), mentioned above. W^* is the barrier height, r_c the critical droplet radius, γ_∞ is surface tension per unit area over a flat interface, g^* is the number of molecules present in the critical nucleus, and $\Delta\mu$ is the bulk free energy change per molecule driving the phase transition:

$$W^* = 4\pi r_c^2 \gamma_\infty / 3 = g^* \Delta\mu / 2. \quad (1)$$

CNT is the simplest model capable of handling a range of nucleation phenomena from bubble nucleation in superheated liquids (Blander and Katz, 1975) to crystallization of ice. Still its limited: In addition to not addressing curvature-dependent surface tension, it cannot explain the vanishing barrier at a spinodal [Oxtoby, 1998]. With these limitations in mind, we turn to an examination of molecular-based theories.

Figure 1 shows calculations based on the density functional method (Oxtoby and Evans, 1988). These were carried out by Ari Laaksonen as a test of Eq. 1 vs. a new molecular-based scaling theory (McGraw and Laaksonen, 1996; Laaksonen and McGraw, 1996). The left panel shows the Kelvin relation doing well for g^*, even when approaching the molecular cluster scale. On the other hand the right hand panel shows $W^*/(g^*\Delta\mu)$ falling well below 1/2 – clearly in violation of Eq. 1. Both panels show the molecular-based theory doing well. Key to the molecular-based theory turns out to be the dividing surface concept of Gibbs – so he's protected either way!

Nucleation near a spinodal: Not long after our papers appeared, Vicente Talanquer demonstrated that the new theory accommodated a vanishing nucleation barrier at the spinodal – to us an encouraging surprise (Talanquer, 1997).

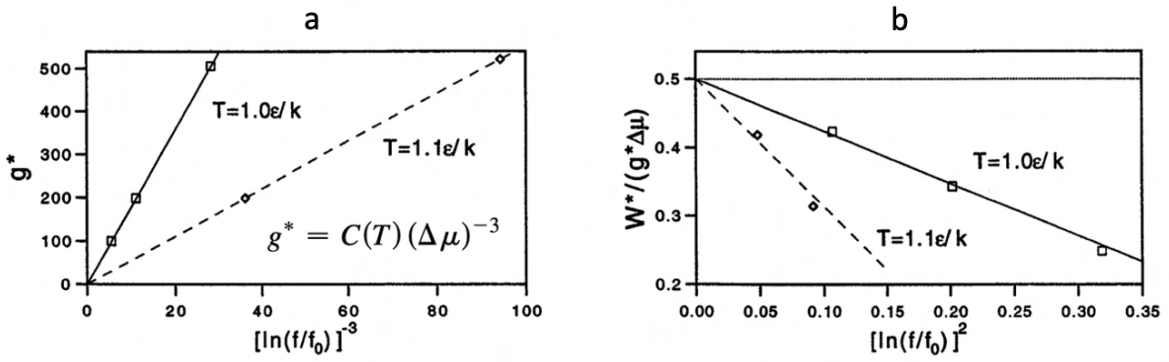


Figure 1. (a) Density functional calculations for g* (markers) and comparison with the Kelvin relation for g^* (inset equation and lines). (b) Density functional results for $W^*/g^* \Delta\mu$ (markers) and comparison with the prediction from CNT (horizontal line at 0.5). The slanted lines in both panels are from the new scaling theory. Temperatures are shown in reduced units kT/ε where ε is the characteristic energy for the Lennard-Jones system and k is Boltzmann's constant, f and f_0 are actual and saturated vapor pressures.

ROLE OF TEMPERATURE FLUCTUATIONS IN NUCLEATION THEORY

Beginning with a publication of Ian Ford (Ford and Clement, 1989), suggesting a many orders of magnitude discrepancy between calculated and measured nucleation rates - the calculated rate being much reduced from measurement - several independent groups got involved to have a look. At a nucleation symposium held at Lehigh University in June of 1990 there were at least two talks on the subject, that I remember, followed by active discussion moderated by Barbara Hale. By 1993 the problem was resolved by the original authors themselves (Barrett, et al., 1993). Citing Blatt and Weisskopf's *Theoretical Nuclear Physics* (1952), they observed a key analogy between the evaporation of a single molecule from a small molecular cluster and the evaporation of a single nucleon from an atomic nucleus. In both cases the particle comes off taking a sizable fraction of the total energy of the cluster/nucleus with it. As a result, the temperature at which the molecule (or nucleon) evaporates is significantly lower than the temperature of the bath, thereby slowing evaporation and increasing nucleation rate, in line with measurement.

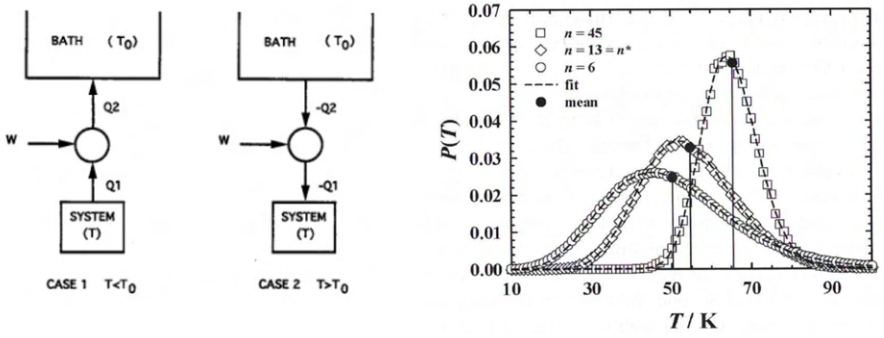


Figure 2. Left: Carnot engine coupling of a small system to a heat bath (McGraw and LaViolette, 1995)
Figure 3. Right: Cluster temperature distributions for subcritical, critical, and post-critical sized clusters (Wedekind et al., 2007)

Figures 2 and 3 show two independent approaches to the distribution of temperature distributions in molecular clusters. Figure 2 shows how these can be computed analytically by considering a small system, the cluster, at temperature T coupled to a large heat bath at T_0 through a Carnot

engine (McGraw and LaViolette, 1995). In either case, heating (case 1) or cooling (case 2), we have:

$$dW = -C_v\,(T_0 - T)/T\;\; dT. \tag{2}$$

Integrating from T_0 to T gives $W(T) = C_v(T_0 - T) + C_v T_0 \ln(T_0/T)$ and the temperature distribution:

$$P(T) = K_1 \exp[-W(T)/kT_0], \tag{3}$$

where K_1 is the normalization constant and C_v is heat capacity. Figure 3 compares temperature distributions from Eq. 3 for sub-critical, critical, and post-critical sized clusters against molecular dynamics simulations. For large clusters C_v is large, fluctuations small, and the distribution can be approximated by a Gaussian. For the larger (non-Gaussian) fluctuations of small clusters, Eq. 3 and the integrated form of Eq. 2 should be used.

APPLICATION OF NUCLEATION KINETICS TO DRIZZLE INITIATION IN CLOUDS

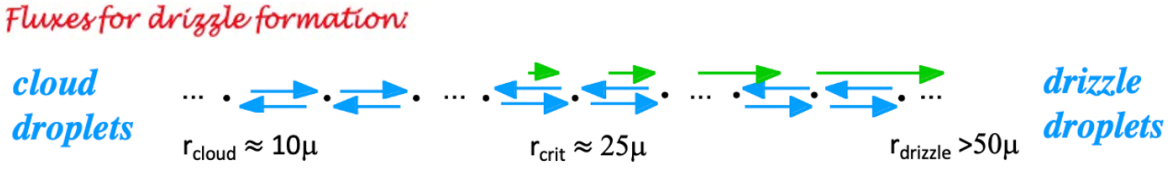


Figure 4. From cloud droplets to drizzle: Prior to collection, droplet growth occurs through the effect of fluctuations in saturation ratio (Kulmala et. al., 1997; Lenschow et al., 1976, 1994). For definition of the kinetic potential see (Wu, 1997).

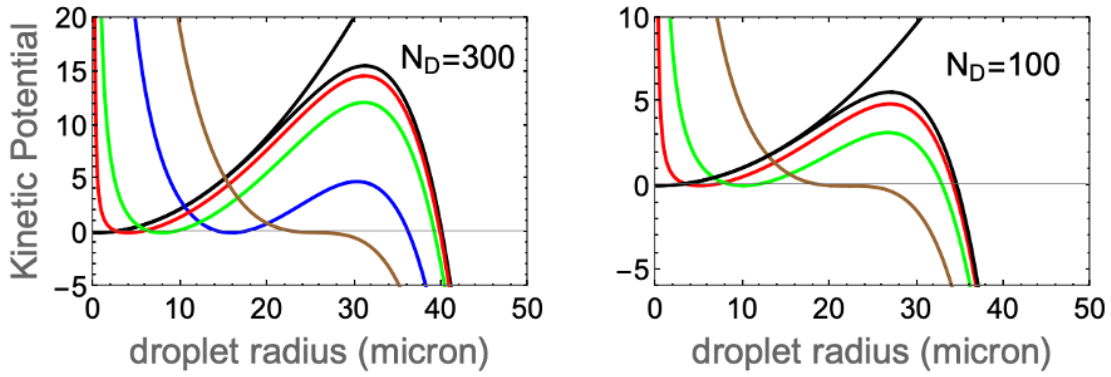


Figure 5. Impact of salt (NaCl) particles of varying size on shaping the kinetic potential. Cloud liquid water fraction is fixed at $L = 0.5 \times 10^{-6}$ (cm^3/m^3). Left panel, $N_d = 300 cm^{-3}$: Upper black curve, reference potential in absence of drizzle based on the saturation fluctuation model of Kulmala et al., this parabolic potential gives rise to a stable cloud droplet distribution of Weibull form that is in excellent agreement with measurements (McGraw and Liu, 2006); lower black curve, limiting result for drizzle formation in presence of ordinary cloud condensation nuclei (CCN); remaining curves from giant CCN (GCCN): red, $r_{dry} = 0.5\mu m$ (threshold size for GCCN); green, $r_{dry} = 1.0\mu m$; blue, $r_{dry} = 2.0\mu m$; brown, $r_{dry} = 2.83\mu m$. Right panel, $N_d = 100 cm^{-3}$: Upper black curve: reference potential; lower black curve, limiting result for drizzle formation in presence of ordinary CCN; remaining curves from GCCN: red, $r_{dry} = 0.5\mu m$; green, $r_{dry} = 1.0\mu m$; brown, $r_{dry} = 1.90\mu m$ (McGraw, Liu and Ghate submitted for publication 2025).

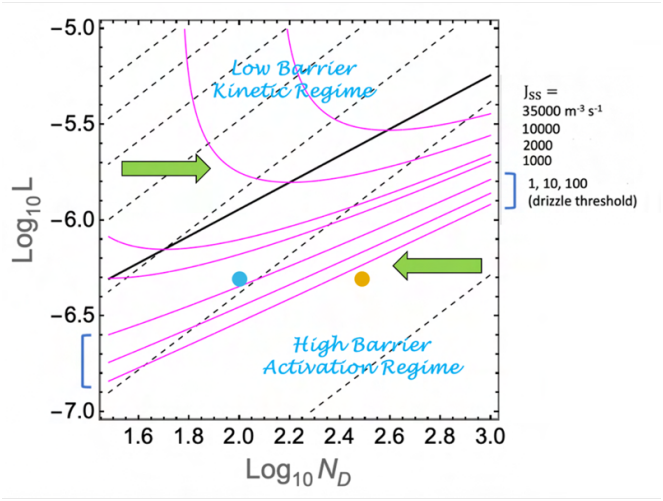


Figure 6. Regime diagram for drizzle rate in absence of GCCN: Figure shows contours of steady-state drizzle rate as functions of cloud liquid water fraction L and droplet number concentration N_D (magenta). Green arrows show direction of increasing drizzle rate with change in cloud droplet number concentration. The solid line marks the locus of conditions where d Log Jss /d Log N_D = 0 at constant L, separating the two regimes. Along this transition line, the dimensionless barrier height has the value 2 and the line itself has slope of 7/10 as do other contours of constant dimensionless barrier height. Dashed lines are contours of constant radius for droplets having mean droplet volume (L/N_D). These range from 5 μm radius (lower right) to to 35 μm radius (upper left) in steps of 5 μm. The two markers, blue and brown, mark the continental and marine/coastal conditions shown in the left and right panels of Fig. 5, respectively (McGraw, Liu and Ghate submitted for publication 2025).

COMING FULL CIRCLE BACK TO EQ. 1 AND GIBBS

The speaker had the good fortune being able to spend a three-month sabbatical in Vienna working with Professors Paul Winkler and Paul Wagner. Here he had the opportunity to (finally) learn heterogeneous nucleation, not only learning it but giving a course on it! Results from our first two papers were discussed at the ICNAA Conference in Helsinki in 2017 and need not be repeated here. Instead I will focus on our third paper (McGraw, Winkler and Wagner, 2018), this one resulted directly from discussions generated throughout the course lectures, to which Profs. Winkler and Wagner contributed diligently.

A unifying identity is derived relating the reversible work of cluster formation (W), its molecular number content (n), and its surface work (Φ) components, each ratioed to the corresponding values for a spherical capillarity drop of critical size in classical nucleation theory. The result is a relationship that generalizes Eq. 1 and connects these ratios. Specifically:

$$f_W = -2f_N + 3f_S \tag{4}$$

where $f_W = W/W^*_{CNT}$ (reversible total work ratio), $f_N = n/n^*_{CNT}$ (volume work/number ratio) and $f_S = \Phi/\Phi^*_{CNT}$ (surface work ratio). Note that the three identical terms of Eq. 1 have been moved, together with their coefficients, to the corresponding denominators of Eq. 4 while the three numerators $W, n,$ and Φ satisfy a much more general result which applies to any cluster size, not just the critical size, and to non-classical theories:

$$W(n) = -n\,\Delta\mu + \Phi. \tag{5}$$

Shown as a generalization of Eq. 1 the new result is demonstrated here for Fletchers's model of heterogeneous nucleation, resulting in a unified treatment of condensation on flat and curve surfaces and smooth passage to the homogeneous limit (Figure 7). Additional applications are made in the cited reference to non-critical as well as critical clusters and to the molecular-based extension of classical theory described in the first section, both omitted here for space.

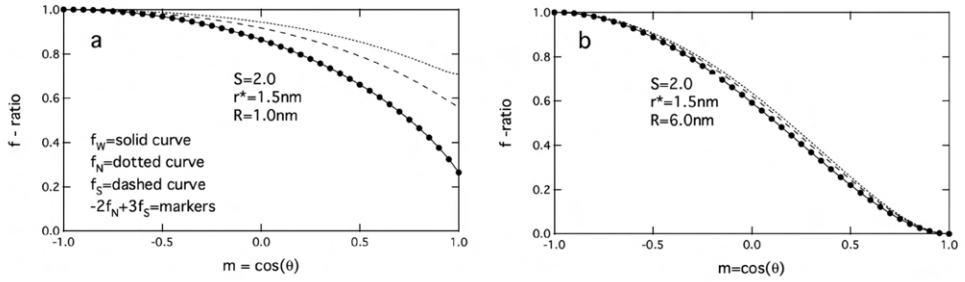


Figure 7. Illustrating *f*-ratios at two different values of the seed particle radius, R, and the same values of saturation ratio and cap radius of curvature r*. (a) R=1.0nm, (b) R=6.0nm with curve labeling indicated in panel (a). These ratios depend only on $x = R/r^*$ and the substance dependent contact angle. Note superposition of the solid curve and markers in agreement with Eq. 4.

ACKNOWLEDGEMENTS

R. McGraw acknowledges the Atmospheric Systems Research (ASR) Program of the U.S. Department of Energy (Grant No: DE-SC0012704) for financial support.

REFERENCES

Barrett, J. C., C. F. Clement and I. J. Ford (1993), Energy fluctuations in homogeneous nucleation theory for aerosols. *J. Phys. Math. Gen. 26*, 529-548.

Blander, M. and J. L. Katz (1975), Bubble nucleation in liquids. *AIChE Journal 21*, 833-848.

Bowles, R. K, R. McGraw, P. Schaaf, B. Senger, J.-C. Voegel and H. Reiss (2000), A molecular based derivation of the nucleation theorem. *J. Chem. Phys. 113*, 4524-4532.

Ford, I. J. and C. F. Clement (1989), The effects of temperature fluctuations in homogeneous nucleation theory. *J. Phys. Math. Gen. 22*, 4007-4018.

Gibbs, J. W. (1878), On the equilibrium of heterogeneous substances. Trans. CT Acad. III.

Katz, J. L., H. Saltsburg and H. Reiss (1966), Nucleation in associated vapors. *J. Coll. Interface Sci. 21*, 560-568.

Kulmala, M., U. Rannik, E. L. Zapadinsky and C. F. Clement (1997), The effect of saturation fluctuations on droplet growth, *J. Aerosol Sci. 28*, 1395-1409.

Laaksonen, A. and R. McGraw (1996), Thermodynamics, gas-liquid nucleation, and size-dependent surface tension, *Europhys. Lett., 35*, 367-372.

Lenschow, D. H., J. Mann and L. Kristensen (1994), How long is long enough when measuring fluxes and other turbulence statistics? *J. Atmos and Oceanic Tech. 11*, 661-673.

Lenschow, D. H. and E. M. Agee (1976), Preliminary results from the Air Mass Transformation Experiment (AMTEX), *Bull. Amer Meteor. Soc., 57*, 1346-1355.

McGraw R. and A. Laaksonen (1996), Scaling properties of the critical nucleus in classical and molecular-based theories of vapor-liquid nucleation, *Phys. Rev. Letts. 76*, 2754.

McGraw, R. and R. LaViolette (1995), Fluctuations, temperature, and detailed balance in classical nucleation theory, J. Chem. Phys. 102, 8983-8994.

McGraw, R. and Y. Liu (2006), Brownian drift-diffusion model for evolution of droplet size distributions in turbulent clouds, *Geophys. Res. Lett. 33*, L03802, doi:10.1029/2005GL023545.

McGraw, R., P. M. Winkler and P.E. Wagner (2018), A unifying identity for the work of cluster formation in heterogeneous and homogeneous nucleation theory. *J. Chem. Phys 146,* 084702.

Oxtoby, D.W. and R. Evans (1988), Nonclassical nucleation theory for the gas-liquid transition, *J. Chem. Phys. 89*, 7251-7230.

Talanquer, V. (1997), A new phenomenological approach to gas-liquid nucleation based on the scaling `properties of the critical nucleus, *J. Chem. Phys. 106*, 9957-9960.

Wedekind, J., D. Reguera and R. Strey (2007), The temperature of nucleating droplets. In *Nucleation and Atmospheric Aerosols, 17th International Conference, Galway, Ireland*, 102-106.

Wu, D. T. (1997), Nucleation Theory, *Solid State Physics 50*, 37-187.

TOWARDS UNDERSTANDING ICE NUCLEATION ON MICROCLINE FELDSPAR BY MEANS OF MACHINE LEARNING AB INITIO SIMULATIONS

P. MONTERO DE HIJES[1] and C. DELLAGO[1]

[1]*Faculty of Physics, University of Vienna, Vienna, Austria.*

Keywords: molecular-dynamics, nucleation, surface, water, ab-initio, machine-learning.

INTRODUCTION

Ice nucleation on mineral surfaces plays a crucial role in cloud formation and climate processes. Among various minerals, microcline feldspar has been identified as an exceptionally efficient ice nucleating material in the atmosphere. However, the molecular mechanisms underlying its ice-nucleating ability remain poorly understood. Previous computational studies using classical force fields have failed to reproduce experimental observations of ice nucleation on microcline surfaces, highlighting the need for more accurate modeling approaches. Here, we present a computational approach combining ab initio simulations with machine learning. We develop a neural network potential trained on revPBE/D3/zd density functional theory calculations to enable molecular dynamics simulations of the water-feldspar interface towards investigating ice nucleation. Our approach allows us to explore the structure and kinetics of water at the mineral surface and by means of metadynamics we investigate the free energetics of ice nucleation. This advanced potential allows us to probe the structural organization and dynamic behavior of water molecules at the mineral surface with quantum mechanical accuracy. Through metadynamics simulations, we explore the free energy landscape governing ice nucleation pathways, identifying key surface features and water configurations that facilitate the initial stages of ice formation.

METHODS

First-principles calculations were performed using density functional theory (DFT) as implemented in the Vienna Ab initio Simulation Package (VASP). The revised Perdew-Burke-Ernzerhof functional with Grimme's D3 dispersion correction (revPBE/D3) and zero damping was employed, which has been shown to accurately describe water. A kinetic energy cutoff of 1000 eV was used for the plane-wave basis set expansion. Various configurations of water molecules on the feldspar surface were sampled, including isolated molecules, small clusters, interfacial layers, and full liquid slabs to ensure diverse training data for the machine learning model. The neural network potential (NNP) was developed using n2p2, which implements a high dimensional neural network architecture specifically designed for representing atomic interactions. The network was trained on approximately 12,000 configurations obtained from the ab initio simulations, encompassing diverse water arrangements on different surface sites of microcline feldspar. The training dataset included energies and forces from the DFT calculations. To ensure robust predictions, we employed an ensemble of four neural networks with different initializations, allowing for committee disagreement analysis to identify regions of configurational space requiring additional sampling. The final NNP achieved a root-mean-square error of less than 0.8 meV/atom for energies and 80 meV/Å for forces compared to the reference DFT calculations. Molecular dynamics simulations were performed using the trained neural network potential implemented through the LAMMPS simulation package. To enhance sampling of rare events such as ice nucleation, we employed metadynamics using the PLUMED software. Collective variables were tested first on bulk water using the mW coarse grained model.

CONCLUSIONS

Our ongoing work represents a significant step toward understanding the molecular mechanisms of ice nucleation on microcline feldspar surfaces. By developing a neural network potential trained on high-accuracy ab initio calculations, we have established a computational framework that overcomes many limitations of classical force fields. Our preliminary investigations of water structure at the feldspar interface suggest promising directions for elucidating the exceptional ice-nucleating properties of this mineral. The neural network potential we've developed demonstrates excellent accuracy in reproducing DFT energies and forces, providing a solid foundation for our molecular dynamics simulations. Initial analysis of water organization near the surface reveals interesting structural motifs that may play a role in facilitating ice formation. Our metadynamics approach has been validated on simpler systems and is now being applied to explore the free energy landscape of water configurations at the feldspar interface. While our research is still in progress, this computational approach offers unprecedented opportunities to investigate heterogeneous ice nucleation with quantum mechanical accuracy at experimentally relevant scales. The ongoing simulations and analyses are expected to yield valuable insights into the specific surface features and water arrangements that contribute to microcline's exceptional ice-nucleating efficiency.

ACKNOWLEDGEMENTS

This research was funded by the Austrian Science Fund (FWF) through the 10.55776/I6467 project.

EVALUATING THE PROPERTIES OF THE CRITICAL NUCLEUS BY SIMULATIONS IN A SMALL SYSTEM

D. REGUERA[1,2], A. LLAMAS[1], and I. LATELLA[1]

[1]*Departament de Física de la Matèria Condensada, Universitat de Barcelona, Martí i Franquès 1, 08028 Barcelona, Spain.*

[2]*Universitat de Barcelona Institute of Complex Systems (UBICS), Martí i Franquès 1, 08028 Barcelona, Spain.*

Keywords: Nucleation theory, Critical cluster, Monte Carlo Simulation.

ABSTRACT

Nucleation is the fundamental mechanism driving first-order phase transitions and is crucial in many scientific and technological contexts. It involves the formation of an unstable critical cluster or nucleus, whose size and energy dictate the onset and rate of phase transformation. A primary challenge in nucleation theory is to accurately determine the work of formation of this critical embryo, as the nucleation rate depends exponentially on this quantity. Even minor inaccuracies in its value can lead to deviations of several orders of magnitude between theoretical predictions and experimental results.

At the theoretical level, Classical Nucleation Theory (CNT) estimates the work of formation using the capillarity approximation, which assumes the surface tension of a planar interface. While CNT provides qualitatively correct predictions for pure fluids, it exhibits systematic deviations from experiments, with errors reaching up to 20 orders of magnitude in cases such as argon condensation. One of the most promising approaches to resolving these discrepancies is by incorporating curvature corrections to the surface tension. When integrated into CNT, these corrections significantly improve the agreement with experimental results for water (Wilhelmsen *et al* 2015) and solve some of the inconsistencies that arise when CNT is extended to multi-component systems (Aasen *et al* 2020). However, the accurate determination of these curvature corrections is challenging, especially for small nucleating clusters (Aasen *et al* 2023).

In this work, we introduce a novel simulation technique to evaluate the free energy of formation and properties of small critical clusters (Llamas et al 2025). Our method is an adaptation of Monte Carlo simulations in a small system with carefully chosen constraints, allowing direct simulation of the critical cluster without the need to sample intermediate states or reconstruct the full free energy landscape. We apply this approach to study critical clusters of various sizes in a truncated and shifted Lennard-Jones fluid at 2.5σ. We compare our results with CNT and previous studies using Umbrella Sampling simulations. Our findings suggest that this new technique is particularly promising for investigating small critical clusters relevant to experimental conditions and complex atmospheric fluids, where traditional methods are computationally demanding.

ACKNOWLEDGEMENTS

This work was supported by the project PID2021-126570NB-I00 financed by MICIU/AEI/10.13039/ 501100011033 and FEDER, UE.

REFERENCES

Aasen, A., Reguera, D. and Wilhelmsen, Ø. (2020). Curvature Corrections Remove the Inconsistencies of Binary Classical Nucleation Theory. *Phys. Rev. Lett.* **124**, 045701.
Aasen, A., Wilhelmsen, Ø., Hammer, M. and Reguera, D. (2023) Free energy of critical droplets—from the binodal to the spinodal. *J. Chem. Phys.* **158**, 114108.
Llamas, A., Latella, I. and Reguera, D. (2025) in preparation.
Wilhelmsen, Ø., Bedeaux, D. & Reguera, D. (2015) Communication: Tolman length and rigidity constants of water and their role in nucleation. *J. Chem. Phys.* **142**, 171103.

GAS-PHASE COLLISION RATE ENHANCEMENT FACTORS FOR ACID-BASE CLUSTERS UP TO 2 NM IN DIAMETER FROM ATOMISTIC SIMULATION AND THE INTERACTING HARD SPHERE MODEL

B. REISCHL[1], V. TIKKANEN[1], H. YANG[2] and H. VEHKAMÄKI[1]

[1]*Institute for Atmospheric and Earth System Research/Physics, Faculty of Science, University of Helsinki, Helsinki, Finland.*

[2]*Max-Planck Institute for Chemistry, Mainz, Germany.*

Keywords: atmospheric new particle formation, collision rate coefficients, molecular dynamics simulations, interacting hard sphere model.

INTRODUCTION

Collisions of neutral molecules and clusters is the most prevalent pathway in atmospheric new particle formation (NPF), with direct implications on air quality and climate (Gordon *et al.*, 2017). A large portion of newly formed aerosols (i.e. secondary aerosols) are born starting from collisions between acid (such as sulfuric acid) and base (e.g. amines) molecules. Such acid-base cluster collisions are important in supplying condensation cores for other atmospheric vapors (such as organic compounds) to grow on. Until recently, these collisions have been modeled mainly using non-interacting hard sphere (NHS) models, which systematically underestimate collision and particle formation rates due to omission of long-range interactions (Stolzenburg *et al*., 2020). Recently, atomistic simulations which account for long-range interactions have been used to study neutral molecule-molecule (Yang *et al.*, 2018; Halonen *et al*., 2019) and molecule-cluster collisions (Yang *et al.*, 2023), but studies on cluster-cluster collisions have still been lacking despite the relevant role they can play, e.g., in haze formation in polluted urban areas (Guo *et al*., 2014).

METHODS

We have studied collisions between same-sized neutral clusters of N bisulphate and N dimethylammonium ions at $T = 300$ K up to $N = 32$, visualized in Fig.1, using atomistic molecular dynamics (MD) simulations with the LAMMPS MD code (Thompson *et al.*, 2022) and interaction parameters from Loukonen *et al.* (2010). The clusters were first equilibrated and equipartition of energy over the internal degrees of freedom insured. Then, two clusters were positioned at a large distance along the x axis and an impact parameter b along the z axis and given relative velocities $\pm v/2$ along the x axis to send them on a potential collision course. The collision rate coefficient was calculated by sampling the collision probability $P(v,b)$ over the relevant range of relative velocities v, and impact parameters b (Yang *et al.*, 2018; Halonen *et al.*, 2019). Simulation results have then been compared against both the traditional NHS model and the newly proposed interacting hard sphere (IHS) variant. The IHS model recently introduced by Yang *et al.* (2023), is built upon a central field model, but the collision criterion based on point particles collapsing into each other is relaxed to a physically more intuitive condition: in the IHS model, a collision is thought to have happened if the center of mass distance between the colliding particles is at any point below the sum of the hard sphere radii. In contrast to the NHS model, a collision may occur even if the colliding partners have an impact parameter larger than the sum of their hard sphere radii. The effective cluster-cluster interaction potential for the IHS model was obtained from the "monomer-monomer" interaction through a Hamaker approach (Hamaker, 1937). The monomer-monomer potential was obtained from a fit to the potential of mean force between two bisulphate-dimethylammonium heterodimers ($N = 1$), obtained from an umbrella sampling simulation (Torrie and Valleau, 1977) using LAMMPS with the PLUMED plug-in, and the same atomistic models and interactions as for the collision trajectory simulations.

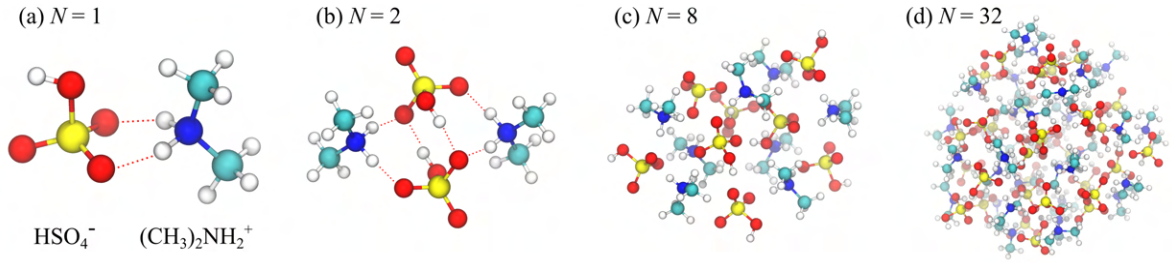


Figure 1. Atomistic models of neutral bisulphate-dimethylammonium clusters $[HSO_4^- \cdot (CH_3)_2NH_2^+]_N$ for $N = 1$, 2, 8 and 32. For $N = 1$ and 2, hydrogen bonds are indicated by dashed red lines.

CONCLUSIONS

We find the collision rates given by the NHS to be enhanced by a factor of $W_{MD} = 2.18\text{-}5.61$ in the atomistic MD simulations, with enhancement decreasing with cluster size, and an asymptotic limit ≈2 (see Fig. 2a). In contrast, the IHS model yields a constant enhancement factor of W_{IHS}=3.36 over the NHS model for collisions between same-sized clusters, which decreases with increasing cluster size ratio (see Fig. 2b). Our results demonstrate how even collisions between clusters of tens of acid-base pairs at a relatively high temperature cannot be accurately modeled by neglecting long-range interactions. We also show that the MD results cannot be reproduced by simple point-particle models, highlighting the importance of atomistic details of intermolecular interactions. The substantial collision rate enhancement factor due to long-range interactions found for clusters containing a single acid-base pair is certainly relevant for atmospheric new particle formation. However, for collisions between larger, same-sized clusters, the enhancement factors quickly drop below 3, which is comparable in magnitude to the collision rate enhancement of "monomers", such as two sulfuric acid molecules, obtained from similar atomistic MD simulations (Halonen *et al.*, 2019). To quantitatively assess the effect of enhancement factors for collisions of molecules and/or clusters on the actual particle formation rates in polluted environments, the complete cluster size distribution dynamics would need to be simulated for the different growth pathways, using either the standard rate coefficients from kinetic gas theory, or those obtained from atomistic simulations, for all relevant collisions.

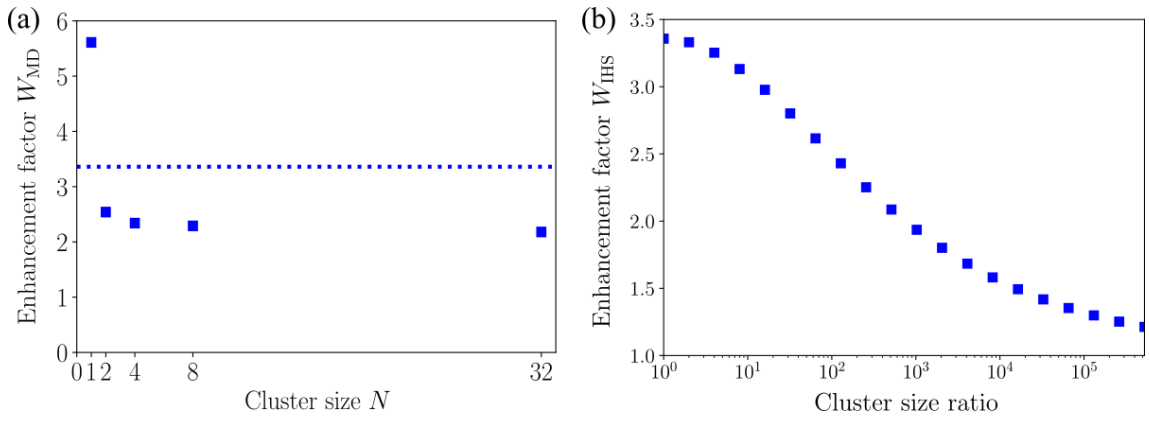


Figure 2. (a) Collision rate enhancement factor W for cluster-cluster collisions as a function of cluster size N from atomistic collision (MD, shown as squares) and the interacting hard sphere model (IHS, shown as the dashed line). (b) IHS enhancement factor as a function of the size ratio of colliding clusters.

ACKNOWLEDGEMENTS

This research has been supported by the European Research Council (project no. 692891 DAMOCLES), the Academy of Finland flagship programme (grant no. 337549) and Centres of Excellence programme (CoE VILMA). Computational resources were provided by the CSC –IT Center for Science Ltd., Finland. The authors wish to thank the Finnish Computing Competence Infrastructure (FCCI) for supporting this project with computational and data storage resources.

REFERENCES

Gordon, H., J. Kirkby, U. Baltensperger, F. Bianchi, M. Breitenlechner, J. Curtius, A. Dias, J. Dommen, N. M. Donahue, E. M. Dunne, *et al.* (2017). Causes and importance of new particle formation in the present-day and preindustrial atmospheres, *J. Geophys. Res.: Atmospheres* **122**, 8739.

Guo, S., M. Hu, M. L. Zamora, J. Peng, D. Shang, J. Zheng, Z. Du, Z.Wu, M. Shao, L. Zeng, *et al.* (2014). Elucidating severe urban haze formation in China, *Proc. Natl. Acad. Sci. USA* **111**, 17373.

Halonen, R., E. Zapadinsky, T. Kurtén, H. Vehkamäki, and B. Reischl (2019). Rate enhancement in collisions of sulfuric acid molecules due to long-range intermolecular forces, *Atmos. Chem. Phys.* **19**, 13355.

Hamaker, H. (1937). The London—van der Waals attraction between spherical particles, *Physica* **4**, 1058.

Loukonen, V., T. Kurtén, I. K. Ortega, H. Vehkamäki, A. A. H. Pádua, K. Sellegri, and M. Kulmala (2010). Enhancing effect of dimethylamine in sulfuric acid nucleation in the presence of water - a computational study, *Atmos. Chem. Phys.* **10**, 4961.

Stolzenburg, D., M. Simon, A. Ranjithkumar, A. Kürten, K. Lehtipalo, H. Gordon, S. Ehrhart, H. Finkenzeller, L. Pichelstorfer, T. Nieminen, *et. al.* (2020). Enhanced growth rate of atmospheric particles from sulfuric acid, *Atmos. Chem. Phys.* **20**, 7359.

Thompson, A. P., H. M. Aktulga, R. Berger, D. S. Bolintineanu, W. M. Brown, P. S. Crozier, P. J. in 't Veld, A. Kohlmeyer, S. G. Moore, T. D. Nguyen, R. Shan, M. J. Stevens, J. Tranchida, C. Trott, and S. J. Plimpton (2022). LAMMPS - a flexible simulation tool for particle-based materials modeling at the atomic, meso, and continuum scales, *Comput. Phys. Commun.* **271**, 108171.

Torrie, G. M. and J. P. Valleau (1977). Nonphysical sampling distributions in Monte Carlo free-energy estimation: Umbrella sampling, *J. Comput. Phys*. **23**, 187.

Yang, H., E. Goudeli, and C. J. Hogan (2018). Condensation and dissociation rates for gas phase metal clusters from molecular dynamics trajectory calculations, J. Chem. Phys. **148**, 164304.

Yang, H., I. Neefjes, V. Tikkanen, J. Kubečka, T. Kurtén, H. Vehkamäki, and B. Reischl (2023). Collision-sticking rates of acid–base clusters in the gas phase determined from atomistic simulation and a novel analytical interacting hard-sphere model, *Atmos. Chem. Phys.* **23**, 5993.

FINITE ELEMENT-BASED EXTENDED KALMAN FILTER AND SMOOTHER FOR RETRIEVAL OF AEROSOL SIZE DISTRIBUTIONS AND PROCESS RATES

T. SALMINEN[1], M. NISKANEN[1], P. MÖNKKÖNEN[2], A. SEPPÄNEN[1], K.E.J. LEHTINEN[1]

[1] *Department of Technical Physics, University of Eastern Finland, Kuopio, Finland.*

[2] *Computing Sciences, Tampere University, Tampere, Finland.*

Keywords: AEROSOL PROCESS RATE ESTIMATION, BAYESIAN STATE-SPACE ESTIMATION, GENERAL DYNAMIC EQUATION, FINITE ELEMENT METHOD.

INTRODUCTION

Aerosol particles have a major effect on the climate as they reflect and absorb incoming solar radiation and act as cloud condensing nuclei, thus both directly and indirectly affecting the albedo of the Earth. However, the magnitude of these effects is highly uncertain partly due to uncertainties in the modelling of aerosol dynamics in global climate models as both aerosol process rate approximations and the applied aerosol dynamics models are typically rather crude. Currently, accurate modelling of aerosol dynamics in global climate models is infeasible due to the high computational cost (Schultze and Rockel, 2018).

Temporal evolution of an aerosol size distribution can be described with the General Dynamic Equation of aerosols (GDE), which accounts for particle growth, nucleation and other particle sources, removal processes and coagulation (Seinfeld & Pandis, 2016). Generally, aerosol process rates (condensation rate, formation rate, and deposition rate) are somewhat unknown as physical mechanisms behind these phenomena are not yet fully understood (Seinfeld & Pandis, 2016). However, these phenomena drive the temporal evolution of the aerosol size distribution, and hence, to estimate the size distribution evolution accurately, the magnitude of these effects should be known in different atmospheric conditions.

In our research, we apply Bayesian state-space estimation methods, the Extended Kalman Filter (EKF) and Extended Kalman Smoother (EKS), to estimate the temporal evolution of the aerosol size distribution and the aerosol process rates, which drive the evolution of the size distribution. We use the finite element method (FEM) to numerically solve the GDE. The main advantages of EKF and EKS compared to the traditional methods are that it is possible to account for the uncertainties related to the measurement devices and the processes into the estimation. The obtained estimates for the size distribution and the process rates are posteriori probability distributions with known expected values and variances.

METHODS

In this study, we use the EKF to estimate the state of the system, i.e., the expected values of the size distribution and process rates. Along with the state, the EKF can also estimate the uncertainty (posterior covariance) of the state, providing credibility intervals for the estimate. At each time step, the EKF predicts the next state based on a linearized model of the system dynamics (the evolution step) and updates this prediction with new measurements (the update step) (Gelb et. al 1974). In the evolution step, we use a FEM approximation of the GDE together with the Crank-Nicolson time-stepping scheme to predict the state of the system at the next timestep (Salminen et. al 2022). We model the process rates as multivariate random processes. Each process rate is expected to have smoothness both with respect to particle size and time; this is accounted for by modeling the evolutions of the process rates by 2nd order vector autoregressive (VAR(2)) models. In this work, the measurements consist of time-series of counts given by differential mobility particle sizer (DMPS) or a scanning mobility particle sizer (SMPS).

The EKS, more specifically extended Fixed-Interval Kalman smoother (FIKS), refines the past state estimates by combining the EKF estimates with a backward pass that incorporates information of future observations to reduce uncertainty.

In this work, the inference of process rate using EKF and FIKS was tested both with synthetic and experimental data. The simulated DMPS data are generated by transforming a known aerosol distribution evolution to the output of DMPS with a system matrix which maps particle number concentrations to counts measured by a condensation particle counter. The obtained counts are corrupted by Poisson distributed noise to mimic a real-world measurement. To apply the methodology for the real data, it is important to know, for the validation of the EKF and FIKS estimates, the exact methodology how the device calculates the size distribution ($dN / d \log(D_p)$) from the raw counts measured by the condensing particle counter (CPC). Sometimes, these are not readily given by the device manufacturers.

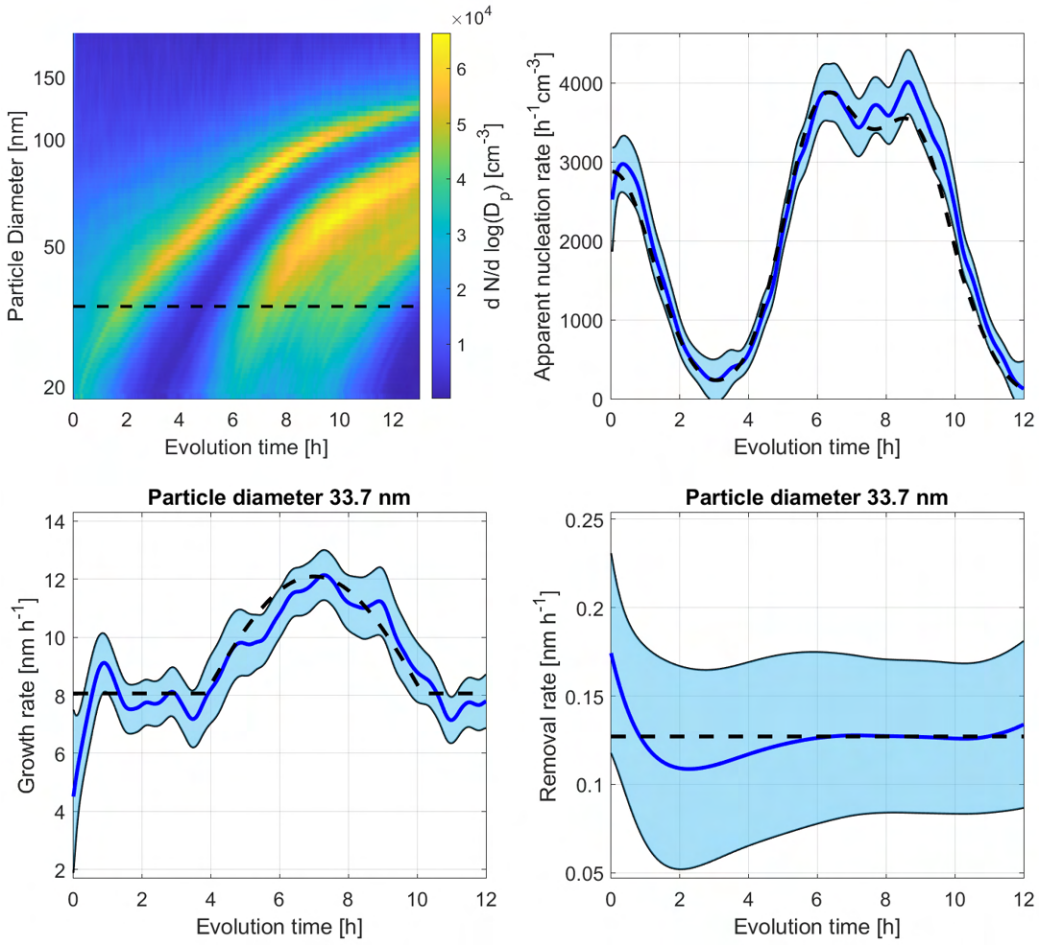


Figure 1. Top left: The Extended Kalman Smoother estimate for the time evolution of aerosol size distribution. The black dashed line corresponds to a diameter of 33.1 nm for which the process rates are presented at the bottom figure tiles. Top right: The apparent nucleation rate at the smallest size class. The black dashed line is true value, the blue line is the EKS estimate, and the light blue areas are the 95 % credibility intervals for the estimate. The bottom figures are the growth rate (left) and removal rate (right) for the particle with a diameter of 33.7 nm. The black dashed line is the true value, the blue line is the EKS estimate, and the light blue areas are the 95 % credibility intervals for the estimate.

RESULTS

As an example case, demonstrating the strengths of our method, we analyze a simulated measurement for which we know the true process rates behind the evolution. Figure 1 shows the EKS estimates for the evolution of the size distribution, the apparent nucleation rate, the growth rate and the removal rate. The process rates are estimated for each time and particle size, but demonstration purposes in the figure the growth and removal rates are only shown for particles of diameter 33.7 nm, together with 95 % credibility intervals. The true values of the process rates are inside the 95 % credibility intervals for the duration of the simulation.

CONCLUSIONS

The capability of EKF and EKS to estimate the aerosol size distribution evolution and process rates from both simulated and measured DMPS data has been demonstrated. In contrast to the traditional methods based on linear regression, the obtained estimates are both time and size dependent. Furthermore, a major strength of these methods is that, in addition to estimates of the mean values, credibility intervals for the variables of interest are obtained.

ACKNOWLEDGEMENTS

This research was funded by the Research Council of Finland (Centre of Excellence of Inverse Modelling and Imaging, 2018–2025, Centre of Excellence of Virtual Laboratory for Molecular Level Atmospheric Transformations), and the Flagship Programmes ACCC and FAME, and a personal grant from Maj and Tor Nessling Foundation, Finland.

REFERENCES

Schultze, M., Rockel, B. Direct and semi-direct effects of aerosol climatologies on long-term climate simulations over Europe. *Clim Dyn* **50**, 3331–3354 (2018).

Seinfeld, J. H., Pandis, S.N. Atmospheric chemistry and physics, from air pollution to climate change, New York, John Wiley & Sons, 2016

Gelb A, et al. Applied optimal estimation. MIT press, 1974.

Salminen, T., Lehtinen, K.E.J., Kaipio, J.P., Russell, V., Seppänen, A., (2022), *J. Aerosol Sci.*, 160.

New particle formation from isoprene in the free troposphere

J. Shen[1], D.M. Russell[2], J. DeVivo[3], F. Kunkler[4], R. Baalbaki[1], B. Mentler[5], CLOUD collaboration, H. Harder[4], A. Hansel[5], N.M. Donahue[3], D.R. Worsnop[1], M. Kulmala[1], J. Kirkby[6], J. Curtius[2], X.C. He[1]

[1]*Institute for Atmospheric and Earth System Research, University of Helsinki, 00014, Finland*
[2]*Institute for Atmospheric and Environmental Sciences, Goethe University Frankfurt, 60438, Germany*
[3]*Department of Chemical Engineering, Carnegie Mellon University; Pittsburgh, 15213 PA, USA*
[4]*Atmospheric Chemistry Department, Max Planck Institute for Chemistry, 55128 Mainz, Germany*
[5]*Institute of Ion Physics and Applied Physics, University of Innsbruck, 6020 Innsbruck, Austria*
[6]*CERN, European Organisation for Nuclear Research, 1211, Geneva, Switzerland*

Keywords: Isoprene, nucleation, free troposphere, acids

INTRODUCTION

Isoprene is the most abundant non-methane biogenic volatile organic compound in the atmosphere, primarily emitted by plants, especially deciduous and broad-leaved evergreen trees. The loss of isoprene from the atmosphere is mainly due to oxidation by hydroxyl radicals (OH) and, at slower rates, by O_3 and NO_3 radicals (Wennberg et al., 2018). Under low nitrogen oxide (NO_x) conditions, the first-generation isoprene peroxy radicals react with hydroperoxyl radicals (HO_2) to produce organic hydroperoxides (ISOPOOH). ISOPOOH can further react with OH to form isoprene epoxydiols (IEPOX) and other oxidation products. These oxidation products can partition into into pre-existing particles by condensation and reactive uptake, thereby contributing to secondary organic aerosol mass (Paulot et al., 2009). Since isoprene contains two carbon-carbon double bonds, the final products involve two successive OH oxidations. In the presence of NO_x, these second-generation products comprise non-nitrates, nitrates and dinitrates, containing zero, one or two nitrogen atoms, respectively.

High concentrations of freshly nucleated particles are observed in the upper free troposphere over the Amazon (Andreae et al., 2018) and the tropical Atlantic and Pacific Oceans (Williamson et al., 2019). Monoterpenes have been proposed to explain these new particles, but aircraft measurements find insufficient monoterpenes to explain the rapid particle nucleation and growth rates (Curtius et al., 2024). On the other hand, recent satellite observations have shown elevated night-time concentrations of isoprene of up to around 1 ppbv in the upper troposphere over tropical South America, central Africa, and Southeast Asia (Palmer et al., 2022). The isoprene is lofted in deep convective clouds and mixed with NO_x from lighting. During the daytime, isoprene concentrations decrease due to high OH concentrations, resulting in an isoprene lifetime of about one hour.

These observations suggest that isoprene, accumulated overnight in the upper troposphere, is rapidly oxidised by OH radicals at sunrise to generate high concentrations of isoprene oxidation products, which may contribute to new particle formation. However, this raises the important question of what could be the underlying mechanism since the ability of isoprene to from new particles has so far been considered to be negligible and, indeed, isoprene is known to suppress new particle formation from monoterpenes.

METHODS

In this study (Shen et al., 2024), we used the CERN CLOUD chamber to investigate new particle formation from the oxidation of isoprene under free tropospheric conditions at temperatures of −10 °C and −50 °C. Isoprene vapour was purified using a cryo-trap before injection to remove low-volatility contaminants, such as monoterpenes. The chamber was maintained at atmospheric pressure and the chemical conditions were precisely controlled. A combination of ammonium, nitrate, and bromide chemical ionisation mass spectrometry was employed to detect the full range of isoprene oxidation products, together with other relevant trace gas measurements and, importantly, OH and HO_2 radicals were measured by fluorescence

spectroscopy. The experimental conditions, including NO_x, OH, HO_2 and the presence of sulfuric acid and iodine oxoacids, were varied to explore their influence on particle formation and growth.

CONCLUSIONS

Our study demonstrates for the first time that isoprene oxidation products drive rapid particle nucleation and early growth in the upper troposphere (Shen et al., 2024), revising the prevailing view that isoprene merely suppresses particle nucleation (Kiendler-Scharr et al., 2009). Our measurements show that isoprene oxidation products can nucleate without requiring additional vapours and that the presence of extremely low concentrations of sulfuric acid or iodine oxoacids strongly enhances nucleation rates. Our study further finds that these newly-formed particles grow rapidly by further condensation of isoprene oxidation products and acids. Upon descent of air masses, these particles represent a major source of cloud condensation nuclei for shallow marine clouds at low latitudes, which are critical for Earth's radiative balance (Figure 1).

In this presentation, I will also show results exploring environmental conditions in the lower free troposphere, suggesting that new particle formation from isoprene may have an even greater impact than previously thought. Additionally, I will discuss quantum chemical calculations that support our proposed mechanism and provide new molecular-level insights.

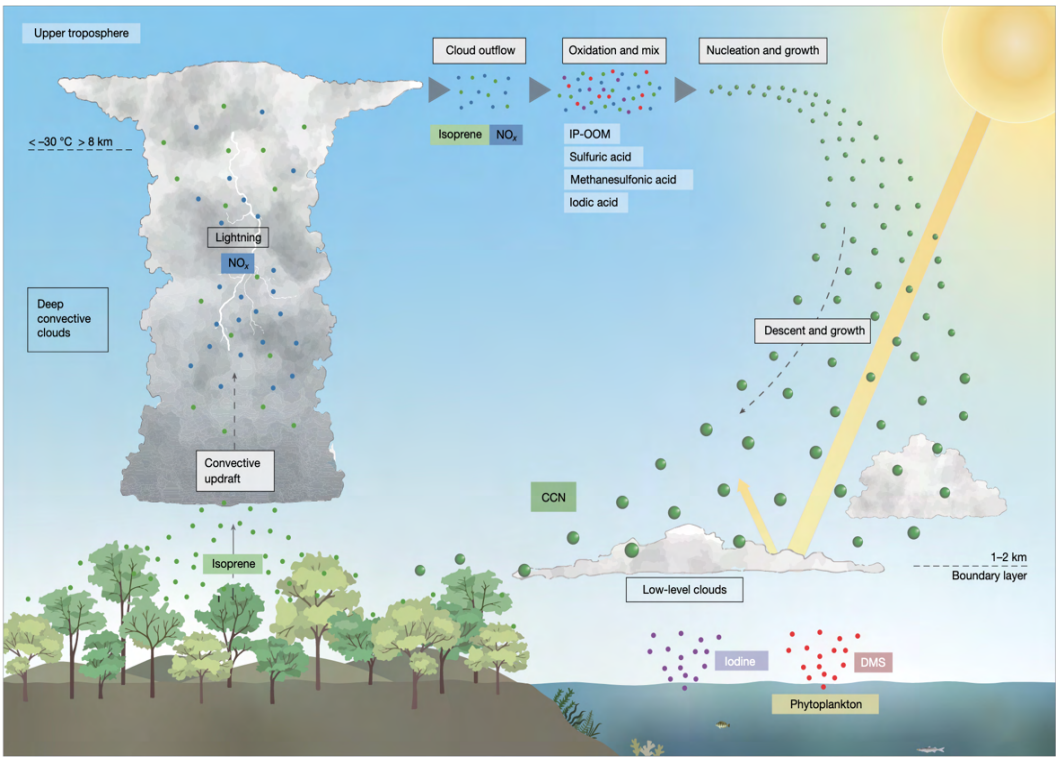


Figure 1. Schematic of new particle formation from isoprene in the upper troposphere.

ACKNOWLEDGEMENTS

This work was supported by MSCA Doctoral Networks (Project 101073026 - CLOUD-DOC - HORIZON-MSCA-2021-DN-01) and Research Council of Finland grant no. 359331.

REFERENCES

Andreae, M. O., Afchine, A., Albrecht, R., Holanda, B. A., Artaxo, P., Barbosa, H. M. J., Borrmann, S., Cecchini, M. A., Costa, A., Dollner, M., Fütterer, D., Järvinen, E., Jurkat, T., Klimach, T., Konemann, T.,

Knote, C., Krämer, M., Krisna, T., Machado, L. A. T., Mertes, S., Minikin, A., Pöhlker, C., Pöhlker, M. L., Pöschl, U., Rosenfeld, D., Sauer, D., Schlager, H., Schnaiter, M., Schneider, J., Schulz, C., Spanu, A., Sperling, V. B., Voigt, C., Walser, A., Wang, J., Weinzierl, B., Wendisch, M., and Ziereis, H.: Aerosol characteristics and particle production in the upper troposphere over the Amazon Basin, Atmos. Chem. Phys., 18, 921–961, 2018.

Curtius, J., Heinritzi, M., Beck, L. J., Pöhlker, M. L., Tripathi, N., Krumm, B. E., Holzbeck, P., Nussbaumer, C. M., Hernández Pardo, L., Klimach, T., Barmpounis, K., Andersen, S. T., Bardakov, R., Bohn, B., Cecchini, M. A., Chaboureau, J.-P., Dauhut, T., Dienhart, D., Dörich, R., Edtbauer, A., Giez, A., Hartmann, A., Holanda, B. A., Joppe, P., Kaiser, K., Keber, T., Klebach, H., Krüger, O. O., Kürten, A., Mallaun, C., Marno, D., Martinez, M., Monteiro, C., Nelson, C., Ort, L., Raj, S. S., Richter, S., Ringsdorf, A., Rocha, F., Simon, M., Sreekumar, S., Tsokankunku, A., Unfer, G. R., Valenti, I. D., Wang, N., Zahn, A., Zauner-Wieczorek, M., Albrecht, R. I., Andreae, M. O., Artaxo, P., Crowley, J. N., Fischer, H., Harder, H., Herdies, D. L., Machado, L. A. T., Pöhlker, C., Pöschl, U., Possner, A., Pozzer, A., Schneider, J., Williams, J., and Lelieveld, J.: Isoprene nitrates drive new particle formation in Amazon's upper troposphere, Nature, 636, 124–130, 2024.

Kiendler-Scharr, A., Wildt, J., Maso, M. D., Hohaus, T., Kleist, E., Mentel, T. F., Tillmann, R., Uerlings, R., Schurr, U., and Wahner, A.: New particle formation in forests inhibited by isoprene emissions, Nature, 461, 381–384, 2009.

Palmer, P. I., Marvin, M. R., Siddans, R., Kerridge, B. J., and Moore, D. P.: Nocturnal survival of isoprene linked to formation of upper tropospheric organic aerosol, Science, 375, 562–566, 2022.

Paulot, F., Crounse, J. D., Kjaergaard, H. G., Kürten, A., St. Clair, J. M., Seinfeld, J. H., and Wennberg, P. O.: Unexpected Epoxide Formation in the Gas-Phase Photooxidation of Isoprene, Science, 325, 730–733, 2009.

Shen, J., Russell, D. M., DeVivo, J., Kunkler, F., Baalbaki, R., Mentler, B., Scholz, W., Yu, W., Caudillo-Plath, L., Sommer, E., Ahongshangbam, E., Alfaouri, D., Almeida, J., Amorim, A., Beck, L. J., Beckmann, H., Berntheusel, M., Bhattacharyya, N., Canagaratna, M. R., Chassaing, A., Cruz-Simbron, R., Dada, L., Duplissy, J., Gordon, H., Granzin, M., Große Schute, L., Heinritzi, M., Iyer, S., Klebach, H., Krüger, T., Kürten, A., Lampimäki, M., Liu, L., Lopez, B., Martinez, M., Morawiec, A., Onnela, A., Peltola, M., Rato, P., Reza, M., Richter, S., Rörup, B., Sebastian, M. K., Simon, M., Surdu, M., Tamme, K., Thakur, R. C., Tomé, A., Tong, Y., Top, J., Umo, N. S., Unfer, G., Vettikkat, L., Weissbacher, J., Xenofontos, C., Yang, B., Zauner-Wieczorek, M., Zhang, J., Zheng, Z., Baltensperger, U., Christoudias, T., Flagan, R. C., El Haddad, I., Junninen, H., Möhler, O., Riipinen, I., Rohner, U., Schobesberger, S., Volkamer, R., Winkler, P. M., Hansel, A., Lehtipalo, K., Donahue, N. M., Lelieveld, J., Harder, H., Kulmala, M., Worsnop, D. R., Kirkby, J., Curtius, J., and He, X.-C.: New particle formation from isoprene under upper-tropospheric conditions, Nature, 636, 115–123, 2024.

Wennberg, P. O., Bates, K. H., Crounse, J. D., Dodson, L. G., McVay, R. C., Mertens, L. A., Nguyen, T. B., Praske, E., Schwantes, R. H., Smarte, M. D., St Clair, J. M., Teng, A. P., Zhang, X., and Seinfeld, J. H.: Gas-Phase Reactions of Isoprene and Its Major Oxidation Products, Chem. Rev., 118, 3337–3390, 2018.

Williamson, C. J., Kupc, A., Axisa, D., Bilsback, K. R., Bui, T., Campuzano-Jost, P., Dollner, M., Froyd, K. D., Hodshire, A. L., Jimenez, J. L., Kodros, J. K., Luo, G., Murphy, D. M., Nault, B. A., Ray, E. A., Weinzierl, B., Wilson, J. C., Yu, F., Yu, P., Pierce, J. R., and Brock, C. A.: A large source of cloud condensation nuclei from new particle formation in the tropics, Nature, 574, 399–403, 2019.

WATCHING AT THE MOLECULAR LEVEL HOW GASES NUCLEATE AT LOW TEMPERATURE

R. SIGNORELL[1]

[1]*Department of Chemistry and Applied Biosciences, ETH Zurich, Zurich, Switzerland.*

Keywords: Intermolecular interactions, Chaperon complex, Laval expansion, mass spectrometry.

INTRODUCTION

Low-temperature vapor nucleation is relevant to aerosol and cloud formation in extraterrestrial atmospheres such as those of Mars or Titan, as well as for low-temperature gas separation, including natural gas separation or carbon dioxide capture technologies. To better understand the mechanisms of the underlying processes and to develop models that enable predictions, experimental studies at the molecular level are crucial. One would therefore like to have information about how the smallest molecular clusters are built up, molecule by molecule, over time.

METHODS

For nucleation studies of weakly interacting gases, experimental methods with sufficient time-resolution are required that initiate nucleation under well-controlled conditions and gently detect small, weakly-bound molecular clusters. We have developed a nucleation instrument that meets these requirements [Ferreiro, 2016; Li, 2021; Feusi, 2024]. A nucleation zone with uniform temperature and pressure is created in the postnozzle flow of a Laval expansion. The size, chemical composition and number concentration of the nucleating clusters are determined by mass spectrometry using ultrasoft, near-threshold single-photon ionization.

CONCLUSIONS

The talk will give an overview of the various atmospheric and industrially relevant gas systems that our research group has investigated with this nucleation instrument in recent years. The focus will be on gas mixtures containing carbon dioxide, water and various hydrocarbons that are relevant to cloud formation on Mars and for natural gas separation, and on the question how the volatility of different vapor components affects the nucleation kinetics. An important result of our study is that certain gas components ("mediator") can accelerate the nucleation of other gas components ("nucleating compound"), although the different gases interact only weakly with each other. Kinetic analysis suggests that the formation of transient heteromolecular clusters (chaperone complexes), consisting of a mediator molecule and a molecule of the nucleating compound, is the reason for the acceleration of nucleation. In other words, the mediator acts as a catalyst for nucleation. This new homogeneous nucleation pathway could compete with heterogeneous pathways under certain condition, e.g. in extraterrestrial atmospheres. Further aspects will address the question how the transition from barrier-controlled nucleation to the collision limit can be investigated (Dingilian, 2021) and how early cluster growth proceeds via homogeneous and heterogeneous processes (Li, 2021).

ACKNOWLEDGEMENTS

This work was supported by the Swiss National Science Foundation under grants 200020_2002306 and 200021-236446.

REFERENCES

Ferreiro, J.J., Chakrabarty, S., Schlaeppi, B. and R. Signorell (2016). Observation of propane cluster size distributions during nucleation and growth in a Laval expansion. *J. Chem. Phys*., **145**, 211907.

Li, C., Krohn, J., Lippe, M and R. Signorell (2021). How volatile components catalyze vapor nucleation". *Sci. Adv.*, **7**, eabd9954.

Feusi, S., Graber, F., Khatri, J., Li, C. and R. Signorell (2024). How CO2 gas accelerates water nucleation at low temperature. *J. Chem. Phys*. **161**, 184304.

Dingilian, K., Lippe, m., Kubečka, J., Krohn, J., Li, C., Halonen, R., Keshavarz, F., Reischl, B., Kurtén, T., Vehkamäki, H., Signorell, R. and B. Wyslouzil (2021). New Particle Formation from the Vapor Phase: From Barrier Controlled Nucleation to the Collisional Limit. *J. Phys. Chem. Lett.,* **12**, 4593-4599

CHEMICALLY RESOLVING THE GROWTH OF GAS PHASE CLUSTERS INTO NANOPARTICLES

J.N. SMITH,[1] C.E. MILLER,[1] V. PERRAUD[1] and N. MYLLYS[2]

[1]*Department of Chemistry, University of California, Irvine, CA USA*

[2]*Department of Chemistry, University of Helsinki, Helsinki, Finland*

Keywords: nucleation, aerosol nanocluster, acid-base chemistry

INTRODUCTION

Particle formation in the atmosphere from gas-phase precursors has been observed around the world; however, our fundamental understanding of the key species responsible and mechanisms involved remains uncertain. In this presentation, I will present laboratory and computational studies that seek to bridge the gap in our understanding of the evolution of clusters into nanoparticles. I will present novel experimental approaches used to directly observe compositional changes that occur in aerosol nanoclusters (AN), which we define as molecular aggregates suspended in a gas with dimensions between 2 and 10 nm (Smith et al., 2021).

METHODS

This project is our first attempt to "bridge the gap" between the measurement of cluster composition, which is typically directly measured by mass spectrometry, and nanoparticle composition, which we measure with thermal desorption chemical ionization mass spectrometry (TDCIMS) (Voisin et al., 2003). Thus far, we have characterized size resolved AN composition from reactions of methanesulfonic acid (MSA) with 4 different gas phase bases: 4-amino-1-butanol (4AB), monoethanolamine (Perraud et al., 2024), methylamine (Perraud et al., 2020), and putrescine. Below, we focus on the properties of AN produced by MSA + 4AB chemistry, but similar data will be presented on all of the above systems.

Figure 1a is a plot of cluster mass-to-charge ratio vs. inverse mobility for singly charged MSA + 4AB clusters with mobility diameters up to 2.4 nm. The singly charged clusters were generated using a bipolar electrospray source, which combines two oppositely charged electrosprays of solutions of the same salt and generates singly charged acid-base clusters, with minor contributions from higher charge states (Fernandez de la Mora and Barrios-Collado, 2017). These clusters were analyzed using a tandem setup featuring a Half-Mini high resolution Differential Mobility Analyzer (Half-Mini DMA; SEADM) (Rosser and de la Mora, 2005) and an Atmospheric Pressure interface Time of Flight Mass Spectrometer (APiTOF-MS using an HTOF mass analyzer; Tofwerk AG). Figure 1b shows the complete mass spectrum of these positively charged clusters, demonstrating that the most stable cluster configuration is one in which there are equal numbers of MSA and 4AB molecules with an additional protonated 4AB providing the charge up to n = 12 (MSA, 4AB) units. Figure 1c shows TDCIMS results of the MSA:4AB molar ratios in size-selected AN with mobility diameter 3.5–8 nm. These were made possible by nucleating neutral AN in a flow reactor from the reaction of the gas phase reactant MSA and 4AB, utilizing the Half-Mini DMA at the inlet of the TDCIMS, as well as other modifications such as higher sampling flow rates. TDCIMS measurements confirm that the most stable configuration of MSA + 4AB AN is one with equal numbers of MSA and 4AB molecules (Acid:Base Molar Ratio = 1.0).

We also have measured the stability of singly charged acid-base clusters by combining the bipolar electrospray, Half-Mini DMA, and an ultrahigh resolution Orbitrap mass spectrometer (Q Exactive Plus, Thermo Fisher Scientific). Figure 2 shows a typical example, again using the MSA + 4AB system as an example, of the data that we are able to obtain with this setup. Clusters fragment by losing a full (MSA,

4AB) heterodimer rather than individual acid or base molecules. In addition, the smallest cluster (MSA, 4AB)-[4AB+H]+ fragments losing first an MSA molecule, then the amine.

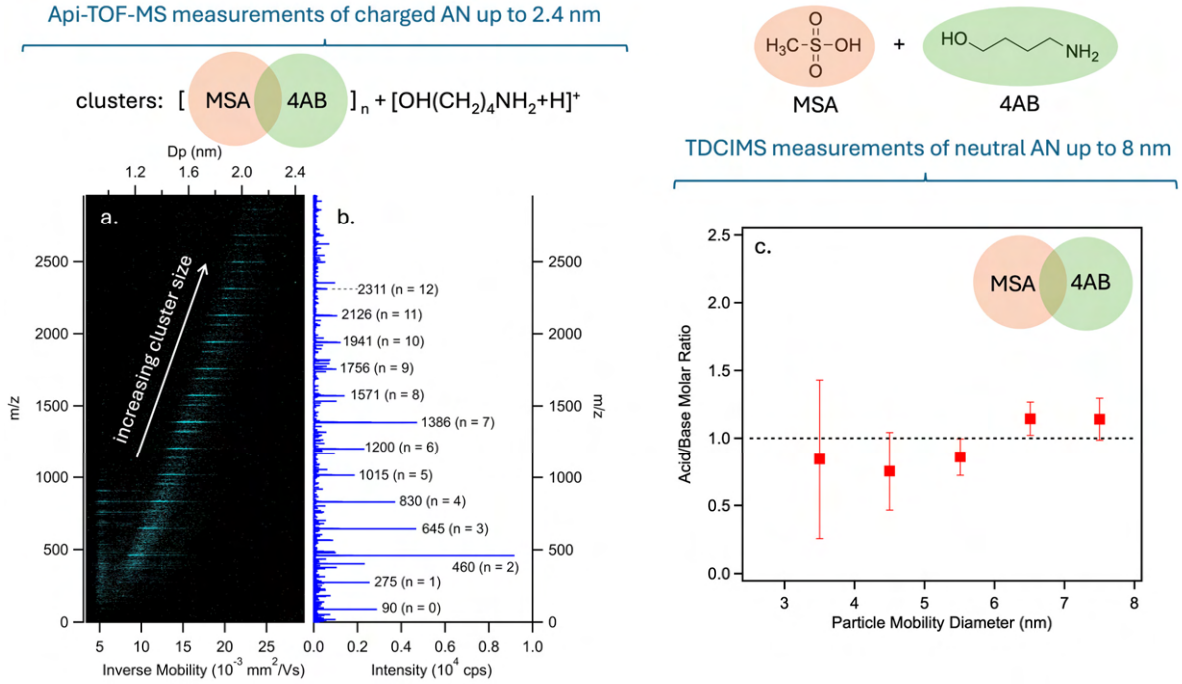


Figure 1. *Composition of AN from MSA+4AB reaction. (a) cluster inverse mobility (equivalent mobility diameter shown at top) vs. cluster m/z as measured by ion mobility-APiTOF-MS; (b) average mass spectrum (c) Size-resolved particulate MSA:4AB ratio in as measured by TDCIMS.*

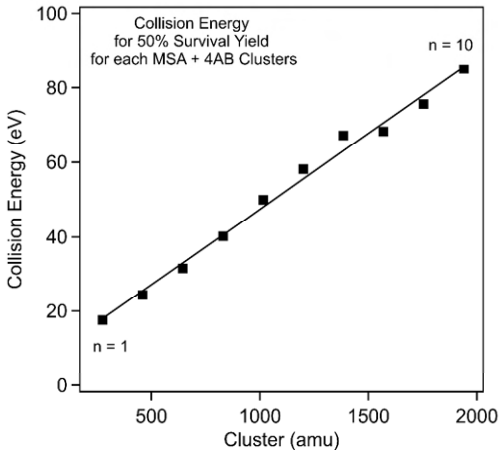


Figure 2. *Collision energy associated with a 50% survival yield of MSA-4AB singly charged clusters. Each point represents a $(MSA)_n(4AB)_n$ cluster. The line is a linear fit to the data.*

CONCLUSIONS

Our studies of AN formation from reactions of MSA with 4AB have shown that this alkanolamine is quite efficient at forming particles with MSA. In addition, nanoparticles formed from MSA + 4AB are neutral (acid:base ratio of 1), with no size dependence. Cluster stability measurements show a linear dependence with cluster size. Ongoing work includes expanding into sulfuric acid + base systems, as well as collaborating with a theory group to gain further fundamental insights into these clusters.

ACKNOWLEDGEMENTS

This work was supported by the National Science Foundation under grant 2004066.

REFERENCES

Fernandez de la Mora, J. et al., 2017. Aerosol Sci. Technol. 51, 778–786.
Perraud, V. et al., 2020. ACS Earth Space Chem 4, 1182–1194.
Perraud, V. et al., 2024. Phys. Chem. Chem. Phys. 26, 9005–9020.
Rosser, S. et al., 2005. Aerosol Sci. Technol. 39, 1191–1200.
Smith, J.N. et al., 2021. J Aerosol Sci 153, 105733.
Voisin, D. et al., 2003. Aerosol Sci. Technol. 37, 471–475.

New particle formation from alpha pinene and trace sulfuric acid

E. Sommer[1, 2*], J. Almeida[1, 3], M. Simon[4], L. Caudillo-Plath[4], W. Yu[5], H. Junninen[6], Z. Zheng[7, 8], B. Judmaier[7], C. Xenofontos[9], A. Pozzer[10], J. Kirkby[1, 4] and the CLOUD collaboration

[1]CERN, European Organisation for Nuclear Research, 1211 Geneva, Switzerland
[2]Faculty of Physics, University of Vienna, 1090 Vienna, Austria
[3]Faculty of Sciences of the University of Lisbon, 1749-016 Lisbon, Portugal
[4]Institute for Atmospheric and Environmental Sciences, Goethe University Frankfurt, 60438 Frankfurt, Germany
[5]INAR, Faculty of Science, University of Helsinki, 00014 Helsinki, Finland
[6]Institute of Physics, Faculty of Science and Technology, University of Tartu, 50411 Tartu, Estonia
[7]Institute of Ion Physics and Applied Physics, University of Innsbruck, 6020 Innsbruck, Austria
[8]Ionicon Analytik Ges.m.b.H., 6020 Innsbruck, Austria
[9]The Cyprus Institute, 2121 Nicosia, Cyprus
[10]Max Planck Institute for Chemistry, 55128 Mainz, Germany

New particle formation (NPF) contributes to about half of all cloud condensation nuclei worldwide (Gordon et al. 2017) and plays a critical role in understanding anthropogenic climate change (IPCC, 2021). A key mechanism driving atmospheric NPF is acid-base nucleation, primarily involving anthropogenic sulfuric acid and ammonia (Kirkby, 2023). Nonetheless, oxygenated organic molecules (OOM), produced from oxidation of terpenes like alpha-pinene (Kirkby et al. 2016) or – in the upper troposphere – isoprene (Shen et al. 2024), can drive rapid particle nucleation in the complete absence of sulfuric acid, a process known as pure biogenic nucleation.

Shen et al. (2024) found that that the addition of trace amounts of sulfuric acid to isoprene-driven NPF enhanced the nucleation rates up to 100-fold. However, so far, a synergistic effect of sulfuric acid with alpha-pinene OOM (AP-OOM) has not been reported.

This study focuses on measurements from the CERN CLOUD chamber, examining NPF from alpha-pinene in the presence of trace sulfuric acid concentrations ranging from 10^4 to 10^6 cm^{-3}, levels that are commonly found in pristine regions. Experiments were conducted at -10°C and +5°C, typical of the cool boundary layer of boreal forest regions, and in the absence of any base vapors such as ammonia or amines.

Gas-phase concentrations were monitored using various CI-Time-Of-Flight mass spectrometers (Nitrate-CIMS, Fusion PTR, STOF PTR-MS, FIGAERO), while naturally charged nucleating clusters were analyzed using an APi-TOF. Aerosol particle distributions were characterized with an array of particle measurement instruments (scanning PSM, CPC, NAIS, nSMPS, lSMPS, DMA-Train). Nucleation and growth rates were determined under varying concentrations of alpha-pinene OOMs and sulfuric acid.

This study presents nucleation and growth rates from AP-OOM in the presence of trace sulfuric acid and compares the rates with those from pure AP-OOM and pure sulfuric acid, respectively.

Gordon, H. et al. (2017) Causes and importance of new particle formation in the present-day and preindustrial atmospheres. *J. Geophys. Res. Atmos.* **122**, 8739-8760.

IPCC (2021) Climate Change 2021 – The Physical Science Basis: Working Group I Contribution to the Sixth Assessment Report of the Intergovernmental Panel on Climate Change. *Cambridge University Press.*

Kirkby, J. et al. (2016) Ion-induced nucleation of pure biogenic particles. *Nature* **533**, 521-526.

Kirkby, J. et al. (2023) Atmospheric new particle formation from the CERN CLOUD experiment. *Nature Geoscience* **16,** 948-957.

Shen, J. et al. (2024) "New particle formation from isoprene under upper-tropospheric conditions." *Nature* 636.8041, 115-123.

NEW PARTICLE FORMATION MEASUREMENTS – NAIS, nanoSMPS, AND PSM COMPARISON

A. ŠPALOVÁ[1,2], A. HOLUBOVÁ ŠMEJKALOVÁ[3], P. ROZTOČIL[1], J. ONDRÁČEK[1], N. ZÍKOVÁ[1,2], V. ŽDÍMAL[1]

[1]*Institute of Chemical Process Fundamentals of the CAS, Prague, Czechia, spalova@icpf.cas.cz*

[2]*Faculty of Science, Charles University, Prague, Czechia*

[3]*Air Quality Department, Košetice Observatory, Czech Hydrometeorological Institute, Košetice, Czechia*

Keywords: new particle formation, nanoSMPS, NAIS, PSM, clusters

INTRODUCTION

Aerosol particles are a key component of Earth's atmosphere, affecting human health, climate, and radiation balance. They enter the atmosphere through direct emissions or form from gaseous precursors. Under favourable conditions, molecules cluster together, growing into aerosol particles. These clusters vary in concentration throughout the day, forming in the morning and either growing or disappearing. However, the exact processes behind the new particle formation (NPF) remain unclear. The NPF events significantly affect the particle concentration in the atmosphere. NPF depends on environmental conditions, for example gaseous precursors, UV radiation, precipitation, wind speed and direction, atmospheric boundary layer characteristics, and the origin of interacting air masses (Kulmala, 2003).

There is quite a small number of devices able to measure small particles, such as 1 nm in diameter, which are able to monitor the beginning of the NPF event, for example, PSM (Particle Size Magnifier) or nanoSMPS (nano Scanning Mobility Particle Sizer) measuring all particles regardless of their original charge. NAIS (Neutral and Air Ion Spectrometer) is able to measure neutral particles and also charged clusters, giving the idea about the charge distribution in the atmosphere. (Kangasluoma, 2020).

METHODS

Measurements take place at NAOK (National Atmospheric Observatory Košetice, Czechia), which features a 250-meter-tall tower. Various instruments, including NAIS (Neutral and Air Ion Spectrometer), PSM (Particle Size Magnifier), SMPS (Scanning Mobility Particle Sizer), and nanoSMPS, is used to measure particle size distribution.

As a part of the larger study, PSM, SMPS, and NAIS are operating on the top of the tower at 230 m above the ground level. SMPS, NAIS, and nano SMPS are operating at the ground level (Tab. 1). The data from the two different heights will be evaluated and compared. The meteorological and other parameters affecting the NPF mentioned above will be monitored and taken into account when describing NPF.

Tab. 1: The list of devices used and their planned placement

	Device	*Device Range*
Ground level	**PSM**	1–12 nm
	NAIS	0,8–40 nm
	SMPS	10–800 nm

	Device	*Device Range*
Tower 230 m above ground level	**nanoSMPS**	from 1,2 nm
	NAIS	0,8–40 nm
	SMPS	10–800 nm

The initial study has been made, comparing the data from PSM, NAIS and nanoSMPS (Tab. 1, bold) placed at the ground level. The study shows data from the devices able to measure the smallest particles, which describe the very beginning of the NPF.

CONCLUSIONS

A comparison of the data obtained by NAIS, nanoSMPS and PSM (Tab. 1, bold) is presented. The devices are placed at a ground level in the NAOK and operating for several weeks simultaneously. The subtle differences between the NPF visualisation by these three devices will be presented. Additionally, the data from NAIS regarding the charge of the particles will be shown.

ACKNOWLEDGEMENTS

This work is supported by a project funded by the Ministry of Education, Youth and Sports of the Czech Republic (MŠMT) through targeted support for large research infrastructures (ACTRIS-CZ: LM2023030).

REFERENCES

Kulmala, M. (2003). How particles nucleate and grow. Science, 302 (5647), 1000–1001.

Kangasluoma, J., Cai, R., Jiang, J., Deng, C., Stolzenburg, D., Ahonen, L. R., Chan, T., Fu, Y., Kim, C., Laurila, T. M., Zhou, Y., Dada, L., Sulo, J., Flagan, R. C., Kulmala, M., Petäjä, T., & Lehtipalo, K. (2020). Overview of measurements and current instrumentation for 1–10 nm aerosol particle number size distributions, Journal of Aerosol Science, 148, 105584.

THE EFFECT OF CHEMICAL SUBSTITUTION ON THE TRANSFORMATION OF ORGANOSULFATES

N. TSONA TCHINDA[1] and L. DU[1]

[1]*Qingdao Key Laboratory for Prevention and Control of Atmospheric Pollution in Coastal Cities, Environment Research Institute, Shandong University, China.*

Keywords: ORGANOSULFATE, OXIDATION, AEROSOL, CLIMATE.

INTRODUCTION

Organosulfates have been widely detected in aerosol particles from various environments around the world (Surratt et al., 2008; Nguyen et al., 2014). Due to the presence of $-OSO_3^-$ or $-OSO_3H$ functional group in their structure, organosulfates are acidic and highly water-soluble, which enables them to enhance the hygroscopicity of aerosols, with potential climate impacts. Despite organosulfates have generally been detected in the particle-phase due to their high partitioning towards the particle-phase, previous studies measured and detected some organosulfates as free species in the gas-phase (Ehn et al., 2010; Le Breton et al., 2018). Organosulfates derived from organic acids were recently identified and characterized in fine particulate matter samples collected in the southeastern U.S., with glycolic acid sulfate being the most abundant (Hettiyadura et al., 2017).

Despite extensive research on the concentration, composition, and formation mechanisms of organosulfates, the limited knowledge of molecular-level mechanisms of their transformations hinders further understanding of their atmospheric processes as well as their physico-chemical properties. Organosulfates primarily exists in the particulate phase due to their low volatility, and can react continuously with gas-phase oxidants (e.g., HO• radicals, O_3, and NO_3 radicals) at or near particle surfaces. The transformation of organosulfates generates not only new organic matter, but also inorganic sulfur species, such as HSO_4^- and SO_4^{2-}. Consequently, the conversion of organosulfates can significantly alter the composition and physico-chemical properties of atmospheric particulate. However, little is known in this regard. A few recorded studies include the chemical transformation of methyl sulfate, ethyl sulfate and an α-pinene-derived organosulfate by heterogeneous HO• oxidation (Kwong et al., 2018; Xu et al., 2022). Based on their observed reaction products, the authors suggested a mechanism proceeding through the formation of an alkoxy radical intermediate followed by fragmentation, yet the mechanism remains not fully elucidated. Moreover, organosulfates that can allow hydrogen abstraction at the β-position to the sulfate group could give rise to more complex mechanisms driven by Russell mechanism and Bennett and Summers reaction. While the presence of functional groups can exhibit specific features in the chemical transformation of organosulfates due to their complexity, their potential impact has not yet been thoroughly investigated.

This study explores the reactions of some prevalent organosulfates, specifically methyl sulfate and glycolic acid sulfate, with HO• in both gas-phase and aqueous-phase environments. The aim is to examine the effect of the carboxyl group in the decomposition process and assess the impact thereof on aerosol chemical composition.

METHODS

This study uses quantum chemical calculations based on density functional theory to explore the reactions of methyl sulfate and glycolic acid sulfate with HO• in the gas-phase and aqueous-phase. Geometry optimizations and vibrational frequency analysis of all reaction states on the energy surface were performed with density functional theory using the Gaussian 09 package (https://gaussian.com) at the M06-2X/6-311+g(2df,2pd) level of theory. To model the aqueous-phase reactions, the continuum solvation model based on the solute electron density was used. The kinetics were evaluated by assuming pseud-steady state approximation on the reactant complex formed from the interaction between initial

reactants (organosulfate (OS) and HO•) according to the following reaction (reaction (R1)) and applying the transition state theory.

OS + HO• ↔ reactant complex → transition state → product complex . (R1)

The rate constants for reaction (R1) are calculated with the following equations for the gas-phase (Eq. (1)) and aqueous-phase (Eq. (2)) reactions

$k_{\text{bim}} = K_{\text{eq}} k_{\text{uni}}$, (1)

$k_{\text{overall}} = \frac{k_{bim} \times k_D}{k_{bim} + k_D}$. (2)

In above equations, K_{eq} is the equilibrium constant of formation of the reactant complex, k_{uni} is the unimolecular rate constant of the transformation of the reactant complex to the product complex, respectively expressed by the following equations:

$$K_{\text{eq}} = \frac{1}{c^0} \times \exp\left(-\frac{\Delta G_{eq}}{RT}\right), \quad (3)$$

$$k_{\text{uni}} = \frac{k_B T}{h} \times \exp\left(-\frac{\Delta G^{\#}}{RT}\right), \quad (4)$$

where ΔG_{eq} is the Gibbs free energy of formation of the reactant complex from initial reactants, h is Planck's constant, k_{B} is Boltzmann's constant, $\Delta G^{\#}$ is the Gibbs free energy of the barrier separating the reactant complex from the product complex, R is the molar gas constant, T is the absolute temperature, and c^0 is the standard concentration (with values of 1 M and 2.46×10^{19} molecule cm^{-3} in the aqueous-phase and in the gas-phase, respectively, at 1 atm and 298.15 K).

k_{D} is the steady-state Smoluchowski rate constant calculated as

$k_{\text{D}} = 4\pi R_{OS,HO} D N_A$. (5)

In Eq. (5), $R_{\text{OS,OH}}$ stands for the reaction distance between the organosulfate and hydroxyl radical, defined as the sum of their respective radii, R_{OS} and R_{OH}. N_{A} is the Avogadro number and D is the sum of the diffusion coefficients of reactants. For a reactant i in water, the diffusion coefficient D_{i} is given by the Stokes-Einstein approach as follows:

$D_{\text{i}} = \frac{k_B}{6\pi\eta R_i}$. (6)

The radii of reactants (organosulfate and hydroxyl radical), assumed to be spherical, were calculated using the Multiwfn software (Lu and Chen, 2012).

CONCLUSIONS

Results indicate that all reactions initiate with hydrogen abstraction by HO• from CH_3- or -CH_2- groups adjacent to the sulfate group, followed by the further reaction of the resulting radical through self-decomposition or interactions with O_2 and O_3. It was shown that the reaction of glycolic acid sulfate in the gas-phase is more kinetically favorable than that of methyl sulfate, which can be attributed to the effect of -COOH substitution that stabilizes the intermediate reactant complex from glycolic acid. In addition, it was found that for glycolic acid sulfate, hydrogen abstraction from the -COOH group could lead to decarboxylation and eventually form similar products as methyl sulfate. The primary reaction products are inorganic sulfate, carbonyl compounds and formic sulfuric anhydride. Rate constants of 1.14×10^{-13} cm^3

molecule^{-1} s^{-1} and 6.17×10^{-12} cm^3 molecule^{-1} s^{-1} at 298.15 K were determined for the gas-phase reaction of methyl sulfate and glycolic acid sulfate, respectively. The former value is consistent with a previous experimental report. Additionally, while prior studies suggested O_2 as primary oxidant in the fragmentation of organosulfates, this study unveils O_3 as a complementary oxidant in the intermediate steps of this process. Overall, this study elucidates mechanisms for HO•-initiated transformation of organosulfates and highlights the potential role of chemical substitution, thereby enhancing our understanding of their atmospheric chemistry and implication for inorganic sulfate formation, which are vital for evaluating their impact on aerosol properties and climate processes.

ACKNOWLEDGEMENTS

This work was supported by National Key Research and Development Program of China (2023YFC3706203), National Natural Science Foundation of China (22376121), and Natural Science Foundation of Shandong Province (ZR2023MD041). The authors acknowledge the Wuxi Hengding Supercomputing Center Co., LTD and National Supercomputer Center in Tianjin for providing the computational resources.

REFERENCES

Ehn, M., Junninen, H., Petaja, T., Kurten, T., Kerminen, V. M., Schobesberger, S., Manninen, H.E., Ortega, I.K., Vehkamaki, H., Kulmala, M., and Worsnop, D.R. (2010). Composition and temporal behavior of ambient ions in the boreal forest, *Atmos. Chem. Phys.* **10**, 8513-8530.

Hettiyadura, A.P.S., Jayarathne, T., Baumann, K., Goldstein, A.H., de Gouw, J.A., Koss, A., Keutsch, F.N., Skog, K., and Stone, E.A (2017). Qualitative and quantitative analysis of atmospheric organosulfates in Centreville, Alabama, *Atmos. Chem. Phys.* **17**, 1343-1359.

Kwong, K.C., Chim, M.M., Davies, J.F., Wilson, K.R., and Chan, M.N. (2018). Importance of sulfate radical anion formation and chemistry in heterogeneous OH oxidation of sodium methyl sulfate, the smallest organosulfate, *Atmos. Chem. Phys.* **18**, 2809-2820.

Le Breton, M., Wang, Y., Hallquist, Å.M., Pathak, R.K., Zheng, J., Yang, Y., Shang, D., Glasius, M., Bannan, T.J., Liu, Q., Chan, C.K., Percival, C.J., Zhu, W., Lou, S., Topping, D., Wang, Y., Yu, J., Lu, K., Guo, S., Hu, M., and Hallquist, M. (2018). Online gas- and particle-phase measurements of organosulfates, organosulfonates and nitrooxy organosulfates in Beijing utilizing a FIGAERO ToF-CIMS, *Atmos. Chem. Phys.*, **18**, 10355-10371.

Lu, T. and Chen, F. (2012). Multiwfn: A multifunctional wavefunction analyzer, *J. Comput. Chem.* **33**, 580-592.

Nguyen, Q.T., Christensen, M.K., Cozzi, F., Zare, A., Hansen, A.M.K., Kristensen, K., Tulinius, T.E., Madsen, H.H., Christensen, J.H., Brandt, J., Massling, A., Nøjgaard, J.K., and Glasius, M. (2014). Understanding the anthropogenic influence on formation of biogenic secondary organic aerosols in Denmark via analysis of organosulfates and related oxidation products, *Atmos. Chem. Phys.* **14**, 8961-8981.

Surratt, J.D., Gomez-Gonzalez, Y., Chan, A.W.H., Vermeylen, R., Shahgholi, M., Kleindienst, T.E., Edney, E.O., Offenberg, J.H., Lewandowski, M., Jaoui, M., Maenhaut, W., Claeys, M., Flagan, R.C., and Seinfeld, J.H. (2008). Organosulfate formation in biogenic secondary organic aerosol, *J. Phys. Chem. A* **112**, 8345-8378.

Xu, R., Ng, S.I.M., Chow, W.S., Wong, Y.K., Wang, Y., Lai, D., Yao, Z., So, P.K., Yu, J.Z., and Chan, M.N. (2022). Chemical transformation of α-pinene-derived organosulfate via heterogeneous OH oxidation: implications for sources and environmental fates of atmospheric organosulfates, *Atmos. Chem. Phys.* **22**, 5685-5700.

ON THE MEAN DIAMETER OF SMALL IONS: INSIGHT INTO ION CLUSTER COMPOSITION AND GROWTH

S. TUOVINEN[1], C. LIU[1], N. SARNELA[1], Y. LIU[2], V-M. KERMINEN[1] and M. KULMALA[1,2]

[1]*Institute for Atmospheric and Earth System Research, Faculty of Science, University of Helsinki, Helsinki, Finland.*
[2]*Aerosol and Haze Laboratory, Beijing Advanced Innovation Center for Soft Matter Science and Engineering, Beijing University of Chemical Technology, Beijing, China*

Keywords: small ions, mobility diameter, cluster formation.

INTRODUCTION

In the atmosphere, charged molecules and clusters of molecules with electrical mobility diameters below 2 nanometer are always present (Hirsikko *et al.*, 2011). The smallest of these so-called small ions consist only from one to a couple of molecules, while the largest, nearing 2 nm, might be composed of over a dozen molecules. Various studies have been made both into the number concentration of small ions or into their chemical composition, with less attention paid to their mobility distribution. In this study, we use atmospheric measurement data to investigate the mean mobility diameter of small ions to get new insight into the connections between small ion mobility diameter distribution, their chemical composition and cluster formation and growth.

METHODS

Data from two contrasting sites, SMEAR II in Hyytiälä, Finland and BUCT measurement site in Beijing, China, was utilized. Data measured with Neutral cluster and Air Ion Spectrometer (NAIS; Mirme & Mirme, 2013), an instrument that measures both the total and charged particle distributions, was used as the main focus of the analysis. The measured ion number size distribution data were used to calculate the mean mobility diameter (d_{mean}) of small ions. Weighted mean, using the number concentrations at different mobility diameters as weights, was used to derive d_{mean}. We used atmospheric low volatility vapor concentrations measured by a chemical ionization mass spectrometer for both sites. Atmospheric sulfuric acid ion cluster concentrations for Hyytiälä were also used. In addition, condensation sink (CS) and NPF ranking (Aliaga et al. 2023) data was used for both sites. NPF ranking was derived based on the number concentration of total particles in the diameter range from 2.5 to 5 nm.

RESULTS AND CONCLUSIONS

The mean mobility diameter (d_{mean}) was found to vary seasonally, and to lesser extend diurnally, in both Hyytiälä and Beijing. In Hyytiälä, d_{mean} of negative small ions varied from less than 1 nm to around 1.15. In Beijing, d_{mean}, of negative small ions varied approximately from 1.05 to 1.15 nm. Positive ions were typically around 0.15 to 0.2 nm negative small ions.

In Hyytiälä, d_{mean} of both positive and negative small ions were found to be strongly positively correlated with the concentrations of atmospheric sulfuric acid and highly oxidized molecules (HOMs). Our results indicate that sulfuric acid and HOMs might contribute to the formation of larger ion clusters, while HOMs could in addition increase d_{mean} simply due to their large molecular size. The correlation of d_{mean} with sulfuric acid ion monomers, dimers and trimers was found to be generally weakly positive in Hyytiälä. During March and April there was a good positive correlation between d_{mean} and the signal from the

sulfuric acid ion clusters. However, more in depth analysis is needed due to the complex seasonal and diurnal patterns of the correlation between d_{mean} and sulfuric acid ion clusters.

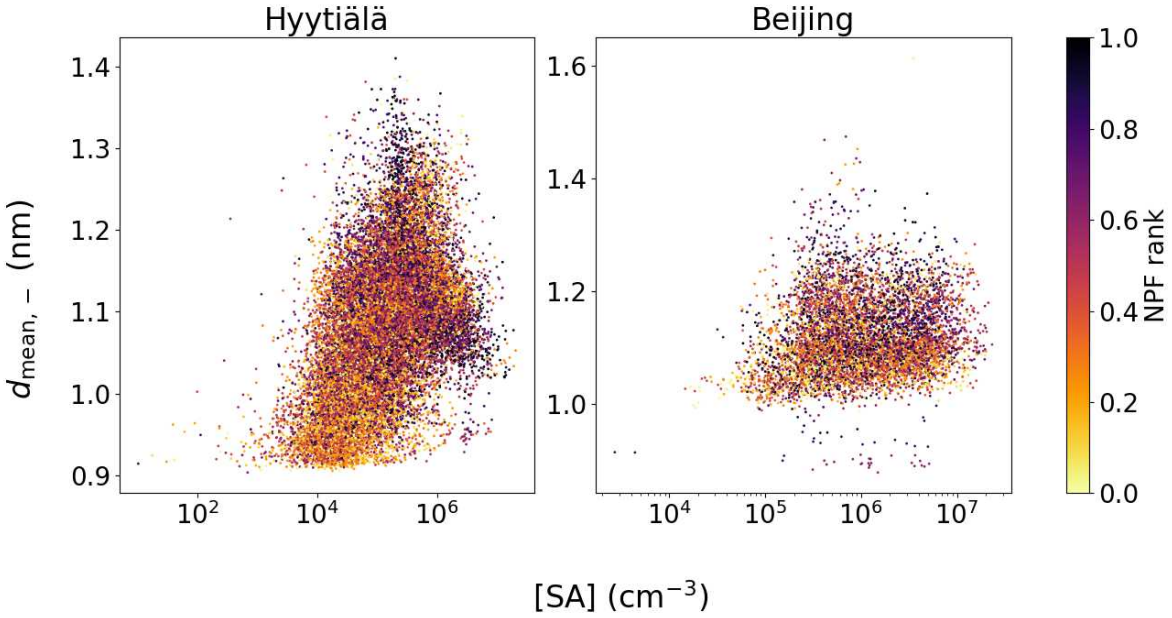


Figure 1. Mean diameter of negative small ions (d_{mean}) versus sulfuric acid vapor concentration [SA]. The value of the daily NPF ranking is indicated by color.

In Beijing, the correlation between d_{mean} of either polarity and both atmospheric sulfuric acid and organic compounds was found weak. However, in both Beijing and Hyytiälä, d_{mean} had a clear positive correlation with NPF ranking (Figure 1). NPF ranking indicates the probability and intensity of atmospheric new particle formation. This results shows that in both locations the small ions seem to be larger when NPF is more intense, indicating their growth to larger sizes. This positive correlation between ranking and small ion mobility diameter was especially clear when CS was low, and therefore the clusters were probably more likely to grow to larger sizes.

Next, to gain a better understanding of the implications of our results on the relationship between small ion mobility diameter and ion composition, more in depth analysis using the sulfuric acid ion cluster data and the sub-2 nm ion number size distribution data will be made.

ACKNOWLEDGMENTS

This work was supported by “Towards climate positive agriculture - The contribution of new particle formation to the climate impact of agriculture” co-research project funded by Business Finland and ACCC Flagship funded by the Academy of Finland grant number 37549.

REFERENCES

Aliaga et al. (2023). Nanoparticle ranking analysis: determining new particle formation (NPF) event occurrence and intensity based on the concentration spectrum of formed (sub-5 nm) particles, *Aerosol Research*, 1, 81–92, https://doi.org/10.5194/ar-1-81-2023.

Hirsikko et al. (2011). Atmospheric ions and nucleation: a review of observations, *Atmospheric Chemistry and Physics*, 11(2), 767-798, https://doi.org/10.5194/acp-11-767-2011.
Mirme, S. & Mirme, A (2013). The mathematical principles and design of the NAIS – a spectrometer for the measurement of cluster ion and nanometer aerosol size distributions, *Atmospheric Measurement Techniques*, 6, 1061–1071, https://doi.org/10.5194/amt-6-1061-2013.

EVAPORATION RATES OF COMPLEX ORGANIC CLUSTERS DEPEND STRONGLY ON MOLECULAR FLEXIBILITY

H. VEHKAMÄKI[1], J. KÄHÄRÄ[1], L. FRANZON[2], S. INGRAM[1] and T. KURTÉN[2]

[1]*Institute for Atmospheric and Earth System Research, University of Helsinki, Finland.*

[2]*Department of Chemistry, University of Helsinki, Finland.*

Keywords: particle formation, organic molecules, molecular modelling

INTRODUCTION

Oxygenated organic molecules (OOMs) form in the atmosphere by oxidation of volatile organic compounds from both natural and anthropogenic sources. Highly oxygenated organic molecules are likely to take part in new particle formation, but it is unclear to what extent they can form particles without the involvement of inorganic acids or ions, and whether they have a significant contribution to the initial formation of molecular clusters, or only to the growth of these clusters. Traditionally, most atmospheric particle formation models have relied on macroscopic thermodynamic properties, in particular saturation vapour pressures. However, experimental data for the saturation vapour pressures of OOMs that can form particles in atmospheric conditions do not exist. Also modelling approaches have large uncertainties when applied to predicting saturation vapour pressures of realistic OOM candidates. More fundamentally, saturation vapor pressures may be relatively poor predictors of the evaporation rates of small clusters which are the true parameters governing particle formation rates. In this work, we use quantum chemical methods to generate optimized OOM cluster configurations and calculate their stabilities.

METHODS

Experimental research suggests that OOMs with 15-20 carbon atoms can contribute to atmospheric cluster formation. However, generating sufficient amounts of accurate data even for dimer (two molecule) clusters of such compounds is computationally prohibitively expensive. Thus we have studied 50 C10-C14 sized OOM accretion products from isoprene and toluene oxidation. These were obtained using Gecko-AP (Franzon et al., 2024), a RO2 + RO2 accretion product generator based on the Gecko-A software. The saturation vapour pressures of these OOMs were calculated with SIMPOL (Pankow and Asher 2008). The framework for configurational sampling, optimizing, and analysing of molecular clusters is provided by JKCS program (Kubečka, Besel, et. al., 2023). Initial sampling of cluster configurations was done at semi-empirical level of theory. Local and global minimum energy configurations were found through successive rounds of filtering a subset of results and re-optimization at higher DFT levels of theory. OOMs were observed to cluster in configurations which maximise the number of hydrogen bonds. As we found that even an extensive sampling of cluster configuration space does not guarantee that the global minimum is found, we introduced constraints to initial sampling which force hydrogen bond formation between molecules. We also used metadynamics simulations to search for additional local minima. Finally, we selected the lowest energy structures to calculate the binding free energies for each cluster type which can be converted into evaporation rates using statistical mechanics. For validation purposes we also performed calculations on dimers of differently sized polyethylene glycol molecules (PEGs), for which the configurational sampling is relatively straightforward, and the saturation vapor pressures are available both from quantum chemistry (via COSMOTherm) and experimentally (Krieger et al. 2018).

CONCLUSIONS

We discovered that our predicted binding free energies of the homodimers of the studied OOMs were almost uncorrelated with their SIMPOL predicted saturation vapour pressures. There is also no obvious trend between the number of hydrogen bonds within the cluster and either binding free energy or vapour pressure. To understand this, we turned to the simpler test case of PEGs. Based on known saturation vapour pressure values, we would expect the binding free energy to decrease when PEG sizes increase. Instead, the dimer binding free energies were found to strongly depend on the configurations used to calculate the monomer free energies. Using the minimum monomer energies as the baseline, the predicted cluster dimer formation free energies in fact increase slightly with increasing molecular mass, opposite to the trend of vapour pressures. Yet, if we instead optimize the dimers tarting from a linear structure (a configuration which better reflects the situation in a bulk liquid, where all the molecules are surrounded from all side by similar molecules, and is thus the setting relevant to saturation vapour pressure definition) we recover a trend in binding energies which is in line with the behaviour of the saturation vapour pressures. The difference is explained by lowest energy PEGs folding inwards onto themselves and forming intramolecular hydrogen bonds, leading to weaker binding to other molecules. The ability to form intramolecular hydrogen bonds depends highly on the structure and flexibility of the molecule. For example, existence of double bonds in the carbon chains is likely to impede the formation of intramolecular hydrogen bonds. In our dataset of C10-C14 molecule clusters we find that the most strongly binding molecules all contain double bonds, but not all molecules with double bonds bind strongly. Promise for developing a transferable machine learning model for predicting the stabilities of OOM clusters is given by our finding that the binding energies of mixed dimers can be estimated by taking the averages of the binding energies of the corresponding homodimers. Furthermore, flexibility is ultimately a unimolecular property, and thus more easily amenable to machine learning approaches which necessitate the production of enormous amounts of training data.

ACKNOWLEDGEMENTS

This work was supported by Academy of Finland Centre of Excellence “VILMA – Virtual Laboratory for Molecular Level Atmospheric Transformations”. Computational resources were provided by CSC-IT Centre for Science, Ltd., Espoo, Finland. We thank Nanna Myllys for the suggestion to use PEGs as test case.

REFERENCES

Kubečka, J., Besel, V., Neefjes, I., Knattrup, Y., Kurtén, T., Vehkamäki, H. and Elm, J. (2023) *ACS Omega*, **8**, 45115.

Krieger,U.K., F. Siegrist, C. Marcolli, E. U. Emanuelsson, F. M. Gøbel, M. Bilde, A. Marsh, J. P. Reid, A. J. Huisman, I. Riipinen, N. Hyttinen, N. Myllys, T. Kurtén, T. Bannan, C. J. Percival, and D. Topping. *AtmosphericMeasurement Techniques*, 11(1):49–63, 2018.

Franzon, L., Camredon, M., Valorso, R., Aumont, B. and Kurten T. (2024) *Atmos. Chem. Phys.*, 24, 11679–11699.

Pankow J.F.and. Asher W.E. *Atmospheric Chemistry and Physics*, 8(10):2773–2796, 2008.

INTERNATIONAL CONFERENCES ON NUCLEATION AND ATMOSPHERIC AEROSOLS (ICNAA) A BRIEF HISTORY

PAUL E. WAGNER
University of Vienna, Austria

INTRODUCTION

The current 22nd International Conference on Nucleation and Atmospheric Aerosols (ICNAA) is commemorating 70 years of the ICNAA Series and 60 years of the Committee on Nucleation and Atmospheric Aerosols (CNAA) being responsible for the organisation of the Conferences. These anniversaries justify a historical retrospect. An earlier review on the ICNAA Series has been provided by O'Connor (2007).

THE CONDENSATION NUCLEI HYPOTHESIS

Already during the late 19th century studies of the processes leading to formation of fogs, clouds and precipitation in the atmosphere have been reported (see reviews by Podzimek, 1989; Spurny, 2000). From the work reported by Tyndall (1869) it is known that fine particles exist in the air. The role of fine airborne particles in vapor condensation processes was first discovered by Paul-Jean Coulier (1875). Series of experiments by Coulier on expanding saturated air using a specially developed apparatus (Figure 1) led to the following conclusion:

Condensation Nuclei Hypothesis:

Fine solid particles suspended in air are necessary for the production of fogs.

Further experiments considering systems at elevated temperatures, however, caused Coulier to doubt the general validity of his Condensation Nuclei Hypothesis, so his work remained widely unnoticed.

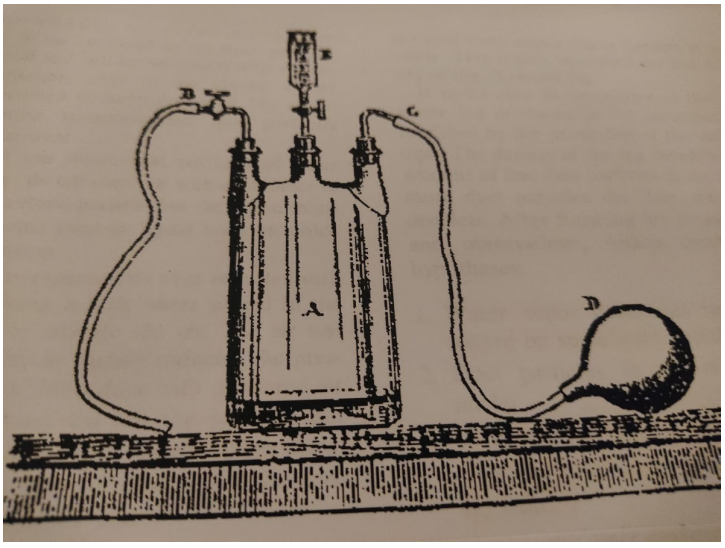


Figure 1. Expansion chamber apparatus presented by P.J. Coulier (1875).
A: Glass flask with some water, D: Rubber ball, E: Filter.

A few years later Aitken (1880, see Figure 2) independently started similar experiments using somewhat different expansion chamber arrangements. He confirmed Couliers Condensation Nuclei Hypothesis. Coulier's doubts were shown to be unjustified. Aitken (1890) designed the famous **Pocket Dust Counter** (Figure 3), a prototype for Condensation Particle Counters. In the Pocket Dust Counter the number concentration of the condensing drops was determined by visually counting drops sedimented to a glass plate. Notably, Aitken (1917) performed experiments with expansion ratios ranging from 1.01 to 1.08 to estimate a nuclei activation threshold. So Aitken already understood the concept of onset saturation ratio for activating atmospheric nuclei.

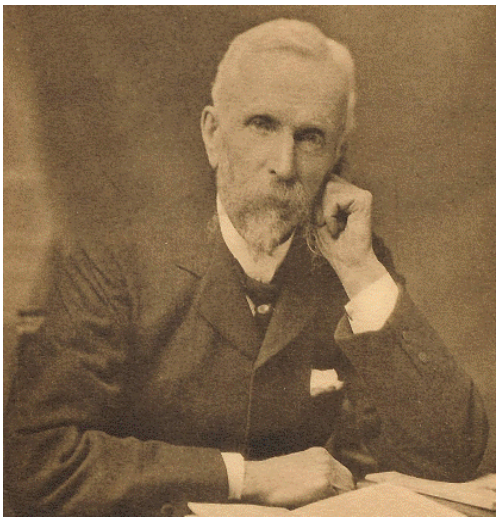


Figure 2. John Aitken (1839 – 1919). Scottish scientist (Meteorology, Physics).
Picture: Wikipedia.

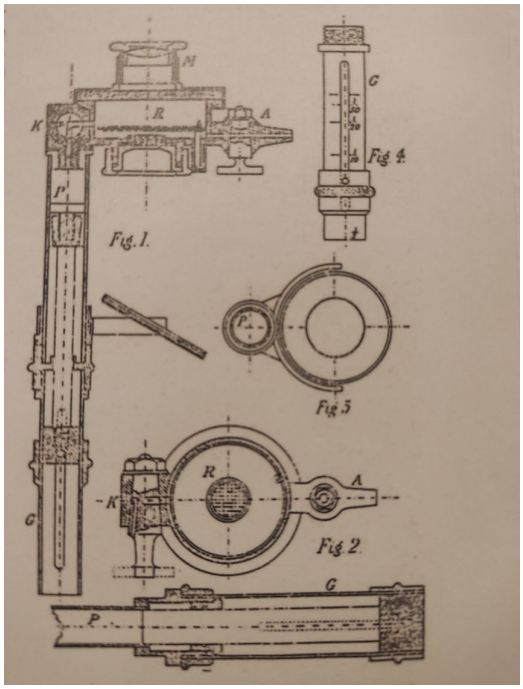


Figure 3. Pocket Dust Counter designed by John Aitken (1890).
R: Expansion chamber, M: Magnifying glass, P: Expansion cylinder.

COORDINATION OF INTERNATIONAL SCIENTIFIC STUDIES AND CONFERENCES

During the early 20th century it became evident that scientific progress is increasingly dependent on international cooperation. Hence several International Scientific Unions were established to promote and coordinate studies in various scientific fields and organize international conferences. Among the first International Unions to be established were
International Union of Pure and Applied Chemistry (IUPAC) established 1919
International Union of Pure and Applied Physics (IUPAP) established 1922
International Union of Geodesy and Geophysics (IUGG) established 1919.

Informations on structure and programs of IUGG are provided by Ismail-Zadeh and Joselyn (2019).
The IUGG holds General Assemblies at four-year intervals, the first IUGG General Assembly was held in 1922. The IUGG is a federation of eight semi-autonomous Associations. One of these Associations was originally established already in 1919 as the Meteorology Section of IUGG. This Association has later been renamed as International Association of Meteorology and Atmospheric Sciences (IAMAS).

IAMAS consists of ten Commissions, among them the following should be particularly noted here:
International Commission on Atmospherical Chemistry and Global Pollution (ICACGP)
International Commission on Climate (ICCL)
International Commission on Clouds and Precipitation (ICCP).

The Executive Committee of the IUGG has the particular responsibility of overseeing the scientific programs of the Assemblies and the numerous Symposia, Commission and Working Group Meetings.

ESTABLISHING A SERIES OF CONFERENCES ON CONDENSATION (AND ICE) NUCLEI – THE FIRST DECADE

Around the middle of the 20th century studies concerning condensation nuclei have received considerable interest at various places.

Since 1955 Helmut K. Weickmann has successfully organised Woods Hole Conferences on Physics of Cloud and Precipitation Particles at Woods Hole Oceanographic Institution, Massachusetts, USA. In 1963 Weickmann founded the International Commission of Clouds and Precipitation (ICCP) within the International Association of Meteorology and Atmospheric Sciences (IAMAS). H.K. Weickmann was the first President of ICCP (Podzimek, 1993). The ICCP is responsible for the organisation of the quadrennial International Conferences on Clouds and Precipitation. The first Conference of this series was held in 1954 at Zurich.

Up to this point studies of condensation nuclei have generally been performed using Aitken's Pocket Dust Counter of 1890 or some modifications. In these instruments the droplets are visually or photographically counted. An important improvement was achieved by Nolan and Pollak (1946, see Figure 4) and Pollak and Murphy (1952, 1953). The **Nolan-Pollak Counter** (see Figure 5) allows to determine the drop concentration from the light extinction due to the drop cloud formed inside the fog tube of the counter.

During the 10th General Assembly of the IUGG in Rome in September 1954 L.W. Pollak (Ireland), H. Israel, R. Mühleisen (Federal Republic of Germany), M. Bider (Switzerland) and R. Siksna (Sweden) met in a small café. In an informal lecture Pollak provided informations on his work in Dublin regarding design, construction and calibration of an improved Condensation Nucleus Counter. This small meeting is sometimes referred to as the Zeroth Conference (Siksna, 1966). The people attending in this meeting prevailed on Pollak to organise a symposium on condensation nuclei.



Figure 4. Leo Wenzel Pollak (1888 Prague - 1964 Dublin).
L.W. Pollak together with P.J. Nolan, T. Murphy and others
developed the Nolan-Pollak Condensation Nucleus Counter.
Photo: Proceedings, First Int. Symposium on Condensation Nuclei, 1955.

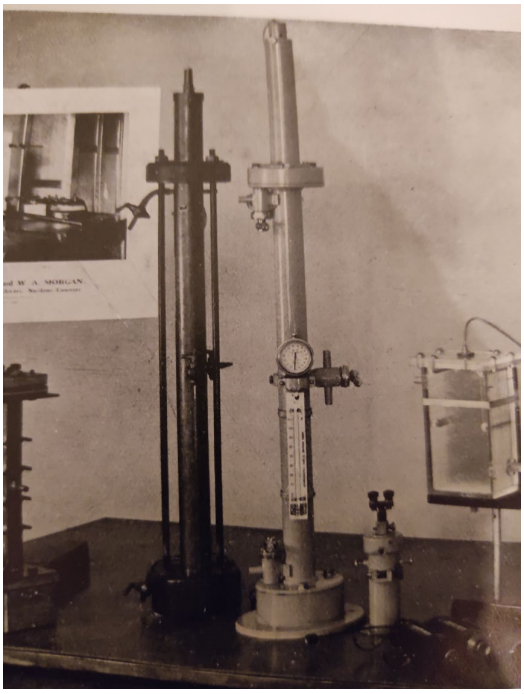


Figure 5. Nolan-Pollak Condensation Nucleus Counters shown during the
First Int. Symposium on Condensation Nuclei, Dublin.
Photo: Proceedings, 1955.



Figure 6. Participants in First Int. Symposium on Condensation Nuclei. Photo: Proceedings, 1955.

1955. The First International Symposium on Condensation Nuclei (see Figure 6) was held during 26-28 April 1955 at Dublin, Ireland – **70 years ago**. It was attended by 34 delegates from 8 countries: France, Germany, Ireland, Italy, Sweden, Switzerland, United Kingdom, USA. 26 papers were presented. Photoelectric Condensation Nucleus Counters were exhibited and demonstrated during the Symposium. Main organizers: L.W. Pollak, P.J. Nolan. Proceedings published in a Special Volume, Geofis. Pura e Appl. Vol. 31 (1955/II).

1956. The Second Symposium on Condensation Nuclei was held during 1-4 October 1956 at Basle and Locarno, Switzerland. 50 scientists from 12 countries have attended, 28 papers were presented. Main Organizers: F. Verzár, M. Bider and J.C. Thams.

1958. The Third International Symposium on Condensation Nuclei was held during 16-18 July 1958 at Cavendish Laboratory, University of Cambridge, UK. 50 scientists from 9 countries have attended, 24 papers were presented. Main organizer: T.W. Wormell.

1961. The 4th Int. Conference on Atmospheric Condensation Nuclei was held during 24-28 May 1961 in Germany at Frankfurt/Mainz and at Heidelberg. 74 scientists from 14 countries have attended, 37 papers were presented. Main Organizers: H.W. Georgii and G. Schumann.

1963. The 5th Int. Conference on Condensation Nuclei and Ice Nuclei was held during 13-17 May 1963 in France at University of Clermont-Ferrand with topic Ice Nuclei, at University of Toulouse with topic Condensation Nuclei and featuring a visit to l'Institut de Physique de l'Atmosphere at Lannemezan. 54 scientists from 14 countries have attended, 34 papers were presented. At this Conference **for the first time Ice Nuclei were mentioned in the title**. Main organizer: H. Dessens.

1966. The 6th Int. Symposium on Condensation Nuclei was held during 9-13 May 1966 in the USA at State University of New York, Albany, NY, and at Pennsylvania State University, University Park, PA. 86 scientists from 14 countries have attended, 55 papers were presented. This Conference was **the first of this Series held outside of Europe**. Main organizers: V.J. Schaefer, C.L. Hosler. Proceedings published in a Special Volume, J. Rech. Atmos. Vol. 2, pp. 50-436 (1966). The Proceedings Volume is dedicated to the memory of L.W. Pollak, who died November 1964.

FOUNDING THE COMMITTEE ON NUCLEATION AND ATMOSPHERIC AEROSOLS

Over the first decade the Conferences have been organized by interested individuals on a voluntary basis without statutes, rules or officers. Clearly an incorporation of the series of conferences into the already existing international cooperation of scientists in the field of atmospheric nucleation was considered desirable. As mentioned by Josef Podzimek (2000), the founding ICCP President Helmut K. Weickmann supported the idea of establishing a Standing Subcommittee of ICCP. Hence it was decided to found the Committee on Nucleation. The ICCP Committee on Nucleation was established in November 1965 - **60 years ago**. Josef Podzimek (Figure 7) was its first Chair. In 1984 the Committee on Nucleation has been renamed as Committee on Nucleation and Atmospheric Aerosols (CNAA). The CNAA is responsible for the organization of the quadrennial International Conferences on Condensation and Ice Nuclei, later International Conferences on Nucleation and Atmospheric Aerosols (ICNAA). The official status of CNAA within ICCP within IAMAS within IUGG facilitates wider publicity of the conferences and can provide support for international conference participation. Close links of personal friendship had in fact become a feature of these conferences.

Members and Chairs of the CNAA are elected in conjunction with Conferences for 1 term, i.e. time interval between two successive Conferences, typically 4 years. Members are eligible for re-election for a maximum of 1 more term. After this their term ends. For practical reasons an exception from this rule is provided for election of a CNAA-Chair. A person nominated for election as CNAA-Chair will usually be already a Member of CNAA and could according to the above rule serve as Chair for only 1 more term. However, it is often desirable to re-elect a Chair for a second term. This requires an exception from the above mentioned rule. Upon nomination a person, usually Member or former Member of CNAA, can be elected as an Honorary Member of CNAA.



Figure 7. Josef Podzimek (1923 Prague - 2007 Rolla, Missouri).
Founding Chair of CNAA.
Picture: Obituary notice.

1969. The 7th Int. Conference on Condensation and Ice Nuclei was held during 18-24 September 1969. According to suggestions by Helmut K. Weickmann and Josef Podzimek it was held at two locations in Central Europe – Prague, Czechoslovakia and Vienna, Austria. The host institutions were the Czechoslovak Academy of Science and the University of Vienna. Scientists from 26 countries have attended, 80 papers were presented. This Conference was **for the first time held in two different countries**. Hence even scientists, who could not travel from Czechoslovakia to Austria, were able to attend the Conference. Main organizers: J. Podzimek, K. Spurny and O. Preining.

1973. The 8th Int. Conference on Nucleation was held during 24-29 September 1973 at Leningrad, USSR. Scientists from 18 countries have attended, 74 papers were presented. These were published, mainly in English. This Conference was **for the first time almost entirely devoted to the topic of Ice Nucleation**. Main organizer: I.I. Gaivoronsky.

1977. The 9th Int. Conference on Atmospheric Aerosols, Condensation and Ice Nuclei (Figure 8) was held during 21-27 September 1977 at Galway, Ireland. 142 scientists from 22 countries have attended, 101 papers were presented. The **topic Atmospheric Aerosols was added** to the title. Main organizers: T.C. O'Connor and A.F. Roddy. Proceedings published by Galway University Press.

1981. The 10th Int. Conference on Condensation and Ice Nuclei was held during 26-28 August 1981 at Hamburg, Germany as part of the 3rd IAMAS Assembly. 58 papers were presented. Program and Abstracts were included in the IAMAS Proceedings. Main organizer: H.W. Georgii.

1984. The 11th Int. Conference on Atmospheric Aerosols, Condensation and Ice Nuclei was held during 3-8 September 1984 at Budapest, Hungary. 110 papers were presented. Main organizers: E. Meszaros and G. Vali.

1988. The 12th Int. Conference on Atmospheric Aerosols and Nucleation was held during 22-27 August 1988 at University of Vienna, Austria. 180 scientists from 28 countries have attended, 167 papers were presented. This Conference was **for the first time held jointly with the Nucleation Symposium (American Chemical Society)** to stimulate contacts and an exchange of information between scientists in closely related disciplines. Main organizers: P.E. Wagner and G. Vali. Proceedings published in a book entitled *Atmospheric Aerosols and Nucleation*, Lecture Notes in Physics 309 (Springer-Verlag, Berlin, Heidelberg, New York, London, Paris, Tokyo, 1988).



Figure 8. Participants in the 9th Int. Conference on Atmospheric Aerosols, Condensation and Ice Nuclei, Galway, Ireland, 1977.

1992. The 13th Int. Conference on Nucleation and Atmospheric Aerosols (**ICNAA**) was held during 24-28 August 1992 at University of Utah, Salt Lake City, USA, again in conjunction with the ACS Nucleation Symposium. Scientists from 22 countries have attended, 114 papers were presented. Main organizers: N. Fukuta and P.E. Wagner. Proceedings published by A. Deepak Publishing, Hampton, Virginia, 1992.

1996. The 14th ICNAA was held during 26-30 August 1996 at University of Helsinki, Finland, again in conjunction with the ACS Nucleation Symposium. 264 scientists from 32 countries have attended, 198 papers were presented. **Nobel Laureate P.J. Crutzen gave the opening lecture** on *The Role of Particulate Matter in Ozone Photochemistry*. Main organizers: M. Kulmala and P.E. Wagner. Proceedings published in a book entitled *Nucleation and Atmospheric Aerosols 1996* (Pergamon, Elevier Science, Oxford, New York, Tokyo, 1996).

2000. The 15th ICNAA was held during 6-11 August 2000 at the University of Missouri, Rolla, MO, again jointly with the Nucleation Symposium. Scientists from 27 countries have attended, 207 papers were presented. A **Special Symposium honoring Howard Reiss** was organized. Main Organizers: B.N. Hale and M. Kulmala. Proceedings were electronically generated by American Institute of Physics as AIP Conference Proceedings Vol. 534, Melville, NY 2000.

2004. The 16th ICNAA was held during 26-30 July 2004 at Kyoto University, Japan. 174 papers were presented. This conference was **the first of this Series held in Asia.** Main organizers: M. Kasahara and M. Kulmala. Proceedings were published by Kyoto University Press, 2004.

2007. The 17th ICNAA (Figure 9) was held during 13-17 August 2007 at National University, Galway, Ireland. 245 papers were presented. The conference marks **the third time a Conference of this Series was held in Ireland.** Main organizers: C.D. O'Dowd and P.E. Wagner. Proceedings were published by Springer-Verlag 2007.

2009. The 18th ICNAA was held during 10-14 August 2009 at Prague, Czech Republic. 253 scientists from 39 countries have attended, 247 papers were presented. A **Special Symposium on Biological Aerosols** was organized. Main organizers: J. Smolik and Colin O'Dowd.

2013. The 19th ICNAA was held during 23-28 June 2013 at Colorado State University, Fort Collins, CO, USA, again jointly with the Nucleation Symposium. 247 papers were presented. A **Special Symposium on the CLOUD Project at CERN** was organized. Main Organizers: P.J. DeMott and C.D. O'Dowd, American Institute of Physics Publishing, AIP Conference Proceedings Vol. 1527, Melville, NY 2013.

2017. The 20th ICNAA was held during 25-30 June 2017 at University of Helsinki, Finland. 220 papers were presented. Main organizers: H. Vehkamäki, P.J. DeMott and Antti Lauri. Papers published in Report Series in Aerosol Science No. 200 (Helsinki 2017) entitled Proceedings of the 20th ICNAA.

The subsequent Conference was delayed by 2 years because of the Covid Pandemic.

2023. The 21st ICNAA was held during 26-30 June 2023 at Brisbane, Australia. 133 papers were presented. This conference was **the first of this series held in Australia.** Main organizer: Zoran Ristovski. Papers published in Report Series in Aerosol Science No. 267 (Helsinki 2023) entitled Abstract Book of the 21st ICNAA, 26th-30th June 2023, Brisbane, Australia.

2025. The 22nd ICNAA is held during 24-29 August 2025 at University of Vienna, Austria. The conference marks **the third time a Conference of this Series was held at University of Vienna, Austria.**

Global distribution of the Conferences:

Europe (16) USA (4) Asia (1) Australia (1)



Figure 9. Participants in the 17th ICNAA, Galway, Ireland, 2007.

Chairs of the Committee on Nucleation and Atmospheric Aerosols (CNAA):

1965-1973: Josef Podzimek (founding Chair)
1973-1981: Hans-Walter Georgii
1981-1988: Gabor Vali
1988-1996: Paul Wagner
1996-2004: Markku Kulmala
2004-2013: Paul DeMott and Colin O'Dowd (co-Chairs)
2013-2018: Barbara Hale (stepped down for health reasons 22 November 2018)
2018-2025: Markku Kulmala (e-mail election 17 December 2018)

SUMMARY

The Series of ICNAA was started with gatherings of scientists interested in measurement of condensation nuclei in the atmosphere. Over the years investigations of ambient atmospheric aerosols were complemented by laboratory studies of nucleation applying new experimental techniques and theoretical models. The range of interest expanded to encompass topics from prenucleation clusters to global measurement and modeling of aerosols and their impact on clouds, precipitation and climate. Notably, Aitken's (1917) questions about activating atmospheric nuclei of different size and nature remain subject of current research.

In the spirit of Tom O'Connor (2007): Be part of this history.

REFERENCES

Aitken, J. (1880). On Dusts, Fogs and Clouds, *Proc. Roy. Soc. Ed.* **11**, 14.

Aitken, J. (1890). On a Simple Pocket Dust Counter, *Proc. Roy. Soc. Ed.* **18**, 39.

Aitken, J. (1917). On Some Nuclei of Cloudy Condensation. Part III, *Proc. Roy. Soc. Ed.* **37**, 215.

Coulier, P.J. (1875). Note sur une nouvelle propriete de l'air, *J. de Pharmacie et de Chimie, Paris (Ser. 4)* **22**, 165.

Ismail-Zadeh, A. and J.A. Joselyn (2019). IUGG: Beginning, Establishment and Early Development (1919-1939), *Hist. Geo- and Space Sci,* **10**, 25.

Nolan, P.J. and L.W. Pollak (1946), The Calibration of a Photo-Electric Nucleus Counter, *Proc. Roy. Irish Acad. Dublin (A)* **51**, 9.

O'Connor, T. (2007). International Nucleation and Atmospheric Aerosol Conference Series: A Brief History 1954-2007, in Proc. 17th International Conference on Nucleation and Atmospheric Aerosols, Galway, ed. by C.D. O'Dowd and P. Wagner (Springer), XIII.

Podzimek, J. (1989). John Aitken's Contribution to Atmospheric and Aerosol Sciences - One Hundred Years of Condensation Nuclei Counting, *Bull. Am. Meteor. Soc.* **70**, 1538.

Podzimek, J. (1993). In Memoriam Helmut Weickmann – A man and a scientist, *Atmos. Res.* **29**, 1.

Podzimek, J. (2000). Private communication.

Pollak, L.W. and T. Murphy (1952). Sampling of Condensation Nuclei by means of a Mobile Photo-Electric Counter, *Arch. Meteor. Geophys. Bioklimat. (A)* **5**, 100.

Pollak, L.W. and T. Murphy (1953). Comparison of Photoelectric Nuclei Counters, *Geofisika Pura e Appl.* **25**, 44.

Siksna, R. (1966). The 0 (Zeroth) International Symposium on the Condensation Nuclei – in Memory of L.W. Pollak, *J. Rech. Atmos.* **2**, 51.

Spurny, K.R. (2000). Atmospheric Condensation Nuclei - P.J. Coulier 1875 and J. Aitken 1880, *Aerosol. Sci. Technol.* **32**, 243.

Tyndall, J. (1869). On a New Series of Chemical Reactions Produced by Light, *Proc. Roy. Soc.* **17**, 93.

IMPACT OF HUMIDITY ON THE AEROSOL GROWTH BY METHANESULFONIC ACID

W. YU[1], R. BAALBAKI[1,2], J. DEVIVO[3], J. SHEN[1], L. CAUDILLO[4], E. SOMMER[5,6], X-C. HE[1], K. LEHTIPALO[1,7], and THE CLOUD COLLABORATION

[1]Institute for Atmospheric and Earth System Research/Physics, Faculty of Science, University of Helsinki, 00014 Helsinki, Finland

[2]Climate and Atmosphere Research Center (CARE-C), The Cyprus Institute, 2121, Nicosia, Cyprus

[3]Center for Atmospheric Particle Studies, Carnegie Mellon University, Pittsburgh, PA, USA

[4]Institute for Atmospheric and Environmental Sciences, Goethe University Frankfurt, Frankfurt am Main, Germany

[5]CERN, the European Organization for Nuclear Research, 1211 Geneva, Switzerland

[6]Faculty of Physics, University of Vienna, 1090 Vienna, Austria

[7]Finnish Meteorological Institute, 00560 Helsinki, Finland

Keywords: Methanesulfonic acid, Relative humidity, New particle formation, CLOUD experiment.

INTRODUCTION

The ocean absorbs approximately 90% of the excess heat trapped by greenhouse gases (Intergovernmental Panel on Climate Change (IPCC) AR5 WG1 2013), underscoring its significant role in the Earth's energy balance. Marine clouds further influence this balance by affecting the ocean's albedo through their high infrared emission and reflectivity. In the remote marine atmosphere, their formation depends largely on cloud condensation nuclei (CCN), which originate from airborne aerosol production and serve as the seeds of clouds (Twomey 1974, Murphy et al. 1998, de Jonge et al. 2024). One of the important contributors to aerosols in the marine atmosphere is dimethyl sulfide (DMS; CH_3SCH_3), an organic sulfur compound (Bates et al. 1992, Quinn et al. 2015).

Dimethyl sulfide is emitted into the atmosphere through the degradation of phytoplankton-produced dimethyl thiopropionate (Bates et al. 1992, Stefels et al. 2007, Carpenter et al. 2012). Its major oxidation products - sulfuric acid (H_2SO_4) and methanesulfonic acid ($CH_3S(O)_2OH$, MSA) (Andreae et al. 1985, Charlson et al. 1987, Bates et al. 1992, Ayers et al. 1996) - are key precursors for new particles formation in the marine and polar atmosphere (Kreidenweis & Seinfeld 1988, Covert et al. 1992, McMurry et al. 2005, Dawson et al. 2012, Beck et al. 2021). Understanding the mechanisms driving the new particle formation and initial growth from H_2SO_4 and MSA is therefore essential.

While most previous studies have focused on identifying the molecules responsible for new particle formation, the impact of environmental conditions such as temperature and humidity has received less attention. Among these factors, many earlier studies have investigated the effect of temperature on particle formation (Wyslouzil et al. 1991, Bork et al. 2014, Rörup et al. 2024). However, a quantitative understanding of how humidity influences particle growth remains scarce. Previously, one flowtube experiment conducted by Kreidenweis (Kreidenweis et al. 1989) investigated the RH effect qualitatively for MSA-H_2O system, showing that the measured particle number concentration increase by a factor of 10^4 with RH increase from 10 % to 50 %. However, the condition is not clear for the vapour concentration, and NH_3 level. Later, flowtube experiments further demonstrated that water plays an important role in particle formation within MSA (3×10^{10} to 5×10^{10} cm^{-3})

and NH_3 (18 ppb) or amines (TMA: 2.5 ppb and DMA: 2.5 ppb) system (Chen et al. 2015, 2016). However, due to experiment limitations, these studies could not eliminate NH_3, and the vapour concentrations used were significantly higher than those found in the real atmosphere. As a result, no direct, atmospheric-relevant experimental evidence exists for the role of RH in the new particle formation and early growth of MSA-H_2SO_4-H_2O clusters under low NH_3 conditions. This is particularly important in polar environments and the upper troposphere, where NH_3 concentrations are extremely low and MSA-H_2SO_4-H_2O may play a critical role in particle formation. Closing this gap will improve our understanding of atmospheric particle formation in these regions. Here, we used the CLOUD chamber to study the effect of RH on particle formation for MSA-H_2SO_4 under atmospherically relevant conditions.

METHODS

In this study, we conducted experiments in the CERN Cosmics Leaving Outdoor Droplets (CLOUD) chamber at different temperatures (+10°C, -10°C and -30°C) to investigate the effect of RH on particle formation and initial growth in the MSA-H_2SO_4-H_2O system.

The precursor gases (DMS and O_3) were continuously injected into the chamber. Once conditions stabilized, the lights in the chamber were switched on. Photolysis of O_3 initiated the oxidation of DMS, producing MSA and H_2SO_4. Particles were allowed to form in the chamber until a stable nucleation rate and the desired particle size growth were achieved. The intensity of the lights was varied to adjust MSA and H_2SO_4 concentrations in the chamber. Experiment 1,2 and 3 in **Figure 1** were under different ionization conditions: neutral (all ions swept from the chamber by high-voltage electrodes) and GCR (natural ionization from galactic cosmic rays, high-voltage electrodes off).

Relative humidity was measured using a chilled dew-point mirror Hygrometer (DewMaster; Edgetech Instruments). The DewMaster measured the dew point (above 0°C) or frost point (below 0°C) in the chamber. Relative humidity was then calculated as the ratio of the saturation vapour pressure at the dew point or frost point to the saturation vapour pressure at the actual chamber temperature, multiplied by 100. MSA and H_2SO_4 concentrations were measured using a nitrate chemical-ionization mass spectrometer. A Filter Inlet for Gases and AEROsols (FIGAERO) coupled with a chemical ionization mass spectrometer was used to analyse the chemical composition of particles. A wide range of aerosol instrumentation, including a scanning Particle Size Magnifier coupled with a butanol Condensation Particle Counter (PSM+CPC, Airmodus Ltd.), a Scanning Mobility Particle Sizer (SMPS, TSI Inc.), and a Neutral cluster and Air Ion Spectrometer (NAIS, Airel Ltd.) were deployed for a full-size range (1-530 nm) measurements of particle and ion size distributions.

RESULTS AND CONCLUSIONS

We present the experiments conducted at +10 °C in the CLOUD chamber, as shown in **Figure 1**. Panel A shows the particle size distribution measured by NAIS in negative particle mode, which was used to calculate the 3.2-8 nm growth rate. Panel B shows acid concentrations and particle nucleation rate at 1.7 nm ($J_{1.7}$).

The transition from neutral conditions (stage 1) to GCR (stage 2) did not affect the growth rate, as particles continued to grow at the same slope. The growth rate from stage 2 (GCR) at 16% RH is 5.3 nm h^{-1}, lower than the growth rate from stage 3 (GCR) at 50% RH, which is 7.4 nm h^{-1}, although the concentrations of H_2SO_4 and MSA were clearly higher in stage 2. If only the contribution of H_2SO_4 to particle growth is considered, the kinetic growth rate should be 5.23 nm h^{-1} and 3.33 nm h^{-1} for experiments 2 and 3, respectively (Stolzenburg et al. 2020, Yu et al. 2017). This accounts for the growth rate observed under the 16% RH condition. However, H_2SO_4 alone cannot explain the

growth rate under the 50% RH condition, suggesting that MSA also contributes to particle growth. This is further supported by FIGAERO measurements, which show a significantly higher fraction of MSA in the particle phase in experiment 3. In addition, the nucleation rate in experiment 3 was almost an order of magnitude higher than in experiment 2, indicating that RH also affects the initial clustering step in this chemical system.

In addition, we compared these results to a nano particle growth model (MABNAG). The model was used to simulate the particle growth under the experimental conditions and the results were compared with the measured values. The comparison revealed that the growth model could not accurately predict particle growth. Specifically, the model simulations using pure H_2SO_4 simulation could explain the measured growth rate at low RH, but not at high RH. When H_2SO_4 was combined with MSA, either treated as organic monoacid or H_2SO_4, the model could only replicate the growth rate at high RH. Our finding suggests that the current treatment of MSA in models is inadequate. To improve the growth model, further experiments are necessary to better constrain the growth rate and refine the treatment of MSA in simulations.

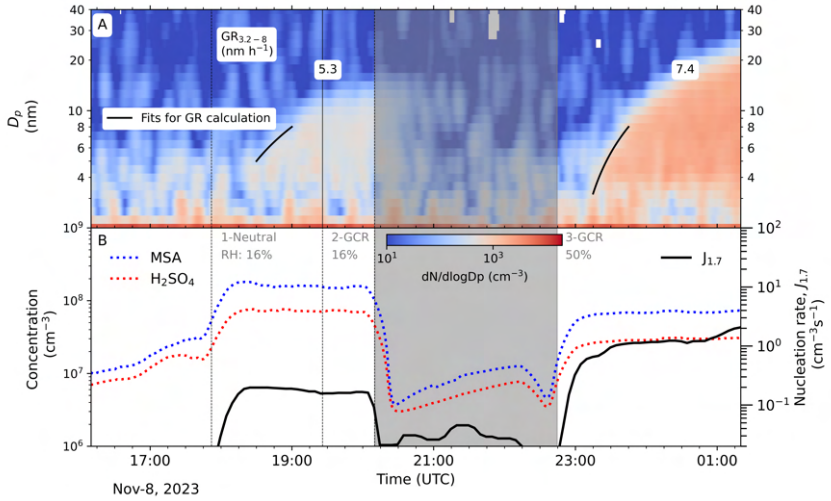


Figure 1: New particle formation experiment from DMS oxidation at +10°C. (A) The black lines depict the linear fits of 50 % appearance time of particles between 3.2 and 8.0 nm. (B) The concentration of MSA and H_2SO_4 in gas phase and particle nucleation rates at 1.7 nm. The vertical grey dashed lines and labels in panels A and B indicate the start of a new stage at which the experimental conditions were adjusted and the grey shadow represents cleaning stage.

The results are presented only at +10 °C here, further analysis at -10°C and -30°C will be showcasing later in the session.

ACKNOWLEDGEMENTS

This work was supported by European Organization for Nuclear Research (CERN), EU MSCA Project 101073026 — CLOUD-DOC. We thank everyone for contributing to the measurements at CLOUD.

REFERENCES

Andreae, M., Ferek, R., Bermond, F., Byrd, K., Engstrom, R., Hardin, S., Houmere, P., LeMarrec, F., Raemdonck, H. & Chatfield, R. (1985), 'Dimethyl sulfide in the marine atmosphere', *Journal of Geophysical Research: Atmospheres* **90**(D7), 12891–12900.

Ayers, G., Cainey, J., Granek, H. & Leck, C. (1996), 'Dimethylsulfide oxidation and the ratio of methanesulfonate to non sea-salt sulfate in the marine aerosol', *Journal of atmospheric chemistry* **25**, 307–325.

Bates, T., Lamb, B., Guenther, A., Dignon, J. & Stoiber, R. (1992), 'Sulfur emissions to the atmosphere from natural sourees', *Journal of Atmospheric Chemistry* **14**, 315–337.

Beck, L. J., Sarnela, N., Junninen, H., Hoppe, C. J., Garmash, O., Bianchi, F., Riva, M., Rose, C., Peräkylä, O., Wimmer, D. et al. (2021), 'Differing mechanisms of new particle formation at two arctic sites', *Geophysical Research Letters* **48**(4), e2020GL091334.

Bork, N., Elm, J., Olenius, T. & Vehkamäki, H. (2014), 'Methane sulfonic acid-enhanced formation of molecular clusters of sulfuric acid and dimethyl amine', *Atmospheric Chemistry and Physics* **14**(22), 12023–12030.

Carpenter, L. J., Archer, S. D. & Beale, R. (2012), 'Ocean-atmosphere trace gas exchange', *Chemical Society Reviews* **41**(19), 6473–6506.

Charlson, R. J., Lovelock, J. E., Andreae, M. O. & Warren, S. G. (1987), 'Oceanic phytoplankton, atmospheric sulphur, cloud albedo and climate', *Nature* **326**(6114), 655–661.

Chen, H., Benny, G. R. et al. (2016), 'Reactions of methanesulfonic acid with amines and ammonia as a source of new particles in air'.

Chen, H., Ezell, M. J., Arquero, K. D., Varner, M. E., Dawson, M. L., Gerber, R. B. & Finlayson-Pitts, B. J. (2015), 'New particle formation and growth from methanesulfonic acid, trimethylamine and water', *Physical Chemistry Chemical Physics* **17**(20), 13699–13709.

Covert, D. S., Kapustin, V. N., Quinn, P. K. & Bates, T. S. (1992), 'New particle formation in the marine boundary layer', *Journal of Geophysical Research: Atmospheres* **97**(D18), 20581–20589.

Dawson, M. L., Varner, M. E., Perraud, V., Ezell, M. J., Gerber, R. B. & Finlayson-Pitts, B. J. (2012), 'Simplified mechanism for new particle formation from methanesulfonic acid, amines, and water via experiments and ab initio calculations', *Proceedings of the National Academy of Sciences* **109**(46), 18719–18724.

de Jonge, R. W., Xavier, C., Olenius, T., Elm, J., Svenhag, C., Hyttinen, N., Nieradzik, L., Sarnela, N., Kristensson, A., Petaja, T. et al. (2024), 'Natural marine precursors boost continental new particle formation and production of cloud condensation nuclei', *Environmental Science & Technology* **58**(25), 10956–10968.

Intergovernmental Panel on Climate Change (IPCC) AR5 WG1 (2013), *Climate Change 2013: The Physical Science Basis*, Cambridge University Press.

Kreidenweis, S. M., Flagan, R. C., Seinfeld, J. H. & Okuyama, K. (1989), 'Binary nucleation of methanesulfonic acid and water', *Journal of aerosol science* **20**(5), 585–607.

Kreidenweis, S. M. & Seinfeld, J. H. (1988), 'Nucleation of sulfuric acid-water and methanesulfonic acid-water solution particles: implications for the atmospheric chemistry of organosulfur species', *Atmospheric Environment (1967)* **22**(2), 283–296.

McMurry, P., Fink, M., Sakurai, H., Stolzenburg, M., Mauldin III, R., Smith, J., Eisele, F., Moore, K., Sjostedt, S., Tanner, D. et al. (2005), 'A criterion for new particle formation in the sulfur-rich atlanta atmosphere', *Journal of Geophysical Research: Atmospheres* **110**(D22).

Murphy, D., Anderson, J., Quinn, P., McInnes, L., Brechtel, F., Kreidenweis, S., Middlebrook, A., Pósfai, M., Thomson, D. & Buseck, P. (1998), 'Influence of sea-salt on aerosol radiative properties in the southern ocean marine boundary layer', *Nature* **392**(6671), 62–65.

Quinn, P. K., Collins, D. B., Grassian, V. H., Prather, K. A. & Bates, T. S. (2015), 'Chemistry and related properties of freshly emitted sea spray aerosol', *Chemical reviews* **115**(10), 4383–4399.

Rörup, B., He, X.-C., Shen, J., Baalbaki, R., Dada, L., Sipilä, M., Kirkby, J., Kulmala, M., Amorim, A., Baccarini, A. et al. (2024), 'Temperature, humidity, and ionisation effect of iodine oxoacid nucleation', *Environmental science: atmospheres* **4**(5), 531–546.

Stefels, J., Steinke, M., Turner, S., Malin, G. & Belviso, S. (2007), 'Environmental constraints on the production and removal of the climatically active gas dimethylsulphide (dms) and implications for ecosystem modelling', *Biogeochemistry* **83**, 245–275.

Stolzenburg, D., Simon, M., Ranjithkumar, A., Kürten, A., Lehtipalo, K., Gordon, H., Ehrhart, S., Finkenzeller, H., Pichelstorfer, L., Nieminen, T. et al. (2020), 'Enhanced growth rate of atmospheric particles from sulfuric acid', *Atmospheric Chemistry and Physics* **20**(12), 7359–7372.

Twomey, S. (1974), 'Pollution and the planetary albedo', *Atmospheric Environment (1967)* **8**(12), 1251–1256.

Wyslouzil, B., Seinfeld, J., Flagan, R. & Okuyama, K. (1991), 'Binary nucleation in acid–water systems. i. methanesulfonic acid–water', *The Journal of chemical physics* **94**(10), 6827–6841.

Yu, H., Dai, L., Zhao, Y., Kanawade, V. P., Tripathi, S. N., Ge, X., Chen, M. & Lee, S.-H. (2017), 'Laboratory observations of temperature and humidity dependencies of nucleation and growth rates of sub-3 nm particles', *Journal of Geophysical Research: Atmospheres* **122**(3), 1919–1929.

Main Topic 2: Tropospheric & Stratospheric Aerosols

AEROSOLS IN AMAZONIA: PRIMARY PARTICLES, NEW PARTICLE FORMATION, CHEMICAL PRODUCTION, AND THE COMPLEX MIXTURE OF ALL THESE COMPONENTS

P. ARTAXO[1,2], L. V. RIZZO[1] L. A. MACHADO[1,4], B. B. MELLER[1], R. VALIATI[1], M. A. FRANCO[3], C. POHLKER[4]

[1]*Institute of Physics, University of São Paulo, Brazil*
[2] *Center for Amazonian Sustainability Studies, University of São Paulo, Brazil*
[3] *Institute of Astronomy, Geophysics and Atmospheric Sciences, University of São Paulo, Brazil*
[4] *Max Planck Institute for Chemistry, Mainz, Germany*

Keywords: AMAZONIA, BIOGENIC PARTICLES, NEW PARTICLE FORMATION.

INTRODUCTION

Amazonia is a complex region for understanding aerosol sources and deposition. In central Amazonia, aerosol sources, weather, and chemical processes create a highly variable aerosol population. The aerosols' optical properties, shaped by composition and size, determine sunlight interaction and the regional radiation budget, in addition to being a critical ingredient in carbon uptake by photosynthesis. The formation of these particles in pristine environments is not well understood. Climate change is altering various processes in the Amazonian atmosphere, characterized by reduced precipitation and an increase in extreme weather events (Artaxo et al., 2019, 2022).

Over the last decade, numerous large-scale airborne experiments, including SAMBBA, GoAmazon, Acridicon-Chuva, and CAFE-Brazil, among others, have generated a substantial amount of information on aerosol production and processing. Trace gases, such as ozone, NOx, and VOCs, are essential for interpreting aerosol processes. Convection and cloud vertical transport are also key ingredients of the aerosol population. The long-term operation of the 325-meter-tall Amazon Tall Tower Observatory (ATTO) is generating a great amount of information on aerosol properties (Andreae et al., 2015). At ATTO, we have been collecting data on optical properties and aerosol composition for more than a decade. We have also been continuously operating for 22 years, with seven AERONET sunphotometer sites providing a large number of inversion products. Remote sensing enables large-scale measurements of Aerosol Optical Depths across the entire basin. The wet season in Amazonia shows a very low aerosol concentration and is dominated by SOA from the oxidation of VOCs, as well as with primary biological particles. During the wet season, we also observe frequent events of Saharan dust transport that reach Central Amazonia, significantly increasing aerosol concentrations, especially in the coarse mode. In the dry season, the long-range transport of biomass-burning particles dominates the picture for the whole basin.

It is clear that deforestation and climate change are reducing the Amazon rainforest's capabilities to capture carbon and release moisture, disrupting its critical role in Earth's climate system. At the same time, biomass burning is altering the cloud regime with feedback mechanisms that are still not fully understood (Davidson et al., 2012).

METHODS

At the ATTO tower, measurements are being taken at several tower heights, as well as at the leading platforms at 325 and 60 meters. Aerodyne Aerosol Chemical Speciation Monitoring (ACSM) measures aerosol composition. Aethalometers and nephelometers measure light absorption and scattering. SMPS measures the aerosol size distribution. Reactive trace gases such as ozone, VOCs, and greenhouse gases are also measured continuously at several levels of the tower.

We also operate at ATTO a site called ATTO-Campina, a permanent observational site located in the central Amazon, approximately 4 km from the ATTO towers. Operational since 2020, ATTO-Campina focuses on characterizing atmospheric, cloud, and rainfall properties through remote sensing. The main instruments are: 1) Cloud Radar Profiler; 2) Radar Wind Profile; 3) Optical disdrometer; 4) Dual-

polarization X-band radar; 5) Microwave profiling radiometer; 6) Electric Field Mill; 7) Ceilometer; 8) CIMEL Solar/Lunar Photometer, among others. The site has been operational for four years.

RESULTS

Such an extensive long-term set of measurements is changing the way science knows the formation mechanisms as well as the deposition and processing of aerosol particles in Amazonia. New particle formation happens differently than in boreal forests (as discussed by Franco et al., 2022, and Machado et al., 2021). Sources that could explain growth events in the absence of deep convection are perhaps related to primary biogenic aerosols emitted by the forest, smooth entrainment of air masses from the free troposphere into the PBL in the early morning or even different meteorological mechanisms such as gravity waves and particle production by lightning in the free troposphere, as reported by Machado et al. (2021). Recent work also shows how rainfall events modify trace gas mixing ratios at ATTO (Machado et al., 2024). The production of nanoparticles in the upper troposphere has been well documented by Curtius et al. (2024) and Andreae et al. (2018). The primary biological aerosol particles produced directly by plants are also an important component in the aerosol population in Amazonia (Pöhlker et al., 2012) and can act as ice nuclei, feeding deep convective clouds.

Figure 1 illustrates the complex link between particle production close to the forest canopy to the vertical transport of VOCs (mostly isoprene), particle production at high troposphere (Curtis et al., 2024), and the cloud processing of these formed particles.

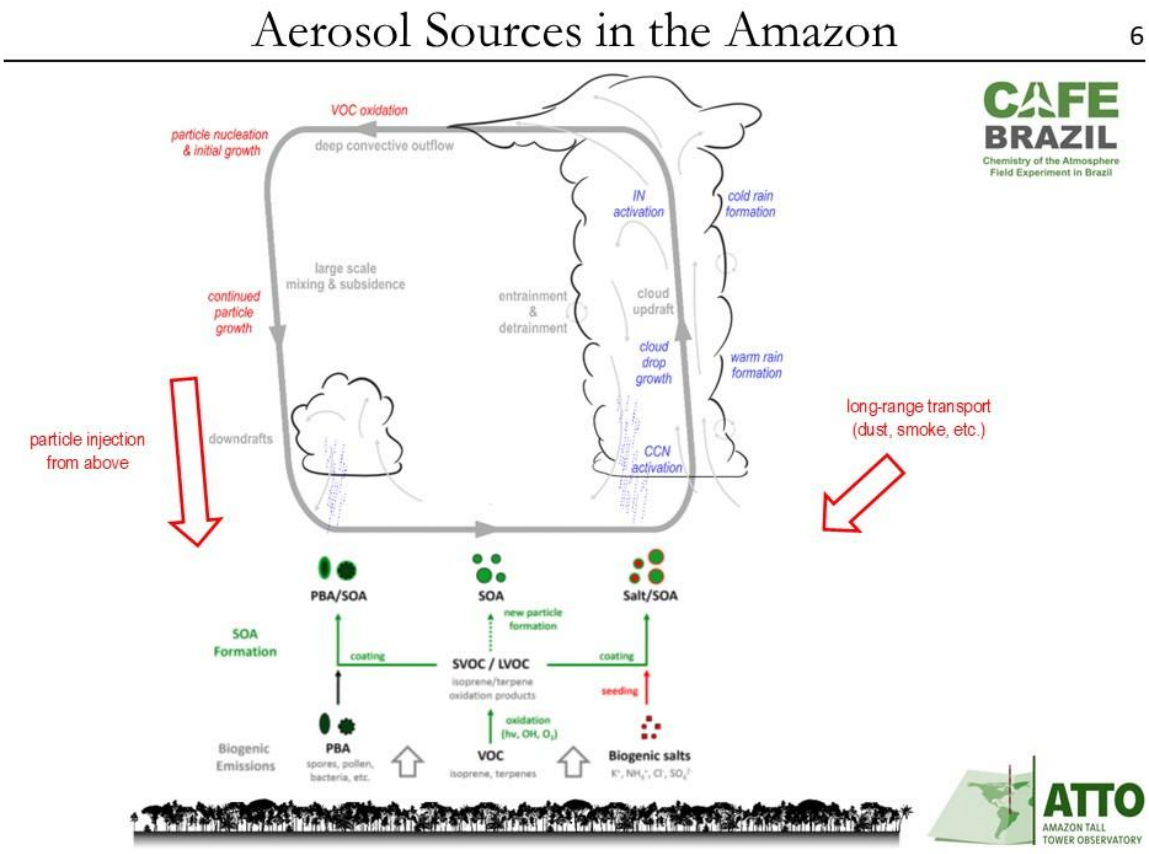


Figure 1. Aerosol sources and processing in Amazonia, derived from ATTO and CAFÉ-Brazil observations (From Christopher Pöhlker).

CONCLUSIONS

The production and evolution of Amazonian aerosols are highly complex, involving a range of biological and chemical processes, including cloud transport and processing. Recently, we have begun to understand the mechanisms of new particle formation in aerosols in Amazonia. Interactions with reactive trace gases, such as NOx produced by lightning, as well as ozone, also play a critical role in aerosol dynamics in Amazonia. We hope to continue operating the ATTO and ATTO-Campina sites in a collaborative manner (Artaxo et al., 2019), thereby establishing the connections between aerosol populations and ecosystem properties, as well as the intense hydrological cycle.

ACKNOWLEDGEMENTS

This work was supported by the São Paulo Research Foundation (FAPESP) (grants 2017-17047-0, 2022/07974-0, and 2023-04358-9) and the Conselho Nacional de Desenvolvimento Científico e Tecnológico (CNPq). ATTO and the work of Max Planck is supported by the Bundesministerium für Bildung und Forschung (BMBF contract nos. 01LB1001A, 01LK1602B, 01LK1602C, and 01LK2101B).

REFERENCES

Andreae, M. O. et al. Aerosol characteristics and particle production in the upper troposphere over the Amazon basin. Atmospheric Chem. Phys. 18, 921–961, DOI: 10.5194/acp-18-921-2018 (2018).

Andreae, M. O. et al. The Amazon Tall Tower Observatory (ATTO): Overview of pilot measurements on ecosystem ecology, meteorology, trace gases, and aerosols. Atmospheric Chem. Phys. 15, 10723–10776, DOI: 10.5194/acp-15-10723-2015 (2015).

Artaxo, P., Working together for Amazonia. Editorial Science Magazine, Vol. 363, Issue 6425, doi: 10.1126/science.aaw6986, (2019).

Artaxo, P. et al. Tropical and Boreal Forest – Atmosphere Interactions: A Review. Tellus B: Chem. Phys. Meteorol. 74, 24–163, DOI: 10.16993/tellusb.34 (2022).

Artaxo, P., et al., Atmospheric aerosols in Amazonia and land-use change: from natural biogenic to biomass burning conditions. Faraday Discussions, DOI:10.1039/C3FD00052D. (2013)

Curtius, J, et al., Isoprene nitrates drive new particle formation in Amazon's upper troposphere, Nature, 636, 124-130, 10.1038/s41586-024-08192-4, 2024.

Davidson, E. A. et al. The Amazon basin in Transition. *Nature* 481, 321–328 (2012).

Franco, M. A. et al. Occurrence and growth of sub-50nm aerosol particles in the Amazonian boundary layer. Atmospheric Chem. Phys. 22, 3469–3492, DOI: 10.5194/acp-22-3469-2022 (2022).

Machado, L. A. T. et al. How weather events modify aerosol particle size distributions in the Amazon boundary layer. Atmospheric Chem. Phys. 21, 18065–18086, DOI: 10.5194/acp-21-18065-2021 (2021).

Machado, L. A. T. et al. How rainfall events modify trace gas mixing ratios in central Amazonia. Atmos. Chem. Phys., 24, 8893–8910, 2024.

Pöhlker, C. et al. Biogenic potassium salt particles as seeds for secondary organic aerosol in the Amazon. Science 337, 1075–1078 (2012).

Wang, J. et al. Amazon boundary layer aerosol concentration sustained by vertical transport during rainfall. Nature 539, 416–419 (2016).

AEROSOL CHEMICAL COMPOSITION MEASURED IN THE UTLS OVER GERMANY IN WINTER 2018

PHILIPP BRAUNER[1], OLIVER APPEL[1,2], OLIVER EPPERS[1], FRANZISKA KÖLLNER[1,2], HANS-CHRISTIAN CLEMEN[1], KATHARINA KAISER[1], JOHANNES SCHNEIDER[1], HANS-CHRISTOPH LACHNITT[2], ANTONIS DRAGONEAS[1], ANDREAS HÜNIG[1,+], SERGEJ MOLLEKER[1], HANS SCHLAGER[3], CHRISTIANE VOIGT[2,3], YAFANG CHENG[4], BRUCE E. ANDERSON[5,*], and STEPHAN BORRMANN[1,2]

[1]*Particle Chemistry Department, Max Planck Institute for Chemistry, Mainz, Germany.*

[2]*Institute for Atmospheric Physics, Johannes Gutenberg University Mainz, Mainz, Germany.*

[3]*Institute of Atmospheric Physics, German Aerospace Center (DLR), Oberpfaffenhofen, Germany.*

[4]*Aerosol Chemistry Department, Max Planck Institute for Chemistry, Mainz, Germany.*

[5]*Science Directorate, NASA Langley Research Center, Hampton, USA.*

[+]*now at SCHOTT AG, Mainz, Germany.*

[*]*retired.*

Keywords: MASS SPECTROMETRY, AEROSOL, CHEMICAL COMPOSITION, CONTRAIL, UTLS.

INTRODUCTION

Aerosol particles have an impact on the Earth's radiation budget in two ways: they interact with solar and terrestrial radiation in a direct way but they can also act as cloud or ice nuclei forming clouds that affect the incoming shortwave and outgoing longwave radiation (Arias *et al.*, 2021). Besides aerosols of natural sources, anthropogenic sources such as commercial aircraft emissions contribute to the aerosol population in the extratropical upper troposphere and lower stratosphere (UTLS). However, the role of UTLS aerosol particles and the contribution of aircraft exhaust on the formation of e.g. cirrus and condensation trails (contrails) still needs further investigation. These cloud types can have positive as well as negative effect on climate forcing (Forster *et al.*, 2021). Here, we present chemical composition measurements of single particles in the UTLS region over Northern Germany in winter. We performed aircraft borne measurements in cloud-free air as well as inside cirrus and compare the results with those from aircraft exhaust plumes and contrails. In addition, mass concentrations of non-refractory species such as ammonium, chloride, nitrate, organics, and sulphate are analyzed.

METHODS

Airborne measurements were conducted during the "NASA and DLR Multidisciplinary Airborne eXperiments" (ND-MAX) in January and February 2018. The Advanced Technology Research Aircraft (ATRA) of the German Aerospace Center (DLR) was fueled with different blends of standard kerosene and alternative bio-based jet fuel. The ATRA, its exhaust plume and contrail were "chased" by the NASA DC-8 aircraft which was equipped with a comprehensive suite of instruments to measure trace gases, water vapor, and the chemicophysical properties of aerosol particles. In total, eight research flights were conducted out of the US and NATO Air Base Ramstein in Germany. The main sampling area was located over Northern Germany in two restricted air space areas close to the seaside. Interstitial aerosol particles

were sampled using a standard aerosol inlet, whereas cloud residual measurements were achieved using a counterflow virtual impactor. The hybrid mass spectrometer ERICA (ERC Instrument for the Chemical composition of Aerosols; Hünig *et al.*, 2022; Dragoneas *et al.*, 2022) was deployed for airborne measurements of the aerosol chemical composition. Single particles were detected in a size range of 174 nm to 3.2 µm by the laser ablation mass spectrometer ERICA-LAMS. Also, bulk measurements of non-refractory aerosol species were conducted for particles larger than 110 nm in diameter based on thermal desorption and subsequent electron-impact ionization (ERICA-AMS). We characterized different air masses of interest (exhaust plumes, contrails, atmospheric background, and cirrus) based on complementary measurements of aerosol as well as ice particle number concentrations and trace gas concentrations.

CONCLUSIONS

Our results reveal that biomass burning (BB) and carbon-containing particles dominated the wintertime UTLS region over Northern Germany. BB particles are partly assigned to North American wild fires using backward trajectory analysis. During measurements inside cirrus clouds, particle types like sea spray, mineral dust, and BB were most abundant in the cloud residuals. In contrast, particle types like elemental carbon, coated soot, and engine oil residues with sizes between 100 and 200 nm can be attributed to aircraft exhaust based on a distance analysis of the two involved airplanes. Besides this chemical signature of aircraft emissions, contrail residuals further contained aerosol particles of natural origin which were also dominant in cirrus clouds. We thus hypothesize that a significant fraction of contrail formation takes place under conditions of low supersaturation, only activating potential ice-nucleating particles. Under stratospheric influence, we observed an increase of organics and sulphate mass concentrations in the atmospheric background. While the origin of sulphur-containing particles in the stratospheric Junge layer is well-known (Kremser et al., 2016), the presence of organic material in the extratropical lower stratosphere is still matter of current research.

ACKNOWLEDGEMENTS

This research was supported by the Deutsche Forschungsgemeinschaft (grant nos. SSP HALO 1294, VO 1504/10-1, and TRR 301 – Project-ID 428312742). NASA support was provided by the NASA Aeronautics Advanced Air Transport Technologies Project within the Advanced Air Vehicles Program and the NASA Airborne Science Program within the Earth Science Division. Additional ground testing support was provided by the U.S. FAA Office of Energy and the Environment as well as Transport Canada. The work on ERICA was financed by the European Research Council under the EU's Seventh Framework Program (FP/2007-2013)/ERC Grant Agreement No.321040 ("EXCATRO") and supported by the Max Planck Society. Further financial support was received from the Max Plank Graduate Center. The authors thank the technical coordinators and all teams that were engaged in the field experiments.

REFERENCES

Arias, P., Bellouin, N., Coppola, E., *et al.* (2021). *"Technical Summary." Climate Change 2021: The Physical Science Basis. Contribution of Working Group I to the Sixth Assessment Report of the Intergovernmental Panel on Climate Change,* (Cambridge University Press, Cambridge, U.K. and New York, NY, USA), https://doi.org/10.1017/9781009157896.002.

Forster, P., Storelvmo, T., Armour, K., et al. (2021). "*The Earth's Energy Budget, Climate Feedbacks, and Climate Sensitivity*." *Climate Change 2021: The Physical Science Basis. Contribution of Working Group I to the Sixth Assessment Report of the Intergovernmental Panel on Climate Change*, (Cambridge University Press, Cambridge, U.K. and New York, NY, USA), https://doi.org/10.1017/9781009157896.009.

Hünig, A., Appel, O., Dragoneas, A., *et al.* (2022). Design, characterization, and first field deployment of a novel aircraft-based aerosol mass spectrometer combining the laser ablation and flash vaporization techniques, *Atmos. Meas. Tech.* **15**, 2889-2921, https://doi.org/10.5194/amt-15-2889-2022.

Dragoneas, A., Molleker, S., Appel, O., *et al.* (2022). The realization of autonomous, aircraft-based, real-time aerosol mass spectrometry in the upper troposphere and lower stratosphere, *Atmos. Meas. Tech.* **15**, 5719–5742, https://doi.org/10.5194/amt-15-5719-2022.

Kremser, S., Thomason, L.W., von Hobe, M., *et al.* (2016). "Stratospheric aerosol—Observations, processes, and impact on climate." *Rev. Geophys.* **54**, 278–335, https://doi.org/10.1002/2015RG000511.

MODELLING THE IMPACT OF ANTHROPOGENIC AEROSOLS ON CCN CONCENTRATIONS OVER A RURAL BOREAL FOREST ENVIRONMENT

P. CLUSIUS[1], M. BAYKARA[2], C. XAVIER[3,4], P. ZHOU[1], J. TYREE[1], B. FOREBACK[1,6], M. ÄIJÄLÄ[6,1], F. GRAEFFE[1], T. PETÄJÄ[1], M. KULMALA[1], P. PAASONEN[1], P. I. PALMER[5], M. BOY[1,6,7]

[1]*Institute for Atmospheric and Earth Systems Research, University of Helsinki, P.O. Box 64, 00014 Helsinki, Finland*
[2]*Climate and Marine Sciences Department, Eurasia Institute of Earth Sciences, Istanbul Technical University, Maslak, Istanbul, 34469, Turkey*
[3]*Department of Physics, Lund University, SE-22100 Lund, Sweden*
[4]*Research Department, Swedish Meteorological and Hydrological Institute, SE-60176 Norrköping, Sweden*
[5]*School of GeoSciences, University of Edinburgh, Edinburgh, UK*
[6]*Atmospheric Modelling Centre – Lahti, Lahti University Campus, Lahti, Finland*
[7]*School of Energy Systems, Lappeenranta-Lahti University of Technology, Lappeenranta, 53850, Finland*

Keywords: Atmospheric modelling, CCN, new particle formation, SOA, aerosol emissions.

INTRODUCTION

The radiative properties of clouds depend partially on the cloud droplet number concentration, which is determined by the concentration of cloud condensation nuclei (CCN) when the clouds are formed. In turn, CCN concentrations are determined by the atmospheric particle size distribution and their chemical composition. New particle formation from atmospheric cluster formation and their eventual growth by organic and inorganic compounds over boreal forest is estimated to account for 10–90 % of observed particle number concentrations. Consequently, the cloud condensation nuclei (CCN) concentrations are affected by the secondary aerosol formation. There is observational evidence that increased temperatures and BVOC emissions in the environments where SOA is formed correlate with increased downstream CCN concentration (e.g. Riipinen *et al.*, 2011; Paasonen *et al*., 2013; Petäjä *et al*., 2021; Yli-Juuti *et al*., 2021). This could result into longer cloud lifetime and negative aerosol indirect forcing. However, increased temperatures, BVOC and aerosol emissions often correlate with geographical origins and consequently with long distance transport. In this work we test the coupling of SOA mass and CCN concentrations, and investigate how much CCN is affected by new particle formation and anthropogenic aerosol emissions. We use a Lagrangian model SOSAA-FLEXPART to investigate the origins and composition of the CCN that are observed at the SMEAR II station during March–October 2018.

METHODS

The SOSAA-FLEXPART model uses backwards airmass trajectories and emission data together with detailed atmospheric chemistry scheme and aerosol dynamics, and allows pinpointing the various sources and processes that lead to observed CCN downstream. The model framework combines: a) global emission datasets, b) backward trajectories from the FLEXible PARTicle dispersion model (FLEXPART, Pisso *et al.*, 2019) airmass dispersion model, c) a detailed description of atmospheric chemistry and aerosol dynamics from the Model to Simulate the Concentration of Organic Vapours, Sulphuric Acid and Aerosol Particles (SOSAA, e.g., Chen *et al.* 2021). We apply this SOSAA-FP (FP standing for FLEXPART) framework to simulate a period from March to October 2018 with one hour time resolution, focusing on the concentrations of CCN between 0.1–1.2 % maximum supersaturation as calculated by the κ-Köhler theory (with respective dry particle diameter of activation ca. 175–35 nm).

RESULTS

We find that the model PM_1 fraction of primary particles, sulfates and secondary organic aerosol correlate well with the observed organic aerosol and sulfate trends and explain most of the observed organic aerosol and sulfate PM_1 mass. Our results show that primary particle emissions play a considerable role in CCN concentrations even at a rural site such as SMEAR II, particularly for the lower supersaturation (0.1%–0.4%), where the anthropogenic aerosol emissions accounted for more than half of the CCN.

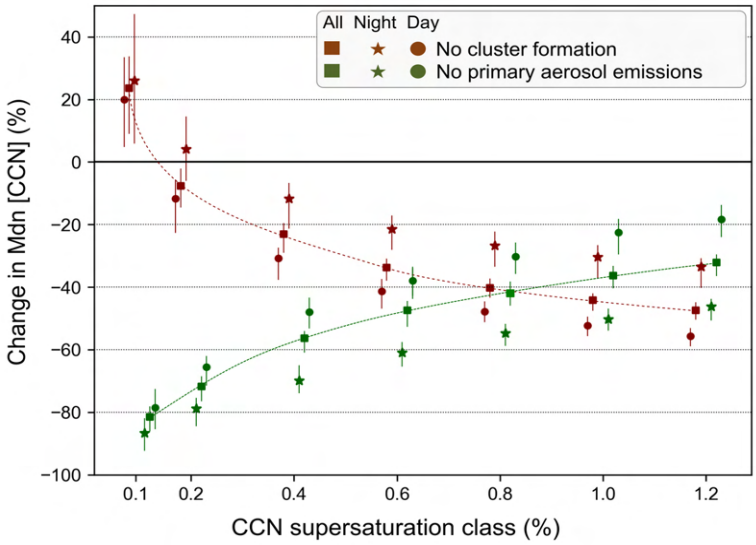


Figure 1: Relative change in median CCN number concentrations during the study period, when cluster formation (red markers) or anthropogenic particle emissions (green markers) were turned off in the model. The data is aggregated to nighttime (21–07 local time, marked with star symbol), daytime (08–20 local time, marked with round symbol) and daily concentrations (marked with squares). The vertical range represents 95 % confidence intervals of the median, obtained from bootstrapping. The spline fits for daily change of medians are provided for visual aid only.

Changes in atmospheric cluster formation rates had a relatively weak impact on the CCN concentrations in the sensitivity runs. Enhanced cluster formation increased (decreased) the CCN concentrations for the highest (lowest) maximum supersaturation. Without any cluster formation our modelled median CCN concentrations changed by –48 % and +23 % for supersaturations of 1.2 % and 0.1 %, respectively, whereas omitting primary particle emissions had a decreasing effect in all calculated CCN supersaturation classes (–82 % and –33 % decrease in median CCN of 1.2 % and 0.1 % supersaturation, respectively, Fig. 1). While the enhancing effect of cluster formation to high supersaturation (i.e., small diameter) CCN concentrations is unsurprising, the weak sensitivity to cluster formation rates and the decreasing effect to lowest supersaturation CCN was unexpected, as was the strong influence of anthropogenic primary emissions.

CONCLUSIONS

The Lagrangian model framework showed its power, as it was possible to identify different modes of CCN formation. The CCN concentrations were affected by both new particle formation and aerosol emissions, with distinct periods where one process was dominating. For example, high SOA and CCN was seen when airmasses arrived from the south-easterly direction, with relatively weak new particle formation but increased primary emissions. On other occasions, airmasses from westerly direction showed stronger new particle formation and subsequent growth to CCN sizes. Primary aerosol emissions affected strongly

on the accumulation mode concentrations, and consequently suppress new particle formation. Primary aerosols contributed substantially to PM_1, especially outside growth season.

ACKNOWLEDGEMENTS

The authors wish to thank the Finnish CSC – IT Center for Science Ltd. for providíng invaluable HPC resources for this study. PC gratefully acknowledges the University of Edinburgh and University of Helsinki Partnership Programme on Forests. We acknowledge the FLEXPART development team (FlexTeam, University of Vienna; flex team.univie.ac.at).

REFERENCES

Chen, D., Xavier, C., Clusius, P., Nieminen, T., Roldin, P., Qi, X., Pichelstorfer, L., Kulmala, M., Rantala, P., Aalto, J., Sarnela, N., Kolari, P., Keronen, P., Rissanen, M. P., Taipale, D., Foreback, B., Baykara, M., Zhou, P. and Boy, M.: A modelling study of OH, NO3 and H2SO4 in 2007–2018 at SMEAR II, Finland: analysis of long-term trends, Environmental Science: Atmospheres, 1, 449-472, 10.1039/d1ea00020a, 2021.

Paasonen, P., Asmi, A., Petäjä, T., Kajos, M. K., Äijälä, M., Junninen, H., Holst, T., Abbatt, J. P. D., Arneth, A., Birmili, W., van der Gon, H. D., Hamed, A., Hoffer, A., Laakso, L., Laaksonen, A., Richard Leaitch, W., Plass-Dülmer, C., Pryor, S. C., Räisänen, P., Swietlicki, E., Wiedensohler, A., Worsnop, D. R., Kerminen, V.-M. and Kulmala, M.: Warming-induced increase in aerosol number concentration likely to moderate climate change, Nat. Geosci., 6, 438-442, 10.1038/ngeo1800, 2013.

Petäjä, T., Tabakova, K., Manninen, A., Ezhova, E., O'Connor, E., Moisseev, D., Sinclair, V. A., Backman, J., Levula, J., Luoma, K., Virkkula, A., Paramonov, M., Räty, M., Äijälä, M., Heikkinen, L., Ehn, M., Sipilä, M., Yli-Juuti, T., Virtanen, A., Ritsche, M., Hickmon, N., Pulik, G., Rosenfeld, D., Worsnop, D. R., Bäck, J., Kulmala, M. and Kerminen, V.-M.: Influence of biogenic emissions from boreal forests on aerosol–cloud interactions, Nat. Geosci., 15, 42-47, 10.1038/s41561-021-00876-0, 2021.

Pisso, I., Sollum, E., Grythe, H., Kristiansen, N. I., Cassiani, M., Eckhardt, S., Arnold, D., Morton, D., Thompson, R. L., Groot Zwaaftink, C. D., Evangeliou, N., Sodemann, H., Haimberger, L., Henne, S., Brunner, D., Burkhart, J. F., Fouilloux, A., Brioude, J., Philipp, A., Seibert, P. and Stohl, A.: The Lagrangian particle dispersion model FLEXPART version 10.4, Geosci. Model Dev., 12, 4955-4997, 10.5194/gmd-12-4955-2019, 2019.

Riipinen, I., Pierce, J. R., Yli-Juuti, T., Nieminen, T., Häkkinen, S., Ehn, M., Junninen, H., Lehtipalo, K., Petäjä, T., Slowik, J., Chang, R., Shantz, N. C., Abbatt, J., Leaitch, W. R., Kerminen, V.-M., Worsnop, D. R., Pandis, S. N., Donahue, N. M. and Kulmala, M.: Organic condensation: a vital link connecting aerosol formation to cloud condensation nuclei (CCN) concentrations, Atmos. Chem. Phys., 11, 3865-3878, 10.5194/acp-11-3865-2011, 2011.

Yli-Juuti, T., Mielonen, T., Heikkinen, L., Arola, A., Ehn, M., Isokääntä, S., Keskinen, H.-M., Kulmala, M., Laakso, A., Lipponen, A., Luoma, K., Mikkonen, S., Nieminen, T., Paasonen, P., Petäjä, T., Romakkaniemi, S., Tonttila, J., Kokkola, H. and Virtanen, A.: Significance of the organic aerosol driven climate feedback in the boreal area, Nat. Commun., 12, 10.1038/s41467-021-25850-7, 2021.

DEEP CONVECTION LEADS TO ULTRAFINE PARTICLE FORMATION AND GROWTH AT CONTINENTAL MID-LATITUDES

M. E. COOKE [1] and J. N. SMITH[1]

[1]*Department of Chemistry, University of California at Irvine, California, United States.*

Keywords: upper-troposphere, sulfuric acid, new particle formation

INTRODUCTION

Ultrafine aerosol particles, particles with an aerodynamic diameter (d_a) less than 100 nm, have significant impacts on global climate and weather due to their ability to nucleate cloud formation. Cloud droplet nucleation by ultrafine particles results in the formation of a large number of small cloud droplets, influencing the cloud reflectivity and lifetime (Rosenfeld 2000). The majority of ultrafine particles are formed from new particle formation events, in which low-volatility vapors (e.g., sulfuric acid, highly oxidized organic compounds) condense to form molecular clusters (Ehn, Thornton et al. 2014). Subsequent condensation results in growth to nanoparticles, which can act as cloud nuclei after growing to d_a of ~50 nm. In the upper troposphere, with limited sources of aerosol particles, up to 91% of cloud condensation nuclei are estimated to originate from new particle formation (Gordon, Kirkby et al. 2017).

Ultrafine particles in the upper troposphere have been measured across the globe. Numerous studies have measured large concentrations of ultrafine particles in the tropical upper troposphere, including the Amazon (Krejci, Ström et al. 2003, Andreae, Afchine et al. 2018, Shen, Russell et al. 2024), the Pacific and Atlantic Oceans (Williamson, Kupc et al. 2019), and Central America (Weigel, Borrmann et al. 2011). Despite the number of studies conducted on ultrafine particle formation in the upper troposphere, the majority of research has focused on tropical regions and few measurements have been conducted on ultrafine particles in the upper troposphere at mid-latitudes (Twohy, Clement et al. 2002, Young, Benson et al. 2007).

Many campaigns that measured ultrafine particle number concentrations in the upper troposphere include supporting measurements of particle composition (Twohy, Clement et al. 2002, Andreae, Afchine et al. 2018) or gas-phase precursors (Curtius, Heinritzi et al. 2024), indicating these particles originate from new particle formation events rather than transport from the boundary layer. For example, several studies have demonstrated that deep convection over the Amazon can transport biogenic volatile organic compounds from the boundary layer to the upper troposphere, and that these vapors can condense to form new particles in the convective outflow (Andreae, Afchine et al. 2018, Curtius, Heinritzi et al. 2024). Deep convection occurs nearly daily across the central United States during the summertime (Carbone 2002), and it is possible that analogous processes result in substantial new particle formation in the upper troposphere of this region. However, it remains unclear the extent to which convection influences ultrafine particle formation and composition in this region.

METHODS

The Deep Convective Clouds and Chemistry Campaign (DC3) was conducted from May to June of 2012. Flights were performed across the Southeastern, Midwestern, and Great Plains region of the United States with two research aircrafts, the NSF-NCAR-GV and the NASA-DC8. The goal of the campaign was to assess how deep convection influences the chemistry of the upper troposphere. For the majority of the flights, the DC-8 aircraft transversed the inflow region of the storm, and the GV followed the outflow of the air parcel from the convection event. A detailed list of instruments aboard each aircraft were previously provided (Barth, Cantrell et al. 2015). This study focuses on measurements conducted aboard the GV aircraft.

A custom-built scanning mobility particle sizer (SMPS) was used to conduct aircraft measurements of ultrafine particles with aerodynamic diameter (d_a) ranging from 8 to ~200 nm. In short, the SMPS measures particle size distributions using electrical mobility (Wang and Flagan 1990). This instrument's

design as well as an evaluation of its operation at high altitudes was discussed in detail previously (Ortega, Snider et al. 2019). Several modifications were made to the SMPS to adjust for flight measurements. At high altitudes, changes in pressure impact the stability of the flows of a traditional SMPS. For the GV-SMPS, the sheath air is controlled using a mass flow controller, which can successfully adjust the flows to steady state quickly with changing pressure, as shown previously (Ortega, Snider et al. 2019). The polydisperse, monodisperse, and excess flows are controlled using a series of flow restrictors. The condensation particle counter (CPC) was adjusted for high altitude operation to more efficiently measure nanoparticles under low pressure conditions (M. Hermann 2001).

A suite of instruments aboard both aircrafts (DC8 and GV) additionally monitored the composition of atmospheric gases, and a detailed list of these measurements was described previously (Barth, Cantrell et al. 2015). In this work, gas-phase measurements are used to assess the factors contributing to ultrafine particle formation and growth. The measurements analyzed include SO_2, from the Georgia Tech Chemical Ionization Mass Spectrometer (GTCIMS); CO, from the Aero-Laser VUV Resonance Fluorescence Carbon Monoxide instrument; and OH, from the Thermal Dissociation Laser Induced Fluorescence instrument.

Direct measurements of sulfuric acid were not conducted during the DC3 campaign. Therefore, to assess the potential for sulfuric acid to contribute to the observed formation and growth of ultrafine particles, [H_2SO_4] was estimated based on a proxy method described previously (Dada, Ylivinkka et al. 2020). The proxy calculation is based on the assumption that H_2SO_4 formation and loss processes are in steady state and that the formation of H_2SO_4 in the atmosphere predominantly occurs from the reaction of SO_2 and OH. As previously, two loss processes were included in the estimate: condensation to existing particles and loss due to molecular cluster formation. Overall, the sulfuric acid concentrations during the flights were estimated using the equation below.

$$[H_2SO_4] = -\frac{CS}{2k_3} + \sqrt{(\frac{CS}{2k_3})^2 + \frac{[SO_2]}{k_3}(k_1[OH])} \quad \textbf{(Eqn. 1)}$$

CONCLUSIONS

Across the DC3 campaign, a total of twenty-one flights were conducted with the GV aircraft, and all twenty-one included measurements of ultrafine particles using the custom-built SMPS described above. For the majority of the flights (~70%), an average $N_{8\text{-}100nm}$ between 10 – 500 cm^{-3} was measured. Three flights had elevated $N_{8\text{-}100nm}$ (> 1000 cm^{-3}), reaching maximum $N_{8\text{-}100nm}$ values of 5 $\times 10^3$ cm^{-3} (RF6), 9 $\times 10^3$ cm^{-3} (RF7), and 2 $\times 10^4$ cm^{-1} (RF16). A similar trend was observed for the smallest class of particles measured, $N_{8\text{-}20nm}$, with an average $N_{8\text{-}20nm}$ between 10 – 500 cm^{-3} for ~60% of the flights. Flights with elevated $N_{8\text{-}100nm}$ exhibited a similar trend for $N_{8\text{-}20nm}$, reaching values up to 1 $\times 10^3$ cm^{-3} (RF6), 7 $\times 10^3$ cm^{-3} (RF7), and 2 $\times 10^4$ cm^{-3} (RF16). Across all flights, the greatest number concentration of particles was measured in the upper troposphere from ~8 – 12 km. Overall, trends for $N_{8\text{-}100nm}$ and $N_{8\text{-}20nm}$ appear similar, with slightly higher $N_{8\text{-}20nm}$ populated in this region of the upper troposphere.

To investigate the factors contributing to the formation of the ultrafine particles measured during DC3 flights in the upper-troposphere, four case study days were selected for in-depth analysis. To select the case study flights in which upper-tropospheric new particle formation most likely occurred, the percentage of SMPS measurements for each flight for which $N_{8\text{-}20nm} > 100$ # cm^{-3} at an altitude > 8 km. Three case study flights were selected in which the majority of the measurements met these criteria (RF6, 60%; RF7, 50%; and RF16, 96%).

The first case study day, RF6, took place on 29 May 2012 in northern Oklahoma. On this day, intense convection occurred in northern and central Oklahoma, including supercell storms characterized by strong winds and an enhanced Fujita scale 1 tornado. The second case study day, RF7, took place the following day, 30 May 2012. On this flight, instrumentation on the GV measured the aged outflow from the previous day's convection; the flight trajectory of RF7 followed the air parcel as it moved towards the southeastern United States. The third case study day, RF16, took place on 21 June 2012. Similar to RF7, the purpose of this flight was to measure aged outflow from the previous day's multicell convection system, which developed overnight in Nebraska and dissipated in Missouri in the early morning. Overall, the case

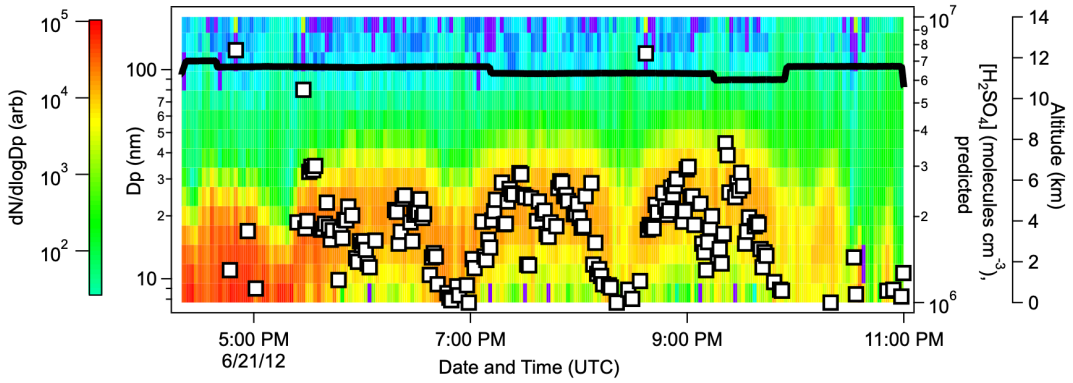


Figure 1. Size-resolved particle counts across the research flights for an example case study day, RF16. Square boxes overlayed on the image plot represent the time-resovled estimate [H_2SO_4] during the flights. The black line shows the altitude.

study days include a flight that occurred during a convection event (RF6) and two flights targeting measurements of aged outflow the day after an event occurred (RF7, RF16).

An example of the size-resolved concentrations (dN/dlogDp) of ultrafine particles measured during the one of the case study days, RF16, is shown in Figure 1. This flight exhibits high concentrations of ultrafine particles at high altitudes. All of the case study research flights show a clear increase in the concentration of ultrafine particles at altitudes > 8 km. For RF6, the majority of the particles are in the smallest size range d_a < ~20 nm. In contrast, larger particles are observed for the two flights that measured the aged outflow the day after an event occurred, RF7 and RF16. For these flights, high concentrations observed at particle sizes up to d_a ~ 40nm.

For all three flights, high levels of SO_2 were measured in these high-altitude regions with elevated number concentrations of ultrafine particles. It is possible that this SO_2, after being transported from the polluted boundary layer to the upper-troposphere from deep convection, can react with OH to form sulfuric acid. As described above, the [H_2SO_4] was estimated based on that previously described (Dada, Ylivinkka et al. 2020). The estimate [H_2SO_4] is overlayed onto the image plot of the size-resolved particle number concentrations for RF16 in Figure 1. Interestingly, the predicted [H_2SO_4] seems to follow the same trends as the particle counts, with elevated [H_2SO_4] predictions coinciding with measurements of elevated ultrafine particle counts.

Overall, these results demonstrate that deep convection likely influences ultrafine particle formation in the mid-latitude regions, particularly in the summertime in the Southeastern United States, when thunderstorm events occur frequently. Our results suggest that sulfuric acid plays a part in the particle formation, potentially participating in nucleation and/or subsequent growth. Future measurements are needed to constrain the role that sulfuric acid plays in these events, particularly measurements of ultrafine particle composition.

ACKNOWLEDGEMENTS

Data provided by NCAR EOL under the sponsorship of the National Science Foundation. https://data.eol.ucar.edu. The National Science Foundation is acknowledged for funding M.E.C. under grant number # 2324901.

REFERENCES

Andreae, M. O., et al. (2018). "Aerosol characteristics and particle production in the upper troposphere over the Amazon Basin." Atmospheric Chemistry and Physics **18**(2): 921-961.

Barth, M. C., et al. (2015). "The Deep Convective Clouds and Chemistry (DC3) Field Campaign." Bulletin of the American Meteorological Society **96**(8): 1281-1309.
Carbone, R. E. T., J. D.; Ahijevych, D. A.; Trier, S. B. (2002). "Inferences of Predictability Associated with Warm Season Precipitation Episodes." Journal of the Atmospheric Sciences **59**(13): 2033-2056.
Curtius, J., et al. (2024). "Isoprene nitrates drive new particle formation in Amazon's upper troposphere." Nature **636**(8041): 124-130.
Dada, L., et al. (2020). "Sources and sinks driving sulfuric acid concentrations in contrasting environments: implications on proxy calculations." Atmospheric Chemistry and Physics **20**(20): 11747-11766.
Ehn, M., et al. (2014). "A large source of low-volatility secondary organic aerosol." Nature **506**(7489): 476-479.
Gordon, H., et al. (2017). "Causes and importance of new particle formation in the present-day and preindustrial atmospheres." Journal of Geophysical Research: Atmospheres **122**(16): 8739-8760.
Krejci, R., et al. (2003). "Evolution of aerosol properties over the rain forest in Surinam, South America, observed from aircraft during the LBA-CLAIRE 98 experiment." Journal of Geophysical Research: Atmospheres **108**(D18).
M. Hermann, A. W. (2001). "Counting efficiency of condensation particle counters at low-pressures with illustrative data from the upper troposphere." Journal of Aerosol Science **32**: 975-991.
Ortega, J., et al. (2019). "Comparison of aerosol measurement systems during the 2016 airborne ARISTO campaign." Aerosol Science and Technology **53**(8): 871-885.
Rosenfeld, D. (2000). "Suppression of rain and snow by urban and industrial air pollution." Science **287**(5459): 1793-1796.
Shen, J., et al. (2024). "New particle formation from isoprene under upper-tropospheric conditions." Nature **636**(8041): 115-123.
Twohy, C. H., et al. (2002). "Deep convection as a source of new particles in the midlatitude upper troposphere." Journal of Geophysical Research: Atmospheres **107**(D21).
Wang, S. C. and R. C. Flagan (1990). "Scanning Electrical Mobility Spectrometer." Aerosol Science and Technology **13**(2): 230-240.
Weigel, R., et al. (2011). "In situ observations of new particle formation in the tropical upper troposphere: the role of clouds and the nucleation mechanism." Atmospheric Chemistry and Physics **11**(18): 9983-10010.
Williamson, C. J., et al. (2019). "A large source of cloud condensation nuclei from new particle formation in the tropics." Nature **574**(7778): 399-403.
Young, L. H., et al. (2007). "Enhanced new particle formation observed in the northern midlatitude tropopause region." Journal of Geophysical Research: Atmospheres **112**(D10).

ISOPRENE DRIVES NEW PARTICLE FORMATION IN THE TROPICAL UPPER TROPOSPHERE

J. CURTIUS[1], M. HEINRITZI[1], L. BECK[1], M.L. PÖHLKER[2,3], N. TRIPATHI[4], B.E. KRUMM[4], P. HOLZBECK[4], C. M. NUSSBAUMER[4], L. HERNÁNDEZ PARDO[1], T. KLIMACH[4], K. BARMPOUNIS[2,4,5], R.I. ALBRECHT[6], M. O. ANDREAE[4,7,8], P. ARTAXO[9], J. N. CROWLEY[4], H. FISCHER[4], H. HARDER[4], D. L. HERDIES[10], M. HEWSON[11], L. A. T. MACHADO[12,4], C. PÖHLKER[4], U. PÖSCHL[4], A. POSSNER[1], J. SCHNEIDER[4], J. WILLIAMS[4,13], J. LELIEVELD[4,13], AND THE CAFE-TEAM

[1]*Institute for Atmospheric and Environmental Sciences, Goethe University Frankfurt, Frankfurt, Germany*
[2]*Atmospheric Microphysics Department, Leibniz Institute for Tropospheric Research, Leipzig, Germany*
[3]*Faculty of Physics and Earth Sciences, Institute for Meteorology, Leipzig University, Leipzig, Germany*
[4]*Max Planck Institute for Chemistry, Mainz, Germany*
[5]*Lemon Labs Ltd., Nicosia, Cyprus*
[6]*Institute of Astronomy, Geophysics and Atmospheric Sciences, University of São Paulo, São Paulo, Brazil*
[7]*Department of Geology and Geophysics, King Saud University, Riyadh, Saudi Arabia*
[8]*Scripps Institution of Oceanography, UCSD, La Jolla, California, USA*
[9]*Center for Amazonian Sustainability, CEAS - University of São Paulo, Brazil*
[10]*National Institute for Space Research, Cachoeira Paulista, SP, Brazil*
[11]*CQUniversity Australia, Rockhampton, North QLD, Australia*
[12]*Instituto de Física da USP, Cidade Universitária, São Paulo, Brazil*
[13]*Climate and Atmosphere Research Center, The Cyprus Institute, Nicosia, Cyprus*

Keywords: Isoprene, nucleation, new particle formation, outflow, tropical upper troposphere.

INTRODUCTION

Global isoprene emissions by vegetation amount to more than 500 million tons per year, which represents by far the largest emission of biogenic volatile organic compounds (Guenther *et al.*, 2012). The largest fraction of these emissions occurs in tropical rain forests (Sindelarova *et al.*, 2014). Until now, it was assumed that the volatility of the isoprene oxidation products is not low enough to form new particles in the atmosphere, and that isoprene rather inhibits aerosol nucleation (Kiendler-Scharr, 2009).
Strong new particle formation has been observed to occur in the tropical upper troposphere over the Amazon (Andreae *et al.*, 2018). It was hypothesized that these particles are formed from organic precursors such as isoprene (Ekman *et al.*, 2008), or monoterpenes like alpha-pinene or limonene (Kirkby *et al.*, 2016, Andreae *et al.*, 2018), but no direct measurements of the chemical precursors were available. Satellite observations combined with model calculations revealed that large amounts of isoprene can be transported at night by deep convective clouds into the upper troposphere, and the isoprene oxidation products were postulated to contribute to SOA formation in the free troposphere (Palmer *et al.*, 2023). Here we report on several research flights, which we carried out in the outflow of deep convection over tropical rain forests (Amazon and Papua New Guinea), as well as eucalyptus forests (North-Eastern Australia). We were able to track the detailed evolution of the isoprene oxidation as well as the new particle formation and growth by performing quasi-Lagrangian measurements operating a set of sensitive *in situ* instrumentation (Curtius *et al.*, 2024). The particles formed in this way may also serve as important CCN for cloud formation at lower altitudes in the tropics (Wang, 2016; Andreae *et al.*, 2018; Williamson *et al.*, 2019).

METHODS

The measurements were carried out with the German research aircraft HALO as part of the missions CAFE-Brazil (Chemistry of the Atmosphere Field Experiment in Brazil, Manaus, Dec 2022-Feb 2023)

and CAFE-Pacific (Cairns, Australia, Jan-Feb 2024). The flights took off about 2 hours before local sunrise, and were continued until the early afternoon. The HALO payload included instrumentation for the measurement of isoprene, various isoprene oxidation products, OH and HO_2, nitrogen oxides NO and NO_2, ozone, water vapour, nucleation mode particle concentration in the size range of 2 to 5 nm, total particle concentration, and many other species and meteorological parameters. A comprehensive description of the instrumentation and detection methods, the flight planning and the meteorological situation is given in Curtius *et al.*, 2024.

RESULTS

Our measurements allowed to track the chemical evolution in the aging cloud outflow in the upper troposphere over several hours. In several flights we observed the production of large quantities of second generation oxidation products of isoprene, which result from two reactions with OH radicals and subsequent termination reactions with NO (from lightning) or HO_2. Organonitrates such as $C_5H_{11}O_4(ONO_2)$ and $C_5H_{10}O_2(ONO_2)_2$ form, which we identified as extremely low volatile products. The occurrence of the organonitrates was highly correlated with the massive formation of nucleation mode particles of 2-5 nm size. We observed new particle formation to occur in large regions (several 100 km horizontal extent and >1 km vertical thickness) with concentrations frequently exceeding 10,000 particles cm^{-3}. We will present a detailed comparison of new particle formation events observed in the upper troposphere over tropical rain forests in different regions of the world as well as over eucalyptus forest. Our observations are consistent with complementary chamber studies from the CLOUD experiment at CERN (Shen *et al.*, 2024; Allen, 2024) as well as a modelling study by Bardakov *et al.*, 2024.

CONCLUSIONS

Our investigations reveal isoprene as a potent precursor for new particle formation in the outflow of deep convection in the continental tropical upper troposphere. Highly oxidized second generation oxidation products form in the aging cloud outflow. These compounds have an extremely low volatility and dominate the new particle formation. This new particle formation is a highly efficient process, which represents an important source of aerosol in the upper troposphere. The newly formed particles are likely to influence cloud formation in the tropics.

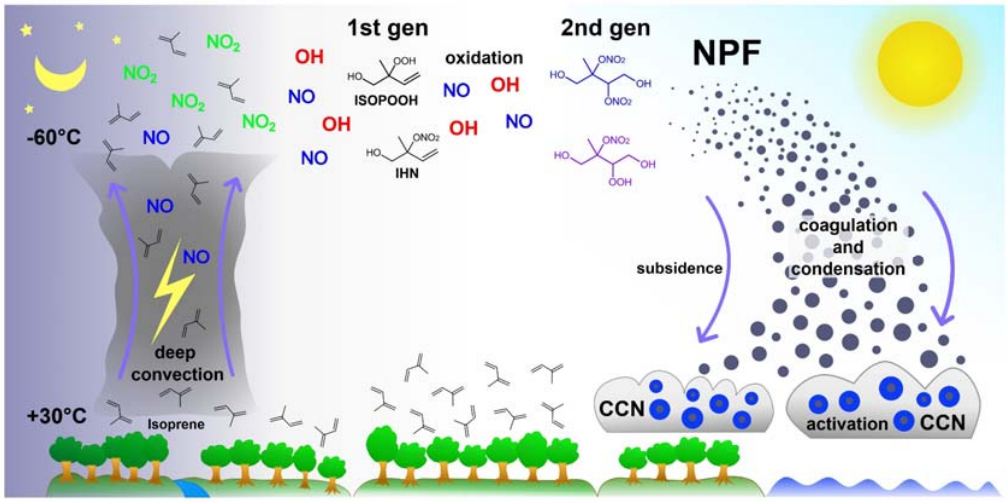


Figure 1. Schematic representation of the upper tropospheric isoprene oxidation forming second generation products of extremely low volatility in the upper troposphere and subsequent new particle formation. Figure from Curtius *et al.*, 2024.

ACKNOWLEDGEMENTS

This work was conducted under authorization 002785/2019-51 and 1.043/2022 of the Brazilian National Council for Scientific and Technological Development (CNPq). We thank the German Aerospace Center Flight Experiments facility (DLR-FX) for operating HALO, specifically the pilots, engineers, technicians, the operations team, and the project management. We thank the CLOUD team for providing intercomparison data and discussion. This research has received funding from the Max Planck Society and the German Research Foundation (DFG) within the SPP 1294 HALO (316646266, 442647232, 461448963, 461450470, 461450583), the TRR 301 TP-Change (428312742, projects A03, A04 and C06), the São Paulo Research Foundation (FAPESP) (grants 2017-17047-0 and 2023-04358-9), the Conselho Nacional de Desenvolvimento Científico e Tecnológico (CNPq) (438638/2018-2, 313355/2021-5, and 440171/2022-9), and the Dr. Hans Messer Foundation. N.T. received funding by the Humboldt Foundation.

REFERENCES

Allan, J: Abundant plant gas forms aerosol particles at high altitude - and could affect the climate, *Nature*, 636, 51-52, 10.1038/d41586-024-03844-x, 2024.

Andreae, MO, A Afchine, R Albrecht, BA Holanda, P Artaxo, HMJ Barbosa, S Borrmann, MA Cecchini, A Costa, M Dollner, D Fütterer, E Järvinen, T Jurkat, T Klimach, T Konemann, C Knote, M Krämer, T Krisna, LAT Machado, S Mertes, A Minikin, C Pöhlker, ML Pöhlker, U Pöschl, D Rosenfeld, D Sauer, H Schlager, M Schnaiter, J Schneider, C Schulz, A Spanu, VB Sperling, C Voigt, A Walser, J Wang, B Weinzierl, M Wendisch, and H Ziereis: Aerosol characteristics and particle production in the upper troposphere over the Amazon Basin, *Atmos. Chem. Phys.*, 18, 921-961, 10.5194/acp-18-921-2018, 2018.

Bardakov, R, JA Thornton, AML Ekman, R Krejci, ML Pöhlker, J Curtius, J Williams, J Lelieveld, and I Riipinen: High Concentrations of Nanoparticles From Isoprene Nitrates Predicted in Convective Outflow Over the Amazon, *Geophys. Res. Lett.*, 51, 10.1029/2024GL109919, 2024.

Curtius, J, M Heinritzi, LJ Beck, ML Pöhlker, N Tripathi, BE Krumm, P Holzbeck, CM Nussbaumer, L Hernández Pardo, T Klimach, K Barmpounis, ST Andersen, R Bardakov, B Bohn, MA Cecchini, J-P Chaboureau, T Dauhut, D Dienhart, R Dörich, A Edtbauer, A Giez, A Hartmann, BA Holanda, P Joppe, K Kaiser, T Keber, H Klebach, OO Krüger, A Kürten, C Mallaun, D Marno, M Martinez, C Monteiro, C Nelson, L Ort, SS Raj, S Richter, A Ringsdorf, F Rocha, M Simon, S Sreekumar, A Tsokankunku, GR Unfer, ID Valenti, N Wang, A Zahn, M Zauner-Wieczorek, RI Albrecht, MO Andreae, P Artaxo, JN Crowley, H Fischer, H Harder, DL Herdies, LAT Machado, C Pöhlker, U Pöschl, A Possner, A Pozzer, J Schneider, J Williams, and J Lelieveld: Isoprene nitrates drive new particle formation in Amazon's upper troposphere, *Nature*, 636, 124-130, 10.1038/s41586-024-08192-4, 2024.

Ekman, AML, R Krejci, A Engstrom, J Strom, M de Reus, J Williams, and MO Andreae: Do organics contribute to small particle formation in the Amazonian upper troposphere?, *Geophysical Research Letters*, 35, -, Artn L17810, Doi 10.1029/2008gl034970, 2008.

Guenther, AB, X Jiang, CL Heald, T Sakulyanontvittaya, T Duhl, LK Emmons, and X Wang: The Model of Emissions of Gases and Aerosols from Nature version 2.1 (MEGAN2.1): an extended and updated framework for modeling biogenic emissions, *Geoscientific Model Development*, 5, 1471-1492, 10.5194/gmd-5-1471-2012, 2012.

Kirkby, J, J Duplissy, K Sengupta, C Frege, H Gordon, C Williamson, M Heinritzi, M Simon, C Yan, J Almeida, J Tröstl, T Nieminen, IK Ortega, R Wagner, A Adamov, A Amorim, A-K Bernhammer, F Bianchi, M Breitenlechner, S Brilke, X Chen, J Craven, A Dias, S Ehrhart, RC Flagan, A Franchin, C Fuchs, R Guida, J Hakala, CR Hoyle, T Jokinen, H Junninen, J Kangasluoma, J Kim, M Krapf, A Kürten, A Laaksonen, K Lehtipalo, V Makhmutov, S Mathot, U Molteni, A Onnela, O Peräkylä, F Piel, T Petäjä, AP Praplan, K Pringle, A Rap, NAD Richards, I Riipinen, MP Rissanen, L Rondo, N Sarnela, S Schobesberger, CE Scott, JH Seinfeld, M Sipilä, G Steiner, Y Stozhkov, F Stratmann, A Tomé, A Virtanen, AL Vogel, AC Wagner, PE Wagner, E Weingartner, D Wimmer, PM Winkler, P

Ye, X Zhang, A Hansel, J Dommen, NM Donahue, DR Worsnop, U Baltensperger, M Kulmala, KS Carslaw, and J Curtius: Ion-induced nucleation of pure biogenic particles, *Nature*, 533, 521-526, 10.1038/nature17953, 2016.

Palmer, PI, MR Marvin, R Siddans, BJ Kerridge, and DP Moore: Nocturnal survival of isoprene linked to formation of upper tropospheric organic aerosol, *Science*, 375, 562-566, doi:10.1126/science.abg4506, 2022

Shen, J, DM Russell, J DeVivo, F Kunkler, R Baalbaki, B Mentler, W Scholz, W Yu, L Caudillo-Plath, E Sommer, E Ahongshangbam, D Alfaouri, J Almeida, A Amorim, LJ Beck, H Beckmann, M Berntheusel, N Bhattacharyya, MR Canagaratna, A Chassaing, R Cruz-Simbron, L Dada, J Duplissy, H Gordon, M Granzin, L Große Schute, M Heinritzi, S Iyer, H Klebach, T Krüger, A Kürten, M Lampimäki, L Liu, B Lopez, M Martinez, A Morawiec, A Onnela, M Peltola, P Rato, M Reza, S Richter, B Rörup, MK Sebastian, M Simon, M Surdu, K Tamme, RC Thakur, A Tomé, Y Tong, J Top, NS Umo, G Unfer, L Vettikkat, J Weissbacher, C Xenofontos, B Yang, M Zauner-Wieczorek, J Zhang, Z Zheng, U Baltensperger, T Christoudias, RC Flagan, I El Haddad, H Junninen, O Möhler, I Riipinen, U Rohner, S Schobesberger, R Volkamer, PM Winkler, A Hansel, K Lehtipalo, NM Donahue, J Lelieveld, H Harder, M Kulmala, DR Worsnop, J Kirkby, J Curtius, and X-C He: New particle formation from isoprene under upper-tropospheric conditions, *Nature*, 636, 115-123, 10.1038/s41586-024-08196-0, 2024.

Sindelarova, K, C Granier, I Bouarar, A Guenther, S Tilmes, T Stavrakou, JF Müller, U Kuhn, P Stefani, and W Knorr: Global data set of biogenic VOC emissions calculated by the MEGAN model over the last 30 years, *Atmospheric Chemistry and Physics*, 14, 9317-9341, 10.5194/acp-14-9317-2014, 2014.

Wang, J, R Krejci, S Giangrande, C Kuang, HMJ Barbosa, J Brito, S Carbone, X Chi, J Comstock, F Ditas, J Lavric, HE Manninen, F Mei, D Moran-Zuloaga, C Pöhlker, ML Pöhlker, J Saturno, B Schmid, RAF Souza, SR Springston, JM Tomlinson, T Toto, D Walter, D Wimmer, JN Smith, M Kulmala, LAT Machado, P Artaxo, MO Andreae, T Petäjä, and ST Martin: Amazon boundary layer aerosol concentration sustained by vertical transport during rainfall, *Nature*, 539, 416-419, 10.1038/nature19819, 2016.

Williamson, CJ, A Kupc, D Axisa, KR Bilsback, T Bui, P Campuzano-Jost, M Dollner, KD Froyd, AL Hodshire, JL Jimenez, JK Kodros, G Luo, DM Murphy, BA Nault, EA Ray, B Weinzierl, JC Wilson, FQ Yu, PF Yu, JR Pierce, and CA Brock: A large source of cloud condensation nuclei from new particle formation in the tropics, *Nature*, 574, 399-+, 10.1038/s41586-019-1638-9, 2019.

REACTIVE CONDENSATION PROCESSES MEASURED USING FIGAERO BIPOLAR SWITCHING TIME-OF-FLIGHT MASS SPECTROMETRY

J. DEVIVO[1], M. ALTON[2], M. CANAGARATNA[2], N.M. DONAHUE[1]

[1]*Carnegie Mellon University, Department of Chemistry, Pittsburgh, PA, USA*

[2]*Aerodyne Research Inc., Billerica, MA, USA*

Keywords: Aerosol chemical composition, FIGAERO, reactive uptake, acid-base

INTRODUCTION

Understanding new particle formation (NPF) and growth is largely an analytical instrumentation challenge. Measuring tiny particles (1-2 nm) and how they grow is difficult. We often learn about the mechanisms of early particle growth by connecting physical properties of aerosol (e.g. mobility diameter, number concentration) with the chemical make-up of the gas-phase. Aerosol chemical composition during early growth must often be inferred because there is insufficient mass. This works well for non-reactive condensation. The volatility basis set is suitable for predicting how ultra and extra low volatile organic compounds contribute to NPF (Donahue *et al*., 2011). However, reactive condensation processes are not easily extrapolated from the gas-phase since they involve chemistry between the gas and particle phase. Additionally, multiphase chemistry occurs within the particle phase. Aerosol properties, such as hygroscopicity, acidity, and phase state, may also enhance or inhibit uptake. For these reasons we need direct and speciated chemical composition measurements.

Thermal programmed desorption (TPD) is a well-characterized method for measuring the binding energy of atoms or molecules on a surface (Schmid *et al*., 2023). The Filter Inlet for Gases and AEROsols (FIGAERO) is designed to collect atmospheric aerosol particles on a PTFE filter and use TPD to evaporate molecular constituents (Lopez Hilfiker *et al*., 2014). It can measure small aerosol concentrations (pg m^{-3}) and diameters (8-10 nm) relevant to early growth because it concentrates mass over time on the filter (Ye *et al*., 2019). Evaporated molecules are typically measured using I^- chemical ionization time-of-flight mass spectrometry. The temperature of maximum desorption signal (T_{max}) correlates with the enthalpy of vaporization. TPD has been an important experimental estimation of the saturation concentration (log $C°_{300K}$) of highly oxygenated organic molecules (Stark *et al*., 2017, Schobesberger *et al*., 2018).

The correlation between vapor pressure and T_{max} works well for molecules bound solely by intermolecular forces. Nevertheless, TPD in atmospheric applications has not yet considered contributions to binding energy beyond non-reactive condensation processes. One of the most studied aerosols, ammonium sulfate, is not held together by intermolecular forces (H_2SO_4 and NH_3 alone are quite volatile), but rather the result reactive uptake via a proton transfer. The binding energy of the resulting salt is influenced by stronger, ionic bonds that make it essentially resistant to evaporation under the conditions it was formed. This study investigates how salt decomposition and fragment evaporation can be used to characterize reactive condensation processes via Temperature Programmed Reaction Spectroscopy (TPRS).

METHODS

Experiments were conducted at Aerodyne Research Inc. in Billerica, MA. A FIGAERO inlet was coupled to a Bipolar Time-of-Flight mass spectrometer (BToF) that has rapid switching between positive and negative modes every 0.5 second with two separate time-of-flight chambers. Over two seconds, the BToF collects mass spectra for four chemical ionization reagents: oxygen (O_2^-), acetone ($C_3H_6O^+$), iodide (I^-), and benzene ($C_6H_6^+$).

Salt solutions (e.g. $(NH_4)_2SO_4$ in HPLC H_2O) were atomized to create aerosols. The particles were passed through an aerosol dryer, size selected to 100 nm using a Differential Mobility Analyzer (TSI Inc) and quantified using a condensation particle counter (TSI Inc). For different aerosol make-ups, the dilution flow and particle collection time were varied to control the mass loading on the filter. The filter mass loading varied between 0.05 and 1 µg, depending on the reagent sensitivity to the specific analytes. The filter was automatically moved in front of the mass spectrometer pinhole where room temperature N_2 carrier gas flowed over it for one minute. For the remaining fourteen minutes, the N_2 carrier gas was heated, reaching a maximum temperature of 160 °C at the filter.

RESULTS & CONCLUSIONS

Here we report FIGAERO thermal desorption spectra for several inorganic and organic acid-base systems. FIGAERO BToF allows for simultaneous monitoring of acid and base desorption by using fast bipolar switching. I^- FIGAERO has previously only been used to measure organic and inorganic acids. In addition, we report base desorption including ammonia, methylamine, dimethylamine, and trimethylamine; all measured using positive ion modes.

Figure 1 presents a FIGAERO BToF thermal desorption spectrum for ammonium sulfate aerosol. We observe three modes in the NH_3 thermograms corresponding with increasing temperature to the decomposition of ammonium sulfate, letovicite, and ammonium bisulfate. Only in the third mode of ammonium bisulfate decomposition do we observe the main mode of sulfuric acid desorption. Simultaneous desorption of H_2SO_4 and NH_3 at 121 °C is evidence that a chemical process, specifically proton transfer of reactive uptake in reverse, is the energetically rate-limiting step to desorption. Chemical processes alone cannot explain thermal desorption. The three NH_3 modes indicate that the internal structure of the aerosol also matters. We must consider the entire lattice energy, encompassing both chemical reactions as well as physicals properties, when interpreting T_{max} for reactive condensation systems.

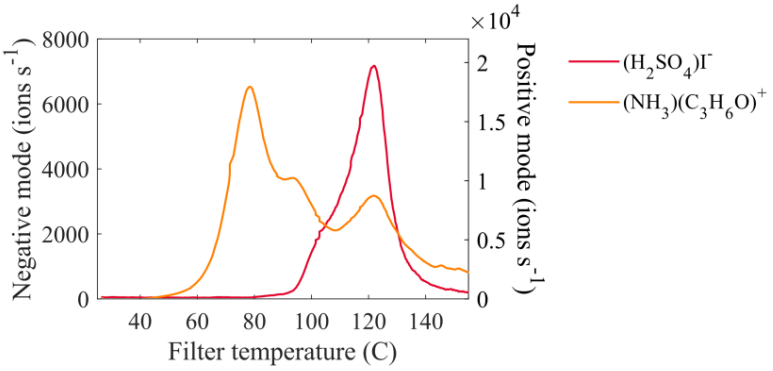


Figure 1. FIGAERO thermal desorption spectra for ammonium sulfate aerosol. The x-axis shows the filter temperature which is analogous to time while ramping the heated N_2 from room temperature up to 160 °C. The left y-axis shows the H_2SO_4 signal measured in negative mode using I^- chemical ionization. The right y-axis shows the NH_3 signal measured in positive mode using acetone chemical ionization.

We will present additional examples for a variety of mixed organic acid and base systems. We interpret the TPD spectra of aerosolized standards representing common acid base systems found in the atmosphere. This lays the groundwork for understanding more complex aerosol interactions. This work has implications for multiphase chemistry, such as cloud processing, where volatile, organic fragments are deprotonated in the particle phase and may be misidentified as thermal decomposition products in TPD techniques. Lastly, we present new results on other chemical transformations within the particle phase arising from reactions with one or both ions.

ACKNOWLEDGEMENTS

This work was supported by NSF grant CHE-2336463.

REFERENCES

Donahue, N. M., Epstein, S. A., Pandis, S. N. & Robinson, A. L. (2011). A two-dimensional volatility basis set: 1. organic-aerosol mixing thermodynamics. Atmospheric Chem. Phys. 11, 3303–3318.

Schmid, M., Parkinson, G. S. & Diebold, U. (2023). Analysis of Temperature-Programmed Desorption via Equilibrium Thermodynamics. ACS Phys. Chem. Au 3, 44–62.

Lopez-Hilfiker, F. D. et al. (2014). A novel method for online analysis of gas and particle composition: description and evaluation of a Filter Inlet for Gases and AEROsols (FIGAERO). Atmospheric Meas. Tech. 7, 983–1001.

Ye, Q. et al. (2019). Molecular Composition and Volatility of Nucleated Particles from α-Pinene Oxidation between −50 °C and +25 °C. Environ. Sci. Technol. 53, 12357–12365.

Stark, H. et al. (2017). Impact of Thermal Decomposition on Thermal Desorption Instruments: Advantage of Thermogram Analysis for Quantifying Volatility Distributions of Organic Species. Environ. Sci. Technol. 51, 8491–8500.

Schobesberger, S., D'Ambro, E. L., Lopez-Hilfiker, F. D., Mohr, C. & Thornton, J. A. (2018). A model framework to retrieve thermodynamic and kinetic properties of organic aerosol from composition-resolved thermal desorption measurements. *Atmospheric Chem. Phys.* **18**, 14757–14785.

TYPE-RESOLVED RETRIEVAL OF CLOUD CONDENSATION NUCLEI AND ICE-NUCLEATING PARTICLE NUMBER CONCENTRATIONS FROM CALIPSO AEROSOL TYPING AND AERONET INVERSION DATA

E. GIANNAKAKI[1], A. KARAGEORGOPOULOU[1]

[1]*Department of Environmental Physics and Meteorology, Faculty of Physics, University of Athens*

Keywords: CCN, INP, CALIPSO, AERONET.

INTRODUCTION

Previous research has shown that polarization lidar systems are effective in retrieving vertically resolved aerosol characteristics, which are essential for estimating cloud condensation nuclei and ice-nucleating particle concentrations. These estimates are derived using correlations between aerosol optical thickness (AOT) and column-integrated particle size distributions obtained from long-term measurements by the Aerosol Robotic Network (AERONET). This study integrates aerosol classification data from CALIPSO with microphysical properties retrieved from AERONET to estimate particle number concentrations relevant to Cloud condensation nuclei and ice nucleation partiles.

METHODS

We used AERONET Version 3, Level 1.5 inversion data spanning 2006–2021 from five selected European stations (Figure 1). These sites represent diverse aerosol environments, including urban-industrial, marine-influenced, and dust-affected regions.



Figure 1. Map of Selected AERONET stations in Europe

To improve aerosol type attribution, we selected CALIPSO overpasses within a 100 km radius of each AERONET site. Only profiles classified as "pure aerosol" types—dust, polluted continental, marine, and smoke—were considered to ensure robust linkage between aerosol properties and their sources.
We interpolated AOD values at 532 nm and 1064 nm from AERONET measurements using Ångström exponents (AE) as follows:
AOD at 532 nm: estimated from 440 nm AOD using the 440–870 nm AE.
AOD at 1064 nm: interpolated from 1020 nm AOD using the 870–1020 nm AE.

AERONET provides particle volume size distributions across 22 logarithmically spaced radius bins. The column-integrated number concentrations were derived by summing bins 4–22 (*i.e.* radii > 98 nm) for desert dust and marine particles. For polluted continental aerosols we sum up of bins 2–22 (*i.e.* radii > 57 nm), while for smoke the bins 2–22 (radii > 57 nm) were summed up (Mamouri and Ansmann, 2015; Mamouri and Ansmann, 2016; Ansmann *et al.*, 2021).
To estimate vertical profiles, we computed mean values over a 1 km atmospheric layer by dividing the AOD at 532 nm by 1000 m, yielding extinction coefficient (σ).

RESULTS

In total we identified 243 cases for all aerosol CALIPSO types across the five AERONET sites. These were analyzed per aerosol type. The results are presented in Table 1.

Desert dust	No. of Data	c_{100} (cm^{-3})	x_d	c_{250} (Mm cm^{-3})
Thessaloniki	25	16.1 ± 4.6	0.83 ± 0.12	0.259±0.026
Barcelona	14	12.1 ± 3.3	0.83 ± 0.12	0.239±0.021
Ispra	12	3.9± 0.8	1.10 ± 0.09	0.278±0.037
Leipzig	5	_	_	_
Limassol	19	64.8± 24.1	0.49 ± 0.16	0.261±0.016
All stations	75	11.8 ± 1.8	0.86 ± 0.07	0.256±0.013
Polluted continental	No. of Data	c_{60} (cm^{-3})	x_{pc}	c_{290} (Mm cm^{-3})
Thessaloniki	22	61.6 ± 23.3	0.79 ± 0.16	0.075±0.023
Barcelona	18	34.0 ± 12.2	0.81 ± 0.16	0.130±0.020
Ispra	23	56.9 ± 19.9	0.74 ± 0.15	0.169±0.021
Leipzig	45	67.1± 24.8	0.66 ± 0.16	0.237±0.028
Limassol	8	106.7 ± 131.0	0.65 ± 0.53	0.093±0.026
All stations	116	44.2± 8.9	0.78 ± 0.09	0.156±0.014
Marine	No. of Data	c_{100} (cm^{-3})	x_m	c_{500} (Mm cm^{-3})
Thessaloniki	3	7.6 ± 2.2	1.07 ± 0.13	0.015±0.004
Barcelona	4	8.4 ± 5.8	0.97 ± 0.30	0.007±0.016
Limassol	23	8.3 ± 4.1	0.99 ± 0.21	0.005±0.004
All stations	30	7.7 ± 3.0	1.01 ± 0.17	0.007±0.003
Smoke	No. of Data	c_{50} (cm^{-3})	x_s	c_{250} (Mm cm^{-3})
Thessaloniki	9	14.7± 10.5	1.02 ± 0.31	0.483±0.073
Barcelona	3	_	_	_
Ispra	4	77.6± 61.5	0.70 ± 0.34	0.782±0.244
Leipzig	3	75.0± 69.5	0.71 ± 0.40	0.510±0.169
Limassol	3	50.1± 21.5	0.78 ± 0.19	0.498±0.165
All stations	22	38.6± 12.2	0.83 ± 0.14	0.459±0.055

Table 1. Conversion parameters required in the conversion of particle extinction coefficients into particle number concentrations. The values are given for 532 nm. and are obtained from the regression analysis.

CONCLUSIONS

This study confirms the capability of combining satellite-based aerosol typing from CALIPSO with long-term AERONET microphysical data to estimate CCN and INP concentrations. By focusing on pure aerosol types (dust, smoke, marine, and polluted continental), we derived empirical conversion factors linking extinction at 532 nm to size-resolved particle number concentrations.

AERONET inversion data provided n_{60}, n_{100}, n_{250}, and n_{290} values, which were matched with CALIPSO aerosol types to assess particle-cloud interaction potential. Distinct differences in conversion factors across aerosol types were evident: dust showed lower CCN values ($c_{100} = 11.8 \pm 1.8$ cm^{-3}) but higher INP scaling ($c_{250} = 0.256 \pm 0.013$ Mm cm^{-3}), while smoke displayed high CCN and INP conversion values ($c_{50} = 38.6 \pm 12.2$ cm^{-3}; $c_{250} = 0.459 \pm 0.055$ Mm cm^{-3}), aligning with known particle composition characteristics.

This framework sets the stage for global CCN and INP estimation using satellite data, grounded in validated relationships from ground-based networks. Future work will focus on expanding the aerosol dataset, refining uncertainty estimates, and validating the results with in-situ observations from airborne and surface platforms.

ACKNOWLEDGEMENTS

The research work was supported by the Hellenic Foundation for Research and Innovation (H.F.R.I.) under the "Basic Research Financing (Horizontal support for all Sciences), National Recovery and Resilience Plan (Greece 2.0)" (Project Number: 015144).

REFERENCES

Ansmann, A., Ohneiser, K., Mamouri, R.-E., Knopf, D. A., Veselovskii, I., Baars, H., Engelmann, R., Foth, A., Jimenez, C., Seifert, P., and Barja, B. (2021). Tropospheric and stratospheric wildfire smoke profiling with lidar: mass, surface area, CCN, and INP retrieval. *Atmospheric Chemistry and Physics*, **21(12)**, 9779–9807.

Mamouri, R. E. and Ansmann, A. (2015). Estimated desert-dust ice nuclei profiles from polarization lidar: methodology and case studies, *Atmospheric Chemistry and Physics*, **15**, 3463-3477.

Mamouri, R. E., and Ansmann, A.(2016). Potential of polarization lidar to provide profiles of CCN- and INP-relevant aerosol parameters, *Atmospheric Chemistry and Physics*, **16(9)**, 5905–5931.

TRACING LOW-VOLATILITY OXIDATION PRODUCTS OF MONOTERPENES IN ATMOSPHERIC AEROSOLS

M. GLASIUS[1], Þ.N. BJÖRGVINSDÓTTIR[1], K.O.M. ÅBOM[1], D. THOMSEN[1], E.M. IVERSEN[1], J. ELM[1] AND M. BILDE[1]

[1]*Center of Excellence for Chemistry of Clouds, Department of Chemistry, Aarhus University, Aarhus, Denmark.*

Keywords: AEROSOL FORMATION, CHEMICAL ANALYSIS, DIMER ESTERS.

INTRODUCTION

Formation of atmospheric aerosols is initiated by nucleation followed by condensation of low-volatility compounds, leading to growth of aerosol particles into sizes of climatic relevance. Oxidation of monoterpenes form a multitude of semivolatile and low-volatile products including highly oxygenated organic molecules (HOM), carboxylic acids and covalently bonded dimers of carboxylic acid monomeric units. Of particular interest are compounds, such as dimers of HOM or carboxylic acid units, that classify as extremely low volatile organic compounds (ELVOCs) as these may contribute to growth of even very small aerosol particles.

The presentation will provide an overview of our recent work on formation and analysis of dimers of carboxylic acid units from oxidation of monoterpenes. These dimers have been hypothesized to form both in the gas phase (Peräkylä *et al.*, 2023) and through particle phase accretion reactions (Kenseth *et al*., 2023), leading to low-volatility products potentially supporting particle formation and growth. Often the carboxylic acid units are joined by an ester bond, and the resulting dimers are thus called dimer esters.

METHODS

A range of monoterpenes, including α-pinene, Δ^3-carene and sabinene, were oxidized by ozonolysis in the AURA chamber (Kristensen *et al*., 2017) at different environmental conditions, in particular varying temperatures, without seed aerosols. Aerosol samples were collected either on filters or using a sequential spot sampler. After extraction, samples were analyzed by high performance liquid chromatography coupled to high resolution mass spectrometry (MS), either quadrupole time-of-flight MS or Orbitrap MS. Identification was based on analysis of mass spectra, comparison with literature and analysis of authentic synthesized compounds.

CONCLUSIONS

We have observed dimer esters of all investigated monoterpenes (Kristensen *et al*., 2017; Thomsen *et al*., 2024). Time-resolved analysis shows formation of dimer esters shortly after mixing the monoterpene and ozone, without significantly increasing (or decreasing) levels during hours of experiment (Thomsen *et al.*, 2022). When α-pinene and Δ^3-carene were mixed, we found a cross-product dimer ester composed of a carboxylic acid unit from oxidation of α-pinene and one from Δ^3-carene (Thomsen *et al.*, 2022). Recent results on formation of dimer esters from ozonolysis of sabinene, as well as analysis of dimer esters in ambient atmospheric aerosol samples will be presented.

ACKNOWLEDGEMENTS

This work was funded by the Danish National Research Foundation through the Center of Excellence for Chemistry of Clouds (Grant Agreement No. DNRF172) and the Carlsberg Foundation.

REFERENCES

Kenseth, C.M., Hafeman, N.J., Rezgui, S.P., Chen, J., Huang, Y., Dalleska, N.F., Kjaergaard, H.G., Stoltz, B.M., Seinfeld, J.H., Wennberg, P.O. (2023) Particle-Phase Accretion Forms Dimer Esters in Pinene Secondary Organic Aerosol, *Science* **382**, 787.

Kristensen, K., L. N. Jensen, M. Glasius and M. Bilde (2017) The Effect of Sub-Zero Temperature on the Formation and Chemical Composition of Secondary Organic Aerosol from Ozonolysis of Alpha-Pinene, *Environ. Sci. Proc. Impacts* **19**, 1220.

Peräkylä, O., Berndt, T., Franzon, L., Hasan, G., Meder, M., Valiev, R.R., Daub, C.D., Varelas, J.G., Geiger, F.M., Thomson, R.J., Rissanen, M., Kurtén, T., Ehn, M. (2023) Large Gas-Phase Source of Esters and Other Accretion Products in the Atmosphere, *J. Am. Chem. Soc.* **145**, 7780.

Thomsen, D., L.D. Thomsen, E.M. Iversen, Þ.N. Björgvinsdottir, S.F. Vinther, J.T. Skønager, T. Hoffmann, J. Elm, M. Bilde, and M. Glasius. Ozonolysis of α-pinene and Δ^3-carene mixtures: Identification of cross-product dimers, *Environ. Sci. Technol.* **56**, 16643.

Thomsen, D., Iversen, E.M., Skønager, J.T., Luo, Y., Li, L., Roldin, P., Priestley, M., Pedersen, H.B., Hallquist, M., Ehn, M., Bilde, M., Glasius, M. (2024) The Effect of Temperature and Relative Humidity on Secondary Organic Aerosol Formation from Ozonolysis of Δ^3-Carene, *Environ. Sci.: Atmos*. **4**, 88.

PRIMARY EMISSIONS AND SECONDARY FORMATION OF ORGANIC AEROSOL IN OPEN BOREAL FOREST FIRE

L. HAO[1], S. KOMMULA[1], T. KOKKOLA[2], M. SOMERO[2], A. HARTIKAINEN[2], M. IHALAINEN[2], K. KÖSTER[2], P. YLI-PIRILA[2], P. MIETTINEN[1], S. PELTOKORPI[1], A. BUCHHOLZ[1], M. SHAHZAIB[2], A. MUKHERJEE[2], S. SCHOBESBERGER[1], O. SIPPULA[2] and A. VIRTANEN[1]

[1]*Department of Technical Physics, University of Eastern Finland, Kuopio, 70211, Finland*

[2]*Department of Environmental and Biological Sciences, University of Eastern Finland, Kuopio, 70211, Finland*

Keywords: Open biomass burning, Secondary organic aerosol, OA mass enhancement ratio, Aerosol mass spectrometer.

INTRODUCTION

Open biomass burning (BB), such as forest fires, is the largest source of primary organic aerosol (POA) on a global scale. Biomass burning also emits substantial amounts of organic gases and vapors, some of which react in the atmosphere to form secondary organic aerosol (SOA) (Andreae, 2019). The annual burned biomass in open fires is estimated to be 450 Tg in boreal forest fires, making it a potentially significant source of atmospheric aerosols. In 2024, we carried out a laboratory campaign "Boreal Forest Fire (BoFF)" at the ILMARI combustion facility in Kuopio, Finland. The BoFF campaign aims to characterize the primary emissions and secondary formation of organic aerosols upon aging from combustion of boreal forest surface biomass.

METHODS

The biomass samples were taken from a coniferous forest in Eastern Finland. They were ignited using an electrical heating element in an open fire burner. In each experiments, either dry biomass samples (96 – 285g in mass) or moist samples (157 -487g) were used. Depending on the combution phases, the emissions from full-flaming stage, the pre-flaming phase, or after-smouldering phase were introduced to a 29 m^3 Teflon smog chamber separately. After stabilization of primary emissions in the chamber for about 50mins, they were aged with either day or nighttime atmospheric oxidants.

The size-resolved mass concentration and chemical composition of nonrefractory aerosol components and refractory black carbon were measured by a soot-particle aerosol mass spectrometer (SP-AMS). Particle size distributions were measured by a scanning mobility particle sizer. The light absorption of particles was measured by Aethalometers (9-λ AE36 & 7-λ AE33, Magee). A combined of other different instruments for measuring gas and particles are also used and will not be listed here.

CONCLUSIONS

In the full flaming experiments of dry biomass material, the total aerosol mass concentration of primary emissions is 68.4 ± 2.4 and 35.2 ± 25.2 ug m^{-3} in the chamber for dry and moist biomass materials, respectively. In both cases, organic aerosol dominated the aerosol mass, accounting for 97.4 % of the total mass, which is consistent with the reported values observed in the boreal forest surface biomass burning experiment (Vakkari et al., 2025; Peltokorpi et al., 2025). For the organic aerosol in the dry biomass, the family of hydrocarbon ions contributed to 64% of the organic aerosol mass (64%, Fig.1), while oxygenated organic compounds have also

been observed in the primary emission. On the other hand, hydrocarbon ions account for a higher fraction of the total organic mass in the mosit biomass experiments, and oxygenated organic ion is less when compared to the dry biomass experiments (Fig. 1).

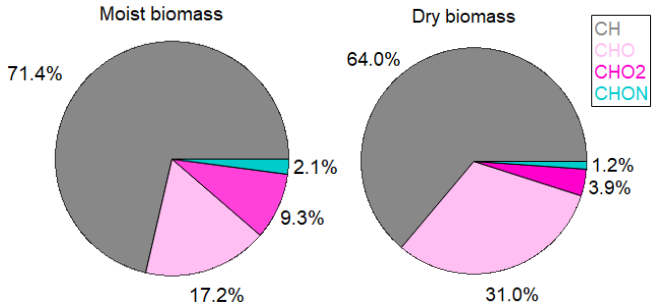


Fig. 1. The chemical compositon of organic aerosol in the primary emissions of full flaming experiment of dry biomass material (right) and moist materials (left).

Upon daytime or nighttime aging, OA production, expressed as a mass enhancement ratio (ratio of OA to primary OA (POA) mass), was highly variable. Photooxidation of primay emission from aftersmoulding stage results in more than two times increase in OA mass for both dry and fresh biomass materials (Fig. 2). In contrast, photooxidation of emissions from preflaming stage lead to a 17% loss of the OA mass. The work highlights the importance of studing OA formation potential in different combustion stages.

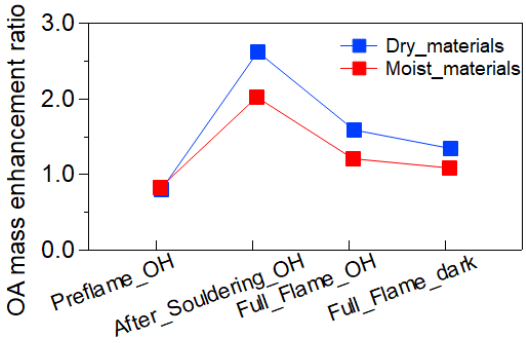


Fig.2. The organic aerosol mass enhancement ratios in two types of biomass materials: dry (blue) and fresh(red). OA formation was studied for photooxidation of primary emissions in three different combustion stages: preflaming, after smouldering and full burning stages, and dark aging of emissions from full burning stages.

ACKNOWLEDGEMENT

This work was supported by the Jane and Aatos Erkko Foundation.

REFERENCE

Andreae, M. O. (2009). Emission of trace gases and aerosols from biomass burning – an updated assessment, *Atmos. Chem. Phys.*, 19, 8523–8546.

Vakkari, V. et al. (2025). Laboratory experiments on savannah and European boreal forest fire emission, *Atmos. Chem. Phys.* to be submitted.

Peltokorpi, S. et al., (2025). Savannah and boreal biomass burning as a source of cloud condensation nuclei, *Atmos. Chem. Phys.* to be submitted.

The influence of small-scale processes on the chemical composition of aerosol particles in the extratropical UTLS

Philipp Joppe[1,3], Johannes Schneider[3], Katharina Kaiser[3], Jonas Wilsch[3], Heiko Bozem[1], Anna Breuninger[4], Joachim Curtius[4], Martin Ebert[5], Nicolas Emig[1], Horst Fischer[6], Peter Hoor[1], Sadath Ismayil[5], Konrad Kandler[5], Daniel Kunkel[1], Matthias Kohl[6], Isabel Kurth[1], Hans-Christoph Lachnitt[1], Yun Li[7], Andreas Marsing[9], Annette Miltenberger[1], Andrea Pozzer[6], Sarah Richter[4], Lenard Röder[6], Christian Rolf[8], Hans Schlager[9], Lisa Schneider[5], Cornelis Schwenk[1], Nicole Spelten[8], Laura Tomsche[1,9], Christiane Voigt[1,9], Alexander L. Vogel[4], Andreas Zahn[10], Stephan Borrmann[1,2] and Yafang Cheng[3]

[1]*Institute for Atmospheric Physics, Johannes Gutenberg University Mainz, Mainz, Germany.*
[2]*Particle Chemistry Department, Max Planck Institute for Chemistry, Mainz, Germany.*
[3]*Aerosol Chemistry Department, Max Planck Institute for Chemistry, Mainz, Germany.*
[4]*Institute for Atmospheric and Environmental Sciences, Goethe University Frankfurt, Frankfurt, Germany.*
[5]*Institute for Applied Geoscience, Technical University Darmstadt, Darmstadt, Germany.*
[6]*Atmospheric Chemistry Department, Max Planck Institute for Chemistry, Mainz, Germany.*
[7]*ICE-3: Troposphere, Forschungszentrum Jülich, Jülich, Germany.*
[8]*ICE-4: Troposphere, Forschungszentrum Jülich, Jülich, Germany.*
[9]*Institute of Atmospheric Physics, Deutsches Zentrum für Luft- und Raumfahrt (DLR), Oberpfaffenhofen, Germany.*
[10]*Karlsruhe Institute of Technology, Institute of Meteorology and Climate Research, Karlsruhe, Germany.*

Keywords: mixing, volcanic eruptions, biomass burning, tropopause, airborne measurements

INTRODUCTION

Aerosol particles in the extratropical upper troposphere and lower stratosphere (UTLS) play a crucial role in the Earth`s radiative budget. Changes in the chemical composition of the extratropical UTLS, especially the composition of aerosol particles, have a large impact on the Earth`s surface temperature due to its radiative sensitivity (Riese et al., 2012; Murphy et al., 2021). The chemical composition of the UTLS is influenced by a variety of processes, like the lower branch of the Brewer-Dobson circulation (Ploeger et al., 2021), quasi-horizontal, turbulent mixing, and vertical transport within warm conveyor belts (WCBs) or convective systems (Joppe et al., 2024). These mixing processes result in the formation of the extratropical transition layer, which is mainly derived by vertical trace gas profiles of carbon monoxide (CO) (Hoor et al., 2004).

METHODS

We use in situ airborne measurements over Europe to investigate small-scale mixing processes across the tropopause. More precisely, we use data from the CAFE-EU/BLUESKY mission from May/June 2020 on board the two research aircrafts HALO (High Altitude and Long Range Research Aircraft) and DLR-Falcon. These measurements were conducted during the COVID-19 pandemic lockdown in Europe and represent the atmosphere in a very clean period with reduced anthropogenic emissions. The measurements range from the planetary boundary layer up to the lower most stratosphere (LMS) in 14 km altitude and therefore offer a detailed coverage of the UTLS. As additional data set which covers also Central Europe, we use measurements from the Tropopause composition gradients and mixing Experiment (TPEx) mission in June 2024. The measurements during TPEx were conducted on board a Learjet 35A that was capable to deploy a towed sensor shuttle (TOSS) on a steel cable below the aircraft with partly redundant measurements on the Learjet and the TOSS. This setup offers the unique opportunity to take highly resolved measurements with a vertical distance of about 200 m, especially vertical gradients within the tropopause region. During TPEx, the meteorological conditions resulted in a highly variable tropopause structure with enhanced

possibility for cross-tropopause mixing due to a series of low-pressure systems associated with warm conveyor belt (WCB) outflow.

CONCLUSIONS

We show that the use of aerosol measurements, especially particulate sulfate, can determine troposphere-stratosphere-exchange. Furthermore, we identified a non-stratospheric volcanic eruption as source for enhanced particulate sulfate in the LMS over Europe (Figure 1). This observed sulfate anomaly is caused by continuous cross-tropopause mixing of the precursor gas SO_2, followed by gas-to-particle conversion. In addition, we analyzed the volcanic eruption in the EMAC model (e.g., Jöckel et al., 2005; Roeckner at al., 2006) and are able to reproduce the observations. This also explains why the sulfate anomaly occurred only during one research flight and was not spread over the whole campaign phase.

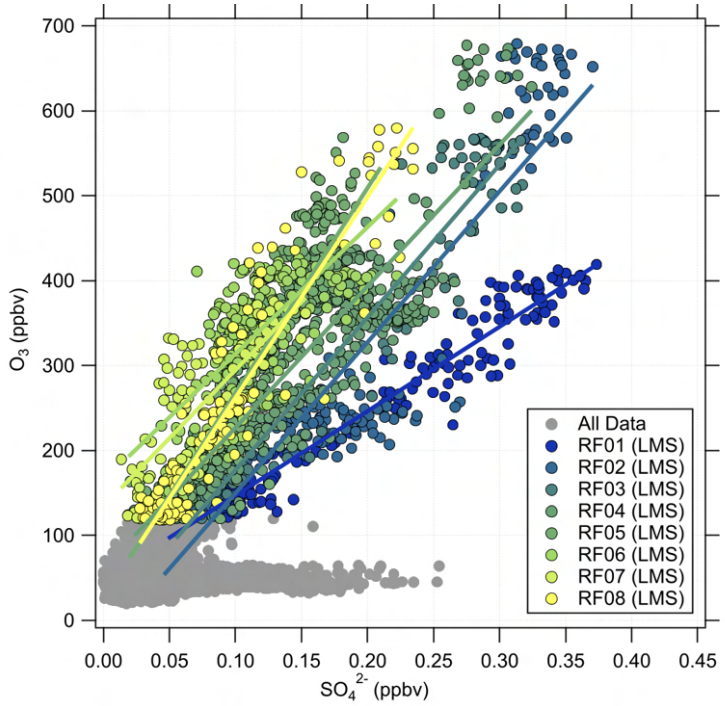


Figure 1. Correlation between the particulate sulfate mixing ratio and the O_3 mixing ratio for the full CAFE-EU/BLUESKY dataset. The color-coded data points indicate the stratospheric data derived from the chemical tropopause O_3 mixing ratios above 120 ppbv. The grey data show the complete dataset, including the tropospheric part. The solid color-coded lines represent the linear regressions for the individual flights (from Joppe et al., 2024).

Additionally, to the identification of cross-tropopause mixing after volcanic eruptions, we present that WCBs including moist uplift bring long-range transported biomass burning (BB) aerosol from low altitudes over Canada into the UTLS over Europe and cause cross-tropopause mixing (Figure 2). Related to this mixing of BB aerosol, we observe changes in the static stability (vertical gradient of potential temperature) of the tropopause region, which is most presumably caused by transported refractory black carbon from the Canadian fires.

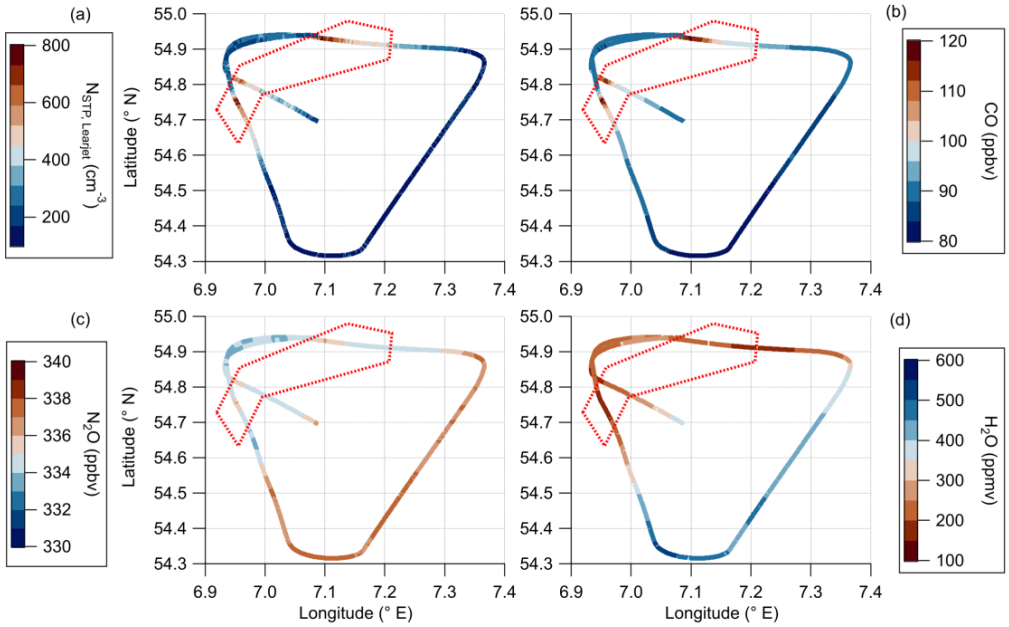


Figure 2. Horizontal view on the flight pattern with deployed TOSS within the restricted air space over the North Sea during TPEx flight F07. The pattern was flown at FL240 (approx. 7400 m) between 07:24 and 07:47 UTC. The color-code represents different in situ measurements of (a) total aerosol number concentration between 0.1 µm and 1µm, (b) CO, (c) N_2O, and (d) H_2O. The red lines surround the region of the polluted streamer (from Joppe et al., 2025, submitted)

ACKNOWLEDGEMENTS

This research has been supported by the Deutsche Forschungsgemeinschaft TRR 301 – project ID 428312742, “The tropopause region in a changing atmosphere”.

REFERENCES

Hoor, Peter, et al. "Seasonality and extent of extratropical TST derived from in-situ CO measurements during SPURT." Atmospheric Chemistry and Physics 4.5 (2004): 1427-1442.

Jöckel, P., et al. "the modular earth submodel system (MESSy)-a new approach towards earth system modeling." Atmospheric Chemistry and Physics 5.2 (2005): 433-444.

Joppe, Philipp, et al. "The influence of extratropical cross-tropopause mixing on the correlation between ozone and sulfate aerosol in the lowermost stratosphere." Atmospheric Chemistry and Physics 24.13 (2024): 7499-7522.

Murphy, Daniel M., et al. "Radiative and chemical implications of the size and composition of aerosol particles in the existing or modified global stratosphere." Atmospheric Chemistry and Physics Discussions 2020 (2020): 1-32.

Ploeger, Felix, et al. "The stratospheric Brewer–Dobson circulation inferred from age of air in the ERA5 reanalysis." Atmospheric Chemistry and Physics 21.11 (2021): 8393-8412.

Riese, Martin, et al. "Impact of uncertainties in atmospheric mixing on simulated UTLS composition and related radiative effects." Journal of Geophysical Research: Atmospheres 117.D16 (2012).

Roeckner, E., et al. "Sensitivity of simulated climate to horizontal and vertical resolution in the ECHAM5 atmosphere model." Journal of Climate 19.16 (2006): 3771-3791.

IDENTIFICATION OF NEW PARTICLE FORMATION EVENTS USING DEEP LEARNING ALGORITHM

V.P. KANAWADE[1], R. BHANDARI[2], C. SARANGI[2], M. SEBASTIAN[2], R.K. HOODA[2,3], A.-P. HYVÄRINEN[3], E. ASMI[3], V. VAKKARI[3,4], G. PANDITHURAI[5], S.N. SINGH[6], V.K. SONI[7], T. NIEMINEN[8,9], P.G. VAN ZYL[4], K. JAARS[4], L. LAAKSO[3,4], D.C.S. BEDDOWS[10], R.M. HARRISON[10,11], J.P. BEUKES[4], N. KALIVITIS[12], N. MIHALOPOULOS[12,13], I. SALMA[14], M. VÖRÖSMARTY[15], L.-H. YOUNG[16], Z. WATSON[17], S.-H. LEE[17], M. PIKRIDAS[1], J. SCIARE[1], T. JOKINEN[1]

[1]*Climate and Atmosphere Research Centre (CARE-C), The Cyprus Institute, Nicosia, Cyprus*
[2]*Department of Civil Engineering, Indian Institute of Technology Madras, Chennai, India*
[3]*Finnish Meteorological Institute, Erik Palmenin Aukio 1, Helsinki, Finland*
[4]*Atmospheric Chemistry Research Group, Chemical Resource Beneficiation, North-West University, Potchefstroom, South Africa*
[5]*Indian Institute of Tropical Meteorology, Ministry of Earth Sciences, Pune, India*
[6]*CSIR-National Physical Laboratory, New Delhi, Delhi, India*
[7]*India Meteorological Department, Ministry of Earth Sciences, New Delhi, India*
[8]*Institute for Atmospheric and Earth System Research (INAR) / Physics, Faculty of Science, University of Helsinki, Helsinki, Finland*
[9]*Department of Physics, Faculty of Science, University of Helsinki, Helsinki, Finland*
[10]*School of Geography, Earth and Environmental Sciences, University of Birmingham, Birmingham, UK*
[11]*Department of Environmental Sciences/Center of Excellence in Environmental Studies, King Abdulaziz University, Jeddah, Saudi Arabia*
[12]*Department of Chemistry, University of Crete, Heraklion, Greece*
[13]*Institute for Environmental Research and Sustainable Development, National Observatory of Athens, Lofos Koufou, P. Penteli, Athens, Greece*
[14]*Institute of Chemistry, Eötvös Loránd University, Budapest, Hungary*
[15]*Hevesy György Ph.D. School of Chemistry, Eötvös Loránd University, Budapest, Hungary*
[16]*Department of Occupational Safety and Health, College of Public Health, China Medical University, Taichung, Taiwan*
[17]*Department of Atmospheric and Earth Sciences, University of Alabama in Huntsville, Huntsville, Alabama, USA*

Keywords: NEW PARTICLE FORMATION, OBJECT DETECTION, DEEP LEARNING, YOLO ALGORITHM.

INTRODUCTION

Atmospheric new particle formation (NPF), involving the formation of nanometer-sized molecular clusters and their subsequent growth to larger particle diameters, significantly impacts air quality, weather, climate and human health. NPF events are primarily identified through visualization of particle number size distributions, which is a subjective and time-consuming process. Here, we utilized a fast object detection deep learning algorithm, You Only Look Once (YOLO) version 8, to identify the features of NPF events. The YOLO algorithm was trained to automatically identify and annotate the visual appearance of particle size distributions and classify a given day into NPF event. A few previous studies have attempted to detect NPF events using deep learning methods (Fogwill *et al.,* 2024; Joutsensaari *et al.,* 2018; Su *et al.,* 2022). Joutsensaari *et al.* (2018) were the first to apply transfer learning with a convolutional neural network (CNN) to classify NPF events from particle size distributions using a 15-year dataset from San Pietro Capofiume, Italy. Later, Su *et al.* (2022) applied a Mask R-CNN to localize the spatial patterns of NPF events and Zaiden *et al.* (2018) applied Bayesian classification to long-term data from the Station for Measuring Ecosystem-Atmosphere Relations (SMEAR) II station in Hyytiälä, Finland. Recently, Fogwill *et al.* (2024) used a statistical algorithm, Hidden Markov Models (HMM), to detect NPF events objectively and efficiently with reduced complexity. The primary goal of this work is to demonstrate the applicability and robustness of

YOLO in detecting NPF event features in global data. This approach can be extended to new datasets from additional locations, further improving the algorithm's performance over time.

METHODS

Here, we used the fast object detection deep learning algorithm, You Only Look Once (YOLO) version 8, to automatically identify the characteristic banana-shaped features of NPF events in contour plots of particle size distributions. We used at least one year of asynchronous particle size distribution measurements from 20 diverse sites worldwide, including India, Taiwan, the UK, Finland, Greece, Hungary, Cyprus, South Africa, and the USA. The YOLO algorithm was trained to detect NPF event features, validated, and evaluated across 20 global sites. We also assessed its performance using key metrics and calculated its accuracy for each site. Additionally, for detected NPF events, the algorithm estimates the event start time (local time) and size-segregated particle growth rates (<25 nm, 25–50 nm, and 50–80 nm).

We first trained and validated the YOLO algorithm using approximately 20 contour plot images of particle size distributions depicting both NPF events and non-events, and then evaluated its performance on the remaining data for NPF event detection. The details of Indian measurement sites; Ranichauri (RNC), Delhi (DEL), Hyderabad (HYD), and Mahabaleshwar (MBL) and aerosol instrumentation are given in Sebastian *et al.* (2022), Agia Marina Xyliatou (AMX), Cyprus in Baalbaki *et al.* (2021), Athens (ATH), Greece in Kalkarvouras *et al.* (2020), Chilbolton (CBT), Marylebone Road (MLB) and North Kensington (NKT), the UK in Stacey *et al.* (2020), Kent (KNT), USA in Kanawade *et al.* (2012), Huntsville (HSV), USA in Watson *et al.* (2023), Taichung (TCG), Taiwan in Young *et al.* (2023) and the remaining measurement sites; Botsalano (BOT), Budapest (BpART, BUD), Finokalia (FKL), Hyytiälä (HYY), Marikana (MAR), Värriö (VÄR), and Welgegund (WGD) are given in Nieminen *et al.* (2018).

CONCLUSIONS

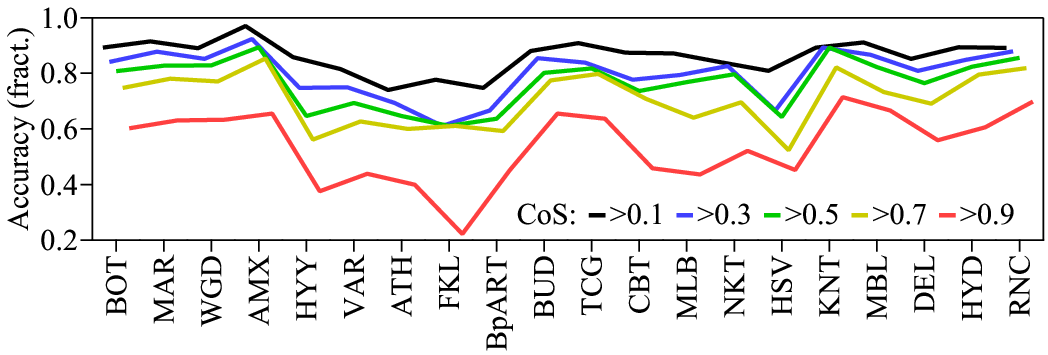


Figure 1. The YOLO algorithm accuracy to detect NPF event features at different confidence scores (>0.1, >0.3, >0.5, >0.7 and >0.9) for all evaluated 20 global sites.

Considering 20 global sites, the model's accuracy ranged from 0.74 to 0.97 at confidence score (CoS) > 0.1 but declined as the CoS score increased, dropping to 0.22–0.71 at CoS > 0.9. Among the 20 global sites, 12 achieved an accuracy above 0.50 at CoS > 0.9, while all sites exceeded 0.60 accuracy at CoS > 0.7 (Fig. 1). This demonstrates the model's robustness and adaptability across diverse global locations, highlighting its potential for generalization under varying conditions. Additionally, training the YOLO algorithm with more data from new locations is expected to enhance its performance over time. Compared to previous studies, our model was evaluated against diverse global sites and achieved higher accuracy, reaching up to 97%, indicating the model's applicability globally. Moreover, the estimated NPF event characteristics, including event starttime and size-segregated particle growth rates, are well within the observed ranges. The YOLO algorithm's precise feature recognition and low classification errors highlight its value for automated NPF event detection in diverse datasets and conditions. However, challenges such as the algorithm's dependence on high-quality and comprehensive training data, can lead to suboptimal results. These limitations could be

addressed through large training with more data, data augmentation, and fine-tuning of model parameters in future studies.

ACKNOWLEDGEMENTS

CS and RB acknowledge the funding support from the Research Council of Finland under CO-ENHANCIN project. VPK and MS acknowledge the funding support from the Science and Engineering Research Board, Government of India (grant no. ECR/2016/001333) and the Institute of Eminence, University of Hyderabad (grant no. UoH/IoE/RC1/RC1-20-014). RKH, APH, EA and VV acknowledge the Academy of Finland Flagship funding (grant no. 357904 and 359342). IS acknowledges the funding support from the Hungarian Research, Development and Innovation Office (contract: Advanced 150835). RKH and APH also acknowledge the Research Council of Finland under CO-ENHANCIN (project 360113). MP, JS, TJ, and VPK acknowledge the funding support by the European Union's Horizon 2020 Research and Innovation Programme under grant agreement No. 856612 and the Cyprus Government. TJ acknowledge the funding support by the European Union ERC-2022-STGERC-BAE-Project: 101076311. LHY acknowledges the funding support from Taiwan's Ministry of Environment and the National Science and Technology Council. CS and RKH also acknowledge support from the Vaishvik Bharatiya Vaigyanik (VAIBHAV) for this research. NK acknowledges support by Horizon Europe project Net4Cities Contract No. 101138405. The authors thank all technical and scientific personnel working at the observational station who contributed to ambient data collection and handling.

REFERENCES

Baalbaki, R., et al. (2021), Towards understanding the characteristics of new particle formation in the Eastern Mediterranean, Atmos. Chem. Phys., 21(11), 9223-9251.

Fogwill, G. P., P. Pelle, and E. Asmi (2024), Identification of New Particle Formation Events With Hidden Markov Models, paper presented at 2021 XIX Workshop on Information Processing and Control (RPIC), 3-5 Nov. 2021.

Joutsensaari, J., M. Ozon, T. Nieminen, S. Mikkonen, T. Lähivaara, S. Decesari, M. C. Facchini, A. Laaksonen, and K. E. J. Lehtinen (2018), Identification of new particle formation events with deep learning, Atmos. Chem. Phys., 18(13), 9597-9615.

Kalkavouras, P., A. Bougiatioti, G. Grivas, I. Stavroulas, N. Kalivitis, E. Liakakou, E. Gerasopoulos, C. Pilinis, and N. Mihalopoulos (2020), On the regional aspects of new particle formation in the Eastern Mediterranean: A comparative study between a background and an urban site based on long term observations, Atmospheric Research, 239, 10491.

Kanawade, V. P., D. R. Benson, and S.-H. Lee (2012), Statistical analysis of 4-year observations of aerosol sizes in a semi-rural continental environment, Atmospheric Environment, 59, 30-38.

Nieminen, T., et al. (2018), Global analysis of continental boundary layer new particle formation based on long-term measurements, Atmos. Chem. Phys., 18(19), 14737-14756.

Sebastian, M., et al. (2022), Observations of particle number size distributions and new particle formation in six Indian locations, Atmos. Chem. Phys., 22(7), 4491-4508.

Stacey, B., R. M. Harrison, and F. Pope (2020), Evaluation of ultrafine particle concentrations and size distributions at London Heathrow Airport, Atmospheric Environment, 222, 117148.

Su, P., et al. (2022), New particle formation event detection with Mask R-CNN, Atmos. Chem. Phys., 22(2), 1293-1309.

Watson, Z., L. Tiszenkel, A. Pour Biazar, K. Knupp, and S.-H. Lee (2023), Effects of boundary layer dynamics and meteorology on ultrafine particle formation and growth, Atmospheric Environment, 309, 119952.

Young, L.-H., C.-S. Hsu, T.-C. Hsiao, N.-H. Lin, S.-C. Tsay, T.-H. Lin, W.-Y. Lin, and C.-R. Jung (2023), Sources, transport, and visibility impact of ambient submicrometer particle number size distributions in an urban area of central Taiwan, Science of The Total Environment, 856, 159070.

Zaidan, M. A., V. Haapasilta, R. Relan, H. Junninen, P. P. Aalto, M. Kulmala, L. Laurson, and A. S. Foster (2018), Predicting atmospheric particle formation days by Bayesian classification of the time series features, Tellus B: Chemical and Physical Meteorology, 70(1), 1-10.

Sulfuric Acid and Methanesulfonic Acid Measurements in the Tropical Troposphere

H. KLEBACH[1], L. BECK[1], M. HEINRITZI[1], S. RICHTER[1], K. KAISER[2], M. ZAUNER-WIECOREK[1], M. GRANZIN[1], T. KEBER[1], D. RUSSELL[1], L. CAUDILLO-PLATH[1], J. SCHNEIDER[2] and J. CURTIUS[1]

[1]*Institute for Atmospheric and Environmental Research, Goethe University Frankfurt, Frankfurt am Main, Germany*.

[2]*Max-Planck-Institute for Chemistry, Particle Chemistry Department, Mainz, Germany*.

Keywords: Aircraft Measurements, Methanesulfonic Acid, Nitrate CIMS, Marine Aerosol.

INTRODUCTION

Dimethyl sulfide is emitted by phytoplankton in the ocean and accounts for the largest natural sulfur source to the atmosphere (Tesdal *et al.*, 2016). DMS can be oxidized to form sulfuric acid (SA) or methanesulfonic acid (MSA), which are essential precursors for atmospheric particle nucleation and growth. Deep convective systems can transport DMS to the upper troposphere in the tropics, providing precursors for aerosol formation in a highly pristine environment.
Previous studies have observed high particle concentrations in the tropical upper troposphere (Williamson *et al.*, 2019; Andreae *et al.*, 2018). While these were related to isoprene oxidation above the Amazon during the CAFE Brazil campaign (Curtius *et al.*, 2024) in situ observations of nucleators in the marine environment are still sparse. The CAFE Pacific campaign (January-February 2023, Cairns Australia) studied the tropical atmosphere above the Indo-Pacific and the Australian continent with a focus on the upper troposphere and the possibility of observing conditions above tropical rainforests as well as the pristine Pacific.

METHODS

Measurements were conducted with the HALO aircraft operated by the German Aerospace Center (DLR) which allows measurements in altitudes ranging from the boundary layer up to 14 km and covering a wide area from the Indo-Pacific warm pool to Papua New Guinea and continental Australia.
Here, we present nitrate CIMS measurements obtained with an instrument specifically optimized for aircraft-based operation. At low altitudes our data represents gas-phase SA and MSA. At higher altitudes (mostly above 9km) a temperature difference between our inlet and the ambient causes particle evaporation, enabling the analysis of combined gas- and particle-phase concentrations. This instrumental behaviour was characterized with additional lab studies at the CERN CLOUD chamber.
A comparison with the AMS (Aerosol Mass Spectrometer) on board the aircraft confirms the efficient evaporation in the instrument and complements the particle phase analysis. The HYSPLIT Lagrangian particle model developed by the National Oceanic and Atmospheric Administration (NOAA) can be used to trace back the air mass origin for certain periods of interest.

CONCLUSIONS

Our measurements show high gas-phase values of SA and MSA in the marine and coastal boundary layer, often in the range of 4×10^6 to 3×10^7 cm^{-3} with similar concentrations for both acids. The particle composition above the oceans is also strongly influenced by these acids with MSA mostly dominating over SA. Both acids are significantly enhanced over the warm pool region compared to regions further

inland, as shown in Figure 1. The comparison with the sulfate values reported by the AMS suggests a large number of small particles in the marine upper troposphere consisting of SA and MSA, which can be linked to convective activity using ozone values and trajectory analysis.
These results offer valuable insights into particle formation and composition in the marine upper troposphere. While SA is well recognized in global aerosol models, MSA remains largely overlooked. The findings presented here contribute to a deeper understanding of MSA's role in atmospheric chemistry, particularly in the vast and understudied tropical upper troposphere - one of the few regions that still closely resembles pre-industrial conditions.

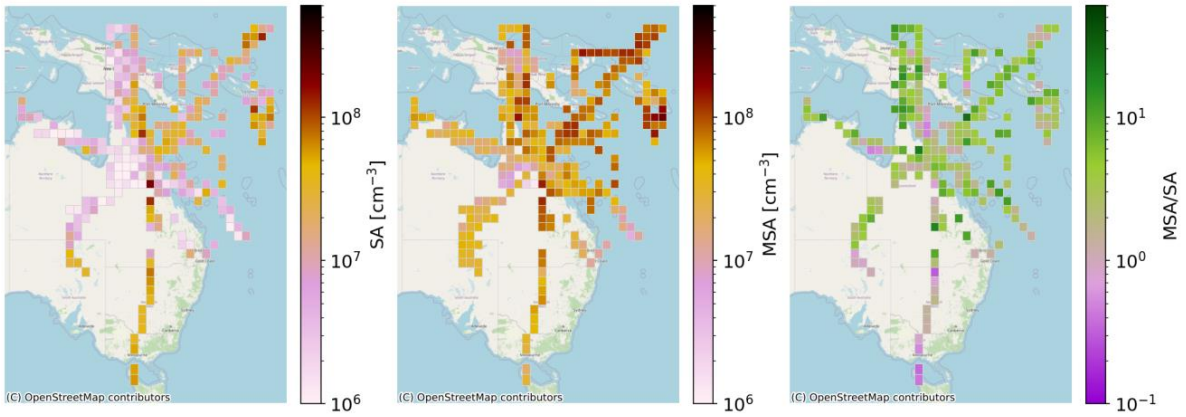


Figure 1. Combined gas- and particle-phase MSA and SA measured by the nitrate CIMS during the CAFE Pacific campaign. Shown are median ambient concentrations in 1° bins.

ACKNOWLEDGEMENTS

We would like to thank the German Aerospace Center (DLR) for their support and operation of the HALO aircraft. This work was supported by the DFG via SPP 1294 "HALO" (CU 126/19-1 (502266535) and CU 126/20-1 (502272415)) and TRR 301 "TP-Change" (A03 and C06, 428312742).

REFERENCES

Tesdal, J.-E.; Christian, J. R.; Monahan, A. H. and von Salzen, K. (2016). Evaluation of diverse approaches for estimating sea-surface DMS concentration and air–sea exchange at global scale, *Environmental Chemistry* **13**, 390-412

Williamson, C. J.; Kupc, A.; Axisa, D.; Bilsback, K. R.; Bui, T.; Campuzano-Jost, P.; Dollner, M.; Froyd, K. D.; Hodshire, A. L.; Jimenez, J. L.; Kodros, J. K.; Luo, G.; Murphy, D. M.; Nault, B. A.; Ray, E. A.; Weinzierl, B.; Wilson, J. C.; Yu, F.; Yu, P.; Pierce, J. R. and Brock, C. A. (2019). A large source of cloud condensation nuclei from new particle formation in the tropics, *Nature* **574(7778)**, 399-403.

Andreae, M. O.; Afchine, A.; Albrecht, R.; Holanda, B. A.; Artaxo, P.; Barbosa, H. M. J.; Borrmann, S.; Cecchini, M. A.; Costa, A.; Dollner, M.; Fütterer, D.; Järvinen, E.; Jurkat, T.; Klimach, T.; Konemann, T.; Knote, C.; Krämer, M.; Krisna, T.; Machado, L. A. T.; Mertes, S.; Minikin, A.; Pöhlker, C.; Pöhlker, M. L.; Pöschl, U.; Rosenfeld, D.; Sauer, D.; Schlager, H.; Schnaiter, M.;

Schneider, J.; Schulz, C.; Spanu, A.; Sperling, V. B.; Voigt, C.; Walser, A.; Wang, J.; Weinzierl, B.; Wendisch, M.; Ziereis, H. (2018). Aerosol characteristics and particle production in the upper troposphere over the Amazon Basin, *Atmospheric Chemistry and Physics*, **18**, 921-961.

Curtius, J.; Heinritzi, M.; Beck, L. J.; Pöhlker, M. L.; Tripathi, N.; Krumm, B. E.; Holzbeck, P.; Nussbaumer, C. M.; Hernández Pardo, L.; Klimach, T.; Barmpounis, K.; Andersen, S. T.; Bardakov, R.; Bohn, B.; Cecchini, M. A.; Chaboureau, J.-P.; Dauhut, T.; Dienhart, D.; Dörich, R.; Edtbauer, A.; Giez, A.; Hartmann, A.; Holanda, B. A.; Joppe, P.; Kaiser, K.; Keber, T.; Klebach, H.; Krüger, O. O.; Kürten, A.; Mallaun, C.; Marno, D.; Martinez, M.; Monteiro, C.; Nelson, C.; Ort, L.; Raj, S. S.; Richter, S.; Ringsdorf, A.; Rocha, F.; Simon, M.; Sreekumar, S.; Tsokankunku, A.; Unfer, G. R.; Valenti, I. D.; Wang, N.; Zahn, A.; Zauner-Wieczorek, M.; Albrecht, R. I.; Andreae, M. O.; Artaxo, P.; Crowley, J. N.; Fischer, H.; Harder, H.; Herdies, D. L.; Machado, L. A. T.; Pöhlker, C.; Pöschl, U.; Possner, A.; Pozzer, A.; Schneider, J.; Williams, J.; Lelieveld, J. (2014). Isoprene nitrates drive new particle formation in Amazon's upper troposphere, *Nature* **636**, 124-130.

Long-range transport and mixing of aerosol from the Asian Tropopause Aerosol Layer (ATAL) into the northern latitude lower stratosphere

F. KÖLLNER[1,2], M. KOHL[2], F. EKINCI[1], O. EPPERS[2], J. SCHNEIDER[2], A. DRAGONEAS[2], S. MOLLEKER[2], S. JOHANSSON[3], J. UNGERMANN[4], E.KRETSCHMER[3], M. HÖPFNER[3], V. LAUTHER[5], C. M. VOLK[5], O. APPEL[1,2], P. BRAUNER[2], D. KUNKEL[1], H.-C. LACHNITT[1], H. BOZEM[1], F. WEYLAND[1], N. EMIG[1], L. ORT[2], A. ZAHN[3], L. TOMSCHE[1,6], A. POZZER[2,7], J. LELIEVELD[2,7], Y. CHENG[2], M. RIESE[4,5], P. HOOR[1], and S. BORRMANN[1,2]

[1] *Institute for Atmospheric Physics, Johannes Gutenberg University, Mainz, Germany.*

[2] *Max Planck Institute for Chemistry, Mainz, Germany.*

[3]*Institute of Meteorology and Climate Research – Atmospheric Trace Gases and Remote Sensing (IMK-ASF), Karlsruhe Institute of Technology, Karlsruhe, Germany*

[4]*Institute of Climate and Energy Systems – Stratosphere (ICE-4), Forschungszentrum Jülich, Jülich, Germany*

[5] *Institute for Atmospheric and Environmental Research, University of Wuppertal, Wuppertal, Germany*

[6]*German Aerospace Center, Weßling, Germany*

[7]*The Cyprus Institute, Climate and Atmosphere Research Center, Nicosia, Cyprus*

Keywords: ammonium nitrate, stratospheric aerosol, Asian summer monsoon, long-range transport.

INTRODUCTION

Stratospheric aerosol particles have been studied for many decades, with sulfuric acid recognized as their primary component of the Junge layer. This layer, spanning altitudes of 15 to 25 km, is mainly formed from natural sources such as volcanic eruptions and tropical carbonyl sulfide injection (Kremser *et al*., 2016). However, recent research highlights the growing importance of the Asian Tropopause Aerosol Layer (ATAL), a unique aerosol layer at altitudes of 13 to 18 km (Vernier *et al.*, 2011). The ATAL is primarily composed of ammonium nitrate, sulfate and organic aerosol, which is formed after the monsoonal uplift of precursor gases from Asian ground-level sources into the upper troposphere (Höpfner *et al.*, 2019; Appel *et al.*, 2022; Weigel *et al.*, 2021; Mahnke *et al.*, 2021). The ATAL can affect regions from the eastern Mediterranean to eastern China annually from June to September. While the ATAL significantly influences the aerosol composition and chemistry in the upper troposphere and lower stratosphere (UTLS) regionally, its broader impact across the Northern Hemisphere is less understood.

METHODS

Motivated by the limited knowledge of the influence of the Asian summer monsoon (ASM) on the extratropical UTLS region, we conducted the PHILEAS mission (Probing High Latitude Export of air from the Asian Summer Monsoon). This aircraft-based mission took place in August/September 2023, operating out of Oberpfaffenhofen, Germany, and Anchorage, Alaska. Our study utilized in-situ and remote sensing aerosol and gas measurements taken onboard the German research aircraft HALO.

Specifically, we conducted vertically-resolved submicron aerosol composition measurements up to a potential temperature of 400 K (approximately 14.5 km altitude) using the ERICA aerosol mass spectrometer (Hünig *et al.*, 2022; Dragoneas *et al.*, 2022). The measurements are complemented by global simulations using the global chemistry-climate model EMAC (Jöckel *et al.*, 2006). Our investigation focused on the sources, transport pathways, and persistence of aerosol in the extratropical UTLS towards the end of the ASM season.

RESULTS AND DISCUSSION

Our analysis reveals that particulate ammonium nitrate and organic compounds are prevalent in the extratropical lower stratosphere (ExLS) in summer and autumn, alongside elevated methane and dichloromethane mixing ratios. Previous studies have shown that Asia is the primary source of global methane and dichloromethane emissions (An *et al.*, 2021; Saunois *et al*., 2020). We thus conclude that the presence of ammonium nitrate and organic aerosol in the ExLS is linked to ground-level Asian sources, combined with the ASM convection, and followed by long-range northward transport above 370 K potential temperature within the stratosphere. Global simulations using the EMAC model indicate that this transport pathway recurs annually during the ASM season. Additional observational and modeling evidences indicate that the aerosol from the ASM is mixed into the stratospheric background air and can persist there for several months. This process affects aerosol neutralization in the ExLS, as ammonium can modify the highly acidic stratospheric composition. In summary, the ASM serves as an efficient yet overlooked pathway for transporting ammonium nitrate and organic aerosol into the Northern Hemisphere stratosphere, with significant potential to alter stratospheric aerosol composition and chemistry.

ACKNOWLEDGEMENTS

The PHILEAS mission was funded by the Deutsche Forschungsgemeinschaft (DFG, German Research Foundation) (HALO-SPP495 1294, project no: 461449927, HO 4225/17-1). The funding for individual projects within PHILEAS was provided by the DFG (KO 6470/1-1, HO 4225/19-1, HO 4120/4-1, VO 1530/9-1). The study was supported by TRR 301 "TPChange" (Project-ID 428312742). This research has received support from the Max Planck Society (MPG) and the Max Planck Graduate Centre (MPGC). The design and construction of the ERICA instrument was financed by the FP7/2013-2019 ERC Advanced Research Grant "EXCATRO" (grant no. 321040). Jörn Ungermann, Sören Johansson, and Michael Höpfner received support from the ESA CARITEX project (4000141036/23/NL/FF/ab). Laura Tomsche acknowledges the support by the project MEFKON (20F2202B) funded by the German Federal Ministry for Economic Affairs and Climate Action within LuFo 6-3.

REFERENCES

An, M., Western, L.M., Say, D. *et al.* (2021). “Rapid increase in dichloromethane emissions from China inferred through atmospheric observations.” *Nat Commun* **12**, 7279. https://doi.org/10.1038/s41467-021-27592-y.

Appel, O., Köllner, F., Dragoneas, A., *et al.* (2022). “Chemical analysis of the Asian tropopause aerosol layer (ATAL) with emphasis on secondary aerosol particles using aircraft-based in situ aerosol mass spectrometry.” *Atmos. Chem. Phys.*, **22**, 13607–13630, https://doi.org/10.5194/acp-22-13607-2022.

Dragoneas, A., Molleker, S., Appel, O., *et al.* (2022). “The realization of autonomous, aircraft-based, real-time aerosol mass spectrometry in the upper troposphere and lower stratosphere”, *Atmos. Meas. Tech.* **15**, 5719–5742, https://doi.org/10.5194/amt-15-5719-2022.

Höpfner, M., Ungermann, J., Borrmann, S. *et al.* (2019). "Ammonium nitrate particles formed in upper troposphere from ground ammonia sources during Asian monsoons." *Nat. Geosci.*, **12**, 608–612, https://doi.org/10.1038/s41561-019-0385-8.

Hünig, A., Appel, O., Dragoneas, A., *et al.* (2022). Design, characterization, and first field deployment of a novel aircraft-based aerosol mass spectrometer combining the laser ablation and flash vaporization techniques, *Atmos. Meas. Tech.* **15**, 2889-2921, https://doi.org/10.5194/amt-15-2889-2022.

Jöckel, P., Tost, H., Pozzer, A., *et al.* (2006). "The atmospheric chemistry general circulation model ECHAM5/MESSy1: consistent simulation of ozone from the surface to the mesosphere." *Atmos. Chem. Phys.*, **6**, 5067–5104, https://doi.org/10.5194/acp-6-5067-2006.

Kremser, S., Thomason, L.W., von Hobe, M., *et al.* (2016). "Stratospheric aerosol—Observations, processes, and impact on climate." *Rev. Geophys.* **54**, 278–335, https://doi.org/10.1002/2015RG000511.

Mahnke, C., Weigel, R., Cairo, F., *et al.* (2021). "The Asian tropopause aerosol layer within the 2017 monsoon anticyclone: microphysical properties derived from aircraft-borne in situ measurements." *Atmos. Chem. Phys.*, **21**, 15259–15282, https://doi.org/10.5194/acp-21-15259-2021.

Saunois, M., Stavert, A. R., Poulter, B., *et al.* (2020). "The Global Methane Budget 2000–2017." *Earth Syst. Sci. Data*, **12**, 1561–1623, https://doi.org/10.5194/essd-12-1561-2020.

Vernier, J.-P., Thomason, L. W., and Kar, J. (2011). "CALIPSO detection of an Asian tropopause aerosol layer." *Geophys. Res. Lett.*, **38**, L07804, https://doi.org/10.1029/2010GL046614.

Weigel, R., Mahnke, C., Baumgartner, M., *et al.* (2021). "In situ observation of new particle formation (NPF) in the tropical tropopause layer of the 2017 Asian monsoon anticyclone – Part 1: Summary of StratoClim results." *Atmos. Chem. Phys.*, **21**, 11689–11722, https://doi.org/10.5194/acp-21-11689-2021.

DERIVATION OF CLOUD CONDENSATION NUCLEI VERTICAL DISTRIBUTIONS FROM CALIOP LIDAR DATA IN THE CAPO VERDE REGION

I. KOUTOUNIDIS[1], E. GIANNAKAKI[1]

[1]*Department of Environmental Physics and Meteorology, Faculty of Physics, University of Athens*

Keywords: CCN, CALIPSO, AERONET, aerosols, dust, smoke.

INTRODUCTION

Large uncertainties in weather and climate projections are driven by limited understanding of aerosol-cloud interactions, particularly the roles of aerosols in liquid, mixed-phase, and cirrus cloud formation. Aerosol particles can act as cloud condensation nuclei (CCN) and/or ice-nucleating particles (INP), with the latter contributing to ice crystal formation via immersion freezing mechanisms.
Ground-based active remote sensing systems, such as lidar and radar, provide high-resolution vertical profiles of aerosol and cloud properties, offering valuable insights into aerosol-cloud interactions under real atmospheric conditions. Several studies have demonstrated that aerosol optical properties can be used to estimate CCN concentrations [1]. More recent efforts have extended this approach to estimate CCN and INP vertical profiles using lidar observations [2], [3].
This work investigates the capability of retrieving CCN and INP profiles for biomass burning and desert dust aerosols across CALIPSO lidar track observations, supported by long-term AERONET.

METHODS

For the retrieval of CCN we need to know the relationship between the observed (ambient) microphysical properties of particle number concentrations considering dry particles with radius: > 50nm (n50, reservoir of biomass burning aerosols); > 100 nm (n100, reservoir of dust aerosols); > 250 nm (n250, reservoir of favorable INP) and the ambient particle extinction coefficient for biomass burning and desert dust aerosol conditions [e.g. 2,3]. The observed correlations of n100, n250 for pure dust conditions (Ångström exponents < 0.5) at Capo Verde are shown in Figure 1.

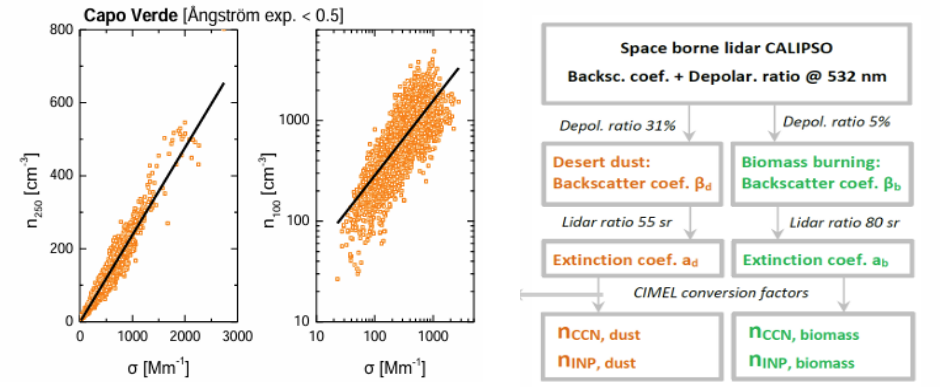


Figure 1 Left: Particle number concentrations n250 and n100 vs 532 nm particle extinction coefficient for Capo Verde Right: Overview of the data analysis scheme.

Table 1. Conversion parameters required in the conversion of particle extinction coefficients into particle number concentrations. The values are given for 532 nm. $c_{50,b}$, $c_{100,d}$ (in cm^{-3} for $\sigma i = 1 Mm^{-1}$), and x_i and respective standard deviations (SD) are obtained from the log-log regression analysis. The mean values and SD of $c_{250,d}$ (in $Mmcm^{-3}$) are computed are also given.

Desert dust	$c_{100,d}$	$x_{d,100}$	$c_{250,d}$
Capo Verde	9.3±1.1	0.74±0.01	0.24±0.001
Biomass burning	$c_{50,b}$	$x_{b,50}$	$c_{250,b}$
Bujumbura	1683.8±1.7	0.35±0.08	0.23 ± 0.008

A deep aerosol layer up to 3.5 km is observed from CALIPSO observations on 31st of January 2008 between 01:44-02:30 UTC that is classified as dust or polluted dust. Six days HYSPLIT backward trajectories ending at three different points of CALIPSO orbit on 31st of January 2008, 02:00 UTC are also shown in the right panel of Figure 2. MODIS fires are superimposed. For each of our backscatter profile along CALIPSO track we perform the aerosol typing. The backscatter coefficients of smoke and dust particles are then converted to extinction coefficients using appropriate lidar ratios.

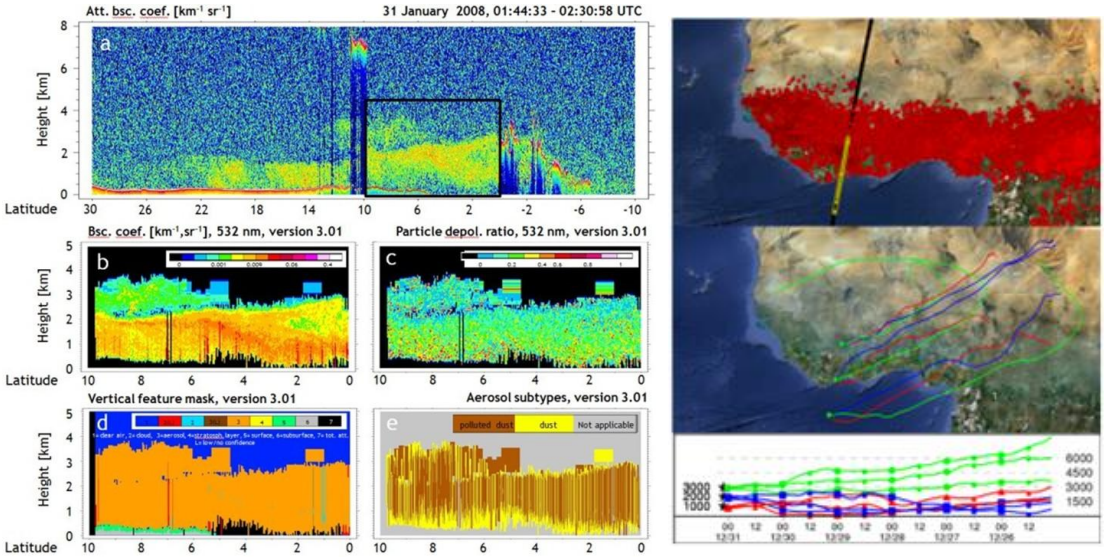


Figure 2 Left: CALIPSO measurement during an overpass on the East of Praia at around 02:30 UTC on 31 January 2008 in terms of latitude-height plots of the Right: MODIS 10 day fire map that shows all locations of fires detected during 21 – 30 January period and six days HYSPLIT backward trajectories ending at three different points of CALIPSO orbit on 31 January 2008, 02:00 UTC.

Each extinction coefficient is then converted to CCN by using the corresponding conversion factors that were calculated from AERONET sunphotometer data and shown in Table 1. The methodology is presented in the right panel of Figure 1.

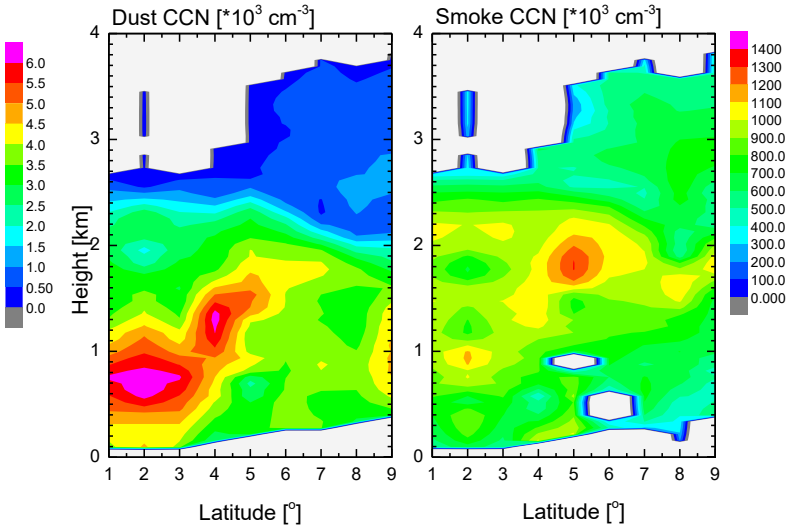


Figure 3 CCN of dust and smoke aerosols for 1o average along CALIPSO track

CONCLUSIONS

This study demonstrates the feasibility of retrieving vertical CCN profiles from CALIPSO lidar observations by applying aerosol-type separation and conversion factors derived from AERONET sun photometer data. CCN-relevant number concentrations (n_{50} for biomass burning, n_{100} for dust) were retrieved along a CALIPSO overpass, showing good agreement with expected spatial distributions and aerosol transport pathways. Although INP estimation was not feasible for the selected case due to temperature constraints, the methodology is readily applicable under colder conditions. Future efforts will focus on expanding the dataset, validating retrievals with in situ observations, and quantifying associated uncertainties to refine space-based aerosol-cloud interaction assessments.

ACKNOWLEDGEMENTS

The research work was supported by the Hellenic Foundation for Research and Innovation (H.F.R.I.) under the “Basic Research Financing (Horizontal support for all Sciences), National Recovery and Resilience Plan (Greece 2.0)” (Project Number: 015144).

REFERENCES

[1] Shinozuka, Y., Clarke, A. D., Nenes, A., Jefferson, A., Wood, R., McNaughton, C. S., Ström, J., Tunved, P., Redemann, J., Thornhill, K. L., Moore, R. H., Lathem, T. L., Lin, J. J., and Yoon, Y.J.: The relationship between cloud condensation nuclei (CCN) concentration and light extinction of dried particles: indications of underlying aerosol processes and implications for satellite-based CCN estimates, Atmos. Chem. Phys. 15, 7585–7604, 2015.
[2] Mamouri, R. E. and Ansmann, A.: Estimated desert-dust ice nuclei profiles from polarization lidar: methodology and case studies, Atmos. Chem. Phys. 15, 3463–3477, 2015.
[3] Mamouri, R. E. and Ansmann, A.: Potential of polarization lidar to provide profiles of CCN- and INP-relevant aerosol parameters, Atmos. Chem. Phys. 16, 5905–5931, 2016.
[4] Winker, D. M., Vaughan, M. A., Omar, A., Hu, Y., Powell, K. A., Liu, Z., Hunt, W. H. and Young, S. A.: Overview of the CALIPSO mission and CALIOP data processing algorithims, J. Atmos. Oceanic Technol. 26, 2310-2323, 2009.
[5] Tesche, M., Ansmann, A., Müller, D., Althausen, D., Engelmann, R., Freudenthaler, V., and Groß, S.: Vertically resolved separation of dust and smoke over Cape Verde using multiwavelength Raman and polarization lidars during Saharan Mineral Dust Experiment 2008, J. Geophys. Res. 114, D13202, 2009.

[6] Groß, S., Tesche, M., Freudenthaler, V., Toledano, C., Wiegner, M., Ansmann, A., Althausen, D., and Seefeldner, M.: Characterization of Saharan dust, marine aerosols and mixtures of biomass burning aerosols and dust by means of multi-wavelength depolarization and Raman lidar measurements during SAMUM 2, Tellus B 63, 706–724, 2011.
[7] Müller, D., Ansmann, A., Mattis, I., Tesche, M., Wandinger, U., Althausen, D., and Pisani, G.: Aerosol-type-dependent lidar ratios observed with Raman lidar, J. Geophys. Res. 112, D16202, 2007.
Alexander, F.R. and J.O. Nathan (1986). *An Introduction to Ultrasonic Nebulisation,* (Cambridge University Press, Cambridge, U.K.).

INSIGHTS FROM THE COMPARISON BETWEEN HYYTIÄLÄ AND BEIJING

M. KULMALA[1,2,3], W. DU[2] , X. ZHANG[2], T. ZHANG[2], M. XIA[1,2], Y. WANG[1], Z. ZOU[2], F. ZHENG[1], Y. ZHANG[1], Q. ZHA[3], C. YAN[3], Q. YUAN[1,2], L. QI[2], T. PETÄJÄ[2], N. SARNELA[2], I. YLIVINKKA[2], D. ALIAGA[2], R. CAI[2,5], M. AGRO'[2], L. AHONEN[2], P. SCHIESTL-AALTO[2], S. TUOVINEN[2], J. CAI[1,2], J. KUJANSUU[1,2], G. CIARELLI[2], Y. CHENG[6], A. DING[3], K. DÄLLENBACH[7], L. DADA[7], D. WORSNOP[2], F. BIANCHI[2], J. JIANG[4], Y. LIU[1], V.-M. KERMINEN[2] and T. KOKKONEN[2]

[1]*Aerosol and Haze Laboratory, Beijing Advanced Innovation Center for Soft Matter Science and Engineering, Beijing University of Chemical Technology, Beijing 100029, China.*

[2]*Institute for Atmospheric and Earth System Research, Faculty of Science, University of Helsinki, Helsinki 00014, Finland.*

[3]*Nanjing-Helsinki Institute in Atmospheric and Earth System Sciences, Nanjing University, Nanjing, 210023, China and Joint International Research Laboratory of Atmospheric and Earth System Sciences, School of Atmospheric Sciences, Nanjing University, Nanjing, 210023, China.*

[4]*School of Environment, State Key Joint Laboratory of Environment Simulation and Pollution Control, Tsinghua University, Beijing, China.*

[5]*Shanghai Key Laboratory of Atmospheric Particle Pollution and Prevention (LAP[3]), Department of Environmental Science and Engineering, Jiangwan Campus, Fudan University, 200438 Shanghai, China.*

[6]*Max Planck Institute for Chemistry, 55128 Mainz, Germany.*

[7]*PSI Center for Energy and Environmental Sciences, Paul Scherrer Institute, 5232 Villigen PSI, Switzerland.*

Keywords: BEIJING, HYYTIÄLÄ, AEROSOL PROCESSES, NEW PARTICLE FORMATION.

INTRODUCTION

Transport and chemical production of particles in the atmosphere are crucial for both air quality and climate. We performed continuous comprehensive measurements of meteorological conditions, trace gases, condensable vapors and characteristics of clusters, ions and aerosol particles in Hyytiälä which is a forestry site in Finland, and Beijing, and urban megacity in China, from 2018 to 2022. Hyytiälä and Beijing represent contrasting locations, motivating a detailed comparison between the two locations. We summarize here our main findings of the comparison for selected variables.

METHODS

SMEAR II in Hyytiälä in the boreal forests of Finland (61°50′N, 24°17′E), is representating clean environments (Hari *et al.*, 2005). Aerosol and Haze Lab (BUCT/AHL), located on the west campus of Beijing University of Chemical and Technology in Beijing, China (39°94′N, 116°30′E), is a typical polluted megacity (Liu *et al.*, 2020). Comprehensive measurements were performed simultanuously in both stations to obtain detailed information on meteorological conditions and gas and particle phase pollutants. To ensure that these instruments performed steadily, inter-comparisons and/or instrument calibration were conducted during the observations.

We analyzed how biogenic and anthropogenic emissions influence some of these variables in aging air masses by utilizing time over land (TOL) in Hyytiälä and time over populated land (TOPL) with high anthropogenic emissions in Beijing. For variables relevant to atmospheric new particle formation (NPF) and growth, we combined the above analysis with a new method that ranks individual days based on a simple metric that describes the intensity of NPF on that day (higher ranking indicates higher NPF intensity) (Aliaga *et al.,* 2023).

CONCLUSIONS

The median concentrations of major air pollutants were approximately 4 (for CO) to 40 (for NO) times higher in Beijing than in Hyytiälä, except ozone, which showed a very similar median concentration level at both sites, but considerably larger diurnal and seasonal variability in Beijing. Similar to the particle mass concentration ($PM_{2.5}$) and condensation sink, median particle number concentrations in different size ranges were roughly ten times higher in Beijing than in Hyytiälä. Organic material dominated the particle mass in Hyytiälä, while the mass fraction of nitrate was on the same order of magnitude compared with organics in Beijing. We confirmed the expectation that the days with higher NPF-related rankings had higher new particle formation rates at both sites, and that NPF tended to be more intense at fresher air masses having lower pre-existing particle loadings. Our results suggest that NPF is associated with sulphuric acid and highly oxygenated organic molecules (HOMs) in Hyytiälä, while in Beijing NPS is typically associated with sulphuric acid dimers indicative of sulfuric acid-base (ammonia/amines) clustering

These massive datasets could help the modelling community in evaluating and understanding model simulation results. Observational datasets for model evaluation are usually very fragmented, limiting our capability of understating what is going right/wrong in models. These types of collaborative efforts forming the next level of observational datasets can bringing our modelling prediction capability to another level of understanding.

ACKNOWLEDGEMENTS

We acknowledge the following projects: ACCC Flagship funded by the Academy of Finland grant number 337549**,** Academy professorship funded by the Academy of Finland (grant no. 302958), Academy of Finland projects no. 325656, 311932, 334792, 316114, 325647, 325681, 333397, 328616, 357902, 345510, 347782, "Quantifying carbon sink, CarbonSink+ and their interaction with air quality" INAR project funded by Jane and Aatos Erkko Foundation, "Gigacity" project funded by Wihuri foundation, European Research Council (ERC) project ATM-GTP Contract No. 742206, and European Union via Non-CO2 Forcers and their Climate, Weather, Air Quality and Health Impacts (FOCI), and CRiceS (No 101003826), RI-URBANS (101036245), EMME-CARE (856612) and FORCeS (821205). The Technology Industries of Finland Centennial foundation via urbaani ilmanlaatu 2.0 -project is gratefully acknowledged. University of Helsinki support via ACTRIS-HY is acknowledged. Support of the technical and scientific staff in Hyytiälä and BUCT/AHL are acknowledged. L.D. acknowledges funding from the Swiss National Science Foundation (grant number 216181).

REFERENCES

Hari, P. and M. Kulmala (2005). Station for measuring ecosystem-atmosphere relations (SMEAR II), *Boreal Environ Res* **10**, 315-322.

Liu, Y. *et al.* (2020). Continuous and comprehensive atmospheric observations in Beijing: a station to understand the complex urban atmospheric environment, *Big Earth Data* **4**, 295-321.

Aliaga, D. *et al.* (2023). Nanoparticle ranking analysis: determining new particle formation (NPF) event occurrence and intensity based on the concentration spectrum of formed (sub-5nm) particles, *Aerosol Research* **1**, 81-92.

AUTOMATIC ESTIMATION OF PARTICLE GROWTH RATES USING CROSS CORRELATION TECHNIQUE

J. LAMPILAHTI, S. TUOVINEN, K. LEHTIPALO, P. PAASONEN, V-M. KERMINEN AND M. KULMALA

Institute for Atmospheric and Earth System Research, University of Helsinki, Helsinki, Finland

Keywords: growth rate, new particle formation

INTRODUCTION

Particle growth rate (GR), defined as the rate of change of particle diameter, is a key parameter determined during new particle formation (NPF) event analysis. Conventionally GR is estimated from size-resolved aerosol particle measurements by sequentially fitting functions to the part of the data where the particles are growing and following the fitted peak values (Kulmala et al. 2012) or leading edges (Lehtipalo et al. 2014).

Traditional GR analysis is time consuming because the fitting is done manually one NPF event day at a time. As atmospheric aerosol data sets grow in size, so does the need for automatic methods to determine the particle GRs. Here we introduce the cross correlation method for calculating GRs.

METHODS

Finding the time delay between concentration peaks in successive size channels has been used before to successfully quantify the particle GR (Riccobono et al. 2012). Here we automate this process by applying a cross correlation technique. Cross correlation measures the similarity between two signals as a function of time delay. We choose the two signals to be normalized concentration size channels represented by diameters d_1 and d_2 during one day. The time delay at maximum cross correlation (t_max) is chosen for the GR calculation in the given size range according to GR = (d_2-d_1)/t_max.

CONCLUSIONS

We tested the cross correlation method on multiple data sets. Figure 1a and 1b show the GR distributions obtained for 2-3 nm negative ions from Värriö, Finland and Hyytiälä, Finland respectively. The GR distributions from the two sites are very similar. In both cases the median GR was 1.9 nm/h. The GRs from both NPF and background NPF (Kulmala et al. 2022) are included in the GR distribution. The cross correlation method is a step towards automatic data driven GR analysis that is applicable to large data sets.

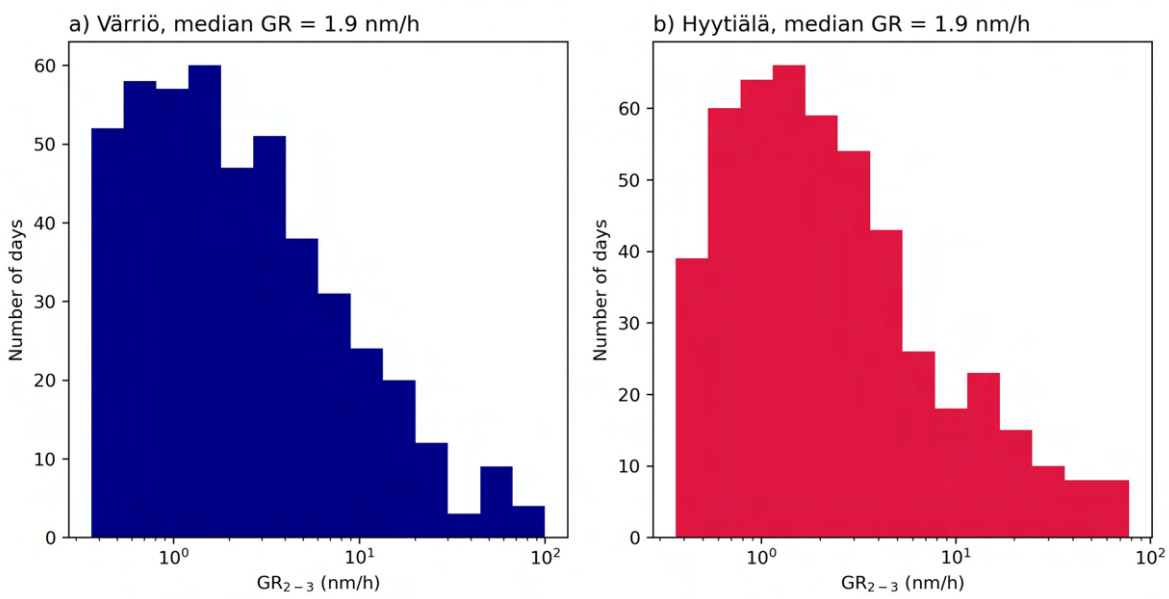


Figure 1. GR distributions obtained from a) Värriö and b) Hyytiälä for negative ions in the 2-3 nm size range. The data is from 2018 onwards and is measured by the Neutral cluster and Air Ion Spectrometer (NAIS, Airel Ltd).

ACKNOWLEDGEMENTS

This work was supported by the Research Council of Finland University Profiling funding InterEarth (grant no. 353218)

REFERENCES

Kulmala, M., et al. (2012). Measurement of the nucleation of atmospheric aerosol particles, *Nat. Protocols*, **7**, 1651–1667.

Lehtipalo, K., et al. (2014). Methods for determining particle size distribution and growth rates between 1 and 3 nm using the Particle Size Magnifier, *Boreal Env. Res.*, **19** (suppl. B), 215–236.

Kulmala, M., et al. (2022). Quiet new particle formation in the atmosphere, *Front. Environ. Sci.* **10**, 912385.

Riccobono, F., et al. (2012). Contribution of sulfuric acid and oxidized organic compounds to particle formation and growth. *Atmos. Chem. Phys.,* **12**, 9427–9439.

ADVANCED SOURCE APPORTIONMENT OF CARBONACEOUS AEROSOLS: INTEGRATING PMF AND MACHINE LEARNING FOR OA AND BC ATTRIBUTION

L. LEI[1], W. XU[2], C. LIN[3], B. CHEN[2], K.N. FOSSUM[1], D. CEBURNIS[1], C. O'DOWD[1] and J. OVADNEVAITE[1]

[1]School of Natural Sciences, Ryan Institute's Centre for Climate & Air Pollution Studies, University of Galway, Galway, Ireland
[2]Center for Excellence in Regional Atmospheric Environment, Institute of Urban Environment, Chinese Academy of Sciences, Xiamen, China
[3]CAS Center for Excellence in Quaternary Science and Global Change & State Key Laboratory of Loess and
Quaternary Geology, Chinese Academy of Sciences, Xi'an 710061, China

Keywords: CARBONACEOUS AEROSOL, SOURCE APPORTIONMENT, MACHINE LEARNING.

INTRODUCTION

Particulate matter (PM) in the atmosphere significantly degrades air quality, impacts regional and global climate [1], and poses severe health risks, causing millions of premature deaths every year [2-3]. Carbonaceous aerosols, comprising organic aerosol (OA) and black carbon (BC), play critical roles in anthropogenic air pollution and climate impacts, particularly in urban areas where residential heating is a major contributor to pollution events. OA, accounting for 20–90% of submicron PM [4], is more toxic than inorganic species but remains poorly understood due to its complex composition, sources, and formation processes. BC, a major light-absorbing component of PM, contributes to atmospheric warming and is a key pollutant in combustion-related emissions. Positive Matrix Factorization (PMF) has long been a powerful and widely used tool for OA source apportionment [5], providing detailed insights into primary and secondary sources. It has also been applied to BC source apportionment, offering an alternative to the traditional Aethalometer model, which relies on fixed absorption coefficients for fossil fuel and biomass burning emissions. While PMF is a powerful tool for source apportionment, real atmospheric processes can be highly nonlinear and complex, involving overlapping sources and secondary formation. As a result, PMF alone may not always be sufficient to fully resolve these intricate interactions.

Machine learning (ML) has emerged as a powerful tool for air quality analysis, successfully applied in pollution forecasting and PM source apportionment [6-7]. ML can capture nonlinear interactions and subtle patterns that traditional models miss. In this study, we integrate supervised ML models with PMF analysis to enhance OOA source apportionment and further differentiate BC from fossil fuels into traffic and heating oil sources. By combining PMF with machine learning, we improve the identification and quantification of carbonaceous aerosols from mixed sources, addressing key limitations of conventional PMF analysis.

METHODS

Submicron PM (PM_1) composition was measured at an urban background site in Dublin, Ireland, from August 2016 to December 2023. OA and other non-refractory PM_1 (NR-PM_1) species were quantified using a Quadrupole Aerosol Chemical Speciation Monitor (Q-ACSM), while equivalent black carbon (eBC) was retrieved from a 7-wavelength Aethalometer (AE33) using attenuation at 880 nm.

Positive Matrix Factorization (PMF) was applied to both OA and BC. For OA, a rolling-PMF approach (14-day window, 1-day step) was performed to account for potential temporal variability in OA profiles and sources over time, resolving six factors. Primary OA (POA) was constrained using reference spectra from burning experiments (peat, wood, coal) and hydrocarbon-like OA (HOA) from the AMS UMR database. For BC, conventional PMF analysis identified fossil fuel and solid fuel sources, with the fossil fuel BC profile constrained using kerbside site measurements dominated by traffic emissions.

To enhance source apportionment, supervised machine learning models were developed. For OOA, the model leveraged correlations with primary species during local pollution events to distinguish local and regional contributions. For BC, machine learning further separated fossil fuel BC into traffic and heating oil sources based on their distinct diurnal patterns, with traffic emissions remaining stable year-round and heating oil emissions appearing only during winter heating hours.

CONCLUSIONS

This study demonstrated the effectiveness of integrating machine learning with PMF analysis to enhance the source apportionment of carbonaceous aerosols in Dublin. While rolling-PMF identified OOA as a major OA component (47–74%), it could not differentiate local and transboundary contributions. The machine learning model successfully attributed OOA to these sources, aligning well with PMF results during local pollution events. During local emission-dominated episodes, the model attributed the majority of OOA to local sources, while during transboundary episodes, most of OOA was attributed to regional transport, suggesting the robustness of the machine learning model. Applying the model to a mixed-pollution episode underscored that, despite transboundary contributions, local emissions from residential heating remained the dominant OA source, highlighting the need to reduce local OA emissions and differentiate OOA sources for effective air pollution control.

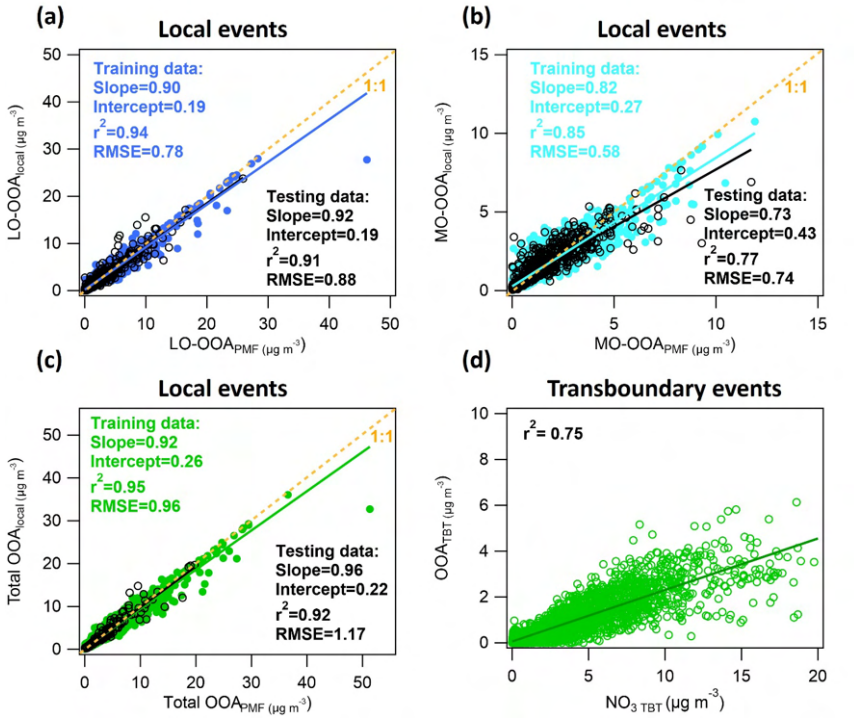


Figure 1. Scatter plots comparing predictions from the machine learning model and rolling-PMF analysis for (a) LO-OOA, (b) MO-OOA, and (c) total OOA during selected local events. Panel (d) shows the scatter plot of OOA from transboundary transport (OOA_{TBT}) calculated from the model versus measured NO_3 filtered for transboundary transport ($NO_{3\ TBT}$).

For BC, PMF effectively distinguished fossil fuel and biomass burning sources, with AAE values as model outputs rather than inputs, improving reliability of the source apportionment over the Aethalometer model. BC exhibited strong seasonality, with fossil fuel BC prevailing year-round and biomass burning contributions increasing in winter. Machine learning further refined BC attribution by separating fossil fuel BC into traffic and heating oil sources, identifying heating oil as the dominant contributor during heating hours. This integration of PMF and machine learning provides a more precise framework for carbonaceous aerosol source apportionment, with direct implications for air quality management and policy.

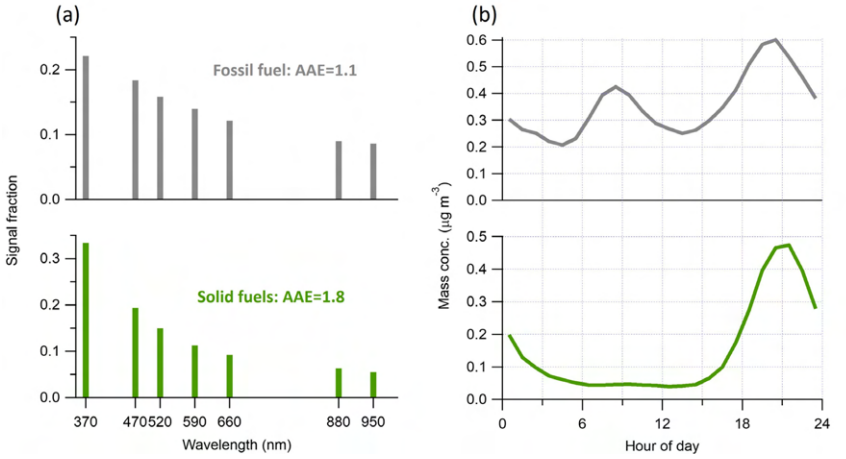


Figure 1. (a) Spectral dependence of black carbon (BC) from fossil fuel (gray) and solid fuel (green) sources, with AAE values of 1.1 and 1.8, respectively. Panel (b) shows the distinct diurnal variations of BC from fossil fuel and solid fuels.

ACKNOWLEDGEMENTS

This work has received funding from European Union's Horizon Europe Research and Innovation programme under HORIZON-CL5-2022-D1-02 (grant no. 101081430 – PARIS). This publication has also emanated from research jointly funded by Taighde Éireann – Research Ireland under Grant number [22/FFP-A/10611], and by National Key R&D Program of China (2023YFC3705503), Hundred Talents Program of Chinese Academy of Sciences, EPA-Ireland, the Department of Environment, Climate and Communications.

REFERENCES

1. IPCC, Intergovernmental Panel on Climate Change (2021), Climate Change 2021: The Physical Science Basis. Working Group I contribution to the Sixth Assessment Report of the Intergovernmental Panel on Climate Change. **2021**.
2. Pope, C. A.; Dockery, D. W., Health effects of fine particulate air pollution: lines that connect. *Journal of the Air & Waste Management Association* **2012,** *56* (6), 709-742.
3. Shiraiwa, M.; Ueda, K.; Pozzer, A.; Lammel, G.; Kampf, C. J.; Fushimi, A.; Enami, S.; Arangio, A. M.; Frohlich-Nowoisky, J.; Fujitani, Y.; Furuyama, A.; Lakey, P. S. J.; Lelieveld, J.; Lucas, K.; Morino, Y.; Poschl, U.; Takahama, S.; Takami, A.; Tong, H.; Weber, B.; Yoshino, A.; Sato, K., Aerosol health effects from molecular to global scales. *Environmental Science & Technology* **2017,** *51* (23), 13545-13567.
4. Jimenez, J. L.; Canagaratna, M. R.; Donahue, N. M.; Prevot, A. S. H.; Zhang, Q.; Kroll, J. H.; DeCarlo, P. F.; Allan, J. D.; Coe, H.; Ng, N. L.; Aiken, A. C.; Docherty, K. S.; Ulbrich, I. M.; Grieshop, A. P.; Robinson, A. L.; Duplissy, J.; Smith, J. D.; Wilson, K. R.; Lanz, V. A.; Hueglin, C.; Sun, Y. L.; Tian, J.; Laaksonen, A.; Raatikainen, T.; Rautiainen, J.; Vaattovaara, P.; Ehn, M.; Kulmala, M.; Tomlinson, J. M.; Collins, D. R.; Cubison, M. J.; Dunlea, J.; Huffman, J. A.; Onasch, T. B.; Alfarra, M. R.; Williams, P. I.; Bower, K.; Kondo, Y.; Schneider, J.; Drewnick, F.; Borrmann, S.; Weimer, S.; Demerjian, K.; Salcedo, D.; Cottrell, L.; Griffin, R.; Takami, A.; Miyoshi, T.; Hatakeyama, S.; Shimono, A.; Sun, J. Y.; Zhang, Y. M.; Dzepina, K.; Kimmel, J. R.; Sueper, D.; Jayne, J. T.; Herndon, S. C.; Trimborn, A. M.; Williams, L. R.; Wood, E. C.; Middlebrook, A. M.; Kolb, C. E.; Baltensperger, U.; Worsnop, D. R., Evolution of organic aerosols in the atmosphere. *Science* **2009,** *326* (5959), 1525-1529.
5. Paatero, P.; Hopke, P. K., Discarding or downweighting high-noise variables in factor analytic models. *Analytica Chimica Acta* **2003,** *490* (1-2), 277-289.

6. Zhu, J. J.; Yang, M.; Ren, Z. J., Machine Learning in Environmental Research: Common Pitfalls and Best Practices. *Environmental Science & Technology* **2023,** *57* (46), 17671-17689.
7. Zhong, S.; Zhang, K.; Bagheri, M.; Burken, J. G.; Gu, A.; Li, B.; Ma, X.; Marrone, B. L.; Ren, Z. J.; Schrier, J.; Shi, W.; Tan, H.; Wang, T.; Wang, X.; Wong, B. M.; Xiao, X.; Yu, X.; Zhu, J. J.; Zhang, H., Machine Learning: New Ideas and Tools in Environmental Science and Engineering. *Environmental Science & Technology* **2021,** *55* (19), 12741-12754.

RESEARCH ON NEW PARTICLE FORMATION (NPF) IN THE EARTH'S TROPOSPHERE: A HISTORICAL AND PERSONAL PERSPECTIVE

P.H. MCMURRY[1]

[1]*Professor Emeritus, Department of Mechanical Engineering, University of Minnesota, Minneapolis, Minnesota, USA.*

Keywords: Nucleation, New Particle Formation, Instrumentation, History

INTRODUCTION

New particles are formed in the atmosphere by chemical processes that lead to the formation of stable molecular clusters and their subsequent growth (e.g., Kulmala et al., 2004). It is currently estimated that new particle formation (NPF) accounts for about half of the cloud condensation nuclei in the atmosphere (Gordon, 2017). I will describe some early work on new particle formation in the troposphere that I think was remarkably insightful, focusing particularly on the work of John Aitken (1839-1919). I will follow this with a brief discussion of important developments in recent decades and conclude with highlights from my 40-year research adventure on this topic. The literature shows that the development of new instrumentation, experimental studies in both the atmosphere and laboratory, and theoretical analyses have played essential roles in advancing our understanding of NPF.

DISCUSSION

Seminal research on NPF in the troposphere was done by the Scottish scientist, John Aitken (1839-1919). In his early work, Aitken (1880-1881) showed that clouds are formed when steam is mixed with ambient air. Until he made those observations, most previous work on atmospheric aerosols focused on particle mass concentrations and composition. Based on that work he concluded that particle number concentrations were also important, and that there "seems to be a possibility of some relation between dust and certain questions of climate, rainfall, etc." About a decade later he invented an instrument for quantitative measurements of particle number concentrations (Aitken, 1888), and two years after that a "simple pocket dust counter…a little larger than a well-filled cigar case" (Aitken, 1890-91) that could easily be used for atmospheric observations. This led to a series of papers on factors that affect ambient particle concentrations, including new particle formation by photochemical processes. He showed that NPF occurred near Kingairloch, Scotland, an estate on the Firth of Lorne (Aitken,1911): "The dust counter was used just as a dog uses its nose when quartering the ground in search for game" and "the sun born nuclei are produced by some changes taking place on the foreshore." He followed up these observations with laboratory experiments where he explored the possibility that salt, iodine or oxidants (H_2O_2 and O_3) might be contributing to NPF. His experiments were less definitive than he might have preferred, and he concluded that "The great difficulty in investigations of this kind is the extremely minute quantities of matter which produce surprising results and make the work full of pitfalls for the hasty…" He also showed (Aitken, 1911-12) that SO_2 and NH_3 contribute to new particle formation, and that NPF is more likely to occur in polluted air than in clean background air: "I find that SO_2, so long as it is in good company, - that is, in pure air - shows no tendency to produce any kind of nuclei.". Surprisingly, I found relatively few references to Aitken's work until recently. Regrettably, that includes my early papers.

There were occasional studies of atmospheric particle number concentrations in the following decades, although I am not aware of work that focused on NPF. The discovery by Haagen-Smit and coworkers that oxidants are formed by photochemical processes that include organic compounds in polluted Los Angeles air (e.g., Haagen-Smit et al, 1953) led to research on chemical processes that produce secondary aerosol mass from SO_2, oxides of nitrogen, and organic compounds. In an early study that led to further work by others, Went (1960) suggested that plant-derived secondary organic particulate matter "is a material for petroleum formation." Smog chamber studies carried out in the 1970s often made use of TSI's electrical

aerosol analyzer (Liu and Pui, 1975). However, most of those chamber studies focused on chemical processes, not on aerosol dynamics. Theoretical studies on "heteromolecular nucleation," especially involving sulfuric acid and water, were also published in this period (e.g., Reiss, 1950; Stauffer and Kiang, 1974). This eventually led to a renewed interest in atmospheric NPF. Noteworthy for me was the work of Austin Hogan and coworkers. Hogan (1968) reported on measurements made at a rural site using an automated GE CNC "at the Crawford Hill Observatory, located atop a 1400 ft hill, 8 miles NW of Schenectady, New York, in a rural area generally free from local contamination." He showed that with the switch from Daylight to Standard time in October 1967, the characteristic increase in Aitken nucleus concentrations typically observed during mornings at this site followed the sun and not human activity. He concluded that photochemically-driven NPF often occurs during the mornings at this site. During my doctoral research at Caltech in the mid 1970s I attempted without success to replicate this result for Pasadena air. I was unable to find any clear evidence for NPF, almost certainly because human activities and not photochemical NPF dominated particle concentrations at this polluted urban location. Hogan and coworkers also reported on a comprehensive study of both aircraft and surface particle concentrations in and around Greenland (Flyger et al., 1976). They found no evidence for NPF on the surface but, for air aloft, "The size spectra strongly indicate that formation of fresh nuclei by gas phase reactions is a common phenomenon."

The modern era for research on new particle formation in the earth's troposphere arguably began with the work of Charlson et al. (1987), who discussed the possible link between cloud-condensation nuclei produced by dimethyl sulphide produced by planktonic algae in sea water and the earth's radiation balance. This led to a series of studies using aircraft (e.g., Hegg et al, 1991; Clarke, 1992), which showed evidence for widespread nucleation in the marine boundary layer and in cloud outflows.

Of great significance since the mid 1990s are continuous, long-term measurements, first carried out in the boreal forest site at Hyytiälä, Finland beginning in 1996 and continuing today (Kulmala et al., 2023). There are now four stations in Finland that provide continuous measurements as well as international stations based on this model, including one in Beijing. These measurements, which include occasional intensive measurement campaigns often done in collaboration with scientists from around the world, have added tremendously to our understanding of meteorological, biological, physical and chemical processes that influence NPF in the atmosphere. For example, these data clearly show the long-term trends in concentrations of trace gas precursors, particle concentrations and the effects of aerosols and clouds on radiation over this 30-year period. The impacts of the global shut down during the COVID epidemic are also evident. An early result from Hyytiälä is the publication of a "banana" plot providing an easily understood graphical demonstration of new particle formation and growth for data acquired during several days in 1996 (Mäkelä, 1997). This soon became a standard way to present such data. Hypotheses raised by that and other work have been studied since 2009 in the CLOUD chamber studies headquartered at CERN (e.g., Kirkby et al, 2023). This work has been carried out under very well controlled conditions using a suite of the world's most innovative instrumentation and has led to many high-profile publications that have had a tremendous impact on our understanding of the global impact of NPF. The CLOUD program has carried out series of campaigns that have focused on issues that include the impact of cosmic rays on particle production, the significance of ion-induced nucleation, and the roles of sulfuric acid, ammonia, amines, iodine, and various organic compounds including biogenic compounds, etc. Results from these studies have often been applied in global models to determine the effects of various processes on atmospheric NPF. An important byproduct of the CLOUD program has been the nurturing of a large community of talented young atmospheric scientists.

I will dedicate part of my talk to describing my journey on NPF. My work on NPF began in 1972 when my doctoral advisor at Caltech, Sheldon Friedlander, suggested that I study nucleation in the presence of a preexisting aerosol. He had been working on his book, "Smoke, Dust, and Haze: Fundamentals of Aerosol Dynamics," which included a chapter on classical nucleation theory. That theory does not include a term for vapor depletion by condensation on preexisting particles which would be important if NPF were to occurr in the atmosphere. I thought a lot about the problem and came to understand how I wanted to approach it, but did not have access to the numerical or experimental tools I needed to pursue many of my ideas. However, at about the same time, William Clark (1972, 1975) was working on his doctoral research

with Ken Whitby at the University of Minnesota. Clark used a Whitby Aerosol Analyzer (Whitby and Clark, 1966) to measure size distributions of particles produced photochemically from SO_2 in a Teflon film chamber using air that was initially particle-free. Although he took care to remove impurities from the air using a charcoal adsorption system, we now know that the air likely contained trace levels of many compounds that may have contributed to particle formation and/or growth. Nevertheless, he was able to acquire high quality measurements of size distributions. The aerosol volume (mass) formation rates observed in these experiments were reasonably constant. Furthermore, by varying the initial SO_2 concentration, Clark was able to vary those aerosol formation rates over a wide range. If it is assumed that 100% of the particle mass consisted of oxidized SO_2 (i.e., sulfates), which I did when analyzing his data, estimates of the rate of sulfuric acid formation, R, could be estimated. Also significant for my work was the doctoral research of Fred Gelbard under the supervision of John Seinfeld at Caltech. Fred's work included the development of accurate numerical methods for solving the aerosol general dynamic equation in chemically reacting systems, including the formation of clusters by nucleation (Gelbard and Seinfeld, 1978). Beginning in 1977, when I was an Assistant Professor at the University of Minnesota, I used Gelbard's numerical methods to analyze Clark's chamber data for aerosol nucleation and growth from SO_2.

I cast the general dynamic equation for aerosols in a nucleating system in a nondimensional form that was independent of the rate at which the condensing vapor (presumably H_2SO_4) was being formed from SO_2 and used Gelbard's software to solve those equations (McMurry, 1980). My theory predicted that following a burst of nuclei formation, NPF soon ceased followed by growth of particles that were formed early in the process. The total concentration of particles formed was predicted to vary in proportion to $R^{1/2}$, and that was in good prediction with Clark's data as was the absolute value of particle concentrations produced. This was a surprising result, as my theoretical approach was conceptually simplistic: I assumed that all collisions were 100% effective, i.e., that nucleation is a coagulation process with no subsequent evaporation from clusters. Under the conditions of Clark's experiments, evaporation of H_2SO_4 from nucleated clusters would have been significant if classical binary nucleation of H_2O and H_2SO_4 was responsible for particle production. I thought it likely that some additional species reacted with nucleated clusters that increased their stability. Shortly before I retired, Chenxi Li, a doctoral student, and I revisited this numerical work (McMurry and Li, 2017). Clark's work provided some evidence that at low R values, the number of particles produced was less than is predicted by collision-limited particle formation. McMurry and Li's more comprehensive analysis uses dimensionless rate constants to determine the effects of wall deposition, scavenging by preexisting particles, and evaporation from clusters, considering both classical and chemical nucleation processes, on the concentrations of particles formed in a chamber. When the values of those rate constants are large enough (or, equivalently, when R is small enough), those processes begin to have a significant impact on NPF observed in a chamber.

While I did not understand why the collision-controlled NPF model so accurately explained Clark's observations (especially at high R) it identified the questions my research team and I pursued during the coming 40 years, including new methods to measure concentrations and sizes of nanoparticles formed by NPF (Stolzenburg and McMurry, 1991; Saros et al, 1996; Iida et al, 2009). Eventually, I established collaborations with Fred Eisele, Jim Smith, Dave Hanson and others that enabled us to measure concentrations of gas phase precursors including sulfuric acid and amines, molecular clusters, and the composition of freshly nucleated particles. We focused our research on learning why NPF rates were often so high (Kuang et al. (2008), Kuang et al (2009), Zhao et al. (2010), Chen et al. (2012), Jen et al. (2016)) and why freshly nucleated particles grew so fast (Smith et al., (2010), Kuang et al., (2012)) and obtained results that answered some of the questions we'd identified. Of course, others have also provided many answers, and much more work remains to be done.

ACKNOWLEDGEMENTS

I wish to express my deep appreciation to the graduate students, postdocs, and senior colleagues who have been so integral to my work on NPF. Those associations have been a highlight of my life. I also greatly

appreciate the financial support from research agencies that have funded this work, including the US NSF, US DOE, and US EPA.

REFERENCES

Aitken, J. (1880-1881), "On dust, fogs, and clouds," *Transactions of the Royal Society of Edinburgh* **XXX**; Collected Scientific Papers of John Aitken, 34.

Aitken, J. (1890-91) "On a simple pocket dust counter," *Proceedings of the Royal Society of Edinburgh* **XVIII**; Collected Scientific Papers of John Aitken, 236.

Aitken, J. (1911) "On some nuclei of cloudy condensation," *Proceedings of the Royal Society of Edinburgh* **XXXI;** Collected Scientific Papers of John Aitken, 495.

Aitken, J. (1911-12) "The sun as a fog producer," Proceedings of the Royal Society of Edinburgh **XXXII**, Collected Scientific Papers of John Aitken, 512.

Charlson, R. J., J. E. Lovelock, M. O. Andreae, S. G. Warren (1987) "Oceanic phytoplankton, atmospheric sulphur, cloud albedo and climate," *Nature* **326**, 655.

Chen, M., M. Titcombe, J. Jiang, C. Jen, C. Kuang, M. L. Fischer, F. L. Eisele, J. I. Siepmann, D. R. Hanson, J. Zhao, P. H. McMurry, (2012) "An acid-base chemical reaction model for nucleation rates in the polluted atmospheric boundary layer," *PNAS* **109**, 18713.

Clark, W. E. (1972) "Measurements of aerosols produced by the photochemical oxidation of SO_2" PhD Thesis, University of Minnesota, Minneapolis, Minnesota, USA

Clark, W. E. and K. T. Whitby (1975) "Measurements of aerosols produced by the photochemical oxidation of SO_2," *J. Colloid Interface Sci.* **51**, 477.

Clarke, A.D. (1992) "Atmospheric nuclei in the remote free troposphere," *J. Atmos. Chem.*, **1**, 479.

Flyger, H., N. Z. Heidam, K.,Hansen, W. J.Megaw, E. G. Walther, and A. W. Hogan (1976) "The background level of the summer tropospheric aerosol, sulphur dioxide, and ozone over Greenland and the North Atlantic Ocean," *J. Aerosol Sci.* **7**, 103.

Gelbard, F. and J. H. Seinfeld (1978) "Numerical solution of the dynamic equation for aerosol systems," *Journal of Computational Physics* **28**, 357.

Gordon, J. Kirkby, U. Baltensperger, F. Bianchi, M. Breitenlechner, J. Curtius, A. Dias, J. Dommen, N. M. Donahue, E. M. Dunne, J. Duplissy, S. Ehrhart, R. C. Flagan, C. Frege, C. Fuchs, A. Hansel, C. R. Hoyle, M. Kulmala, A. Kürten, K. Lehtipalo, V. Makhmutov, U. Molteni, M. P. Rissanen, Y. Stozkhov, J. Tröstl, G. Tsagkogeorgas, R. Wagner, C. Williamson, D. Wimmer, P. M. Winkler, C. Yan, K. S. Carslaw. (2017) "Causes and importance of new particle formation in the present-day and preindustrial atmospheres," *JGR: Atmospheres* **122**, 8739.

Haagen-Smit, A. C. E. Bradley and M. M. Fox (1953) "Ozone formation in photochemical oxidation of organic substances," *Indust. Eng. Chem.* **45**, 2086.

Hegg, D.A., L. F Radke, and P. V Hobbs (1991) "Measurements of Aitken nuclei and cloud condensation nuclei in the marine Atmosphere and their relation to the DMS-cloud-climate hypothesis," *J. Geophys. Res.*, **96**, 18727.

Hogan, A. W. (1968) "An experiment illustrating that gas conversion by solar radiation is a major influence in the dirunal variation of Aitiken nucleus concentrations," *Atmos. Environ.* **2** 599.

Iida, K., M. R. Stolzenburg, and P. H. McMurry (2009) "Effect of working fluid on sub-2 nm particle detection with a laminar flow ultrafine condensation particle counter," *AST* **43**, 81.

Jen, C. N., R. Bachman, J. Zhao, P. H. McMurry, D. R. Hanson (2016) "Diamine-sulfuric acid reactions are a potent source of new particle formation," *GRL.* **43**, 867.

Kirkby, J., A. Amorim, U. Baltensperger, K. S. Carslaw, T. Christoudias, J.Curtius, N. M. Donahue, I. E. Haddad, R. C. Flagan, H. Gordon, A. Hansel, H. Harder, H. Junninen, M. Kulmala, A. Kürten, A. Laaksonen, K. Lehtipalo,, J. Lelieveld, O. Möhler, I. Riipinen, F. Stratmann, A. Tomé, A.Virtanen, R. Volkamer, P. M. Winkler, D. R. Worsnop (2023) "Atmospheric new particle formation from the CERN cloud experiment," *Nature Geoscience* **16**, 948.

Kuang, C., P. H. McMurry, A. V. McCormick, F. L. Eisele (2008) "Dependence of nucleation rates on sulfuric acid vapor concentration in diverse atmospheric locations," *JGR Atmospheres* **113**, D10209.

Kuang, C. I. Riipinen, T.Yli-Juuti, M. Kulmala, A. V. McCormick, P. H. McMurry (2010) "An improved criterion for new particle formation in diverse atmospheric environments," *ACP* **10**, 8469.

Kuang, C., N. Chen, J., Zhao, J., Smith, P. H., McMurry, J., Wang (2012) "Size and time-resolved growth rate measurements of 1 to 5 nm freshly formed atmospheric nuclei," *ACP* **12**, 3573.

Kulmala, M., H. Vehkamaki, T. Petajda, M. Dal Maso, A. Lauri, V. M. Kerminen, W. Birmili, P. H. McMurry (2004) "Formation and growth rates of ultrafine atmospheric particles: a review of observations," *J. Aerosol Sci.* **35**, 143.

Kulmala, M., A. Lintunen, H. Lappalainen, A. Virtanen, C. Yan, E. Ezhova, T. Nieminen, I. Riipinen, R. Makkonen, J. Tamminen, A.-M. Sundström, A. Arola, K. Hansel, A., Lehtinen, T. Vesala, T. Petäjä, J. Bäck, T. Kokkonen, V.-M. and Kerminen (2023) "Opinion: The strength of long-term comprehensive observations to meet multiple grand challenges in different environments and in the atmosphere," *Atmos. Chem. Phys*., **23**, 14949.

Liu, B. Y. H. and D. Y. H. Pui (1975) "The performance of the electrical aerosol analyzer," *J. Aerosol Sci*. **6**:249.

Mäkelä, J.M., P.Aalto, V. Jokinen, T. Pohja, A. Nissinen, S. Palmroth, T. Markkanen, K. Seitsonen, H. Lihavainen, M. Kulmala(1997) "Observations of ultrafine aerosol formation and growth in boreal forest," *Geophysical Research Letters* **24**,1219.

McMurry, P. H. (1980) "A theoretical analysis of smog chamber data," *JCIS* **78**, 513.

McMurry, P. H. and C. Li (2017) "The dynamic behavior of nucleating aerosols in constant rate systems: Dimensional analysis and generic numerical solutions," *AST* **51**,1057.

Reiss, H. (1950) "The kinetics of phase transitions in binary systems," *J. Chem. Phys.***18**, 840.

Saros, M. T., R. J. Weber, J. J. Marti, P. H. McMurry (1996) "Ultrafine aerosol measurement using a condensation nucleus counter with pulse height analysis," *AS&T.* ***25***, 200.

Smith, J. N., K. C. Barsanti, H. R. Friedli, M. Ehn, M. Kulmala, D. R. Collins, J. H. Scheckman, B. J. Williams, P. H. McMurry (2010) "Observations of aminium salts in atmospheric nanoparticles and possible climatic implications," *PNAS* **107**, 6634.

Stauffer, D. and C. S. Kiang (1974) "Heteromolecular nucleation for multicomponent gas mixtures," *Tellus*, **XXVI**, 295.

Stolzenburg, M. R. and P. H. McMurry (1991) "Ultrafine CPC design: Optimizing nanoparticle transport," *AS&T.* ***14***, 48.

Weber,R. J., F. L. Eisele, P. H McMurry et al. (1998) "Measured atmospheric new particle formation rates: Implications for nucleation mechanisms." *Chem. Eng. Comm.* **151**, 53.

Went, F. W. (1960) "Organic matter in the atmosphere and its possible relation to petroleum formation," *PNAS* **46**, 212.

Whitby, K. T. and W. E. Clark (1966) "Electric aerosol particle counting and size distribution measuring system for the 0.0156 to 1 μm size range," *Tellus* **XVIII**, 573.

Zhao, J., F. L. Eisele, M. Titcombe, C. Kuang, P. H. McMurry, P. H. (2010) "Chemical ionization mass spectrometric measurements of atmospheric neutral clusters using the Cluster-CIMS," J*GR* **115**, D08205.

ANTARCTIC CONTINENTAL OUTFLOW AS A TRANSPORT PATHWAY OF BIOGENICALLY DOMINATED AEROSOLS

B.MILJEVIC[1], M. MALLET[2], J.ALROE[1], A.SARASWATHY[1], C.G. OSUAGWU[1], , Z.RISTOVSKI[1], R.HUMPHRIES[3], P. SELLECK[3], M.KEYWOOD[3], S.TAYLOR[3]

[1]International Laboratory for Air Quality and Health, School of Earth and Atmospheric Sciences, Queensland University of Technology, Brisbane, 4001 Australia
[2] Institute for Marine and Antarctic Studies (IMAS), University of Tasmania, Hobart, 7004, Australia
[3]Climate Science Centre, Oceans and Atmosphere, CSIRO, Melbourne, Victoria, Australia

Keywords: marine aerosols, Antarctica, Southern Ocean, sulfuric acid, methanesulfonic acid.

INTRODUCTION

Dimethyl sulfide (DMS) is the largest natural source of sulfur in the atmosphere, in particular in remote marine environments. It originates primarily from dimethylsulfoniopropionate (DMSP), an organosulfur compound produced by marine phytoplankton. After emission into the atmosphere, DMS is chemically transformed through different pathways and oxidation steps, ultimately leading to the production of sulfuric acid (SA; H_2SO_4) and methanesulfonic acid (MSA; CH_3SO_3H).SA is well known to participate in particle nucleation and growth. MSA can contribute to particle growth, but so far there is no in situ observational evidence of its role in particle nucleation. DMS oxidation is complex and dependent on oxidant type and availability as well as environmental conditions (T and Relative Humidity (RH)), resulting in relative yields of its oxidation products being still uncertain. Polar marine environments and in particular Southern Ocean are a significant source of DMS during austral summer (Hulswar et al., 2022). This presentation will primarily discuss MSA and SA in particle and gas phase measured during two summer Southern Ocean voyages with a focus on air masses origin.

METHODS

CAPRICORN-2 (Clouds, Aerosols, Precipitation, Radiation, and atmospheric Composition Over the southeRn ocean; Jan-Feb 2018) and MISO (Multidisciplinary Investigation of the Southern Ocean; Jan – March 2024)) were both campaigns aboard the RV Investigator and both took place in the western Pacific sector of the Southern Ocean (110° – 150° E).Gaseous SA and MSA were measured using a nitrate Chemical Ionisation Mass Spectrometer (NO_3-CIMS); PM1 composition was measured using aerosol mass spectrometers (ACSM during CAPRICORN-2 and compact ToF-AMS during MISO) as well as ~24hr filters. Aerosol size distribution was measured using electrical mobility particle size spectrometers (Grimm and TSI Inc SMPS during CAPRICORN-2 and TROPOS MPSS during MISO). Cloud Condensation Nuclei (CCN) number concentration was measured using CCN counter (Droplet measurement technologies). Standard meteorological variables, such as air temperature, pressure, relative humidity, wind speed and direction were measured as a part of the ongoing underway systems. Periods influenced by ship exhaust have been identified according to (Humphries et al., 2019) and removed from the dataset. It was found that less than around 15% of the data was contaminated by the ship's exhaust. Five day air mass backtrajectories were calculated using HYSPLIT for every hour of the ship's position at a height of 100 m above sea level. For CAPRICORN-2 backtrajectories the Global Data Assimilation System (GDAS) 0.5° meteorological data was used and Global Forecast System (GFS) 0.25° meteorological data was used for the MISO backtrajectories calculations.

CONCLUSIONS

There are some strong similarities between the two voyages: 1) both voyages show an increase in gaseous MSA with latitude (and particularly in the polar cell; Figure 1), while this is not the case for SA; 2) both voyages result in in periods substantially elevated gaseous MSA concentrations with these "high MSA" periods being in duration of 1 to 7 days; 3) "high MSA" periods for both voyages coincide with aerosols having a prominent and persistent accumulation mode and consequently the highest CCN concentrations; 4) During all periods of high gaseous MSA particle composition was strongly dominated by species of biogenic origin (SO_4^{2-}, MS^-).

The periods of high gaseous MSA and biogenically dominated aerosols coincided with a sharp and sustained decrease in both absolute humidity and temperature. Such dry and cold air masses are frequently associated with Antarctic katabatic outflow. Antarctic continental influence of strong directional constancy was confirmed by HYSPLIT backtrajectory analysis. We suggest that this enrichment in biogenic gases (i.e. MSA) and biogenically dominated aerosols during continental outflow results from atmospheric uplift over Antarctic coastal waters, followed by subsidence over the Antarctic continent.

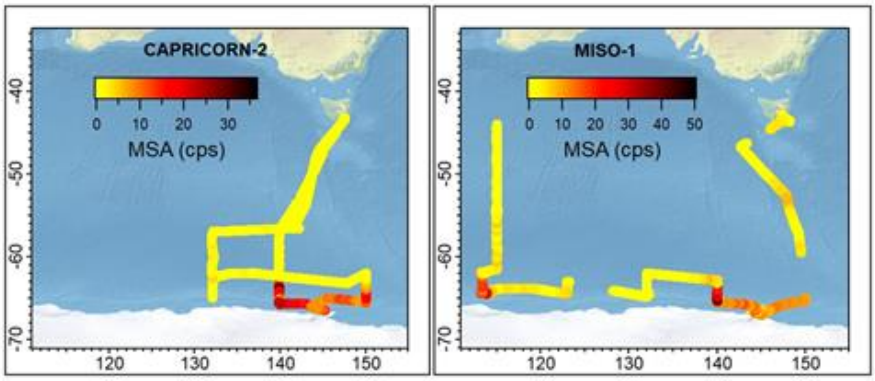


Figure 1. CAPRICORN-2 (Jan-Feb 2018) and MISO (Jan – March 2024) voyage tracks color-coded by the MSA counts.

ACKNOWLEDGEMENTS

The authors wish to thank the CSIRO Marine National Facility (MNF) for their support in the form of sea time on RV Investigator and associated support personnel, scientific equipment and data management during both voyages.

The MISO voyage was supported by the Australian Research Council Discovery project (DP240100389).

REFERENCES

Hulswar, S., Simó, R., Galí, M., Bell, T. G., Lana, A., Inamdar, S., Halloran, P. R., Manville, G., & Mahajan, A. S. (2022). Third revision of the global surface seawater dimethyl sulfide climatology (DMS-Rev3). *Earth Syst. Sci. Data, 14*(7), 2963-2987. https://doi.org/10.5194/essd-14-2963-2022

Humphries, R. S., McRobert, I. M., Ponsonby, W. A., Ward, J. P., Keywood, M. D., Loh, Z. M., Krummel, P. B., & Harnwell, J. (2019). Identification of platform exhaust on the RV Investigator. *Atmos. Meas. Tech., 12*(6), 3019-3038. https://doi.org/10.5194/amt-12-3019-2019

LONG-TERM TRENDS OF PARTICLE NUMBER-SIZE DISTRIBUTIONS AND NEW PARTICLE FORMATION AT SAN PIETRO CAPOFIUME, ITALY

T. NIEMINEN[1], J. JOUTSENSAARI[2], T. YLI-JUUTI[2], V. LEINONEN[3], P. MIETTINEN[2], A. VIRTANEN[2], S. MIKKONEN[4], A. LAAKSONEN[5], S. DECESARI[6], M. C. FACCHINI[6]

[1] *Institute for Atmospheric and Earth System Research INAR, University of Helsinki, Helsinki, Finland*
[2] *Department of Technical Physics, University of Eastern Finland, Kuopio, Finland*
[3] *Tampere University, Faculty of Engineering and Natural Sciences, Tampere, Finland*
[4] *Department of Environmental and Biological Sciences, University of Eastern Finland, Kuopio, Finland*
[5] *Finnish Meteorological Institute, Helsinki, Finland*
[6] *Institute of Atmospheric Sciences and Climate (ISAC) of the Italian National Research Council (CNR), Bologna, Italy*

Keywords: new particle formation, particle growth, long-term trends

INTRODUCTION

Formation and growth of secondary aerosol particles is a major source of atmospheric aerosols. However, only few long-term datasets (at least 10 years of continuous measurements) of atmospheric new particle formation (NPF) exist. Observations in the Finnish boreal forest and at two Arctic sites in Finnish Lapland indicate very small changes in NPF over the past 25 years (Asmi *et al.*, 2011; Kyrö *et al.*, 2014; Nieminen *et al.*, 2014). In Central Europe a clear decrease in NPF occurrence has been reported (Hamed *et al.*, 2010). Comparisons with global model simulations of aerosol number size distributions show similar trends as observed in Europe (Leinonen *et al.*, 2022). In this work we analyze trends in aerosol number size distributions and in NPF characteristics at San Pietro Capofiume in Po Valley region, Northern Italy.

METHODS

The number size distributions of 3–630 nm particles have been measured at the station in 2002–2017 with a twin-DMPS setup. The station is influenced by emissions of local anthropogenic pollutants (such as SO_2) as well as long-range transport from Central and Eastern Europe (Sogacheva *et al.*, 2007), and can therefore provide important information on the impact of anthropogenic activities on aerosol number size-distributions and atmospheric NPF.

The particle number size distribution data was classified into NPF event, non-event, and undefined days (Kulmala *et al.*, 2012). To quantify the NPF events, formation rates of nucleation mode particles (3–25 nm) were calculated from the measured number size-distribution data. Particle growth rates were calculated by fitting log-normal modes to the measured size-distribution data and following the time evolution of the geometric mean size of the fitted nucleation mode.

RESULTS AND CONCLUSIONS

Figure 1 shows the number concentrations of nucleation mode particles measured in 2002–2017. An overall decreasing linear trend of –4.9 %/year is observed, although after 2010 this decrease is not as clear as in the early part of the time series. Also accumulation mode particle (100–630 nm) and particulate matter (PM_{10}) concentrations have declined. Frequency of NPF occurrence did not show any clear trend, varying between 20% and 40% of the days in a year. Both the formation and growth rates of nucleation mode particles had decreasing trends. This indicates that while the sink for the newly formed nucleation-

mode particles has decreased (due to decrease in particulate matter concentrations), a simultaneous decrease in emissions of nucleation precursor vapours (such as SO_2, ammonia, amines, organics) has also occurred.

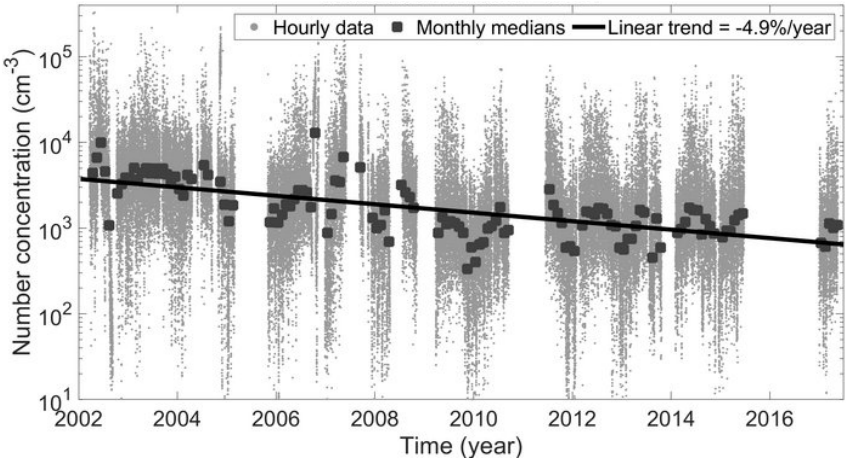


Figure 1. Number concentration of 3–25 nm particles in San Pietro Capofiume 2002–2017. Grey points show the hourly concentrations, black markers indicate the monthly medians, and black line shows the linear trend.

ACKNOWLEDGEMENTS

This work was supported by Research Council of Finland (grants number 307331, 311932, 337549) and EU Horizon Europe funded FOCI project (grant agreement 101056783).

REFERENCES

Asmi, E. *et al.* (2011). Secondary new particle formation in Northern Finland Pallas site between the years 2000 and 2010, *Atmos. Chem. Phys.* 11, 12959–12972.

Hamed, A. *et al.* (2010). Changes in the production rate of secondary aerosol particles in Central Europe in view of decreasing SO_2 emissions between 1996 and 2006, *Atmos. Chem. Phys.* 10, 1071–1091.

Kulmala, M. *et al.* (2012). Measurement of the nucleation of atmospheric aerosol particles, *Nat. Protocols* 7, 1651–1667.

Kyrö, E.-M. *et al.* (2014). Trends in new particle formation in eastern Lapland, Finland: effect of decreasing sulfur emissions from Kola Peninsula, *Atmos. Chem. Phys.* 14, 4383–4396.

Leinonen, V. *et al.* (2022). Comparison of particle number size distribution trends in ground measurements and climate models, *Atmos. Chem. Phys.* 22, 12873–12905.

Nieminen, T. *et al.* (2014). Trends in atmospheric new-particle formation: 16 years of observations in a boreal-forest environment, *Boreal Env. Res.* 19 (suppl. B), 191–214.

Sogacheva, L. *et al.* (2007). Relation of air mass history to nucleation events in Po Valley, Italy, using back trajectories analysis, *Atmos. Chem. Phys.* 7, 839–853.

CHARACTERIZATION OF PRESCRIBED FIRE EMISSIONS IN A FINNISH BOREAL FOREST

S. PELTOKORPI[1], A. BUCHHOLZ[1], L. HAO[1], S. KOMMULA[1], P. MIETTINEN[1], I. PULLINEN[1], T. KOKKOLA[2], M. IHALAINEN[2], V. VAKKARI[3,4], E. ASMI[4], O. SIPPULA[2,5] and A. VIRTANEN[1]

[1]*Department of Technical Physics, University of Eastern Finland, Kuopio, Finland*

[2]*Department of Environmental and Biological Sciences, University of Eastern Finland, Kuopio, Finland*

[3]*Atmospheric Chemistry Research Group, Chemical Resource Beneficiation, North-West University, Potchefstroom, South Africa*

[4]*Atmospheric Composition Unit, Finnish Meteorological Institute, Helsinki, Finland*

[5]*Department of Chemistry, University of Eastern Finland, Joensuu, Finland*

Keywords: PRESCRIBED FIRE, BOREAL FOREST, EMISSION FACTORS, CCN ACTIVITY.

INTRODUCTION

Wildfires emit substantial amount of primary organic aerosol, black carbon (BC), secondary organic aerosol precursors as well as greenhouse gases (e.g. Andreae, 2019). These compounds have a great potential to alter the radiative balance of earth, decrease the air quality and cause adverse health effects on humans. The characterization of wildfire emissions in real life conditions is challenging due to the spontaneous nature of fire and the safety hazards. Hence, limited measurements have been conducted in the vicinity of wildfires, especially in European boreal forests. The fresh and aged biomass burning (BB) emissions of various fuel types have been measured widely in laboratories using an atmospheric chamber, however, the burning conditions may be different from the field and therefore not be representable of real wildfires.

For this study, we have cooperated with the Finnish Forest Administration (Metsähallitus) to measure the emissions and their properties from a prescribed fire in a Finnish boreal forest. We aim to determine the CCN activity, emission factors, chemical composition, and other important properties of the aerosol emitted in wildfires.

METHODS

As part of the Boreal Forest Fire (BoFF) project, field measurements on prescribed fire emissions were carried out in June 2024 in a Finnish boreal forest. An 8-ha area was burned by the Finnish Forest Administration (Metsähallitus) as part of a project aiming to restore forests to their natural state. A container including various instruments to measure aerosol and gas properties was placed in the middle of the burned area to ensure sufficient capture of the emitted smoke. To study the effects of burning condition (smoldering/flaming) on the emission properties, the modified combustion efficiency (MCE = ΔCO_2 / (ΔCO_2 + ΔCO)) was calculated with the background corrected CO_2 and CO concentrations measured with a cavity ringdown spectrometer (model G2401, Picarro, Inc.).

For this study, an online high-resolution time-of-flight soot particle aerosol mass spectrometer (HR-ToF-SP-AMS, abbreviated as AMS) was used to quantify the particle composition and calculate emission factors for various species emitted in wildfires. The BC concentration was measured with a micro-aethalometer (model MA-200, AethLabs). Size resolved CCN activity measurements were conducted

using a CCN counter (CCNC, model CCN-100, Droplet Measurement Technologies Inc.) along with a differential mobility analyser (DMA, coaxial Vienna-type) and a condensational particle counter (CPC, model 3775, TSI Inc.). High variability in wind direction impacted the data quality of especially the CCN measurements, as the size distribution and hygroscopicity was changing during a scan. For CCN data, this was accounted for by grouping the available data into bins based on MCE value and calculating an average hygroscopicity parameter κ within these bins instead of analyzing individual CCN scans.

RESULTS

In total, the gaseous and particulate emissions and their properties were measured during the open flame burning and the subsequent smoldering for almost 22 hours. In addition to the smoke emissions, the background air and aerosol properties were measured prior to the burning. In Figure 1b, we present the MCE values throughout the burning as a function of time. The burned forest consisted of two areas isolated from their surroundings by a clearance (see Fig 1a). Both the areas were burned starting close to the container; hence MCE is high (indicating flaming combustion) immediately or soon after the burn start and decreases as the flames move away from it. Overall, the mean MCE was 0.84 suggesting the dominance of smoldering in boreal forest surface fires. However, the changing wind directions and the fixed location of the container may have affected the amount of smoldering and flaming combustion captured by the measurements.

The average background aerosol was organic dominated with some influence from sulphate and minor influence from ammonium and BC. During the burning, the relative contribution of organic material to the aerosol composition increased to above 95 %. The overall mass concentration of aerosol was up to 1000 times higher during burning relative to the background. The highest mass concentration was measured during the flaming period.

The average hygroscopicity parameter κ (Petters & Kreidenweis, 2007) was determined for the background aerosol and for the smoke aerosol within each MCE bin. Background aerosol had moderate hygroscopicity with κ value of 0.19 for supersaturation of 0.32 % and 0.16 for supersaturation of 0.49 %. During burning, κ value ranged from 0.09 to 0.13 for supersaturation of 0.32 % and from 0.1 to 0.14 for supersaturation of 0.49 % suggesting that wildfires decrease the hygroscopicity of ambient aerosol in European boreal forests. Despite the decrease in hygroscopicity, the CCN number concentration was higher during burning compared to the background due to the elevated aerosol number concentration. No clear trend with MCE was seen for κ, although more detailed analysis is needed.

CONCLUSIONS

We have investigated the properties of gaseous and particulate emissions from a prescribed fire to characterize the atmospherically relevant properties of wildfire emissions. Due to the proximity of the fire to the measuring container, we were able to successfully capture the emitted smoke during the measurements. This study provides novel insights on the less studied European boreal forest surface fires and their potential impacts on the climate.

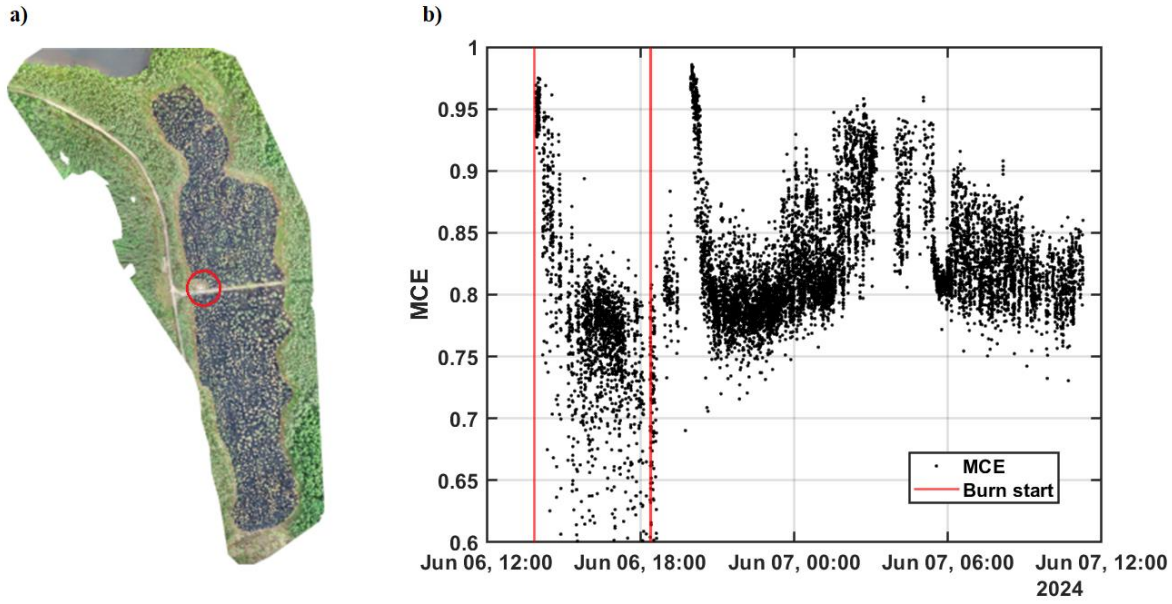


Figure 1. (a) The burned area from above. The red circle shows the location of the container. **(b)** Modified combustion efficiency (MCE) as a function of time. The starting time of burning of the Southern and Northern area are shown with red vertical lines. The data points with no smoke influence have been removed.

ACKNOWLEDGEMENTS

This work was supported by the Jane and Aatos Erkko Foundation (decision 230026).

REFERENCES

M. O. Andreae, (2019). Emission of trace gases and aerosols from biomass burning – an updated assessment, *Atmospheric Chemistry and Physics*, **19**(13), 8523-8546.

M. Petters and S. Kreidenweis, (2007). A single parameter representation of hygroscopic growth and cloud condensation nucleus activity, *Atmospheric Chemistry and Physics*, **7**(8), 1961-1971.

CHANGING PEATLANDS: EFFECTS ON AEROSOL FORMATION POTENTIAL

I. PULLINEN[1], A. BUCHHOLZ[1], A. KORRENSALO[2,3], O. SKALDINA[2], E. MÄNNISTÖ[4], AND A. VIRTANEN[1]

[1]*Department of Technical Physics, University of Eastern Finland, Kuopio, 70211, Finland*
[2]*Department of Environmental and Biological Sciences, University of Eastern Finland, Joensuu, 80101, Finland*
[3]*Natural Resources Institute Finland (Luke), Joensuu, 80100, Finland*
[4]*School of Forest Sciences, University of Eastern Finland, Joensuu, 80101, Finland*

Keywords: PEATLANDS, SOA, AEROSOL YIELDS, ECOSYSTEM CHANGE.

INTRODUCTION

Currently, the Biogenic Volatile Organic Compound (BVOC) emissions from boreal peatlands are inaccurately represented in the global climate simulations, although peatlands cover 18-28 % of boreal region (Kauppi et al., 1997). These emissions have been shown to increase with higher temperatures (Lindwall et al., 2016) and decrease with lowered water tables (Faubert et al., 2010), both of which are the likely outcomes of climate change in the peatlands. With changing climate and human land use, peatlands are experiencing a drying trend with open, sedge-dominated fen ecosystems transitioning towards shrub-dominated bogs or even forests (Magnan et al., 2022; Tahvanainen, 2011).
Simultaneously, peatland drainage for agriculture and forestry has led to wide-scale drying of peatlands, a development which is currently attempted to be reversed through restoration efforts. Taken together, the changes in peatland ecosystems can be expected to alter also the BVOC emissions, and with them the amount and type of secondary organic aerosols (SOA) that are formed from these emissions. Aerosols play a crucial role in the atmosphere as they are directly interacting with incoming solar radiation as well as acting as nuclei for cloud formation. In our study, we investigate how much SOA is formed from the BVOC emissions of the different peatland types to understand the potential impact of changing peatland ecosystems.

METHODS

We used an oxidative flow reactor to investigate the SOA formation on ammonium sulphate seed aerosol. VOC concentrations, aerosol bulk mass and properties, and particle size distribution were monitored to determine aerosol yield curves for each investigated precursor. We utilise previously published data about the VOC emissions from a fen and a bog site in Finland (Männistö et al., 2023) to identify the VOCs typical for these two ecosystems. Two synthetic VOC mixtures were created from the 15 most prominent compounds (referred to as "FEN" and “BOG”). To identify which VOCs enhance SOA formation and which may suppress it, we also studied SOA formation of each individual compound and of the mixtures without isoprene (referred to as “BOG no isoprene” and “FEN no isoprene”).

CONCLUSIONS

Figure 1 shows the organic aerosol mass formed as a function of precursor VOC concentration. The suppressing role of isoprene for the SOA formation seems evident, as has been shown in previous studies (McFiggans et al., 2019). FEN which has >90% isoprene content shows clearly lower SOA formation potential than Bog (50% isoprene). Additionally, while the presence of isoprene suppressed SOA formation for the other VOCs in the FEN mixture, the BOG mixtures behaved very similarly with and

without isoprene. It may be that the high sesquiterpene fraction in the BOG mixture leads to a situation where even low SOA potential isoprene oxidation products lead to formation of condensable gases.

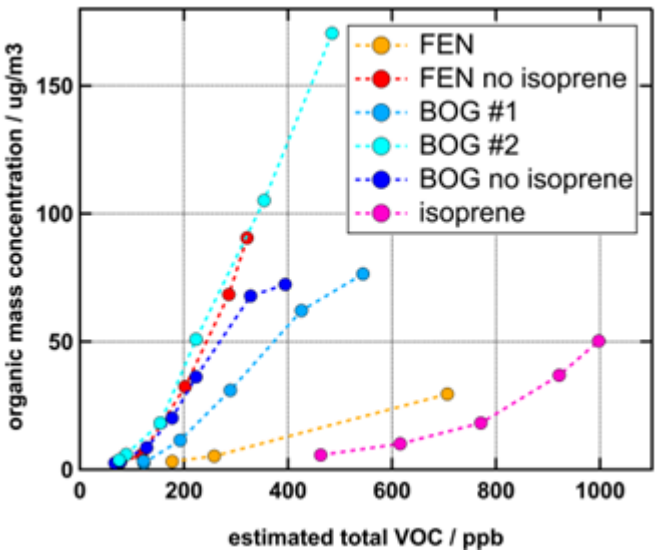


Figure 1. Produced SOA for different VOC mixtures as a function of precursor concentration.

When comparing the FEN and BOG cases (i.e., the actual observed BVOC mixtures), the difference in yields implies that a shift towards higher amount of peatlands dominated by vegetation typical of bogs may increase their particle formation potential. However, for the effect on regional climate and potential feedback loops, the magnitude of total VOC emissions and their temperature sensitivity need to be considered as well, as the higher overall emissions from the fen may compensate for the lower aerosol yield.

ACKNOWLEDGEMENTS

This work was supported by the Academy of Finland Flagship programme ACCC (grant no. 337550), and Academy of Finland grant 338980 to Aino Korrensalo.

REFERENCES

Faubert, P., Tiiva, P., Rinnan, Å., Räty, S., Holopainen, J. K., Holopainen, T., & Rinnan, R. (2010). Effect of vegetation removal and water table drawdown on the non-methane biogenic volatile organic compound emissions in boreal peatland microcosms. *Atmospheric Environment*, *44*(35), 4432–4439. https://doi.org/10.1016/J.ATMOSENV.2010.07.039

Kauppi, P. E., Posch, M., Hänninen, P., Henttonen, H. M., Ihalainen, A., Lappalainen, E., Starr, M., Kauppi, P. T., Lappalainen, A., & Starr, E. (1997). Carbon reservoirs in peatlands and forests in the boreal regions of Finland. *Silva Fennica*, *31*(1). https://doi.org/10.14214/SF.A8507

Lindwall, F., Svendsen, S. S., Nielsen, C. S., Michelsen, A., & Rinnan, R. (2016). Warming increases isoprene emissions from an arctic fen. *Science of The Total Environment*, *553*, 297–304. https://doi.org/10.1016/J.SCITOTENV.2016.02.111

Magnan, G., Sanderson, N. K., Piilo, S., Pratte, S., Väliranta, M., van Bellen, S., Zhang, H., & Garneau, M. (2022). Widespread recent ecosystem state shifts in high-latitude peatlands of northeastern Canada and implications for carbon sequestration. *Global Change Biology*, *28*(5), 1919–1934. https://doi.org/10.1111/GCB.16032

Männistö, E., Ylänne, H., Losoi, M., Keinänen, M., Yli-Pirilä, P., Korrensalo, A., Bäck, J., Hellén, H., Virtanen, A., & Tuittila, E. S. (2023). Emissions of biogenic volatile organic compounds from adjacent boreal fen and bog as

impacted by vegetation composition. *Science of The Total Environment*, *858*, 159809. https://doi.org/10.1016/J.SCITOTENV.2022.159809

McFiggans, G., Mentel, T. F., Wildt, J., Pullinen, I., Kang, S., Kleist, E., Schmitt, S., Springer, M., Tillmann, R., Wu, C., Zhao, D., Hallquist, M., Faxon, C., Le Breton, M., Hallquist, Å. M., Simpson, D., Bergström, R., Jenkin, M. E., Ehn, M., … Kiendler-Scharr, A. (2019). Secondary organic aerosol reduced by mixture of atmospheric vapours. *Nature 2019 565:7741*, *565*(7741), 587–593. https://doi.org/10.1038/s41586-018-0871-y

Tahvanainen, T. (2011). Abrupt ombrotrophication of a boreal aapa mire triggered by hydrological disturbance in the catchment. *Journal of Ecology*, *99*(2), 404–415. https://doi.org/10.1111/J.1365-2745.2010.01778.X

A KINETIC MODEL OF MULTIPHASE CHEMISTRY INTEGRATING NEW PARTICLE FORMATION AND SIZE DISTRIBUTION DYNAMICS IN SECONDARY ORGANIC AEROSOL FORMATION (KM3C-NPF)

M. W. RADECKA[1], H. G. KANG[1], Z. ZHANG[1], U. PÖSCHL[1] and T. BERKEMEIER[1]

[1]*Max Planck Institute for Chemistry, Multiphase Chemistry Department, Hahn-Meitner-Weg 1, 55128 Mainz, Germany.*

Keywords: SOA, new particle formation, multiphase chemistry, kinetic modelling

INTRODUCTION

Organic aerosols are one of the largest natural and anthropogenic aerosol sources. Secondary organic aerosol (SOA) from monoterpene precursors can constitute almost 50 % of organic aerosol mass in the summer (Zhang *et al*. 2018). However, there still remain discrepancies between the growth rates of nanoparticles measured in the laboratory, the ambient atmosphere, and those predicted in model calculations (Stolzenburg *et al.* 2025). Furthermore, there is a lack of kinetic models that explicitly describe particle-phase diffusion and chemistry, as well as new particle formation (NPF) and size distribution dynamics.

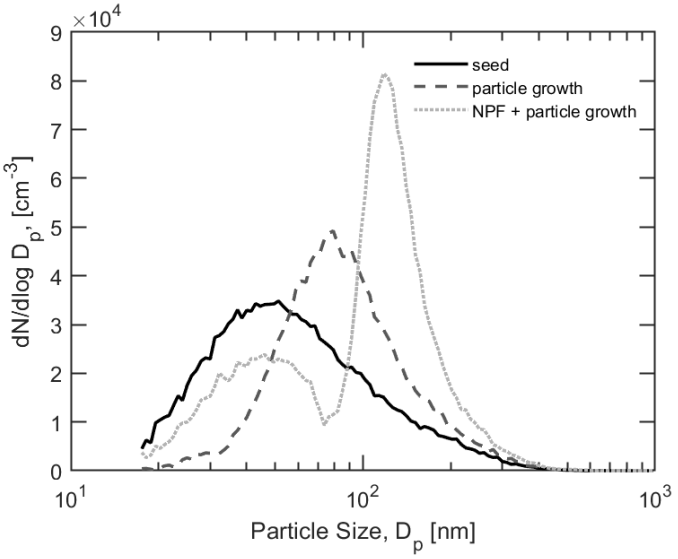


Figure 1: Time evolution of the particle size distribution of limonene-derived secondary organic aerosol particles in a chamber oxidation experiment from Berkemeier *et al.* 2020. In addition to growth onto ammonium sulfate seed particles, a second mode of newly formed particles appears.

METHODS

We use the kinetic multilayer model for multiphase chemistry (KM3C) and investigate the evolution of particle size distributions during oxidation of α-pinene and limonene with the NO_3 radical in the presence of seed aerosol in a laboratory chamber. KM3C explicitly treats gas-phase chemistry, gas-particle partitioning into bins of different particle sizes, as well as condensed-phase chemistry and diffusion in each particle size bin over time. In the limonene - nitrate radical oxidation system, homogeneous

nucleation of new particles occurred in the chamber, which is modelled by a newly developed nucleation scheme (KM3C-NPF). The results are compared with previous modelling efforts that did not explicitly treat NPF and assumed a single, effective particle size (Berkemeier *et al*., 2020).

CONCLUSIONS

We demonstrate the capability of the newly developed model to describe the experimental data. We find that particle-phase chemistry and diffusion have pronounced effects on the formation and evaporation rate of SOA. We investigate the effect of oligomerization and phase state on mass growth and evolution of size distribution. We explore how nanoparticle growth rates are affected by these processes.

REFERENCES

H. Zhang, L.D. Yee, B.H. Lee, M.P. Curtis, *et al.* (2018), Monoterpenes are the largest source of summertime organic aerosol in the southeastern United States, *Proc. Natl. Acad. Sci. U.S.A.* **115 (9)** 2038-2043, https://doi.org/10.1073/pnas.1717513115.

Stolzenburg, D., Sarnela, N., Bianchi, F. *et al*. (2025) Incomplete mass closure in atmospheric nanoparticle growth. *npj Clim Atmos Sci* **8**, 75. https://doi.org/10.1038/s41612-025-00893-5

Berkemeier, T., Takeuchi, M., Eris, G., and Ng, N. L. (2020): Kinetic modeling of formation and evaporation of secondary organic aerosol from NO_3 oxidation of pure and mixed monoterpenes, *Atmos. Chem. Phys.*, **20**, 15513–15535, https://doi.org/10.5194/acp-20-15513-2020, 2020.

VERTICAL DIFFERENCES IN NR-PM$_1$ ATMOSPHERIC AEROSOL COMPOSITION

J. SCHWARZ[1], P. VODIČKA[1], R. LHOTKA[1,2], N. ZÍKOVÁ[1], S. MBENGUE[3], and V. ŽDÍMAL[1]

[1]*Research Group of Aerosol Chemistry and Physics, Institute of Chemical Process Fundamentals CAS, Prague, Czechia.*
[2]*Air Quality Department, Košetice Observatory, Czech Hydrometeorological Institute, Prague, Czechia.*
[3]*Global Change Research Institute, CAS, Brno, Czechia.*

Keywords: Tall tower, NR-PM$_1$, Chemical composition, AMS.

INTRODUCTION

Atmospheric aerosols are mostly measured near ground. Vertical measurements are usually either short-term using various types of flights or long-term using remote sensing that cannot directly assess aerosol chemical composition. To overcome this lack of knowledge, measurement at tall tower can be used. One of them (250 m) was set-up at National Atmospheric Observatory Košetice (NAOK) in Czechia.

METHODS

Compact Time of Flight Aerosol mass spectrometer (C-ToF AMS, Drewnick *et al*. 2005) was used to measure NR-PM$_1$ chemical composition in a 5-min time resolution. To measure NR-PM$_1$ from 4 m and 230 m a.g.l. using a single instrument placed at the ground level, a switching valve was installed so that three consecutive samples were taken from the inlet at 4 m and three samples from the other 230 m long inlet. An example of time series obtained using this approach is shown in Fig 1. This measurement was complemented with several other instruments, including Aethalometer AE33 which provides the concentration of the equivalent black carbon (eBC), a most important refractive component of PM$_1$.

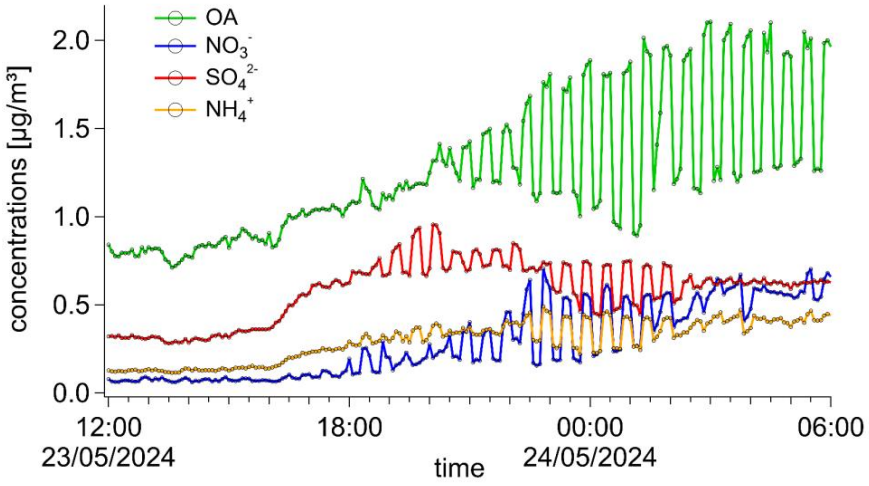


Figure 1. An example of time series of major NR-PM$_1$ chemical species (uncorrected by CE) obtained by C-ToF AMS using a switching valve. Higher concentrations are usually found near the ground.

RESULTS

In general, differences in the concentrations of atmospheric aerosol are strongly dependent on the vertical mixing. However, not only overall concentration is changing when mixing is not sufficient enough, but

also chemical composition is changing, as can be seen already in Fig 1, especially in early morning on 24/05/2024. The reasons for these changes are mainly position of sources of individual compounds but also differences in chemical thermodynamics at different height that can cause changes in aerosol composition. This is probably valid mainly for ammonium nitrate because of its thermal instability that can be also influenced by different relative humidity. Although less than 24 h time series shown in Fig 1 are not representative of longer period, it actually agrees well with average diurnal pattern of all components over spring season shown in Fig 2.

There is a clear difference in the diurnal pattern of organics measured near ground and at 230 m. While at 4 m organics exhibit minimum in the afternoon and the highest concentration during night, at 230 m they have flat diurnal profile with small maximum before noon. The behavior of nitrates is somewhat different. They have also higher concentration near the ground but they have early morning maxima and minima in late afternoon at both heights. On the other hand, sulphates have similar concentrations and diurnal profiles at both heights with small maxima during midday. Finally, ammonium results are in between those of nitrates and sulphates, thanks to their prevailing content in nitrate and sulphate salts.

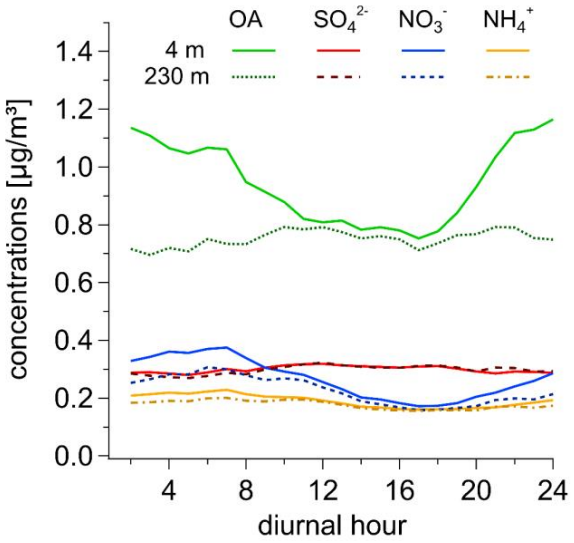


Figure 2. Average diurnal concentrations of NR-PM_1 chemical species (uncorrected by CE) at 4 m and 230 m above the ground during spring season.

CONCLUSIONS

Vertical differences in NR-PM_1 atmospheric aerosol composition were studied and significant differences were found especially during night when atmospheric mixing is often limited. Different behavior was found for every major studied component of NR-PM_1.

ACKNOWLEDGEMENTS

This work was supported by the Czech Science Foundation under grant 24-10768S.

REFERENCES

Drewnick, F. et al., (2005). A new Time-of-Flight Aerosol Mass Spectrometer (TOF-AMS)—Instrument description and first field deployment. *Aerosol Sci. Technol*. **39**, 637.

AEROSOL-RADIATION INTERACTIONS OF COASTAL AEROSOLS IN SCANDINAVIA

J. T. SKØNAGER[1], Z. TENG[1], M. SALTER[2], M. BILDE[1], A. MASSLING[3], H. SKOV[3], B. ROSATI [1,4]

[1]*Department of Chemistry, Aarhus University, Aarhus, Denmark*

[2]*Department of Environmental Science, Stockholm University, Stockholm, Sweden*

[3]*Department of Environmental Science, iClimate, ARC, Aarhus University, Roskilde, Denmark*

[4]*Institute of Meteorology and Climatology, BOKU University, Vienna, Austria*

Keywords: optical properties, coastal aerosol, scattering, absorption, Ångström.

INTRODUCTION

Assessing the role of atmospheric aerosols for climate change is key to decrease uncertainties related to it and improve future climate predictions. Aerosol particles can directly interact with radiation by either light absorbing or scattering of the incoming sunlight. These aerosol-radiation interactions are dictated by the size and shape of the particles as well as their chemical composition.
Coastal areas are strongly influenced by natural processes and anthropogenic activities as they are in close proximity to the oceans, the largest aerosol source by mass globally, and impacted by shipping as well as local vehicular traffic and emissions from other human activities. As approximately 40 % of the total population worldwide is located in coastal areas (UNEP), it is imperative to investigate coastal aerosol properties and their impacts on climate and human health.

METHODS

Coastal aerosols were measured at two locations in Scandinavia: i) at Aarhus Bay during March - April 2023 and ii) on the island Askö, located approximately 80 km south of Stockholm between September 2024 – March 2025. Aarhus Bay, is next to Kattegat, which is located North of Zeeland, east of Jutland and west of Sweden. The Bay is directly influenced by the urban activities in Aarhus (about 200000 inhabitants) but also by agriculture in the vicinity and natural sources including the sea and the forests nearby. Askö (Sweden), on the other hand, is a nature reserve facing the Baltic Sea and expected to be influenced by mostly natural and long-range transported aerosols.
The optical properties of the aerosols were probed with a nephelometer (AURORA 3000, Ecotech) for their scattering potential and an aethalometer (AE33 / AE36s) for their absorbing potential. Additional information on the particle number size distributions was obtained with a white-light optical particle spectrometer (WELAS 2300, Palas GMbH) and/or a scanning mobility particle sizer (SMPS). Figure 1 illustrates the time series of scattering coefficients and absorption coefficients measured at Aarhus Bay at three different wavelengths.
The optical measurements were analyzed regarding their wavelength dependent behavior, described by the Ångström exponent. By comparing scattering (SAE) and absorption Ångström exponents (AAE), the source of the aerosol particles can be assessed (Cazorla et al., 2013; Cappa et al., 2016).

CONCLUSIONS

Preliminary results reveal quite large variabilities in both scattering and absorption potential at both locations. Results from Aarhus Bay point towards a complex mixture of sources including local events described by larger absorbing fractions and long-range transported aerosols containing more processed particles. Measurements at Askö, were also characterized by different sources with some events pointing towards local carbonaceous particles, but also towards larger sized particles potentially originating from local sea spray and/or long-range transport. The single sources will be analyzed in more detail to assess to which extent different types of aerosols, originating from specific sources, contribute to the aerosol load at the coastal sites. This study will serve to better quantify aerosol emissions in Scandinavia and in particular at coastal areas to assess their influence on climate and air quality in populated areas.

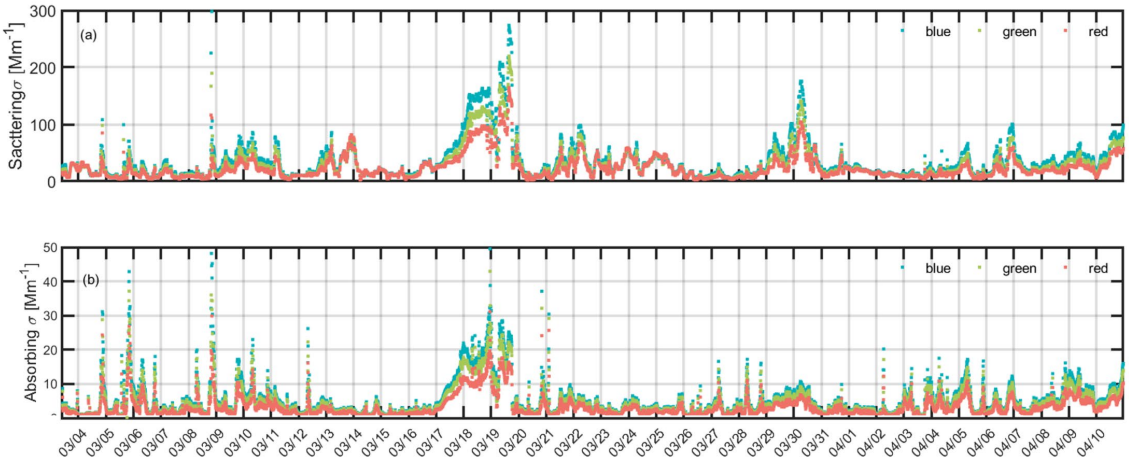


Figure 1. Time series of scattering and absorption coefficients as measured during the Aarhus Bay campaign in spring 2023.

ACKNOWLEDGEMENTS

This work was supported by a research grant from Villum Fonden (42128), and the aethalometer in Aarhus Bay (AE33, MAGEE) was loaned from Villum Research Station. We acknowledge the support of the Center of Excellence for Chemistry of Clouds (C3), funded by the Danish National Research Foundation (DNRF172). We acknowledge the Danish National Center for Environment and Energy at Aarhus University, for providing data and support for this study.

REFERENCES

United Nations Environment Programme (UNEP) Global Programme of Action for the Protection of the Marine Environment From Land-based Activities (GPA) Coordination Office.

Cazorla, A., Bahadur, R., Suski, K. J., Cahill, J. F., Chand, D., Schmid, B., Ramanathan, V., and Prather, K. A. (2013): Relating aerosol absorption due to soot, organic carbon, and dust to emission sources determined from in-situ chemical measurements, Atmos. Chem. Phys., 13, 9337–9350, https://doi.org/10.5194/acp-13-9337-2013.

Cappa, C. D., Kolesar, K. R., Zhang, X., Atkinson, D. B., Pekour, M. S., Zaveri, R. A., Zelenyuk, A., and Zhang, Q. (2016): Understanding the optical properties of ambient sub- and supermicron particulate matter: results from the CARES 2010 field study in northern California, Atmos. Chem. Phys., 16, 6511–6535, https://doi.org/10.5194/acp-16-6511-2016.

TRACEABLE CALIBRATION OF ULTRAFINE PARTICLE COUNTERS

G. STEINER[1], C. KUNATH[1], E. MERKER[1], L. KECK[1], C. KRAUSE[2] and M. GÖTZ[2]

[1] *Grimm Aerosol Technik GmbH, Muldestausee, 06744, Germany*
[2] *Physikalisch Technische Bundesanstalt, Braunschweig and Berlin, Germany*

Keywords: UFP, FCAE, CPC, CALIBRATION.

INTRODUCTION

Ultrafine particle (UFP) measurements have a long-standing history, with initial efforts dating back to the late 19th century (Aitken, 1880). Over the decades, measurement techniques have evolved significantly, leading to highly refined and standardized methods that are now routinely employed at scientific monitoring stations worldwide. With the adoption of the new Ambient Air Quality Directive (Directive 2024/2881) to closer align to recommendations by WHO (2021), the measurement of UFPs will become a mandatory component of national ambient air quality monitoring networks across the European Union. This regulatory shift underscores the critical importance of frequent and traceable calibration of measurement equipment to ensure data accuracy, comparability, and long-term reliability.

METHODS

Currently, the only harmonized European standards for ambient UFP measurement are EN 16976 (CEN, 2024), which specifies the use of a condensation particle counter (CPC) for determining particle number concentration in the size range below 100 nm and CEN/TS 17434 (CEN, 2020) that describes the measurement of the particle number size distribution from 10 – 800nm in the ambient air. To ensure traceability and accuracy, CPCs are calibrated by comparing their response to either a reference CPC or a reference-grade Faraday Cup Aerosol Electrometer (FCAE). This calibration approach is described in ISO 27891 (ISO, 2015), which provides a standardized method for determining the counting efficiency of CPCs using monodisperse aerosol particles. The calibration process involves generating particles of known size and charge, measuring their concentration with the FCAE, and adjusting the CPC response accordingly. This ensures that the CPC provides reliable and reproducible measurements across different monitoring sites and over time.

Although FCAEs serve as reference instruments for the calibration of CPCs, they themselves require precise calibration. Since both the volumetric flow rate and the measured electric current are directly traceable to the SI system, FCAEs are particularly well-suited for establishing metrological traceability of particle number concentrations. Until now, FCAE calibration has only been possible at national metrology institutes (NMIs), requiring the use of highly precise, stationary, and costly equipment. These constraints have limited the availability and frequency of FCAE calibrations in practice, thereby hindering widespread traceability of UFP measurements.

CONCLUSIONS

We present a novel and practical method for calibrating Faraday Cup Aerosol Electrometers (FCAEs) using the Ultra-stable Low-noise Current Amplifier (ULCA), which is now commercially available. This approach enables precise and traceable current calibration by applying a series of well-defined, stable

femtoampere-level currents to the FCAE under test. As illustrated in Figure 1, the calibration factor is derived from the ratio of the ULCA-generated current to the current measured by the FCAE. Ideally, this ratio remains constant across the full measurement range, confirming the linearity and accuracy of the instrument.

As both a CPC and FCAE manufacturer, we recognize the value of having calibration equipment readily available—not only for final calibration of customer instruments but also for routine quality assurance checks during production. The integration of this method into our calibration workflow enhances traceability, improves production efficiency, and supports compliance with emerging regulatory requirements for ultrafine particle measurements.

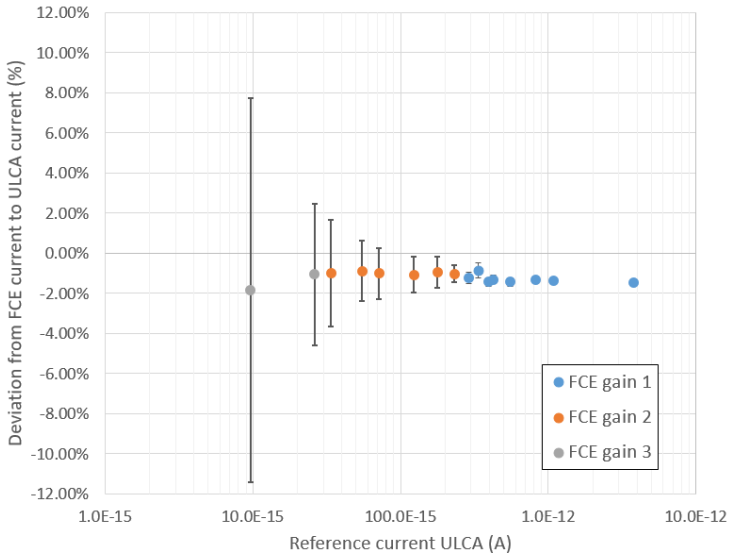


Figure 1. Experimentally determined deviation of FCAE current to ULCA reference current

REFERENCES

Aitken, J., On Dust, Fogs, and Clouds, Trans. R.S.E., 1880- 81.

CEN (Comité Européen de Normalisation), EN 16976:2024, Ambient air - Determination of the particle number concentration of atmospheric aerosol.

CEN (Comité Européen de Normalisation), CEN/TS 17434:2020, Ambient air - Determination of the particle number size distribution of atmospheric aerosol using a Mobility Particle Size Spectrometer (MPSS)

Directive 2024/2881. Directive (EU) 2024/2881 of the European Parliament and of the Council of 23 October 2024 on ambient air quality and cleaner air for Europe

ISO (International Organization for Standardization), ISO 27891:2015, Aerosol particle number concentration — Calibration of condensation particle counters

WHO (World Health Organization) global air quality guidelines. Geneva: World Health Organization; 2021

FORMATION AND CHARACTERISTICS OF ATMOSPHERIC AEROSOLS IN AN ALASKAN BOREAL FOREST

STEVEN JOB THOMAS[1], JAMES CAMPBELL[2], WANG CONGRONG[2], FEDERICO BIANCHI[1], and JINGQIU MAO[2]

[1]*Institute for Atmospheric and Earth System Research / Physics, Faculty of Science, University of Helsinki, Helsinki, 00560, Finland.*

[2]*Geophysical Institute and Department of Chemistry and Biochemistry, University of Alaska Fairbanks, Fairbanks, AK 99775, USA.*

Keywords: AEROSOLS, BOREAL FOREST, NEW PARTICLE FORMATION, ALASKA.

INTRODUCTION

Aerosols, particularly fine particles, have significant impacts on system and human health by influencing radiative forcing, cloud formation, and air quality. These particles, from both natural and anthropogenic sources, contribute to atmospheric processes with regional and global effects. Boreal forests, which cover 27% of the world's forested area, are key contributors to atmospheric aerosols (Shrivastava, et al. 2017; FAO, 2020). Observations from Hyytiälä, Finland, show that biogenic volatile organic compound (BVOC) emissions in boreal forest play a major role in atmospheric chemistry, with variability influenced by temperature and meteorological conditions (Petäjä et al., 2022). Differences between European and North American boreal forests—such as species composition and climate—affect the types and quantities of BVOCs emitted, which in turn influences aerosol formation. Boreal forests in North America are predominantly isoprene-emitting (Zhao et al., 2022), whereas those in Europe, particularly Finland, are more monoterpene-dominant (Oderbolz et al., 2013). These variations in BVOC emissions contribute to distinct aerosol dynamics and atmospheric chemistry in each region.

METHODS

SITE DESCRIPTION

To better understand aerosol dynamics in boreal forests, observations have been ongoing since 2023 at a site in Delta Junction, Alaska (63°52'58"N, 145°45'02"W). Located in a scrubby evergreen forest primarily composed of black and white spruce and American dwarf birch, Delta Junction is co-located with a terrestrial National Ecological Observatory Network (NEON) field site in central Alaska. This site offers a unique opportunity to investigate boreal forest-atmosphere interactions. In addition to the comprehensive environmental monitoring provided by NEON, the site is also part of NASA's AERONET network, which monitors aerosol optical properties. Furthermore, Delta Junction is included in the newly established long-term Atmospheric Science and Chemistry Measurement Network (ASCENT), a U.S.-based initiative aimed at characterizing aerosol chemical composition and physical properties.

INSTRUMENTATION

An Aerosol Chemical Speciation Monitor (ACSM) measures the chemical composition of non-refractory aerosol particles, while a Scanning Mobility Particle Sizer (SMPS) characterizes aerosol size distributions in the nanometer-to-micrometer range. An Aethalometer continuously monitors black carbon concentrations, providing insights into both natural and anthropogenic combustion sources. Additionally, since November 2024, a Neutral cluster and Air Ion Spectrometer (NAIS) has been operational at the site. NAIS is crucial for detecting both neutral and charged particles down to a few nanometers, making it a valuable tool for studying new particle formation (NPF) events in the boreal forest environment.

CONCLUSIONS

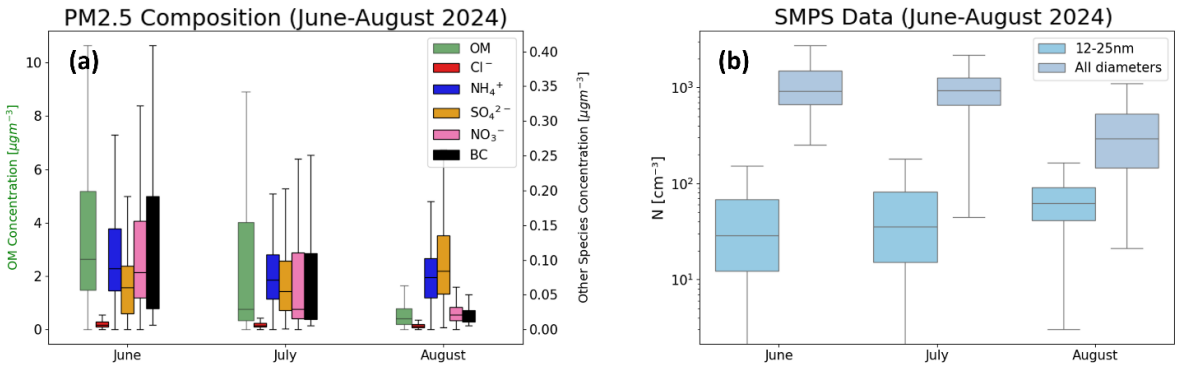


Figure 1. Box plots of (a) PM2.5 chemical species (Cl^-, OM, NH_4^+, NO_3^-, SO_4^{2-}, BC) and (b) total number concentration for aerosol particles in the 12–25 nm diameter range and for all diameters, across different months during the summer of 2024.

In the summer of 2024, the composition of PM2.5 aerosols was primarily dominated by organic matter (OM), with significant fluctuations observed throughout the season. From late June to early July, both aerosol number concentrations and the levels of chemical species rose, largely driven by wildfire activity in Canada. The higher concentrations of PM2.5 chemical species, particularly OM, in June are clearly reflected in the bar plots (Fig. 1). By August, however, the levels of OM, black carbon (BC), and total aerosol number concentrations had decreased compared to June. The highest accumulation-mode particle concentrations were observed in June, coinciding with peak wildfire emissions. By August, the relative contribution of OM declined, while sulphate (SO_4^{2-}) and ammonium (NH_4^+) concentrations increased, suggesting shifts in atmospheric processing or source contributions. SMPS data reveal that while total aerosol number concentrations decreased in August, the 12–25 nm particle concentration was notably higher, indicating possible new particle formation (NPF) events during this period. Further analyses will be conducted using the full dataset, incorporating the extended time series to better understand seasonal trends, wildfire influences, and aerosol formation processes. Additionally, NAIS data will be examined to provide deeper insights into NPF and particle growth dynamics at Delta Junction

ACKNOWLEDGEMENTS

This work was supported by the U.S. National Science Foundation (AGS-2131914).

REFERENCES

FAO. (2020). *Global Forest Resources Assessment 2020 – Key Findings*, Food and Agriculture Organization of the United Nations. Rome, Italy.

Oderbolz, D. C., et al. (2013). A comprehensive emission inventory of biogenic volatile organic compounds in Europe: improved seasonality and land-cover, Atmos. Chem. Phys., 13, 1689–1712.

Petäjä, T., et al. (2022). Influence of biogenic emissions from boreal forests on aerosol–cloud interactions, *Nature Geoscience*, *15*, 42–47.

Zhao, T., et al. (2022). Source and variability of formaldehyde (HCHO) at northern high latitudes: an integrated satellite, aircraft, and model study, Atmos. Chem. Phys., 22, 7163–7178.

Shrivastava, M., et al. (2017). Recent advances in understanding secondary organic aerosol: Implications for global climate forcing, *Rev. Geophys.*, 55, 509–559.

TOWARDS A MORE DETAILED REPRESENTATION OF MONOTERPENE OXIDATION IN CLIMATE MODELS – BIAS CORRECTION OF VBS WITH NEURAL NETWORKS

A. VARTIAINEN[1,2], P. ROLDIN[3], M. IRFAN[1], A THOMASSON[3], H. KOKKOLA[1,4] and T. YLI-JUUTI[1]

[1]*Department of Technical Physics, University of Eastern Finland, Kuopio, Finland.*

[2]*Advanced Computing Facility, CSC - IT Center for Science Ltd, Espoo, Finland.*

[3]*Department of Physics, University of Lund, Lund, Sweden.*

[4]*Finnish Meteorological Institute, Kuopio, Finland.*

Keywords: VBS, α-pinene, oxidation, neural network, global climate model.

INTRODUCTION

The oxidation of volatile organic compounds (VOCs) constitutes an important step in the formation of secondary organic aerosol (SOA), as it produces compounds with lower volatilities that can condense into the particle phase. Among the main VOCs influencing atmospheric SOA formation are monoterpenes emitted by vegetation, which are commonly described through the properties of α-pinene in large-scale models. Biogenic SOA is involved in a negative climate feedback mechanism where increasing surface temperatures lead to increases in VOC emissions, SOA formation, and cloud condensation nuclei (Yli-Juuti et al., 2021). In addition to the temperature dependent VOC emissions, the strength of this mechanism may be influenced by the temperature dependence of both gas-particle partitioning and atmospheric oxidation chemistry. Especially the unimolecular peroxy radical autoxidation reaction rates that govern the formation of highly oxygenated organic molecules (HOM) show a strong positive temperature dependence (Quéléver et al., 2019; Roldin et al., 2019). To improve the accuracy of simulated SOA in a changing climate, it is essential to represent the volatility of the products from monoterpene oxidation under varying conditions in global climate models. Currently, VOC oxidation in climate models is either highly simplified or absent. For example, the sectional aerosol module SALSA, which is one of the most advanced models for aerosol microphysics in global-scale models and implemented in global model ECHAM-HAMMOZ, contains a simplified VOC oxidation scheme with e.g. constant stoichiometric coefficients for condensing vapors (Kokkola et al., 2018; Schultz et al., 2018; Irfan et al., 2024).

Recent experimental studies in combination with quantum chemically calculated reaction rates and gas-phase kinetic simulations have allowed an improved understanding of α-pinene oxidation chemistry, consequently leading to more precise descriptions of it in process-scale models. Such detailed chemical models, with numerous model compounds and reactions, are generally not suitable for global-scale simulations, as the computational costs involved would be excessive. However, with statistical methods, it may be possible to simplify the complex models enough to enable their use in climate models. In our study, the aim is to develop a hybrid model for α-pinene oxidation that combines the simplified scheme of SALSA with a neural network (NN) capable of correcting the resulting volatility distributions of oxidation products based on atmospheric conditions. The NN is trained to learn the difference between the outputs of SALSA and a state-of-the-art atmospheric chemistry model. By utilizing knowledge of varying oxidation conditions, the NN can learn to predict the biases caused by the simplified formulation in SALSA. Ultimately, our goal is to implement the hybrid SALSA+NN framework into a global climate model, such as ECHAM-HAMMOZ.

METHODS

To simulate α-pinene oxidation in various conditions, we have used ADCHAM, an advanced model for aerosol chamber studies containing the gas-phase chemistry model MCM (Roldin et al., 2014). In

ADCHAM, the complex autoxidation chain of monoterpenes and the consequent formation of HOMs is described by the Peroxy Radical Autoxidation Mechanism (PRAM), which extends the number of reactions in MCM by 1773 (Roldin et al., 2019). We have chosen eight variables, deemed relevant based on simulations with ADCHAM, to represent atmospheric oxidation conditions and to act as input variables to the NN. These are the concentrations of α-pinene and the three oxidants in SALSA (O_3, OH, and NO_3), the concentrations of other gases (NO, NO_2 and CO), and temperature. According to our analysis of ADCHAM simulations, CO mainly affects the oxidation process indirectly through formation of HO_2, as the effect of CO is greatly diminished by fixing HO_2 to a constant value. However, HO_2 is less often represented in global-scale climate models, so we have used CO as a proxy for it.

To generate a large number of potential oxidation conditions, combinations of the eight variables were produced using Latin hypercube sampling, which is designed to cover a multidimensional sample space more uniformly than a pure Monte Carlo sampling does (McKay et al., 1979). The upper and lower bounds for sampling each variable were chosen based on the CAMS EAC4 reanalysis data (Inness et al., 2019), focusing our analysis on the lowest ten levels of the L47 vertical resolution used by ECHAM-HAMMOZ (corresponding to approximately 3 km in altitude). In higher altitudes, the α-pinene oxidation rates from the SALSA scheme were considered too small to be relevant for SOA formation.

For each of the generated oxidation conditions, both SALSA and ADCHAM were used to simulate volatility distributions after 7.5 minutes of chemistry, corresponding to the internal timestep of ECHAM-HAMMOZ. The volatility distribution was represented by a 3-bin VBS (*volatility basis set)* setup, which is the default configuration in SALSA. Conditions that resulted in a below 1 $cm^{-3}s^{-1}$ total production rate of the three VBS bins were dropped from the dataset (as seen in the vertical cutoff of SALSA values in Figure 1), as these were considered non-relevant for SOA formation. Because ADCHAM produces concentrations for individual compounds, these compounds were categorized into VBS bins based on their volatilities estimated using functional group contribution methods. Finally, differences in production rates between ADCHAM and SALSA for each bin were calculated, which together constitute the three target variables of the NN. For training the NN to model the difference between VBS bins for SALSA and ADCHAM, the dataset composed of the oxidation conditions and corresponding VBS differences was further split into training (80%) and testing (20%) subsets. Hyperparameters of the NN were optimized using a randomized search with 5-fold cross-validation on the training set. For example, networks with one to four hidden layers were compared to select the best model architecture. As a baseline model, we additionally fitted a linear regression model (*ordinary least squares*, OLS) to each bin of the training data.

RESULTS AND CONCLUSIONS

Figure 1 shows the preliminary results of the bias correction of SALSA by NN and OLS. In this visualization, the production rates of all three VBS bins have been summed together, and only the test subset is shown. Especially for small rates from ADCHAM, SALSA tends to significantly overestimate the production rates compared to the detailed chemistry model, in some cases by more than 10 orders of magnitude. However, it should be noted that most of the SALSA rates are still situated close to the 1:1 – line, though point density may not be clear from the figure. The linear model is already able to correct most of the overestimation and improve all fit metrics, although considerable variability around the perfect fit line remains. On the other hand, the NN correction produces a highly accurate correspondence to ADCHAM outputs, a clear improvement to the OLS fit. Individual bins behave similarly to the total, though there are some slight differences. Overall, these preliminary results showcase the ability of NNs to learn from advanced chemistry models like ADCHAM and to use this knowledge for correcting the biases present in simpler schemes. Although the computational demands of the NN have not yet been considered, our optimal network configuration only has two hidden layers, which are both of reasonable size. This might enable its implementation into a global climate model, particularly if its size is further optimized. Before this ultimate goal, however, we plan to evaluate the performance of our bias correction models against ADCHAM in various scenarios of box model simulations.

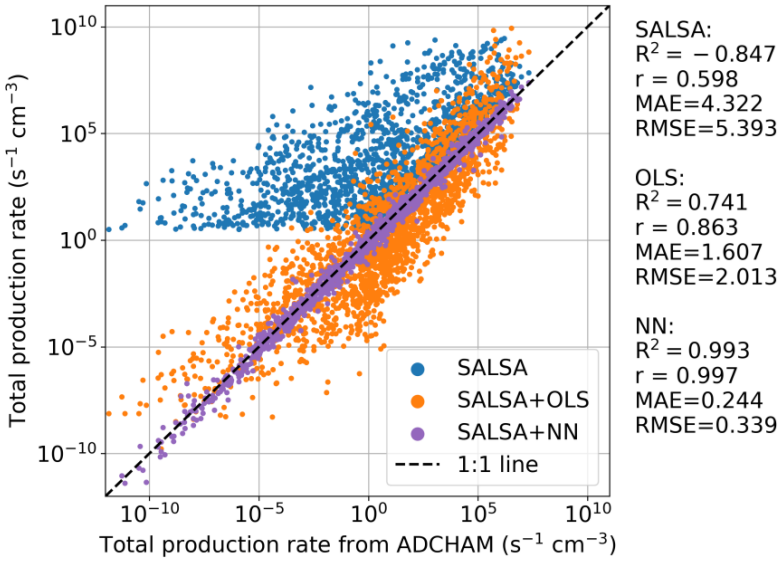


Figure 1. Production rates, in molecules per cm³ per second, of condensable α-pinene oxidation products calculated by SALSA (blue dots) and corrected using OLS (orange dots) or a NN (purple dots) as a function of corresponding production rates from ADCHAM. All three VBS bins, corrected separately, have been aggregated for this figure. The test set fit metrics shown are means calculated across the three bins, after a base 10 log-transformation. The abbreviations refer to the coefficient of determination (R^2), the Pearson correlation coefficient (r), mean absolute error (MAE), and root mean squared error (RMSE).

ACKNOWLEDGEMENTS

This research was funded by the Research Council of Finland (grant nos. 337550 and 337552). Sampling bounds for input variables were chosen based on Copernicus Atmosphere Monitoring Service Information from year 2015, last access 21 March 2025. Neither the European Commission nor ECMWF is responsible for any use that may be made of the information it contains.

REFERENCES

Inness et al. (2019). The CAMS reanalysis of atmospheric composition, *Atmos. Chem. Phys.* **19,** 3515–3556.

Irfan et al. (2024). A model study investigating the sensitivity of aerosol forcing to the volatilities of semi-volatile organic compounds, *Atmos. Chem. Phys*. **24**, 8489–8506.

Kokkola et al. (2018). SALSA2.0: The sectional aerosol module of the aerosol–chemistry–climate model ECHAM6.3.0-HAM2.3-MOZ1.0, *Geosci. Model Dev*. **11**, 3833–3863.

McKay et al. (1979). A Comparison of Three Methods for Selecting Values of Input Variables in the Analysis of Output from a Computer Code, *Technometrics* **21,** 239–245.

Quéléver et al. (2019). Effect of temperature on the formation of highly oxygenated organic molecules (HOMs) from alpha-pinene ozonolysis, *Atmos. Chem. Phys*. **19**, 7609–7625.

Roldin et al. (2014). Modelling non-equilibrium secondary organic aerosol formation and evaporation with the aerosol dynamics, gas- and particle-phase chemistry kinetic multilayer model ADCHAM, *Atmos. Chem. Phys*. **14**, 7953–7993.

Roldin et al. (2019). The role of highly oxygenated organic molecules in the Boreal aerosol-cloud-climate system, *Nat. Commun.* **10**, 4370.

Schultz et al. (2018). The chemistry–climate model ECHAM6.3-HAM2.3-MOZ1.0, *Geosci. Model Dev*. **11**, 1695–1723.

Yli-Juuti et al. (2021). Significance of the organic aerosol driven climate feedback in the boreal Area, *Nat. Commun.* **12**, 5637.

SOURCE APPORTIONMENT OF ORGANIC AEROSOLS IN FIVE EUROPEAN LOCATIONS

V. PRABHU[1], K.N. FOSSUM[1], L. LEI[1], V. MOSCHOS[1], C. LIN[1,3], N. KORHALE[1], L. COLEMAN[1], J.-E. PETIT[2], P. ACHARJA[8], M. RINALDI[4], J. VASILESCU[5], A.V. DANDOCSI[5,7], K. PETRIONOLI[6], A. BOUGIATIOTI[6], N. MIHALOPOULOS[6] and J. OVADNEVAITE[1]

[1]*School of Natural Sciences, Physics, Centre for Climate and Air Pollution Studies, Ryan Institute, University of Galway, University Road, Galway H91 CF50, Ireland.*

[2]*Laboratoire des Sciences du Climat et de l'Environnement (LSCE), CNRS-CEA-UVSQ (UMR 8212), 91191 Gif-sur-Yvette, France.*

[3]*Center for Excellence in Quaternary Science and Global Change, Institute of Earth Environment, Chinese Academy of Sciences, Xi'an 710061, China.*

[4]*Institute of Atmospheric Sciences and Climate (ISAC), National Research Council (CNR), 40129 Bologna, Italy.*

[5]*National Institute of Research and Development for Optoelectronics INOE 2000, 77125 Magurele, Romania.*

[6]*Institute for Environmental Research & Sustainable Development, National Observatory of Athens, 15236 Athens, Greece.*

[7]*UNST Politehnica of Bucharest, Bulevardul Iuliu Maniu 1-3, Bucharest, 061071, Bucharest, Romania.*

[8]*Laboratoire Interuniversitaire des Systèmes Atmosphériques (LISA), Univ Paris Est Creteil and Université Paris Cité, Créteil, 94010, France.*

Keywords: AEROSOLS, BLACK CARBON, ORGANIC MATTER, SOURCE APPORTIONMENT.

INTRODUCTION

Particulate matter, including organic matter (OM) aerosols and black carbon (BC), plays a critical role in influencing both climate and air quality (Lin *et al*., 2020). As a key component of PM_1 (particulate matter with aerodynamic diameter $\leq$1 μm), OM and BC act as short-lived climate forcers with complex and sometimes opposing effects on the climate (CCAC, 2019). However, diverse aerosol sources and limited atmospheric data create challenges in aligning bottom-up emission inventories with observations, necessitating advancements in data analysis, source attribution, and atmospheric modelling.
Under the EU Horizon Process Attribution of Regional Emissions (PARIS) project, five European sites exhibiting significant discrepancies between ground-based PM_1 measurements and model estimates were identified. Source apportionment studies of these locations, using advanced rolling positive matrix factorization (PMF) revealed key PM_1 sources.

METHODS

For the study, four sites (Athens, Bologna, Bucharest and Sirta) with urban/sub-urban land use characteristics and one site (Carnsore point) with rural background were selected. Organic PM_1 data measured using a Quadrupole Aerosol Chemical Speciation Monitor was collected from these sites for the period (2022-23). Igor Pro software with SoFi Pro tool was utilized to perform source apportionment. The Primary organic aerosols (POAs) such as hydrocarbon-like OA (HOA), cooking-OA (COA), coal-OA, peat-OA, and biomass burning-OA (BBOA) were constrained with *a* values ranging between 0 and 0.5.

Also, a bootstrap-based resampling strategy was used to examine statistical uncertainty. The identification of the optimal number of sources at each site was guided by multiple criteria, including the *Q/Qexp* ratio, the diurnal residual patterns of key marker species, and the correlation of factors with external tracers such as BC, NO*x*, *etc*. were investigated to decide on the meaningful number of sources from each site.
Air mass back trajectories along with spatial mapping of restaurants, fire spots, and road networks around the sites were conducted to understand the possible sources that can affect the receptor location.

CONCLUSIONS

Figure 1 presents the percentage contribution of OA components across the five study locations. The HOA, a primary pollutant associated with vehicular emissions and oil burning was observed in all sites, but most prominently in urban sites, where they contribute 10 to 13% of OA. Secondary OA such as less oxidized oxygenated OA (LO-OOA) and more oxidized oxygenated OA (MO-OOA) dominate the OA composition in all the sites, indicating the prevalence of regional secondary aerosol formation. This process is sometimes driven by photochemical aging and long-range transport, but also has diurnal patterns indicating sources from nighttime biomass burning.
The presence of a substantial BBOA component at Sirta (16.3%) and Bucharest (16.5%) underscores the influence of residential wood burning and possibly episodic agricultural burning activities. Similarly, the presence of peat, coal and wood burning-OA at Carnsore Point (CRP) suggests seasonal residential heating patterns in rural areas. Overall, this analysis shows the presence of both primary and secondary aerosols, the relative importance of either component fluctuation depending on the season.

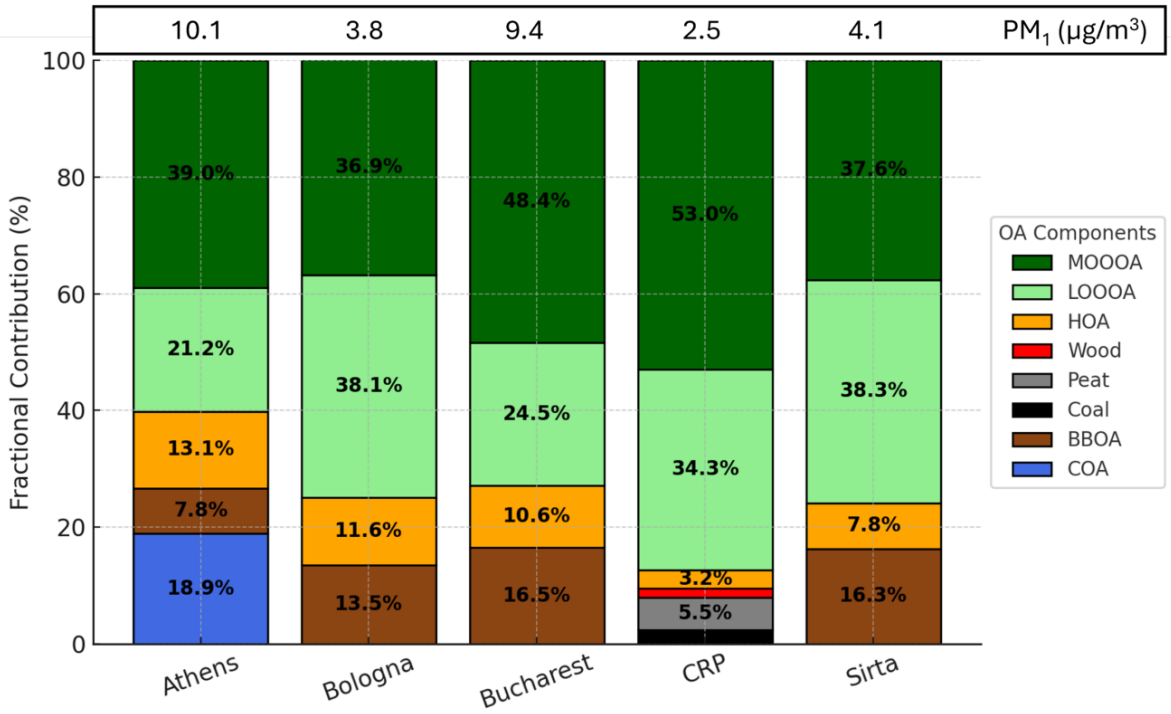


Figure 1. Percentage contribution of OA sources in the study sites

The seasonal fluctuations in concentrations of different OA components were observed across all locations which emphasize the importance of local sources and seasonal patterns in influencing OA concentrations and would be highly valuable for evaluating emission inventories with the regional model.

ACKNOWLEDGEMENTS

This work was supported by the European Union's Horizon Europe Research and Innovation programme under HORIZON-CL5-2022-D1-02 (grant no. 101081430-PARIS). We also thank EPA Ireland and Department of the Environment, Climate and Communications for CRP data. INOE acknowledge the support of the Core Program within the Romanian National Research Development and Innovation Plan 2022-2027, carried out with the support of MCID, project no. PN 23 05.

REFERENCES

CCAC (2019). *Air Pollution in Asia and Pacific: Science-Based Solution*, (United Nations Environment Programme (UNEP)). ISBN 978-9-2807-3725-7.

Lin, C., Darius, C., Xu, W., Heffernan, E., Hellebust, S., Gallagher, J., Huan, R.J., O'Dowd, C., and Jurgita, O. (2020). The impact of traffic on air quality in Ireland: Insights from the simultaneous kerbside and suburban monitoring of submicron aerosols, Atmos. Chem. Phys. 20, 10513–10529.

ON THE QUEST FOR THE FIRST EVER MEASURED "BANANA" IN THE ATMOSPHERE

P. M. WINKLER[1], G. STEINER[2], A. MORAWIEC[1], A. E. VRTALA[3] and W. WINKLMAYR[4]

[1]*Faculty of Physics, University of Vienna, Vienna, Austria*

[2]*Grimm Aerosol Technik GmbH, Ainring, Germany*

[3]*Ingenieurbüro Dr. Vrtala e.U., Freistadt, Austria*

[4]*tapcon GmbH, Ludwigsburg, Germany*

Keywords: NEW PARTICLE FORMATION, PARTICLE SIZE DISTRIBUTION, DIFFERENTIAL MOBILITY ANALYZER, "BANANA".

INTRODUCTION

The spontaneous formation of aerosol particles in the atmosphere from the transition of trace gases into particle phase is usually referred to as new particle formation (NPF). Modelling results suggest that NPF globally accounts for one of the largest contributions to the budget of cloud condensation nuclei (e.g., Gordon *et al*., 2017). The associated indirect radiative effect and its uncertainty in climate predictions thus makes NPF a primary topic in aerosol research. Elucidating the formation mechanisms is key for quantification of the particulate outcome and impact.

The global importance of NPF was first recognized by a work published ~20 years ago (Kulmala *et al*., 2004). However, the existence of NPF was known for more than a century before and can be traced back to the pioneering work of John Aitken in the late 19th century. With the instruments available at that time Aitken could distinguish periods of elevated particle concentrations and he even suggested formation mechanisms (Aitken, 1880). Since then improvements of experimental techniques have led to the monitoring of time dependent particle number size distributions which nowadays allow recognition of new particle formation almost in real time. In this abstract we are revisiting the historic evolution of NPF studies tracing back the origin of ambient particle number size distribution measurements as we know them today. Specifically, we want to highlight early work that measured the typical shape of the growing aerosol mode during NPF, which is commonly referred to as "banana". These early studies can be viewed as the foundation of modern experimental NPF research aimed at the quantitative interpretation of nucleation and growth rates.

METHODS

Size distribution measurements are typically based on electrical mobility analysis utilizing a differential mobility analyser (DMA) in combination with a detector. The Vienna-type DMA designed by Georg P. Reischl from the Vienna aerosol group has been a standard in aerosol sizing for the past couple of decades. Not surprisingly, this principle was employed in atmospheric measurements of particle number size distribution early on. During NPF a new mode of very small nanoparticles appears in the size spectrum which shifts towards larger sizes over time due to particle growth. This characteristic behavior is known from 2D contour plots or 3D representation of the time evolution of particle size distributions and goes back to Jyrki Mäkelä, who published the first report on NPF at the Hyytiälä measurement station in southern Finland in 1997 (Mäkelä *et al*., 1997). Due to the bowed shape characteristic for NPF in contour plots this is typically referred to as a "banana plot". The term is mentioned in a review on NPF by Kulmala & Kerminen (2008) but likely also can be attributed to Jyrki Mäkelä as the founder of modern NPF representation. It is thus oftentimes believed that Mäkelä *et al.* (1997) contains the first ever measured "banana". Remarkably, in this paper a reference is made to a paper from the Vienna aerosol group (Temnitschka *et al*., 1989) highlighting the first visual representation of NPF and its contribution to the

Aitken mode in the atmosphere. Indeed, data taken during the South California Air Quality Study in 1987 were published in a 3D plot and clearly show a banana-like shape (see Figure 1). To our knowledge it is the first 3D representation of NPF from the Vienna Aerosol Group. The question is: was it the first banana on record?

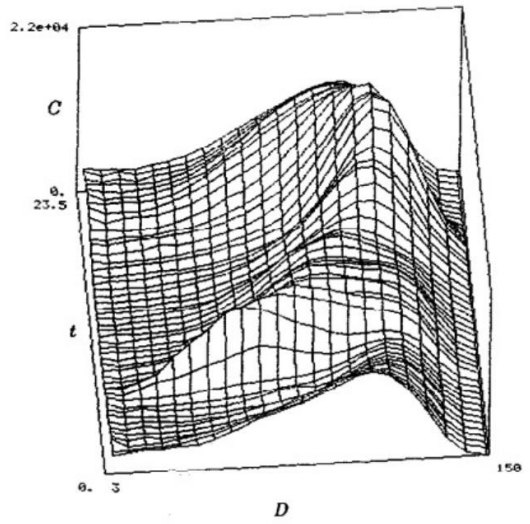


Figure 1. Earliest known 3D representation of a new particle formation event measured by the Vienna aerosol group (Temnitschka *et al*., 1989). X-axis (D) shows particle diameter in nm, y-axis shows time (t) of the day. Concentration (C) is displayed on the z-axis in units of cm^{-3}.

The paper by Temnitschka *et al*. (1989) was published in the conference proceedings from the European Aerosol Conference 1989 which took place in Vienna, Austria. Astonishingly, in the same issue a paper was published by Girgzdys *et al*. (1989) entitled "Atmospheric Aerosol Formation Research". The paper reports on size distribution measurements taken in the suburbs of Vilnius, Lithuania, between 1985 and 1989. Figure 2 shows an NPF event observed in August 1987, practically at the exact same time that the measurements from Temnitschka et al. (1989) took place in California.

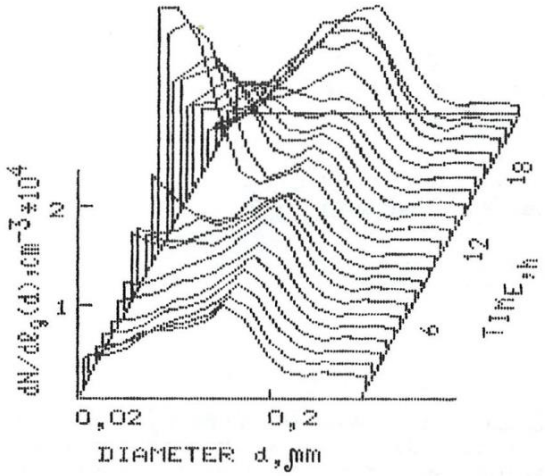


Figure 2. 3D representation of an NPF event reported by Girgzdys *et al*. (1989). The size distribution function (vertical axis) is plotted against diameter and time. Clearly, the appearance of a new mode at around 20 nm can be seen during midday that shifts towards larger sizes in the afternoon.

Apparently, bananas were known since the late 1980s. It should be pointed out that computers available at that time allowed automated data collection, however, graphical display was still a challenging task. We therefore speculate that these are among the earliest ever published bananas that we know of. Nevertheless, measurements of size resolved NPF have been taken by the Lithuanian group since 1985 which is also true for the Vienna aerosol group. In fact, measurements from the Vienna aerosol group of ambient particle number size distribution were taken in a semi-continuous way from a balcony in the second floor of the Faculty of Physics building in the 9th district in Vienna sampling urban background air. The typical set-up used by Wolfgang Winklmayr in his doctoral thesis (1987) was made up of the EMS-VIE-06 covering the size range between 3 and 150 nm, the same size range that was reported by Temnitschka *et al*. (1989). Details on instrument performance and characterization can be found in the paper by Reischl (1991). In brief, a Faraday cup electrometer was used as detector and sampling time intervals of ~10 minutes were achieved.

These measurements for which data are on record can be traced back to the year 1985. Unfortunately, none of these data have ever been published but are available from several seminar talks in the form of slides. As an example, Figure 3 below shows size distribution evolution during April 27, 1986, the day after the Chernobyl disaster had happened. While in the morning aerosol concentration was comparatively low indicating clean conditions before arrival of the radioactive cloud, a new mode of small nanoparticles appeared at high concentrations before noon. This mode disappeared subsequently showing growth of particles to larger sizes.

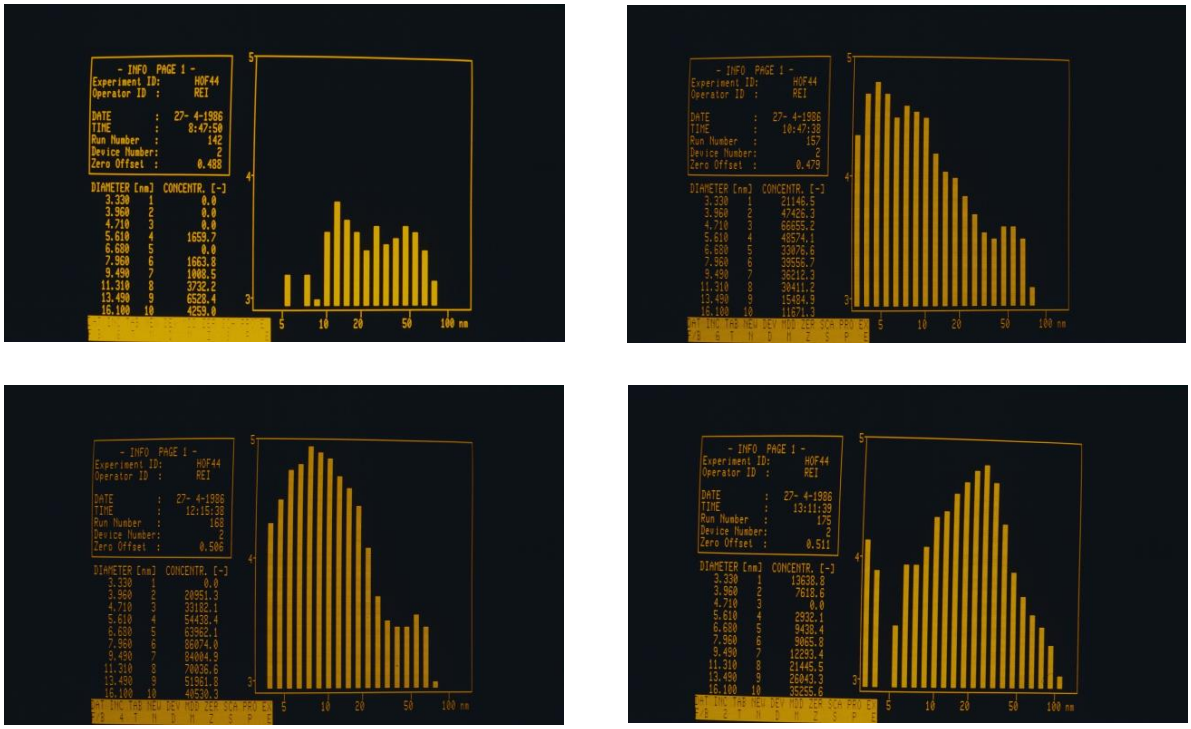


Figure 3. Ambient size distributions measured in Vienna on April 27, 1986. The sequence illustrates clear evolution of particle formation with pristine conditions in the morning (upper left panel), appearance of a new mode of sub-10 nm particles (upper right panel) and shift of the new mode to larger sizes during the day (bottom left and right panels).

It can be concluded from these figures that NPF was clearly observed by the Vienna aerosol group as early as 1986, possibly even in 1985. Nevertheless, the characteristic representation as a banana plot was not yet possible at that time.

CONCLUSIONS

While NPF research dates back to the time of John Aitken in the late 1800s, modern NPF research utilizes time-resolved monitoring of particle number size distributions starting at sizes well below 10 nm. Here we have demonstrated that the banana-shaped representation of NPF from atmospheric observations was first available in the late 1980s, with a tight match between the research groups from Lithuania and Austria. It should be noted though, that seminal work by others, e.g., Heisler&Friedlander (1977), McMurry & Wilson (1982), has already focused on the microphysical understanding of NPF well before, but sizing capabilities either were not sufficient to measure below ~20-30 nm or were lacking time resolution. The electrical mobility measurement as the standard in NPF research was fully established with the paper by Flagan *et al*. (1991). In any case, the global implications of the observations were not yet clear at that time.

ACKNOWLEDGEMENTS

PMW and AM acknowledge funding by the EU MSCA Doctoral Network CLOUD-DOC 101073026.

REFERENCES

Gordon et al. (2017), *J. Geophys. Res. Atmos*., **122**, doi:10.1002/2017JD026844.
Kulmala, M. et al. (2004), *J. Aerosol Sci.* **35**, 143-176.
Aitken, J., *On Dust, Fogs, and Clouds*, Trans. R.S.E., 1880- 81.
Mäkelä, J.M. et al. (1997) *Geophys. Res. Lett*. **24**, 10, 1219-1222.
Kulmala, M. and Kerminen, V.-M. (2008), *Atmos. Res*. **90**, 132-150.
Temnitschka et al. (1989) *J. Aerosol Sci.* **20**, 1173-1176.
Girgzdys *et al*. (1989), *J. Aerosol Sci.* **20**, 1107-1109.
Winklmayr, W. (1987). Ph.D. Thesis, University of Vienna, Vienna.
Reischl, G.P. (1991) *Aerosol Sci. Technol*. **14**, 5-24.
Heisler, S. L. and Friedlander, S. K. (1977), *Atmos. Environ*. **11**, 157-168.
McMurry, P. H. and Wilson, J. C. (1982), *Atmos. Environ*. **16**, 121-134.
Flagan, R. C. et al. (1991), *Environ. Sci. Technol*. **25**, 883-890.

CHARACTERISATION OF A THERMODENUDER-TYPE INLET USING NANOPLASTIC AEROSOL

P.J. WLASITS[1], D. KUNZE[1], R. KONRAT[1], A. JACOBSHAGEN[1] and P.M. WINKLER[1]

[1]*Faculty of Physics, University of Vienna, Vienna, Austria.*

Keywords: nanoplastic aerosol, thermal decomposition, tube furnace, differential mobility analyser.

INTRODUCTION

In recent years, nanoplastic pollution has been identified to be a problem on a global scale (Velimirovic *et al.*, 2021). Numerous studies addressed the dispersion of these anthropogenic pollutants across various ecosystems (e. g. Amobonye *et al.*, 2021; Materić *et al.*, 2022a; Materić *et al.*, 2022b). Despite a steadily increasing number of studies, atmospheric transport processes of plastic-derived nanoparticles are still poorly understood (Petersen and Hubbart, 2021).
As shown by Wlasits *et al.* (2022) nanoplastic aerosol can be generated in a controlled way using a tube furnace. This method enabled research on fundamental interactions of the generated particles with water vapor (Wlasits *et al.*, 2023). Most recently, tube furnace-generated Polyethylene terephthalate (PET) nanoplastic particles have been analysed using a high-resolution time-of-flight mass spectrometer (Tawadrous *et al.*, 2024).
Here, we present the characterisation of a thermodenuder-type inlet using nanoplastic aerosol. The aim of our work is to investigate the potential use of thermodenuder-type aerosol inlets in combination with APi-ToF mass spectrometers for the characterisation of nanoplastic aerosol.

METHODS

Characterisation experiments were conducted using two identically constructed thermodenuder-type inlets. The centrepiece of each inlet is a stainless steel tube that is heated using a heating band (Zhao *et al.*, 2024). The set point temperature of the heating band is controlled using a PID temperature controller (LabHEAT KM-RX1001).
Nanoplastic aerosol is generated by controlled evaporation-condensation using a tube furnace following Wlasits *et al.* (2022). PET pellets of known composition are placed onto a quartz glass-crucible and inserted into the working tube of the tube furnace (Nabertherm R50/250/13). The generated aerosol is put into charge equilibrium using a soft X-ray charger (TSI Advanced Aerosol Neutralizer 3088) and size-selected using a Vienna-type nano-DMA. Downstream of the nano-DMA (e. g. Wlasits *et al.*, 2023) a Y-splitter is used to feed the aerosol into the two inlets under investigation. Each inlet is connected to a particle detector monitoring the particle number concentration. Consequently, the effect of various temperature set points, aerosol flow rates, and particle number concentrations can be studied by comparing the readings of the detectors downstream of the inlets.

CONCLUSIONS

Our study shows that thermal decomposition of aerosol particles generated by controlled evaporation-condensation in a tube furnace can be achieved using the described inlets. Hence, our results can be a useful aid for the use of APi-ToF mass spectrometers for the chemical characterisation of nanoplastic aerosol.

ACKNOWLEDGEMENTS

This research was funded in whole or in part by the Austrian Science Fund (FWF) [10.55776/PAT5114323].

REFERENCES

Amobonye, A., P. Bhagwat, S. Raveendran, S. Singh and S. Pillai (2021). Environmental Impacts of Microplastics and Nanoplastics: A Current Overview. *Front. Microbiol.*, **12**, 768297.

Materić, D., H.A. Kjær, P. Vallelonga, J.-L. Tison, T. Rockmann and R. Holzinger (2022a). Nanoplastics measurements in Northern and Southern polar ice. *Environ. Res.*, **208**, 112741.

Materić, D., M. Peacock, J. Dean, M. Futter, T, Maximov, F. Moldan, T. Röckmann and R. Holzinger (2022b). Presence of nanoplastics in rural and remote surface waters. *Environ. Res. Lett.*, **17**(5), 054036.

Petersen, F. and J.A. Hubbart (2021). The occurrence and transport of microplastics: The state of the science. *Sci. Total Environ.*, **758**, 143936.

Tawadrous, M.A.R., A.K.Y. Lee and A.W.H. Chan (2024). Characterization of airborne PET nanoplastic particles using Aerosol mass spectrometry. *Aerosol Sci. Technol.*,1-14, doi:10.1080/02786826.2025.2451070.

Wlasits, P.J., A. Stoellner, G. Lattner, K. Maggauer and P.M. Winkler (2022). Size characterization and detection of aerosolized nanoplastics originating from evaporated thermoplastics. *Aerosol Sci. Technol.*, **56**, 176-185.

Wlasits, P.J., R. Konrat and P.M. Winkler. (2023). Heterogeneous Nucleation of Supersaturated Water Vapor onto Sub-10 nm Nanoplastic Particles. *Environ. Sci. Technol.*, **57**(4), 1584-1591.

Zhao, J., V. Mickwitz, Y. Luo, E. Häkkinen, F. Graeffe, J. Zhang, H. Timonen, M. Canagaratna, J.E. Krechmer, Q. Zhang, M. Kulmala, J. Kangasluoma, D. Worsnop and M. Ehn (2024) Characterization of the Vaporization Inlet for Aerosols (VIA) for online measurements of particulate highly oxygenated organic molecules (HOMs). *Atmos. Meas. Tech.*, **17**(5), 1527-1543.

Quantifying HONO Production from Nitrate Photolysis in Polluted Atmosphere

Men Xia[1,2,3], Yifan Jiang[1], Likun Xue[4], Xinfeng Wang[4], Xuelian Zhong[4], Yongchun Liu[3], Markku Kulmala[2,3], Tong Ma[5], Jiaqi Wang[5], Yurun Wang[1], Jian Gao[5], and Tao Wang[1]

[1]Department of Civil and Environmental Engineering, The Hong Kong Polytechnic University, Hong Kong, 999077, China

[2]Institute for Atmospheric and Earth System Research/Physics, Faculty of Science, University of Helsinki, Helsinki, 00014, Finland

[3]Aerosol and Haze Laboratory, Advanced Innovation Center for Soft Matter Science and Engineering, Beijing University of Chemical Technology, 100029, Beijing, China

[4]Environment Research Institute, Shandong University, Qingdao, 266237, China

[5]State Key Laboratory of Environmental Criteria and Risk Assessment, Chinese Research Academy of Environmental Sciences, Beijing, 100012, China

Abstract

The photolysis of particulate nitrate (pNO_3^-) has been suggested to be an important source of nitrous acid (HONO) in the troposphere. However, determining the photolysis rate constant of pNO_3^- ($j_{pNO_3^-}$) suffers from high uncertainty. Prior laboratory measurements of $j_{pNO_3^-}$ using aerosol filters have been complicated by the "shadow effect"—a phenomenon of light extinction within aerosol layers that potentially skews these measurements. We developed a method to correct the shadow effect on the photolysis rate constant of pNO_3^- for HONO production ($j_{pNO_3^-\rightarrow HONO}$) using aerosol filters with identical chemical compositions but different aerosol loadings. We applied the method to quantify $j_{pNO_3^-\rightarrow HONO}$ over the North China Plain (NCP) during the winter haze period. After correcting for the shadow effect, the normalized average $j_{pNO_3^-\rightarrow HONO}$ at 5 °C increased from 5.89×10^{-6} s^{-1} to 1.72×10^{-5} s^{-1}. The $j_{pNO_3^-\rightarrow HONO}$ decreased with increasing pH and nitrate proportions in $PM_{2.5}$ ($R_{NO_3^-}$) and had no correlation with nitrate concentrations. A parameterization for $j_{pNO_3^-\rightarrow HONO}$ was developed for model simulation of HONO production in NCP and similar environments.

Chemical Fingerprints and Source Apportionment of $PM_{2.5}$ at Offshore and Remote Islands in Taiwan and Japan Transported through East and West Channels

Jia-Yi Zhao[1], Yu-Lun Tseng[1], and Chung-Shin Yuan[1*]

[1]*Institute of Environmental Engineering, National Sun Yat-sen University, Kaohsiung, Taiwan, ROC*

Keywords: Marine fine particles ($PM_{2.5}$), chemical fingerprints, spatiotemporal variation, long-range transport (LRT), east and west channels, source apportionment

INTRODUCTION

East Asia has been characterized as one of the worst particulate air quality regions in the world. Asian continental outflow (ACO) was transported from China, Mongolia, and Korea to the leeward waters by a Siberia high during Asian Northeastern Monsoons (ANMs) (Yen et al., 2023; Yuan et al., 2023a). ACO could transport not only crustal dust from natural sources (i.e. Asian dust), but also from anthropogenic sources during the long-range transport (LRT), indicating that natural dust could mix with anthropogenic particles and form complex aerosols (Liu et al., 2019). Moreover, marine fine particles ($PM_{2.5}$) were a mixture of water-soluble ions, metallic elements, carbons, anhydrosugars, and organic acids. World Health Organization (WHO) reports that $PM_{2.5}$ is known as carcinogenic pollutants and could pose adverse effects on human respiratory system (Xing et al., 2016), ambient air quality and atmospheric visibility, and regional and global climates. Additionally, $PM_{2.5}$ could not only affect the tropospheric ozone (O_3) through atmospheric photochemical reactions, but also absorbs and scatters solar radiation, reduces atmospheric visibility, influences the atmospheric radiation budget balance, and changes the global climate.

As ACO passes through the Central Mountain Range (CMR) centered along north-south in the Taiwan Island, air masses can be divided into two separate air currents, namely the East and West Channels. Air masses in the West Channel move along the outer sea of western Taiwan (i.e. Taiwan Strait) down to the northern South China Sea (SCS) (Yuan, et al., 2023b), while those in the East Channel move through the outer seas of eastern Taiwan (i.e. West Pacific Ocean (WPO)) and the Bashi Channel (BC), and then transport to the northern SCS. It would be scientifically valuable if we can quantify the contributions of $PM_{2.5}$ blown from the two channels separately.

Accordingly, this study explored the spatiotemporal variation of $PM_{2.5}$ concentration and chemical characteristics for clustered transport channels/routes of air masses moving toward the leeward remote sites. The potential sources of $PM_{2.5}$ and their contributions were further resolved by CMB receptor modeling.

METHODOLOGIES

In this study, marine $PM_{2.5}$ were simultaneously collected by $PM_{2.5}$ samplers (BGI, PQ-200) at four remote islands, the Penghu Islands (PH), the Dongsha Island (DS), the Okinawa Island (OK), and the Green Island (GR) (Figure 1). During the diurnal sampling periods, 12-hr $PM_{2.5}$ samples were collected at four remote islands. The chemical composition of $PM_{2.5}$ was analyzed to quantify water-soluble ions, metallic elements, carbons, anhydrosugars, and organic acids. Furthermore, HYSPLIT simulation and CMB models were applied to resolve the potential sources of $PM_{2.5}$ and their contributions.

RESULTS AND DISCUSSION

This study investigated the spatiotemporal variation, chemical composition, and source apportionment of marine fine particles ($PM_{2.5}$) in the offshore islands of Taiwan and Japan. It showed that $PM_{2.5}$ concentrations in winter (15.92 μg m^{-3}) and spring (10.37 μg m^{-3}) (i.e., during the period of Asian Northeastern Monsoons; ANMs) were always higher than those in summer (5.62 μg m^{-3}) and fall (13.06 μg m^{-3}) (Figure 2).

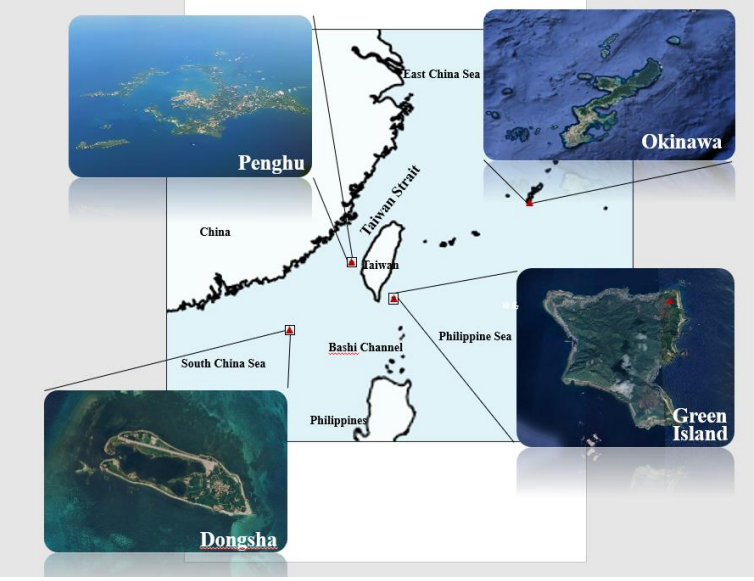


Figure 1. Locations of $PM_{2.5}$ sampling sites at the Penghu Islands, the Dongsha Island, the Okinawa Island, and the Green Island.

In terms of chemical composition of $PM_{2.5}$, secondary inorganic aerosols (SIAs; NO_3^-, SO_4^{2-}, and NH_4^+) (Figure 3) were the dominant component of water-soluble ions (WSIs) accounting for 37.2~52.4% of $PM_{2.5}$. Crustal elements (i.e., Mg, Al, Ca, Fe, and K) (Figure 4) dominated the metallic contents in $PM_{2.5}$. High values of enrichment factor (EF>10) showed that trace metals (i.e., V, Mn, Ni, Cu, and Zn) were potentially contributed from anthropogenic sources. Moreover, organic carbon (OC) (0.98 μg m^{-3}) was superior to elemental carbon (EC) (0.47 μg m^{-3}) in $PM_{2.5}$ (Figure 5). The mass ratios of OC and EC (OC/EC) were higher than 2.0 in all seasons except summer, showing the potential formation of secondary organic aerosols (SOAs) in $PM_{2.5}$ at the offshore islands. High concentrations of anhydrosugars were significantly affected by polluted air masses blown from the north occurred in winter and spring. In terms of spatial distribution, the average concentrations of anhydrosugars were ordered as: PH > DS > GR > OK (Figure 6). The M/S ratios of $PM_{2.5}$ at the four remote sites were similar, but also ordered as: PH> DS > GR > OK (Figure 7).

Backward trajectory simulation indicated that high $PM_{2.5}$ concentrations were mostly originated from North and Central China, Japan islands, and Korea Peninsula (Figure 8). Major sources (contribution percentage) of $PM_{2.5}$ resolved by CMB (Figures 9 and 10) receptor modeling were ordered as: sea salts (19.0%) > fugitive dust (17.9%) > industrial boilers (oil-fired) (9.5%) > secondary sulfate (9.9%) > Others (7.2%) > mobile sources (8.5%) > Biomass Burning (4.6%) > Secondary Nitrate (4.4%) > Fishing Vessel (4.3%) > Secondary Organic Carbon (2.7%) > Petrochemical Industry (2.5%) > Industrial Boilers (Coal-fired) (2.0%) > Steel Plant (1.6%).

Overall, this study in-depth investigated the chemical characteristics of $PM_{2.5}$ at four remote islands for the potential formation of secondary inorganic aerosols (SIAs) and organic carbon (OC). The backward trajectory simulation indicated that most polluted air masses originated from Northern Asia, suggesting that cross-boundary transport may be a key factor for the deterioration of regional air quality. Furthermore, CMB receptor model identified the contributions of industrial emissions, vehicular exhausts, and sea salts. Future research could focus on enhanced source apportionment and pollution control strategies to promote sustainable development and establish a healthy living environment.

CONCLUSIONS

This study sampled and analyzed $PM_{2.5}$ at four remote island sites over eight seasons, showing higher concentrations in winter and spring due to polluted air masses from East Asia. $PM_{2.5}$ levels were the highest at PH, mainly influenced by the LRT of secondary $PM_{2.5}$ in the West Channel. WSIs accounted for 37.2-52.4% of $PM_{2.5}$, with SIAs comprising 59.8% of WSIs. Major sources of metals in $PM_{2.5}$ included crustal elements (58.3%), oceanic spray (16.0%), and anthropogenic activities (13.8%). Higher OC/EC ratios in

winter and spring indicated the formation SOA, and biomass burning significantly impacted $PM_{2.5}$. CMB simulations revealed that West Channel transport was dominated by industrial boilers (oil), fugitive dust, secondary aerosols, and ship exhausts, while the East Channel was influenced by oceanic spray and industrial emissions.

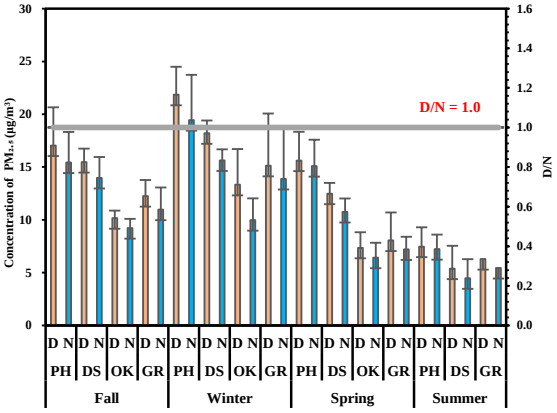


Figure 2. The spatiotemporal variation of $PM_{2.5}$ concentrations at PH, DS, OK, and GR

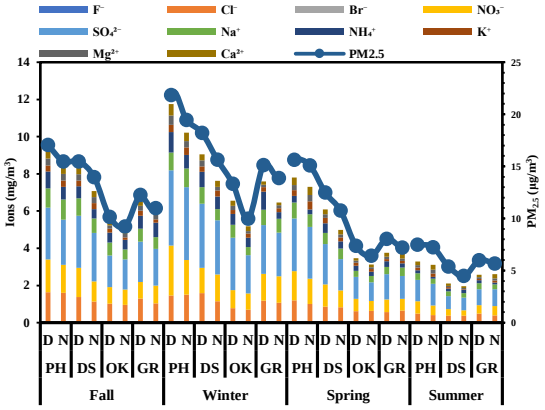


Figure 3. The spatiotemporal variation of water-soluble ion concentrations at PH, DS, OK, and GR.

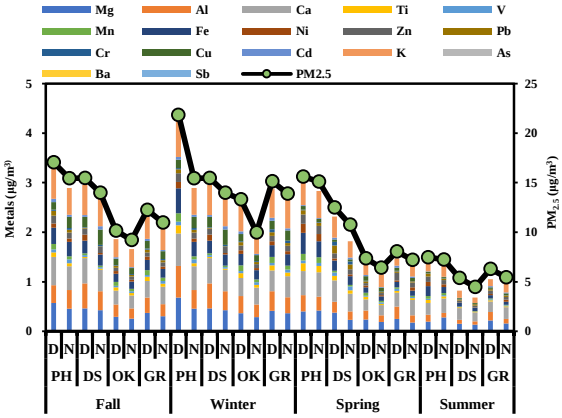


Figure 4. The spatiotemporal variation of metallic element concentrations at PH, DS, OK, and GR.

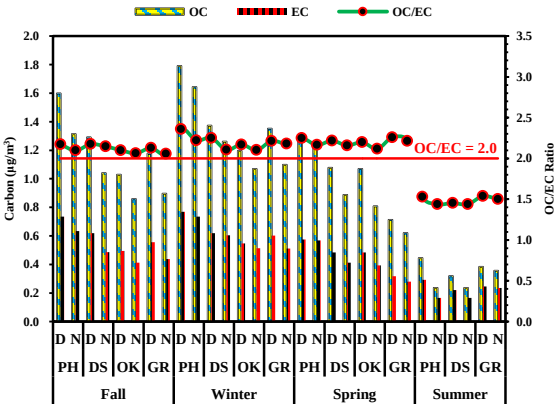


Figure 5. The spatiotemporal variation of carbons concentrations at PH, DS, OK, and GR.

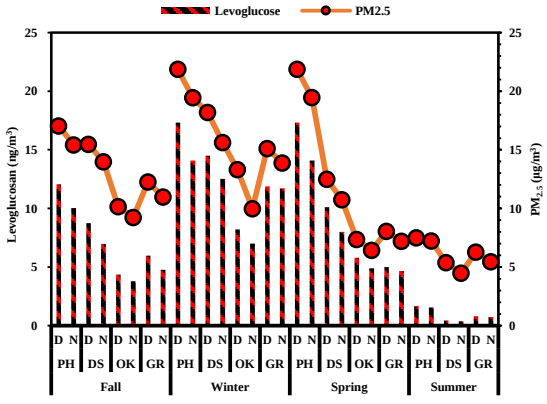


Figure 6. The spatiotemporal and diurnal variation trend of anhydrosugar concentration at PH, DS, OK, and GR.

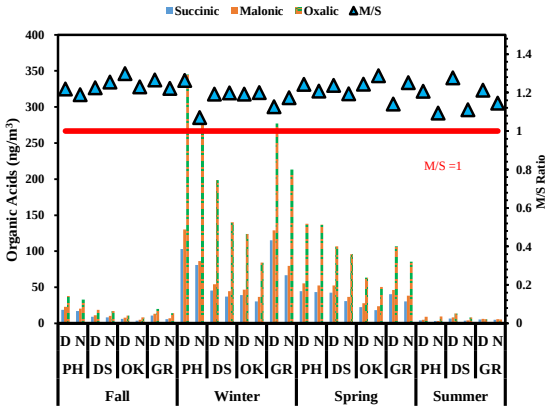
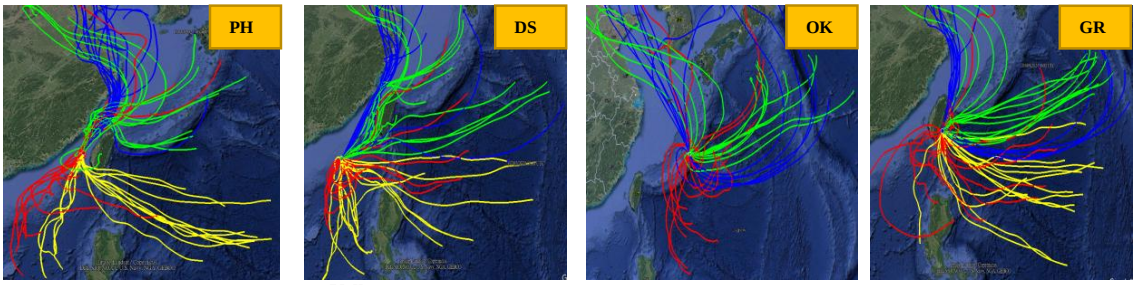


Figure 7. The spatiotemporal variation of organic acid concentrations at PH, DS, OK, and GR.



*Green:Fall; Blue:Winter; Red:Spring; Yellow:Summer

Figure 8. The transport route-based cluster analysis at the remote sites during the sampling periods.

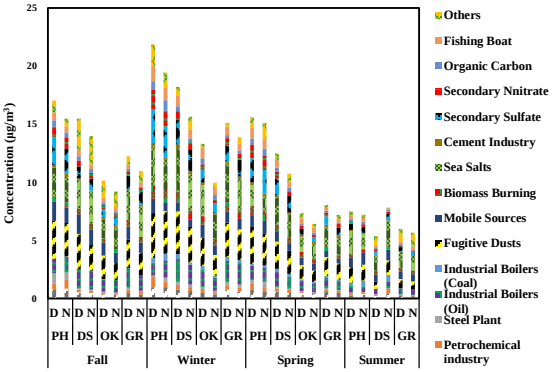


Figure 9. The source apportionment of $PM_{2.5}$ at the remote sites during the sampling periods

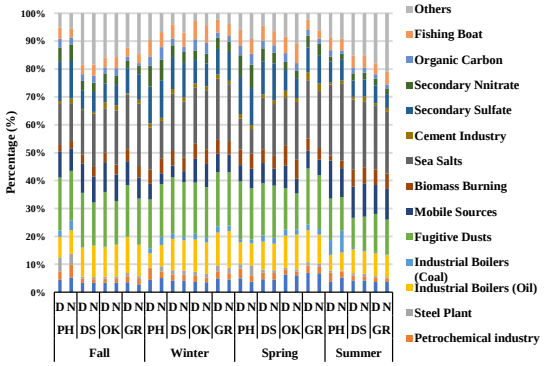


Figure 10. The source apportionment and contribution ratios of $PM_{2.5}$ concentrations at the remote sites during the sampling periods

ACKNOWLEDGEMENTS

This study was performed under the auspices of National Science and Technology Council (MOST) of Taiwan, ROC. The authors are grateful to MOST for its constant financial support. Special thanks go to the Biodiversity Research Center of the Academia Sinica, Marine Research Station in the Dongsha Atoll of MOST, and Weather Wings of Taiwan Navy and Air Force for their administrative assistance in meteorological observations and $PM_{2.5}$ sampling at the Green and Dongsha Islands.

REFERENCES

Liu, H., Yan, Y., Chang, H., Chen, H., Liang, L., Liu, X., Qiang, X., & Sun, Y. (2019). Magnetic signatures of natural and anthropogenic sources of urban dust aerosol. *Atmospheric Chemistry and Physics*, *19*(2), 731-745.

Xing, Y.-F., Xu, Y.-H., Shi, M.-H., & Lian, Y.-X. (2016). The impact of $PM_{2.5}$ on the human respiratory system. *Journal of Thoracic Disease*, *8*(1), E69.

Yen, P.-H., Yuan, C.-S., Lee, C.-W., Ceng, J.-H., Huang, Z.-Y., Chiang, K.-C., Du, I.-C., Tseng, Y.-L., Soong, K.-Y., & Jeng, M.-S. (2023). Chemical characteristics and spatiotemporal variation of marine fine particles for clustered channels of air masses transporting toward remote background sites in East Asia. *Environmental Pollution*, *331*, 121870.

Yuan, C.-S., Chiang, K.-C., Yen, P.-H., Ceng, J.-H., Lee, C.-E., Du, I.-C., Soong, K.-Y., & Jeng, M.-S. (2023a). Long-range transport of atmospheric speciated mercury from the eastern waters of Taiwan Island to northern South China Sea. *Environmental Pollution*, *318*, 120899.

Yuan, C.-S., Ceng, J.-H., Yen, P.-H., Chiang, K.-C., Tseng, Y.-L., Wong, K.-W., & Jeng, M.-S. (2023b). Temporospatial variation, chemical composition, and source resolution of $PM_{2.5}$ in the southeastern Taiwan Island. *Aerosol and Air Quality Research*, *23*(1), 220350.

Main Topic 3: Cloud Drop and Ice Nucleation

ON THE ICE NUCLEATION ACTIVITY OF MOLECULAR ICE NUCLEATORS

C. ALEFF[1] and T. KOOP[1],

[1]*Bielefeld University, Faculty of Chemistry, Bielefeld, Germany.*

Keywords: ICE NUCLEATION, MOLECULAR ICE NUCLEATOR, MICROFLUIDIC DEVICE.

INTRODUCTION

Ice nucleation is important for the formation of ice clouds and the initiation of precipitation. There have been extensive studies on various heterogeneous ice nucleators, both in laboratory experiments as well as in the field or on field-collected samples. Originally, many of these studies had been concerned with particulate ice nucleators, but in recent years it has become clear that ice nucleators of molecular origin can also trigger ice nucleation. A detailed molecular understanding of their way of action, however, is still lacking and, hence, dedicated experiments towards that goal appear essential, both in order to deepen our understanding of the fundamentals of that process as well as regarding an assessment of the relevance of molecular ice nucleators in various ice nucleation processes in nature.

METHODS

First, we prepared aqueous solutions of the ice-nucleating substances at varying concentrations. For the freezing studies, we applied two setups for detecting droplet freezing, see Figure 1. Firstly, the microliter-volume droplet freezing setup BINARY (Bielefeld Ice Nucleation ARraY) introduced several years ago (Budke and Koop, 2015) and, secondly, the recently developed microfluidic device nanoBINARY (nanoliter Bielefeld Ice Nucleation ARraY), in which nanoliter-volume droplets are employed (Eickhoff *et al.*, 2023). The latter is based on the WISDOM setup, developed previously at the Weizmann Institute of Science (Reicher *et al.*, 2018). In combination, these two devices BINARY and nanoBINARY allow the study of freezing processes over a wide range of temperature from the ice melting point down to the homogeneous ice nucleation limit of water droplets, which is about −36.2 °C for the ~100 µm droplets employed in nanoBINARY at a cooling rate of −1 °C min^{-1} (Koop and Murray, 2016). The latter ability is an important prerequisite for studying molecular ice nucleators, which often induce ice nucleation only at low temperature close to the homogeneous ice nucleation limit.

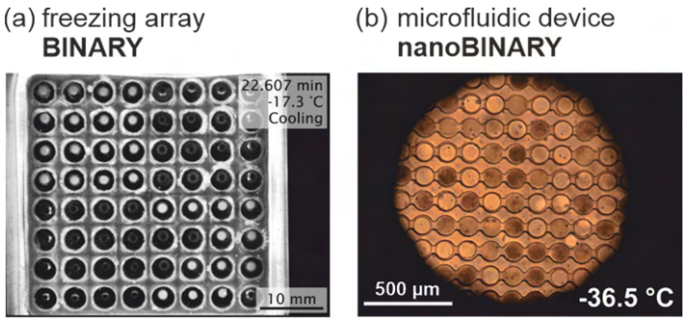


Figure 1. Images of frozen and unfrozen droplets during experiments with (a) the freezing array BINARY and (b) the microfluidic device nanoBINARY. In (a), the top left quarter of water droplets contain Snomax and the bottom right quarter contain birch pollen, while the unfrozen quarters of droplets (top right and bottom left) contain illite and pure water, respectively. In (b) the droplets contain pure water.

RESULTS

We investigated several naturally occurring compounds and also synthetic substances, some of which are also of relevance in nature. The ice nucleation data presented include those of antifreeze proteins, ice-nucleating proteins, polysaccharides as well as monomers, oligomers and polymers of poly(vinyl alcohol) and others (e.g., Eickhoff *et al.*, 2019; Forbes *et al.*, 2022; Eickhoff *et al.*, 2023). Together these data strongly suggest that the ice nucleation temperature within one class of compounds scales with molecular size: the larger the size of a molecular ice nucleator, the higher is its ice nucleation temperature. Moreover, it appears to be important that the ice nucleating moieties present a continuous, uninterrupted motif in order to support the formation of the critical ice cluster. Finally, there is some evidence that the ice nucleation, at least in some cases, may be triggered by clusters of molecules rather than individual molecules, in particular for the smaller molecular ice nucleators.

CONCLUSIONS

We present experimental data that molecules can act as ice nucleators and that their molecular properties are responsible for their high or low ice nucleation activity.

ACKNOWLEDGEMENTS

We thank Carsten Budke and Lukas Eickhoff as well as Naama Reicher and Yinon Rudich for their work and support during the development of the experimental techniques.

REFERENCES

Budke, C. and T. Koop (2015). BINARY: an optical freezing array for assessing temperature and time dependence of heterogeneous ice nucleation. *Atmos. Meas. Tech*. **8**, 689.

Eickhoff, L., K. Dreischmeier, A. Zipori, V. Sirotinskaya, C. Adar, N. Reicher, I. Braslavsky, Y. Rudich and T. Koop, T (2019). Contrasting Behavior of Antifreeze Proteins: Ice Growth Inhibitors and Ice Nucleation Promoters. *J. Phys. Chem. Lett.* **10** (5), 966.

Eickhoff, L., M. Keßler, C. Stubbs, J. Derksen, M. Viefhues, D. Anselmetti, M.I. Gibson, B. Hoge and T. Koop (2023). Ice nucleation in aqueous solutions of short- and long-chain poly(vinyl alcohol) studied with a droplet microfluidics setup. *J. Chem. Phys.* **158** (15), 154504.

Forbes, J., A. Bissoyi, L. Eickhoff, N. Reicher, T. Hansen, C.G. Bon, V.K. Walker, T. Koop, Y. Rudich, I. Braslavsky and P.L. Davies (2022). Water-organizing motif continuity is critical for potent ice nucleation protein activity. *Nat. Commun.* **13** (1), 5019.

Koop, T. and B.J. Murray (2016). A physically constrained classical description of the homogeneous nucleation of ice in water. *J. Chem. Phys.* **145** (21), 211915.

Reicher, N., L. Segev and Y. Rudich (2018). The WeIzmann Supercooled Droplets Observation on a Microarray (WISDOM) and application for ambient dust. *Atmos. Meas. Tech.* **11** (1), 233.

HYGROSCOPICITY AND CLOUD CONDENSATION NUCLEI ACTIVATION OF ATMOSPHERIC AEROSOLS AT A CENTRAL EUROPEAN RURAL SITE

C.S. ANDAN[1,2], P. MORAVEC[1], N. ZÍKOVÁ[1], R. LHOTKA[1,3], S. MBENGUE[4], J. ONDRáčEK[1], J. SCHWARZ[1], P. VODIčKA[1], and V. ŽDíMAL[1]

[1]*Institute of Chemical Process Fundamentals of the Czech Academy of Science, Prague, Czech Republic.*
[2]*Institute of Environmental Studies, Faculty of Science, Charles University, Prague, Czech Republic.*
[3]*Air Quality Department, Košetice Observatory, Czech Hydrometeorological Institute, Prague, Czech Republic.*
[4]*Global Change Research Institute, Czech Academy of Science, Brno, Czech Republic*

Keywords: Cloud Condensation Nuclei, Hygroscopicity, Aerosol Nucleation, Activation Efficiency

INTRODUCTION

Atmospheric aerosol particles play a crucial role in cloud formation by acting as cloud condensation nuclei (CCN), influencing the Earth's radiative balance and hydrological cycle. The ability of aerosols to serve as CCN depends not only on their number concentration but also on their physical and chemical properties, as well as their mixing state (Mochida et al., 2010). Understanding these complex interactions remains a key challenge in atmospheric research. Many studies have explored the relationship between aerosol hygroscopicity under subsaturated conditions and CCN activity under supersaturated conditions (Mochida et al., 2011). Hygroscopicity, which describes a particle's ability to absorb water, is a fundamental property that governs aerosol behavior in the atmosphere. Since aerosol hygroscopic properties evolve throughout their atmospheric lifetime, understanding these changes is essential for assessing their role in cloud activation. This study presents a comprehensive analysis of aerosol physical, chemical, and activation properties measured at the ACTRIS (Aerosol, Clouds, and Trace Gases Research Infrastructure, http://www.actris.eu/) site in Košetice, Czech Republic. Our primary objective is to improve the understanding of aerosol activation processes and ambient hygroscopic properties, with a particular focus on how chemical composition influences CCN activity. This work provides new insights into the complex interactions that govern aerosol-cloud interactions.

METHODS

Atmospheric aerosol measurements were conducted at the National Atmospheric Observatory Košetice (NAOK; 49◦35' N, 15◦05' E; 534 m a.s.l.) in the Bohemian-Moravian Highlands region. NAOK is classified as a rural background site, representing the regional background air pollution of the Czech Republic and, thus, Central Europe. This study focuses on aerosol particles' physicochemical properties and activation ability using the data collected at NAOK from December 2022 to November 2023.

A compact time-of-flight aerosol mass spectrometer (ToF-AMS, Aerodyne) was used to measure the chemical compositions of the non-refractory submicron aerosol particulate matter (nitrate, sulfate, chloride, ammonium, and organics). The mass concentration of equivalent black carbon was measured using the Aethalometer (AE33, Magee). The condensation particle counter (CPC, model 3775, TSI) was used to measure the total number concentration (N_{CPC}) of atmospheric aerosol and the cloud condensation nuclei counter (CCNC, model 200, Droplet Measurement Technologies) was used to measure the CCN number concentration (N_{CCNC}).

The total activated fraction was obtained by getting the ratio of N_{CCNC} over N_{CPC} at every supersaturation (SS) level. At fully stabilized CCNC conditions, five different SS conditions were set in the CCNC instrument (0.1 %, 0.2 %, 0.3 %, 0.5 %, and 1.0 %). A complete SS cycle lasted ~ 1 hour.

The hygroscopicity (κ) was derived from the ACSM chemical composition measurements using the Zdanovskii–Stokes–Robinson (ZSR) mixing rule combined with κ-Köhler theory (Petters and Kreidenweis, 2007). A simple ion-pairing scheme (Gysel et al., 2007) was used in this study, with the κ and ρ values of chemical species adopted by Wu et al. (2015). A κ of 0.1 was used for particulate organics (Gunthe et al., 2011). For black carbon, a κ of 0 was used (Schmale et al., 2018).

The GDAS (Global Data Assimilation System) meteorological data in 1°x1° spatial resolution were downloaded and back trajectories were calculated using the Hybrid Single Particle Lagrangian Integrated Trajectory (HYSPLIT) model (Stein et al., 2015). Air trajectory data were clustered and Kruskal–Wallis test was used to test the significance of inter-cluster variation in aerosol concentration.

CONCLUSIONS

Air masses originating from the continental region or eastern Europe (Cluster 1) is characterized by elevated concentrations of organics, sulfate (SO_4^{2-}), nitrate (NO_3^-), and ammonium (NH_4^+), indicative of anthropogenic pollution from industrial and urban sources (Fig. 1). The high fraction of equivalent black carbon (eBC) was also observed for Cluster 1, suggesting a larger influence of combustion-related emissions. Cluster 2, bringing continental air masses from western Europe, displays moderate levels of organics, SO_4^{2-}, NO_3^-, NH_4^+, and eBC, with a slightly higher κ that may reflect some biomass burning influence. This κ suggests a blend of both anthropogenic and natural sources. Cluster 3, originating from the Atlantic region, likely carries maritime-influenced air masses and is characterized by lower concentrations of most pollutants, except organics. The lower κ in this cluster may result from sub-micron measurement, missing the hygroscopic particles expected in this cluster.

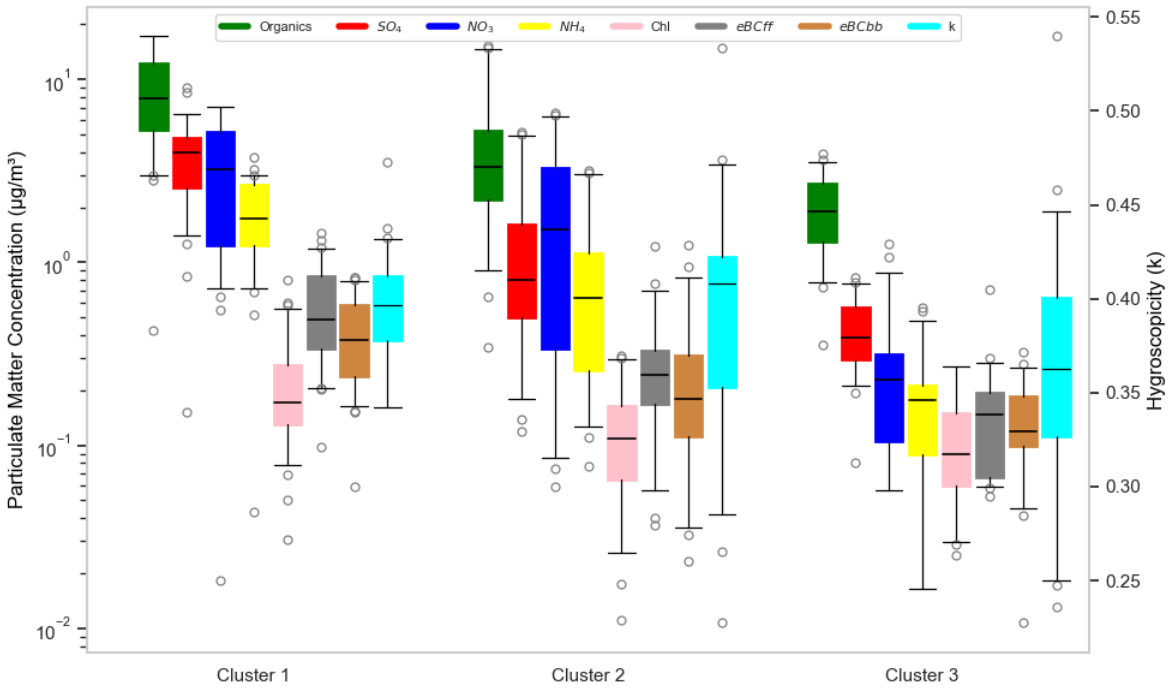


Figure 1. Particulate matter composition and hygroscopicity across clusters. Each box represents the interquartile range (IQR: Q1–Q3), the median (Q2), whiskers (5th and 95th percentiles), and circles indicating outliers.

Kruskal-Wallis tests was conducted to assess the significance of chemical composition differences across clusters. The results indicated significant differences among clusters for all measured components. Notably, SO_4^{2-} and NH_4^+ exhibit the highest H-statistics (65 and 61.9, respectively), suggesting strong variations across air mass clusters. eBC from fossil fuel (eBCff) and organics also show significant differences with H-statistics (51.9 and 51.8, respectively), aligning with the influence of long-range transport of pollution and organic aerosol content. The κ, on the other hand was tested using ANOVA, shows a weaker yet statistically significant difference (F-stat = 3.5, p-value = 0.03), implying that the ability of aerosols to uptake water varies by cluster but to a lesser extent compared to chemical composition.

The ability of aerosols in different clusters to activate as CCN under varying supersaturation levels was also analysed (Fig. 2). As supersaturation increases, activation ratios rise, but cluster-specific differences remain evident. Cluster 1 consistently exhibits higher activation across all supersaturation levels, while Cluster 3 shows reduced activation, in agreement with the κ values calculated from chemical composition (Fig. 1).

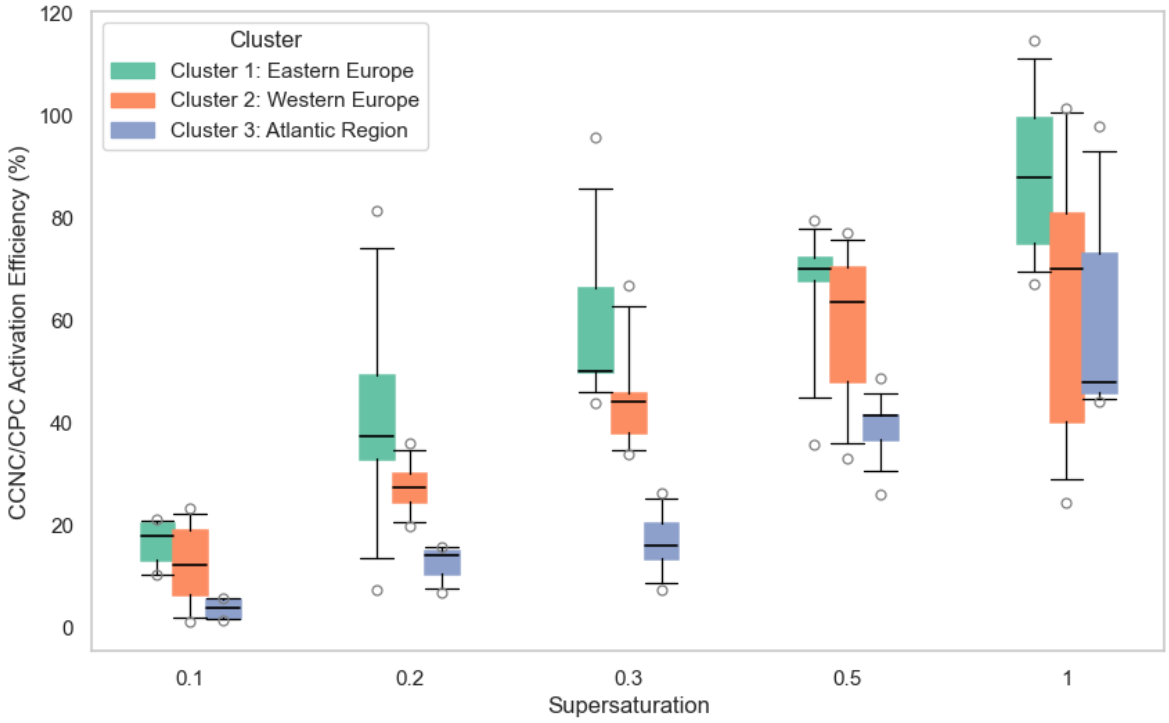


Figure 2. CCN activation ratio as a function of supersaturation for different clusters. Each box represents the interquartile range (IQR: Q1–Q3), the median (Q2), whiskers (5th and 95th percentiles), and circles indicating outliers.

Hygroscopicity plays a key role in CCN activation, with higher κ values corresponding to greater activation potential. This highlights the influence of chemical composition on cloud droplet formation. Cluster 1 contains more hygroscopic components, leading to enhanced CCN activation, whereas Cluster 3, with a higher fraction of hydrophobic organics, demonstrates reduced activation. As supersaturation increases, these differences become more pronounced, further emphasizing the impact of aerosol composition on CCN activation efficiency.

ACKNOWLEDGEMENTS

The authors appreciate the support of the project of the national research infrastructure ACTRIS–CZ (LM2023030) financed by the MEYS of the Czech Republic.

REFERENCES

Stein A.F., R.R. Draxler, G.D. Rolph, B.J.B. Stunder, M.D. Cohen and F. Ngan (2015). NOAA's HYSPLIT Atmospheric Transport and Dispersion Modeling System. *American Meteorological Society*.

Gunthe, S.S., D. Rose, H. Su, R.M. Garland, P. Achtert, A. Nowak, A. Wiedensohler, M. Kuwata, N. Takegawa, Y. Kondo, M. Hu, M. Shao, T. Zhu, M.O. Andreae and U. Pöschl (2011). Cloud condensation nuclei (CCN) from fresh and aged air pollution in the megacity region of Beijing, *Atmos. Chem. Phys.*, 11, 11023–11039.

Gysel, M., J. Crosier, D.O. Topping, J.D. Whitehead, K.N. Bower, M.J. Cubison, P.I. Williams, M.J. Flynn, G.B., McFiggans and H. Coe (2007). Closure study between chemical composition and hygroscopic growth of aerosol particles during TORCH2, *Atmos. Chem. Phys.*, 7, 6131–6144.

Mochida, M., C. Nishita-Hara, Y. Kitamori, S.G. Aggarwal, K. Kawamura, K. Miura and A. Takami (2010). Size-segregated measurements of cloud condensation nucleus activity and hygroscopic growth for aerosols at Cape Hedo, Japan, in spring 2008, *J. Geophys. Res.*, 115, D21207.

Mochida, M., C. Nishita-Hara, H. Furutani, Y. Miyazaki, J. Jung, K. Kawamura, and M. Uematsu (2011), Hygroscopicity and cloud condensation nucleus activity of marine aerosol particles over the western North Pacific, *J. Geophys. Res.*, 116, D06204.

Petters, M.D. and S.M. Kreidenweis (2007). A single parameter representation of hygroscopic growth and cloud condensation nucleus activity, *Atmos. Chem. Phys.*, 7, 1961–1971.

Schmale, J., S. Henning, S. Decesari, B. Henzing, H. Keskinen, K. Sellegri, J. Ovadnevaite, M.L. Pöhlker, J. Brito, A. Bougiatioti, A. Kristensson, N. Kalivitis, I. Stavroulas, S. Carbone, A. Jefferson, M. Park, P. Schlag, Y. Iwamoto, P. Aalto, M. Äijälä, N. Bukowiecki, M. Ehn, G. Frank, R. Fröhlich, A. Frumau, E. Herrmann, H. Herrmann, R. Holzinger, G. Kos, M. Kulmala, N. Mihalopoulos, A. Nenes, C. O'Dowd, P. Petäjä, T., Picard, D., Pöhlker, C., Pöschl, U., Poulain, L., Prévôt, A. S. H., Swietlicki, E., Andreae, M. O., Artaxo, A. Wiedensohler, J. Ogren, A. Matsuki, S.S. Yum, F. Stratmann, U. Baltensperger and M. Gysel (2018). Long-term cloud condensation nuclei number concentration, particle number size distribution and chemical composition measurements at regionally representative observatories, *Atmos. Chem. Phys.*, 18, 2853–2881.

Wu, Z.J., L. Poulain, W. Birmili, J. Größ, N. Niedermeier, Z.B. Wang, H. Herrmann, and A. Wiedensohler (2015). Some insights into the condensing vapors driving new particle growth to CCN sizes on the basis of hygroscopicity measurements, *Atmos. Chem. Phys.*, 15, 13071–13083.

THE ROLE OF CONTACT LINE ICE-NUCLEATION FOR FREEZING OF WATER ON PLASTIC INTERFACES

P. Bieber[1], and N. Borduas-Dedekind[1]

[1]*Department of Chemistry, University of British Columbia, Vancouver, V6T 1Z1, Canada.*

Keywords: Ice nucleation, contact line, plastic, high-speed cryo-microscopy.

INTRODUCTION

The heterogeneous nucleation of ice influences natural and human-induced cloud glaciation events (Lohman & Feichter, 2005), aircraft icing (Yamazaki et al., 2021), and the freezing of biological materials during cryo-preservation (Morris & Acton, 2013). Recently, plastic materials (polypropylene, polyethylene terephthalate) were added to the growing list of known ice-nucleating substances, with potential impact on atmospheric ice nucleation (Seifried et al., 2024; Aeschlimann et al., 2022). In fact, polypropylene microplastics immersed in aqueous droplets nucleated ice at temperatures around -22°C in two independent laboratory studies (Seifried et al., 2024; Busse et al., 2024). It is not clear how and why microplastics nucleate ice, or how a nucleation site might look like. Studying the local distribution and density of nucleation sites on plastic materials can improve the predictive capabilities for plastics induced ice nucleation in cloud models, and in the cryo-preservation and aviation industries. Here we report on high-speed cryo-microscopic investigations of droplets freezing on macroscopic plastic interfaces. We study onset locations of freezing (contact line nucleation vs plastic-water interface) to gain mechanistic insights into the ice-nucleation process induced by the macroscopic plastic interfaces.

METHODS

The ice nucleation locations on flat plastic substrates [polypropylene (PP)] were measured in a cryo-chamber with a high-speed camera (Chronos 1.4, Krontech). The pieces of PP were placed on a gold coated silicon-wafer on a Peltier-element. Thermo-paste served as a heat transporting medium between the pieces and the cooling stage. One droplet of pure water with a volume of 1 µL was pipetted onto the PP piece and the chamber was closed and flushed with nitrogen to remove any aerosols that could induce freezing. To start the experiment the stage was rapidly cooled to -15 °C and thereafter cooled with 1 °C min^{-1} until the droplet froze (example in Figure 1a). Note that no freezing event was observed above -15 °C. The settings of the camera were adjusted to a view of 800 x 800 pixels and a recording rate of 2100 frames per second. The recordings of the camera started prior cooling and stopped after the droplet froze. The videos were cut to show the freezing onset locations of the droplets. The temperature was measured with a K-type thermocouple placed in the thermo-paste next to the PCR tray piece and the freezing temperature was noted once the droplet froze. The experiment was conducted 30 times with individual plastic slides of the same sample type.

RESULTS & DISCUSSIONS

Using the high-time resolution of the camera enabled us to locate the freezing onset for droplets on the investigated PP sheet (see time frames in Figure 1a and Figure 1b for geometry of the droplet). Clearly, nucleation started at the three-phase contact line in 26 out of 30 experiments (Figure 1c). Freezing at the contact line would be very unlikely induced by contaminants which are equally distributed in the bulk of the droplet. For example, hydrophilic INPs from birch pollen nucleated in the bulk of droplets when observed with a high-speed camera between two glass slides (Bieber & Borduas-Dedekind, 2024). Also, nucleation sites on the surface of the substrate, similar to pores or cracks on mineral dust surfaces as observed by Holden et al., 2021, cannot explain why the droplets on the PP substrate freeze at the contact line more often than not.

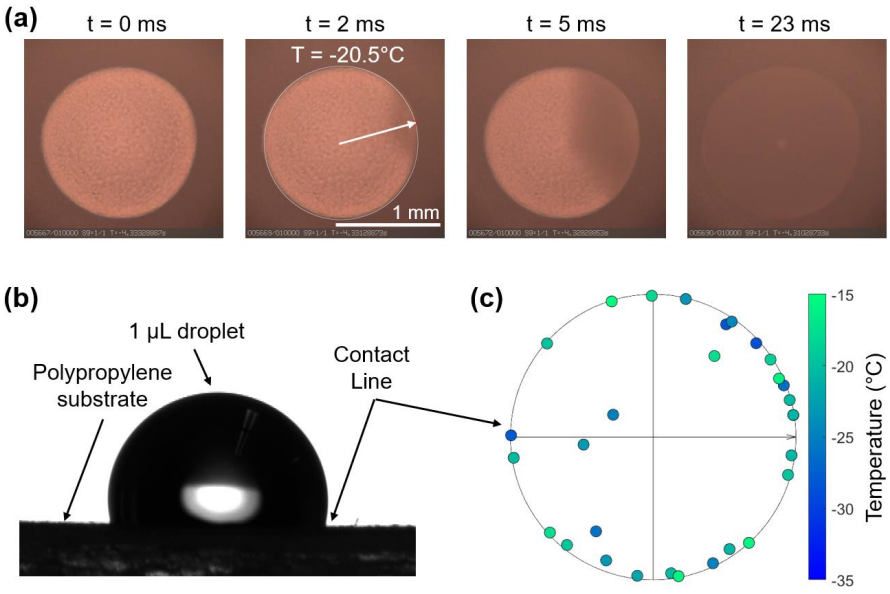


Figure 1. Ice-nucleation initiates at the plastic-water-air contact line. (a) High-speed cryo-microscopy of an aqueous droplet freezing on the plastic interface (top view). The ice scatters the light beam and thus appears dark. (b) Droplet side view on the polypropylene substrate. (c) Results from 30 measurements: the locations of freezing in polar coordinates are depict as color coded markers, the color indicates the freezing temperature.

Ice-nucleation at contact lines has been observed for various substrates, including an aluminum plate (Kart et al., 2021), silicon wavers (Suzuki et al., 2007), and glass fibers (Gurganus et al., 2014). For example, Suzuki et al., found that the ice nucleation of droplets placed on silicon wavers and on fluorinated substrates initiated at the contact-line. However, two contrasting studies found no evidence for contact-line nucleation for similar substrates, but rather that the nucleation sites were randomly distributed on the substrate-water interface (Gurganus et al., 2011; Gurganus et al., 2013). In a follow-up study the same group showed that the surface roughness can lead to contact nucleation. A glass fiber with nanoscale structures predominantly nucleated at the contact line although the immersed surface area is significantly higher than the intersection at the contact line (Gurganus et al., 2014).

What caused nucleation at the contact line for the investigated plastic substrates in this study? We can speculate based on literature about contact line nucleation:

- **Excess free energy at the contact-line**: Ice cluster growth requires the generation of a new interface, the ice-water interface, which is energetically unfavorable. Therefore, the energetically cheapest growth of ice clusters could be at the line where all three phases (air, substrate and water) meet, the contact line (Kart et al., 2021, Sear 2012, Djikaev & Ruckenstein 2008). Indeed, Kart et al., 2021 showed that nucleation at the contact line dominated the nucleation locations for substrates with a contact angle around 90°.
- **Contact line pinning induces negative pressure perturbation:** The surface tension of water increases with decreasing temperatures (Vins et al., 2020). According to the Young equation, the contact angle of a water droplet on a plastic substrate would increase with increasing surface tension (Song & Fan, 2021). Therefore, the contact angle of a droplet on a flat substrate must increase upon cooling. However, some surfaces are known to pin the contact line in place, leading to hysteresis in the system. It has been shown that this distortion of a moving contact line can initiate freezing, most likely due to pressure perturbations (Yang et al., 2018; Yang et al., 2019; Rosky et al., 2022), which may be the reason for nucleation at the air-water-plastic contact line on the investigated samples.

CONCLUSIONS AND OUTLOOK

Ice nucleation was observed at the contact line in most (87%) of the investigated droplets on PP interfaces, suggesting that contact-line nucleation is the primary freezing mode for plastics. In contrast to mineral dust, where cracks and pores serve as nucleation sites, these features do not appear to drive ice nucleation on plastics. The excess free energy at the contact line, or the contact line hysteresis upon cooling associated with pressure perturbations, may provide a physical explanation for this phenomenon. Modifying the contact angle or surface roughness to reduce contact line pinning could help mitigate icing problems. The next phase of this project will focus on extrapolating these findings to microscopic plastic interfaces to assess the atmospheric relevance of contact-line nucleation.

ACKNOWLEDGEMENTS

The authors thank KronTechnologies for providing High-speed cameras for this research. Furthermore, the authors thank Hinrich Grothe and David Schmale III for supporting this research with laboratory equipment to build the setup. P.B. is thankful for a 4YF scholarship from UBC.

REFERENCES

Aeschlimann, M., Li, G., Kanji, Z. A., & Mitrano, D. M. (2022). Potential impacts of atmospheric microplastics and nanoplastics on cloud formation processes. *Nature Geoscience*, 15(12), 967-975.

Bieber, P., & Borduas-Dedekind, N. (2024). High-speed cryo-microscopy reveals that ice-nucleating proteins of Pseudomonas syringae trigger freezing at hydrophobic interfaces. *Science Advances*, 10(27), eadn6606.

Busse, H. L., Ariyasena, D. D., Orris, J., & Freedman, M. A. (2024). Pristine and aged microplastics can nucleate ice through immersion freezing. *ACS ES&T Air*, 1(12), 1579-1588.

Djikaev, Y. S., & Ruckenstein, E. (2008). Thermodynamics of heterogeneous crystal nucleation in contact and immersion modes. *The Journal of Physical Chemistry A*, *112*(46), 11677-11687.

Gurganus, C., Kostinski, A. B., & Shaw, R. A. (2011). Fast imaging of freezing drops: No preference for nucleation at the contact line. *The Journal of Physical Chemistry Letters*, 2(12), 1449-1454.

Gurganus, C., Kostinski, A. B., & Shaw, R. A. (2013). High-speed imaging of freezing drops: Still no preference for the contact line. *The Journal of Physical Chemistry C*, 117(12), 6195-6200.

Gurganus, C. W., Charnawskas, J. C., Kostinski, A. B., & Shaw, R. A. (2014). Nucleation at the contact line observed on nanotextured surfaces. *Physical review letters*, 113(23), 235701.

Holden, M. A., Campbell, J. M., Meldrum, F. C., Murray, B. J., & Christenson, H. K. (2021). Active sites for ice nucleation differ depending on nucleation mode. *Proceedings of the National Academy of Sciences*, 118(18), e2022859118.

Kar, A., Bhati, A., Lokanathan, M., & Bahadur, V. (2021). Faster nucleation of ice at the three-phase contact line: Influence of interfacial chemistry. *Langmuir*, 37(43), 12673-12680.

Lohmann, U., & Feichter, J. (2005). Global indirect aerosol effects: a review. *Atmospheric Chemistry and Physics*, 5(3), 715-737.

Morris, G. J., & Acton, E. (2013). Controlled ice nucleation in cryopreservation–a review. *Cryobiology*, 66(2), 85-92.

Sear, R. P. (2012). The non-classical nucleation of crystals: microscopic mechanisms and applications to molecular crystals, ice and calcium carbonate. *International Materials Reviews*, *57*(6), 328-356.

Seifried, T. M., Nikkho, S., Morales Murillo, A., Andrew, L. J., Grant, E. R., & Bertram, A. K. (2024). Microplastic particles contain ice nucleation sites that can be inhibited by atmospheric aging. *Environmental Science & Technology*, 58(35), 15711-15721.

Suzuki, S., Nakajima, A., Yoshida, N., Sakai, M., Hashimoto, A., Kameshima, Y., & Okada, K. (2007). Freezing of water droplets on silicon surfaces coated with various silanes. *Chemical Physics Letters*, 445(1-3), 37-41.

Vinš, V., Hykl, J., Hrubý, J., Blahut, A., Celný, D., Čenský, M., & Prokopová, O. (2020). Possible anomaly in the surface tension of supercooled water: New experiments at extreme supercooling down to− 31.4° C. *The Journal of Physical Chemistry Letters*, *11*(11), 4443-4447.

Yamazaki, M., Jemcov, A., & Sakaue, H. (2021). A review on the current status of icing physics and mitigation in aviation. *Aerospace*, 8(7), 188.

Yang, F., Cruikshank, O., He, W., Kostinski, A., & Shaw, R. A. (2018). Nonthermal ice nucleation observed at distorted contact lines of supercooled water drops. *Physical Review E*, *97*(2), 023103.

Yang, F., Cantrell, W. H., Kostinski, A. B., Shaw, R. A., & Vogelmann, A. M. (2019). Is contact nucleation caused by pressure perturbation?. *Atmosphere*, *11*(1), 1.

Rosky, E., Cantrell, W., Li, T., & Shaw, R. A. (2022). Homogeneous ice nucleation rate at negative pressures: The role of the density anomaly. *Chemical Physics Letters*, *789*, 139289.

FREE-TROPOSPHERIC ICE-NUCLEATING PARTICLE MEASUREMENTS AT CIRRUS FORMATION TEMPERATURES

P. BOGERT[1], L. LACHER[1], K. HÖHLER[1], E. LUDEWIG[2], C. MAIER[2], J. SCHROD[3], J. CURTIUS[3] AND O. MÖHLER[1]

[1]*Institute of Meteorology and Climate Research, Atmospheric Aerosol Research, Karlsruhe Institute of Technology, Karlsruhe, Germany.*

[2]*Sonnblick Observatory, GeoSphere Austria, Salzburg, 5020, Austria.*

[3]*Institute for Atmospheric and Environmental Sciences, Goethe University Frankfurt, Frankfurt am Main, Germany.*

Keywords: ICE-NUCLEATING PARTICLES, FIELD MEASUREMENTS, CIRRUS CLOIDS.

INTRODUCTION

A minor and strongly temperature-dependent fraction of atmospheric aerosols, called Ice-Nucleating Particles (INPs), is known to impact the weather and climate systems by inducing the formation of ice in mixed-phase and cirrus clouds (Fan et al., 2017; Forster et al., 2021; Murray et al., 2021). There is increasing evidence that INPs not only induce the formation of precipitation in particular over continental areas (Field et al., 2012) but also have an important impact on the radiative properties of a number of cloud types throughout the troposphere (Forster et al., 2021). For cirrus formation, the abundance and types of INPs play important roles in the interplay between heterogeneous and homogeneous ice nucleation pathways, leading to either net cooling or heating of cirrus clouds in the global climate system. Despite their importance, there is a lack of INP measurements in the free troposphere, especially for those INPs that activate ice at cirrus formation temperatures. There are also no aircraft-based INP measurements at temperatures below -40 °C so far. Such measurements are of great importance as they can help to better understand not only the INP concentration of the natural background conditions, but also to understand the influence of aviation emissions on the formation of ice clouds due to contrail formation. Here, the emission of soot aerosol, sulfate aerosol or lubricant oils can impact cloud formation. This topic has received more and more interest in the recent years, as it is known that global air traffic leads to a net warming of the earth's surface and thus enhances anthropogenic climate warming (Lee et al., 2021).

METHODS

During the previous years, the new instrument PINEair (Portable Ice Nucleation Experiment – aircraft-based version, Bogert, 2024) was developed for measuring INPs at cirrus formation temperatures between about -40°C and -65°C and ice supersaturations of up to about 100%. It can also be used to investigate the INP concentration at mixed-phase cloud conditions. The new instrument can be operated both onboard research aircrafts and at high altitude mountain stations. It is based on the PINE (Portable Ice Nucleation Experiment) instrument, which was developed for laboratory experiments on ice nucleation processes and for automated operation during longer-term INP monitoring activities in the field (Möhler et al., 2021). PINEair is developed and optimized for direct sampling in the free troposphere. The main difference between PINEair and PINE is that PINEair consists of three small cloud expansion chambers each with a volume of three liters (Fig. 1), whereas PINE only has a single 10-liter cloud expansion chamber. This allows measurements with an improved time resolution. The three cloud chambers are located inside a vacuum chamber (Fig. 1) which provides both a good thermal insulation of the cooled cloud chambers and a mechanical stabilization of the thin-walled cloud chambers during pressure reduction for cloud droplet and ice activation of the sampled aerosol. Cooling of the cloud chamber walls is achieved with a sterling cooler which needs only electric power but no coolant liquid. Each cloud expansion chamber has its own

inlet, outlet and optical particle counter (OPC) for detecting aerosol particles, liquid droplets and ice crystals (Fig. 1).

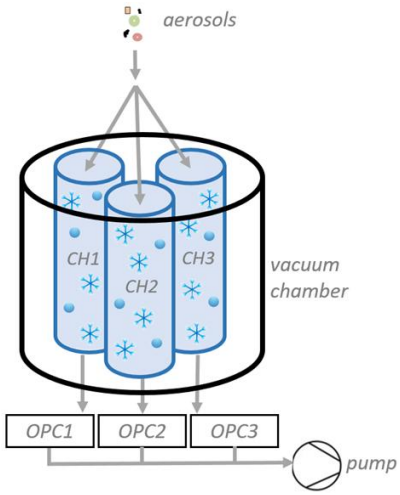


Figure 1. Schematic diagram of PINEair with the three cloud chambers located in the vacuum chamber.

RESULTS AND CONCLUSIONS

While the version of PINEair for HALO (High Altitude and Long Range Research Aircraft) is currently under construction, a prototype version of PINEair was built at KIT to perform characterization experiments and use it for automated long-term measurements at field observatories. In May 2023, the first field campaign with PINEair was successfully conducted at the Sonnblick Observatory (SBO) in Austria, which is located at an altitude of 3106m and is therefore an ideal location to investigate INPs in the free troposphere. Figure 2 shows an example measurement for the INP concentration from May 20, 2023, records between 11:10 h and 15:40 h local time. The colors correspond to the peak ice saturation ratio $S_{ice,p}$ inside the chamber. The gray shaded area shows the INP concentration for a relative humidity scan, with higher concentrations at higher $S_{ice,p}$. The unshaded area shows a series of run by run INP concentrations measured for almost constant $S_{ice,p}$ with only heterogeneous ice formation to occur. Here, the single run data scattered around a mean value of about 3 std L^{-1}. This scatter is mainly caused by the statistical counting uncertainty of a low number of ice crystals detected in each run.

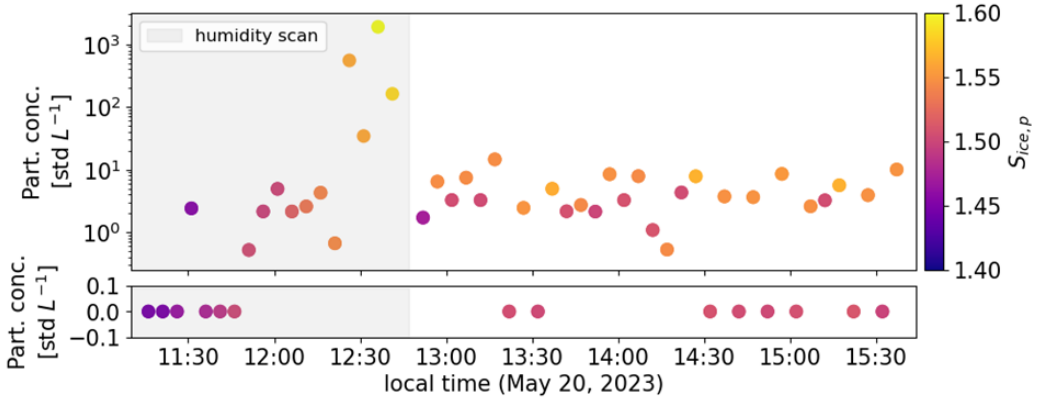


Figure 2. Example measurement with PINEair at a temperature of about -47.8 °C during 20 May 2023 at the Sonnblick Observatory (SBO) in Austria. The grey-shaded area marks the time period of a relative humidity scan, the unshaded area shows a series of single run INP concentrations measured at constant $S_{ice,p}$, where only heterogeneous ice nucleation conditions are reached in the expansion chamber.

The campaign successfully demonstrated that PINEair is a steadily operating instrument and it can be used to measure the INP concentration at both mixed-phase and cirrus cloud formation temperatures. Since August 2019, we also continuously measure the INP concentration at the SBO via aerosol filter collection and offline analysis using INSEKT (Ice Nucleation Spectrometer of the Karlsruhe Institute of Technology, Schneider et al., 2021) with a time resolution of one week. From August 2021 until October 2022, we performed additional measurements with the online INP instrument PINE, which has a time resolution of 5 to 6 min. In this contribution, we show the results from long-term INP measurements at SBO for nucleation temperatures from -10 °C to -30° C, where we found a significant seasonal recurring trend in the INP concentration, as well as the INP measurements with PINE and PINEair.

ACKNOWLEDGEMENTS

The development of PINEair is funded by the German Science Foundation (DFG) as part of the SPP 1294 HALO (project number 667314). Support by the AIDA team at the Karlsruhe Institute of Technology and GeoSphere Austria team during the measurements at Sonnblick Observatory is gratefully acknowledged.

REFERENCES

Bogert, P. Ice-nucleating particles in the free troposphere: long-term observation and first measurements at cirrus formation temperatues using the novel Portable Ice Nucleation Experiment PINEair, Ph.D. thesis, Karlsruhe Institute of Technology, https://doi.org/10.5445/IR/1000174265, 2024.

Fan, J.; Leung, L.R.; Rosenfeld, D.; DeMott, P.J. Effects of cloud condensation nuclei and ice nucleating particles on precipitation processes and supercooled liquid in mixed-phase orographic clouds. Atmos. Chem. Phys. 2017, 17, 1017-1035.

Field, P.R.; Heymsfield, A.J.; Shipway, B.J.; DeMott, P.J.; Pratt, K.A.; Rogers, D.C.; Stith, J.; Prather, K.A. Ice in clouds experiment–layer clouds. Part ii: Testing characteristics of heterogeneous ice formation in lee wave clouds. Journal of the Atmospheric Sciences, 69, 1066-1079, 2012.

Forster, P., T. Storelvmo, K. Armour, et al.W. Collins, J.-L. Dufresne, D. Frame, D.J. Lunt, T. Mauritsen, M.D. Palmer, M. Watanabe, M. Wild, and H. Zhang, 2021: The Earth's Energy Budget, Climate Feedbacks, and Climate Sensitivity. In Climate Change 2021: The Physical Science Basis. Contribution of Working Group I to the Sixth Assessment Report of the Intergovernmental Panel on Climate Change [Masson-Delmotte, V., P. Zhai, A. Pirani, S.L. Connors, C. Péan, S. Berger, N. Caud, Y. Chen, L. Goldfarb, M.I. Gomis, M. Huang, K. Leitzell, E. Lonnoy, J.B.R. Matthews, T.K. Maycock, T. Waterfield, O. Yelekçi, R. Yu, and B. Zhou eds.)]. Cambridge University Press, Cambridge, United Kingdom and New York, NY, USA, pp. 923–1054, doi:10.1017/9781009157896.009.

Lee D.S.; Fahey, D.W.; Skowron, A.; Allen, M.R.; Burkhardt, U.; Chen, Q.; Doherty, S.J.; Freeman, S.; Forster, P.M.; Fuglestvedt, J. et al.: The contribution of global aviation to anthropogenic climate forcing for 2000 to 2018, Atmospheric Environment, 244, 1352-2310, https://doi.org/10.1016/j.atmosenv.2020.117834, 2021.

Möhler, O., Adams, M., Lacher, L., Vogel, F., Nadolny, J., Ullrich, R., Boffo, C., Pfeuffer, T., Hobl, A., Weiß, M., Vepuri, H. S. K., Hiranuma, N., and Murray, B. J.: The Portable Ice Nucleation Experiment (PINE): a new online instrument for laboratory studies and automated long-term field observations of ice-nucleating particles, Atmos. Meas. Tech., 14, 1143–1166, https://doi.org/10.5194/amt-14-1143-2021, 2021.

Murray, B. J., Carslaw, K. S., and Field, P. R.: Opinion: Cloud-phase climate feedback and the importance of ice-nucleating particles, Atmos. Chem. Phys., 21, 665-679, 10.5194/acp-21-665-2021, 2021.

WHAT DRIVES BIOGENIC ICE NUCLEATION?

S.D. Brooks[1], D.C.O. Thornton[2] and R. Sofa[1]

[1]*Texas A&M University, Department of Atmospheric Sciences, College Station, Texas*

[2]*Texas A&M University, Department of Atmospheric Sciences, College Station, Texas*

Keywords: protein, ice nucleation, aerosol, biological aerosol, catalysis

INTRODUCTION

It is now understood that biological aerosols are important contributors to heterogenous nucleation and may even contribute most of the INP at temperatures above -20 degrees C (*Zhang et.al,* 2024). However, "biological aerosol" is a grossly oversimplified description of this group of particles with a variety of sources, compositions and sizes with a similarly diverse range of nucleation temperatures (*Alsante, et al,* 2003&2024; *Thornton et al,* 2023; *Matthews et al,* 2023). On a fundamental level, we lack an understanding of what physicochemical properties are root causes of ice nucleation ability. Beyond the chemical formula, our measurements suggest that the role of aggregation plays is a key role in the ice nucleation ability of certain proteins. Specifically, in high concentration, ice nucleation of the protein RuBisCO (ribulose-1,5-bisphosphate carboxylase/oxygenase) occurs at temperatures above -8 degrees C (*Alsante, Thornton and Brooks,* 2023). in both immersion and contact nucleation mode. In immersion mode, the warmest nucleation events coincided with the formation of large aggregates with a hydrodynamic diameter of $\sim 10^3$ nm. While our results show that many additional proteins, including cytochrome C, thyroglobulin, pyruvate kinase, alkaline phosphatase, lipase, and insulin also aggregate in solution, trends in aggregation and ice nucleation efficiency are not straightforward. Aggregation can be enhanced by the presents of metal cations, which, in turn affect the ice nucleation activity. Additional factors, including concentration effects, surface charge, and pH also influence to ice nucleating temperatures. Here we present recent advances in the fundament drivers of biogenic nucleation activity.

ACKNOWLEDGEMENTS

This work was supported by the National Science Foundation, Award #2128133. Roya Safa acknowledges support from a Texas A&M Hagler Fellowship.

REFERENCES

Alsante, A.N., Thornton, D.C.O. & Brooks, S.D. Ice nucleation catalyzed by the photosynthesis enzyme RuBisCO and other abundant biomolecules. *Commun Earth Environ* **4**, 51 (2023). https://doi.org/10.1038/s43247-023-00707-7

Alsante, A. N., D. C. O. Thornton, S. D. Brooks, J. A. Mirrielees, E. K. Wilbourn, B. H. Matthews, B. Diaz and K. D. Bidle (2025). "Effect of viral infection on the ice nucleation efficiency of marine coccolithophores." *Aerosol Science and Technology* 59(2): 195-213.

Alsante, A. N., D. C. O. Thornton and S. D. Brooks (2024). "Effect of Aggregation and Molecular Size on the Ice Nucleation Efficiency of Proteins." *Environmental Science & Technology* **58**(10): 4594-4605.

Thornton, D. C. O., S. D. Brooks, E. K. Wilbourn, J. Mirrielees, A. N. Alsante, G. Gold-Bouchot, A. Whitesell and K. McFadden (2023). "Production of ice-nucleating particles (INPs) by fast-growing phytoplankton." *Atmospheric Chemistry and Physics* **23**(19): 12707-12729.

Matthews, B. H., Alsante, A. N., & Brooks, S. D. (2023). Pollen Emissions of Subpollen Particles and Ice Nucleating Particles. *ACS Earth and Space Chemistry*, 7(6), 1207-1218. doi:10.1021/acsearthspacechem.3c00014

Zhang, Y., T. Subba, B. H. Matthews, C. Pettersen, S. D. Brooks and A. L. Steiner (2024). "Effects of Pollen on Hydrometeors and Precipitation in a Convective System." J*ournal of Geophysical Research-Atmospheres* 129(6).

Sub-Arctic fungal spores as atmospheric ice-nucleating particles

JÜRGEN GRATZL[1], ALEXANDER BÖHMLÄNDER[2], OTTMAR MÖHLER[2], EIJA ASMI[3], SANNA PÄTSI[4], ANNIKA SAARTO[4], CLARA-E. POGNER[5], MARKUS GORFER[5], DAVID BRUS[3], KONSTANTINOS MATTHAIOS DOULGERIS[3], DOMINIK STOLZENBURG[1], FLORIAN WIELAND[1], HINRICH GROTHE[1]

[1]*Institute of Materials Chemistry, TU Wien, Vienna, 1060, Austria*
[2]*Institute of Meteorology and Climate Research, Atmospheric Aerosol Research (IMK-AAF), Karlsruhe Institute of Technology (KIT), Karlsruhe, 76021, Germany*
[3]*Finnish Meteorological Institute, Atmospheric Composition Research, Helsinki, Fl-00101, Finland*
[4]*Biodiversity Unit, University of Turku, Turku, Finland*
[5]*Center for Health and Bioresources, AIT Austrian Institute of Technology GmbH, Tulln, 3430, Austria*

Keywords: Bioaerosols, Fluorescent aerosols, High temperature INPs, Aerobiology, Boreal Forest

INTRODUCTION

Bioaerosols such as fungal spores, bacteria, and pollen grains represent an important fraction of total aerosol particles, due to their high efficiency as ice-nucleating particles (INPs). While bioaerosols have been identified as key contributors to high-temperature INPs in northern latitudes (Pereira Freitas *et al*., 2023; Šantl Temkiv *et al.*, 2019), pinpointing the exact types of bioaerosols involved in atmospheric ice formation remains challenging. In this study, we investigate whether bioaerosols influence the atmospheric INP population in the Finnish sub-Arctic and identify which types of bioaerosols act as INPs.

METHODS

This study was conducted at the Sammaltunturi station, part of the Pallas Atmosphere-Ecosystem Supersite in the Finnish sub-Arctic, at the northern edge of the boreal forest. We combined measurements of highly fluorescent aerosol particles (HFAPs) using the Wideband Integrated Bioaerosol Sensor (WIBS 5/NEO, Gratzl *et al.*, 2025) with direct fungal spore counts from a Hirst-type volumetric sampler (Hirst, 1952) and eDNA sequence analysis from filter samples. INPs were measured using the Ice Nucleation Spectrometer of the Karlsruhe Institute of Technology (INSEKT, Schneider *et al.*, 2021).

CONCLUSIONS

Our results reveal a positive correlation between a subset of HFAPs and INPs active over a wide temperature range. An exceptionally strong correlation (Pearson $r = 0.94$, $p < 0.001$) was observed for INPs active above -13.5 °C, suggesting that these HFAPs dominate the high-temperature INP population. A detailed analysis of WIBS data showed a strong seasonal pattern in HFAP concentrations, driven by snow cover and ambient temperature, with higher concentrations when the station was within the mixing layer, indicating locally emitted bioaerosols. A comparison of HFAPs with offline direct fungal spore counts and eDNA analysis confirmed the fungal nature of the bio-INPs. However, we could not pinpoint the exact genera or species contributing to INPs, as only 6 out of the 143 genera detected via DNA sequencing have been tested for ice nucleation activity (INA) so far, with most showing little to no INA.
Despite this uncertainty, our study represents a significant step in demonstrating that fungal spores, originating from the local biosphere, dominate the INP population active above -15 °C in the Finnish sub-Arctic.

ACKNOWLEDGEMENTS

This work was supported by ATMO-ACCESS under the ID ATMO-TNA-4-0000000069, by the FFG under the Project Lab on a Drone (888109) and by the Vienna Science and Technology Fund (WWTF) through project VRG22-003.

REFERENCES

Gratzl, J., Brus, D., Doulgeris, K., Böhmländer, A., Möhler, O., and Grothe, H. (2025). Fluorescent aerosol particles in the Finnish sub-Arctic during the Pallas Cloud Experiment 2022 campaign, *Earth System Science Data Discussions*, 2025, 1–20.

Hirst, J. M. (1952) An automatic volumetric spore trap, *Ann Appl Biol*, 39, 257–265.

Pereira Freitas, G., Adachi, K., Conen, F., Heslin-Rees, D., Krejci, R., Tobo, Y., Yttri, K. E., and Zieger, P. (2023), Regionally sourced bioaerosols drive high-temperature ice nucleating particles in the Arctic, *Nat Commun*, 14, 5997.

Šantl Temkiv, T., Lange, R., Beddows, D., Rauter, U., Pilgaard, S., Dall'Osto, M., Gunde-Cimerman, N., Massling, A., and Wex, H. (2019). Biogenic Sources of Ice Nucleating Particles at the High Arctic Site Villum Research Station, *Environ Sci Technol*, 53, 10 580–10 590,

Schneider, J., Höhler, K., Heikkilä, P., Keskinen, J., Bertozzi, B., Bogert, P., Schorr, T., Umo, N. S., Vogel, F., Brasseur, Z., Wu, Y., Hakala, S., Duplissy, J., Moisseev, D., Kulmala, M., Adams, M. P., Murray, B. J., Korhonen, K., Hao, L., Thomson, E. S., Castarède, D., Leisner, T., Petäjä, T., and Möhler, O. (2021). The seasonal cycle of ice-nucleating particles linked to the abundance of biogenic aerosol in boreal forests, *Atmos Chem Phys*, 21, 3899–3918.

ROLE OF ISOPRENE-DERIVED SECONDARY ORGANIC AEROSOLS IN THE GLACIATION OF DEEP CONVECTIVE CLOUDS

MILIN KANIYODICAL SEBASTIAN[1], ROBERT WAGNER[1], ALEXEI KISELEV[1], HARALD SAATHOFF[1], YANXIA LI[1], KRISTINA HOEHLER[1], NSIKANABASI SILAS UMO[1], OTTMAR MOEHLER[1]

1 *Institute of Meteorology and Climate Research - Atmospheric Aerosol Research, Karlsruhe Institute of Technology, Karlsruhe, Germany*

Keywords: Ice nucleation, Isoprene, Cloud-processing, Morphology.

INTRODUCTION

Ice clouds have a global mean coverage of about 30% and can reach a maximum of 70% over the tropics. (Nazaryan et al., 2008), with ice-nucleating particles (INPs) playing a crucial role in their formation. While organic aerosols are generally considered to be less active INPs and often treated as ice-inactive in cloud models (Kasparoglu et al., 2022), their ice nucleation ability (INA) can be influenced by changes in viscosity and morphology. Atmospheric freeze-drying processes can lead to porous particle structures, which in turn impact cloud microphysics (Wagner et al., 2012, Adler et al., 2013, Marcolli et al., 2014, Wagner et al., 2017, Wagner et al., 2024). Recent airborne observations (Curtius et al., 2024), supported by chamber studies (Shen et al., 2024), indicate that isoprene, a biogenic volatile organic compound previously thought to have a negligible role in new particle formation, enhances aerosol concentrations over tropical rainforests. Given its abundance and the strong convective activity in the tropics, understanding how these aerosols are processed in deep convective clouds is critical, particularly regarding their ice nucleation potential.
To investigate this, we utilized the Aerosol Interaction and Dynamics in the Atmosphere (AIDA) chamber for aerosol-cloud processing studies of isoprene-derived secondary organic aerosols (SOA) particles via expansion cooling experiments. The INA of pristine and ice-cloud processed SOA particles was analyzed using the mobile Ice Nucleation Instrument of the Karlsruhe Institute of Technology (mINKA) (Bertozzi, 2021), which is a Continuous Flow Diffusion Chamber (CFDC). Changes in particle morphology upon cloud-processing were evidenced by in-situ light scattering measurements and Environmental Scanning Electron Microscope (ESEM) images of the particles sampled from the AIDA cloud chamber. The chemical composition of the particles was measured with an Aerosol Mass Spectrometer (HR-ToF-AMS, Aerodyne).

EXPERIMENTAL PROCEDURE

Mixtures of isoprene and ozone were introduced into a 4 m^3-sized aerosol preparation chamber (APC) to form freshly nucleated organic aerosol particles at room temperature and under dark conditions. After the particles had grown to a mobility diameter of about 270 nm, they were transferred to the 84 m^3 AIDA chamber, which is located in a thermal housing maintained at cold temperatures. Experiments were started at stable AIDA temperatures of 227 K, 235 K, and 243 K. The pristine aerosol particles were sampled by mINKA via a cooled sampling line to study their INA at cirrus temperatures of 218 K and 222 K. After fully characterizing the unprocessed SOA particles, an AIDA expansion experiment was conducted, during which the chamber pressure was reduced with the help of mechanical pumps located beneath the chamber. The decrease in the gas temperature during expansion led to an increase in the ice saturation ratio, resulting in the formation of supercooled liquid droplets/ice clouds depending on the AIDA temperature. The cloud-processing experiment that started at 243 K mimics the “atmospheric freeze-drying” process described by Adler et al. (2013), as it first led to the formation of supercooled cloud droplets, which then froze to ice crystals below the homogeneous freezing temperature of about 235 K. The expansion cooling experiments that started at 235 K and 227 K directly led to the formation of ice crystals. The ice clouds that were formed during the expansion experiment were then sublimated by refilling the AIDA chamber with dry synthetic air while the AIDA warmed to the initial starting temperatures. The cloud-processed SOA particles were then again sampled by mINKA to investigate whether the INA had changed during the simulated cycle of a deep convective cloud process. In a second processing step, the relative humidity in the AIDA chamber was

again temporarily increased by moderate expansion cooling, leading to a temporary decrease in particle viscosity and an associated re-collapse of porous structures to more compact particle morphologies. The INA of the re-compacted particles was analyzed in a third series of mINKA measurements.

RESULTS AND CONCLUSIONS

Figure 1 shows the activated fraction of SOA particles from the AIDA experiment that started at 243K. Pristine isoprene-derived SOA particles nucleate ice at high ice saturation ratios at or above the homogeneous freezing threshold for aqueous solution droplets (red line in Figure 1). Even though small, a consistent improvement is observed for the INA of cloud-processed aerosol particles at all AIDA temperatures investigated in this study. For the cloud-processing experiment that started at 243 K, a clear morphological change of the aerosol particles was seen in the ESEM images, i.e. a transition from compact particle morphologies for the unprocessed particles to porous, fluffy structures after the atmospheric freeze-drying. The degree of porosity, however, was less than in similar experiments conducted with alpha-pinene derived SOA particles (Wagner et al., 2024). The higher surface area of the freeze-dried particles could explain the increase in the INA (the green lines in Figure 1), together with the presence of pores that could mediate ice formation via the two-step pore condensation and freezing mechanism (Marcolli, 2014). In line with this explanation, the INA again slightly decreased after the re-compaction step (represented by the blue lines in Figure 1). The improved INA in the experiments started at 235 and 227 K, where we did not detect a change in particle morphology, might be explained by a "memory" or pre-activation effect of the preceding ice nucleation event.

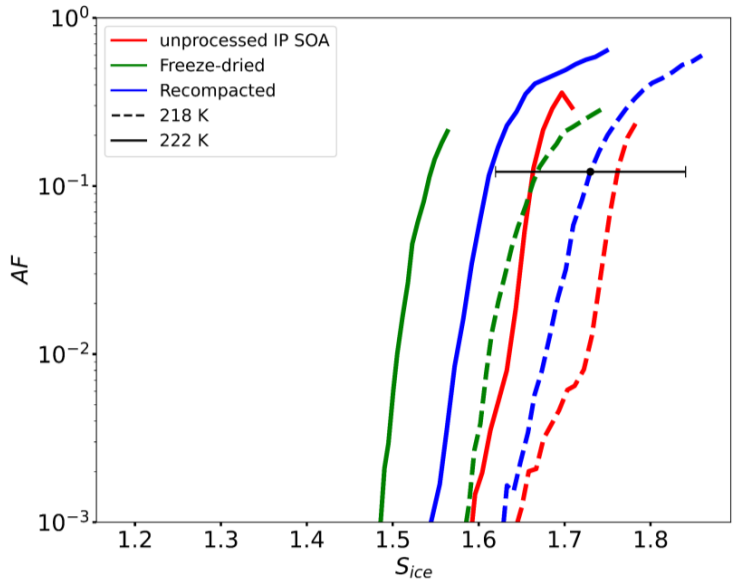


Figure 1. Ice activation spectra from mINKA measurements at 218 and 222 K during the three characterization periods of the AIDA experiments that started at 243 K. The activated fraction (AF) is shown as a function of saturation ratio with respect to ice (S_{ice}). Red: unprocessed isoprene-derived SOA particles, green: freeze-dried particles, blue: recompacted particles. The solid lines correspond to mINKA measurements at 222 K and the dashed lines corresponds to the temperature of 218 K. The black horizontal line represents the error bar.

This contribution aims to highlight the role of isoprene-derived SOA in the formation and glaciation of deep convective clouds, which significantly influence weather phenomena, particularly in the tropics. Our results indicate that cloud processing may alter the morphology and INA of isoprene-derived SOA. These findings

provide new insights into the role of isoprene-derived SOA in atmospheric ice cloud formation and highlight the need for improved representation of the most abundant non-methane hydrocarbon emitted into the atmosphere in cloud models.

ACKNOWLEDGEMENTS

This work was supported by European Union's Horizon 2020 research and innovation programme CLOUD-DOC under the Marie Skłodowska-Curie grant agreement No. 101073026.

REFERENCES

Adler, G., Koop, T., Haspel, C et al. (2013). Formation of highly porous aerosol particles by atmospheric freeze-drying in ice clouds. Proceedings of the National Academy of Sciences of the United States of America, 110(51), 20414–20419.

Bertozzi, B. (2021). Ice nucleation ability of secondary aerosol particles at cirrus cloud conditions. (PhD). Karlsruhe Institute of Technology, Germany

Curtius, J, Heinritzi, M., Beck, Lisa J. et al. (2024). Isoprene nitrates drive new particle formation in Amazon's upper troposphere. Nature, 636(8041):124–130, December 2024.

H. Nazaryan, M.P. McCormick, W.P. Menzel (2008). Global characterization of cirrus clouds using CALIPSO data. J. Geophys. Res. Atmos., 113 (D16)

Kasparoglu, S., Perkins, R., Ziemann et al. (2022). Experimental determination of the relationship between organic aerosol viscosity and ice nucleation at upper free tropospheric conditions. Journal of Geophysical Research:Atmospheres, 127(16), e2021JD036296.

Marcolli, C. (2014). Deposition nucleation viewed as homogeneous or immersion freezing in pores and Cavities. Atmospheric Chemistry and Physics, 14(4), 2071–2104.

Shen, J., Russell, D. M., DeVivo, J et al. (2024). New particle formation from isoprene under upper-tropospheric conditions. Nature, 636(8041):115–123.

Wagner, R., Möhler, O., Saathoff, H., Schnaiter, M et al. (2012). Ice cloud processing of ultra viscous/glassy aerosol particles leads to enhanced ice nucleation ability. Atmospheric Chemistry and Physics, 12(18), 8589–8610.

Wagner, R., Höhler, K., Huang et al. (2017). Heterogeneous ice nucleation of α-Pinene SOA particles before and after ice cloud processing. Journal of Geophysical Research-Atmospheres, 122(9), 4924–4943.

Wagner, R., Hu, Y., Bogert, P et al. (2024). How porosity influences the heterogeneous ice nucleation ability of secondary organic aerosol particles. Journal of Geophysical Research: Atmospheres, 129, e2024JD041576.

COMPETITION BETWEEN DYNAMIC WETTING AND FREEZING OF SUPERCOOLED WATER DROPLETS UPON CONTACT WITH ICE OR ICE-NUCLEATING SURFACE

ALEXEI A. KISELEV[1], JOHANNA S. SEIDEL[1], and SUSAN HARTMANN[2]

1. Institute of Meteorology and Climate Research, Karlsruhe Institute of Technology, Karlsruhe, Germany.
2. Department of Atmospheric Microphysics, Leibniz Institute for Tropospheric Research, Leipzig, Germany

Keywords: heterogeneous ice nucleation, dynamic wetting, supercooled water droplets, secondary ice production.

INTRODUCTION

Freezing of supercooled water in contact with a foreign substrate can be facilitated by the presence of special surface sites assisting the formation of a critical ice embryo. Under stationary conditions (constant temperature or slow cooling ramp), the probability of freezing can be described by the Classical Nucleation Theory (CNT) with account for the properties of such sites and stochastic nature of nucleation. Recent progress in atomistic modeling and experimental research allowed for a significant improvement in the quantitative description of heterogeneous ice nucleation.

The freezing mechanism becomes more complicated under non-equilibrium conditions, for example, if a supercooled droplet experiences a collision with an ice nucleating particle or ice surface (e.g., on collision with a graupel). Depending on the wetting behavior of the substrate and temperature, a droplet requires some time to achieve a stable equilibrium on the substrate. During this transition, freezing kinetics can be influenced by changing properties of the water-substrate interface.

In this contribution, we report experimental measurements of supercooled droplets freezing upon contact with the precooled surfaces of freshly cleaved feldspar, graphite, silicon, and ice. We explore the competition between dynamic wetting and freezing by recording the freezing-upon-collision events with a high-speed video camera under well-defined condition of an electrodynamic trap and in the setup simulating riming-splintering ice multiplication (Seidel et al., 2024). We report measurements of the average time needed to initiate freezing for different types of IN particles and substrates. Surprisingly, this characteristic time delay does not correlate with the efficacy of the ice nucleating substrate, nor does it show a strong correlation with the contact area of water-substrate interface. Finally, we discuss possible mechanisms of such freezing behavior and potential implications for the future ice nucleation research.

METHODS

Our setup is based on a electrodynamic balance of hyperbolic type connected to a thermostat to control the temperature between 0°C and -40°C (Hoffmann et al., 2013). Droplets with an initial diameter of approximately 100 µm were generated using a piezoelectric drop-on-demand dispenser (GeSIM SPIP). The droplets were inductively charged to less than -1 pC by applying a positive voltage to a ring electrode placed in front of the dispenser tip. A single droplet was levitated in the center of the trap for a time required to achieve the temperature of the trap (generally less than 1 min) (Kleinheins et al., 2021). A substrate (cleaved alkali feldspar, exfoliated graphite, or a silicon wafer) connected to a non-conducting rod was inserted into the trap through the central opening in the upper electrode and left there for several minutes to achieve the thermal equilibrium with the trap. The supercooled droplet was brought in contact with the substrate by applying a -1 kV square voltage pulse to the lower electrode for a duration of 20 ms. This pulse accelerates the droplet towards substrate with velocity of approximately 1 m/s.

Spreading and freezing of small droplets (in the range between 2 µm and 40 µm in diameter) has been studied in the Ice Droplets splintEring on FreezIng eXperiment (IDEFIX) setup, which has been developed to study riming under well-controlled atmospheric conditions (Seidel et al., 2024). In IDEFIX,

riming is simulated by exposing a fixed large ice particle (1mm in diameter) to a stream of supercooled water droplets carried by an airflow. The rimer is placed on the intersection of two carbon fibers with a thickness of about 6 µm. The airflow velocity corresponds to the terminal fall velocity of a graupel grain of 1 mm in diameter, which is approximately 1m/s. IDEFIX provides thermodynamic, and flow conditions and allows for the visualization of the riming process, measurement of the graupel surface temperature, and quantification of the production rate of the SI particles. The IDEFIX experiments were carried out in the temperature range between -7°C and -10°C, the temperature range where Hallett-Mossop ice multiplication mechanism was reported to be most active (Mossop, 1976, 1985).

The collision and freezing events in both types of experiments were recorded with the high-speed video camera Phantom VEO 710 (HS Vision) with the frame rate between 20000 and 50000 frames per second. The temperature of the rimer in IDEFIX was measured with the IR thermography system (ImageIR 7340, InfraTec GmbH).

RESULTS AND DISCUSSION

Upon collision with ice surface, supercooled water droplets freeze almost immediately, and the delay time is only limited by our ability to identify the appearance of ice in water (figure 1). This time does not depend on the temperature in the range between -30°C and -15°C. and is n the order of 100 µs. At lower temperature (below -20°C) the spread of water droplets on ice surface is arrested by freezing, so that the initial contact angle is preserved. At higher temperature, the spreading of the supercooled droplet is faster than freezing, so that the droplet spreads to a hemispherical shape before freezing.

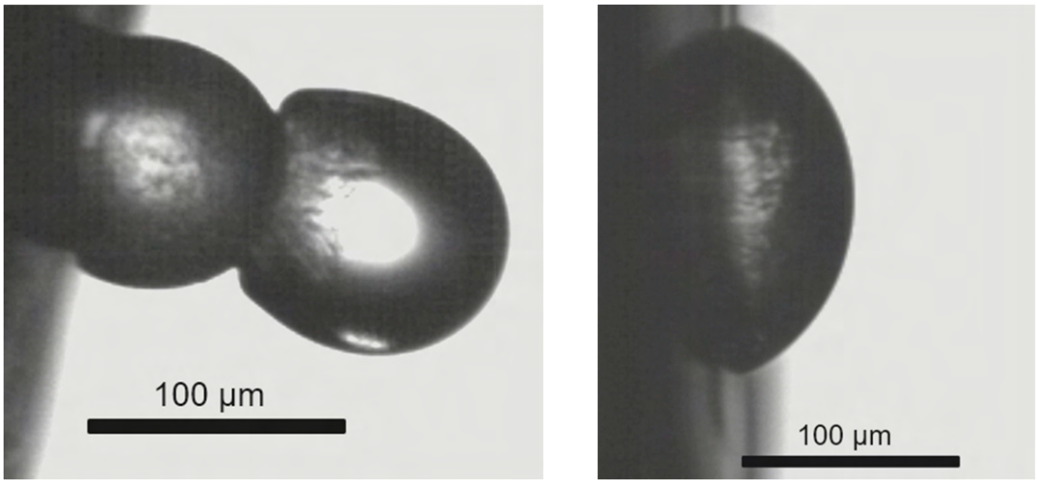


Figure 1. *Droplet freezing upon collision with ice (left) and feldspar mineral surface (right) at -25°C.*

On a mineral substrate (alkali feldspar), freezing initiation is always delayed by some time, during which the droplet spreads to achieve an equilibrium shape defined by water-substrate interface energy (Figure 1, right panel, and Figure 2). For all droplets investigated in this study, freezing was never observed before the droplet has achieved its equilibrium shape. The delay time becomes longer with higher temperature, varying from roughly 2 ms -30°C to almost 1 s at -15°C. Above this temperature droplet evaporation hinders a reliable observation of freezing event.

Smaller droplets colliding on ice surface show different behavior. Upon collision, a droplet starts spreading to assume the equilibrium shape determined by the surface energy relationship between the ice, water, and gas phases. However, the spreading is counteracted by freezing, which is also initiated at the

moment of contact. Contrary to ice growth rate, the rate of spreading does not depend on the temperature in the range of between −3 and −8 °C; the final shape of an accreted droplet is therefore defined by the time required to arrest the spreading by freezing. The HSV records taken at −10 °C in Fig. 3 show spreading and freezing of accreted droplet. Contrary to the previous assumption (Choularton et al., 1978), droplets do not freeze in spherical shape so that the mechanism of ice multiplication on riming remains unclear (Seidel et al., 2024).

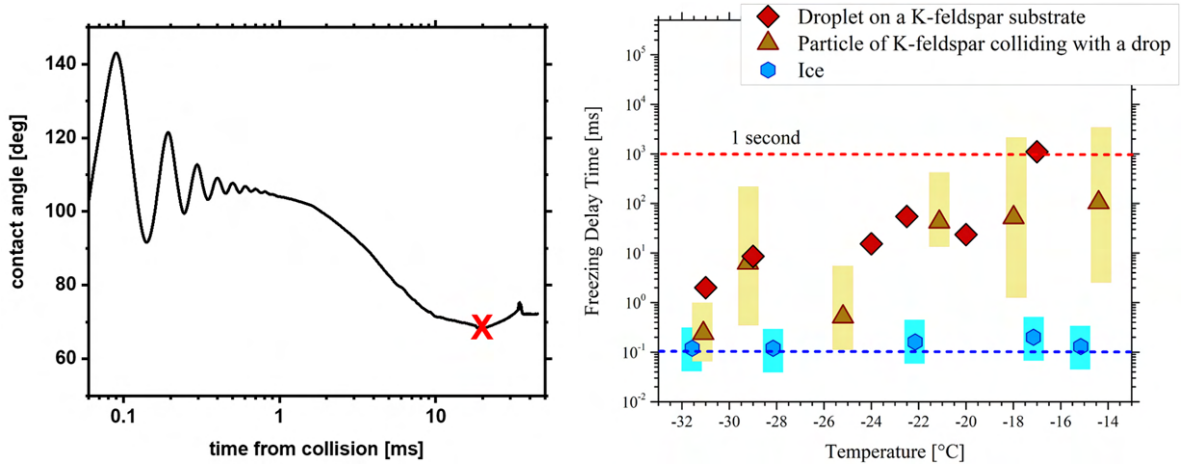


Figure 2. *Left: time evolution of contact angle after collision with feldspar substrate. The red cross indicates the moment of freezing. Right: freezing delay time between initial contact and freezing on feldspar mineral surface measured at different temperatures. Color bars indicate 50% quantiles of data distribution.*

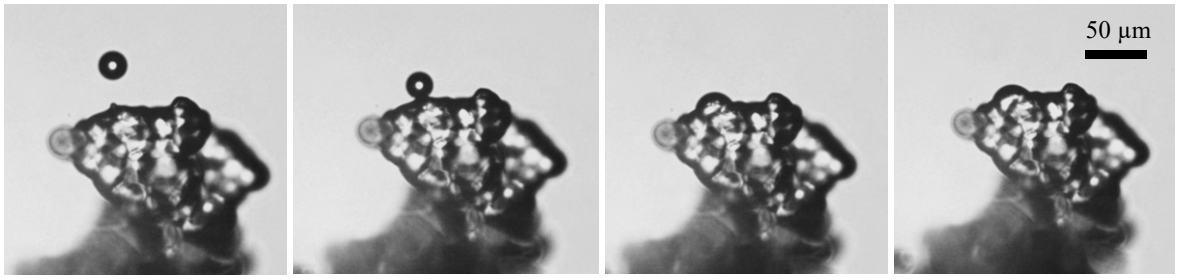


Figure 3. *20 µm droplet spreading upon collision with ice at -10°C. Time delay between frames is 20 µs.*

In conclusion, we do not observe freezing initiated immediately upon contact with ice nucleating substrate (except for ice); and the delay time of freezing initiation does not seem to correlate with the ice nucleating efficiency of the substrate or contact area between supercooled water and substrate. The delay time of freezing initiation was found to be similar for feldspar particles colliding with the droplet and droplets colliding with a flat surface of feldspar, allowing us to conclude the freezing delay is not associated with stochastic nature of freezing (induction time). Most importantly, freezing does not seem to be associated with moving interface line. These findings highlight the gaps in our understanding of heterogeneous nucleation under non-equilibrium conditions and call for further studies.

ACKNOWLEDGEMENTS

This research has been supported by the German Research Foundation (grant nos. HA 8322/1-1 and KI 1997/1-1).

REFERENCES

Choularton, T. W., Latham, J., and Mason, B. J. (1978): *A possible mechanism of ice splinter production during riming*, Nature, 274, 791-792, https://doi.org/10.1038/274791a0.

Hoffmann, N., Duft, D., Kiselev, A., and Leisner, T. (2013): *Contact freezing efficiency of mineral dust aerosols studied in an electrodynamic balance: quantitative size and temperature dependence for illite particles,* Faraday Discussions, 165, 383-390, https://doi.org/10.1039/c3fd00033h.

Kleinheins, J., Kiselev, A., Keinert, A., Kind, M., and Leisner, T. (2021): *Thermal Imaging of Freezing Drizzle Droplets: Pressure Release Events as a Source of Secondary Ice Particles*, Journal of the Atmospheric Sciences, 78, 1703-1713, https://doi.org/10.1175/JAS-D-20-0323.1.

Mossop, S. C. (1976): *Production of secondary ice particles during the growth of graupel by riming*, Q. J. R. Meteorol. Soc., 102, 45-57, https://doi.org/10.1002/qj.49710243104.

Mossop, S. C.:(1985) *The Origin and Concentration of Ice Crystals in Clouds*, Bulletin Am. Meteorol. Soc., 66, 264–273, https://doi.org/10.1175/1520-0477(1985)066<0264:TOACOI>2.0.CO;2:

Seidel, J. S., Kiselev, A. A., Keinert, A., Stratmann, F., Leisner, T., and Hartmann, S. (2024): S*econdary ice production – no evidence of efficient rime-splintering mechanism*, Atmos. Chem. Phys., 24, 5247-5263, https://doi.org/10.5194/acp-24-5247-2024.

THE ROLE OF ORGANIC MATTER FOR ICE NUCLEATION ON MINERAL AND SOIL DUSTS

THOMAS KRAUTWIG & CLAUDIA MARCOLLI

Institute for Atmospheric and Climate Science, ETH Zurich, Zurich, Switzerland.

Keywords: ICE NUCLEATION, ICE NUCLEATING PARTICLES, SOIL DUST, CLAY MINERALS, ORGANIC MATTER, BIOGENIC MACROMOLECULES.

INTRODUCTION

Ice-nucleating particles (INPs) are a tiny fraction of atmospheric aerosols but play a key role in cloud processes by initiating the ice phase and forming precipitation (Pruppacher & Klett, 1997). Mineral dusts are probably the most important and best established type of INPs, but there are still uncertainties concerning their ability to have ice crystals formed on them. Research shows that ice nucleation (IN) on mineral dust occurs on rare sites that do not represent the average mineral surface. Besides the mineral type, different factors influence the IN ability of dusts, including particle size, interaction with solutes and water, adsorption of organic molecules, and freezing mode. In general, soil dusts, which include an organic, biogenic share, nucleate ice at higher temperatures than pure mineral dusts (Kanji et al., 2017). The aim of this study is to identify factors that influence the IN ability of organic matter adsorbed on mineral dust.

METHODS

A top-down approach is applied where collected soil samples from Chile are fractionated and analyzed (Wasner et al., 2024). To gain insights into the IN ability, immersion freezing experiments are conducted with the Super DRoplet Ice Nuclei Counter Zurich (S-DRINCZ) to obtain IN active site densities over a large temperature range. S-DRINCZ replicates DRINCZ (David et al., 2019) yet offers the option of parallel cooling several well plates. In short, the samples – suspended in water – are dispensed into a well plate and gradually cooled within an ethanol-cooled chiller while monitoring freezing events optically with a camera (Figure 1). The fraction of frozen droplets per temperature step is used to derive the INP concentration with the knowledge of the dry sample mass in each well.

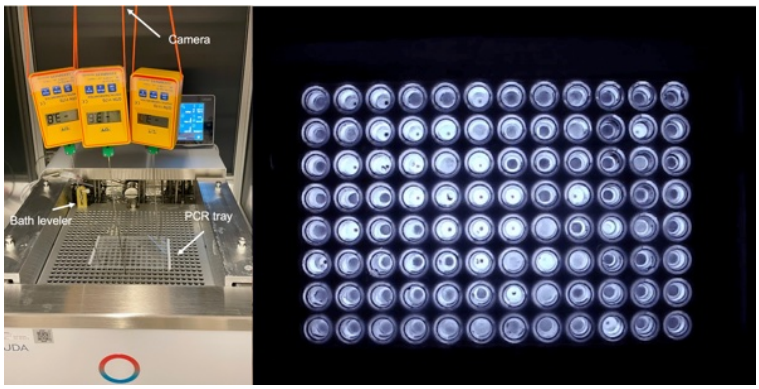
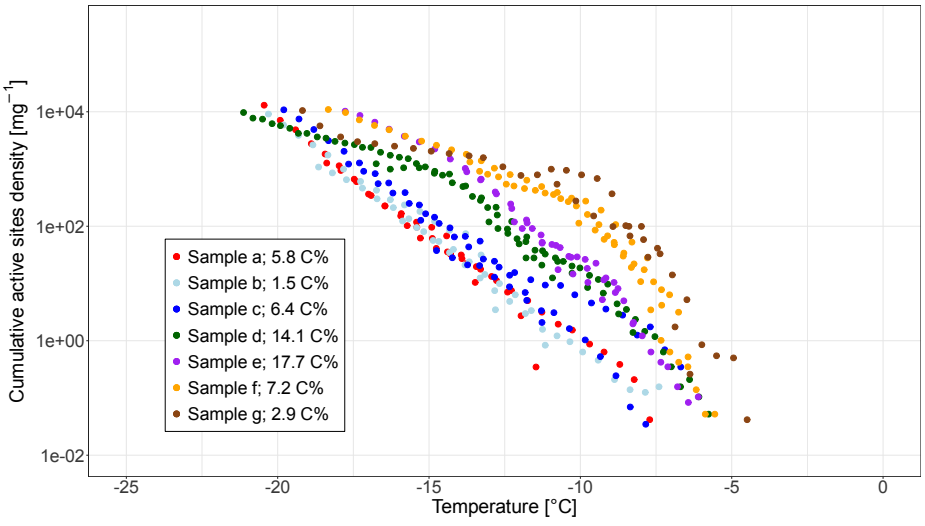


Figure 1. Left image: Setup of S-DRINCZ. Right image: Light transmission during an experiment with frozen (dark) and unfrozen (transparent) droplets.

To trace back the IN active components, different analytical techniques, such as X-ray diffraction (XRD) and thermogravimetric analysis with coupled mass spectrometry (TG-MS) are used. To complement these, nuclear magnetic resonance spectroscopy (NMR) will also be used to get insights into the functional group composition of the organic matter. XRD analyzes the diffraction patterns of X-rays interacting with a sample and characteristic diffraction peaks are used to identify specific minerals. TG-MS tracks mass loss as a function of temperature, with the mass spectrometer providing insights into thermal decomposition and organic content. Functional groups of the organic matter can be inferred from NMR spectroscopy to obtain information about the composition of biogenic macromolecules, such as proteins, carbohydrates and others.
In total, the sieved clay and silt fraction (>63µm) of seven different soil dust samples with organic shares between 1 and 18 %were selected. First, the freezing of the total sample was measured with S-DRINCZ. Second the samples were treated with hydrogen peroxide (H_2O_2) to remove all organic matter (Hamzehpour et al., 2022). Third, the samples were heated in wet solution at 95°C for 30 min to denature heat-labile protein compounds and deteriorate their IN ability (Daily et al., 2022).

RESULTS AND CONCLUSIONS

Figure 2 (top) shows the cumulative ice nucleation active site (INAS) density as a function of temperature for the seven investigated samples with freezing onsets between -4.5 and -7.8°C. It can be seen that samples with higher organic carbon content (samples d, e and f) exhibit higher INAS densities than the samples a, b, and c with a lower organic carbon content. Yet, the sample with the highest INAS density for T > -12°C has one of the lowest organic contents (sample g).
To further assess the contribution of biogenic matter to the observed IN ability, H_2O_2 and heat treatments have been applied to the samples. In Figure 2 (bottom) the results for sample d are shown as an example. This sample displays a decrease in IN ability over the whole investigated temperature range due to the H_2O_2 treatment by almost an order of magnitude at -14°C in terms of INAS density. Furthermore, heating in wet solution decreases its INAS density in the higher temperature range suggesting the relevance of proteins to its IN ability (Daily et al., 2022). These findings will be further related to composition with the help of XRD, TG-MS and NMR measurements and correlated with the C, N, and C:N content.



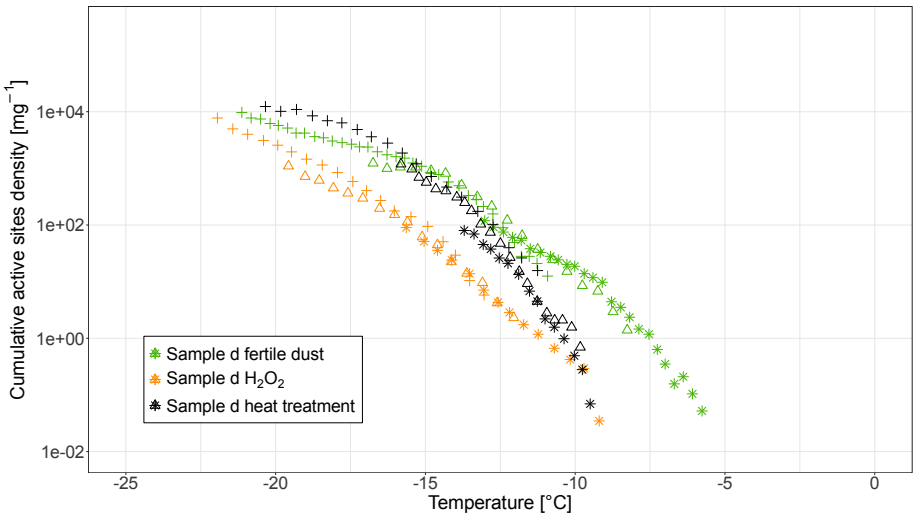


Figure 2. Top panel: INAS density as a function of temperature for the seven investigated samples (silt and clay fraction). Bottom panel: INAS density of sample d without treatment (green), H_2O_2 treated (dark orange) and heated in suspension (black).

ACKNOWLEDGEMENTS

This work is supported by the Swiss National Science Foundation (SNSF) with project number 214909.

REFERENCES

Daily, M. I., Tarn, M. D., Whale, T. F., and Murray, B. J. (2022). An evaluation of the heat test for the ice-nucleating ability of minerals and biological material. Atmos. Meas. Tech., 15, 2635–2665.

David, R. O., Cascajo-Castresana, M., Brennan, K. P., Rösch, M., Els, N., Werz, J., Weichlinger, V., Boynton, L. S., Bogler, S., Borduas-Dedekind, N., Marcolli, C., and Kanji, Z. A. (2019). Development of the DRoplet Ice Nuclei Counter Zurich (DRINCZ): validation and application to field-collected snow samples, Atmos. Meas. Tech., 12, 6865–6888.

Hamzehpour, N., Marcolli, C., Klumpp, K., Thöny, D., and Peter, T. (2022). The Urmia playa as a source of airborne dust and ice-nucleating particles – Part 2: Unraveling the relationship between soil dust composition and ice nucleation activity, Atmos. Chem. Phys., 22, 14931–14956.

Kanji, Z. A., Ladino, L. A., Wex, H., Boose, Y., Burkert-Kohn, M., Cziczo, D. J., Krämer, M. (2017). Overview of Ice Nucleating Particles, Meteorological Monographs, American Meteorological Society, 58, 1.1-1.33.

Pruppacher, H. R., & Klett, J. D. (2010). Microphysics of Clouds and Precipitation. Atmospheric and Oceanographic Sciences Library, Volume 18. Springer, Dordrecht.

Wasner, D., Mainka, M., Sommerauer, L., Haaf, D., Griepentrog, M., Berhe, A. A., & Doetterl, S. (2024). The role of climate, mineralogy and stable aggregates for soil organic carbon dynamics along a geoclimatic gradient. Global Biogeochemical Cycles, 38(7), e2023GB007934.

DEPOSITION ICE NUCLEATION VIA FREEZING OF ADSORBED WATER

A. LAAKSONEN[1,2], G. ROUDSARI[1], A. A PIEDEHIERRO[1] and A. WELTI[2]

[1]*Finnish Meteorological Institute. Helsinki, Finland.*

[2]*Department of Technical Physics, University of Eastern Finland, Kuopio, Finland.*

Keywords: Deposition ice nucleation, Freezing, Adsorption

INTRODUCTION

Heterogeneous vapor-liquid nucleation of water occurs when a sufficiently large number of water molecules come together at a surface, forming a cluster that does not decay but initiates condensation. In the classical view, deposition ice nucleation occurs analogously to vapor-liquid nucleation, with the difference that the water molecules form not only a cluster but a hexagonal crystal. The requirement of the crystalline structure of the cluster obviously greatly decreases the probability of nucleation, and it seems likely that an intermediate liquid phase would facilitate ice nucleation. In the pore condensation and freezing mechanism (Marcolli, 2014), the intermediate liquid phase is capillary condensed water. However, deposition ice nucleation occurs on different nonporous ice nuclei as well, suggesting that multilayer adsorbed water may in these cases act as the intermediate phase. Here we describe a theoretical framework to account for the homogeneous and heterogeneous freezing of adsorbed water films and droplets.

CONCLUSIONS

Water vapor adsorption is described using the FHH adsorption model, which is commonly used in studies of CCN activation of insoluble particles (Sorjamaa and Laaksonen, 2007), and the freezing rates are calculated using the classical nucleation theory. The theory predicts very diverse temperature dependencies of the critical supersaturation that are determined by the adsorption parameters and ice and water contact angles of the ice-nucleating materials, and the requirement that the adsorption layer thickness, or adsorbed droplet size, must be large enough to accommodate the critical ice cluster. The predictions agree remarkably well with laboratory experiments.

ACKNOWLEDGEMENTS

This work was supported by the Research Council of Finland Flagship ACCC (grant no. 337552) and MEDICEN project (grants no. 336557 and 345125).

REFERENCES

Marcolli, C. (2014) Deposition nucleation viewed as homogeneous or immersion freezing in pores and cavities, *Atmos. Chem. Phys*., **14**, 2071–2104.

Sorjamaa, R., and Laaksonen, A. (2007). The effect of H_2O adsorption on cloud drop activation of insoluble particles: a theoretical framework. *Atmos. Chem. Phys*. **7**, 6175–6180.

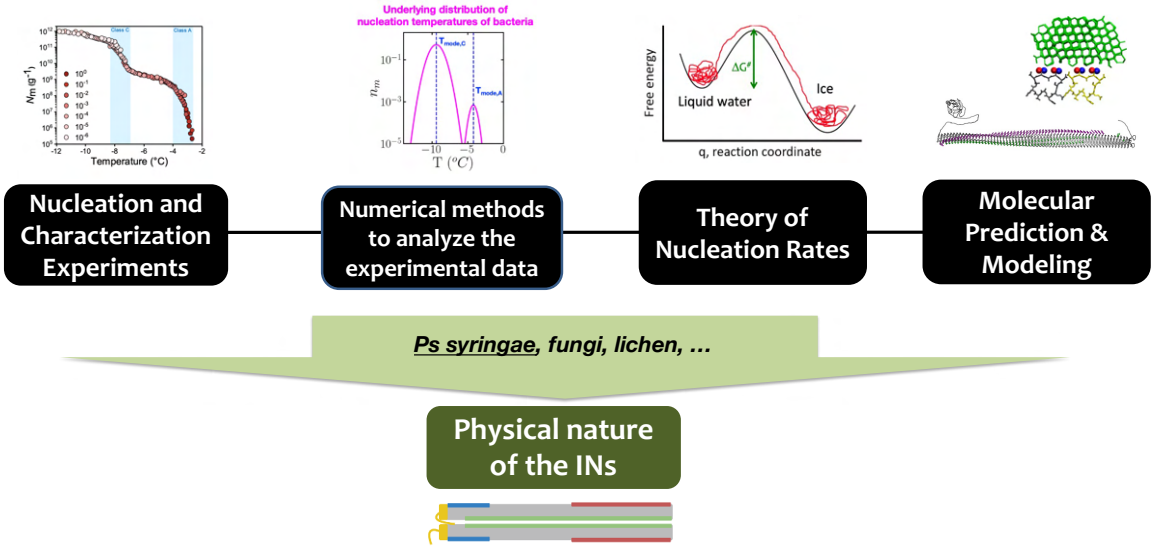
The Most Potent Snow Makers

Valeria Molinero
The University of Utah

Several species of bacteria, fungi, lichen, and insects have evolved proteins that are potent ice nucleants. Bacteria and fungi are aerosolized and uplifted to the clouds, where they contribute to cloud glaciation and precipitation. Indeed, bacteria are so powerful ice nucleants that are routinely used for the synthetic production of snow. Despite the importance of biological ice nucleation for the survival and thriving of organisms and atmospheric processes, little is known about sequence and/or structure of the ice nucleating proteins, the mechanisms by which they promote water crystallization, and what makes them so outstanding. This presentation will discuss our approach to bridge the results of laboratory experiments, theory, numerical and molecular simulations, and artificial intelligence to elucidate the mode of action of biological ice nucleants. Our studies reveal that nature uses a common strategy among organisms in several kingdoms, "E pluribus unum" (out of many, one), to nucleate ice at temperatures close to the 0°C by assembly of ice-nucleating proteins into large functional aggregates.

This work is supported by the MURI project "Unraveling the Mechanisms of Ice Nucleation and Anti-Icing Through an Integrated Multiscale Approach" in collaboration with the groups of Prof. Konrad Meister at Boise State University and Dr. Rajiv Berry at the Air Force Research Laboratory.

Abstract figure:



AEROSOL'S CCN ACTIVITY AND AEROSOL CHEMICAL COMPOSITION DURING FOG AND HAZE EVENTS IN NEW DELHI, INDIA

MRUNAL NAIK, AKASH VISPUTE, CHAITRALI SHINDE, SANDEEP WAGH, SACHIN D. GHUDE

Indian Institute of Tropical Meteorology, Pune 411008, India

Keywords: CCN activation, hygroscopicity, Aerosol composition, air quality.

INTRODUCTION

Delhi experiences severe aerosol loading in winter due to biomass burning, festival emissions, and stagnant meteorological conditions, leading to frequent haze and fog events. Cloud condensation nuclei (CCN) activation plays a crucial role in these transitions, governed by aerosol composition and supersaturation (SS). High aerosol loads during haze increase CCN concentrations but suppress efficient droplet growth due to competition for water vapor. This study provides insights into the mechanisms controlling haze-to-fog transitions in New Delhi, emphasizing the role of aerosol hygroscopicity, CCN activation, and atmospheric thermodynamics in urban air quality and climate.

METHODS

This study investigates the complex interactions between aerosol composition, cloud condensation nuclei (CCN) activation, and atmospheric thermodynamics, collectively regulating the transition between haze and fog episodes and influencing regional cloud microphysics at the India Meteorological Department (IMD) in Delhi, as part of the Winter Fog Experiment (WiFEX) conducted by IITM Pune during January 2024. The primary objective of this study is to investigate the variability in CCN concentrations, their size distribution, and the dominant aerosol sources contributing to CCN activation across different atmospheric conditions. By analyzing CCN properties, aerosol hygroscopicity, chemical composition, PM2.5 concentrations, meteorological parameters, and visibility, this study aims to enhance the understanding of fog dynamics, including the transition between haze and fog episodes and the role of aerosol composition in CCN activation efficiency.

Droplet Measurement Technologies (DMT; www.dropletmeasurement.com) has developed a novel CCN counter based on the design proposed by Roberts and Nenes (2005). This design generates supersaturation in an axisymmetric flow by applying a constant temperature gradient along the stream-wise direction, a concept also independently explored by Rogers and Squires (1977). Like earlier designs (e.g., Hoppel et al., 1979; Chuang et al., 2000), the instrument leverages the difference in heat and water vapor diffusivity to create supersaturation. The total concentration of CCN (N_{CCN}, #/cc) is obtained using equation (1), where 'n' refers to total number of bins 'n_{CCN}' is the number concentration of CCN (#/cc) within a bin. The 'n_{CCN}' is estimated from bin count, C (#/s), sample flow, F (CC/min) as shown in equation (2). Supersaturation depletion correction has been applied for the entire CCN data presented here following the method of Lathem and Nenes (2011).

$$N_{CCN} = \sum_1^n n_{CCN} \quad (1)$$

$$n_{CCN} = \frac{C + \text{Overflow}}{F} * 60 \quad (2)$$

Additionally, hygroscopicity parameter and aerosol chemical composition data were used from Humidified Tandem Differential Mobility Analyzer (HTDMA) and High-Resolution Time of Flight Aerosol Mass Spectrometer (HR-ToF-AMS), respectively. To classify fog, haze, and severe haze events, atmospheric visibility data were analysed throughout the campaign.

CONCLUSIONS

At increasing supersaturation (SS), CCN activation initially rises, as more aerosol particles reach their critical SS and form cloud droplets. However, beyond a threshold (SS ≈ 0.25%), droplet growth dominates over additional activation, leading to an increase in droplet size rather than a significant rise in CCN number concentration. This occurs because most available CCN have already activated, and excess water vapor preferentially condenses onto existing droplets rather than forming new ones. The competition for water vapor and the Kelvin effect further enhance the growth of larger droplets, suppressing the activation of smaller particles. research on CCN characteristics during the Indian summer monsoon observed high CCN concentrations (>1000 cm^{-3}) even at a low SS of 0.2%, highlighting the dominance of droplet growth over new CCN activation at higher SS (Jayachandran et al., 2020). These findings support the idea that while CCN activation initially increases with SS, droplet growth eventually takes precedence due to water vapor competition and the Kelvin effect.

Haze episodes demonstrated elevated concentrations of secondary inorganic aerosols (SIAs), notably nitrate (NO_3^-) and sulfate (SO_4^{2-}), suggesting active secondary aerosol production. Peak nitrate concentrations recorded during haze episodes align with prior findings on heterogeneous and aqueous-phase nitrate formation under conditions of high humidity (Wang et al., 2016; Xie et al., 2020). Ammonium (NH_4^+) concentrations were significantly higher during haze than fog episodes, playing a pivotal role in neutralizing acidic aerosol species. Organic aerosol (OA) composition showed notable differences between fog and haze events. Haze episodes were dominated by oxidized organic aerosols (OOA). Hydrocarbon-like organic aerosol (HOA) and biomass burning organic aerosol (BBOA) showed distinct episodic spikes during haze periods, indicative of primary emissions from vehicular exhaust and biomass combustion, recognized as critical air pollution sources in Delhi during winter (Pant et al., 2015). The elevated HOA and BBOA concentrations highlight significant primary emissions alongside secondary aerosol formation processes in haze episodes.

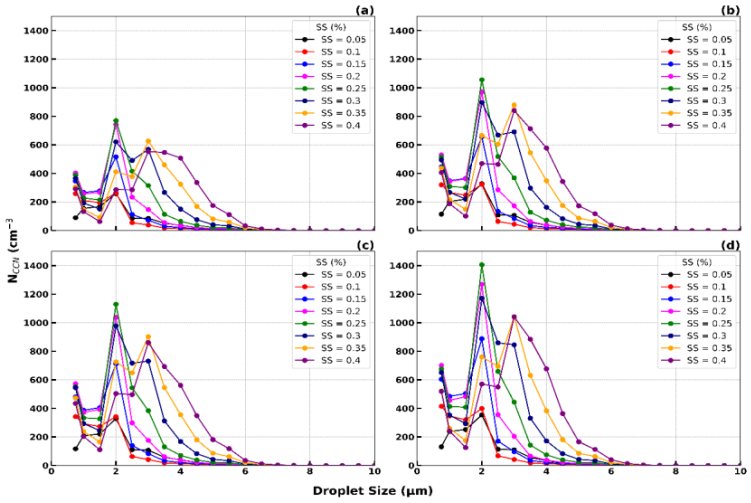


Figure 1. CCN spectra across three different atmospheric conditions (a) during clean period, (b) during Haze period, (c) during Shallow Fog period, (d) during Moderate Fog period.

ACKNOWLEDGEMENTS

I would like to extend my sincere gratitude to the Ministry of Earth Sciences (MoES) and the Director of the Indian Institute of Tropical Meteorology (IITM) for their invaluable support and resources.

REFERENCES

1. Roberts, G. C., & Nenes, A. (2005). A Continuous-Flow Streamwise Thermal-Gradient CCN Chamber for Atmospheric Measurements. *Aerosol Science and Technology*, *39*(3), 206–221. https://doi.org/10.1080/027868290913988
2. Rogers, C. F. (1977). *A New Device for Studies of Cloud Condensation Nuclei Active at Low Supersaturations* (Ph.D. dissertation). University of Nevada, Reno.
3. Hoppel, W. A., Twomey, S., & Wojciechowski, T. A. (1979). A segmented thermal diffusion chamber for continuous measurements of CN. *Journal of Aerosol Science, 10(4)*, 369–373. https://doi.org/10.1016/0021-8502(79)90031-4
4. Chuang, P. Y., Nenes, A., Smith, J. N., Flagan, R. C., & Seinfeld, J. H. (2000). Design of a CCN Instrument for Airborne Measurement. *Journal of Atmospheric and Oceanic Technology*, *17*(8), 1005-1019. https://doi.org/10.1175/1520-0426(2000)017<1005:DOACIF>2.0.CO;2
5. Lathem, T. L., and Nenes, A. (2011). Water Vapour Depletion in the DMT Continuous Flow CCN Chamber: Effect on Supersaturation and Droplet Growth. Aeros. Sci. Tech., 45(5):604–615. DOI: 10.1080/02786826.2010.551146
6. Jayachandran, V. N., Varghese, M., Murugavel, P., Todekar, K. S., Bankar, S. P., Malap, N., Dinesh, G., Safai, P. D., Rao, J., Konwar, M., Dixit, S., and Prabha, T. V.: Cloud condensation nuclei characteristics during the Indian summer monsoon over a rain-shadow region, Atmos. Chem. Phys., 20, 7307–7334, https://doi.org/10.5194/acp-20-7307-2020, 2020.
7. Wang, G., Zhang, R., Gomez, M. E., Yang, L., Zamora, M. L., Hu, M., ... & Molina, M. J. (2016). Persistent sulfate formation from London Fog to Chinese haze. *Proceedings of the National Academy of Sciences***,** 113(48), 13630-13635.
8. Xie, Y., Ding, A., Nie, W., Mao, H., Kerminen, V. M., Zheng, L., ... & Kulmala, M. (2020). Enhanced sulfate formation by nitrogen dioxide: Implications from in situ observations at the SORPES station. *Journal of Geophysical Research: Atmospheres*, 125(3), e2019JD031934.
9. Pant, P., Shukla, A., Kohl, S. D., Chow, J. C., Watson, J. G., & Harrison, R. M. (2015). Characterization of ambient PM2.5 at a pollution hotspot in New Delhi, India and inference of sources. *Atmospheric Environment*, 109, 178-189.

Comprehensive Characterization of the Seasonal Cycles of Ice Nucleating Particles in Complex Mountainous Terrain

Russell Perkins, Ruichen Zhou, Drew Juergensen, Kelton Ayars, Oren Dutton, Paul DeMott, Sonia Kreidenweis

Colorado State University

Ice nucleating particles (INPs) are a critical driver of cloud phase and precipitation but are often under-sampled in the atmosphere. In particular, the spatial variability in INP concentrations is poorly understood, especially in complex terrain environments, as is the balance between local and long-range sources. In order to close this gap, we have analyzed samples and data collected during the Surface Atmosphere Integrated Field Laboratory (SAIL) campaign that took place in the Rocky Mountains near Crested Butte, CO, from September 2021 to June 2023. The INP sample set consists of long-term collections across all seasons from the DOE ARM INP mentor program, as well as spatial dispersed ground site collections by Handix Scientific through their SAIL-NET program and vertically resolved samples collected by the ARM tethered balloon system (TBS). Our preliminary results from analysis of this dataset are: 1) INP concentrations and characteristics are largely regional in nature, despite the complex terrain, 2) Dust is the most prevalent INP source in this region, with spectra similar to those observed in mineral and arable soil dusts, 3) Increased INP concentrations associated with anthropogenic activities are observed, both from cloud seeding and local snowmaking activities, and can greatly perturb monthly average INP concentrations. We are developing parameterization products for INPs for incorporation into numerical models, and relatively simple parameterization methods appear promising so far. This data will be discussed in light of other recent field campaign measurements.

COMPARISON OF THE MEASURED CHEMICAL COMPOSITION OF LOW VOLATILITY ORGANIC COMPOUNDS FROM DIFFERENT AIRCRAFT FUELS LEADING TO NEW PARTICLE AND ICE NUCLEI FORMATION

C. RIGHI[1], T. ELOMAA[1], T. CHAN[1], F. GRAEFFE[1], L.L.J. QUÉLÉVER[1], T. PETÄJÄ[1], A. BERTHIER[2], L. GANEAU[2], I. K. ORTEGA[2], A. VANDESTOC[2], L. ARSICAUD[3], A.S. BADHE[3], C. RENARD[3], J.B. MAY-CARLE[4], N. SARNELA[1] and J. DUPLISSY[1]

[1]*Institute for Atmospheric and Earth System Research (INAR) / Physics, University of Helsinki, FI-00014, Helsinki, Finland*

[2]*Multi-physics for Energetics Department, ONERA Université Paris Saclay, F-91123, Palaiseau, France*

[3]*Airbus Operations SAS, Toulouse, France*

[4]*Safran Aircraft Engines, Rond-point René Ravaud, F-77550, Moissy-Cramayel, France*

Keywords: AIRCRAFT EMISSIONS, HYDROGEN ENGINE, CHEMICAL COMPOSITION, ICE NUCLEATION.

INTRODUCTION

Global aviation operations impact the climate through a combination of processes that lead to net surface warming. Alongside the emission of carbon dioxide (CO_2), key contributors include nitrogen oxides (NOx), water vapor, soot, and sulfur compounds, which are often referred to as non-CO_2 effects. The interactions of these non-CO_2 emissions can result in ice nucleation (IN) and contrail formation. Contrails are of particular concern, as they introduce significant uncertainty into the climate impact of aviation, especially due to their potential to form cirrus clouds, which influence the Earth's radiative balance (Lee *et al.*, 2021).
To mitigate non-CO_2 effects, the aviation industry is exploring various sustainable aviation fuels (SAFs), including hydrogen, which primarily produces water vapor upon combustion. However, the high temperatures involved in this process can still result in the formation of NOx, and aircraft engines – whether powered by hydrogen or conventional fuels – also release lubrication oil vapors. As a result, emissions from hydrogen engines can still influence contrail formation and their properties. In order to assess the climate impact of such emissions, a comprehensive study involving multiple instruments and approaches is required. Among these, understanding the chemical composition of direct aircraft emissions is important to study their role in new particle formation (NPF) and IN.

METHODS

The experimental setup for the study involved a comprehensive set of instruments aimed at characterizing the particle properties and chemical composition of aircraft emissions.
Aerosol generation was achieved using multiple systems, including a sulfate aerosol generator, a humidified air generator, and a combustion system designed to mimic the particle emissions from an aircraft engine (CAST). The aerosol emissions were then directed through a dilution chamber to mix the gases before entering the Potential Aerosol Mass Oxidation Flow Reactor (PAM-OFR), where they were exposed to high concentrations of oxidants to rapidly simulate atmospheric aging and facilitate secondary organic aerosol formation.

The detailed characterization of particle number and size distribution was achieved employing a Particle Size Magnifier (PSM), a Condensation Particle Counter (CPC) and a Scanning Mobility Particle Sizer (SMPS), while the ice nucleation capacity of the generated particles was assessed using the Portable Ice Nuclei Chamber 2 (PINCii). As for chemical composition analysis, an Aerosol Mass Spectrometer (AMS) and a Chemical Ionization Atmospheric Pressure interface Time-of-Flight (CI-APi-ToF) mass spectrometer were used.

The CI-APi-ToF (Figure 1) is a high-resolution mass spectrometer that integrates a specialized inlet for chemical ionization at ambient pressure with an atmospheric pressure interface time-of-flight mass spectrometer. The capabilities and features of the APi-ToF as a versatile tool for measuring atmospheric ion composition have been extensively described by Junninen *et al.* (2010). For this study, the CI inlet used in combination with the APi-ToF was a MION inlet (Rissanen *et al.*, 2019). This configuration allowed for switching between the CI mode, used to study neutral species, and the APi mode, for the analysis of ambient ions. Dibromomethane (CH_2Br_2) was ionized using soft X-ray radiation (Hamamatsu) to produce bromide ions (Br^-), providing a versatile reagent ion capable of detecting a wide range of atmospheric compounds, including hydroxyl radical (OH) and hydroperoxyl radical (HO_2, Sanchez *et al.*, 2016), sulfuric acid (H_2SO_4) and halogens (Wang *et al.*, 2021), and various organic species (Rissanen *et al.*, 2019), primarily through nucleophilic addition (i.e., clustering with the analytes).

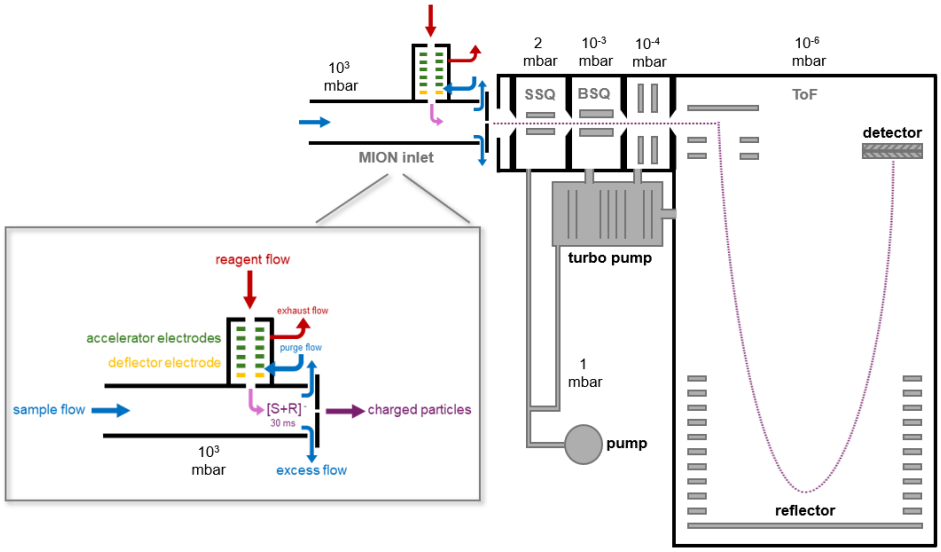


Figure 1. Schematic of CI-APi-TOF. Figure adapted from Junninen *et al.* (2010) and Rissanen *et al.* (2019), reprinted under Creative Common Attribution 3.0 ad 4.0 Licence, respectively.

RESULTS AND OUTLOOK

The chemical analysis of NOx-only experiments – which entailed injecting NOx at various concentrations into the air flow, without introducing any oil vapors – primarily revealed inorganic ions and clusters derived from nitric acid (HNO_3), with no significant presence of organic compounds. No particle formation or ice nuclei activity was observed, even after aging, suggesting that NOx and its oxidation products alone do not contribute to these processes under the tested conditions (i.e., room temperature). When oil vapors were introduced, a substantial increase in the abundance of organic species was detected, particularly in the 150–350 mass-to-charge ratio range. This coincided with the onset of particle formation and subsequent ice nucleation particle (INP) formation, indicating a potential role of oil-derived organics in particle growth and activation.

The strong reagent ion depletion observed in most cases limited a fully quantitative analysis. Therefore, to improve measurement accuracy, future studies should consider additional dilution or the use of an alternative reagent ion to mitigate overconsumption effects.

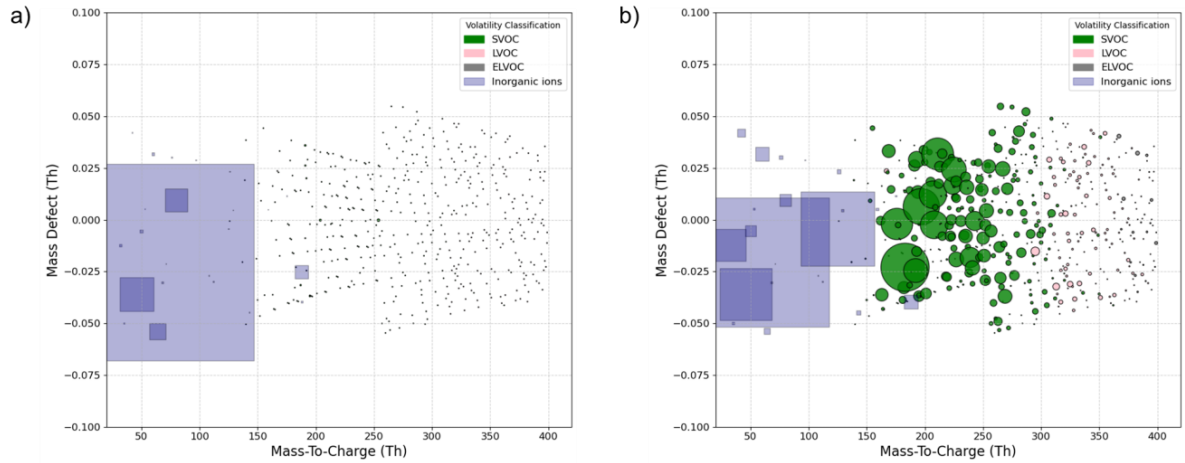


Figure 2. (a) Test point from the NOx-only investigation, involving the injection of 250ppm NOx into the air flow and oxidation induced by the PAM-OFR, mainly resulting in the presence of inorganic ions and clusters derived from HNO_3 (e.g., NO_3^-, $H_2ONO_3^-$, $HNO_3NO_3^-$, etc.). (b) Test point from the Oil-only investigation, involving the injection of oil and oxidation induced by the PAM-OFR, showing a significantly higher abundance of organic species clustered with Br^- (Semi-Volatile Organic Compounds, Low Volatile Organic Compounds, Extremely Low Volatile Organic Compounds).

ACKNOWLEDGEMENTS

This project was funded by SAFRAN, Airbus, and the European Union's Horizon Europe research and innovation programme under grant agreements No. 10119233 and No. 10119259. This work was supported by the French Civil Aviation Authority (DGAC) through the HYCONIC project (CIRRUS-H2 convention No. IA-2020-20-03). We acknowledge ACTRIS CiGas – Centre for Reactive Trace Gases In Situ Measurements for providing operational support. We also extend our gratitude to the INAR staff for their valuable assistance during the campaign.

REFERENCES

Junninen, H. (2010). A high-resolution mass spectrometer to measure atmospheric ion composition, *Atmos. Meas. Tech.*, **3**, 1039–1053.

Lee, D.S. (2021). The contribution of global aviation to anthropogenic climate forcing for 2000 to 2018, *Atmos. Env.*, **244**, 117834.

Rissanen, M.P. (2019). Multi-scheme chemical ionization inlet (MION) for fast switching of reagent ion chemistry in atmospheric pressure chemical ionization mass spectrometry (CIMS) applications, *Atmos. Meas. Tech.*, **12**, 6635–6646.

Sanchez, J. (2016). A new technique for the direct detection of HO2 radicals using bromide chemical ionization mass spectrometry (Br-CIMS): initial characterization, *Atmos. Meas. Tech.*, **9**, 3851–3861.

Wang M. (2021). Measurement of iodine species and sulfuric acid using bromide chemical ionization mass spectrometers, *Atmos. Meas. Tech.*, 14, 4187–4202.

On the identification of ice phases and phase transitions using NIR and MIR spectroscopy

Jonas Schlagin, Christina Tonauer, Klaus R. Liedl, Thomas Loerting

Water is ubiquitous. But it not only plays a crucial role on our own planet but also in the far reaching depths of the observable universe, where it can be found on interstellar dust, comets, nebulas, planets and icy moons, where due to the thermodynamic conditions almost all of it is solidified as ice (1).

All of the solidified states feature different densities and porosities, and vibrational characteristics. In addition, the spectral pattern of each phase is a unique identifier that can be used to detect individual phases in extraterrestrial environments. Furthermore, since the change in local order and the spectral pattern is a function of pressure and temperature, the prevailing thermodynamic conditions can be directly inferred.

While the crystal structures of the known polymorphic forms of ice are well characterized, this is not the case for their infrared absorption characteristics. Following the pioneering work of Bertie and Whalley (2; 3), who recorded MIR and FIR spectra of some ice polymorphs known at the time, the infrared spectroscopy of ice phases was largely neglected for the upcoming five decades. Only recently, Tonauer (4) et al. recorded the previously entirely overlooked NIR spectra of several ice phases. At the same time, the impressive data from infrared space telescopes such as JWST require a solid reference database of spectra to enable accurate detection. We present here the MIR and NIR spectra of different ice phases and their temperature dependence over a range from 108 K up to the phase transition to hexagonal ice I. Furthermore, we demonstrate how knowledge of the vibrational spectrum can be utilized for extraterrestrial detection.

Literaturverzeichnis

1. *Ices in space.* **Grennberg, JM, van de Bult, CEPM and Allamandola, LJ.**,JPC, 1983, Vol. 87.

2. *Infrared Spectra of Ices II, III, and V in the Range 4000 to 350 cm—1.* **Bertie, JE and Whalley, E.**, JCP, 1964, Vol 40.

3. *Far-Infrared Spectra of Ice II, V, and IX.* **Bertie, JE and Labbé, HJ, Whalley, E.**, JCP, 1968, Vol. 49.

4. *Near-Infrared Spectra of High-Density Crystalline H2O Ices II, IV, V, VI, IX, and XII.* **Tonauer, CM, et al.** , JPC A, 2021, Vol. 125.

IN SITU X-RAY DIFFRACTION STUDY OF ICE CRYSTALS GROWING ON NATURAL ALKALI FELDSPAR

J.S. SEIDEL[1], A.A. KISELEV[1], B. KRAUSE[2], M. KAMIŃSKI[2], D.A. HEUSER[3], R. ABART[3], E. PETRISHCHEVA[3]

[1]*Institute of Meteorology and Climate Research Atmospheric Aerosol Research, Karlsruhe Institute of Technology, Karlsruhe, Germany.*

[2]*Institute for Photon Science and Synchrotron Radiation, Karlsruhe Institute of Technology, Karlsruhe, Germany.*

[3]*Department of Lithospheric Research, University of Vienna, Vienna, Austria.*

Keywords: HETEROGENEOUS ICE NUCLEATION, ALKALI FELDSPAR, GRAZING INCIDENCE X-RAY DIFFRACTION.

INTRODUCTION

Understanding the ice formation in clouds is crucial as ice influences precipitation formation and cloud radiation properties, thus being an important factor controlling the Earth's weather and climate system (Cantrell and Heymsfield, 2005). Above -38°C, ice particles are mainly formed via heterogeneous nucleation, whereby certain aerosols can act as ice nucleating particles (INPs) initiating the freezing process by lowering the energy barrier which is hampering spontaneous formation of critical ice embryos (Kanji *et al.*, 2017).

From a variety of freezing experiments conducted in the past decade, it is known that alkali feldspar is one of the most effective ice nucleating components of mineral dust (Atkinson *et al*., 2013, Whale *et al.*, 2017). The high ice nucleation efficiency of alkali feldspar, especially of type microcline, is attributed to its perthitic microstructure, which may result from exsolution of Na-rich and K-rich feldspar during cooling after magmatic or metamorphic crystallization (Smith and Brown, 1988). Subsequent natural ageing in the course of chemical or hydrothermal alteration and weathering may carve out surface defects like step edges, cracks, pores and cavities (Whale *et al.*, 2017). Such features are often aligned with the non-rational Murchison plane with Miller indices ranging from (-801) to (-601), which is sub-parallel to the (100) plane (see Fig. 1). Also, exsolution lamellae follow the Murchison plane to minimise the elastic energy associated with exsolution (Petrishcheva *et al.,* 2023). Kiselev *et al.* (2017, 2021) and Keinert *et al.* (2022) hypothesized that IN-active patches of (100) crystallographic plane might be exposed at such defect sites, thus explaining the epitaxial relationship between feldspar (100) and primary prismatic crystal planes of macroscopic ice crystals, observed in ESEM experiments of Kiselev *et al*. (2017) and Pach and Verdaguer (2019) and immersion experiments of Keinert *et al.* (2022). However, because surfaces parallel to the (100) plane in feldspar cannot be created by cleaving and do not form during crystal growth, direct evidence for an enhanced ice nucleating efficiency of surfaces parallel to the (100) crystallographic plane of feldspar is still missing.

In this study, we complement droplet freezing assay and ESEM ice nucleation experiments with a new in situ X-ray diffraction (XRD) setup to identify the role of liquid water in contact with the feldspar and to elucidate the nature of the epitaxial relationship between ice crystals and feldspar. Unraveling the mechanism underlying the ice nucleation on natural alkali feldspar on the molecular level will allow to characterize the importance of alkali feldspar aerosol in cloud formation and precipitation processes.

METHODS

For our X-ray study of ice formation on alkali feldspar, we use cleaved slabs of (001) and (010) orientation of natural perthitic microcline feldspar from Pakistan exhibiting a complex microstructure with twinning intergrowth and porosity related to hydrothermal alteration. This feldspar type shows an

extraordinarily high ice nucleation activity in droplet freezing assay experiments and ice crystals growing with a preferential orientation from the vapor phase in ESEM experiments. To analyze the role of surface topography and phase composition on the ice nucleation ability, we use a potassium-rich gem quality sanidine with a homogeneous and defect-free surface as a reference. This feldspar type shows a comparatively low IN activity and a random distribution of ice crystal orientations in ESEM deposition freezing experiments. To specifically investigate the importance of either cracks or pores on the ice nucleation ability without facing further microstructural complexity such as twinning intergrowth, we also use samples of the gem-quality feldspar featuring a system of parallel cracks sub-parallel to the Murchison plane produced by chemically induced fracturing (Scheidl *et al.*, 2014, Kiselev *et al.*, 2021), and samples of the gem-quality feldspar which were hydrothermally altered by Na-K-cation exchange at high temperature and pressure (Norberg *et al.*, 2011) to induce micro- and nonscale porosity. During subsequent cooling and recrystallization, cracks and a system of pores aligned with the Murchison plane and thus sub-parallel to (100) are induced in feldspar samples.

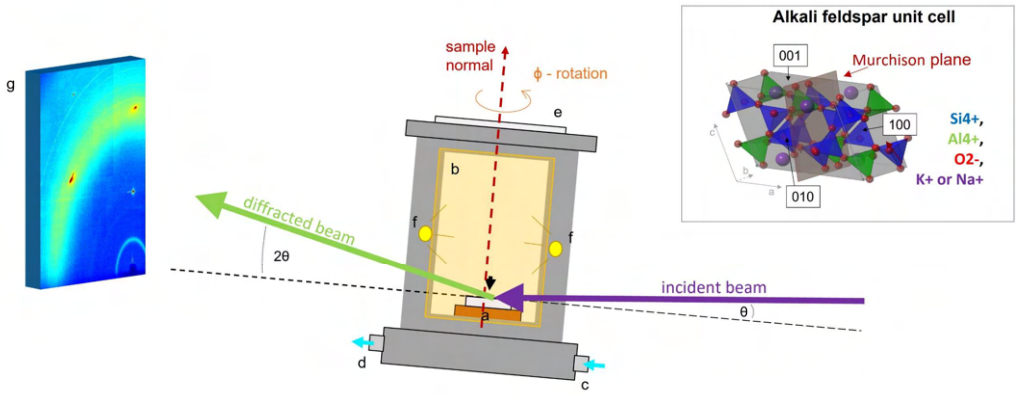


Figure 1: Schematic drawing of the synchrotron X-Ray scattering experiment. The main components of the environmental cell are (a) sample cooling stage with TEC temperature control; (b) X-ray transparent windows (Kapton® foil); (c, d) inlet and outlet for humidified N_2 flow, (e) optical window for video camera, (f) LEDs, (g) X-ray detector. The upper right panel shows the unit cell of alkali feldspar with the Murchison plane indicated in darkred.

The feldspar sample is mounted on top of a thermoelectric cooler (TEC) located in the centre of a custom designed experimental cell with X-ray permeable windows enclosing a model atmosphere of humidified nitrogen gas (Fig. 1). During a typical ice nucleation experiment, we perform grazing incidence XRD while ice crystals are generated from the vapor phase by slowly cooling the feldspar sample down until the ice nucleation onset is reached. From those time scans, we expect to resolve whether adsorbed or liquid water is formed before the onset of ice nucleation. Nucleation and growth of the ice crystals are monitored with a video camera equipped with a long-distance microscope objective lens. At equilibrium (ice crystals do not grow or shrink), larger regions of reciprocal space are mapped to obtain the average ice crystal orientation with respect to the crystallographic axis of the feldspar sample.

RESULTS and DISCUSSION

The first successful in situ X-ray diffraction experiments were conducted at the DESY P08 high resolution diffraction beamline (Seeck *et al.*, 2012) in July 2024. The large area detector used in the setup allowed measurements of the X-ray signal of water condensing on the feldspar surface (Fig. 2).

A preliminary result of an ice crystal growth experiment on a cleaved microcline (010) slab under ambient pressure conditions is shown in Fig. 3. The polar plot shows the distribution of X-ray diffraction maxima for a substrate, which was fully covered with comparatively large ice crystals (~100µm diameter). Peak clusters are observed near the theoretical positions of two ice reflexes, which were calculated based on the assumption of an epitaxial relationship between the feldspar and ice i.e.,

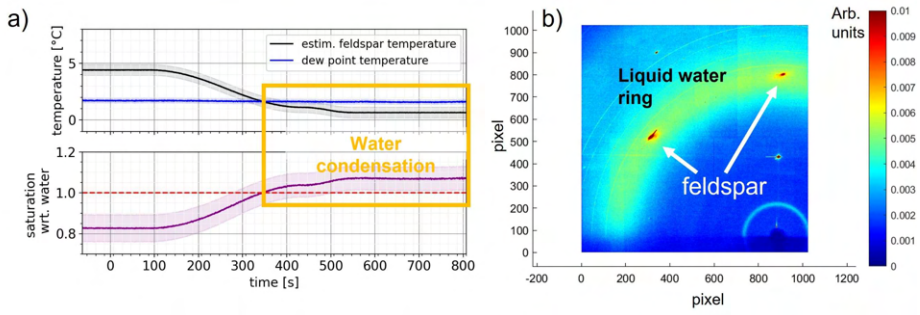


Figure 2: a) Time series of the feldspar surface temperature, ambient dew point temperature and saturation with respect to water during a typical water condensation experiment on a microcline (001) surface. b) X-ray diffraction signal while condensed water was present on the feldspar surface. The liquid water becomes visible in form of a broad ring. Red spots within the water ring are reflexes from the feldspar substrate.

ice (10-10) ‖ to feldspar (100). This finding confirms earlier microscopic observations of a preferential oriented ice crystal growth on the surfaces of perthitic feldspar by Kiselev *et al*. (2017) and Keinert *et al.* (2022). However, the spread of several degrees of the data points in Fig. 3 indicates that there were ice crystals with different orientations present. This is most likely caused by the complexity of the microcline substrate, featuring albite and pericline twinning, exsolution lamellae and lattice strain. Further X-ray diffraction experiments are needed to elaborate this finding in more detail.

Gaining statistical evidence and quantitative information on the average ice crystal orientation on natural perthitic and chemically altered feldspar substrates is one objective of the follow-up beam time at P08 in June 2025. Furthermore, we want to unveil the role of adsorbed or liquid water in pores or cavities prior to ice nucleation.

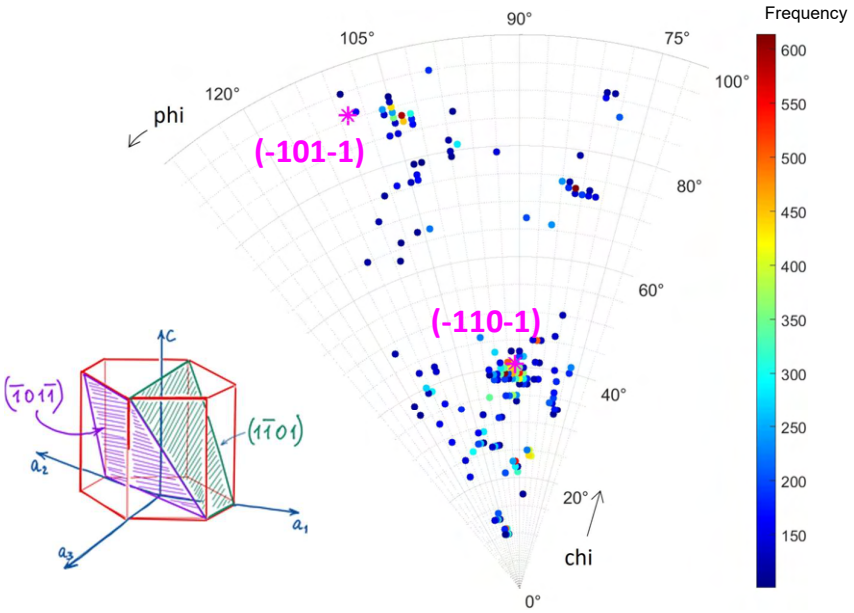


Figure 3: Distribution of the {10-11} X-ray diffraction maxima in polar coordinates. Pink asterisks mark the theoretical position of two ice reflexes resulting from the ice (-101-1) and (-110-1) planes, which were calculated with the assumption of ice (10-10) ‖ to feldspar (100).

ACKNOWLEDGEMENTS

This work was supported by Deutsche Forschungsgemeinschaft (DFG), project number 515700978 and by FWF grant I 6467. We would like to thank the beamline scientists Dr. Florian Bertram and Dr. Chen Shen and the beamline technician Rene Kirchhof for their great support during our stay at the DESY, PETRA III P08 beamline.

REFERENCES

Atkinson, J. D., Murray, B. J., Woodhouse, M. T., Whale, T. F., Baustian, K. J., Carslaw, K. S., Dobbie, S., O'Sullivan, D. and Malkin, T. L. (2013). The importance of feldspar for ice nucleation by mineral dust in mixed-phase clouds. *Nature*, ***498***(7454), 355-358. https://doi.org/10.1038/nature12278.

Cantrell, W., and Heymsfield, A. (2005). Production of Ice in Tropospheric Clouds: A Review. *Bull. Amer. Meteor. Soc.*, ***86***, 795–808. https://doi.org/10.1175/BAMS-86-6-795.

Kanji, Z. A., Ladino, L. A., Wex, H., Boose, Y., Burkert-Kohn, M., Cziczo, D. J., and Krämer, M. (2017). Overview of ice nucleating particles. *Meteorological monographs*, ***58***, 1-1. https://doi.org/10.1175/AMSMONOGRAPHS-D-16-0006.1.

Keinert, A., Deck, K., Gaedeke, T., Leisner, T., and Kiselev, A. A. (2022). Mechanism of ice nucleation in liquid water on alkali feldspars. *Faraday Discussions*, ***235***, 148-161. https://doi.org/10.1039/D1FD00115A.

Kiselev, A., Bachmann, F., Pedevilla, P., Cox, S. J., Michaelides, A., Gerthsen, D., and Leisner, T. (2017). Active sites in heterogeneous ice nucleation—the example of K-rich feldspars. *Science*, ***355***(6323), 367-371.

Kiselev, A. A., Keinert, A., Gaedeke, T., Leisner, T., Sutter, C., Petrishcheva, E., and Abart, R. (2021): Effect of chemically induced fracturing on the ice nucleation activity of alkali feldspar, Atmos. Chem. Phys., 21, 11801-11814, https://doi.org/10.5194/acp-21-11801-2021.

Marcolli, C. (2014). Deposition nucleation viewed as homogeneous or immersion freezing in pores and cavities. *Atmospheric Chemistry and Physics*, ***14***(4), 2071-2104. https://doi.org/10.5194/acp-14-2071-2014

Norberg, N., Neusser, G., Wirth, R., & Harlov, D. (2011). Microstructural evolution during experimental albitization of K-rich alkali feldspar. *Contrib. Mineral. Petrol.*, ***162***(3), 531-546. https://doi.org/10.1007/s00410-011-0610-y.

Pach, E. and Verdaguer, A. (2019): Pores Dominate Ice Nucleation on Feldspars, The Journal of Physical Chemistry C, 123, 20998-21004, https://doi.org/10.1021/acs.jpcc.9b05845.

Petrishcheva, E., Heuser, D., Abart, R. (2023) Coherent lamellar intergrowth in alkali feldspar. *Contrib. Mineral. Petrol.*, **178**, 77. https://doi.org/10.1007/s00410-023-02059-z.

Scheidl K, Schaeffer, AK, Petrishcheva E, Habler G, Fischer FD, Schreuer J, Abart R (2014) Chemically induced fracturing in alkali feldspar. *Phys. Chem. Min.*, **41**: 1-16, https://doi.org/10.1007/s00269-013-0617-1.

Seeck, O. H., Deiter, C., Pflaum, K., Bertam, F., Beerlink, A., Franz, H., Horbach, J., Schulte-Schrepping, H., Murphy, B. M., Greve, M. and Magnussen, O. (2012). The high-resolution diffraction beamline P08 at PETRA III. *J. Synchrotron Rad.* ***19***, 30-38. https://doi.org/10.1107/S0909049511047236

Smith, J. and Brown, W. (1988) *Feldspar Minerals, 1. Crystal Structures, Physical, Chemical and Microtextural Properties.* (Springer-Verlag, Berlin, Heidelberg and New York, 2nd edition).

Whale, T. F., Holden, M. A., Kulak, A. N., Kim, Y. Y., Meldrum, F. C., Christenson, H. K., and Murray, B. J. (2017). The role of phase separation and related topography in the exceptional ice-nucleating ability of alkali feldspars. *Physical Chemistry Chemical Physics*, ***19***(46), 31186-31193. https://doi.org/10.1039/C7CP04898J

EMERGING CONTAMINANTS IN THE AIR: IMPACT OF MICROPLASTICS ON CLOUD FORMATION THROUGH ICE NUCLEATION

T.M. SEIFRIED[1], G. UPPAL[1], S. NIKKHO[1], A. MORALES MURILLO[2], L. J. ANDREW[1], C. VARCOE[3], E. R. GRANT[1] and A. K. BERTRAM[1]

[1]*Department of Chemistry, University of British Columbia, Vancouver, British Columbia, Canada;*

[2]*Faculty of Pharmaceutical Sciences, University of British Columbia, Vancouver, British Columbia, Canada;*

[3]*Department of Mechanical Engineering, University of British Columbia, Vancouver, British Columbia, Canada;*

Keywords: MICROPLASTICS, TIRE & BRAKE WEAR, ICE NUCLEATION, CLOUDS.

INTRODUCTION

Microplastics have emerged as widespread anthropogenic contaminants in the atmosphere, originating from the abrasion and degradation of everyday plastic products as well as from intentionally manufactured particles. Additionally, non-exhaust vehicle emissions, including tire and brake wear, are now recognized as significant sources of airborne microplastics due to their high plastic content. The release of microplastic particles has increased dramatically in recent decades due to the rising global use of plastics and the growing number of vehicles on the road, however with unknown impacts on the atmospheric environment and our climate.

Similar to other aerosols, airborne microplastics can affect climate indirectly by acting as cloud condensation nuclei (Wlasits et al., 2023) or ice-nucleating particles (INPs) thereby influencing cloud formation and precipitation. In the absence of INPs, cloud droplets freeze homogeneously at temperatures below -38°C. However, if INPs are present, freezing is initiated at higher temperatures impacting cloud lifetime, cloud optical properties, and precipitation. However, the role of microplastics as effective INPs and their impact on cloud formation remains poorly understood. Additionally, if microplastics act as INPs, their atmospheric lifetime may be impacted by ice nucleation followed by precipitation, which could affect their transport pathways. In this study, we investigated the ice nucleation activity of several microplastics, brake wear, and tire wear particles in immersion freezing mode, the primary freezing pathway in mixed-phase clouds.

METHODS

We measured the ice nucleation activity of a range of microplastics including polypropylene (PP), polyethylene (PE) and polyethylene terephthalate (PET) samples, as well as brake wear (ceramic, semi-metallic and organic) and tire wear particles suspended in water using droplet freezing techniques. Measurements were conducted using either (i) a cold stage (droplet volume: µL, background freezing: approx. -25°C) or (ii) a cryo-microscope (droplet volume: nL, background freezing: approx. -34.0°C), with the latter used for samples that nucleated around and below -25°C. In the cold stage, 1-2 µL droplets of the corresponding sample suspension were pipetted onto the hydrophobic glass slide, followed by cooling at 3°C/min while freezing was observed through a mounted camera. In contrast, for the cryo-microscope, dry particles were first deposited onto a coverslip before humid air was introduced at 0°C, allowing water to condense until particles were immersed in droplets. The system was then cooled at 5°C/min, and freezing events were monitored through an objective and an attached camera. Figure 1 gives schematic illustrations of the used freezing setups.

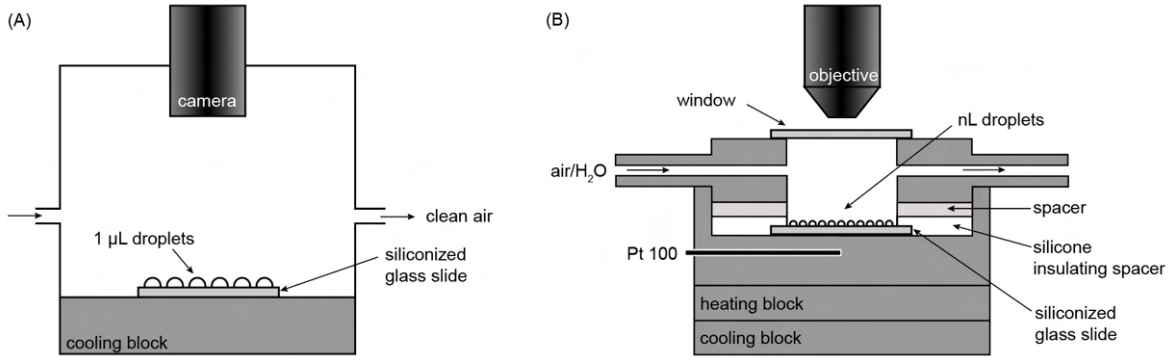


Figure 1. Schematic illustration of (A) the cold stage setup (µL droplets, background freezing at approximately -25°C), and (B) the cryo-microscope (nL droplets, background freezing at approximately -34.0°C).

RESULTS

PP needles, PP fibers and PET fibers nucleated ice heterogeneously with median freezing temperatures ranging from -20.9°C to -23.2°C. The number of ice nucleation sites per surface area, $n_s(T)$, ranged from 10^{-1} to 10^{4} cm^{-2} within the temperature range of -15 to -25°C, similar to volcanic ash and fungal spores. To assess the impact of atmospheric aging, we exposed these ice-active plastics to ozone and a combination of UV light and ozone. The ice nucleation activity either decreased or remained unchanged, suggesting that prolonged atmospheric exposure could reduce their ability to nucleate ice in the atmosphere, potentially influencing their long-range transport (Seifried et al., 2024).

We further demonstrate that non-exhaust road emissions can nucleate ice heterogeneously. The tire wear standard CMTT (cryo-milled tire tread) nucleated ice at -25°C, while the background freezing occurred at -34°C. In addition, we found that brake wear particles nucleated ice at varying efficiencies depending on their composition. Semi-metallic brake wear froze at the highest temperatures with median freezing temperatures of -21.2°C in contrast to ceramic and organic ones. A preliminary comparison showed that semi-metallic brake wear has similar nucleation site densities compared to PP and PET ice-active microplastics (Figure 2).

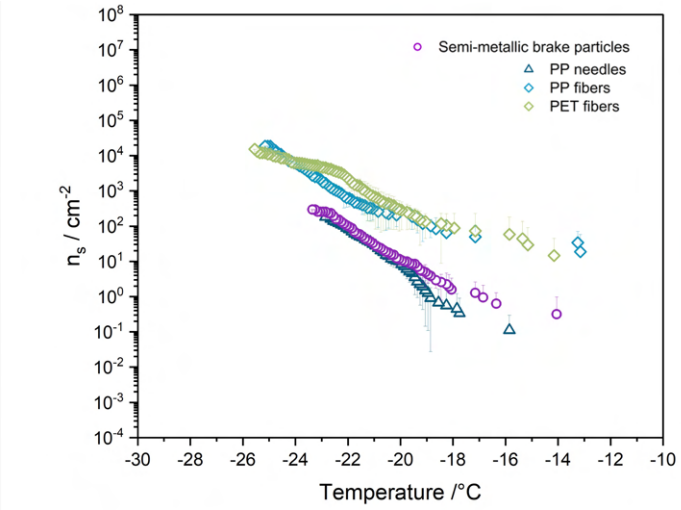


Figure 2. Comparison of the number of ice nucleation sites per surface of semi-metallic brake particles to ice-active microplastics including polypropylene (PP) needles, fibers, and polyethylene terephthalate (PET) fibers (Seifried et al., 2024).

CONCLUSION

The role of microplastics in atmospheric processes, particularly their potential to influence ice nucleation in clouds, remains uncertain. In this study, we show that microplastic samples, specifically PP needles, PP fibers, and PET fibers, nucleate ice in the immersion freezing mode at temperatures ranging from -15°C to -25°C. Recently, Tatsii et al. (2025) incorporated the PET fiber nucleation data into the FLEXPART atmospheric transport model to estimate the contribution of road-related emissions, including tire and brake wear, to INP concentrations, as no experimental data existed for these particles. Their findings suggest that under high-emission scenarios, tire and brake wear could substantially contribute to the INP concentration in tropical regions. Here, we provide the first direct evidence that tire wear and certain brake wear particles can nucleate ice, with the latter freezing similar to PET fibers. We suggest incorporating this new data into models to refine estimates of the impact of road-related microplastics on INP populations. In general, understanding the ice-nucleating ability of microplastics will help us identify their influence on cloud processes and better understand their transport pathways.

ACKNOWLEDGEMENTS

The authors acknowledge the support of the Natural Sciences and Engineering Research Council of Canada (RGPIN-2023-05333). T.M.S. and E.R.G. gratefully acknowledge support by a Discovery Grant from The Natural Sciences and Engineering Research Council of Canada (RGPIN-2019-04242). T.M.S. acknowledges funding by the Austrian Science Fund (FWF) under project number J 4752-N.

REFERENCES

Seifried, T. M., Nikkho, S., Morales Murillo, A., Andrew, L. J., Grant, E. R., & Bertram, A. K. (2024). Microplastic particles contain ice nucleation sites that can be inhibited by atmospheric aging. *Environmental Science & Technology*, 58(35), 15711-15721.

Tatsii, D., Gasparini, B., Evangelou, I., Bucci, S., & Stohl, A. (2025). Do Microplastics Contribute to the Total Number Concentration of Ice Nucleating Particles?. *Journal of Geophysical Research: Atmospheres*, 130(2), e2024JD042827.

Wlasits, P. J., Konrat, R., & Winkler, P. M. (2023). Heterogeneous nucleation of supersaturated water vapor onto sub-10 nm nanoplastic particles. Environmental Science & Technology, 57(4), 1584-1591.

Study of Multicomponent Aerosol-Water Interactions using Molecular Dynamic Simulation: Implications for Cloud Droplet Formation

D.D. VADGAMA[1], R. SRIVASTAVA[1] and S.M. SHINDE[1]

[1]*Department of Physics, School of Energy Technology, Pandit Deendayal Energy University, Raysan, Gandhinagar 382426, Gujarat, India.*

Keywords: Cloud Condensation Nuclei, Cloud Droplet Formation, Dimethyl Sulfide, Palmtic Acid, Molecular Dynamic Simulation.

INTRODUCTION

Clouds play a major role in global weather and climate by reflecting or scattering the incoming solar radiation and absorbing the Earth's heat radiation. The properties of clouds depend on the growth and formation of Cloud droplets, which begins when water vapor condenses on airborne particles, known as Cloud Condensation Nuclei (CCN) (Li et al., 2011). The formation of cloud droplets is influenced by atmospheric aerosols, including organic and inorganic compounds and also prevailing atmospheric conditions (Karadima et al., 2019). Among the various compounds influencing CCN activity, Dimethyl sulfide (DMS) and Palmitic Acid (PA) stand out due to their contrasting chemical properties and atmospheric significance. DMS, predominantly released from marine phytoplankton, is a well-known precursor to sulfate aerosols, which are highly efficient CCN in sulfur-rich environments (Ghahreman et al., 2019). In contrast, PA, a fatty acid commonly found in organic aerosols, exhibits surface active properties that affect droplet growth dynamics and alter cloud optical properties (Garland et al., 1951). These compounds interact with water and ionic species, such as NaCl, potentially influencing CCN activity and cloud microphysics. Despite the importance of these interactions, the molecular-scale mechanism governing the effects of such distinct compounds and how these interactions differ in promoting droplet nucleation and growth remain poorly understood. Previous studies have explored various organic-water (Li et al., 2013) and ions-water (Li et al., 2010; Liu et al., 2022) systems, but the specific interplay between DMS and PA with water ions is less studied. Hence, this study aims to bridge the gap by employing molecular dynamics simulation to investigate the interactions of water and ions (NaCl) with DMS or PA, elucidating their distinct contribution in cloud droplet nucleation and growth. Understanding the interactions that govern this process is necessary for improving the accuracy of climate models and predicting changes in global weather systems.

METHODS

The GROMACS program package was used to perform molecular dynamic simulation, employing NVT and NPT ensembles with the temperature set to 300 K using V-rescale thermostat and pressure set to 1 bar using C-rescale barostat to mimic the atmospheric condition. Four distinct water clusters consisting of 200, 400, 800 and 1000 water molecules with an equal number of Ions and DMS or PA molecules (System I: Water_Ions_DMS and System II: Water_Ions_PA) were constructed. For all the molecules, the OPLS force field was used along with the SPC/E water model, with each cluster contained within a simulation box of 6nm. Short-range interactions were truncated at 1.0 nm cutoff distance, with long-range Coulombic interactions treated using the particle mesh Ewald method. Simulations were performed with a 2 fs time step, beginning with energy minimization followed by 100 ps of equilibration under NVT and NPT, respectively. Following that, a production simulation of 1 ns ran with trajectories saved every 10 ps. Radial distribution function and number density profile were analyzed to understand the molecular level interaction and water clustering around aerosol components.

RESULT AND DISCUSSION

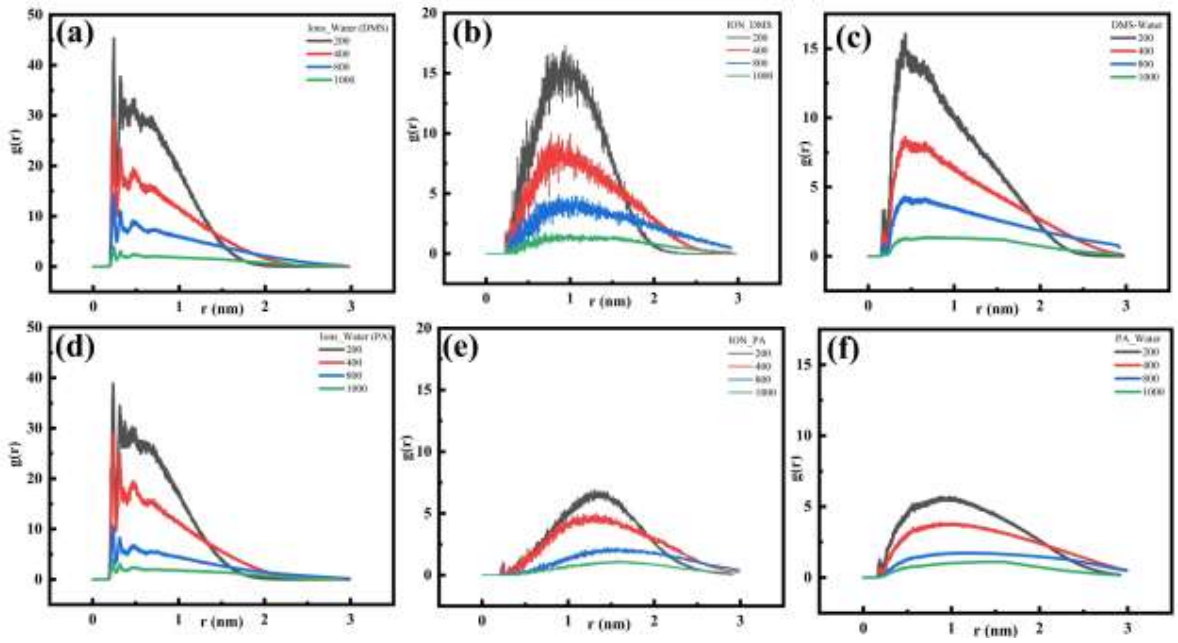


Figure 1. Radial Distribution Function (RDFs) of PA and DMS in the water and ion clusters: (a) Ion-Water, (b) Ion-DMS, and (c) DMS_Water for system I (Water_Ions_DMS), respectively and (d) Ion-Water, (e) Ion-PA, and (f) PA_Water for system II (Water_Ions_PA).

The plots show the radial distribution function (RDF), g(r), for Ion-Water interactions when either DMS or PA (Fig. 1a, d) is present, ion-DMS/PA (Fig. 1b, e) interactions and DMS/PA-Water (Fig. 1c, f) interactions at various hydration levels. The Ion-water interaction exhibits the highest peaks, followed by ion-DMS/PA and then DMS/PA-water interaction, suggesting strong ion-water interactions and formation of structured hydration shells around ions. These observed strong structuring plays a crucial role in attracting water molecules, an initial step in the formation of CCN. The less pronounced peaks of DMS and PA interaction with ion and water indicate moderated hydration enhancement without forming strong bonds with complexes. Furthermore, the interaction of PA with water and ions is weaker compared to DMS due to its hydrophobic tail, which is likely to reduce bulk dynamics. However, PA demonstrates surface-active properties, with water clustering around its polar headgroup, while the hydrophobic tail reduces interaction in bulk water (Shrestha et al., 2018). This highlights the effectiveness of DMS in nucleating small, effective cloud droplets, contributing to CCN efficiency (Fung et al., 2022), while PA may result in fewer, larger droplets due to weaker water structuring, impacts droplet growth dynamics and impacts cloud optical properties. As hydration levels increase, the peak intensities decrease for all the cases, suggesting a dilution effect where hydration shells around molecules become less structured and evenly distributed water molecules. Hence, the behavior of DMS and PA molecules suggests that DMS is a potential CCN precursor, where it facilitates nucleation, especially in rich organic sulfur regions while PA influences droplet formation and growth differently by acting as a surface-active compound.

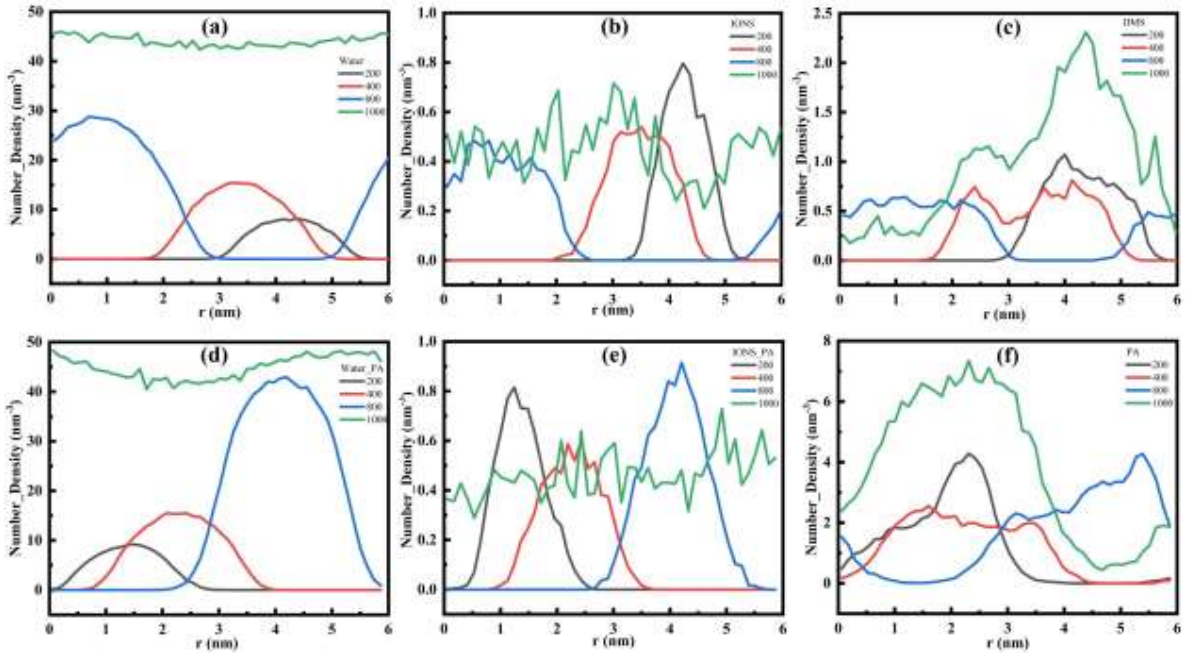


Figure 2. Number Density profile of (a) Water, (b) Ions, and (c) DMS for system I (Water_Ion_DMS) and (d) Water, (e) Ions, and (f) PA for system II (Water_Ion_PA)

The number density profile depicts the molecular distribution within the system. At lower hydration levels (200 and 400 water molecules), the density of water molecules concentrated predominantly on one side of the box, forming dense regions around ions or organic molecules. However, at higher hydration levels (800 and 1000 water molecules), this distribution broadens, indicating a more dispersed hydration dynamic as the system becomes bulkier. Ion density exhibits behaviour consistent with water number density, confirming the role of ions as centers of hydration, which aligns with the observed RDF peaks for ion-water interactions. DMS shows a broader peak compared to water and ion number densities, suggesting stronger interaction with both ion and water molecules, solidifying its role in CCN formation within sulfur-rich marine environments (Fung et al., 2022). On the other hand, PA displays distinct peaks near the air-water interface, reflecting its surface-active properties (Shrestha et al., 2018). While the polar head of PA promotes water clustering at the interface, its hydrophobic tail reduces bulk interactions. This unique combination affects droplet growth and CCN activity, highlighting PA's influence on heterogeneous nucleation.

The analysis further emphasizes the variation of hydration dynamics and molecular interaction with increasing concertation of water molecules. DMS demonstrates efficient CCN activation by enhancing solubility and hydration; this aligns with its role in producing smaller droplets with higher albedo, contributing to short-lived cloud systems often seen in sulfur-rich marine environments. In contrast, PA impacts droplet formation differently by altering surface tension and promoting larger droplet growth, which lowers albedo and affects radiative forcing, potentially altering local temperature patterns. The molecular behaviors highlight their distinct role in influencing cloud microphysics and broader climate processes.

CONCLUSIONS

This study examines Water_Ion_DMS and Water_Ion_PA systems using Molecular dynamic simulation. Analysis of RDF and Number Density suggests that Ion-water interactions are strong at lower hydration levels but weaken with higher hydration. DMS forms localized hydration shells, contributing to hydration-driven droplet nucleation, whereas PA stabilizes aerosol particles more effectively through surface-active effects, impacting droplet growth dynamics. DMS-dominated systems are linked to marine cloud formation, where phytoplankton emits sulfurs and enhances CCN activity and leads to short-lived clouds with higher-albedo droplets over oceans. In contrast, PA emissions from the vegetation and anthropogenic sources,

align with the terrestrial or coastal clouds, fostering longer-lasting clouds with more heterogeneous structures and larger droplets. This different droplet size distribution plays a critical role in cloud lifetime and precipitation patterns; smaller droplets resist coalescence, producing non-precipitating clouds, while larger droplets are more likely to precipitate, shorting cloud lifetime and contributing to local rain events. These findings highlight the distinct role of DMS and PA in influencing the CCN activity, droplet formation and cloud dynamics, particularly in marine and urban environments, where these compounds are prevalent. Incorporating these processes into climate models can improve predictions of cloud cover, albedo effect and their influence on radiative forcing, particularly in regions with high organic aerosols or sulfur compound concentration.

ACKNOWLEDGEMENTS

This work is supported by the SHODH Scheme under the Education Department of Gujarat.

REFERENCES

Fung, K. M., Heald, C. L., Kroll, J. H., Wang, S., Jo, D. S., Gettelman, A., Lu, Z., Liu, X., Zaveri, R. A., Apel, E. C., Blake, D. R., Jimenez, J. L., Campuzano-Jost, P., Veres, P. R., Bates, T. S., Shilling, J. E., & Zawadowicz, M. (2022). Exploring dimethyl sulfide (DMS) oxidation and implications for global aerosol radiative forcing. *Atmospheric Chemistry and Physics*, *22*(2), 1549–1573. https://doi.org/10.5194/acp-22-1549-2022

Garland, R. M., Wise, M. E., Beaver, M. R., Dewitt, H. L., Aiken, A. C., Jimenez, J. L., & Tolbert, M. A. (1951). Impact of palmitic acid coating on the water uptake and loss of ammonium sulfate particles. In *Atmos. Chem. Phys* (Vol. 5). www.atmos-chem-phys.org/acp/5/1951/SRef-ID:1680-7324/acp/2005-5-1951EuropeanGeosciencesUnion

Ghahreman, R., Gong, W., Gal\'{\i}, M., Norman, A.-L., Beagley, S. R., Akingunola, A., Zheng, Q., Lupu, A., Lizotte, M., Levasseur, M., & Leaitch, W. R. (2019). Dimethyl sulfide and its role in aerosol formation and growth in the Arctic summer – a modelling study. *Atmospheric Chemistry and Physics*, *19*(23), 14455–14476. https://doi.org/10.5194/acp-19-14455-2019

Karadima, K. S., Mavrantzas, V. G., & Pandis, S. N. (2019). Insights into the morphology of multicomponent organic and inorganic aerosols from molecular dynamics simulations. *Atmospheric Chemistry and Physics*, *19*(8), 5571–5587. https://doi.org/10.5194/acp-19-5571-2019

Li, X., Hede, T., Tu, Y., Leck, C., & Ågren, H. (2010). Surface-active cis-pinonic acid in atmospheric droplets: A molecular dynamics study. *Journal of Physical Chemistry Letters*, *1*(4), 769–773. https://doi.org/10.1021/jz9004784

Li, X., Hede, T., Tu, Y., Leck, C., & Ågren, H. (2011). Glycine in aerosol water droplets: A critical assessment of Köhler theory by predicting surface tension from molecular dynamics simulations. *Atmospheric Chemistry and Physics*, *11*(2), 519–527. https://doi.org/10.5194/acp-11-519-2011

Li, X., Hede, T., Tu, Y., Leck, C., & Gren, H. Å. (2013). Cloud droplet activation mechanisms of amino acid aerosol particles: Insight from molecular dynamics simulations. *Tellus, Series B: Chemical and Physical Meteorology*, *65*(1). https://doi.org/10.3402/tellusb.v65i0.20476

Liu, L., Guo, S., Zhao, Z., & Li, H. (2022). Free Energy Prediction of Ion-Induced Nucleation of Aqueous Aerosols. *Journal of Physical Chemistry A*, *126*(15), 2407–2416. https://doi.org/10.1021/acs.jpca.1c09787

Shrestha, M., Luo, M., Li, Y., Xiang, B., Xiong, W., & Grassian, V. H. (2018). Let there be light: stability of palmitic acid monolayers at the air/salt water interface in the presence and absence of simulated solar light and a photosensitizer. *Chemical Science*, *9*(26), 5716–5723. https://doi.org/10.1039/C8SC01957F

PHASE TRANSITION IN THIN LAYERS OF ADSORBED WATER ON PbI_2

A. WELTI[1], Y. VIISANEN[1], A.A. PIEDEHIERRO[1] and A. LAAKSONEN[1,2]

[1]*Finnish Meteorological Institute, Helsinki, Finland.*

[2]*Department of Applied Physics, University of Eastern Finland, Kuopio, Finland.*

Keywords: ICE NUCLEATION, WATER ADSORBTION, FREEZING, ICE SURFACE.

INTRODUCTION

To elucidate the mechanisms of ice nucleation on silver iodide, Barnes and Sänger (1961) used proton spin resonance spectroscopy to detect the temperature dependent phase state of surface adsorbed water. Based on the results, they suggested that a substance becomes active at nucleating ice after the adsorbed water on the surface transforms into an ice-like state, and that there should be a correspondence between the temperature of ice nucleation and the temperature at which adsorbed water becomes ice like.
To test this hypothesis, we use diffuse reflectance infrared Fourier transform spectroscopy (DRIFTS) to measure the temperature dependent phase state of water adsorbed on various powders. The DRIFTS signal is compared to the ice nucleation onset temperature of the test substances. We present some preliminary results using lead iodide (PbI_2), a highly active ice nucleating substance.

METHODS

DRIFT spectroscopy was used to simultaneously determine the amount and phase state of adsorbed water based on characteristic absorption peaks. Water molecules in a weakly bound, liquid-like state absorb light at a higher wavenumber than in a strongly bound, solid-like configuration. The measurements are conducted in an environmental chamber that allows exposure of a test substance to a broad range of temperature and humidity levels while recording the diffuse infrared reflectance spectrum of the adsorbed water. Controlling humidity allows the deposition of a specific number of water monolayers on the substrate to study the dependence on adsorption layer thickness.
Ice nucleation experiments are conducted using the modified Spectrometer for Ice Nuclei (SPIN) described in Welti *et al*. (2020). SPIN is a continuous flow diffusion chamber in which test particles are exposed to constant temperature and humidity conditions. Formed ice crystals are detected after a residence time of 8-12 seconds at the exit of the SPIN chamber.

CONCLUSIONS

Ice nucleation experiments confirm the high ice nucleation efficiency of PbI_2. The onset temperature is 263K. However, DRIFTS experiments only show a gradual phase transition at temperatures below 243K, which is not close to the ice nucleation onset, suggesting that there is no simple relationship between the occurrence of more ice-like structures in the adsorbed layers of water and the ice nucleation activity. Surprisingly, at 263K a well-defined, narrow hydroxyl stretching peak that is clearly distinct from the broader stretching peak of hydrogen bonded H_2O in liquid- (ν_3) or ice-like (ν_1) configuration, appears at 3500cm^{-1}. The peak width and wavenumber suggest the presence of not hydrogen bonded OH. Dangling OH can occur on the outermost layer of thin ice if few adsorbed layers do not develop a perfect crystal lattice. The presence of dangling OH groups would make the surface more hydrophilic and could affect how additional water molecules attach and cluster.
The investigation of more substances will show whether a relationship between temperature-dependent properties of adsorbed water and ice nucleation can be identified.

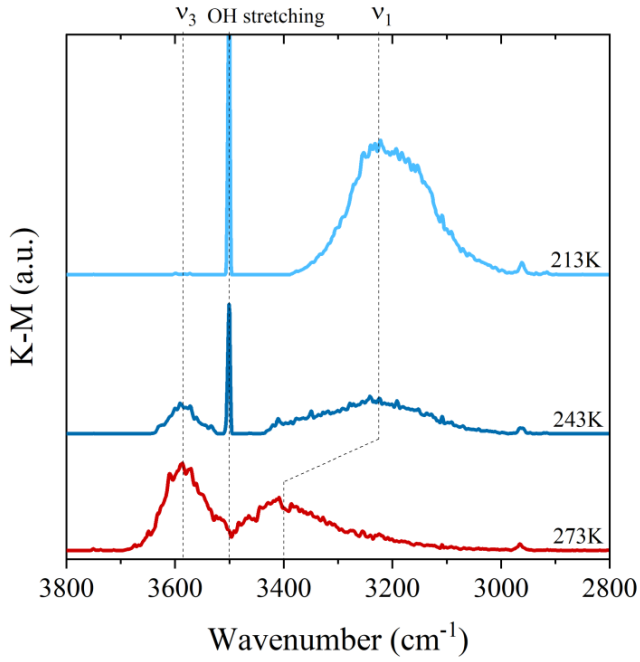


Figure 1. Infrared spectra of adsorbed water on PbI_2 at decreasing temperatures. Temperatures and typical water absorption peaks are marked in the figure. The diffuse reflection was converted to an adsorbent-proportional absorption signal using the Kubelka-Munk function. Note the narrow peak at 3500cm^{-1} in the two upper spectra.

ACKNOWLEDGEMENTS

This work was supported by the Academy of Finland, project MEDICEN (grant no. 345125), and the ACCC Flagship programme (grant no. 337552).

REFERENCES

Barnes, G. T., and R. Sänger (1961). An Investigation into the Mechanism of Ice Crystal Nucleation by Proton Spin Resonance Spectroscopy, *ZAMP*, **12**, 159-163.

Welti, A., Korhonen, K., Miettinen, P., Piedehierro, A. A., Viisanen, Y., Virtanen, A., and A. Laaksonen (2020). SPIN modification for low-temperature experiments, *Atmos. Meas. Tech*., **13**, 7059–7067.

EXPLORING THE ROLE OF AGGREGATION IN BIOLOGICAL ICE-NUCLEATING MACROMOLECULES

F. WIELAND[1] and H. GROTHE[1]

[1] *TU Wien, Institute of Materials Chemistry, Atmospheric physical chemistry, Austria.*

Keywords: ice nucleation, biological, macromolecules, aggregation.

INTRODUCTION

Various aerosols, including mineral dust, soot, and biological particles, can act as ice nuclei and initiate the freezing of supercooled cloud droplets. The freezing of cloud droplets significantly affects cloud properties and, consequently, weather and climate. Homogeneous freezing in cloud droplets occurs around -38°C (Pruppacher 1995). Therefore, ice nuclei can be active between 0°C and -38°C. Some ice nuclei exhibit exceptionally high nucleation temperatures close to 0°C, most of which are biological, making biological ice nucleators of particular interest. Pummer *et al.* (2012; 2015) reported that ice-nucleating macromolecules (INMs) are responsible for the ice-nucleation activity of various bacteria, fungi, and pollen and can often be washed off the respective particle surface. However, the diverse group of biological macromolecules includes a wide variety of substances and lacks a precise definition. In the bacterial species *Pseudomonas syringae,* a membrane-bound protein *InaZ* has been identified as an ice-nucleating agent (Warren and Corotto 1989). Clear evidence is still lacking for many other highly efficient biological ice nucleators. More importantly, it is difficult to identify a common theme in the underlying ice nucleation mechanism of highly efficient biological nucleators due to their diversity and mostly unknown chemical structure. While the idea of tree-based INMs originated from studies on various pollen by Diehl *et al.* (2001; 2002), we found these pollen-based INMs abundant all over the trees' surface for *Betula pendula* and *Pinus sylvestris* species (Seifried et al. 2020; 2023). This suggests that tree-based INMs are abundant in forest areas and represent a large potential source of atmospheric ice nuclei. Our most recent work (Wieland et al. 2025) focused on *Betula pendula* INMs as a proxy to understand the underlying ice nucleation mechanism.

METHODS

We extracted INMs from *Betula pendula* pollen and performed various physical and chemical experiments and analyses. We investigated the ice nucleation activity using two different immersion-freezing ice nucleation assays, namely the twin-plate ice nucleation assay (TINA) and the Vienna optical droplet crystallization assay (VODCA).

Subsequently, we conducted three sets of experiments. The first focused on the behavior of INMs under varying conditions such as freeze-drying, heat-treatments, and freeze-thaw cycles. These experiments specifically focused solely on physical changes to the INMs. In a second set of experiments, we conducted experiments focusing on the size of the INMs, including dynamic light scattering (DLS) and size-selective filtration. In a third set of experiments, we used fluorescence, infrared, and circular dichroism measurements to obtain chemical information about the INMs.

RESULTS

Using our two ice nucleation assays, we identified three distinct ice-nucleation classes within the *Betula pendula* INMs that were active at three discreet ice nucleation temperatures of -8.7°C, -15.7°C, and -17.4°C (see Figure 1).
We then found a correlation between the size, determined by DLS or size-selective filtration, and the onset temperature of ice nucleation, more specifically: The larger the molecules, the higher the onset temperature. Furthermore, the freeze-drying and freeze-thawing experiments suggested that the different sizes were likely aggregates of smaller subunits rather than being different molecules themselves. This is a common theme for biological ice nucleators, as it has been studied for the bacteria *Pseudomonas syringae* (Turner et al. 1990; Southworth et al. 1988; Kozloff et al. 1983) and the fungi *Fusarium acuminatum* (Schwidetzky et al. 2023).

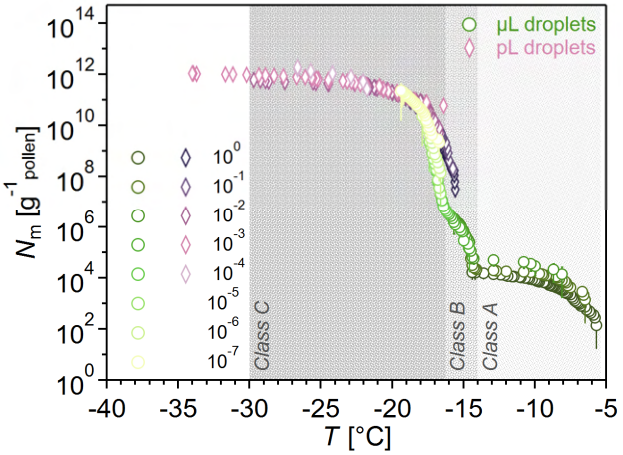


Figure 1. Freezing spectrum of *Betula pendula* INMs from birch pollen washing water (BPWW) measured with two complementary ice nucleation assays, the twin-plate ice nucleation assay (TINA) and the Vienna optical droplet crystallization assay (VODCA) showing three distinct ice nucleation temperatures. Adapted from (Wieland et al. 2025).

CONCLUSIONS

This common theme suggests that the underlying ice-nucleating mechanisms are the same. The popular idea of nucleation sites explains that a larger aggregate has more nucleation sites, leading to higher nucleation temperatures. However, as we present here, *Betula pendula* INMs show three discrete ice nucleation temperatures rather than a continuous transition of ice nucleation temperatures. *Pseudomonas syringae* and *Fusarium acuminatum* show similar behavior as mentioned above.
Combined with the nucleation site theory, this suggests aggregates only form at discreet sizes, which seems rather unlikely. Another explanation could be a different nucleation mechanism that occurs when an aggregate reaches a specific size. According to our understanding, aggregation leading to enhanced ice nucleation activity can be caused by four central physical and chemical reasons. These are water structure on the INM surface, nano-confined geometries, specific water-ordering amino acid motifs, and efficient energy release.
Despite the many questions raised by our studies, this work represents a significant step forward in unraveling the complex nucleation mechanisms of biological ice nuclei.

ACKNOWLEDGEMENTS

We gratefully acknowledge the support from the FFG (Austrian Research Promotion Agency) for funding as part of project no. 888109 (Lab on a Drone).

REFERENCES

Diehl, K., S. Matthias-Maser, R. Jaenicke, and S. K. Mitra. 2002. 'The Ice Nucleating Ability of Pollen: Part II. Laboratory Studies in Immersion and Contact Freezing Modes'. *Atmospheric Research* 61 (2).

Diehl, K., C. Quick, S. Matthias-Maser, S. K. Mitra, and R. Jaenicke. 2001. 'The Ice Nucleating Ability of Pollen Part I: Laboratory Studies in Deposition and Condensation Freezing Modes'. *Atmospheric Research* 58 (2).

Kozloff, L M, M A Schofield, and M Lute. 1983. 'Ice Nucleating Activity of Pseudomonas Syringae and Erwinia Herbicola'. *Journal of Bacteriology* 153 (1): 222–31.

Pruppacher, H. R. 1995. 'A New Look at Homogeneous Ice Nucleation in Supercooled Water Drops', June.

Pummer, B. G., H. Bauer, J. Bernardi, S. Bleicher, and H. Grothe. 2012. 'Suspendable Macromolecules Are Responsible for Ice Nucleation Activity of Birch and Conifer Pollen'. *Atmospheric Chemistry and Physics* 12 (5).

Pummer, B. G., C. Budke, S. Augustin-Bauditz, D. Niedermeier, L. Felgitsch, C. J. Kampf, R. G. Huber, et al. 2015. 'Ice Nucleation by Water-Soluble Macromolecules'. *Atmospheric Chemistry and Physics* 15 (8).

Schwidetzky, Ralph, Ingrid de Almeida Ribeiro, Nadine Bothen, Anna T. Backes, Arthur L. DeVries, Mischa Bonn, Janine Fröhlich-Nowoisky, Valeria Molinero, and Konrad Meister. 2023. 'Functional Aggregation of Cell-Free Proteins Enables Fungal Ice Nucleation'. *Proceedings of the National Academy of Sciences* 120 (46): e2303243120.

Seifried, Teresa M., Paul Bieber, Laura Felgitsch, Julian Vlasich, Florian Reyzek, David G. Schmale, and Hinrich Grothe. 2020. 'Surfaces of Silver Birch (*Betula Pendula*) Are Sources of Biological Ice Nuclei: In Vivo and in Situ Investigations'. *Biogeosciences* 17 (22).

Seifried, Teresa M., Florian Reyzek, Paul Bieber, and Hinrich Grothe. 2023. 'Scots Pines (*Pinus Sylvestris*) as Sources of Biological Ice-Nucleating Macromolecules (INMs)'. *Atmosphere* 14 (2): 266.

Southworth, M W, P K Wolber, and G J Warren. 1988. 'Nonlinear Relationship between Concentration and Activity of a Bacterial Ice Nucleation Protein.' *Journal of Biological Chemistry* 263 (29): 15211–16.

Turner, M A, F Arellano, and L M Kozloff. 1990. 'Three Separate Classes of Bacterial Ice Nucleation Structures'. *Journal of Bacteriology* 172 (5): 2521–26.

Warren, Gareth, and Loren Corotto. 1989. 'The Consensus Sequence of Ice Nucleation Proteins from *Erwinia Herbicola, Pseudomonas Fluorescens* and *Pseudomonas Syringae*'. *Gene* 85 (1): 239–42.

Wieland, Florian, Nadine Bothen, Ralph Schwidetzky, Teresa M. Seifried, Paul Bieber, Ulrich Pöschl, Konrad Meister, Mischa Bonn, Janine Fröhlich-Nowoisky, and Hinrich Grothe. 2025. 'Aggregation of Ice-Nucleating Macromolecules from *Betula Pendula* Pollen Determines Ice Nucleation Efficiency'. *Biogeosciences* 22 (1): 103–15.

SINGLE-PARTICLE ICE-NUCLEATING PARTICLE (INP) CHARACTERIZATION AT MIXED-PHASE AND ICE CLOUD CONDITIONS AT THE HIGH-ALTITUDE STATION JUNGFRAUJOCH (3580 M A.S.L.), SWITZERLAND

CUIQI ZHANG[1], XIAOLI SHEN[2], JUSTIN L. JACQUOT[2], LARISSA LACHER[3], BENJAMIN T. BREM[4], ROBIN L. MODINI[4], VISHNUPRIYA SELVAKUMAR[1], MICHAEL SPRENGER[1], MARTIN STEINBACHER[5], STEPHAN HENNE[5], MARTINE COLLAUD COEN[6], FRANZ CONEN[7], KRISTINA HÖHLER[3], OTTMAR MÖHLER[3], MARTIN GYSEL-BEER[4], DANIEL J. CZICZO[2], AND ZAMIN A. KANJI[1]

[1]*Institute for Atmospheric and Climate Sciences, D-USYS, ETH Zurich, 8092 Zurich, Switzerland.*

[2]*Department of Earth, Atmospheric, and Planetary Sciences, Purdue University, West Lafayette, 47907, Indiana, USA.*

[3]*Institute of Meteorology and Climate Research Atmospheric Aerosol Research, Karlsruhe Institute of Technology, 76344 Eggenstein-Leopoldshafen, Germany.*

[4]*PSI Center for Energy and Environmental Sciences, 5232 Villigen PSI, Switzerland.*

[5]*Empa, Swiss Federal Laboratories for Materials Science and Technology, 8600 Dübendorf, Switzerland.*

[6]*Federal Office of Meteorology and Climatology, MeteoSwiss, 1530 Payerne, Switzerland.*

[7]*Department of Environmental Sciences, University of Basel, 4056 Basel, Switzerland.*

Keywords: ICE-NUCLEATING PARTICLE, SINGLE PARTICLE MASS SPECTROMETRY, PUMPED COUNTERFLOW VIRTUAL IMPACTOR, MIXED-PHASE CLOUDS, ICE CLOUDS.

INTRODUCTION

A scarce fraction of atmospheric aerosol particles (1 in 10^5 at -20 ℃) can act as ice-nucleating particles (INPs), which can facilitate primary ice crystal formation in clouds between -38 and 0 ℃ to form mixed-phase clouds, or below -38 ℃ to contribute to ice cloud formation. Modification of cloud phase by INPs can lead to changes in cloud radiative properties and cloud lifetime, which affect global precipitation distribution and energy budget (e.g., Fan et al., 2017; Storelvmo, 2017).

In previous field observations at the high-altitude station Jungfraujoch (JFJ) located in the Swiss Alps, atmospheric INP number concentration (N_{INP}) were correlated with aerosol particle properties obtained from in-situ measurements (e.g., Lacher et al., 2021) or remote sensing retrievals (e.g., Brunner et al., 2021) to infer the chemical species and sources of INPs. In Brunner et al. (2021), it was shown that the dominant INP over a full year of measurements was mineral dust. Even in the absence of Saharan dust events at the field site, the background aerosol particles contributing to immersion INPs at -30 ℃ were >95% coming from dust. In this work, we specifically characterize the chemical composition and identify the source of ambient INPs at temperatures (T) and relative humidity (RH) corresponding to mixed-phase cloud (T = -30 °C, RH_w = 104%) and ice cloud (T = -40 °C, RH_w = 90%) conditions during a measurement campaign conducted at the JFJ from Jan. 22 to Feb. 14 in 2024.

METHODS

A schematic of the experimental setup is shown in Fig. 1. Ambient air was sampled through a total aerosol inlet, which is 2 m above the roof of the Sphinx Observatory at JFJ (46.33° N, 7.59° E, 3580 m a.s.l.). The

inlet was maintained at 35 °C to prevent ice accumulation and to evaporate cloud droplets at an early stage (Weingartner et al., 1999). The sample flow was then split and pumped to different instruments.

Single-particle INP characterization was achieved by coupling the Automated Horizontal Ice Nucleation Chamber (HINC-Auto, Brunner and Kanji, 2021), Pumped Counterflow Virtual Impactor (PCVI; BMI Model 8100; Boulter et al., 2006), Particle Analysis by Laser Mass Spectrometry-Next Generation (PALMS-NG, Jacquot et al., 2024), and Ultra High Sensitivity Aerosol Spectrometer (UHSAS; DMT), shown as blue solid line in Fig. 1. Ambient INPs were first activated into ice crystals within HINC-Auto under fixed thermodynamic conditions to simulate mixed-phase and ice clouds. Upon exiting HINC-Auto chamber, the ice crystals were separated from liquid droplets and non-activated aerosol particles within a PCVI due to their inertial difference. After sublimating the ice crystals at room temperature, these activated INPs were introduced into PALMS-NG and UHSAS, where their chemical composition and size distribution were measured, respectively.

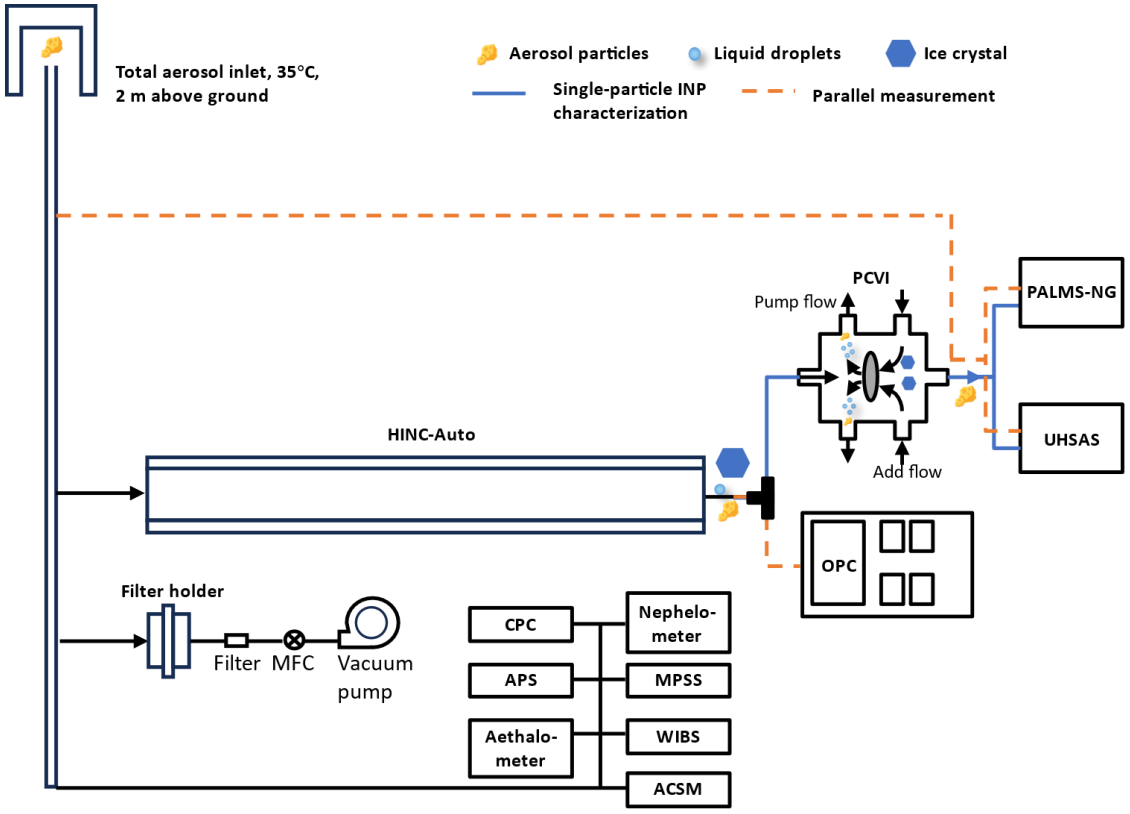


Figure 1. Schematic of the experimental setup (not drawn to scale). HINC-Auto: Automated Horizontal Ice Nucleation Chamber; PCVI: Pumped Counterflow Virtual Impactor; PALMS-NG: Particle Analysis by Laser Mass Spectrometry - Next Generation; UHSAS: Ultra-High Sensitivity Aerosol Spectrometer; OPC: Optical Particle Counter; MFC: Mass Flow Controller; APS: Aerodynamic Particle Sizer; CPC: Condensation Particle Counter; MPSS: Mobility Particle Size Spectrometers; WIBS: Wideband Integrated Bioaerosol Sensor; ACSM: Aerosol Chemical Speciation Monitor.

Continuous aerosol measurements at JFJ are part of the Aerosol, Clouds, and Trace gases Research InfraStructure (ACTRIS). Aerosol properties, including size distribution, total number concentration, absorption and scattering, as well as bulk chemical composition, have been measured by PSI. Reactive trace gases, such as ozone and carbon monoxide, have been measured by Empa as part of the operation of the Swiss National Air Pollution Monitoring Network (NABEL) and the Integrated Carbon Observation System Research Infrastructure (ICOS RI). The Ice Nucleation Spectrometer of the Karlsruhe Institute of Technology (INSEKT, Schneider et al. 2021) determined the N_{INP} in the temperature range above -25 °C

while online INP measurements conducted with HINC-Auto focused on -30 and -40 °C for immersion freezing and deposition nucleation respectively. The black solid lines and the orange dashed lines in Fig. 1 denote the ambient aerosol characterization, when all instruments were directly connected to the total aerosol inlet and ran in parallel.

Meteorology parameters have been measured operationally by MeteoSwiss, including wind speed, wind direction, *RH*, and *T*. Radon-222 has been measured by the University of Basel at JFJ since 2009, and could serve as an indicator for boundary layer influence (Griffiths et al., 2014). Due to its altitude, JFJ is in the free troposphere for a majority of the time in winter, with occasional boundary layer injections during daytime.

CONCLUSIONS

We characterized the chemical composition of ambient aerosol particles and grouped them into five classes (Fig. 2). The fraction of activated ambient INPs at different thermodynamic conditions was obtained based on the direct chemical composition measurement of the ice residuals (Fig. 3).

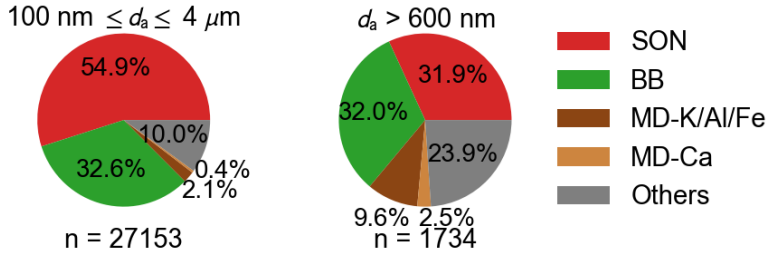


Figure 2. Number fraction of ambient aerosol particle categories with different aerodynamic diameter d_a: 100 nm ≤ d_a ≤ 4 μm (left), and 600 nm < d_a ≤ 4 μm (right). SON – sulfate, organics, and nitrate; BB – biomass burning; MD – mineral dust; MD-K/Al/Fe – MD with high K/Al/Fe signal; MD-Ca – MD with high Ca signal

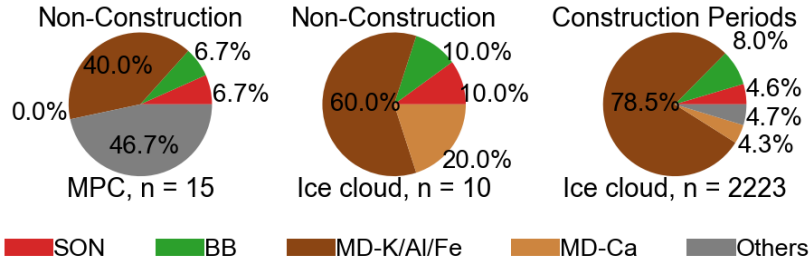


Figure 3. Number fraction of activated ambient INPs with 600 nm ≤ d_a ≤ 4 μm during non-construction periods after processing at T = -30 °C, RH_w = 104% (left) and T = -40 °C, RH_w = 90% (middle), and during construction periods after processing at T = -40 °C, RH_w = 90% (right).

We observed that mineral dust particles were an important source of ice-nucleating particles at both mixed-phase (T = -30 °C, RH_w = 104%) and ice cloud (T = -40 °C, RH_w = 90%) conditions. It is worth noting that the mineral dust particles had two sub-classes, i.e., with high K/Al/Fe (MD-K/Al/Fe) and high Ca (MD-Ca) signal. During our measurement period, construction activities at the field site were a major source of MD- K/Al/Fe. Local construction dust particles (MD-K/Al/Fe) emitted at high altitude acted as effective depositional INP. During the mixed-phase (T = -30 °C, RH_w = 104%) processing experiments, there was no construction activity, but we still sampled MD-K/Al/Fe. The source of these mineral dust particles is still under investigation in combination of back-trajectory calculation.

Sulfate, organics, and nitrate aerosol particles, as well as biomass burning aerosol particles, got depleted downstream of the PCVI, indicating their low ice nucleation activity after both mixed-phase and ice cloud processing.

ACKNOWLEDGEMENTS

This work was supported by ACTRIS-CH through SERI, GAW-CH through MeteoSwiss, and ATMO-ACCESS TNA.

REFERENCES

Boulter, J. E., Cziczo, D. J., Middlebrook, A. M., Thomson, D. S., and Murphy, D. M. (2006). Design and Performance of a Pumped Counterflow Virtual Impactor, *Aerosol Sci. Technol.* **40**, 969-976.

Brunner, C., Brem, B. T., Collaud Coen, M., Conen, F., Hervo, M., Henne, S., Steinbacher, M., Gysel-Beer, M., and Kanji, Z. A. (2021). The contribution of Saharan dust to the ice-nucleating particle concentrations at the High Altitude Station Jungfraujoch (3580 m a.s.l.), Switzerland, *Atmos. Chem. Phys.* **21**, 18029-18053.

Brunner, C., and Kanji, Z. A. (2021). Continuous online monitoring of ice-nucleating particles: development of the automated Horizontal Ice Nucleation Chamber (HINC-Auto), *Atmos. Meas. Tech.* **14**, 269-293.

Fan, J., Leung, L. R., Rosenfeld, D., and DeMott, P. J. (2017). Effects of cloud condensation nuclei and ice nucleating particles on precipitation processes and supercooled liquid in mixed-phase orographic clouds, *Atmos. Chem. Phys.* **17**, 1017-1035.

Griffiths, A. D., Conen, F., Weingartner, E., Zimmermann, L., Chambers, S. D., Williams, A. G., and Steinbacher, M. (2014). Surface-to-mountaintop transport characterised by radon observations at the Jungfraujoch, *Atmos. Chem. Phys.* **14**, 12763-12779.

Jacquot, J. L., Shen, X., Abou-Ghanem, M., Froyd, K. D., Lawler, M., Schill, G. P., Slovacek, K., Thomson, D. S., Cziczo, D. J., and Murphy, D. M. (2024). A new airborne single particle mass spectrometer: PALMS-NG, *Aerosol Sci. Technol.*, 58, 991–1007.

Lacher, L., Clemen, H. C., Shen, X., Mertes, S., Gysel-Beer, M., Moallemi, A., Steinbacher, M., Henne, S., Saathoff, H., Möhler, O., Höhler, K., Schiebel, T., Weber, D., Schrod, J., Schneider, J., and Kanji, Z. A. (2021). Sources and nature of ice-nucleating particles in the free troposphere at Jungfraujoch in winter 2017, *Atmos. Chem. Phys.* **21**, 16925-16953.

Storelvmo, T. (2017). Aerosol Effects on Climate via Mixed-Phase and Ice Clouds, *Annu. Rev. Earth Planet. Sci.* **45**, 199-222.

Weingartner, E., Nyeki, S., and Baltensperger, U. (1999). Seasonal and diurnal variation of aerosol size distributions (10<D<750 nm) at a high-alpine site (Jungfraujoch 3580 m asl), *J. Geophys. Res. Atmos.* **104**, 26809-26820.

Main Topic 4: Aerosol-Climate Interactions

INFLUENCE OF AIR PARCEL HISTORY ON THE THERMODYNAMIC PHASE OF LOW-LEVEL ARCTIC CLOUDS

L. CASTIN[1], Q. COOPMAN[1], A. DZIDUCH[2], O. JOURDAN[2] and J. RIEDI[1]

[1]*Univ. Lille, CNRS, UMR 8518 - LOA - Laboratoire d'Optique Atmosphérique, F-59000 Lille, France*

[2]*Université Clermont Auvergne, Laboratoire de Météorologie Physique, 63000 Clermont-Ferrand, France*

Keywords: Arctic, aerosol-cloud interactions, back trajectory, mixed-phase clouds, ice nucleation, space-based measurements

INTRODUCTION

The Arctic is warming at unprecedented rates, yet climate models struggle to represent key processes like aerosol-cloud interactions - particularly in polar regions. The evolution of the thermodynamic phase of arctic clouds and the impact of aerosols, which can act as ice-nucleating particles, remain poorly understood due to complex microphysical processes. Previous studies often co-locate cloud phases to aerosol content, ignoring the physico-chemical modifications of the air parcel during long-range transport. We propose analysing trajectories of aerosols before cloud observation - a novel approach to unravel how aerosol transport pathways and ageing can determine cloud phase transitions.

METHODS

Our study builds upon the work of Mioche et al. (2015) and Dziduch et al. (2025), focusing on low-level clouds at altitudes lower than 3000 m. Our dataset uses DARDAR retrieval products, based on the synergy of the data from the Cloud-Aerosol Lidar with Orthogonal Polarization (CALIOP) and the CloudSat Cloud Profiling Radar (CPR), both part of the "A-Train" constellation. Cloud thermodynamic phases are derived from DARDAR-MASKv2 products (Ceccaldi et al. 2013), in which each atmospheric pixel (60 m vertically, 1.7 km along track) is assigned to a specific class (e.g. warm rain, clear sky or ice cloud).

We use DARDAR-SOCP classification algorithm (Bazantay et al. 2024) : if there are at least three vertical adjacent cloudy pixels in the DARDAR-MASK product, then a cloud event is counted and added in our dataset. Our analysis region spans from 60°N to 82°N, with a spatial resolution of 0.5° by 0.5°. We discriminate clouds into five categories, excluding warm clouds (above 0°C): ice clouds, unglaciated supercooled liquid clouds, and three types of mixed-phase clouds based on the top pixel class, (i) ice, (ii) supercooled + ice, or (iii) supercooled.

Our objective is to compare air parcel pathways before observations of clouds which are in similar meteorological states but different categories. In order to do that, three basic meteorological quantities have been identified as being correlated with cloud microphysical properties (Matsui et al., 2006; Mauger and Norris, 2007): lower tropospheric stability (LTS), specific humidity (SH), and temperature. We first constrain for LTS and SH distributions.

With this constrained dataset, we are left with hundreds of thousands of pixels in which a cloud was observed by CALIPSO and CloudSat. For each pixel, we compute a 120-hour back trajectory that starts at the centre of the pixel and at the cloud top altitude using NOAA's Hybrid Single-Particle Lagrangian Integrated Trajectory model (HYSPLIT) with the National Centers for Environmental Prediction and National Center for Atmospheric Research (NCEP/NCAR) reanalysis as input meteorological data.

We co-locate along the back trajectories several parameters: sea ice concentration from the Advanced Microwave Scanning Radiometer satellite observations (AMSR2), meteorological parameters from the European Centre for Medium-Range Weather Forecasts Reanalysis v5 (ERA5) and aerosol mixing ratios from the Modern-Era Retrospective analysis for Research and Applications, v2 (MERRA2). This results in a robust dataset with hourly information on the surface below the air parcel, its meteorological state, and aerosol content. Our goal is to analyse clouds within the same temperature bin and understand which parameters (e.g. aerosols) influence the most the thermodynamic phase of clouds that are in a similar meteorological state.

RESULTS

Our initial findings show that during the transport of air parcels, the three key meteorological parameters (LTS, SH, and temperature) evolve similarly for all cloud categories. We constrained these three parameters for t=0, but it is significant to note that during the days before cloud observation, the air parcels were already in a similar meteorological state. This suggests that the differences in cloud thermodynamic phases are likely due to non-meteorological factors.

When examining the dust mixing ratio over time, we observe a consistent offset between air parcels that will form ice clouds and those that will become supercooled clouds at the time of CALIPSO/CloudSat observation. The dust content in air parcels that will form ice clouds is approximately 40% higher than in those that will become supercooled clouds. This parameter might have an influence on the thermodynamic phase of the observed clouds but since this offset remains constant along the trajectories, it indicates minimal impact from transport.

For other parameters, such as sea salt, the offset between cloud categories varies over time. Five days before observation, the sea salt content in parcels that will become mixed-phase clouds is similar to that in parcels that will form ice clouds. However, during the trajectory, the sea salt content in parcels that will become mixed-phase clouds increases, while it remains constant in those that will form ice clouds. This suggests that sea salt content influences the thermodynamic phase of air parcels under similar meteorological conditions and that transport plays a role in this process.

In summary, some aerosol parameters, like dust, exhibit consistent behaviour with minimal transport impact, while others, such as sea salt, show dynamic changes influenced by transport. Both types of parameters may affect the thermodynamic phases of Arctic clouds. Further thorough analysis is necessary to fully understand the role of each parameter.

ACKNOWLEDGMENTS

This project was funded by Université de Lille and by the (MPC)² project supported by the French Agence Nationale de la Recherche under the grant ANR-22-CE01-0009. We would like to acknowledge LaMP and AERIS/ICARE for providing the data. Finally, we gratefully acknowledge the NOAA Air Resources Laboratory (ARL) for the provision of the HYSPLIT transport and dispersion model used in this publication.

REFERENCES

Bazantay, C., O. Jourdan, G. Mioche, J. Uitz, A. Dziduch, J. Delanoë, Q. Cazenave, R. Sauzède, A. Protat, and K. Sellegri (2024). *Relating Ocean Biogeochemistry and Low-Level Cloud Properties Over the Southern Oceans*, Geophysical Research Letters, 51(10).

Ceccaldi, M., J. Delanoë, R. J. Hogan, N. L. Pounder, A. Protat, and J. Pelon (2013). *From CloudSat-CALIPSO to EarthCare: Evolution of the DARDAR Cloud Classification and Its Comparison to Airborne Radar-Lidar Observations*, Journal of Geophysical Research: Atmospheres, 118(14), 7962-81.

Delanoë, J., and R. J. Hogan (2010). *Combined CloudSat-CALIPSO-MODIS Retrievals of the Properties of Ice Clouds*, Journal of Geophysical Research: Atmospheres 115(4) .

Dziduch, A., G. Mioche, Q. Coopman, C. Bazantay, J. Delanoë, and O. Jourdan (2025). *Environmental Drivers of Arctic Low-Level Clouds: Analysis of the Regional Dependencies Using Space-Based Lidar and Radar*.

Matsui, T., H. Masunaga, S. M. Kreidenweis, R. A. Pielke Sr., W.-K. Tao, M. Chin, and Y. J. Kaufman (2006). *Satellite-Based Assessment of Marine Low Cloud Variability Associated with Aerosol, Atmospheric Stability, and the Diurnal Cycle*, Journal of Geophysical Research: Atmospheres, 111(D17).

Mauger, G. S., and J. R. Norris (2007). *Meteorological Bias in Satellite Estimates of Aerosol-Cloud Relationships*, Geophysical Research Letters, 34(16).

Mioche, G., O. Jourdan, M. Ceccaldi, and J. Delanoë (2015). *Variability of Mixed-Phase Clouds in the Arctic with a Focus on the Svalbard Region: A Study Based on Spaceborne Active Remote Sensing*, Atmospheric Chemistry and Physics, 15(5), 2445-61.

Stein, A. F., R. R. Draxler, G. D. Rolph, B. J. B. Stunder, M. D. Cohen, and F. Ngan (2015). *NOAA's HYSPLIT Atmospheric Transport and Dispersion Modeling System*, Bulletin of the American Meteorological Society, 96(12), 2059-77.

DEVELOPMENT OF MACHINE LEARNING MODEL TO PREDICT CCN NUMBER CONCENTATION IN THE ARCTIC

H. CHO[1], H. KANG[2], Y. YOON[2], K. PARK[1]

[1]*Department of and Environment and Energy Engineering, Gwangju Institute of Science and Technology,*

123 Cheomdangwagiro, Buk-gu, Gwangju, Republic of Korea

[2]*Korea Polar Research Institute, Incheon, Republic of Korea*

Keywords: CCN, NPF, MACHINE LEARNING, PREDCTION, ARCTIC

INTRODUCTION

Cloud condensation nuclei (CCN) are crucial for the Arctic cloud formation and climate system, influencing cloud persistence, surface energy balance, and sea ice extent (Sterzinger et al., 2024). In the Arctic, relatively low aerosol concentrations exist to become the CCN, and new particle formation (NPF) can be considered as one of important factors to enhance the CCN level under various environmental conditions. The CCN prediction models from routine measurement parameters should be so useful to predict CCN at the region with extreme conditions like the Arctic where the measurement is so difficult, and to better understand complex interactions among aerosols, meteorological variables, and CCN. In this study, various measurement parameters such as meteorological variables, NPF parameters, and gases obtained from the Arctic site were used to train and test various machine learning models. The non-linear machine learning models should be so useful to determine important factors and to understand their interactions, affecting the CCN number concentration. Several feature selection procedures have been conducted to find the most important features and to minimize multi-collinearity among features, and then model evaluation and interpretation have been conducted with explainable AI techniques.

METHODS

The Arctic site (Zeppelin observatory) is located in Ny-Ålesund, Svalbard, Norway (78.54°N and 11.53°E). The CCN number concentrations were measured by using the CCN counter (CCNC: CCN-100, Droplet Measurement Technologies, USA) at five different super-saturation levels of 0.2%, 0.4%, 0.6%, 0.8%, and 1.0% every 30 mins. The number size distribution of particles from 3 nm to 60 nm was measured with the nano-scanning mobility particle sizer (SMPS) consisting of a nano-differential mobility analyzer (nano-DMA) (model 3085, TSI, USA) and a condensation particle counter (CPC) (model 3776, TSI, USA). Gas data (NH_3 and SO_2) and meteorological parameters (solar radiation (SRAD), temperature (T), relative humidity (RH), wind, and pressure) were obtained from the Norwegian National Monitoring Program site via the EBAS database (http://ebas.nilu.no/). The concentrations of ionic species (Na^+, Mg^{2+}, K^+, NH_4^+, NO_3^-, SO_4^{2-}, and Cl^-) in particulate matter less than 10 μm (PM10) were also obtained from the database. The site information including sampling periods (2018-2022) has been described in details in the previous study (Lee et al., 2020).

The minimum redundancy maximum relevance (mRMR) and the feature importance in tree-based feature selection procedure were employed to find the best input features. The first selected features were growth rate of 3-25 nm particles ($GR_{3\text{-}25}$) during NPF event days, T, pressure, RH, SRAD, wind speed, wind direction, SO_2, and NH_3. The measurement data were randomly divided into training dataset (80%) and testing dataset (20%), and used five-fold cross validation. The machine learning models employed here include decision tree regression (DT), random forest regression (RF), gradient boosting regression (GBM), general linear regression (GLM), and ensemble (GBM + RF). The schematic for the whole methodology is shown in Figure 1.

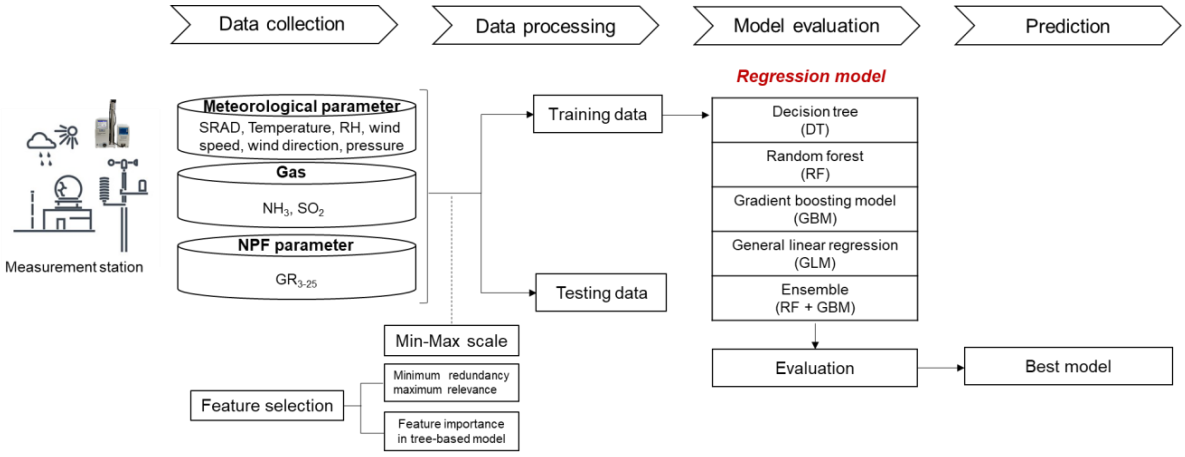


Figure 1. A schematic of CCN prediction models by using machine learning methods.

CONCLUSIONS

We evaluated five different machine learning models to predict the CCN number concentrations from the SRAD, RH, pressure, NH_3 and $GR_{3\text{-}25}$. The ensemble model (92%) was found to be best model to predict the CCN number concentration as shown in Figure 2. The random forest model also had a good performance. Further selection of various combinations of features including NPF parameters and employment of explainable AI techniques are being conducted in the future.

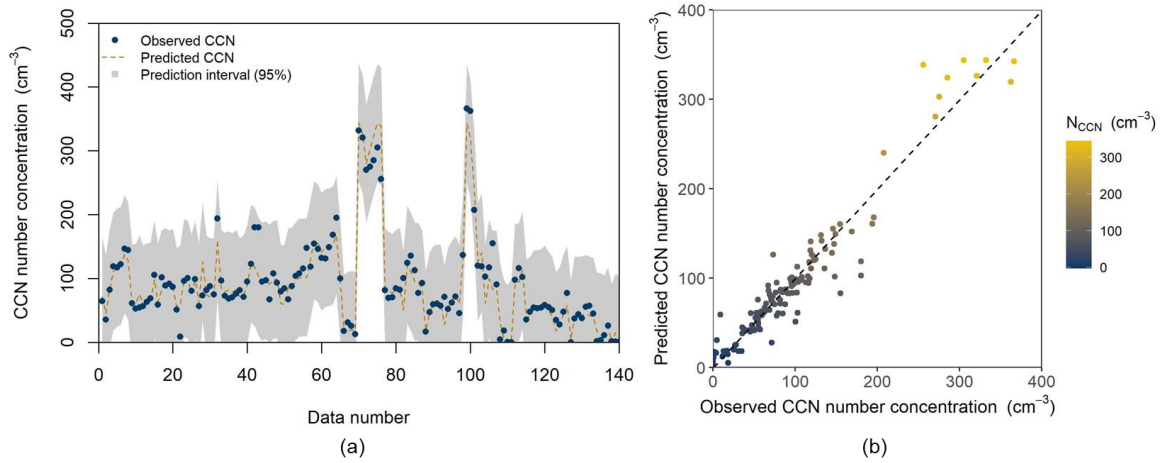


Figure 2. (a) Time series of predicted (ensemble model) and measured CCN number concentrations and (b) relationship between predicted and measured CCN number concentrations.

ACKNOWLEDGEMENTS

This research was supported by a National Research Foundation of Korea Grant from the Korean Government (MSIT; the Ministry of Science and ICT) (NRF-2021M1A5A1065667) (KOPRI-PN21011), and Samsung Advanced Institute of Technology (SAIT).

REFERENCES

Sterzinger, L.J. and A.L. Igel (2024). Above-cloud concentrations of cloud condensation nuclei help to sustain some Arctic low-level clouds, Atmos. Chem. Phys. 24, 3529–3540. https://doi.org/10.5194/acp-24-3529-2024.

Lee, H., Lee, K., Lunder, C. R., Krejci, R., Aas, W., Park, J., Park, K.-T., Lee, B. Y., Yoon, Y. J., and Park, K.: Atmospheric new particle formation characteristics in the Arctic as measured at Mount Zeppelin, Svalbard, from 2016 to 2018, Atmos. Chem. Phys., 20, 13425–13441, https://doi.org/10.5194/acp-20-13425-2020, 2020.

The Influence of Various Aerosol Types on Cloud microphysical processes: An Examination of Arctic Aerosol-Cloud Interactions in Relation to WRF-Chem Parameterization Sensitivity.

P. FATTAHI MASROUR, Q. COOPMAN

Univ. Lille, CNRS, UMR 8518 - LOA - Laboratoire d'Optique Atmosphérique, F-59000 Lille, France

Keywords: AEROSOL-CLOUD INTERACTION, ARCTIC, WRF_CHEM, AEROSOL TYPES, RADIATIVE FEEDBACK, CLOUD PARAMETERIZATION, MODEL SENTIVITY.

INTRODUCTION

The Arctic is one of the most climate-sensitive places on Earth, with warming rates more than double the world average known as the Arctic amplification (Rantanen et al., 2022). This rapid warming is influenced by intricate interactions among radiation, clouds, and aerosols (Schmale et al., 2021).

Aerosols serve as cloud condensation nuclei (CCN) or ice nucleating particles (INP) and influence cloud properties such as droplet size, albedo and lifetime, which in turn influence the Arctic's radiation balance (Abbatt et al., 2019). Changes in Arctic cloud cover are crucial for managing the region's energy balance because they modulate both shortwave and long-wave radiation. Because of the naturally low background levels of CCN in the Arctic, clouds are especially sensitive to changes in aerosol concentrations. According to studies, Arctic clouds are essential for controlling surface heat exchange, and low-level clouds have a major impact on the long-wave radiation effects that control atmospheric dynamics and ice melt (Eirund et al., 2019). Study by van den Heever et al. (2006) showed that the precipitation increases as the IN-value increases. However, some studies have shown that IN does not significantly influence the intensity of convection (Connolly et al., 2006; Yin and Chen, 2007), but it does have a significant effect on the microphysical properties of clouds and leads to their increased brightness (Fan et al., 2010).

Arctic aerosol sources include long-range pollution transfer from mid-latitudes, marine biogenic emissions, and growing local sources (e.g., ship traffic; Stapf et al., 2020). These aerosols affect clouds more or less efficiently depending on their composition and concentration, causing differences in cloud optical depth and thermodynamic phase partitioning between liquid and ice clouds (Filioglou et al., 2019). For example, high aerosol loading can increase cloud optical thickness, enhancing cloud reflectivity and contributing to a warming effect due to trapped long-wave radiation (Sterzinger et al., 2022). In pristine Arctic conditions, mixed-phase clouds are more prone to glaciation, which can contribute to higher precipitation and cloud dissipation (Karlsson et al., 2022). Despite improvements in observational and modeling methodologies, major uncertainties remain in determining these processes because to the complexity of aerosol-cloud interactions and limited in situ data (Petäjä et al., 2022). Addressing these knowledge gaps is critical for enhancing climate models and producing more accurate projections of Arctic climate change under future emission scenarios (Gordon et al., 2023).

Weather Research and Forecasting model with Chemistry (WRF-Chem) is a regional atmospheric model which simultaneously simulates meteorological and chemical processes and is thus apt for the study of aerosol-cloud interactions in the Arctic (Grell et al., 2005). Because of the extreme sensitivity of the Arctic to aerosol perturbations and the complex microphysics of clouds, WRF-Chem provides researchers with a unique opportunity for integrating dynamical, physical, and chemical processes in order to better represent aerosol emissions, transport, and deposition (Fast et al., 2006).

METHODS

Aerosol-cloud interactions in atmospheric models must be improved with knowledge of the Arctic region's distinct climate sensitivity, wherein mixed-phase clouds and aerosols transported over long distances substantially affect energy balance. The study shall address the influence of different aerosol types, such as sulfate, black carbon, sea salt, and organics, on two important aspects of cloud microphysics, namely cloud droplet activation and ice nucleation in relation to the partitioning of cloud phases. The project will also include evaluations of the radiative effects under both anthropogenic and natural aerosol scenarii while factoring in their contributions to cloud albedo, cloud lifetime, and surface energy balance.

The present study presents several innovations that distinguish it from the earlier research. Firstly, it will use a multi-scheme comparison approach that thoroughly assesses the performance of different WRF-Chem microphysics schemes (Morrison and Thompson-Eidhammer) alongside aerosol chemistry models (MOSAIC, CBMZ, and SORGAM) in modeling Arctic aerosol-cloud interaction. This approach will allow a detailed appraisal of how parameterization choices affect the model performance, a significant uncertainty in climate predictions. This research will specifically focus on the climatic effects due to the longwave and shortwave responses related to aerosol cloud modifications in the Arctic. In the process, the objective is to gain insight into the cloud radiative forcing mechanisms in the rapidly warming Arctic. With respect to that, by inspecting aerosol-cloud-radiation interactions under different pollution scenarii, this study aims to provide relevant information for improving aerosol-cloud interaction representations in models.

In addition, this research will eventually address the role of the secondary organic aerosol (SOA) and their impact on cloud formation in the Arctic, which has not been a widely studied subject. Using SORGAM together with WRF-Chem will provide novel evidence on the roles of both biogenic and anthropogenic SOAs in CCN and INP concentrations. This work is fundamental for the formation and lifetime of clouds in both pristine and polluted Arctic regions. Considering the importance of clouds in Arctic climate dynamics, understanding aerosol-cloud interaction through fine-scale modeling approaches like WRF-Chem will greatly reduce uncertainty in climate prediction and inform mitigation strategies.

CONCLUSIONS

Aerosol changes can produce complex effects on cloud formation and radiation in the Arctic. The alteration of the chemical composition of aerosols in these regions can exert a profound influence on radiation and alter cloud nature. This effect is most pronounced in regions with extreme variations in humidity and specific weather conditions. Recent research, for instance, has demonstrated that a higher supercooling needed for cloud freezing is correlated with smaller cloud droplet sizes. Pollution plumes, however, drastically lower the amount of supercooling needed for freezing, even though there is a noticeable decrease in cloud cover in polluted air (Coopman et al., 2018). Therefore, precise modeling of cloud microphysics and their interactions with aerosols is necessary to understand how aerosols affect radiation and precipitation.

Both the Morrison scheme, with two-moment cloud microphysics, and the Thompson-Eidheimer scheme, with finer aerosol activation processes, are suitable for this. At the same time, aerosol schemes such as MOSAIC, with multispecies aerosol tracking, provide a more comprehensive aerosol-cloud treatment, while CBMZ and SORGAM provide computationally less expensive alternatives to investigate organic and simple aerosol processes. By comparing these models, we can find the best setting for simulating the effect of aerosols such as black carbon and sulfate on cloud characteristics and radiative forcing in the Arctic. The accuracy of such models can be tested by comparison of cloud microphysical properties, aerosol activation,

and radiative forcing within the Arctic atmosphere. We are able to gain further insight into how aerosols affect Arctic clouds, which in turn can lead to more accurate climate models and better projections of the region's response to global change.

ACKNOWLEDGEMENTS

This work was supported by the University of Lille and (MPC)² project supported by the French Agence Nationale de la Recherche under the grant ANR-22-CEO1-0009.

REFERENCES

Abbatt, J. P., Leaitch, W. R., Aliabadi, A. A., Bertram, A. K., Blanchet, J. P., Boivin-Rioux, A., ... & Yakobi-Hancock, J. D. (2019). Overview paper: New insights into aerosol and climate in the Arctic, *Atmospheric Chemistry and Physics 19*(4), 2527-2560.

Coopman, Q., Garrett, T. J., Finch, D. P., & Riedi, J. (2018). High sensitivity of Arctic liquid clouds to long-range anthropogenic aerosol transport, *Geophysical Research Letters*, *45*(1), 372-381.

Connolly, P. J., Choularton, T. W., Gallagher, M. W., Bower, K. N., Flynn, M. J., & Whiteway, J. A. (2006). Cloud-resolving simulations of intense tropical Hector thunderstorms: Implications for aerosol–cloud interactions, *Quarterly Journal of the Royal Meteorological Society: A journal of the atmospheric sciences, applied meteorology and physical oceanography 132*(621C), 3079-3106.

Eirund, G. K., Possner, A., & Lohmann, U. (2019). Response of Arctic mixed-phase clouds to aerosol perturbations under different surface forcings, *Atmospheric Chemistry and Physics 19*(15), 9847-9864.

Fan, J., Comstock, J. M., & Ovchinnikov, M. (2010). The cloud condensation nuclei and ice nuclei effects on tropical anvil characteristics andwater vapor of the tropical tropopause layer, *Environmental Research Letters 5*(4), 044005.

Fast, J. D., Gustafson Jr, W. I., Easter, R. C., Zaveri, R. A., Barnard, J. C., Chapman, E. G., ... & Peckham, S. E. (2006). Evolution of ozone, particulates, and aerosol direct radiative forcing in the vicinity of Houston using a fully coupled meteorology-chemistry-aerosol model, *Journal of Geophysical Research: Atmospheres 111*(D21).

Filioglou, M., Mielonen, T., Balis, D., Giannakaki, E., Arola, A., Kokkola, H., ... & Romakkaniemi, S. (2019). Aerosol effect on the cloud phase of low-level clouds over the Arctic, *Journal of Geophysical Research: Atmospheres 124*(14), 7886-7899.

Gordon, H., Glassmeier, F., & T. McCoy, D. (2023). An Overview of Aerosol-Cloud Interactions, *Clouds and Their Climatic Impacts: Radiation, Circulation, and Precipitation* 13-45.

Grell, G. A., Peckham, S. E., Schmitz, R., McKeen, S. A., Frost, G., Skamarock, W. C., & Eder, B. (2005). Fully coupled “online” chemistry within the WRF model, *Atmospheric environment 39*(37), 6957-6975.

Karlsson, L., Baccarini, A., Duplessis, P., Baumgardner, D., Brooks, I. M., Chang, R. Y. W., ... & Zieger, P. (2022). Physical and chemical properties of cloud droplet residuals and aerosol particles during the Arctic Ocean 2018 expedition, *Journal of Geophysical Research: Atmospheres 127*(11), e2021JD036383.

Petäjä, T., Tabakova, K., Manninen, A., Ezhova, E., O’Connor, E., Moisseev, D., ... & Kerminen, V. M. (2022). Influence of biogenic emissions from boreal forests on aerosol–cloud interactions, *Nature Geoscience 15*(1), 42-47.

Rantanen, M., Karpechko, A. Y., Lipponen, A., Nordling, K., Hyvärinen, O., Ruosteenoja, K., ... & Laaksonen, A. (2022). The Arctic has warmed nearly four times faster than the globe since 1979, *Communications earth & environment 3*(1), 168.

Schmale, J., Zieger, P., & Ekman, A. M. (2021). Aerosols in current and future Arctic climate, *Nature Climate Change 11*(2), 95-105.

Stapf, J., Ehrlich, A., Jäkel, E., Lüpkes, C., & Wendisch, M. (2020). Reassessment of shortwave surface cloud radiative forcing in the Arctic: consideration of surface-albedo–cloud interactions. *Atmospheric Chemistry and Physics*, *20*(16), 9895-9914.

Sterzinger, L. J., Sedlar, J., Guy, H., Neely III, R. R., & Igel, A. L. (2022). Do Arctic mixed-phase clouds sometimes dissipate due to insufficient aerosol? Evidence from comparisons between observations and idealized simulations, *Atmospheric Chemistry and Physics 22*(13), 8973-8988.

Van den Heever, S. C., Carrió, G. G., Cotton, W. R., DeMott, P. J., & Prenni, A. J. (2006). Impacts of nucleating aerosol on Florida storms. Part I: Mesoscale simulations, *Journal of the atmospheric sciences 63*(7), 1752-1775.

Yin, Y., & Chen, L. (2007). The effects of heating by transported dust layers on cloud and precipitation: a numerical study, *Atmospheric Chemistry and Physics 7*(13), 3497-3505.

Shortcomings in ultrafine particle measurement and source attribution, major sources and environmental impact

W. JUNKERMANN[1], J.M. HACKER[2,3] and A. McGRATH[2,3]

[1]*Karlsruhe Institute of Technology, IMK-IFU, Garmisch-Partenkirchen.*

[2] *Airborne Research Australia, Parafield Airport, SA, Australia*
[3]*Flinders University, College of Science and Engineering, Bedford Park, SA.Australia*

Keywords: CCN, SOURCE APPORTIONMENT, CLIMATE IMPACT.

INTRODUCTION

Ultrafine particles (UFP, aerosols <100 nm diameter) are highly important for cloud microphysics, affecting the environment through cloud droplet size, cloud albedo, cloud cover and lifetime, raindrop formation and the amount of liquid and gas phase water (latent energy) in the atmosphere. However, UFP are not amenable to remote sensing because of their size much less than the wavelengths of light, and so knowledge of their budget and 3D distribution is limited. It is believed that a significant fraction of UFPs are produced from gas to particle conversion not only in the PBL, but also in elevated layers, either in the residual layer, the lower free troposphere (LFT) or even up in the upper troposphere, from where these particles are transported down to cloud-relevant altitudes, i.e. below cloud base. Observations show that global and regional aerosol models often underestimate the particle concentrations found in or directly above the planetary boundary layer. This suggests that either not all chemical production pathways are considered, or that primary emissions are missing. Here we report recent airborne measurements within the PBL and the LFT, focusing on particle numbers and size distributions, that reveal several dominant anthropogenic sources of primary particles. These ultrafine particles, traveling aloft in layers exceeding PBL concentrations by more than an order of magnitude and over distances up to > 2500 km can be characterized based on their size distribution and their transport pathways according to case studies using meteorological data and HYSPLIT backtrajectory analysis. We used also regional scale Lagrangian flight patterns to quantify these dominant particle sources and to characterize their emission patterns.

CONCLUSIONS

The results indicate that the anthropogenic sources, emitting primary nano- and Aitken-particles into mid elevations of the PBL, the nocturnal residual layer or even the lower free troposphere are highly relevant for the global particle number and cloud condensation nuclei budget, however, often not visible for ground based monitoring stations. Correspondingly, most monitoring studies tend to underestimate the total particle / CCN budget at cloud base. To match both observations and model calculations for closure studies requires also an update of model emission scenarios. This could improve calculations of the atmospheric water cycle relevant for drought and flood extremes in agreement with observed decadal rainfall trends. .

REFERENCES

Junkermann, W. & Hacker, J., 2022, Unprecedented levels of ultrafine particles, major sources, and the hydrological cycle, Nature Scientific Reports, 12:7410 | https://doi.org/10.1038/s41598-022-11500-5

HOW ATMOSPHERIC NEW PARTICLE FORMATION AFFECTS INTERLINKED ENVIRONMENTAL GRAND CHALLENGES?

M. KULMALA[1], T. PETÄJÄ[1], A. LINTUNEN[1], A. LAAKSO[2], M. EHN[1], K. LEHTIPALO[1], AND V.-M. KERMINEN[1]

[1]*Institute for Atmospheric and Earth System Research, University of Helsinki, Helsinki, Finland*
[2]*Finnish Meteorological Institute, P.O. Box 1627, FI-70211 Kuopio, Finland*

Keywords: comprehensive observations, local clustering, air quality, climate, CarbonSink+, solar radiation modification, science diplomacy

BACKGROUND

The accelerating growth of the global population, coupled with rapid urbanization and increasing gross domestic product (GDP), has led to a substantial rise in energy demand. This escalating consumption contributes significantly to a complex web of environmental grand challenges, including climate change, resource depletion, and ecosystem degradation. As humanity expands its footprint, it faces the urgent need to secure vital resources—clean air, fresh water, nutritious food, and sustainable energy—amid a rapidly changing climate. There are also other environmental grand challenges such as air quality, biodiversity, chemicalisation, deforestation, acidification and pandemics. Since these grand challenges are highly connected and interlinked, sustainable solutions to tackle these challenges are tightly coupled with each other and thus cannot be solved separately. To meet these challenges, we need everyone: all disciplines, all countries, governments, industries, Non-Governmental Organizations and individual people. It is crucial to discuss, to listen to each other and disseminate result and information on problems so that we are able to provide scientifically, economically and societally effective and sustainable solutions.

In recent years, substantial advances have been made in understanding atmospheric processes, particularly the mechanisms of atmospheric new particle formation (NPF) and subsequent aerosol growth. These insights offer promising avenues for tackling climate-related challenges, as aerosols play a critical role in cloud formation and Earth's radiative balance and furthermore also other grand challenges (Kulmala et al., 2024a). In this work we showcase, how such fundamental knowledge with continuous scientific inquiry can contribute to addressing the pressing sustainability issues facing the global community.

ON GLOBAL CLIMATE CHALLENGE AND SOLAR RADIATION MANAGEMENT (SRM)

The global greenhouse gas concentrations are increasing ca 3 ppm/year. This is mainly due to the continuing use of fossil fuels, leading to rapid climate warming. If we are able to reduce global CO_2 emissions 2 % per year, and at the same time enhance continental sinks by 2% year (including technical sinks) it would take 23 years before the annual maximum of atmospheric CO_2 concentration starts to decrease. However, today there is no indication that this will happen. First, global emissions are still increasing. Second, natural and technical sinks are not enhancing significantly, and there are even risks of reductions of natural sinks in various land ecosystems (e.g. Pan et al., 2024; See et al. 2024). Besides reducing emissions and enhancing sinks, also solar radiation modification (SRM) has been suggested as a potential tool helping to mitigate climate change. Stratospheric aerosol injection (SAI) was suggested as means to slow down climate warming already in mid 70's (Budyko, 1977). Since then, it has been the most widely studied method for solar radiation modification (SRM). As the idea for SAI originated from observations of long-lasting global cooling after large volcanic eruptions, sulfur injections have been the primal focus of SAI studies. However, sulfur might not be the optimal selection for SAI. By understanding NPF we are – at least, in principle – able to master SAI. In fact, without rigorous scientific approach and

comprehensive understanding it is not possible. Therefore, a long-term comprehensive research program is needed.

Recently proposed geoengineering approaches for mitigating global warming include a potential for large magnitude feedbacks which can have significant, yet unpredictable influence the other processes. Risks related to uncontrolled geoengineering without international laws and the manipulation of the atmosphere highlight the value of continuous, comprehensive measurements detecting the changes. For example, operational SRM deployment would introduce new environmental and socio-economic threats like damaging the ozone layer and overcompensating climate change at regional scales (UNEP, 2023).

In relation to SRM and generally, Earth surface and the atmosphere are in constant interaction with each other as energy and material are exchanged between them. Ecosystems act as sources or sinks of various greenhouse gases (GHGs) and sources of volatile organic compounds (VOCs) that contribute to formation of atmospheric aerosol particles and further cloud condensation nuclei that are needed to form clouds. By acting as a sink of GHGs and a source of VOCs, ecosystems can mitigate climate change. The climate mitigation potential of ecosystems in terms of GHGs lies in storing GHGs in the ecosystems (in plant structures and soil) and this way keeping the GHG away from the atmosphere, where they would absorb solar radiation and warm the planet. The climate mitigation potential of ecosystems in terms of VOCs lies in the ability of aerosol particles through new particle formation and growth and therefore influence the properties of clouds (Petäjä et al. 2022) that can reflect solar radiation back to space and therefore cool the planet. Here NPF is the key process to understand to be able to quantify the potential.

THE NEEDED APPROACH

Tackling the environmental grand challenges is crucial for humankind and for our planet. These challenges are strongly interlinked and to meet them we need several tools including open data, open science, science diplomacy and Artificial Intelligence tools. Since the challenges are enormous, we need to work over boundaries wherever they exist. We need open big data to meet the present grand challenges, and we need to collect comprehensive data to be prepared to answer questions which do not even exist today. The questions can be societal, economic or scientific, or any combination of these.

Recently, we have started to build a holistic understanding of different ecosystems to global climate. In the holistic approach, not only GHG sources and sinks are considered, but also aerosol formation potential of different ecosystems is accounted for (Kulmala et al., 2024b). These comprehensive measurements, combined with increased process understanding and modeling, will allow us to assess a holistic climate impact of different ecosystems. To quantify these effects, we define the concept of CarbonSink+ (Kulmala et al., 2024b), which includes all radiative forcers. Furthermore, according to our present understanding atmospheric production new particles and aerosol mass dominates the global aerosol and CCN (cloud condensation nuclei) load.

Currently, the speed of climate change along with its unpredictable consequences are challenging the capacities of existing observation systems. In addition, the ability to analyze the yet unknown questions and challenges, calls for comprehensive continuous observations (Kulmala, 2018, Kulmala et al., 2021). For example, COVID19 gave an unexpected opportunity to demonstrate the effect of exceptional reductions in anthropogenic emissions on air quality and climate. Other examples of this type of unusual and extraordinary events could be volcanic eruptions, gas pipe attacks, extreme weather events, forest fires, exceptionally dry periods, economic collapses or chemical weapons. All these events have both short- and long-term dynamic effects on air quality and the climate system as well as on the functioning of societies. Also, the possibility of realized global tipping points, such as permafrost loss or boreal forest shift towards north, may lead to unexpected environmental episodes, events and feedbacks. The key questions are whether the majority of current observation systems contain sufficiently comprehensive set

of variables to capture these events, and whether we have the preparedness to detect, analyze and quantify these events.

However, the more open, comprehensive data we have the more we understand. E.g. based on data (e.g. Kulmala et al., 2013, 2024a) we know that the higher the atmospheric new particle formation rate is the higher is CarbonSink+ and more CCN, cloud droplets and haze particles are produced.

ACKNOWLEDGEMENTS

This work was supported by the Research Council of Finland University Profiling funding InterEarth (grant no. 353218)

REFERENCES

Budyko, M. I. (1977). Climatic changes (transl. Izmeniia Klimata Leningrad: Gidrometeoizdat, 1974). Washington, DC: American Geophysical Union.

Kulmala, M. Build a global Earth observatory Nature 553, 21-23 (2018) doi: 10.1038/d41586-017-08967-y

Kulmala, M., Lintunen, A., Ylivinkka, I., Mukkala, J., Rantanen, R., Kujansuu, J., Petäjä, T., and Lappalainen, H.K. (2021). Atmospheric and ecosystem big data providing key contributions in reaching United Nations' sustainable development goals, Big Earth Data, 5, 3, 277-305, doi: 10.1080/20964471.2021.1936943.

Kulmala, M., Kontkanen, J., Junninen, H., Lehtipalo, K., Manninen, H.E., Nieminen, T., Petäjä, T., Sipilä, M., Schobesberger, S., Rantala, et al. (2013). Direct observations of atmospheric aerosol nucleation. Science 339, 943-946, doi: 10.1126/science.1227.

Kulmala, M., Aliaga, D., Tuovinen, S., Cai, R., Junninen, H., Yan, C., Bianchi, F., Cheng, Y., Ding, A., Worsnop, D. R., Petäjä, T., Lehtipalo, K., Paasonen, P. and Kerminen V.-M.: (2024a). Opinion: A paradigm shift in investigating the general characteristics of atmospheric new particle formation using field observations. Aerosol Res., 2, 49-58.

Kulmala, M., Ke, P., Lintunen, A., Peräkylä, O., Lohtander, A., Tuovinen, S., Lampilahti, J., Kolari, P., Schiestl-Aalto, P., Kokkonen, T., Nieminen, T., Dada, L., Ylivinkka, I., Petäjä, T., Bäck, J., Lohila, A., Heimsch, L., Ezhova, E., and Kerminen, V-M. (2024b). A novel concept for assessing the potential of different boreal ecosystems to mitigate climate change (CarbonSink+ Potential). Boreal Environment Research 29, 1-16, https://www.borenv.net/BER/archive/pdfs/ber29/ber29-001-016.pdf.

Pan, Y., Birdsey, R. A., Phillips, O. L., Houghton, R. A., Fang, J., Kauppi, P. E., Keith, H., Kurz, W., A., Ito, A., Lewis, S. L., Nabuurs, G.-J., Shvidenko, A., Hashimoto, S., Lerink, B., Schepaschenko, D., Castanho, A. & Murdiyarso, D.: The enduring world forest carbon sink, Nature, 631, 563-569, https://doi.org/10.1038/s41586-024-07602-x, 2024.

Petäjä, T., Tabakova, K., Manninen, A., Ezhova, E., O'Connor, E., Moisseev, D., Sinclair, V.A., Backman, J., Levula, J., Luoma, K., Virkkula, A., Paramonov, M., Räty, M., Äijälä, M., Heikkinen, L., Ehn, M., Sipilä, M., Yli-Juuti, T., Virtanen, A., Ritsche, M., Hickmon, N., Pulik, G., Rosenfeld, D., Worsnop, D.R., Bäck, J., Kulmala, M. and Kerminen, V.-M. (2022) Influence of biogenic emissions from boreal forests on aerosol–cloud interactions, Nature Geosci. 15, 42-47, doi.org/10.1038/s41561-021-00876-0.

See, C. R., Virkkala, A.-M., Natali, S. M., Rogers, B. M., Mauritz, M., Biasi, C., Boike, J., Bret-Harte, M. S., Celis, G., chae, N.Christensen, T. R.Murner, S. J., Dengel, S., Dolman, H., Edgar, C. W., Elberling, B., Emmerton, C A., Euskirchen, E. S., Gockede, M., Grelle, A., Heffernan, L., Helbig, M., Holl, D., and Schuur, E. G. R.: Decadal increases in carbon uptake offset by respiratory losses across northern permafrost ecosystems, Nat. Clim. Change, 14, 853-862, https://doi.org/10.1038/s41558-024-02057-4, 2024.

UNEP, United Nations Environment Programme. One Atmosphere: An independent expert review on Solar Radiation Modification research and deployment. Kenya, Nairobi, 2023.

EMITTED NUCLEATION MODE PARTICLES – HOW TO DISTINGUISH FROM NEW PARTICLE FORMATION AND TO INLCUDE IN MODELS?

P. PAASONEN[1], XIANG LI[1], S. BASYAL[1], M. OKULJAR[1,*], D. DING[1], P. CLUSIUS[1], B. FOREBACK[1,2], A. OVASKA[1], XIAOYU LI[1], H. PORTIN[3], J. NIEMI[3], V.-V. PAUNU[4], N. KARVOSENOJA[4], J.-P. JALKANEN[5], Z. KLIMONT[6], V.-M. KERMINEN[1], M. KULMALA[1], T. PETÄJÄ[1] AND K. LEHTIPALO[1,5]

[1]*Institute for atmospheric and Earth system research (INAR/Physics), University of Helsinki, Finland*
[2]*Atmospheric Modelling Centre – Lahti, Lahti University Campus, Lahti, Finland*
[3]*Helsinki region environmental services authority (HSY), Helsinki, Finland*
[4]*Finnish environment institute (SYKE), Helsinki, Finland*
[5]*Finnish meteorological institute (FMI), Helsinki, Finland*
[6]*International institute for applied systems analysis (IIASA), Laxenburg, Austria*
[*]*Now at: Queensland University of Technology (QUT), Australia*

Keywords: ultrafine particle emissions, new particle formation, aerosol-cloud interactions.

INTRODUCTION

Growth of nucleation mode particles (with initial diameter D_P < 25 nm) contributes strongly to accumulating aerosol pollution (e.g., $PM_{2.5}$) and cloud condensation nuclei concentrations in polluted urban and clean boreal terrestrial environments (Hakala *et al*., 2022; Räty *et al*., 2023). In addition to atmospheric new particle formation (NPF) process, occurring both in strong atmospheric NPF events (NPFEs) and with lower rate outside these discernible NPFEs, nucleation mode particles down to sub-3 nm sizes are emitted in large numbers from traffic combustion (Rönkkö *et al*., 2017). These emissions are not captured by the existing emission inventories (Foreback *et al*., 2025) but including them in GAINS emission scenarios (Paasonen *et al*., 2016) is on the way. However, implementing the anthropogenic nucleation mode emissions directly to large scale models is expected to severely overestimate their contribution on the particle concentrations, if the sub-grid scale aerosol processes occurring near the strong sources, e.g., in urban areas, are not considered. Distinguishing NPF and traffic sources in the observed urban particle number (PN) size distribution data and including them in large scale models with proper sub-grid scale parameterisations is crucial for quantifying their roles in urban air quality and climate.

Here, we present two methods that we are currently developing for distinguishing nucleation mode particles originating from NPF and traffic. We also describe how the primary particle number emissions in GAINS emission scenarios will be improved and the approach we are using to develop sub-grid scale aerosol process parameterisations.

METHODS

First, we present a detailed classification procedure for elevated PN concentration events in nucleation mode size range. This procedure is further developed from the NPFE classification scheme developed by Dal Maso *et al*. (2005). In addition to more detailed classes for NPFEs with different spatial connection to the observation site (NPFEs occurring both *in situ* and wide upwind area, NPFEs occurring *in situ* but limited upwind area and NPEFs occurring in wide area upwind but not *in situ*), the procedure classifies different Undefined Events (UEs) as events that are likely related to nearby primary emissions, e.g., traffic. The UEs are defined as appearing modes that do not show clear growth and either appear only in sizes larger than 5 nm or, if extending to sub-5 nm range, appear simultaneously in sizes over 25 nm. This

method is applied for the data collected at two coastal sites in Southern Finland, urban background site SMEAR III in Helsinki (Järvi *et al*., 2009) and agricultural site in Qvidja (Olin *et al*. 2022).

Second, we utilise NO_x concentration as a tracer for traffic emissions and develop further the methodologies developed by Rodrigues and Cuevas (2007), Okuljar *et al*. (2021), and Chen *et al*. (2023). We investigate long time series of PN and NO_x concentrations in traffic-influenced environment, starting with data recorded at the HSY supersite at Mäkelänkatu in Helsinki (Kuuluvainen *et al*., 2018) and investigating next the data from urban background site SMEAR III. The typical contribution of traffic to PN concentration is determined based on the occurrence (frequency) distribution of different PN concentrations observed with given NO_x concentrations. A lognormal mode is used to reproduce the occurrence of lower end and intermediate PN concentrations and the PN concentrations exceeding this mode are considered as being influenced by NPF. With this method we can both determine the overall contribution of traffic on the observed particle concentration and estimate the probabilities of traffic and NPF contributions to the observed concentrations at each time step.

The particle number emissions in GAINS emission scenarios, introduced by Paasonen *et al*. (2016), are being updated with ECLIPSE v6b scenarios (Klimont *et al*., 2025) and augmented with international shipping emissions based on the STEAM model (Jalkanen *et al*., 2009). The updated GAINS output is annual particle number emissions with 0.1°×0.1° spatial resolution globally with distribution to >20 size bins and 11 main activity sectors. Including the nucleation mode emissions in GAINS traffic emissions has been tested in a LES modelling study in the surroundings of an urban street canyon in Beijing (Li *et al*., 2025). The sub-grid scale (SGS) aerosol process parameterisations – required for implementing the nucleation mode emissions to the coarse spatial resolution of regional or global models – are developed with point-source parameterisations by Ramnarine *et al*. (2019) and SGS heterogeneity of the emissions based on GAINS output and ultra-high resolution emission scenario model FRES (Karvosenoja, 2008).

RESULTS

The updated NPFE classification procedure showed that at both the costal sites, the NPFEs with wide upwind NPFE area were originating from airmasses arriving from inland. On the contrary, the NPFEs occurring on the marine airmasses showed limited upwind NPFE area, suggested that the events start when the air masses arrive from the sea to the coast or to its vicinity. The classification showed frequent UEs in Helsinki but rarely in Qvidja, which agrees with the assumption of them being related to traffic emissions. However, many of the modes appearing at the rush hour time and being connected to elevated NO_x concentration were classified as NPFEs with limited upwind NPFE area. This underlines the difficulty of separating the traffic and NPFE as sources of sub-5 nm particles.

The method utilizing the NOx concentration as a tracer for traffic related nucleation mode particles produced reasonable preliminary results. In the Mäkelänkatu street canyon, the occurrence of the PN concentrations in diameter range 5-15 nm showed roughly a lognormal distribution, with PN concentration of maximum occurrence increasing steadily with NO_x concentration (Figure 1). Yet, the lognormal mode did not capture the occurrence of higher PN concentrations, and the positive residual was interpreted as the contribution of NPF. The cumulative occurrence of NPF influenced concentrations was notably lower than that of only traffic related concentrations, which can be expected as strong NPF source is presumed for only few hours per clear sky day. However, NPFs contributed significantly to the total PN budget due to the roughly an order of magnitude higher PN concentrations when NPF is producing particles in addition to traffic.

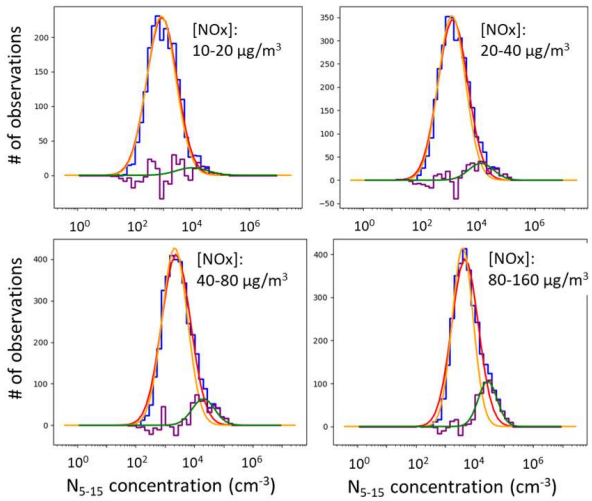


Figure 1. Occurrence distributions of PN concentrations in diameter range 5-15 nm ($N_{5\text{-}15}$) under different ranges of NO_x concentrations in June 2017 and 2018. The blue histogram is the original occurrence data, and the red line the lognormal mode fitted to it. The yellow line is lognormal mode fitted to the lower end and intermediate PN concentrations (from minimum to maximum occurrence and until the occurrence goes below ¾ of the maximum) and it is interpreted as the occurrence mode of solely traffic related particles. Magenta histogram shows the residual of the blue histogram after subtracting the (yellow) traffic mode and green line is a lognormal mode fitted to it, interpreted as concentrations during intense NPF.

The global PN emissions with ECLIPSE v6b CLE emission scenario (available by now for Europe; Figure 2) and the influence of added nucleation mode emissions will be presented in the conference, as well as the methodology and initial results of the SGS aerosol process parameterisations.

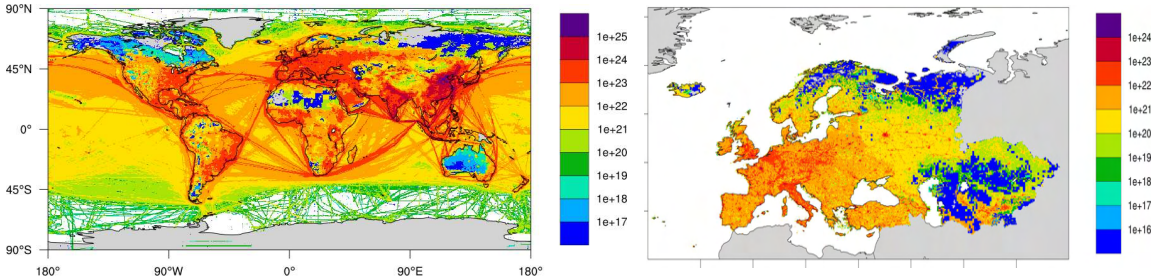


Figure 2. Left: annual particle number emissions in particles per 0.5°×0.5° grid cell for year 2015, based on ECLIPSE v5a CLE scenario as in Paasonen *et al*. (2016) for the continental area and based on STEAM model for international shipping. Right: annual particle number emissions in Europe in particles per 0.1°×0.1° grid cell for year 2015, based on ECLIPSE v6b CLE scenario.

CONCLUSIONS

To quantify the impact of anthropogenic emissions and atmospheric NPF on ambient particle number concentrations and aerosol-cloud interactions we need to understand better our observations and be able to implement the spatially heterogenous nucleation mode emissions in regional and global models. In this presentation we describe our recent work in determining the contributions of emissions and NPF on the observed nucleation mode particle number concentrations, in producing particle number emission data with high spatial and diameter resolution, and in deriving parameterisations for sub-grid scale aerosol processes required for implementing the emissions in regional and global models.

ACKNOWLEDGEMENTS

This work was supported by the Academy of Finland (grants: 337549, 357902, 358647, 359340, 367739, 360114) and European Commission (grants: 101056783, FOCI; 821205, FORCeS). We acknowledge CSC - IT Centre for Science, Finland, for providing computational resources.

REFERENCES

Chen, L., *et al*. (2023). High concentration of atmospheric sub-3 nm particles in polluted environment of eastern China: New particle formation and traffic emission. *Journal of Geophysical Research: Atmospheres*, 128.

Dal Maso, M., *et al.* (2005). Formation and growth of fresh atmospheric aerosols: Eight years of aerosol size distribution data from SMEAR II, Hyytiälä, Finland. *Boreal Environ. Res.*, *10*(5), 323–336.

Foreback, B, *et al.* (2025). Severe haze episodes in Beijing may be influenced by emissions in far western China, *Air quality, atmosphere & health, in review*.

Hakala, S., *et al*. (2022). Observed coupling between air mass history, secondary growth of nucleation mode particles and aerosol pollution levels in Beijing, *Environmental Science: Atmospheres*, 2.

Jalkanen, J.-P., *et al.* (2009). A modelling system for the exhaust emissions of marine traffic and its application in the Baltic Sea area, *Atmos. Chem. Phys.*, 9, 9209–9223.

Järvi, L., *et al.* (2009). The urban measurement station SMEAR III: continuous monitoring of air pollution and surface-atmosphere interactions in Helsinki, Finland, *Boreal Environ. Res*., 14 (A), 86–109.

Karvosenoja, N. (2008). Emission scenario model for regional air pollution. *Monographs of the Boreal Environment Research*, 32.

Klimont, Z., *et al.* (2025). Global scenarios of anthropogenic emissions of air pollutants: ECLIPSE, *Geosci. Model Dev., in preparation*.

Kuuluvainen, H., *et al*. (2018). Vertical profiles of lung deposited surface area concentration of particulate matter measured with a drone in a street canyon, *Environ. Pollut.*, 241, 96–105.

Li, Xiaoyu, *et al*. (2025). Sensitivity of the Sectional Aerosol Module SALSA in the PALM Model System to Vehicle Emissions in Beijing, *Atmospheric Environment, in review.*

Okuljar, M., *et al*. (2021). Measurement report: The influence of traffic and new particle formation on the size distribution of 1–800 nm particles in Helsinki—A street canyon and an urban background station comparison. *Atmos. Chem. Phy.*, *21*(13), 9931–9953.

Olin, M., *et al.* (2022). Measurement report: Atmospheric new particle formation in a coastal agricultural site explained with binPMF analysis of nitrate CI-APi-TOF spectra, *Atmos. Chem. Phys.*, 22, 8097–8115.

Ramnarine, E., *et al*. (2019). Effects of near-source coagulation of biomass burning aerosols on global predictions of aerosol size distributions and implications for aerosol radiative effects, *Atmos. Chem. Phys.*, 19, 6561–6577.

Rodríguez, S. and Cuevas, E. (2007). The contributions of "minimum primary emissions" and "new particle formation enhancements" to the particle number concentration in urban air, *Journal of Aerosol Science*, 38, 12, 1207-1219.

Räty, M., *et al*. (2023). Dynamics of aerosol, humidity, and clouds in air masses travelling over Fennoscandian boreal forests, *Atmos. Chem. Phys*., 23, 3779–3798.

Rönkkö, T., *et al*. (2017). Traffic is a major source of atmospheric nanocluster aerosol. *Proceedings of the National Academy of Sciences of the United States of America*, *114*(29), 7549–7554.

Influence of Aerosol Mixing State on Hygroscopic Growth and Fog Formation in New Delhi: Insights from HTDMA Measurements

CHAITRALI.D. SHINDE[1], SANDEEP WAGH[1], AKASH VISPUTE[1], SHRAVAN DESHMUKH[2]

SACHIN GHUDE[1]

[1]Indian Institute of Tropical Meteorology, Ministry of Earth Sciences, Pune, India.

[2]Leibniz Institute for Tropospheric Research, e.V. (TROPOS), Permoserstrasse 15, 04318 Leipzig, Germany

Keywords: HYGROSCOPICITY, KAPPA, GROWTH FACTOR, AEROSOL MIXING STATE.

INTRODUCTION

Delhi experiences severe aerosol loading, especially during winter, due to its geography and pollution sources such as biomass burning and Diwali celebrations. These factors significantly deteriorate air quality (AQI) and contribute to dense fog events. Understanding aerosol hygroscopicity is crucial, as it influences fog formation and visibility by determining how particles absorb water vapor, swell, and scatter light. This study investigates the role of aerosol mixing state—internal or external—in modulating hygroscopic growth during peak pollution and fog events, providing insights into fog formation mechanisms in New Delhi.

METHODS

This study investigates the hygroscopic properties of aerosols using the Humidified Tandem Differential Mobility Analyzer (HTDMA) at the India Meteorological Department (IMD) in Delhi. As part of the Winter Fog Experiment (WiFEX) conducted by IITM Pune, a comprehensive field campaign was carried out from October 2024 to January 2025 at IMD Delhi. The primary objective is to analyse the aerosol mixing state by plotting Growth Factor Probability Density Functions (GF-PDF) during pollution and fog events and evaluate the hygroscopic properties of aerosols. HTDMA data are correlated with Aerodyne Aerosol Mass Spectrometer (AMS) measurements to determine the hygroscopicity parameter (κ), based on the chemical composition of aerosol particles.

HTDMA operates in both constant and varying humidity modes, with the present study utilizing the varying humidity mode. Aerosol particles in the size range of 100 nm to 600 nm were subjected to relative humidity (RH) variations from 70% to 90%. The hygroscopicity parameter κ was calculated using k-Köhler theory, following the equation by Petters & Kreidenweis (2007):

$$\kappa = (Gf^3 - 1)\left(\frac{exp\left(\frac{A}{D_d Gf}\right)}{RH} - 1\right)$$

Additionally, the chemical hygroscopicity parameter (κ_{chem}) was determined using the Zdanovskii-Stokes-Robinson (ZSR) rule, incorporating AMS data.

To classify fog, haze, and severe haze events, atmospheric visibility data were analysed throughout the campaign.

CONCLUSIONS

The Growth Factor Probability Density Function (GF-PDF) provides insights into aerosol hygroscopicity and mixing state by analyzing the probability distribution of growth factors. To assess the variability in growth factors and classify internal and external mixing states, we employed the standard deviation of the growth factor (σ_{GF}) as a metric, as suggested by Sjogren et al. (2008). Based on our analysis for November 2024, aerosols with $\sigma_{GF} \geq 0.12$ were categorized as externally mixed, while those with $\sigma_{GF} \leq 0.05$ were classified as internally mixed.

A detailed examination of GF-PDF distributions revealed significant seasonal variations. In December 2024, a secondary peak was observed but was not very prominent, and the primary peak appeared between GF = 1 and 1.2, indicating limited aerosol growth. In January 2025, however, a more distinct bimodal distribution was evident, with the first peak slightly shifted to GF = 1.2 and a prominent second peak at GF = 1.6, signifying the presence of more hygroscopic aerosols. These findings align with our classification of months into two major periods—pollution (November and December) and fog (January)—where more hygroscopic aerosols were expected during the fog period, particularly in January.

November 2024, categorized as a pollution period, did not show significant variations at a coarse temporal resolution. To gain deeper insights, we plan to identify specific peak pollution events and analyze their corresponding aerosol mixing states. Following this, AMS data will be examined to determine the chemical composition of aerosols during these events. Finally, the hygroscopicity parameter will be calculated using both HTDMA and AMS data, enabling a direct comparison of measured and chemically derived hygroscopicity.

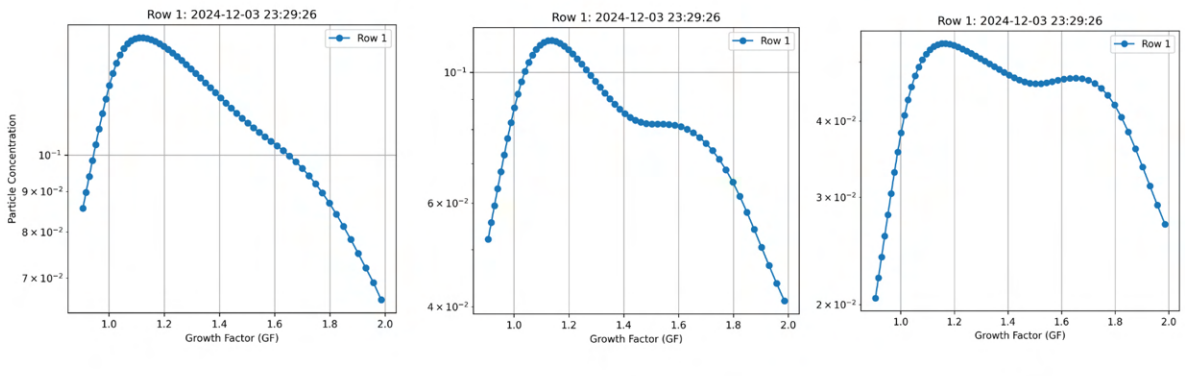


Figure 1. GF- Distribution for month of Nov 2024, Dec 2024 and Jan 2025 respectively.

ACKNOWLEDGEMENTS

I would like to extend my sincere gratitude to the Ministry of Earth Sciences (MoES) and the Director of the Indian Institute of Tropical Meteorology (IITM) for their invaluable support and resources.

REFERENCES

Petters, M.D., Kreidenweis, S.M., 2007. A single parameter representation of hygroscopic growth and cloud condensation nucleus activity. Atmos. Chem. Phys. 1961–1971.

Sjogren, S., Gysel, M., Weingartner, E., Alfarra, M. R., Duplissy, J., Cozic, J., Crosier, J., Coe, H., and Baltensperger, U.: Hygroscopicity of the submicrometer aerosol at the high-alpine site Jungfraujoch, 3580 m a.s.l., Switzerland, Atmos. Chem. Phys.,8, 5715–5729, https://doi.org/10.5194/acp-8-5715-2008, 2008.

Impact of Anthropogenic Ammonia on Upper Tropospheric Aerosol Composition and Climatic Implications

C. Xenofontos[1], M. Kohl[2], S. Ruhl[2], A. Pozzer[2,1], J. Lelieveld[2,1], T. Christoudias[1]

[1]*Climate and Atmosphere Research Center (CARE-C), The Cyprus Institute, Nicosia, Cyprus*

[2]*Atmospheric Chemistry Department, Max Planck Institute for Chemistry, Mainz, Germany*

Keywords: New Particle Formation, Anthropogenic NH_3, UTLS, CCN, AOD

INTRODUCTION

Anthropogenic ammonia (NH_3) plays a central role in atmospheric new particle formation (NPF) (Yu et al., 2006). NH_3 is predominantly emitted from agricultural sources and anthropogenic emissions are expected to double by 2100 (Panther et al., 2014). While the impact of NH_3 on near-surface air quality is well documented, its contribution to aerosol formation and cloud-relevant properties under the cold temperatures of the upper troposphere and lower stratosphere (UTLS) remains poorly constrained. NH_3 can be transported to the UTLS in convective clouds. MIPAS detected NH_3 in the UTLS of up to 30 ppt (Hopfner et al., 2016) and ammonium nitrate particles were measured in the upper troposphere from ground ammonia sources during Asian monsoons (Hopfner et al, 2019).

Recent CLOUD experiments have demonstrated that NH_3 significantly enhances nucleation rates through mechanisms involving H_2SO_4 and HNO_3 under UTLS conditions (Dunne et al., 2016; Wang et al., 2022). These findings highlight the need to quantify the global influence of NH_3 on particle formation and its implications for the climate .

In this study, we use the EMAC Earth system model with nucleation parameterisations from CLOUD experiments to simulate the impact of anthropogenic NH_3 emissions on global UTLS NPF, aerosol composition and optical properties, and CCN concentrations. We compare simulations with and without NH_3 emissions to quantify their role in modifying aerosol properties and assess implications for cloud microphysics and climate.

METHODS

We use the EMAC (ECHAM5/MESSy Atmospheric Chemistry) Earth system model (Jockel, et al., 2010) with parameterizations of ternary (H_2SO_4–NH_3–H_2O) and synergistic (H_2SO_4–NH_3–HNO_3–H_2O) nucleation derived from the CERN CLOUD experiment (Dunne et al., 2016; Wang et al., 2022). These mechanisms are implemented in the NAN submodel (Ehrhart, et al., 2018) and coupled with aerosol microphysics via GMXe and the ISORROPIA-II thermodynamic equilibrium model (Pringle et al. 2010)). The model resolves aerosol size distributions, including growth to CCN, aerosol chemical composition, , and optical depth (AOD).

Global simulations are conducted for the period 2003–2019 under two emission scenarios: one including CEDS anthropogenic NH_3 emissions and one with the anthropocentric emissions component removed. Model output NH_3 concentrations are evaluated against satellite observations from MIPAS and IASI (Blumstein, et al., 2004).

RESULTS

Our model simulations show good agreement in space and time with MIPAS UTLS retrievals, and reveal a substantial enhancement of NPF in the upper troposphere due to anthropogenic NH_3 emissions, especially in regions affected by deep convection. Over the Asian Monsoon region, ternary NH_3–H_2SO_4–H_2O nucleation rates ($J_{1.7}$) increase by up to three orders of magnitude compared to the baseline scenario without anthropogenic NH_3. This enhancement is particularly pronounced during the summer monsoon season, driven by efficient vertical transport of NH_3 under deep convective conditions to altitudes of 10–17 km,. where the Asian Tropopause Aerosol Layer (ATAL) is formed (Vernier et al. 2011), as shown in Figure 1.

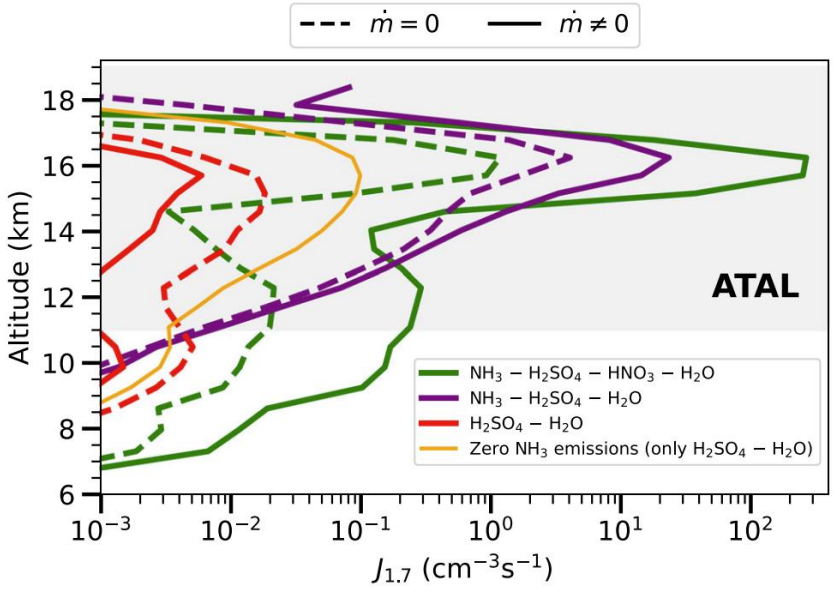


Figure 1. Simulated Nucleation Rates and the Influence of Convection in the ATAL. Nucleation rates at 1.7 nm ($J_{1.7}$), calculated under ambient conditions, are presented across different altitudes over the South Asian monsoon region for the summer of 2017. The simulations include four nucleation pathways: synergistic NH_3–H_2SO_4–HNO_3–H_2O (green), ternary NH_3–H_2SO_4–H_2O (purple), and binary H_2SO_4–H_2O both with (red) and without (orange) anthropogenic NH_3 emissions. Solid lines represent conditions with convective updrafts ($\dot{m} \neq 0$), indicative of active deep convection, while dashed lines reflect quiescent atmospheric conditions without convection ($\dot{m} = 0$). The grey-shaded band highlights the vertical extent of the ATAL, where nucleation rates are most sensitive to the presence of convective transport (Adapted from Xenofontos et al. 2024).

Overall, Anthropogenic NH_3 emissions also enhance upper tropospheric $J_{1.7}$ by one to three orders of magnitude over other major source regions such as the US, Europe, East Asia. Globally, we find a doubling of aerosol number concentrations and a significant increase in the abundance of ammonium nitrate and aerosol water in the UTLS. This compositional shift enhances the AOD by 20–40% regionally, with up to 80% change in total column AOD over emission-intensive areas. Additionally, CCN concentrations at 0.4% supersaturation in the upper troposphere increase by a factor of 2.5, with potential impacts on cirrus cloud formation and the climate.

CONCLUSIONS

Our results highlight the need for global climate models to include NH_3-driven aerosol-climate interactions in the upper troposphere. While reduction of agricultural NH_3 emissions is expected to improve surface air quality, this can also lead to a depletion of the UTLS aerosol layer. This underscores the importance of incorporating these findings into future emission and climate policy frameworks to ensure a complete assessment of environmental and climate outcomes.

ACKNOWLEDGEMENTS

This work was supported by the EU MSCA Doctoral Network CLOUD-DOC 101073026 and the European Union's Horizon 2020 research and innovation programme under grant agreement No. 856612.

REFERENCES

F Yu, Effect of ammonia on new particle formation: A kinetic H2SO4 − H2O − NH3 nucleation model constrained by laboratory measurements. J. Geophys. Res. Atmospheres 111 (2006).

Höpfner, M., Ungermann, J., Borrmann, S. et al. Ammonium nitrate particles formed in upper troposphere from ground ammonia sources during Asian monsoons. Nat. Geosci. 12, 608–612 (2019).

M Wang, et al., Rapid growth of new atmospheric particles by nitric acid and ammonia condensation. Nature 581, 184–189 (2020).

C Xenofontos, et al., The impact of ammonia on particle formation in the Asian Tropopause Aerosol Layer. npj Clim. Atmospheric Sci. 7, 215 (2024).

M Wang, et al., Synergistic HNO3–H2SO4–NH3 upper tropospheric particle formation. Nature 605, 483–489 (2022).

EM Dunne, et al., Global atmospheric particle formation from CERN CLOUD measurements. Science 354, 1119–1124 (2016).

M Hopfner, et al., First detection of ammonia (NH3) in the Asian summer monsoon upper troposphere. Atmospheric Chem. Phys. 16, 14357–14369 (2016).

M Prather, et al., Climate system scenario tables. (2014).

P Jockel, et al., Development cycle 2 of the modular earth submodel system (MESSy2). Geosci. Model. Dev. 3, 717–752 (2010).

K Pringle, et al., Description and evaluation of GMXe: a new aerosol submodel for global simulations (v1). Geosci. Model. Dev. 3, 391–412 (2010).

S Ehrhart, et al., Two new submodels for the Modular Earth Submodel System (MESSy): New Aerosol Nucleation (NAN) and small ions (IONS) version 1.0. Geosci. Model. Dev. 11, 4987–5001 (2018).

D Blumstein, et al., IASI instrument: technical overview and measured performances in Infrared Spaceborne Remote Sensing XII, ed. M Strojnik. (International Society for Optics and Photonics, SPIE), Vol. 5543, pp. 196 – 207 (2004).

Vernier, J.-P., Thomason, L. & Kar, J. CALIPSO detection of an Asian tropopause aerosol layer. *Geophys. Res. Lett.* **38**, L07804 (2011).

Special Session 1: Global observations of aerosols, clouds and trace gases: longterm monitoring networks and research infrastructure

NEW PARTICLE FORMATION EVENTS OBSERVED DURING THE AIRCRAFT MEASUREMENT OF THE ASIA-AQ CAMPAIGN

CHANWOO AHN[1], PYOSUK SEO[1, 2] , SEONG SOO YUM[1, 2], and RICHARD H. MOORE[3]

[1] Department of Atmospheric Science, Yonsei University, Seoul, Republic of Korea

[2]Climate Environmental Research Institute, Korea Institute of Science and Technology, Seoul, Republic of Korea

[3]NASA Langley Research Center, Hampton, VA, USA

Keywords: ASIA-AQ campaign, aircraft measurement, new particle formation

INTRODUCTION

Atmospheric aerosols play a critical role in climate and visibility (Charlson 1969; Ramanathan et al, 2001) and can also act as cloud condensation nuclei (CCN). A large proportion of these aerosols is directly emitted by human activities (Streets et al., 2003). However, Yu and Luo (2009) reported that at least 50% of aerosols were estimated to be formed through new particle formation (NPF) events in East Asia. NPF events generally consist of two main steps (Kulmala et al., 2012): (i) the formation of clusters from precursor gases and (ii) the subsequent growth of these clusters to larger sizes. They are also considered a major natural source of CCN in the atmosphere, since the grown particles can readily act as CCN (Yue et al., 2011). NPF events can occur in any environment as long as certain conditions are met (Kulmala et al., 2014); however, their characteristics, such as spatial extent and the growth pattern of newly formed particles, vary significantly depending on the atmospheric environment (Crumeyrolle et al., 2010; Šmejkalová et al., 2021). This highlights the need for comprehensive studies on NPF events across diverse regions and altitudes to better understand their effects on clouds and climate.

The ASIA-AQ (Airborne and Satellite Investigation of Asian Air Quality)

campaign was carried out in February and March 2024 under the supervision of the National Aeronautics and Space Administration (NASA), as an international cooperative effort aimed at enhancing the understanding of local air quality across several Asian countries. The DC-8 aircraft was used as the main platform for the campaign, with a total of 26 teams participating in the in-situ measurement of gas- and aerosol-related parameters. We report the characteristics of NPF events occurred in each country using the data collected during a total of 161 hours of research flights. First, the latitude, longitude, and altitude of the NPF events were investigated, and then based on this information, their horizontal and vertical extents were estimated. Since a single research flight typically consisted of two or three laps along similar flight routes, we also analyzed the growth patterns of newly formed particles by comparing each lap. Finally, the country-specific characteristics of several important factors (e.g., temperature, relative humidity (RH), sulfur dioxide (SO_2), and pre-existing aerosols) were examined, which are known to influence NPF events.

METHODS

Here we focus three types of instruments installed on the DC-8 aircraft during the campaign for our analysis: a condensation particle counter (CPC; model 3010, TSI), a scanning mobility particle sizer (SMPS; model 3936 L10, TSI) with another CPC 3010, and a cloud condensation nuclei counter (CCNC; model CCN-100, Droplet Measurement Technologies). The CPC measured aerosol number concentrations larger than 10 nm in diameter every 1 s. The SMPS measured the aerosol number-size distribution in the diameter range 10–300 nm every 3 min. The CCNC measured CCN number concentrations at a supersaturation of 0.37% every 1 s, with the instrument pressure controlled at 675 mb using the constant pressure inlet. The supersaturation calibration of the CCNC using NaCl particles was performed once before and twice during the campaign. All instruments were connected to the community aerosol inlet using conductive tube to minimize aerosol losses. All data were converted to values at standard temperature and pressure (273.15 K and 1013.25 hPa) before analysis.

RESULTS AND CONCLUSIONS

In the Philippines region, NPF events were observed during all four flights. All four NPF events occurred approximately below 1000 m altitude, i.e.,

within the planetary boundary layer (PBL), and appeared regionally over Manila bay and the Taal Volcano. The growth of particles formed by NPF events was notably faster in the Philippine compared to other countries, which is presumed to be associated with the large amounts of SO_2 emitted from the active Taal Volcano. Although the temperature within the PBL was higher than in the upper layers, the RH was sufficiently low (~60 %), which generated favorable conditions for NPF events (Hamed et al., 2011). The low number concentration of accumulation mode particles larger than 100 nm in diameter also facilitated the occurrence of NPF events.

In the Republic of Korea region, a total of three NPF events occurred during five flights. Unlike the NPF events in other countries, these three events all initiated at altitudes above the PBL. Among them, two were observed only over the land, while the remaining one event was observed not only over land area but also over the Yellow Sea. Uniquely for this case, the Gisang 1 research vessel operated by the National Institute of Meteorological Sciences (NIMS) of Korea also observed the NPF event over the Yellow Sea but at a later time than that onboard the aircraft, suggesting that the NPF event that occurred aloft penetrated down to lower altitude as the PBL expanded during the day. Temperature profiles differed slightly among the three event days, but RH remained consistently below 60%.

NPF events were observed in the Thailand region in two of the four flights, and in all three flights in the Taiwan region. The horizontal extent of the NPF events was mostly limited to Bangkok (Thailand) and to Tainan and Chiayi (Taiwan), and vertically, they were primarily confined within the PBL. Except for the first flight in Taiwan, the research flights in both countries consisted of only two laps, and as a result, the growth of newly formed particles could not be clearly identified. More detailed results will be presented at the conference

ACKNOWLEDGEMENTS

This work was supported by the National Institute of Environmental Research (NIER) of Korea grant funded by the Korean Government (MSIT) (NIER-2024-03-02-006) and Yonsei Signature Research Cluster Program of 2023-22-0009. We are grateful to the National Aeronautics and Space Administration (NASA) for the support provided by the DC-8 and its crew.

REFERENCES

Charlson, R.J., 1969. Atmospheric visibility related to aerosol mass concentration: review. Environ. Sci. Technol. 3, 913-918.

Crumeyrolle, S., Manninen, H.E., Sellegri, K., Roberts, G., Gomes, L., Kulmala M., Weigel, R., Laj, P., Schwarzenboeck, A., 2010: New particle formation events measured on board the ATR-42 aircraft during the EUCAARI campaign. Atmos. Chem. Phys. 10, 6721-6735.

Hamed, A., Korhonen, H., Sihto, S.-L., Joutsensaari, J., Järvinen, H., Petäjä, T., Arnold, F., Nieminen, T., Kulmala, M., 2011. The role of relative humidity in continental new particle formation. J. Geophys. Res. Atmos. 116, D03202.

Šmejkalová, H. A., Zíková, N., Ždímal, V., Plachá, H., Bitter, M., 2021. Atmospheric aerosol growth rates at different background station types. Environ. Sci. Pollut. Res. 28, 13352–13364.

Kulmala, M., Petäjä, T., Nieminen, T., Sipilä, M., Manninen, H.E., Lehtipalo, K., Dal Maso, M., Aalto, P.P., Junninen, H., Paasonen, P., 2012. Measurement of the nucleation of atmospheric aerosol particles. Nat. Protoc. 7, 1651-1667.

Ramanathan, V., Crutzen, P.J., Kiehl, J.T., Rosenfeld, D., 2001. Aerosols, climate, and the hydrological cycle. Science. 294, 2119-2144.

Streets, D.G., et al., 2003. An inventory of gaseous and primary aerosol emissions in Asia in the year 2000. J. Geophys. Res. 108, 8809.

Yu, F., Luo, G., 2009. Simulation of particle size distribution with a global aerosol model: contribution of nucleation to aerosol and CCN number concentrations. Atmos. Chem. Phys. 9, 7691–7710.

Yue, D.L., Hu, M., Zhang, R.Y., Wu, Z.J., Su, H., Wang, Z.B., Peng, J.F., He, L.Y., Huang, X.F., Gong, Y.G., Wiedensohler, A., 2011. Potential contribution of new particle formation to cloud condensation nuclei in Beijing. Atmos. Environ. 45, 6070–6077.

Kulmala, M., Petäjä, T., Ehn, M., Thornton, J., Sipilä, M., Worsnop, D.R., Kerminen, V.-M., 2014. Chemistry of atmospheric nucleation: on the recent advances on precursor characterization and atmospheric cluster composition in connection with atmospheric new particle formation. Annu. Rev. Phys. 65, 21–37.

NEW INSIGHTS INTO THE MOLECULAR CHEMICAL CHARACTERISTICS AND SOURCES OF ATMOSPHERIC ORGANIC AEROSOLS IN EAST CHINA

MAOYU CAO[1], CHAO YAN[1,2], YULIANG LIU[1], JUNCHAO YIN[1], DAFENG GE[1], YUANYUAN LI[1], BISEN HAN[2], ZHENNING WANG[1], WEI NIE[1,2], AIJUN DING[1,2]

[1]School of Atmospheric Sciences, Nanjing University, Nanjing, 210046, China
[2] Nanjing-Helsinki Institute in Atmospheric and Earth System Sciences, Nanjing University, Nanjing, 210046, China

Keywords: OOMs, Organic aerosols, source apportionment.

Secondary organic aerosols (SOA) play a critical role in atmospheric chemistry, posing considerable challenges for air quality management and public health (Carslaw et al., 2013). Oxygenated organic molecules (OOMs) have been identified as key precursors in the formation and growth of SOA and new atmospheric particles. Due to their low volatility, OOMs readily condense onto existing particle surfaces, substantially contributing to particle mass growth and influencing aerosol composition, size distribution, and atmospheric lifetime (Nie et al., 2022; Ehn et al., 2014; Riccobono et al., 2014). Recent studies have demonstrated that condensed-phase reactions can rapidly transform the chemical composition of organic aerosols (OA), significantly affecting the contribution of OOMs to particle mass (Pospisilova et al., 2020). Consequently, acquiring detailed information on the composition of OOMs in particulate matter is essential for understanding their condensed-phase reactivity, which is pivotal to elucidating the atmospheric life cycle of particles and the global carbon budget.

In this study, we conducted an intensive 24-day field campaign in Nanjing, China, employing a Vaporization Inlet for Aerosols (VIA) coupled with a nitrate Chemical Ionization Mass Spectrometer (VIA-NO_3-CIMS), alongside a high-resolution time-of-flight aerosol mass spectrometer (HR-TOF-AMS). This comprehensive dataset enabled a detailed characterization of the chemical composition and sources of OOMs in ambient particulate matter. We systematically analyzed the distribution and dominant species of OOMs, and further explored their elemental composition under varying meteorological conditions. By integrating source apportionment results from both AMS and VIA-NO_3-CIMS, we inferred potential particle-phase reaction pathways. Overall, our findings offer new insights into the particle-phase chemistry of OOMs and advance our understanding of the atmospheric evolution and transformation of organic aerosols.

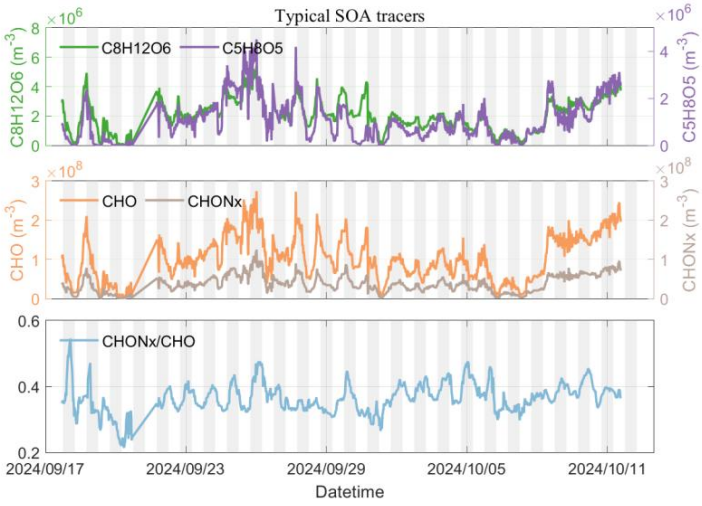


Fig. 1. Time series of CHO and CHONx compounds, their ratios, and SOA tracers in particulate matter.

ACKNOWLEDGEMENTS

This study is funded by the National Natural Science Foundation of China (NSFC) project 42475118.

REFERENCES

Carslaw, K. S. (2013). Large contribution of natural aerosols to uncertainty in indirect for*cing*, *J. Nature*, *503*(7474), 67-71.

Ehn, M. (2014). A large source of low-volatility secondary organic aerosol, *J. Nature*, *506*(7489), 476-479.

Nie, W. (2022). Secondary organic aerosol formed by condensing anthropogenic vapours over China's megacities, *J. Nature Geoscience*, *15*(4), 255-261.

Pospisilova, V. (2020). On the fate of oxygenated organic molecules in atmospheric aerosol particles, *J. Science Advances*, *6*(11), 8922.

Riccobono, F.(2014). Oxidation Products of Biogenic Emissions Contribute to Nucleation of Atmospheric Particles, *J. Science*, *344*(6185), 717-721.

INSIGHTS OF LONG-TERM AEROSOL PARTICLE SIZE DISTRIBUTION MEASUREMENTS DOWN TO 1 NM WITH THE NEW AIRMODUS A12 IN HYYTIÄLÄ, FINLAND

H. G. HARTL[1,2], M. KULMALA[1], J. VANHANEN[2] and K. LEHTIPALO[1,3]

[1]*Institute for Atmospheric and Earth System Research, Faculty of Science, University of Helsinki, Helsinki, Finland.*

[2]*Airmodus Oy, Helsinki, Finland*

[3]*Finnish Meteorological Institute, Helsinki, Finland*

Keywords: AEROSOL MEASUREMENTS, NPF, UFP.

INTRODUCTION

Traditionally, ultrafine aerosol particle size distributions are measured using mobility-based instruments , which classify particles according to their electrical mobility and require these to be electrically charged (Winklmayr et al., 1991). At the lower nanometer scale charging probabilities are negligible and diffusion is dominant causing significant sampling losses (Wiedensohler, 1988). The combination of these effects renders the detection of sub 3 nm particles challenging and makes counting statistics unreliable, ultimately impeding the ability to obtain reliable measurements in this critical regime.

To overcome this limitation, an activation-based approach for measuring particle size distributions was introduced with the Airmodus A11 system (Vanhanen et al., 2011). It operates by counting the number of particles activated to optically detectable sizes in an environment supersaturated by its working fluid's vapor. The activation onset diameter poses a function of the supersaturation and by varying latter the fraction of activated particles varies likewise, yielding particle size distributions in the size range of approximately 1 to 4 nm. Due to its redesigned liquid-handling-, saturator-flow- and flow mixing-system its succeeder – the Airmodus A12 (Sulo et al, 2023) – offers an extended detection size range of around 1 to 12 nm, while also providing improved stability.

In this study, we for the first time present long-term measurements conducted in Hyytiälä, Finland, using the Airmodus A12. We evaluate its performance by comparing it with established measurement techniques, provide insights into its capabilities and limitations in atmospheric nanoparticle detection, bridging the gap between ion- and particle-mode measurements and ultimately discuss observed new particle formation events.

METHODS

We analyzed time series of ambient air data as measured by the novel Airmodus A12 over the course of selected months in the period of February 2024 to February 2025 at SMEAR II station. These results were investigated on overall concentrations, size distribution and new particle formation events. Additionally, we compared these results to the data as gathered by other well-established instruments e.g. its predecessor, the Airmodus A11, as well as a Neutral Cluster and Air Ion Spectrometer (NAIS) and a Differential mobility Particle Sizer (DMPS). The SMEAR II station is located at the remote countryside of Hyytiälä within a boreal forest in southern Finland and is part of the ACTRIS network.

CONCLUSIONS

The first long-term time series of particle size distributions using the Airmodus A12 was obtained, providing new insights into the concentration and size distribution of ultrafine particles and new particle formation events. As shown in Figure 1, a comparison of different instruments demonstrates good overall agreement in particle number concentrations between the Airmodus A11, the novel Airmodus A12 and the Airel NAIS, particularly in the size ranges above 2.5 nm and below 1.5 nm, consistent with the findings of Sulo et al. (2023). Temporal variations were identified to be driven by seasonal and diurnal cycles, as well as NPF events. These aspects will be further explored in the conference sessions.

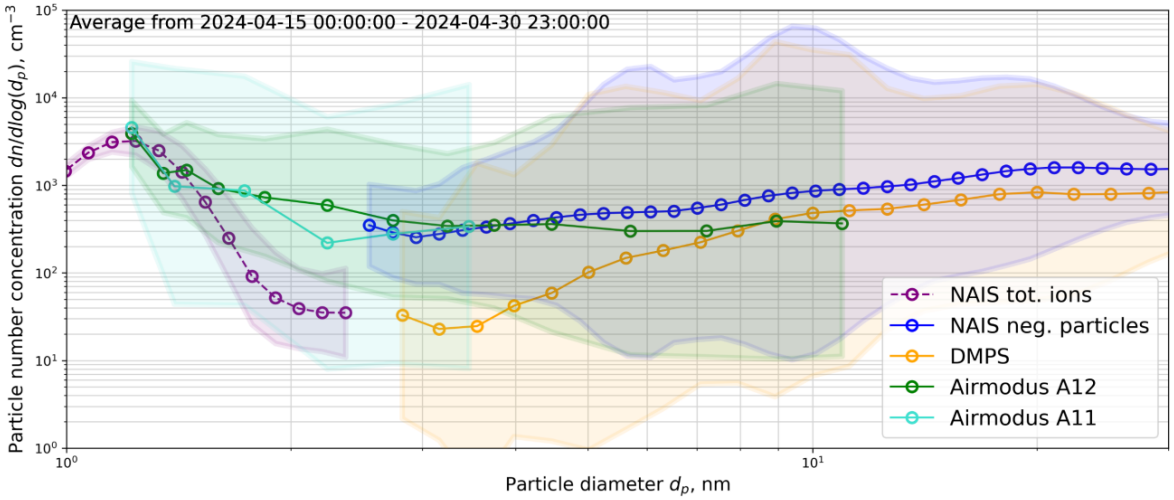


Figure 1. Average size distributions for different instruments at Hyytiälä SMEAR II station in the second half of April 2024. The colored areas represent the temporal variations in the particle size distribution of each instrument over the shown time span.

ACKNOWLEDGEMENTS

This work was supported by the Research Council of Finland, the University of Helsinki through funding for ACTRIS-Finland and the Doctoral School of Industry Innovations (DSII).

REFERENCES

Sulo, J. et al. (2023). Pushing nano-aerosol measurements towards a new decade -- technical note on the Airmodus particle size magnifier 2.0, *Aerosol Research* **2**, 13-20.

Vanhanen, J., et al. (2011). Particle Size Magnifier for Nano-CN Detection, *Aerosol Science and Technology* **45:4**, 533-542.

Wiedensohler, A., et al (1988). An Approximation of the Bipolar Charge Distribution for Particles in the Submicron Size Range, *Journal of Aerosol Science* **19**, 387-389.

Winklmayr, W., et al. (1991). A new Electromobility Spectrometer for the Measurement of Aerosol Size Distributions in the Size Range from 1 to 1000 nm, *Journal of Aerosol Science* **22**, 289-296.

OBSERVING CLOUDS IN A WARMING WORLD: THE ACTRIS TOPICAL CENTRE FOR CLOUD IN SITU MEASUREMENTS

K. HÖHLER[1], T. BACHLEITNER[2], N. BÜTTNER[1], R. FÖSIG[1], A. KARRAIS[1], U. KÄFER[3], L. LACHER[1], E. LUDEWIG[2], C. MAIER[2], O. MÖHLER[1], D. VAN PINXTEREN[3], and A. SCHWARZENBÖCK[4]

[1]*Institute of Meteorology and Climate Research Atmospheric Aerosol Research (IMKAAF), Karlsruhe Institute of Technology (KIT), Karlsruhe, Germany.*

[2]*Sonnblick Observatory, GeoSphere Austria, Salzburg, Austria.*

[3]*Atmospheric Chemistry Department (ACD), Leibniz Institute for Tropospheric Research (TROPOS), Leipzig, Germany.*

[4]*Laboratoire de Météorologie Physique, Université Clermont Auvergne, Clermont-Ferrand, France.*

Keywords: ACTRIS, MONITORING, CLOUDS, CLOUD CLIMATE FEEDBACK

THE IMPORTANCE OF CLOUD OBSERVATIONS

Clouds significantly affect Earth's radiative balance and hydrological cycle, influencing both climate regulation and weather patterns. Changes in cloud properties - such as amount, altitude, opacity, and microphysics - have far-reaching implications for the Earth's energy budget and regional precipitation. Climate models still show large differences in the predicted cloud feedback to increased global temperatures (e.g., Zelinka *et al.*, 2022), especially aerosol-cloud interactions and the role of atmospheric ice-nucleating particles are not well understood (e.g., Burrows *et al.*, 2022). As an example, the global temperature surge in 2023 was recently connected to a non-predicted decline of low-level clouds over the northern mid-latitudes and tropical oceans (Goessling *et al.*, 2025). To better understand cloud-climate feedback and to be able to refine climate projections, long-term cloud data is needed. While remote sensing and satellite observations provide useful large-scale data, *in situ* measurements are crucial for characterizing local cloud properties and for better understanding microphysical cloud processes.

ACTRIS AND THE TOPICAL CENTRE FOR CLOUD IN SITU MEASUREMENTS (CIS)

ACTRIS (Aerosol, Clouds, and Trace Gases Research Infrastructure) is a European Research Infrastructure Consortium (ERIC) dedicated to atmospheric research, providing facilities, data, and services for studying short-lived atmospheric constituents and clouds (Laj *et al.*, 2024). It addresses pressing challenges related to climate change, air quality, and human health by ensuring standardized methodologies and quality assurance / quality control through its so-called Topical Centres. ACTRIS prioritizes high-quality, FAIR (findable, accessible, interoperable, reusable) long-term data to ensure accessibility and usability for both researchers and policymakers.

Within ACTRIS, the Topical Centre for Cloud In Situ Measurements (CIS) focuses on *in situ* measurements of critical cloud properties, which include:

- Liquid water content and cloud droplet effective diameter
- Cloud particle number and size distribution
- Bulk cloud water chemistry
- Ice nucleating particle (INP) concentrations

CIS ensures the quality of cloud in situ data derived by ACTRIS research stations, mobile platforms and atmospheric simulation chambers by providing guidelines for instrumentational setup, measurement procedures and data management. Also, quality audits as part of the ACTRIS evaluation process and training workshops are conducted.

CIS CURRENT STATUS

This presentation will provide an overview of TC CIS's current progress, highlighting the development of standardized measurement protocols and QA/QC procedures. It will present findings from early inter-comparison campaigns, which evaluate cloud in situ instrumentation. These efforts are key for validating instruments, refining operational practices, and ensuring the consistency of TC CIS data.

ACKNOWLEDGEMENTS

This work was supported by the German Federal Ministry of Education and Research (BMBF, grant 01LK2002B) and by the German Federal Ministry for the Environment, Nature Conservation, Nuclear Safety and Consumer Protection (BMUV).

REFERENCES

Burrows, S. M., et al. (2022). Ice-nucleating particles that impact clouds and climate: Observational and modeling research needs. *Reviews of Geophysics*, 60, e2021RG000745.

Goessling, F., et al. (2025). Recent global temperature surge intensified by record-low planetary albedo, *Science* **387**, 68-73.

Laj, P., et.al. (2024). Aerosol, Clouds and Trace Gases Research Infrastructure (ACTRIS): The European Research Infrastructure Supporting Atmospheric Science. *Bull. Amer. Meteor. Soc.*, **105**, E1098–E1136.

Zelinka, M. D., et. al. (2022). Evaluating climate models' cloud feedbacks against expert judgment. *J. of Geophys. Res.: Atmospheres*, 127.

CHARACTERIZING AIRBORNE ULTRAFINE PARTICLES IN CHINA BASED ON A BIPOLAR SMPS NETWORK

JINGKUN JIANG[1], JIN WU[1], YIRAN LI[1], HAO WU[1], QIANG ZHANG[1], HAN LIAO[1], YIYANG WANG[1]

[1]*State Key Joint Laboratory of Environment Simulation and Pollution Control, School of Environment, Tsinghua University, Beijing, 100084, China*

Keywords: Ultrafine Particles, Aerosol Network Measurement, Aerosol Charging, Particle Number Size Distribution

INTRODUCTION

Airborne ultrafine particles (UFPs), which are defined as particles with diameters smaller than 100 nm, can significantly influence global climate, regional air quality, and human health (Kumar et al., 2014; Schraufnagel, 2020). The particle number size distribution (PNSD) is a key parameter for understanding the sources and impacts of UFPs (Cai et al., 2020; Kuwayama, Ruehl, & Kleeman, 2013). The latest directive on ambient air quality and cleaner air of European Union recommends measuring the size distribution of UFPs, especially in urban sites. Considering the complex spatiotemporal variations and potential adverse health impacts of UFPs, the World Health Organization has also recommended integrating ultrafine particles into existing air quality monitoring. Therefore, it is necessary to establish networks that continuously monitor PNSD. There are already some PNSD networks such as Global Atmosphere Watch (GAW) (Rose et al., 2021), EU infrastructure project ACTRIS (Laj et al., 2024), German Ultrafine Aerosol Network (GUAN) (Birmili et al., 2016) and Spanish REDMAAS (Alonso-Blanco et al., 2018).

In this study, we build a bipolar SMPS network in China and have carried out two phases of observation so far. The network consists of 4 urban sites, 3 suburban sites and 7 background sites, covering key regions across China. The positively and negatively charged particles are scanned without conventional neutralizers. A set of harmonized quality assurance procedures including laboratory calibrations and intercomparisons, maintenance and monitoring are adopted during field measurement. We also confirmed that sum inversion is a reliable method to mitigate the deviation resulting from fluctuation of charge fractions.

METHODS

Field measurement was conducted in 14 sites across China (Figure 1). Eight homemade bipolar SMPSs were used in the observation, which can scan negative and positive particles in the size range of 10–700 nm, and measure the total particle number concentration at 5-minutes intervals (Li et al., 2024). We adopted harmonized quality assurance procedures in this network based on existing ones used in GAW and GUAN with some improvements. These instruments were calibrated every year to ensure their comparability.

When performing data inversion, the charge fractions of particles are important parameters, but they can differ significantly from those assumed in approximations or models that use fixed ion properties. To evaluate fluctuation of charge fractions in long-term observation, we analyzed the raw data of positively and negatively charged aerosols conditioned by different neutralizers. We also investigated whether using the concentrations of both positively and negatively charged particles during inversion provides better results than using unipolar data alone (Chen & Jiang, 2018).

CONCLUSIONS

In the network, the number concentration of ultrafine particles (N_{UFP}) dominates the total particle number concentration at most sites. Atmospheric new particle formation (NPF) is an important source of N_{UFP} and contributes more to N_{UFP} at suburban sites than at urban sites. For instance, N_{UFP} on NPF days can be 88% higher than those on non-NPF days at the Kunming site. The diurnal cycles of N_{UFP} and $PM_{2.5}$ are different, the former cannot be captured by the existing national air quality monitoring system. From 2013 to 2023, N_{UFP} has significantly decreased by 55.2% and 66.4% in Beijing and Shanghai, reflecting the effectiveness of air pollution control. To improve the accuracy of inverted PNSD, we recommend using the sum inversion method together with the actual charge fractions retrieved from the raw bipolar data instead of approximation formulae. The raw concentration of positively and negatively charged particles provides information about both charge fractions and ion properties.

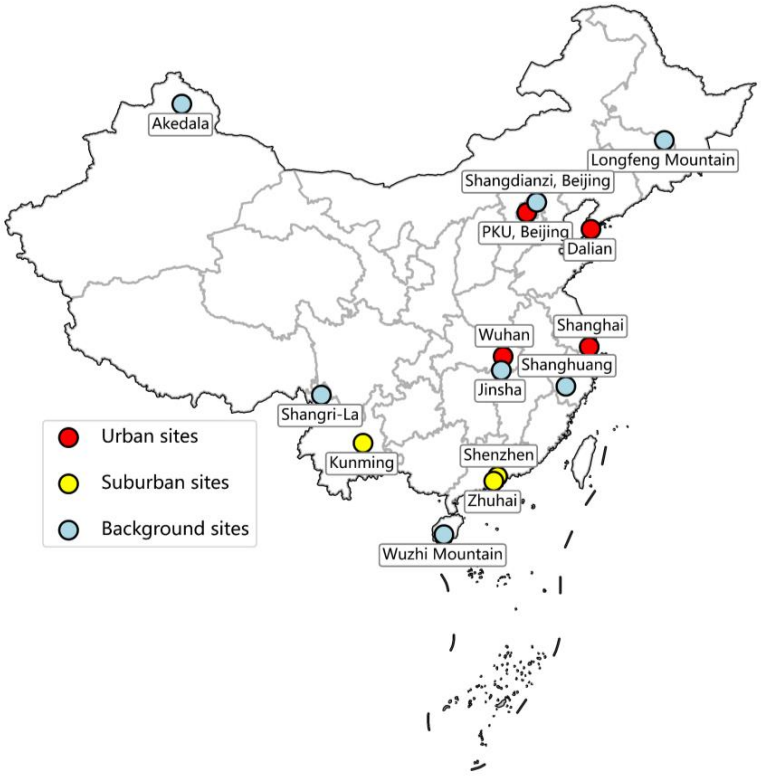


Figure 1. Locations of measurement sites

ACKNOWLEDGEMENTS

This work was supported by the National Natural Science Foundation of China (22327806) and China Postdoctoral Science Foundation (2023M741930).

REFERENCES

Alonso-Blanco, E., Gomez-Moreno, F. J., Artinano, B., Iglesias-Samitier, S., Juncal-Bello, V., Pineiro-Iglesias, M., . . . Alados-Arboledas, L. (2018). Temporal and spatial variability of atmospheric particle number size distributions across Spain. *Atmospheric Environment, 190*, 146-160. doi:10.1016/j.atmosenv.2018.06.046

Birmili, W., Weinhold, K., Rasch, F., Sonntag, A., Sun, J., Merkel, M., . . . Fiebig, M. (2016). Long-term observations of tropospheric particle number size distributions and equivalent black carbon mass concentrations in the German Ultrafine Aerosol Network (GUAN). *Earth System Science Data, 8*(2), 355-382. doi:10.5194/essd-8-355-2016

Cai, J., Chu, B., Yao, L., Yan, C., Heikkinen, L. M., Zheng, F., . . . Daellenbach, K. R. (2020). Size-segregated particle number and mass concentrations from different emission sources in urban Beijing. *Atmospheric Chemistry and Physics, 20*(21), 12721-12740. doi:10.5194/acp-20-12721-2020

Chen, X., & Jiang, J. (2018). Retrieving the ion mobility ratio and aerosol charge fractions for a neutralizer in real-world applications. *Aerosol Science and Technology, 52*(10), 1145-1155. doi:10.1080/02786826.2018.1498587

Kumar, P., Morawska, L., Birmili, W., Paasonen, P., Hu, M., Kulmala, M., . . . Britter, R. (2014). Ultrafine particles in cities. *Environment International, 66*, 1-10. doi:10.1016/j.envint.2014.01.013

Kuwayama, T., Ruehl, C. R., & Kleeman, M. J. (2013). Daily Trends and Source Apportionment of Ultrafine Particulate Mass (PM0.1) over an Annual Cycle in a Typical California City. *Environmental Science & Technology, 47*(24), 13957-13966. doi:10.1021/es403235c

Laj, P., Lund Myhre, C., Riffault, V., Amiridis, V., Fuchs, H., Eleftheriadis, K., . . . Vana, M. (2024). Aerosol, Clouds and Trace Gases Research Infrastructure (ACTRIS): The European Research Infrastructure Supporting Atmospheric Science. *Bulletin of the American Meteorological Society, 105*(7), E1098-E1136. doi:10.1175/bams-d-23-0064.1

Li, Y., Wu, J., Wu, H., Liu, X., Zhou, Q., Lu, Y., . . . Jiang, J. (2024). A bipolar SMPS network for measuring atmospheric aerosols using natural air ions. *Atmospheric Environment, 325*, 120462. doi:https://doi.org/10.1016/j.atmosenv.2024.120462

Rose, C., Collaud Coen, M., Andrews, E., Lin, Y., Bossert, I., Lund Myhre, C., . . . Laj, P. (2021). Seasonality of the particle number concentration and size distribution: a global analysis retrieved from the network of Global Atmosphere Watch (GAW) near-surface observatories. *Atmospheric Chemistry and Physics, 21*(22), 17185-17223. doi:10.5194/acp-21-17185-2021

Schraufnagel, D. E. (2020). The health effects of ultrafine particles. *Experimental and Molecular Medicine, 52*(3), 311-317. doi:10.1038/s12276-020-0403-3

ACTRIS – HIGH QUALITY ATMOSPHERIC DATA TO ALL USERS

N. KIVEKÄS[1], E. JUUROLA[1], G. SAPONARO[1], M. PARAMONOV[1], T. PETÄJÄ[1], C. CORNACCHIA[2], R. PETRACCA ALTIERI[2], A. WIEDENSOHLER[3], R. TILLMANN[4], K. HÖHLER[5], M. HAEFFELIN[6], M. DE MAZIERE[7], D. NICOLAE[8] and C. LUND MYHRE[9]

[1]*ACTRIS ERIC, Helsinki, Finland*

[2] *Institute of Methodologies for Environmental Analysis, National Research Council of Italy, Potenza, Italy*

[3]*Leibniz Institute for tropospheric research, Leipzig, Germany*

[4] *Forschungszentrum Jülich, Jülich, Germany*

[5] *Karlsruhe Institute of Technology, Karlsruhe, Germany*

[6] *French National Centre for Scientific Research, Paris, France*

[7] *Royal Belgian Institute for Space Aeronomy, Brussels, Belgium*

[8] *National Institute of Research and Development for Optoelectronics, Bucharest, Romania*

[9] *NILU – Norwegian institute for air research, Kjeller, Norway*

Keywords: ACTRIS, atmospheric aerosol, measurements, instrumentation, data.

INTRODUCTION

The Aerosol, Cloud and Trace Gases Research Infrastructure (ACTRIS) is a European Research Infrastructure for providing high-quality data and services on short-lived atmospheric constituents: aerosol particles, cloud microphysics and reactive trace gases through in situ measurements and remote sensing of the atmosphere. Additionally, ACTRIS provides physical and remote access to well-equipped observational and exploratory research facilities and training for facilities' staff, students and service users. ACTRIS is not project-based but is funded by participating countries for long-term operation. A thorough description of ACTRIS is available at Laj *et al*. (2024).

METHODS FOR DATA

The origin of ACTRIS data is the currently 78 observational sites, 18 mobile platforms, 14 atmospheric simulation chambers and one laboratory measuring properties of either ambient or artificial atmosphere, measuring more than one hundred atmospheric parameters. These so-called ACTRIS national facilities (NFs) are large-scale research facilities at the cutting edge of scientific discovery that enable both excellence in basic and advanced research - critical to future developments. The locations of ACTRIS measurement sites are shown in figure 1.

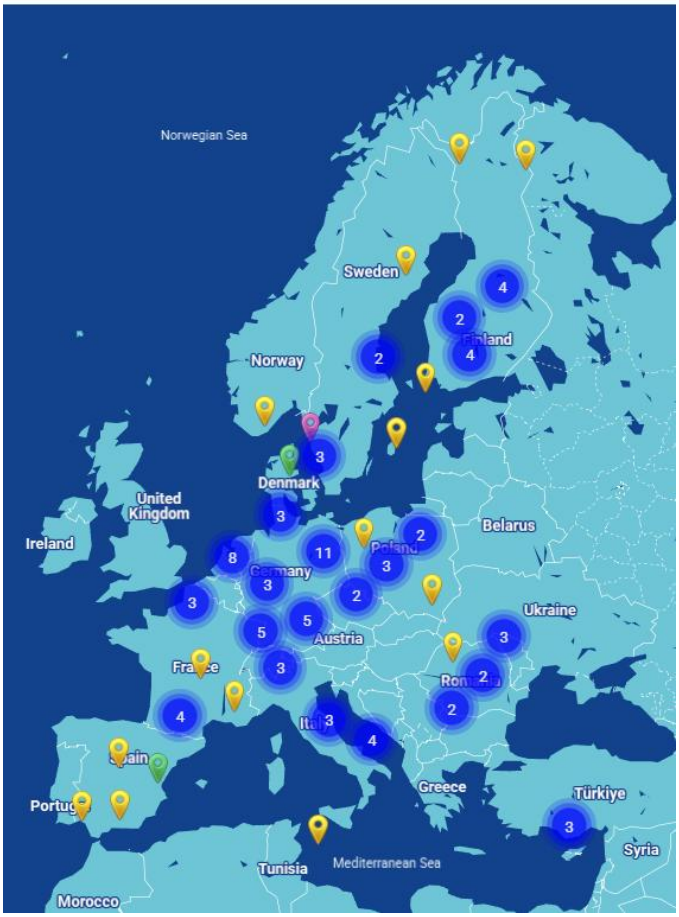


Figure 1. Location of ACTRIS measurement sites across Europe.

The NFs are supported by Central Facilities (CFs), which provide training, standard operation procedures for instruments, instrument calibrations and site evaluations. Six of these are called Topical Centres, each focusing on a specific type of measurements.

Measurements	Topical Centre (acronym)	Web page
Aerosol in situ	CAIS-ECAC	*https://www.actris-ecac.eu/*
Aerosol remote sensing	CARS	*https://www.actris.eu/topical-centre/cars*
Cloud in situ	CIS	*https://www.actris.eu/topical-centre/cis*
Cloud remote sensing	CCRES	*https://www.actris.eu/topical-centre/ccres*
Trace gases in situ	CiGas	*https://www.actris.eu/topical-centre/cigas*
Trace gases remote sensing	CREGARS	*https://www.actris.eu/topical-centre/cregars*

Table 1. Types of measurements and the respective Topical Centres.

The NFs produce measurement data and provide the data to the ACTRIS Data Centre (DC, *https://www.actris.eu/topical-centre/data-centre*), which is responsible for making the data available for users of any kind. The DC collects the data in a pre-defined format with rich meta data. The DC also creates digital identifiers (DOI) for the data sets so that a specific data set can be directly referenced in a publication, acknowledging the persons and institutions that had produced the data. The data centre offers centralized data processing, software and tools for data processing, and centralised quality control of the data to ensure harmonised quality over time and space. The data are openly searchable and available for any user through a user-oriented data portal and through machine-to-machine interface.

ACCESS

ACTRIS is one of the rare Research Infrastructures providing all different types of access to services: virtual access to data, physical, remote and hybrid access for research and innovation, as well as technical and training services provided by the ACTRIS facilities. The access to ACTRIS services can be:
Curiosity-driven, when it supports fundamental or disruptive research in all fields,
Challenge-driven, when it addresses problems that have immediate or future societal relevance, supporting scientific investigations to find practical solutions,
Excellence-driven, when it depends on scientific excellence, originality, quality and technical feasibility of a user project,
Need-driven, when it is required to meet specific needs of users, e.g., technical needs to guarantee quality assurance and high instrument performance, or training needs,
Market-driven: when it satisfies the specific needs of the private sector users and is customized to meet their requirements.

RESULTS

The result of the collaboration of the entities described above is inter-comparable high-quality data from sites across Europe and beyond, provided from a single data portal in a unified format. The high-quality data based on the traceable provision chain are used by organizations such as Copernicus and ESA in their services.
Besides data, the same strict quality control measures apply to instruments and procedures used at the facilities providing access to users, being the simulation chambers, mobile platforms, laboratory and many of the observational platforms. The strict quality control of the entire process from measurements up to the final data products enables the users to properly account for any uncertainties associated with the measurements.
All ACTRIS data and services can be obtained through the ACTRIS web page at ***https://www.actris.eu/***

ACKNOWLEDGEMENTS

ACTRIS is mostly funded by the member countries. Further, ACTRIS and its activities have been supported by numerous EC grants and are currently supported by the EC grants 101008004 (ATMO-ACCESS, 2021-2025), 101036245 (RI-URBANS, 2021-2025), 101131141 (ENVRI-hub NEXT, 2023-2027), 101131426 (ENVRINNOV, 2023-2027), 101132093 (CARGO-ACT, 2024-2027) and 101131261 (IRISCC 2024-2028). We also thank the numerous past and ongoing national projects and programs for providing immense support for long-term atmospheric and aerosol research throughout Europe.

REFERENCES

Laj, P. et al., (2024). Aerosol, Clouds and Trace Gases Research Infrastructure (ACTRIS): The European Research Infrastructure Supporting Atmospheric Science, B. *American Met. Soc.* **23**, E1098-E1136.

ACTRIS CLUSTER CALIBRATION CENTER: TOWARDS STANDARDIZING THE MEASUREMENTS OF SUB-10 NM AEROSOL PARTICLES

K. LEHTIPALO[1,2], J. LAMPILAHTI[1], H. HARTL[1], T. PETÄJÄ[1] and S. HÄME[1]

[1]Institute for Atmospheric and Earth System Research/ Physics, Faculty of Science, University of Helsinki, Finland.
[2]Finnish Meteorological Institute, Helsinki, Finland.

Keywords: aerosol size distribution, calibration, ion spectrometers, mobility particle sizers

INTRODUCTION

Measuring the aerosol particle size distribution down to the size of the nucleating clusters (~1 nm) is crucial for understanding particle formation and growth processes. Moreover, ultrafine particles often dominate the aerosol number concentration especially in urban environments. During so called new particle formation events or close to traffic emissions, even the majority of particles can be smaller than 10 nm (Zhou et al. 2020). However, measuring the smallest particles is difficult due to their high diffusivity and low charging probability. Standard methods for aerosol size distribution measurements, such as mobility particle sizer spectrometers (MPSSs) exhibit large variability in the sub-10 nm size range (Wiedensohler et al. 2012). Therefore, there is an urgent need to improve the instrumentation and methods for determining the sub-10 nm particle concentration and size distribution, as well as to develop the related calibration practices.

METHODS

The Aerosol, Clouds and Trace Gases Research Infrastructure (ACTRIS) is a pan-European distributed research infrastructure for short-lived atmospheric constituents. The Cluster Calibration Center (CCC), hosted by University of Helsinki, is part of the ACTRIS Center for Aerosol In-Situ Measurements (CAIS-ECAC). The CCC provides services to the ACTRIS National Facilities (i.e. measurement stations and platforms) and other users of ACTRIS, who want to perform measurements on aerosol particle concentration and size distribution extending to sizes below 10 nm with instrumentation optimized for this purpose. Such instruments include e.g. ultrafine Condensation Particle Counters (UF-CPCs), Particle Size Magnifiers (PSMs), nano-MPSSs (e.g. nano-scanning mobility particle sizers) and ion spectrometers (e.g. Neutral Cluster and Air Ion Spectrometer NAIS).

The tasks of CCC include developing instructions, standard operation procedures, data tools, organizing instrument calibration and intercomparison workshops and providing training and consultancy. Our aim is to test and validate the methods for measuring sub-10 nm particle concentrations and size distributions and to improve the methods for calibrating the relevant instrumentation. Several steps have been made in this direction, which will be reviewed in this presentation.

RESULTS & CONCLUSIONS

The operational activities of the ACTRIS Cluster Calibration Center have been started and first instrument intercomparison workshops were organized in 2023, separately for ion spectrometers and for instruments relying on CPCs (UF-CPCs, PSMs and nano-MPSSs). During the workshops, the instruments' sizing accuracy and concentration response was tested for size-selected test particles. Additionally, the workshops included an intercomparison of all the participating instruments.

As an example of the CCC activities, Figure 1 presents intercomparison results from the NAIS workshop in 2023. Most instruments compare very well to each other and to the reference NAIS, both in ion and particle

modes. Only Instrument 1 (blue line), which is an older model, show clearly larger concentrations throughout the whole size range. Below ca. 3 nm the instrument-to-instrument variability started to increase. It can also be seen that in the particle mode all the NAISs showed somewhat larger concentrations than the MPSS (dashed line), which has been observed also in earlier NAIS workshops (Gagné et al. 2011). The reasons are under investigation and will be discussed in this contribution.

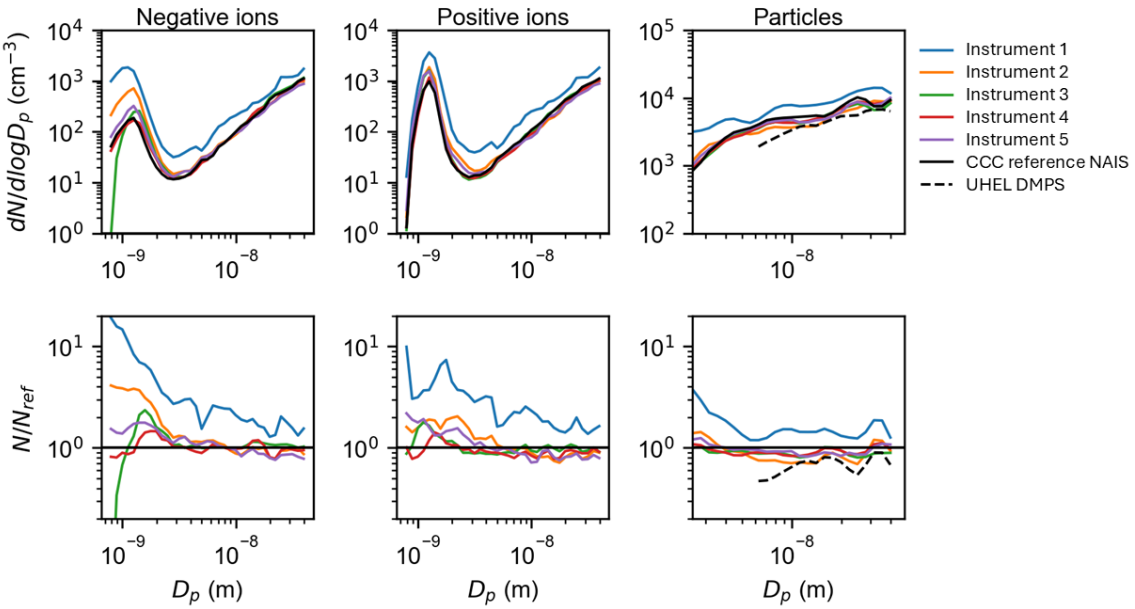


Figure 1. Intercomparison of different NAISs measuring outside air during the ion spectrometer workshop in 2023. Leftmost panels show measurement in the negative ion mode, middle panels positive ion mode and rightmost panels in particle mode. The lower row shows the concentration of test instruments divided by the concentration of the reference NAIS. Dashed line shows simultaneous measurements with the Differential Mobility Particle Sizer (DMPS).

ACKNOWLEDGEMENTS

The funding from the host organization University of Helsinki (UH), Research Council of Finland (ACTRIS Central Facilities 2020-2024 grant no. 329274 and 2025-2027 no. 367784) and ACTRIS ERIC are acknowledged.

REFERENCES

Gagné, S. et al.: Intercomparison of air ion spectrometers: an evaluation of results in varying conditions, Atmos. Meas. Tech., 4, 805–822, https://doi.org/10.5194/amt-4-805-2011, 2011.

Wiedensohler, A. et al.: Mobility Particle Size Spectrometers: Harmonization of Technical Standards and Data Structure to Facilitate High Quality Long-term Observations of Atmospheric Particle Number Size Distributions. *Atmos. Meas. Tech.*, 5:657–685, 2012.

Zhou, Y et al.: Variation of size-segregated particle number concentrations in wintertime Beijing, Atmospheric Chemistry and Physics, 20, 1201-1216, https://doi.org/10.5194/acp-20-1201-2020. 2020

THE INFLUENCE OF ATMOSPHERIC TRANSPORT AND MIXING ON INTERPRETATION OF PM1 AND ORGANIC AEROSOL SOURCE APPORTIONMENT AT A RURAL BACKGROUND SITE IN CENTRAL EUROPE

R. LHOTKA[1], P. POKORNÁ[1], P. VODIČKA[1], N. ZÍKOVÁ[1], G. I. CHEN[2,3], A. S. H. PRÉVÔT[3], S. MBENGUE[4], J. SCHWARZ[1], AND V. ŽDÍMAL[1]

[1]*Research Group of Aerosol Chemistry and Physics, Institute of Chemical Process Fundamentals, CAS, Prague 6, Czech Republic*
[2]*MRC Centre for Environment and Health, Environmental Research Group, Imperial College London, London, UK*
[3]*Laboratory of Atmospheric Chemistry, Paul Scherrer Institute, 5232, Villigen, Switzerland*
[4]*Global Change Research Institute, CAS', Brno, Czech Republic*

Keywords: NR-PM1, AMS, Ventilation index, PMF, Air mass back trajectories.

INTRODUCTION

Organic aerosol (OA) is a major component of atmospheric fine aerosol, however the knowledge of its origin and fate in atmosphere is still prone to high uncertainties. The influence of meteorology on its fate and transport is even less known.

METHODS

Compact Time of Flight Aerosol Mass Spectrometer (C-ToF AMS, Drewnick *et al*. 2005) was used to measure NR-PM1 chemical composition in 5 min time resolution at National Atmospheric Observatory Košetice (NAOK) in the Czech Republic. This measurement was complemented with several other instruments including Aethalometer AE33 to measure of equivalent black carbon (eBC). NO_x, SO_2, and O_3 were monitored by Czech Hydrometeorological Institute network.

RESULTS

We analyzed four seasons' data obtained from January till October 2019. Positive matrix factorization (PMF) method was used using SoFi Pro software (SoFi Pro 6.8, Datalystica Ltd., Villigen, Switzerland) to distinguish 4 – 5 organic aerosol (OA) factors of which hydrocarbon like OA (HOA), biomass burning OA (BBOA) and coal combustion OA (CCOA) are known as primary organic aerosol (POA), while less oxidized oxygenated OA (LO-OOA) and more oxidized oxygenated OA (MO-OOA) are known as OOA factors. All factors were separated in all seasons except for summer, when the CCOA factor was missing. The obtained concentration of individual inorganic compounds and organic factors in individual seasons are described in detail in Lhotka *et al.* (2025); here, we focus on the description of meteorology's influence on the interpretation of the obtained results.

Factor	Winter	Spring	Summer	Autumn
HOA	-0.68	-0.49	-0.55	-0.63
BBOA	-0.68	-0.34	-0.44	-0.31
CCOA	-0.49	-0.29	x	-0.26
LO-OOA	-0.51	-0.45	-0.45	-0.79
MO-OOA	-0.71	-0.07	-0.01	-0.34

Table 1. Correlations of individual OA factors with ventilation index in each season.

Ventilation index (VI, Tennekes, 1974) was calculated hourly and average ventilation index for each cluster for all seasons were determined. Correlation analysis of VI with individual OA factors (Tab 1),

when most of the factors at least partially negatively correlated with VI suggested the significant influence of local or regional sources. The only exception was MO-OOA factor that did not correlate with VI in spring and summer and this further supported, together with the conditional bivariate probability function method (CBPF, Uria-Tellaetxe and Carslaw, 2014) analysis, its long-range transport origin in these seasons.

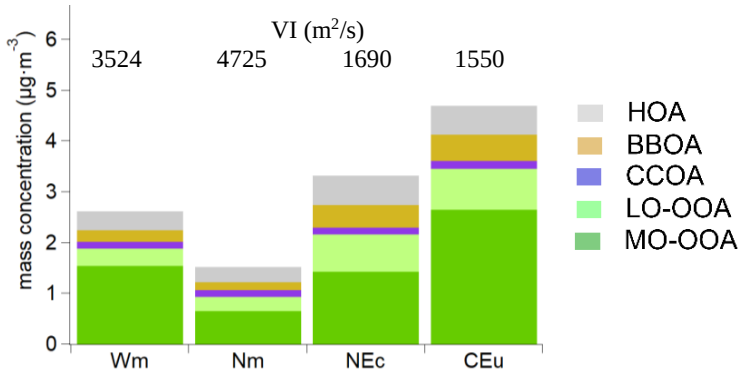


Figure 1. An example of inversion relation between average mass concentrations of OA in individual OA factors and ventilation index for winter season and four AMBT clusters (west marine (Wm), North marine (Nm) North east continental (NEc) and Central European (CEu)).

Air mass back trajectories (AMBT, Stein *et al*., 2015) were calculated for every hour and clustered (Petit *et. al*. 2017) into four to or five clusters depending on a season. Continental and Central European clusters usually exhibited higher concentrations of all OA factors. It appeared that clusters with higher average concentrations were mostly related to low ventilation indexes and vice versa (Figure 1). This confirmed lower influence of long-range transport and higher influence of local and regional organic aerosols during high pollution periods.

CONCLUSIONS

OA factors varied by season, with POA factors most abandoned in winter. Local or regional origin of NR-PM1 OA was observed with exception of MO-OOA in spring and summer based on negative correlations with VI. AMBT cluster analysis should be accompanied with VI analysis to assess real NR-PM1 origin.

ACKNOWLEDGEMENTS

This study was supported by the Ministry of Education, Youth and Sports of the Czech Republic by ACTRIS-CZ LM2023030.

REFERENCES

Drewnick, F. et al. (2005). A new Time-of-Flight Aerosol Mass Spectrometer (TOF-AMS)—Instrument description and first field deployment. *Aerosol Sci. Technol*. **39**, 637.

Lhotka, R. et al. (2025). Influence of meteorological conditions and seasonality on PM1 and organic aerosol sources at a rural background site, *Atmos. Environ.*, **344**, 121028.

Petit, J.E., Favez, O., Albinet, A., Canonaco, F. (2017). A user-friendly tool for comprehensive evaluation of the geographical origins of atmospheric pollution: Wind and trajectory analyses. *Environ. Model. Softw*. **88**, 183.

Tennekes, H. (1974). The Atmospheric Boundary Layer. *Phys. Today*. **27**, 52.

Uria-Tellaetxe, I., and Carslaw, D.C. (2014). Conditional bivariate probability function for source identification. *Environ. Model. Softw*. **59**, 1.

Multi-year measurement of low-volatility vapors and their implications in boreal environment

C. LIU[1], O. PERAKYLA[1], V.S. KOLHINEN[1], L. AHONEN[1], M. EHN[1] and N. SARNELA[1]

[1]*Institute for Atmospheric and Earth System Research, University of Helsinki, Helsinki, Finland*

Keywords: low-volatility vapors, new particle formation, long-term measurement, chemical ionization mass spectrometry

INTRODUCTION

Inorganic and organic vapors with low volatility can either participate in new particle formation or contribute to their subsequent growth. The formed particles can further grow to sizes which have an impact on global climate and human health. Studies show those biogenic low-volatility vapors are formed through autoxidation, that is, a peroxy radical first undergoes an intramolecular hydrogen-atom shift forming a hydroperoxide functionality and an alkyl radical, to which molecular oxygen then rapidly attaches to form a new, more oxidized, peroxy radical (Bianchi et al., 2019). However, the driving factors of this process and detailed formation pathways remains ambiguous, e.g. related to the oxidants that initiate this autoxidation and the pathways to terminate it, as well as the influence of temperature. In this regard, long-term ambient measurement data could help to improve our understanding of autoxidation though recognizing the important influential factors of this process and their implications in the actual atmosphere from a broader temporal perspective. Here, we study the variation of low-volatility vapors concentration from 2019-2022 in a boreal environment, with the focus on how the atmospheric condition affects the behavior of low-volatility vapors and their potential contribution to particle formation.

METHODS

A nitrate-chemical ionization mass spectrometr (CIMS) has been deployed at SMEAR II station (Hyytiälä, southern Finland) since November 2018. In this boreal forest region, oxidation of monoterpenes emitted from Scot pines has been demonstrated to be the main driver of the ultrafine particle's growth (Ehn et al., 2014). Environmental variables, such as temperature vary dramatically between seasons and the nearby forest and soil are often covered by snow during winter months.

The data processing of mass spectra (MS) is challenging and has a lot of uncertainty due to the huge amount of information in the MS. The binPMF method has been introduced to help us better interpret the data (Zhang et al., 2019). In short, the MS data has been binned prior to PMF analysis, reducing the uncertainty by being directly related to the MS data rather than applying PMF to fitted data. It can help to categorize these thousands of peaks in the MS based on their temporal behaviors, highlighting important processes and hence improving the accuracy and efficiency of peak identification.

CONCLUSIONS

Clear seasonal variation was observed for all the low-volatility vapors. Sulfuric acid (SA) concentration shows maximum during both spring and summer because of solar radiation, while biogenic high oxygenated molecules (HOMs) peak in summer due to biogenic emission from the boreal forest. Both SA and HOMs monomers exhibit a diurnal variation pattern with higher concentrations in the day and lower at night, while HOM dimers show the opposite trend.

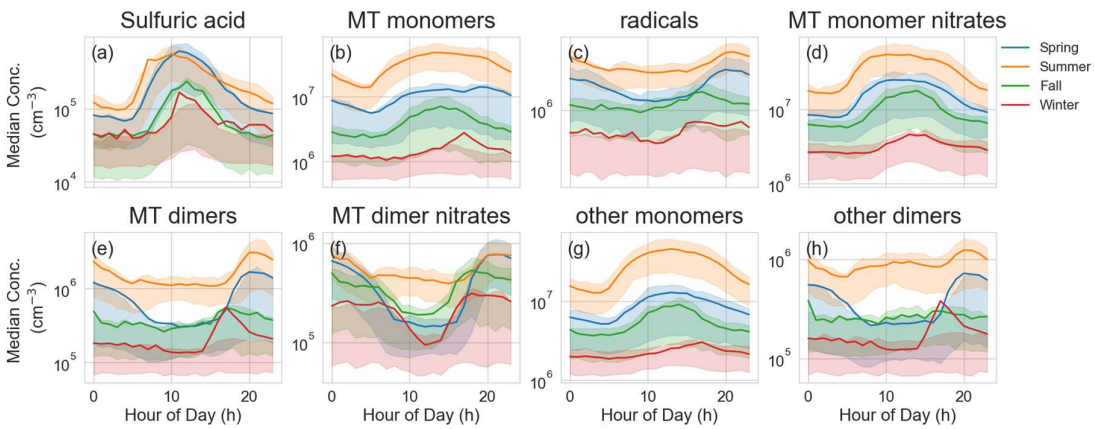


Figure 1. The diurnal variation of low volatility gases across seasons. (a) Sulfuric acid; (b) monoterpene (MT) HOM non-nitrate monomer; (c) HOM radicals; (d) MT HOM monomer nitrates; (e) MT HOM non-nitrate dimers; (f) MT HOM dimer nitrates; (g) other HOM monomers; (h) other HOM dimers. The total HOMs are divided into seven subgroups based on their chemical formula. The band shows the 25th-75th percentile interval.

Indication of temperature-dependent autoxidation rates was observed for the first time in the ambient environment. Fig 2a shows temperature seems to facilitate the autoxidation process by accelerating H-shift to form more oxygenated radicals, potentially lowering the volatility of final products. This trend can also be seen within one season, when temperature fluctuation is relatively minor. This indicates the H-shift rate is sensitive to ambient temperature (Fig 2b). We will further investigate the temperature dependence on other HOM species and its abundance at other measurement sites.

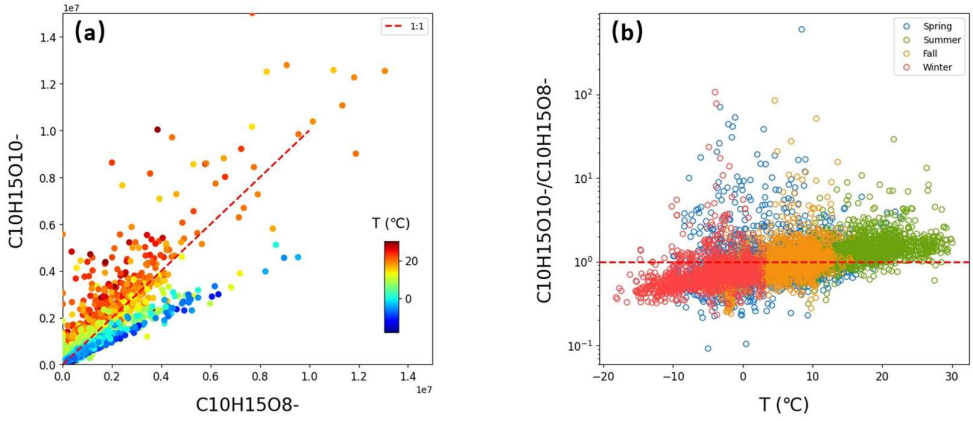


Figure 2. Temperature-dependent HOM oxidation level. $C_{10}H_{15}O_{10}$ and $C_{10}H_{15}O_8$ are two typical radicals detected in the boreal forest. $C_{10}H_{15}O_{10}$ is the main next-step oxidation product of $C_{10}H_{15}O_8$. (a) scatter plot of $C_{10}H_{15}O_{10}$ versus $C_{10}H_{15}O_8$, color-coded by temperature; (b) scatter plot of $C_{10}H_{15}O_{10}$ / $C_{10}H_{15}O_8$ versus temperature, color-coded by seasons.

ACKNOWLEDGEMENTS

Hyytiälä personnel is acknowledged for their help in conducting the measurements. This work is supported by University of Helsinki hosting the ACTRIS Topical Centre Units and Research Council of Finland supporting the implementation and operation of the Units (FIRI funding, ACTRIS Central Facilities 2020-2024, grant no. 329274).

REFERENCES

Federico Bianchi, Theo Kurtén, Matthieu Riva et al., Highly Oxygenated Organic Molecules (HOM) from Gas-Phase Autoxidation Involving Peroxy Radicals: A Key Contributor to Atmospheric Aerosol, *Chemical* Reviews, 2019 119 (6), 3472-3509

Ehn, M., Thornton, J., Kleist, E. et al. A large source of low-volatility secondary organic aerosol, *Nature* **506**, 476–479 (2014).

Zhang, Y., Peräkylä, O., Yan, C., Heikkinen, L., Äijälä, M., Daellenbach, K. R., Zha, Q., Riva, M., Garmash, O., Junninen, H., Paatero, P., Worsnop, D., and Ehn, M.: A novel approach for simple statistical analysis of high-resolution mass spectra, *Atmos. Meas. Tech.*, 12, 3761–3776 (2019).

DECADAL TRENDS AND SOURCE ATTRIBUTION OF ATMOSPHERIC AEROSOLS AT MACE HEAD

V. MOSCHOS[1], E. CHEVASSUS[1], K.N. FOSSUM[1], L. LEI[1], V. PRABHU[1], D. MARTIN[1], D. CEBURNIS[1], C. O'DOWD[1], J. OVADNEVAITE[1]

[1]*Centre for Climate and Air Pollution Studies, Physics, School of Natural Sciences, University of Galway, University Road, Galway H91 CF50, Ireland.*

Keywords: climate change, mass spectrometry, positive matrix factorization, source regions.

Long-term atmospheric measurements at 3 strategically located coastal observatories in Ireland — Mace Head (MHD), Valentia (VAL), and Carnsore Point (CRP) — offer unprecedented insights into marine–continental interactions in the northeastern Atlantic. These observatories monitor a wide range of aerosol and trace gas species, including equivalent black carbon measured by aethalometers (BC), organic aerosol (OA) and major ionic species (e.g., sulphate, nitrate, ammonium) quantified by high-resolution time-of-flight AMS (HR-ToF-AMS) or aerosol chemical speciation monitors (ACSMs), elements, and carbon monoxide (CO). The unique coastal locations of these sites enable sampling of clean marine air masses (Ovadnevaite *et al*, 2014) and pollution episodes from regional or distant sources.

MHD, a long-established Global Atmospheric Watch (GAW) "supersite," has collected decades of aerosol, trace/greenhouse gas and meteorological data, providing a robust baseline for assessing changing emission patterns and climate-driven impacts. VAL and CRP extend this Irish monitoring network to the southwest and southeast coasts, respectively, broadening the spatial coverage of atmospheric observations. Together, these 3 observatories function as a "natural laboratory," where contrasting air masses converge, illuminating a wide spectrum of marine–continental aerosol interactions.

In this study, we leverage these multi-year datasets, including HR-ToF-AMS data at MHD (since 2008) and ACSM data at VAL and CRP, to perform chemical speciation, and OA source apportionment using positive matrix factorization. The factor analysis reveals key contributors to OA variability, including marine biogenic sources, secondary OA derived from both marine and continental precursors, peat burning, and continental pollution outflow. Aerosol species and CO data are integrated with hourly 5-day back-trajectories, using the ZeFir toolkit (Petit *et al*, 2017) and the concentration-weighted trajectory approach, to identify source regions driving episodic pollution events. While marine air masses are more frequent at MHD, episodic long-range transport of the aethalometer-based BC from continental Europe (Figure 1a) indicates the transboundary nature of air quality at this remote coastal region.

A central objective of our work is to evaluate decadal trends in each (aerosol) species, OA factor, and key ratios. We hypothesize that anthropogenic OA at MHD has declined over the past decade (similarly to BC; Figure 1b) due to stringent European emission regulations, while marine biogenic and other natural OA may be increasing in response to climate-driven changes (e.g., warming seas, shifts in oceanic productivity). Assessing whether and how these hypothesized trends are reflected in the data is critical to understanding the shifting balance between primary vs. secondary, marine vs. continental, and natural vs. anthropogenic (organic) aerosol sources in the North Atlantic.

Our multi-year observational dataset and source apportionment provide a foundation for future model–measurement integration. This effort will enhance constraints on aerosol–cloud interactions and feedback mechanisms in climate models. Ultimately, we deliver valuable insights for developing effective emission control strategies, understanding ocean–atmosphere–climate linkages, and predicting how environmental changes may influence air quality in the coming decades.

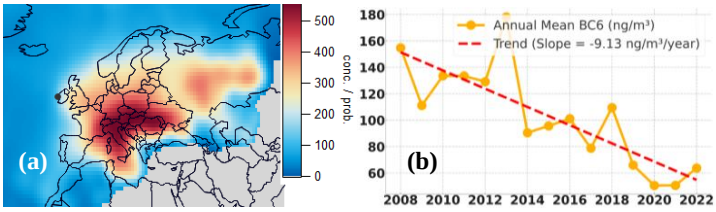


Figure 1. (a) Distant hotspot potential source regions and (b) long-term trend from the Mann-Kendall test, for BC at MHD during 2009-2022 (concentration in ng m^{-3}).

ACKNOWLEDGEMENTS

This work was supported by the EPA-Ireland and Department of the Environment, Climate and Communications (AEROSOURCE); Taighde Éireann – Research Ireland, grant no. 22/FFP-A/10611 (EPIC-AIR); and the University of Galway College of Science and Engineering Postgraduate Fellowship n°127407.

REFERENCES

Ovadnevaite, J., Ceburnis, D., Leinert, S., Dall'Osto, M., Canagaratna, M., O'Doherty, S., Berresheim, H., and O'Dowd, C. (2014) *JGR Atmos.* **119**, 11,850-11,863.

Petit, J.-E., Favez, O., Albinet, A., and Canonaco, F. (2017) *Environ. Model. Softw.* **88**, 183-187.

CAPE-K CHEM: NEW PARTICLE FORMATION AND PRECURSORS VAPORS AT CAPE GRIM

J.B. PERNOV[1], J. ALROE[1], J. SULO[1], Z. LI[1], Z. RISTOVSKI[1], AND B. MILJEVIC [1]

[1]*School of Earth and Atmospheric Sciences, Queensland University of Technology, Brisbane, Australia*

Keywords: AEROSOL PRECURSORS, CAPE K, SOUTHERN OCEAN, KENNAOOK/CAPE GRIM

INTRODUCTION

Understanding the pre-industrial atmosphere is imperative for investigating anthropogenic climate change and the Southern Ocean offers one of the last representative examples of Earth's pre-industrial atmosphere (Hamilton et al., 2014). However, global climate models still exhibit persistent biases in downwelling solar radiation and misrepresentation of natural aerosol particles is a large factor in these shortcomings (Mallet et al., 2023). New particle formation (NPF) represent a large contribution to aerosol loading and cloud condensation nuclei globally, both in the preindustrial and present day atmosphere (Gordon et al., 2017). NPF mechanisms are complex and diverse globally and models struggle to simulate them accurately (Zhao et al., 2024). Incorporating natural RPF processes into climate models can help constrain this uncertainty (Regayre et al., 2014), however there have been few comprehensive studies of RPF and secondary aerosol formation in this region. To address this lack, ongoing in situ measurements of aerosol particles and precursor vapors have been underway since October 2024 during the CAPE-k CHEM campaign.

METHODS

As part of the larger Clouds and Precipitation Experiment at kennaook (CAPE-k) campaign, CAPE-k CHEM performed online measurements of aerosol precursor vapors using a high-resolution chemical ionization mass spectrometer (CIMS), ion and neutral particle number size distributions (PNSDs) using a neutral and air ion spectrometer (NAIS), and non-refractory (NR) aerosol chemical composition using a high-resolution time-of-flight aerosol mass spectrometer (HR-ToF-AMS) for $PM_{2.5}$. Measurements were performed in the U.S. Department of Energy Atmospheric Radiation Management (ARM) Mobile Facility (AMF2) at kennaook/Cape Grim Baseline Air Pollution Station on Tasmania, Australia (40.68 °S, 144.69 °E). CAPE-k CHEM represents the first-time deployment of these state-of-the-art aerosol instrumentation at kennaook/Cape Grim. This abstract shows a first look at early results from October 10, 2024, to January 31, 2025.

CONCLUSIONS

CAPE-k CHEM ultimately aims to elucidate the sources, transformations, and fate of natural aerosols in the Southern Ocean as well as their effects on cloud properties. CAPE-k CHEM offers a unique opportunity to examine the effect of natural RPF from marine as well as anthropogenic sources on cloud properties in detail. This is due to the two dominant modes of wind direction (Fig. 1), either from the baseline sector (190° - 280°) representing natural, pristine Southern Ocean background air masses (55 %) or from easterly directions representing either terrestrial and anthropogenic air masses from Tasmania or mainland Australia (45 %).

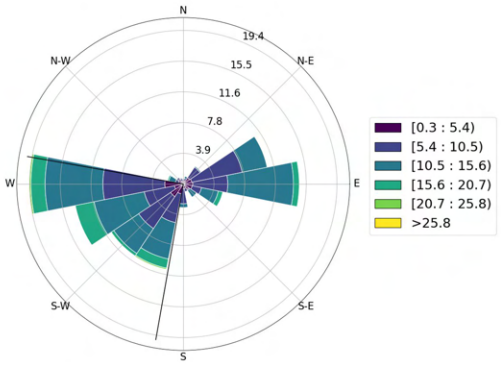


Figure 1. Wind rose for CAPE-k CHEM campaign (October 2024 – January 2025).

Currently, we have observed 13 NPF events during CAPE-k CHEM, with all of them arriving from the non-baseline sector, representing an NPF frequency of ~10 %. An example of one such NPF event is displayed in Fig. 2, which shows the PNSD from 2 to 40 nm, sulfuric, methanesulfonic, and iodic acid on Nov 30, 2024. The presence of nanoparticles appears concurrently with a peak in iodic acid, but the formation and growth intensely develop with the increase in sulfuric and methanesulfonic acid. This suggests multiple precursor vapors are involved in different stages of particle production and growth. The event appears to be initiated by an increase in iodic acid followed by sulfuric acid while the growth coincides with an increase in methanesulfonic acid. Later in the event, sulfuric acid decreases while iodic acid shows an increase with considerable variation. The underlying causes for these variations remain to be elucidated.

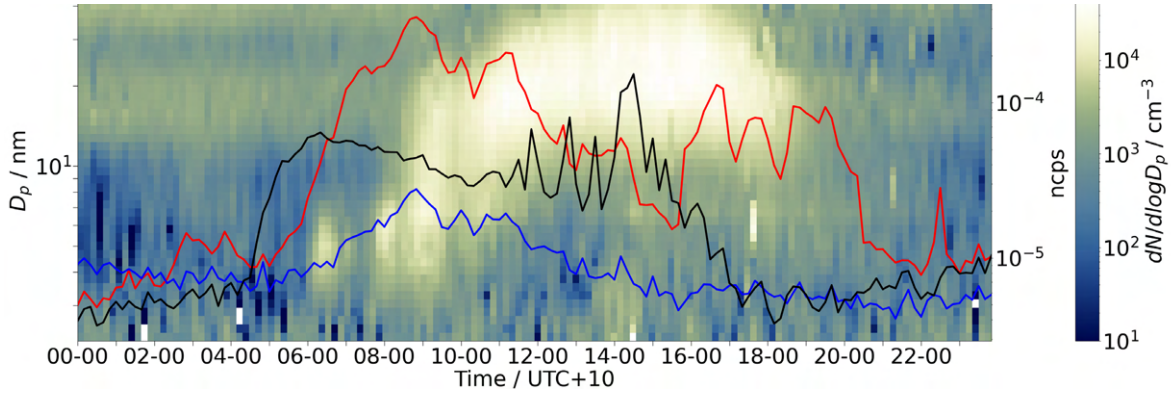


Figure 2. PNSD (2-40 nm) and sulfuric (red), methanesulfonic (blue), and iodic (black) acid in normalized counts per sec on Nov 30, 2024.

We will present a statistical overview of NPF events, precursor vapors, and submicron size distributions, including source regions, environmental drivers, and the effects of cloud properties. This analysis will incorporate air mass back-trajectory modeling, meteorological reanalysis data, and satellite products, alongside statistical tools such as Positive Matrix Factorization and machine learning. The findings will contribute to improving model parameterizations, refining bias correction methods, and enhancing our understanding of the pre-industrial atmosphere.

ACKNOWLEDGEMENTS

This project is funded by the Australian Research Council (ARC Discovery funding scheme, grant number: DP240100389). The U.S. Department of Energy Atmospheric Radiation Management is

acknowledged for use of their mobile container. Technicians Thomas Day and Frank Zurek are acknowledged for their help with installing and maintaining these instruments.

REFERENCES

Gordon, H., Kirkby, J., Baltensperger, U., Bianchi, F., Breitenlechner, M., Curtius, J., Dias, A., Dommen, J., Donahue, N. M., Dunne, E. M., Duplissy, J., Ehrhart, S., Flagan, R. C., Frege, C., Fuchs, C., Hansel, A., Hoyle, C. R., Kulmala, M., Kürten, A., Lehtipalo, K., Makhmutov, V., Molteni, U., Rissanen, M. P., Stozkhov, Y., Tröstl, J., Tsagkogeorgas, G., Wagner, R., Williamson, C., Wimmer, D., Winkler, P. M., Yan, C., and Carslaw, K. S.: Causes and importance of new particle formation in the present-day and preindustrial atmospheres, J. Geophys. Res. Atmospheres, 122, 8739–8760, https://doi.org/10.1002/2017JD026844, 2017.

Hamilton, D. S., Lee, L. A., Pringle, K. J., Reddington, C. L., Spracklen, D. V., and Carslaw, K. S.: Occurrence of pristine aerosol environments on a polluted planet, Proc. Natl. Acad. Sci., 111, 18466–18471, https://doi.org/10.1073/pnas.1415440111, 2014.

Mallet, M. D., Humphries, R. S., Fiddes, S. L., Alexander, S. P., Altieri, K., Angot, H., Anilkumar, N., Bartels-Rausch, T., Creamean, J., Dall'Osto, M., Dommergue, A., Frey, M., Henning, S., Lannuzel, D., Lapere, R., Mace, G. G., Mahajan, A. S., McFarquhar, G. M., Meiners, K. M., Miljevic, B., Peeken, I., Protat, A., Schmale, J., Steiner, N., Sellegri, K., Simó, R., Thomas, J. L., Willis, M. D., Winton, V. H. L., and Woodhouse, M. T.: Untangling the influence of Antarctic and Southern Ocean life on clouds, Elem. Sci. Anthr., 11, 00130, https://doi.org/10.1525/elementa.2022.00130, 2023.

Regayre, L. A., Pringle, K. J., Booth, B. B. B., Lee, L. A., Mann, G. W., Browse, J., Woodhouse, M. T., Rap, A., Reddington, C. L., and Carslaw, K. S.: Uncertainty in the magnitude of aerosol-cloud radiative forcing over recent decades, Geophys. Res. Lett., 41, 9040–9049, https://doi.org/10.1002/2014GL062029, 2014.

Zhao, B., Donahue, N. M., Zhang, K., Mao, L., Shrivastava, M., Ma, P.-L., Shen, J., Wang, S., Sun, J., Gordon, H., Tang, S., Fast, J., Wang, M., Gao, Y., Yan, C., Singh, B., Li, Z., Huang, L., Lou, S., Lin, G., Wang, H., Jiang, J., Ding, A., Nie, W., Qi, X., Chi, X., and Wang, L.: Global variability in atmospheric new particle formation mechanisms, Nature, 631, 98–105, https://doi.org/10.1038/s41586-024-07547-1, 2024.

THE FIRST ACTRIS CHEMICAL IONIZATION MASS SPECTROMETRY INTERCOMPARISON WORKSHOP PROVIDED CRUCIAL INFORMATION ON THE DETECTION OF CONDENSABLE VAPOURS

N. SARNELA[1], P. METTKE[2], M. SIMON[3], T. VERA[4], R. SOLER[4] AND THE INTERCOMPARISON COLLABORATION

[1]Institute for Atmospheric and Earth System Research (INAR), University of Helsinki, 00560, Helsinki Finland.
[2]Atmospheric Chemistry Department (ACD), Leibniz Institute for Tropospheric Research (TROPOS), 04318 Leipzig, Germany.
[3]Institute for Atmospheric and Environmental Sciences, Goethe-University Frankfurt, 60438, Frankfurt am Main, Germany.
[4]EUPHORE Lab, Fundación CEAM, 46980, Paterna, Spain.

Keywords: CONDENSABLE VAPOURS, INTERCOMPARISON, MASS SPECTROMETRY

INTRODUCTION

Advancements in instrument development have enabled a focus on the initial steps of particle formation through particle counters capable of detecting sub-3 nm particles and mass spectrometric methods that can resolve the composition of particles and determine the concentrations of their precursor vapours. The challenge in measuring these condensable precursor vapours arises from their extremely low concentrations—often at parts per trillion or parts per quadrillion volume mixing ratios—and their low volatility. Their tendency to condense and form molecular clusters also makes them prone to sticking to any surface they encounter, requiring special precautions to prevent losses before detection. Among the most important condensable vapours, sulphuric acid is widely present and plays a key role in the initial steps of nucleation (Sipilä et al., 2010). Other inorganic acids, such as methanesulfonic acid (Shen et al., 2024) and iodic acid (He et al., 2022), can also contribute, particularly in specific environments. In addition to these inorganic species, a vast number of organic compounds participate in particle formation (Ehn et al., 2014).

When studying new particle formation, the quantitative data on these vapours is compared with particle formation and growth rates. To fully understand the role of different species, all relevant vapours must be measured quantitatively. However, due to the challenges associated with condensable vapor detection, calibrating these species is not straightforward, and measurement uncertainties remain high. Nitrate ion-chemical ionization mass spectrometry (NO_3-CIMS) is widely used method in atmospheric research to measure condensable vapours but the sensitivity of different instruments and the variation in the detection of them are not well understood as the instruments are generally calibrated only for sulphuric acid. As the studied oxidized organic compounds are a group of thousands different molecules with different functional groups the sensitivity towards them might vary significantly between different molecules.

ACTRIS CiGas-UHEL

CiGas-UHEL is a unit of the ACTRIS Central Facility of reactive trace gases in situ measurement focusing on measurements of condensable vapours. The key-mission of CiGas-UHEL is to offer operational support for continuous long-term measurements of condensable vapours and aerosol precursors such as sulphuric acid and oxygenated organic molecules (OOMs) in the atmosphere. The core activity of CiGas-UHEL is to ensure sustainable and traceable high-quality data and quantification of in-situ measured atmospheric reactive trace gases with known uncertainty and reproducibility. Intercomparison workshops provide crucial information about the individual functionality of the different

instruments and understanding of their characteristic sensitivity and selectivity. Thus, the intercomparison workshops are a great tool towards the general goal of CiGas-UHEL to standardize and harmonize the different measurement methods.

METHODS

CiGas-UHEL arranged the pilot intercomparison workshop of chemical ionization mass spectrometers (CIMS, Eisele and Tanner, 1993; Jokinen et al. 2012, Rissanen et al. 2019) at the twin chamber facility ACDC (Atmospheric Chemistry Department Chamber) at TROPOS in March 2023 in collaboration with the ACTRIS OrGanic Tracers and Aerosol Constituents - Calibration Centre (OGTAC-CC). The intercomparison workshop brought together ten instruments for measuring condensable vapors, each featuring a unique setup. All instruments included an inlet where chemical ionization occurs using specific reagent ions and ionization methods, as well as a time-of-flight mass spectrometer for ion detection at a defined resolution. The instruments varied in their inlet designs and ionization methods, which included corona discharge, X-ray, visible UV, and radioactive sources such as Am-241 and Po-210 (Table 1).

Table 1. The chemical ionization mass spectrometers participating the intercomparison workshop

chamber	inlet	reagent ions	ionization	mass spectrometer
A	EISELE	NO_3^-	corona	L-TOF
A	aircraft CI	NO_3^-	corona	H-TOF
A	AIM	NO_3^-	VUV	L-TOF
A	EISELE	NO_3^-	X-ray	H-TOF
A	EISELE	NO_3^-	X-ray	H-TOF
B	MION	NO_3^-/Br^-	X-ray	L-TOF
B	MION	NO_3^-/Br^-	X-ray	L-TOF
B	EISELE	NO_3^-	X-ray	L-TOF
B	EISELE	NO_3^-	Am241	C-TOF
B	FIGAERO	I^-	Po210	H-TOF

In the experiments, we focused on detecting sulphuric acid and various oxidized organic compounds, which are the target compounds of the CiGas-UHEL unit. Additionally, two calibration compounds, 4-nitrophenol and 1,2-ISOPOOH, were introduced at various concentration levels under both dry and high relative humidity (RH) conditions. We examined different oxidation regimes of α-pinene, using both OH radicals and ozone as oxidants, under high and low nitrogen oxide (NO) conditions. Furthermore, we investigated how variations in relative humidity affected the observed signals during chamber reactions. Lastly, we measured different concentrations of sulfuric acid under dry and high RH conditions, with α-pinene added as a precursor compound in the same system.

RESULTS & DISCUSSION

In the workshop, we calibrated the instruments using a sulphuric acid calibrator and calculated inlet line losses for different molecules. To determine the concentrations of each molecule, we applied the calculated loss factor and the sulphuric acid calibration coefficient. This approach allowed us to assess how well sulphuric acid calibration works for other compounds, as it is widely used as the sole calibration method.

The workshop provided valuable insight into the detection of different molecules and underscored the need for improved characterization of calibration methods and loss calculations. Due to differences in the fragmentation settings of the instruments, we observed variations in the distribution of reagent ions (Fig. 1), sulfuric acid ions, and sensitivity to oxidized organic compounds. We selected a peak list of 40 oxidized organic compounds and categorized them into four groups based on their volatility. The largest

variation in detection between the instruments was observed for semi-volatile organic compounds, while the variation decreased for less volatile compounds.

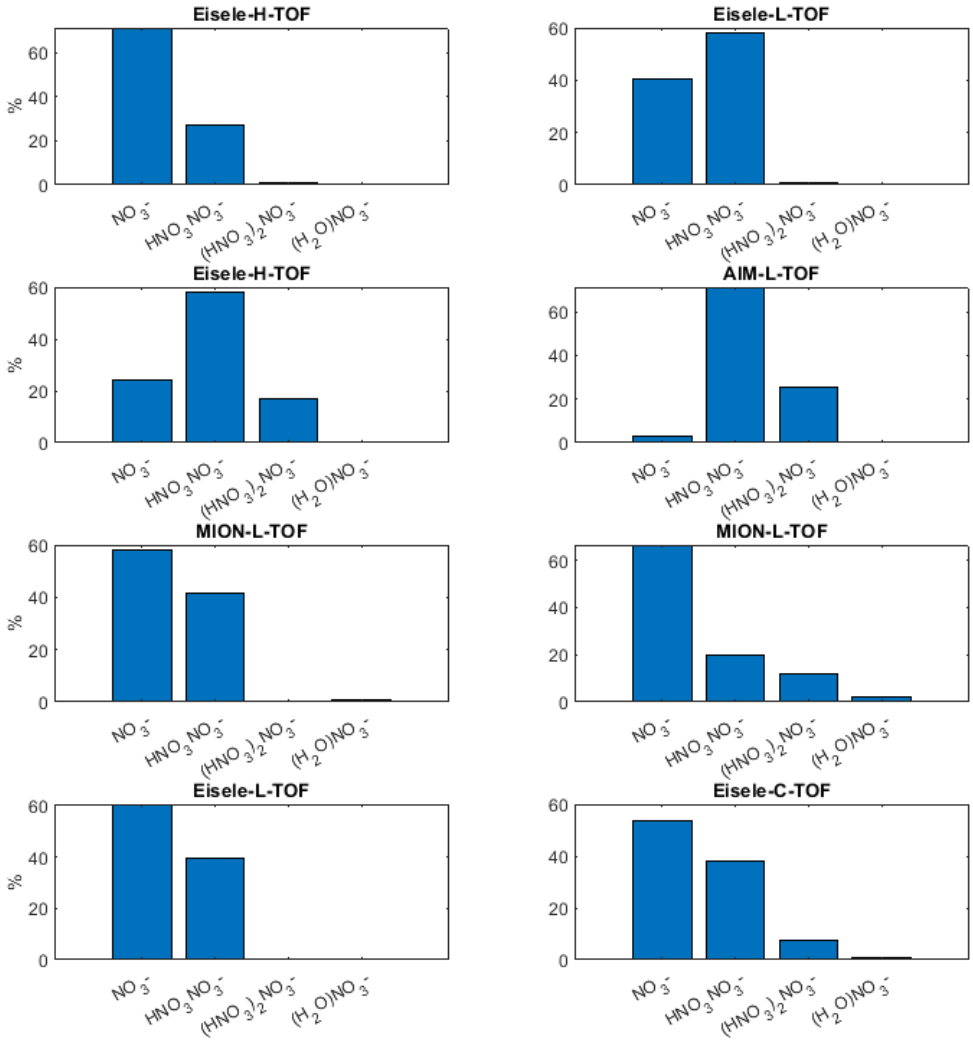


Figure 1. Reagent ion distribution in eight instruments that participated the workshop

CONCLUSIONS

The first ACTRIS intercomparison of chemical ionization mass spectrometers revealed significant variability in condensable vapour detection. The response of the instruments to the changes in chamber conditions did not show uniform agreement, highlighting the importance of this form of intercomparison workshops and further discussion within the network. The knowledge gained will help us to better understand and evaluate the sampled data of condensable vapours in the atmosphere and can provide defined measurement standards and operating procedures of CIMS instruments for the broader atmospheric science community.

ACKNOWLEDGEMENTS

This work is a result of great collaboration with intercomparison participants from Leibniz Institute for Tropospheric Research (TROPOS), Forschungszentrum Jülich, Centre d'Estudis Ambientals del Mediterrani (CEAM), Cyprus Institute, Goethe University Frankfurt, Tampere University and instrument

manufacturers Karsa, Aerodyne and Tofwerk. The intercomparison workshop was organized in collaboration with OGTAC-CC and the Centre is acknowledged for all the arrangements and hosting. This work is supported by University of Helsinki hosting the ACTRIS Topical Centre Units and Research Council of Finland supporting the implementation and operation of the Units (FIRI funding, ACTRIS Central Facilities 2020-2024, grant no. 329274). The ACCC Flagship funding by the Research Council of Finland (grant no. 337549) and Jane and Aatos Erkko Foundation funding are acknowledged.

REFERENCES

Ehn, M., Thornton, J. A., Kleist, E., Sipilä, M., Junninen, H., Pullinen, I., Springer, M., Rubach, F., Tillmann, R., Lee, B., Lopez-Hilfiker, F., Andres, S., Acir, I.-H., Rissanen, M., Jokinen, T., Schobesberger, S., Kangasluoma, J., Kontkanen, J., Nieminen, T., … Mentel, T. F. (2014). A large source of low-volatility secondary organic aerosol. *Nature*, **506**, 476–479.

Eisele, F. L., & Tanner, D. J. (1993). Measurement of the gas phase concentration of H2SO4 and methane sulfonic acid and estimates of H2SO4 production and loss in the atmosphere. *J. Geophys. Res.*, **98**, 9001.

He, X.-C., Tham, Y. J., Dada, L., Wang, M., Finkenzeller, H., Stolzenburg, D., Iyer, S., Simon, M., Kürten, A., Shen, J., Rörup, B., Rissanen, M., Schobesberger, S., Baalbaki, R., Wang, D. S., Koenig, T. K., Jokinen, T., Sarnela, N., Beck, L. J., … Sipilä, M. (2021). Role of iodine oxoacids in atmospheric aerosol nucleation. *Science*, **371**.

Jokinen, T., Sipilä, M., Junninen, H., Ehn, M., Lönn, G., Hakala, J., Petäjä, T., Mauldin, R. L., Kulmala, M., & Worsnop, D. R. (2012). Atmospheric sulphuric acid and neutral cluster measurements using CI-APi-TOF. *Atmos Chem. Phys.*, **12**, 4117–4125.

Rissanen, M. P., Mikkilä, J., Iyer, S., & Hakala, J. (2019). Multi-scheme chemical ionization inlet (MION) for fast switching of reagent ion chemistry in atmospheric pressure chemical ionization mass spectrometry (CIMS) applications. *Atmos. Meas. Tech.*, **12**, 6635–6646.

Shen, J., Scholz, W., He, X.-C., Zhou, P., Marie, G., Wang, M., Marten, R., Surdu, M., Rörup, B., Baalbaki, R., Amorim, A., Ataei, F., Bell, D. M., Bertozzi, B., Brasseur, Z., Caudillo, L., Chen, D., Chu, B., Dada, L., … Worsnop, D. R. (2022). High Gas-Phase Methanesulfonic Acid Production in the OH-Initiated Oxidation of Dimethyl Sulfide at Low Temperatures. *Environ. Sci.Tech.*, **56,** 13931–13944.

Sipilä, M., Berndt, T., Petaja, T., Brus, D., Vanhanen, J., Stratmann, F., Patokoski, J., Mauldin, R. L., Hyvärinen, A. P., Lihavainen, H., & Kulmala, M. (2010). The role of sulfuric acid in atmospheric nucleation. *Science*, **327**, 1243–1246.

INVESTIGATION OF LOW-VISIBILITY ATMOSPHERIC EVENTS AT RADO-BUCHAREST ACTRIS FACILITY, ROMANIA

F. TOANCA[1], A.V. DANDOCSI[1,2], A. ILIE[1,3], J. G. VASILESCU[1], D. NICOLAE[1], A. NEMUC[1]

[1]*National Institute of Research and Development for Optoelectronics, INOE, Măgurele-Bucharest, Romania.*
[2]*UNST Politehnica of Bucharest, Bulevardul Iuliu Maniu 1-3, Bucharest, 061071, Bucharest, Romania*
[3] *Faculty of Geography, University of Bucharest, Bulevardul Nicolae Bălcescu 1, 010041, Bucharest, Romania*

Keywords: LOW-VISIBILITY EVENTS, ATMOSPHERE, REMOTE SENSING.

INTRODUCTION

Low-visibility events (LVEs), including fog and haze, are meteorological phenomena that can significantly affect various sectors such as transportation, public safety, and meteorology. These events are characterized by a substantial reduction in visibility, typically caused by environmental factors such as suspended water droplets, pollutants, and aerosols in the air. Fog, for instance, forms when water droplets become suspended in the air, leading to a significant decrease in horizontal visibility, often dropping below 1 km *(*WMO, 1992). LVEs present considerable challenges, contributing to increased accident rates, travel disruptions, and complications in daily activities, particularly in regions with high levels of air pollution (Gultepe, I. et al., 2007; Zhang et al., 2015; Cornejo-Bueno et al., 2020; Dey et al., 2018). Furthermore, these phenomena can interfere with aviation and also, pose significant risks to public health, underscoring the importance of accurate monitoring and forecasting to mitigate their effects (Pérez-Díaz, J.L. et al., 2017). Previous studies have utilized remote sensing data (e.g. Radiometrics Profiling Microwave Radiometer and Vaisala ceilometer CT25K) to analyze LVEs, providing valuable insights into their characteristics and behavior (Gultepe I. et al., 2009).

METHODS

This study analyzed LVEs using remote sensing instruments as the Lufft CHM15k ceilometer and the HATPRO G5 microwave radiometer, from October 2021 to March 2023. The instruments are located at Măgurele Atmospheric Radiation Studies (MARS) facility (44.344°N, 26.012°E) in Romania, part of the Aerosol, Clouds, and Trace Gases Research Infrastructure (ACTRIS). The experimental site is located in a flat terrain, preurban area of Bucharest. Data analysis focused on LVE frequency, distribution, and seasonal variations. The ceilometer provided real-time measurements of vertical optical range (VOR), sky condition index (SCI), and total cloud cover (TCC). SCI values equal to 2 (fog) and VOR values below 1000 m were considered. TCC values were categorized from 0 (clear sky) to 9 (sky obscured by fog). The microwave radiometer measured vertical relative humidity (RH), with an 80% RH threshold for over two consecutive minutes at one altitude level (0-520 m, across 20 levels). Rainfall periods were excluded. Temperature profiles were generated every three hours to identify thermal inversions associated with fog events. Graphical analyses highlighted fog persistence periods and vertical temperature profiles. Over 80% of fog events were confirmed through human observation.

CONCLUSIONS

Figure 1 illustrates the 53 fog episodes identified over a total of 59 days between October 2021 and March 2023, with some episodes extending across two consecutive days. The distribution of these events highlights

seasonal variations in fog occurrence at our site. Based on the applied methodology, December 2022 had the highest number of recorded fog events (17), which suggests that winter conditions, including lower temperatures and higher humidity levels, contributed to increased fog formation. This was followed by November 2021, with 9 identified episodes, further emphasizing the prevalence of fog during colder months. The observed seasonal pattern aligns with known meteorological conditions that favor fog development, such as thermal inversions and radiative cooling during the night, which are more frequent in late autumn and winter in our region.

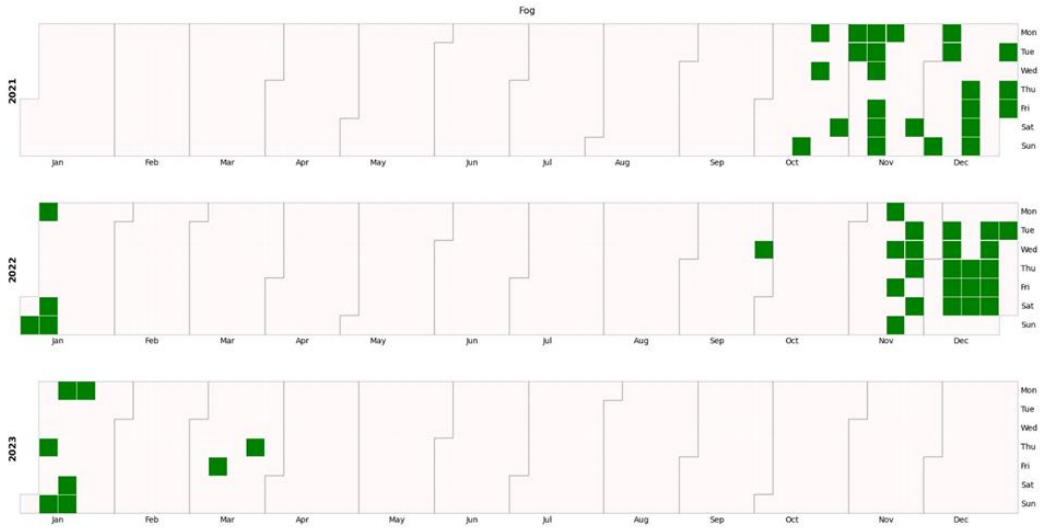


Fig.1 Fog episodes identified during October 2021 - March 2023 at RADO-Bucharest facility, Romania

In terms of seasonal distribution, fog episodes in the 2021-2022 season were observed in October, November, December, and January, whereas in the 2022-2023 season, they occurred in September, November, December, January, and March. More than half of these episodes began in the morning, a typical characteristic of radiation fog.

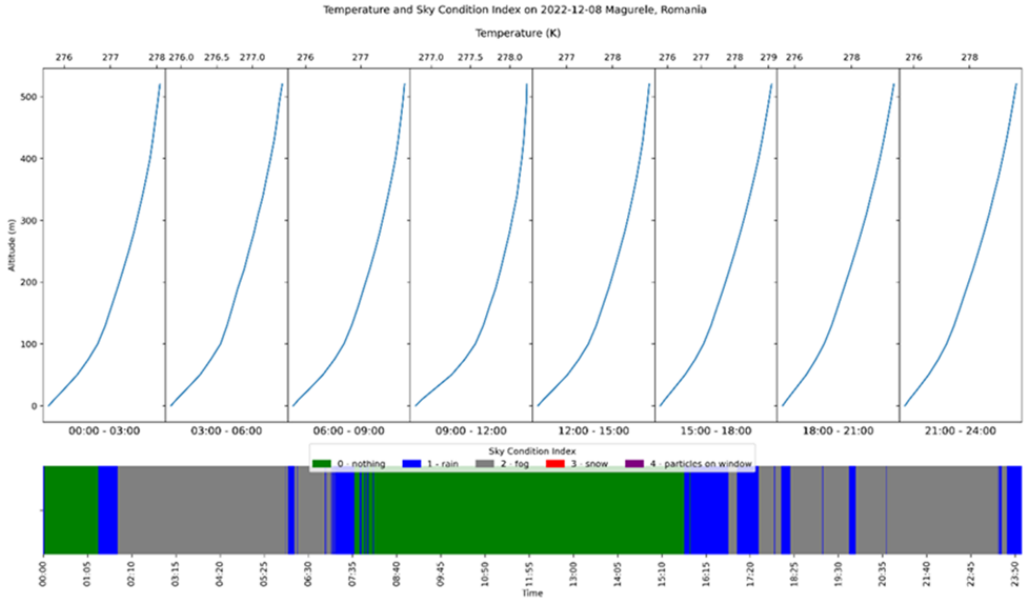


Fig.2 Fog event from December 8, 2022: vertical temperature profiles every 3 hours determined by the HATPRO G5 microwave radiometer (top) and the "sky condition index" parameter determined by the CHM15k ceilometer (bottom) at RADO-Bucharest facility, Romania

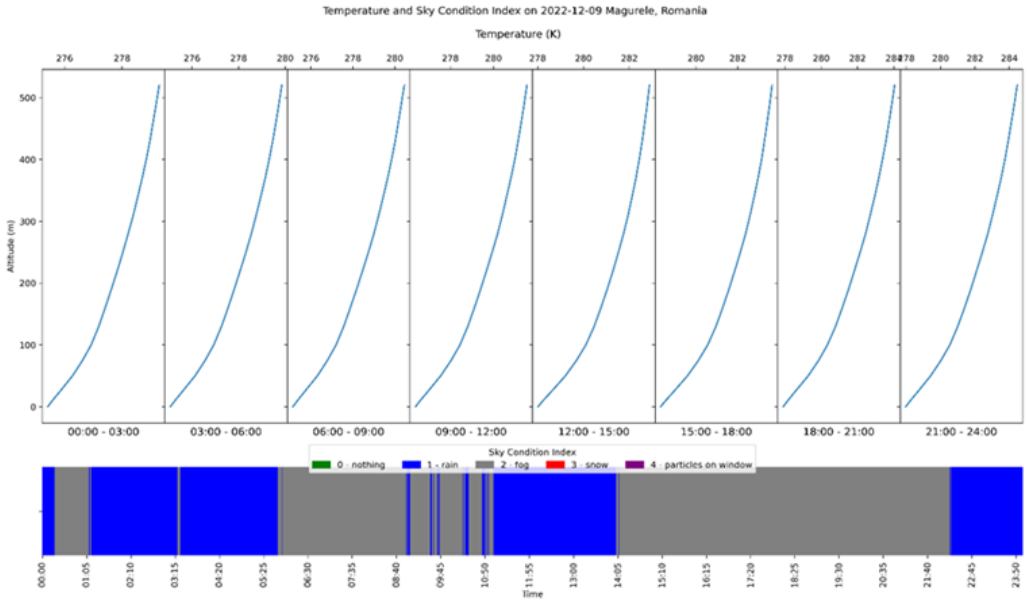


Fig.3 Fog event from December 9, 2022: vertical temperature profiles every 3 hours determined by the HATPRO G5 microwave radiometer (top) and the "sky condition index" parameter determined by the CHM15k ceilometer (bottom) at RADO-Bucharest facility, Romania

Regarding duration and characteristics, fog events were identified with durations ranging from less than 30 minutes to up to 18 hours, following the established methodology. Table 1 and Figures 2 and 3 illustrate the timing and duration of fog episodes recorded on December 8 and 9, 2022, using the synergistic fog episode analysis approach. The vertical temperature profiles (0–500 m) and SCI confirm the presence of fog, with temperature profiles indicating thermal inversion on these days. Typically, thermal inversions occur at night due to radiative surface cooling, as also reflected in Table 1, which details the fog events from December 8–9, 2022.

Fog onset	Fog offset	Event duration
2022-12-08 16:48:43	2022-12-09 00:59:44	8:11:01
2022-12-09 05:52:44	2022-12-09 10:46:15	4:53:31

Table1: Fog events during the period 8-9 December 2022

This study revealed the seasonal and temporal variability of low-visibility events (LVEs) at the RADO-Bucharest ACTRIS facility, emphasizing their increased occurrence during cold months. This is in accordance with the study of Vlad et al 2024 at a location close to North Bucharest and a previous study during 2012-2014 (Toanca et al. 2017). The highest number of fog episodes was recorded in December, with a notable concentration in the early morning hours, highlighting the influence of radiative cooling in fog formation. Temperature inversions were found to be a key factor in fog persistence, as confirmed by vertical temperature profiles obtained from the microwave radiometer. The methodology employed, integrating data from both the ceilometer and microwave radiometer, proved effective in accurately detecting and characterizing fog events. By combining vertical optical range (VOR), sky condition index (SCI), total cloud cover (TCC), and relative humidity profiles, the study provided a detailed assessment of fog onset, duration, and dissipation. This synergistic approach allowed for a more precise identification of fog episodes and their associated meteorological conditions.

ACKNOWLEDGEMENTS

This work was carried out through the Core Program within the National Research Development and Innovation Plan 2022-2027, with the support of MCID, project no. PN23 05/ 3.01.2023 and was financed by Smart Growth, Digitization and Financial Instruments Program (PoCIDIF) 2021-2027, Action 1.3 Integration of the national RDI ecosystem in the European and international Research Space, project -

Supporting the operation of facilities in Romania within the ACTRIS ERIC research infrastructure, SMIS code 309113.

REFERENCES

World Meteorological Organization (1992). International Meteorological Vocabulary, (WMO Publication 182, World Meteorological Organization, Geneva, Switzerland).

Zhang, D., T. Sullivan, N.E. O'Connor, R. Gillespie, and F. Regan (2015). Coastal fog detection using visual sensing, in Proc. OCEANS 2015, Genoa, Italy (IEEE), 1–5.

Gultepe, I., R. Tardif, S.C. Michaelides, J. Cermak, A. Bott, J. Bendix, M.D. Müller, M. Pagowski, B Hansen, G. Ellrod, et al. (2007). Fog research: A review of past achievements and future perspectives, Pure Appl. Geophys. 164, 1121–1159.

Cornejo-Bueno, S., D. Casillas-Pérez, L. Cornejo-Bueno, M.I. Chidean, A.J. Caamaño, J. Sanz-Justo, C. Casanova-Mateo, and S. Salcedo-Sanz (2020). *Persistence analysis and prediction of low-visibility* Events at Valladolid Airport, Spain, Symmetry 12, 1045.

Dey, S. (2018). On the theoretical aspects of improved fog detection and prediction in India, Atmospheric Research 202, 77-80.

Pérez-Díaz, J.L., O. Ivanov, Z. Peshev, M.A. Álvarez-Valenzuela, I. Valiente-Blanco, T. Evgenieva, T. Dreischuh, O. Gueorguiev, P.V. Todorov, and A. Vaseashta (2017). Fogs: Physical basis, characteristic properties, and impacts on the environment and human health, Water 9, 807.

Gultepe, I., and Coauthors (2009) The Fog Remote Sensing and Modeling Field Project. Bull. Amer Meteor. Soc., 90, 341–360.

Vlad, A., Iorga, G., Barbu, N., and Stefan, S. (2024), Examining the fog occurrence over the Bucharest Henri Coandă International Airport and its adjacent area, EGU General Assembly 2024, Vienna, Austria, 14–19, Apr 2024, EGU24-16368, https://doi.org/10.5194/egusphere-egu24-16368.

Toanca, F., Stefan, S., Labzovskii, L., Belegante, L., Andrei, S., Nicolae D. (2017). Study of fog events using remote sensing data. Rom. Rep. Phys. 2017, 69, 703.

LONG TERM IN-SITU OBSERVATIONS REVEAL HIGH SENSITIVITY OF CLOUD FORMATION TO AEROSOL CHANGES

Annele Virtanen[1], Jorma Joutsensaari[1], Harri Kokkola[1,2], Daniel G. Partridge[3], Sara Blichner[4,5], Øyvind Seland[6], Eemeli Holopainen[2#], Emanuele Tovazzi[3], Antti Lipponen[2], Santtu Mikkonen[1], Ari Leskinen[1,2], Antti-Pekka Hyvärinen[7], Paul Zieger[4,5], Radovan Krejci[4,5], Annica M. L. Ekman [4,8], Ilona Riipinen[4,5], Johannes Quaas[9] and Sami Romakkaniemi[2]

[1]*University of Eastern Finland, Department of Technical Physics, 70211 Kuopio, Finland*

[2]*Finnish Meteorological Institute, 70211 Kuopio, Finland*

[3] *Department of Mathematics and Statistics, Faculty of Environment, Science and Economy, University of Exeter, Exeter, United Kingdom*

[4]*Stockholm University, Bolin Centre for Climate Research, Stockholm SE-106 91, Sweden*

[5]*Stockholm University, Department of Environmental Science, Stockholm, SE-106 91, Sweden*

[6]*Research and Development Department, Norwegian Meteorological Institute, Oslo, Norway*

[7]*Finnish Meteorological Institute, 00560 Helsinki, Finland*

[8]*Stockholm University, Department of Meteorology, Stockholm, SE-10691, Sweden*

[9]*Leipzig Institute for Meteorology, Leipzig University, Stephanstr. 3, 04103 Leipzig, Germany*

Keywords: aerosol-cloud interactions, long-term observations, in-situ observations, large scale models

INTRODUCTION

Radiative forcing by aerosols through aerosol cloud interactions (ERFaci) forms the most important component contributing to Earth's radiative forcing by significant negative value, and it still remains as the single largest source of uncertainty in radiative forcing estimates. The susceptibility (S) of cloud droplet number concentration (N_d) to cloud condensation nuclei (CCN) number concentration is one of the major factors controlling the aerosol indirect forcing. In this study we investigate the sensitivity of N_d to CCN concentrations in low level stratiform clouds using long term in-situ observations from three ACTRIS stations and use them to evaluate four global models. (Virtanen et al., 2025)

METHODS

We use long term (3-10 years) in-situ observations from three ACTRIS stations (Puijo, Pallas, Zeppelin) locating in Finland and Arctic. These stations represent semiurban, remote and Arctic remote environments with differences in typical updraft velocity conditions as well as in aerosol number

concentrations. Low level stratiform clouds are ideal to assess the Twomey effect and provide constraints on S because they are usually shallow, mainly non-precipitating and cover large surface areas. We compare the in-situ observations with four large scale models (ECHAM-HAM, ECHAM-SALSA, UKESM and NorESM) having differences in aerosol presentation while the activation parametrization is the same in all three model setups. In the observation-model comparison we use N_d and CCN model outputs of the gridbox corresponding to the vertical and horizontal location of each station. In addition, we compare the updraft velocities from the models and stations when they are available.

CONCLUSIONS

Our analysis of in-situ observations shows higher susceptibility of N_d to CCN for low-level stratiform clouds (0.82-0.89 depending on the site) than values reported for satellite data. This suggests stronger aerosol radiative forcing than assumed based on satellite observations.

In the four investigated climate models, S varied by a factor of 2-3 for the investigated cloud type. This can be expected to result in a large uncertainty in RFaci as RFaci is directly proportional to the susceptibility. Our analysis reveal that even if S in some of the models was relatively close to observations, the underlying physics in the models is unrealistic when compared to observations. We showed that the model difference in S is driven mainly by problems in defining the updrafts and the aerosol number size distributions. In addition, our analysis showed that the cloud droplet activation parametrization does not per se cause the difference.

Overall, this study demonstrates the power of long-term in-situ observations to evaluate and analyse the deficiencies in large scale models and in pin-pointing the specific processes or factors that should be improved to get the cloud activation and aerosol indirect forcing better represented in the models.

ACKNOWLEDGEMENTS

This work was supported by the European Commission grants FORCeS no. 821205, CERTAINTY no. 101137680, INTEGRATE no. 867599, and CleanCloud no. 101137639

REFERENCES

Virtanen, A., Joutsensaari, J., Kokkola, H., Partridge, D.G., Blichner, S.M., Seland, Ø., Holopainen, E., Tovazzi, E., Lipponen, A., Mikkonen, S., Leskinen, A., Hyvärinen, A.-P., Zieger, P., Krejci, R., Ekman, A. M. L., Riipinen, I., Quaas, J, Romakkaniemi S. (2025) High sensitivity of cloud formation to aerosol changes. *Nature Geoscience*, In press.

GASEOUS SULFURIC ACID CONTRIBUTIONS TO SULFATE FORMATION IN URBAN ATMOSPHERE

Zhenning Wang[1], Wei Nie[1,2,*], Yuliang Liu[1,2], Liwen Yang[1], Chong Liu[1,3], Ying Zhang[1], Chao Yan[1,2], Qiaozhi Zha[1,2], Dafeng Ge[1], Ximeng Qi[1,2], Chang Zhou[1], Liangduo Chen[1], Xueyu Zhou[1], Lei Wang[1], Dan Dan Huang[4], Xuguang Chi[1,2,*], Aijun Ding[1,2]

[1] *Joint International Research Laboratory of Atmospheric and Earth System Research, School of Atmospheric Sciences, Nanjing University, Nanjing, 210023, China*

[2] *National Observation and Research Station for Atmospheric Processes and Environmental Change in Yangtze River Delta, Nanjing, 210023, China*

[3] *Hubei Province Academy of Eco-Environmental Sciences, Wuhan, 430072, China*

[4] *State Environmental Protection Key Laboratory of Formation and Prevention of Urban Air Pollution Complex, Shanghai Academy of Environmental Sciences, Shanghai, China*

Keywords: Gaseous sulfuric acid, Condensation, Aerosol sulfate, $PM_{2.5}$ concentration

INTRODUCTION

Sulfate aerosols are critical atmospheric constituents, influencing air quality and climate. Their complex formation processes have been studied predominantly in the context of multiphase chemistry. However, the substantial contribution of gas-phase condensation of sulfuric acid (SA_{cond}) to sulfate aerosol formation has not been fully recognized, primarily due to the challenges associated with the long-term measurement of gaseous sulfuric acid (H_2SO_4). Using the comprehensive dataset from the SORPES station, we elucidated the influence of gaseous H_2SO_4 on sulfate aerosol generation across different meteorological and pollution contexts. Our analysis indicates a marked increase in gaseous H_2SO_4 concentrations enhances its role in sulfate formation, with cumulative five-day production accounting for up to 50% of the total sulfate levels. Detailed analysis of stable meteorological conditions revealed that SA_{cond} initially increases and then stabilizes with higher levels of $PM_{2.5}$, while its relative influence on sulfate formation diminishes. This implies that in high-polluted environments, multiphase reactions primarily drive sulfate formation. Given the ongoing efforts to reduce $PM_{2.5}$ levels in China, the role of SA_{cond} in shaping sulfate aerosol profiles is anticipated to become increasingly significant. This underscores the need for a renewed focus on gas-phase processes within the broader context of aerosol formation and atmospheric chemistry.

METHODS

The observations were conducted at the SORPES station in Nanjing, China (118°57′E, 32°07′N) during 2018-2020. The surrounding environment of the site and detailed descriptions can be found elsewhere(W. Nie et al. 2015; A. Ding et al. 2019). A chemical ionization with the atmospheric pressure interface time-of-

flight mass spectrometer (CI-APi-TOF) with a nitrate source was deployed to measure neutral H_2SO_4 molecules and cluster concentrations. H_2SO_4 molecules were charged by reacting with nitrate (NO_3^-) reagent ions in the reaction chamber of the inlet, and then the sulfuric acid concentration was calculated according to the measured ratio of hydrogen sulfate ions and initial ions(W. Nie et al. 2022). During the measurement period, sulfur dioxide (SO_2) concentration was monitored using a Thermo TEI 43i, and sulfate aerosol concentration was measured with the aerosol chemical speciation monitor (ACSM).

CONCLUSIONS

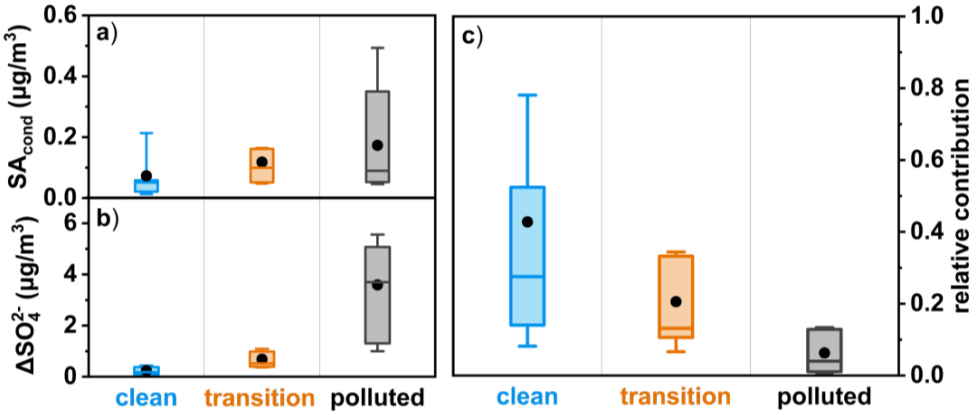


Figure 1. The contribution of daytime SA_{cond} to sulfate aerosols at different $PM_{2.5}$ concentrations.

ACKNOWLEDGEMENTS

We thank the tofTools team for providing programs for data analysis of mass spectrometry. This work was supported by the National Key Research and Development Program of China (2023YFC3706302), the National Natural Science Foundation of China (NSFC) project (42075101), Natural Science Foundation of Jiangsu Province (BK20230773), the Jiangsu Provincial Collaborative Innovation Center of Climate Change and the Fundamental Research Funds for the Central Universities.

REFERENCES

Nie, W., A. J. Ding, Y. N. Xie, Z. Xu, H. Mao, V.-M. Kerminen, L. F. Zheng, et al. 2015. "Influence of Biomass Burning Plumes on HONO Chemistry in Eastern China." *Atmospheric Chemistry and Physics* 15 (3): 1147–59. https://doi.org/10.5194/acp-15-1147-2015.

Ding, Aijun, Xin Huang, Wei Nie, Xuguang Chi, Zheng Xu, Longfei Zheng, Zhengning Xu, et al. 2019. "Significant Reduction of $PM_{2.5}$ in Eastern China Due to Regional-Scale Emission Control: Evidence from SORPES in 2011–2018." *Atmospheric Chemistry and Physics* 19 (18): 11791–801. https://doi.org/10.5194/acp-19-11791-2019.

Nie, Wei, Chao Yan, Dan Dan Huang, Zhe Wang, Yuliang Liu, Xiaohui Qiao, Yishuo Guo, et al. 2022. "Secondary Organic Aerosol Formed by Condensing Anthropogenic Vapours over China's Megacities." *Nature Geoscience* 15 (4): 255–61. https://doi.org/10.1038/s41561-022-00922-5.

ACTRIS Quality Assurance of the New Aerosol Measurements in the European Air Quality Directive: Particle Number Concentration, Particle Number Size Distribution, and Equivalent Black Carbon

[1]A.WIEDENSOHLER, K. WEINHOLD, M. MERKEL, S. PFEIFER, S. DÜSING, T. MÜLLER, M PÖHLKER

World Calibration Center for Aerosol Physics, Leibniz Institute for Tropospheric Research, Leipzig, Germany

Keywords: CALIBRATION, PARTICLE NUMBER CONCENTRATION, PARTICLE NUMBER SIZE DISTRIBUTION, PARTICLE LIGHT ABSORTION COEFFICIENT, EQUIVALENT BLACK CARBON

INTRODUCTION

The Aerosol, Clouds and Trace Gases Research Infrastructure (ACTRIS) is a pan-European Research Infrastructure Consortium (ERIC) dedicated to advancing atmospheric science. Its primary goal is to produce high-quality data on short-lived atmospheric constituents. ACTRIS focuses on understanding the processes that drive the variability of these constituents in both natural and controlled environments. The ACTRIS community comprises more than 100 research organizations across Europe. Officially established by the European Commission in April 2023, ACTRIS ERIC represents a major step forward in coordinated atmospheric research.

ACTRIS CENTRAL FACILITY CAIS-ECAC

The Center of Aerosol In-Situ Measurements – European Center for Aerosol Calibration and Characterization (CAIS-ECAC) has developed standardized procedures for 12 advanced aerosol in-situ measurement variables. These procedures are grounded in ISO and CEN standards, supported by scientific literature, and aligned with WMO-GAW guidelines. To ensure ACTRIS compliance and maintain high-quality data, CAIS-ECAC conducts performance tests on instruments from various manufacturers. Additionally, it provides traceable calibrations against reference instruments and certified standards. All ACTRIS aerosol in-situ instruments are quality-assured at the CAIS-ECAC laboratories on a bi-annual basis.

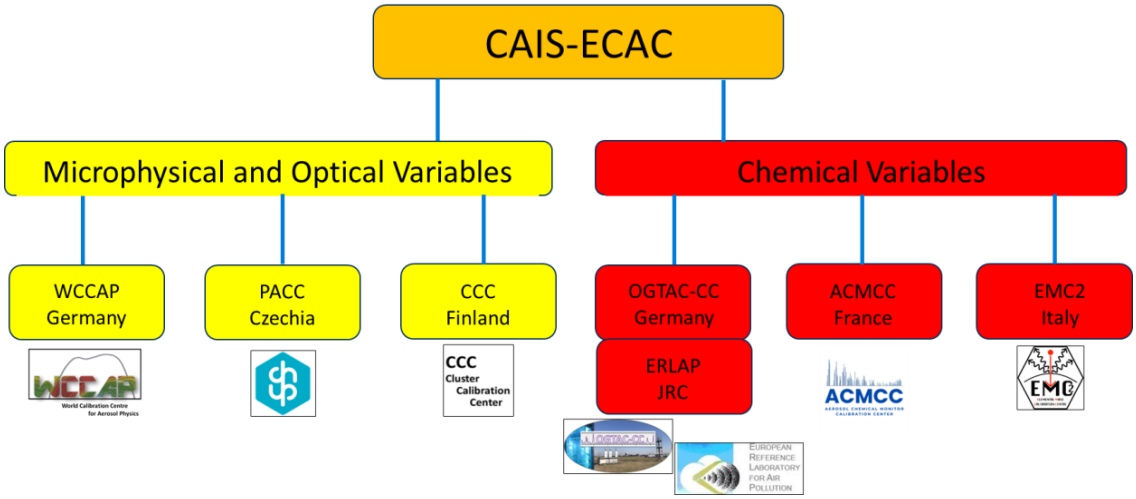


Figure 1. The consortium of the Center of Aerosol In-Situ Measurements – European Center for Aerosol Calibration and Characterization with 7 laboratories for microphysical, optical, and chemical variables.

The revised EU Ambient Air Quality Directive recommends adopting ACTRIS guidelines for measuring ultrafine particles (UFPs), including particle number concentration (PNC), particle number size distribution (PNSD), and the particle light absorption coefficient, also known as equivalent black carbon (eBC). To support this initiative, the Centre for Aerosol In-Situ Measurements – European Centre for Aerosol Calibration (CAIS-ECAC) offers collaboration with the air quality community by providing capacity-building programs focused on quality assurance and calibrations for these measurements & instruments..

EXAMPLES OF CALIBRATION RESULTS OF PNC & PNSD

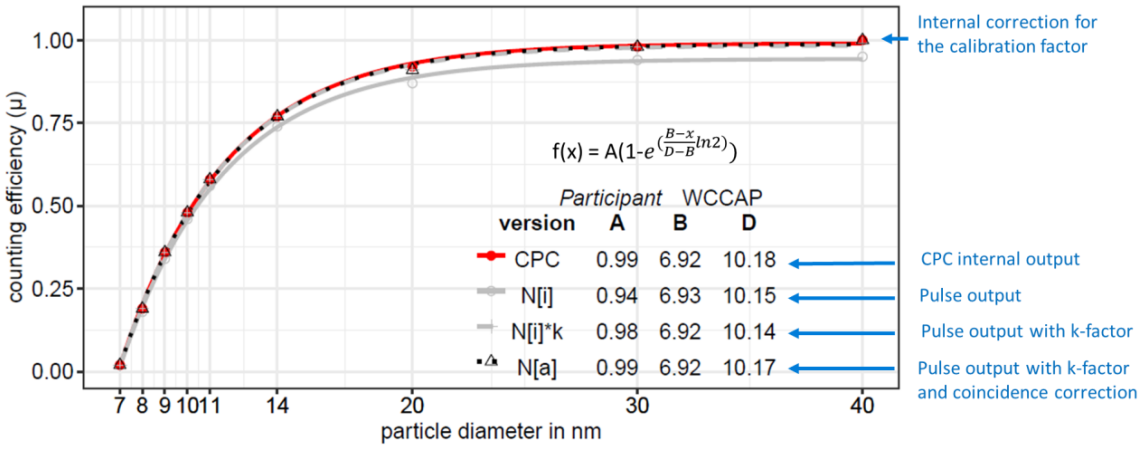


Figure 2. Calibration of a Condensation Particle Counter according to the EN 16976 Ambient air Determination of the particle number concentration of atmospheric aerosol.

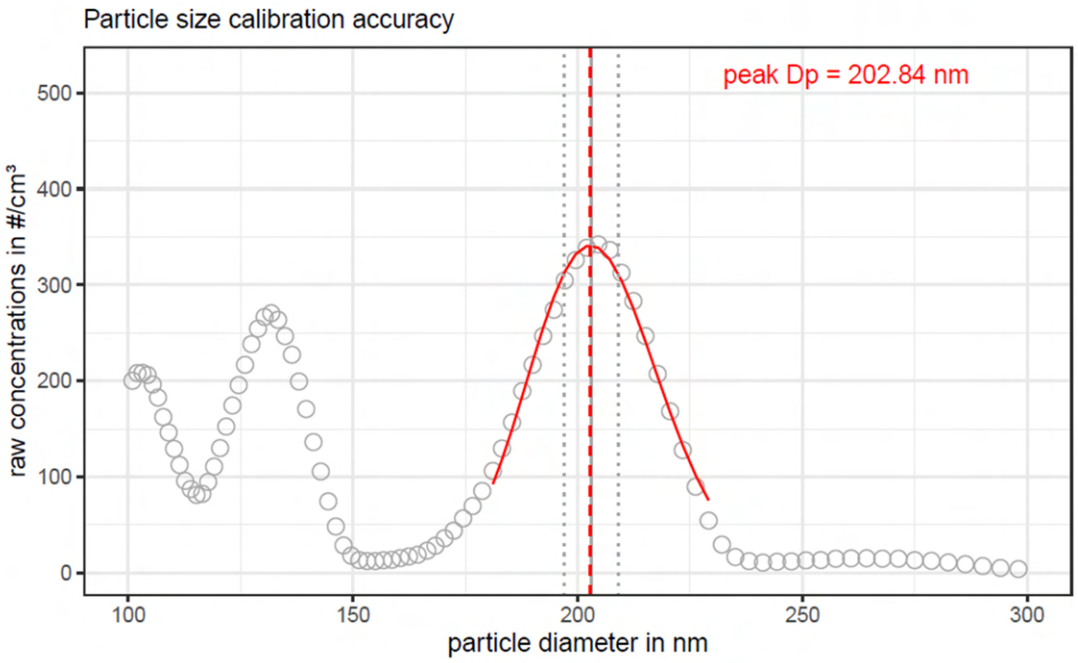


Figure 3. Latex Calibration of a Mobility Particle Size Spectrometer according to the CEN/TS 17434 Ambient air - Determination of the particle number size distribution of atmospheric aerosol using a Mobility Particle Size Spectrometer (MPSS)

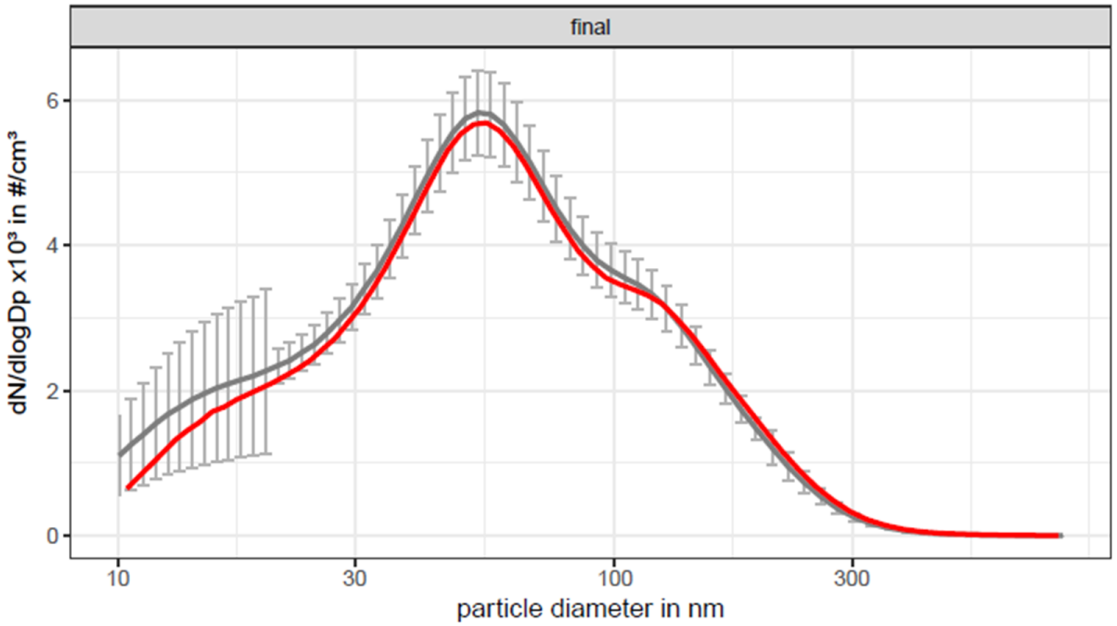


Figure 4. Calibration of a Mobility Particle Size Spectrometer against the reference MPSS according to the CEN/TS 17434 Ambient air - Determination of the particle number size distribution of atmospheric aerosol using a Mobility Particle Size Spectrometer (MPSS)

ACKNOWLEDGEMENTS

The WCCAP as one unit of the Central Facility CAIS-ECAC is funded by the German “Bundesministerium für Bildung und Forschung” (BMBF) for the implementation and by the German “Bundesministerium für Umwelt, Naturschutz, nukleare Sicherheit und Verbraucherschutz” (BMUV) for the operational activities.

REFERENCES

ACTRIS Standard Procedures for In-Situ Aerosol Sampling, Measurements, and Analyses at ACTRIS Observatories at https://www.actris-ecac.eu/

Performance & evaluation criteria for calibration workshops & ACTRIS compatibility at https://www.actris-ecac.eu/

EN 16976 Ambient air - Determination of the particle number concentration of atmospheric aerosol

CEN/TS 17434 Ambient air - Determination of the particle number size distribution of atmospheric aerosol using a Mobility Particle Size Spectrometer (MPSS)

Advancing Vertical Profiling of $PM_{2.5}$ Chemical Components: Integrating Remote Sensing Retrieval with Data Assimilation Systems

Ting Yang [1], Hongyi Li [1], Yifan Song [1,2], Yutong Tian [1,2], Yining Tan [1,2], Yele Sun [1,2] and Zifa Wang [1,2]

[1]*State Key Laboratory of Atmospheric Environment and Extreme Meteorology, Institute of Atmospheric Physics, Chinese Academy of Sciences, Beijing 100029, China*
[2]*College of Earth and Planetary Sciences, University of Chinese Academy of Sciences, Beijing 100049, China*

Keywords: $PM_{2.5}$, Vertical Evolution; Aerosol Component; Remote Sensing; Data Assimilation

INTRODUCTION

$PM_{2.5}$ comprises a diverse mixture of chemical components, including inorganic scattering components such as sulfate (SO_4^{2-}), nitrate (NO_3^-), and ammonium (NH_4^+), alongside organic-absorbing constituents like black carbon (BC) and brown carbon (BrC). $PM_{2.5}$ from various origins possesses unique optical and chemical properties, thus wielding different climatic and health implications. Moreover, the vertical distribution of $PM_{2.5}$ components changes rapidly with the swift variation of the planetary boundary layer. Diverse sources and fast changes induce the complexity of vertical component analysis.

METHODS

We obtained hourly concentration profiles for five components (SO_4^{2-}, NH_4^+, NO_3^-, OM, and BC) covering 150–6000 m, by aerosol component retrieval from remote sensing. The retrieval process is an integration of a novel fine-mode aerosol retrieval algorithm and an optimal deep learning model. A detailed description is given in Wang et al. and Li et al. , respectively. The first part of the retrieval process is retrieving optical component profiles from GRASP-GARRLiC outputs by constructing the aerosol model and microphysical parameterization schemes. GRASP-GARRLiC (Generalized Retrieval of Aerosol and Surface Properties–Generalized Aerosol Retrieval from Radiometer and Lidar Combined data), an open-source model for the joint retrieval of multiple observations, which was built directly on the AERONET inversion algorithm and modified to incorporate LiDAR data, has been widely used to characterize atmospheric aerosol properties and was validated by atmospheric observations in previous studies.

CONCLUSIONS

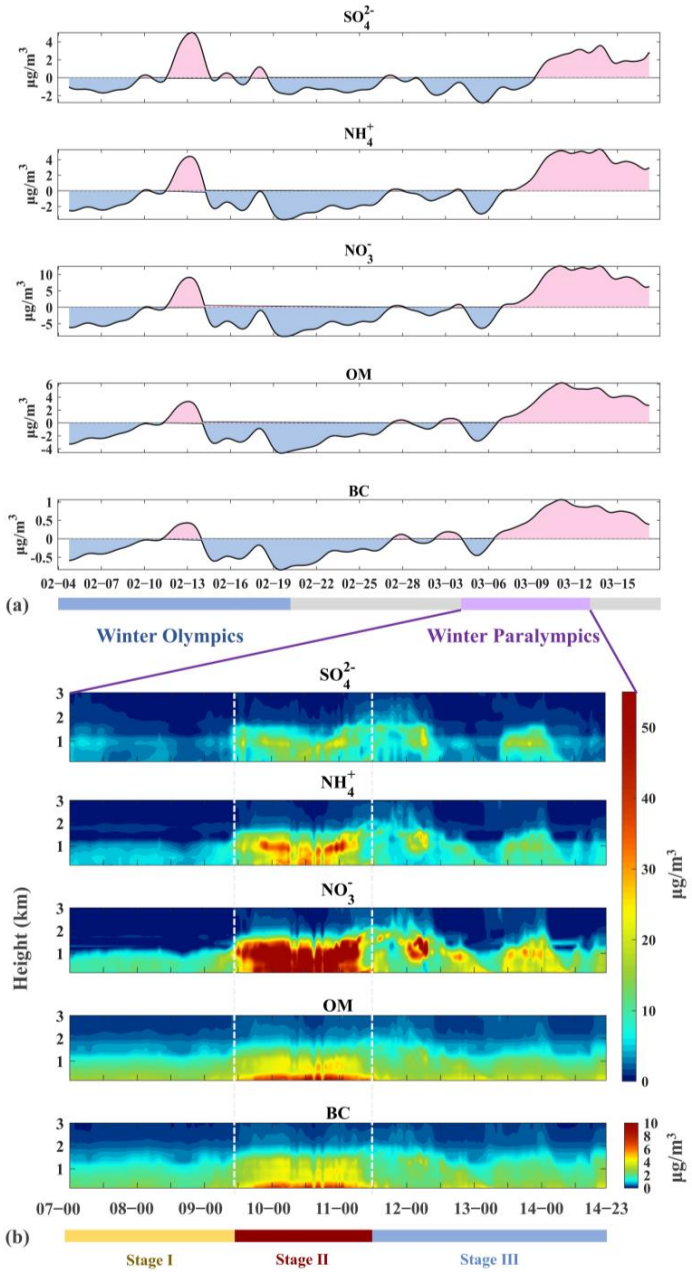


Figure 1. (a) Meteorologically adjusted long-term components from 4 February to 17 March. (b) Vertical concentration evolution of five chemical components in the pollution process of the Winter Paralympics (from 7 March 0:00 to 14 March 23:00). Time is presented as month–day in (a) and day–hour in (b).

ACKNOWLEDGEMENTS

This work was supported in part by the National Key Research and Development Program for Young Scientists of China (No. 2022YFC3704000).

REFERENCES

Wang, F.; Yang, T.; Wang, Z.; Wang, H.; Chen, X.; Sun, Y.; Li, J.; Tang, G.; Chai, W. Algorithm for vertical distribution of boundary layer aerosol components in remote-sensing data. *Atmos. Meas. Technol.* **2022**, *15*, 6127–6144.

Li, H.; Yang, T.; Du, Y.; Tan, Y.; Wang, Z. Interpreting hourly mass concentrations of PM2.5 chemical components with an op-timal deep-learning model. J. Environ. Sci. 2025, 151, 125–139.Chapman, D.H. (1975). Optical scattering from combustion aerosols, *J. Aerosol Science* **36**, 3456.
Finn, P., G.N. Diver and K.T. Wake (1998). Aerosol measurements in Iceland, in Proc. 13th Int. Conf. on Marine Aerosols, Reykjavik (Wiley, New York), 631.

GLOBAL ICE-NUCLEATING PARTICLE NUMBER CONCENTRATION DATABASE: AMBIENT MEASUREMENTS FROM 1948 TO 2025

CUIQI ZHANG[1], YIN HAU LAM[1], ANDRÉ WELTI[2], ROBERT O. DAVID[3], JANN SCHROD[4], LUISA ICKES[5], ERIK S. THOMSON[6], AND ZAMIN A. KANJI[1]

[1]*Institute for Atmospheric and Climate Sciences, D-USYS, ETH Zurich, 8092, Zurich, Switzerland.*

[2]*Finnish Meteorological Institute, Helsinki, Finland.*

[3]*Department of Geosciences, University of Oslo, Oslo, Norway.*

[4]*Institute for Atmospheric and Environmental Sciences, Goethe-University Frankfurt, Frankfurt am Main, Germany.*

[5]*Department of Space, Earth and Environment, Chalmers, Gothenburg, Sweden.*

[6]*Department of Chemistry and Molecular Biology, University of Gothenburg, Gothenburg, Sweden.*

Keywords: ICE-NUCLEATING PARTICLE, MIXED-PHASE CLOUDS, ICE CLOUDS, FIELD OBSERVATION, PARAMETERIZATION.

INTRODUCTION

Atmospheric primary ice crystal formation from supercooled droplets via immersion freezing can only be initiated by ice-nucleating particles (INPs) between -38 and 0 °C (Pruppacher and Klett, 1997). |Ice crystal can also form homogeneously when the temperature is below -38 °C, but the presence of INPs allows ice crystal formation at milder conditions, e.g., higher temperature or lower humidity. Field observations of ambient INP number concentration provide data for parameterization development, which can be implemented in global models to investigate aerosol-ice-cloud interaction feedbacks to climate, as well as to directly validate global climate model output. Despite major community efforts in the past few decades, the spatial and temporal distribution of INPs remains poorly constrained, which further hampers the ability of global models to estimate the sources and transport of INPs in the atmosphere.

More than 420,000 global ambient INP number concentration data points, measured since 1948, have been compiled into an Ice Nucleation DataBase (INDB). The INDB is an archive that includes sampling/measurement time, location, experimental conditions under which INP were measured, INP number concentration, campaign information, and reference information. The INDB attempts to comprehensively consolidate and digitize historical and contemporary ambient INP number concentration data.

METHODS

Figure 1 illustrates the identified global ambient INP number concentration datasets from over 300 publications (published after 1949 till 2025). An additional over 100 publications released after 2020 have been identified using keyword searches (e.g.,“ice-*nucle*”) on the Web of Science and are scheduled to be compiled in 2025.

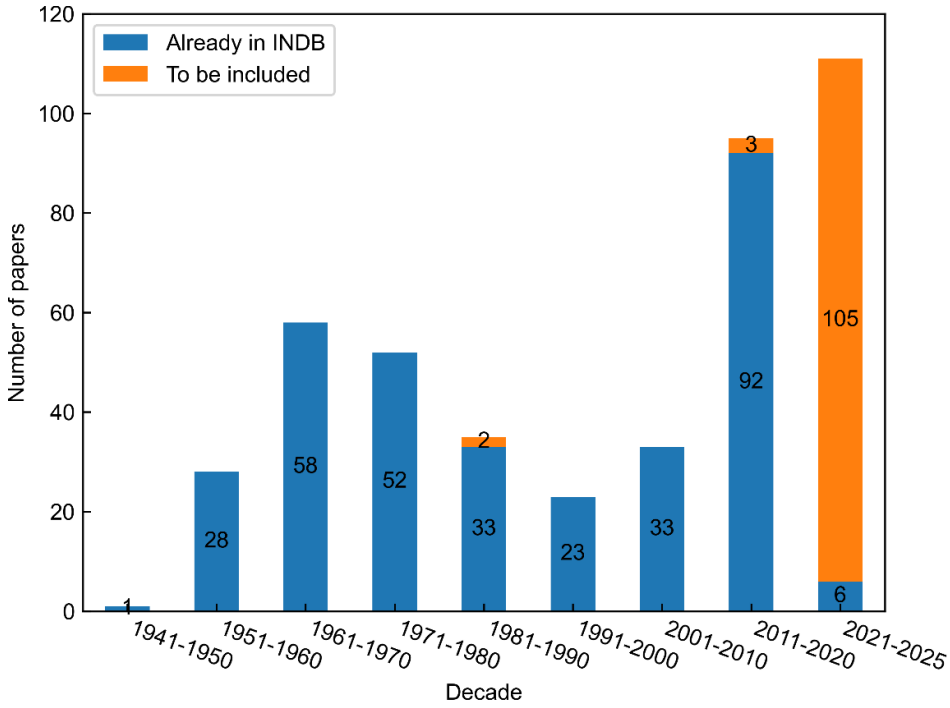


Figure 1. Digitized publications containing ambient INP number concentration data per decade.

CONCLUSIONS

We present an overview of ambient INP number concentration data extracted from more than 300 studies published over the past ≈75 years that are now archived in the INDB. The INDB has the potential to be a convenient resource for the ice nucleation research community to find INP number concentration data obtained at specific locations and times. Moreover, the INDB can be used to investigate the spatial and temporal evolution of INP concentrations, evaluate contemporary measurements and global model output, and to plan future field observations. As shown in Fig. 2, INP data coverage within and around Africa, South America, and Antarctica remains sparse.

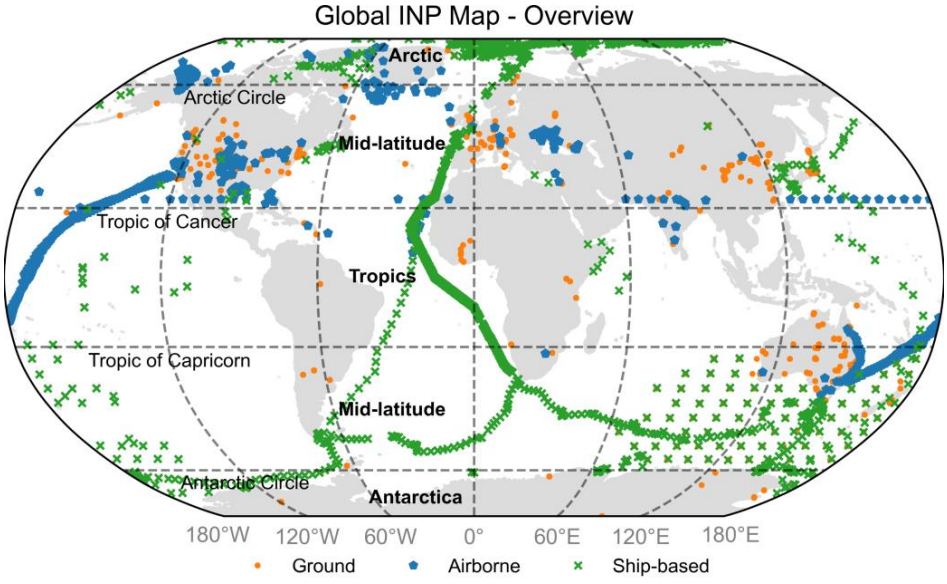


Figure 2. Global ambient INP number concentration measurements from different platforms.

Our next step is to improve global INP parameterizations with geographical information using the INDB. More than 50 existing INP parameterizations in the literature are compiled and categorized into thermodynamic condition (temperature and relative humidity) based (e.g., Meyers et al., 1992) and aerosol aware parameterizations based on the variables used. Aerosol properties, including number concentration above a certain size threshold (e.g., DeMott et al., 2010; DeMott et al., 2015), organic content (e.g., Wilson et al., 2015; McCluskey et al., 2018), and surface area (e.g., Ullrich et al., 2017; Harrison et al., 2019) are commonly utilized to predict INP number concentration within certain atmospheric temperature ranges.

ACKNOWLEDGEMENTS

This work was supported by the Horizon Europe project Cloud-aERosol inTeractions & their impActs IN The earth sYstem (CERTAINTY) under Grant Agreement No 101137680 and the EU FP7 project impact of Biogenic versus Anthropogenic emissions on Clouds and Climate: towards a Holistic UnderStanding (BACCHUS).

REFERENCES

DeMott, P. J., Prenni, A. J., Liu, X., Kreidenweis, S. M., Petters, M. D., Twohy, C. H., Richardson, M. S., Eidhammer, T., and Rogers, D. C. (2010). Predicting global atmospheric ice nuclei distributions and their impacts on climate, *Proceedings of the National Academy of Sciences* **107**, 11217-11222.

DeMott, P. J., Prenni, A. J., McMeeking, G. R., Sullivan, R. C., Petters, M. D., Tobo, Y., Niemand, M., Moehler, O., Snider, J. R., Wang, Z., and Kreidenweis, S. M. (2015). Integrating laboratory and field data to quantify the immersion freezing ice nucleation activity of mineral dust particles, *Atmos. Chem. Phys.* **15**, 393-409.

Harrison, A. D., Lever, K., Sanchez-Marroquin, A., Holden, M. A., Whale, T. F., Tarn, M. D., McQuaid, J. B., and Murray, B. J. (2019). The ice-nucleating ability of quartz immersed in water and its atmospheric importance compared to K-feldspar, *Atmos. Chem. Phys.* **19**, 11343-11361.

McCluskey, C. S., Ovadnevaite, J., Rinaldi, M., Atkinson, J., Belosi, F., Ceburnis, D., Marullo, S., Hill, T. C. J., Lohmann, U., Kanji, Z. A., O'Dowd, C., Kreidenweis, S. M., and DeMott, P. J. (2018). Marine and Terrestrial Organic Ice-Nucleating Particles in Pristine Marine to Continentally Influenced Northeast Atlantic Air Masses, *J. Geophys. Res. Atmos.* **123**, 6196-6212.

Meyers, M. P., DeMott, P. J., and Cotton, W. R. (1992). New Primary Ice-Nucleation Parameterizations in an Explicit Cloud Model, *Journal of Applied Meteorology and Climatology* **31**, 708-721.

Pruppacher, H. R., and Klett, J. D. (1997). *Microphysics of Clouds and Precipitation*, 2 ed., Atmospheric and Oceanographic Sciences Library, 18, (Springer Netherlands), XXII, 954 pp.

Ullrich, R., Hoose, C., Möhler, O., Niemand, M., Wagner, R., Höhler, K., Hiranuma, N., Saathoff, H., and Leisner, T. (2017). A New Ice Nucleation Active Site Parameterization for Desert Dust and Soot, *Journal of the Atmospheric Sciences* **74**, 699-717.

Wilson, T. W., Ladino, L. A., Alpert, P. A., Breckels, M. N., Brooks, I. M., Browse, J., Burrows, S. M., Carslaw, K. S., Huffman, J. A., Judd, C., Kilthau, W. P., Mason, R. H., McFiggans, G., Miller, L. A., Nájera, J. J., Polishchuk, E., Rae, S., Schiller, C. L., Si, M., Temprado, J. V., Whale, T. F., Wong, J. P. S., Wurl, O., Yakobi-Hancock, J. D., Abbatt, J. P. D., Aller, J. Y., Bertram, A. K., Knopf, D. A., and Murray, B. J. (2015). A marine biogenic source of atmospheric ice-nucleating particles, *Nature* **525**, 234-238.

FIVE-YEAR COMPARATIVE SECONDARY INORGANIC AEROSOL STUDY: EMMISSION SOURCES AND TRANSPORT PATTERNS IN FINLAND'S BOREAL FOREST AND BEIJING MEGACITY

Z. ZOU[1,2], W. DU[2], Q. YUAN[1,2], Y. LIU[1], G. CIARELLI[2,3] and T.V. KOKKONEN[2, 3]

[1].*Aerosol and Haze Laboratory, Beijing Advanced Innovation Center for Soft Matter Science and Engineering, Beijing University of Chemical Technology, Beijing 100029, China*

[2] *Institute for Atmospheric and Earth System Research, University of Helsinki, Helsinki, Finland*

[3]*Nanjing-Helsinki Institute in Atmospheric and Earth System Sciences, Nanjing University, Nanjing, China*

Keywords: SECONDARY INORGANIC AEROSOL, SULFATE, NITRATE, BOREAL FOREST, BEIJING.

INTRODUCTION

To our knowledge, there are no studies that would report secondary inorganic aerosol (SIA) pollutants over an extended period in contrasting environments such as Beijing in China, being an anthropogenic dominating region for SIA production, with Hyytiälä in Finland, can be considered to belong to a clean region in certain wind and during extended summer period (Ciarelli et al., 2024; Guo et al., 2023). Even though the air quality in the Beijing area has improved substantially in the latest decade due to the clean air policies implemented, it is still facing significant challenges in mitigating primary gaseous/particulate emissions and further reducing ambient PM levels. Although post-2013 air pollution control measures have substantially lowered primary pollutant concentrations, secondary components slower reduction rates (Cheng et al., 2016; Quan et al., 2015; Xu & Zhang, 2020). This study highlights secondary sulfate and nitrate as dominant contributors to fine particulate pollution, accounting for 33% and 23% of $PM_{2.5}$ mass annually with their formation efficiency strongly modulated by emission controls and atmospheric reactivity(Wang et al., 2019).

METHODS

The sulphate and nitrate concentration data were retrieved from 2 Aerosol Chemical Speciation Monitor (ACSM, Ng et al., 2011) located in Aerosol and Haze Laboratory, Beijing University of Chemical Technology (AHL/BUCT; 39.9428N, 119.2966E, Liu et al., 2020), and SMEAR II station, Hyytiälä, Finland (Hari et al., 2013). The Station for Measuring Ecosystem–Atmosphere relations (SMEAR) II station, located in the boreal forest of Hyytiälä, Finland, is well known for its comprehensive and wide measurements for environmental parameters(Hari et al., 2013). Inorganic species from anthropogenic activities, the majority identified as ammonium sulfate and nitrate, are also transported to the station. Ammonium sulfate represents the dominating inorganic species(Äijälä et al., 2019). Other meteorology variables are measured with an Automatic Weather Station. The concentration was provided in 1 hour temporal resolution, study period was form 2018-2022. The Time over Land (ToL) and Time over Populated Land (ToPL) in short, was the time of airmass arrived when measuring travelled above land or polluted land, it was calculated based on back trajectory calculated by HYSPLIT model.

CONCLUSIONS

This study reveals contrasting pathways of sulfate (SO_4) and nitrate (NO_3) formation between Beijing and Hyytiälä under varying humidity regimes. In Beijing, elevated specific humidity (q_{air} >60%) stabilizes the sulfur oxidation ratio (SOR) at 0.9, compare with local secondary production, SO_4 accumulation was primarily driven by SO_2 oxidation during transportation. The humidity dependent SOR gradient (from 0.4 at q_{air}<30% to 0.9 at q_{air} >60%) underscores aqueous phase SO_2 conversion as the dominant pathway, facilitated by abundant aerosol water content. The diverging Beijing-Hyytiälä SOR ratio after 60-hour transport highlights source-region chemistry differences—Beijing's sulfate derives from land-based SO_2 emissions with homogeneous oxidation dominance at low q_{air}, whereas Hyytiälä's stable SOR reflects pre-aged air masses with depleted SO_2 reactivity.

Nitrate dynamics exhibit distinct humidity sensitivity: high q_{air} conditions (>60%) in Beijing elevate the nitrogen oxidation ratio (NOR) through enhanced N_2O_5 hydrolysis on hydrated aerosol surfaces, contrasting with Hyytiälä's suppressed NO_3 formation under similar q_{air} due to cloud induced OH depletion.

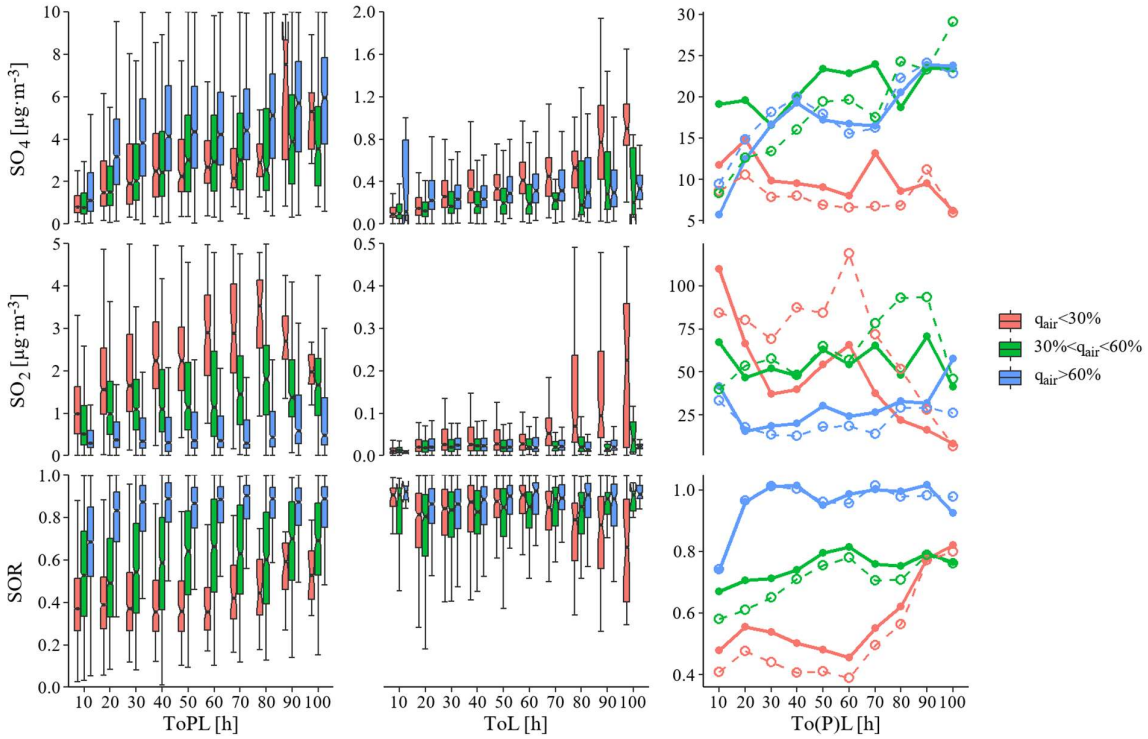


Figure 1. To(P)L affecting Sulfate, SO_2 and SOR with different bins of specific humidity q_{air}

ACKNOWLEDGEMENTS

The ACCC Flagship funded by the Academy of Finland grant number 337549, Academy professorship funded by the Academy of Finland (grant no. 302958), Academy of Finland projects no. 325656, 311932, 334792, 316114, 325647, 325681, 333397, 328616, 357902, 345510, 347782, "Quantifying carbon sink, CarbonSink+ and their interaction with air quality" INAR project funded by Jane and Aatos Erkko Foundation, "Gigacity" project funded by Wihuri foundation, the program of Chinese Scholarship Council (No. 202206380019). University of Helsinki support via ACTRIS-HY is acknowledged. Support of the technical and scientific staff in Hyytiälä and BUCT/AHL are acknowledged. L.D. acknowledges funding from the Swiss National Science Foundation (grant number 216181).

REFERENCES

Äijälä, M., Daellenbach, K. R., Canonaco, F., Heikkinen, L., Junninen, H., Petäjä, T., . . . Ehn, M. (2019). Constructing a data-driven receptor model for organic and inorganic aerosol – a synthesis analysis of eight mass spectrometric data sets from a boreal forest site. *Atmos. Chem. Phys., 19*(6), 3645-3672. doi:10.5194/acp-19-3645-2019

Cheng, Y., Zheng, G., Wei, C., Mu, Q., Zheng, B., Wang, Z., . . . Carmichael, G. (2016). Reactive nitrogen chemistry in aerosol water as a source of sulfate during haze events in China. *Science advances, 2*(12), e1601530.

Ciarelli, G., Tahvonen, S., Cholakian, A., Bettineschi, M., Vitali, B., Petäjä, T., & Bianchi, F. (2024). On the formation of biogenic secondary organic aerosol in chemical transport models: an evaluation of the WRF-CHIMERE (v2020r2) model with a focus over the Finnish boreal forest. *Geoscientific Model Development, 17*(2), 545-565.

Guo, Y., Deng, C., Ovaska, A., Zheng, F., Hua, C., Zhan, J., . . . Xie, J. (2023). Measurement report: The 4-year variability and influence of the Winter Olympics and other special events on air quality in urban Beijing during wintertime. *Atmospheric Chemistry and Physics, 23*(12), 6663-6690.

Hari, P., Nikinmaa, E., Pohja, T., Siivola, E., Bäck, J., Vesala, T., & Kulmala, M. (2013). Station for measuring ecosystem-atmosphere relations: SMEAR. *Physical and physiological forest ecology*, 471-487.

Liu, Y., Chao, Y., Zemin, F., Feixue, Z., Xiaolong, F., Yusheng, Z., . . . and Kulmala, M. (2020). Continuous and comprehensive atmospheric observations in Beijing: a station to understand the complex urban atmospheric environment. *Big Earth Data, 4*(3), 295-321. doi:10.1080/20964471.2020.1798707

Ng, N. L., Herndon, S. C., Trimborn, A., Canagaratna, M. R., Croteau, P. L., Onasch, T. B., . . . Jayne, J. T. (2011). An Aerosol Chemical Speciation Monitor (ACSM) for Routine Monitoring of the Composition and Mass Concentrations of Ambient Aerosol. *Aerosol Science and Technology, 45*(7), 780-794. doi:10.1080/02786826.2011.560211

Quan, J., Liu, Q., Li, X., Gao, Y., Jia, X., Sheng, J., & Liu, Y. (2015). Effect of heterogeneous aqueous reactions on the secondary formation of inorganic aerosols during haze events. *Atmospheric Environment, 122*, 306-312.

Wang, Q., Huang, X. H., Tam, F. C., Zhang, X., Liu, K. M., Yeung, C., . . . Ng, W. M. (2019). Source apportionment of fine particulate matter in Macao, China with and without organic tracers: A comparative study using positive matrix factorization. *Atmospheric Environment, 198*, 183-193.

Xu, X., & Zhang, T. (2020). Spatial-temporal variability of PM2. 5 air quality in Beijing, China during 2013–2018. *Journal of environmental management, 262*, 110263.

Special Session 2: Solar radiation management by aerosols

PRELIMINARY AEROSOL CHARACTERIZATION OF SALINE RAYLEIGH JETS FOR THE PURPOSE OF MARINE CLOUD BRIGHTENING

J. CHAPMAN[1], H. HUNT[1]

[1]*Centre for Climate Repair, Department of Engineering, University of Cambridge, United Kingdom*

Keywords: Rayleigh jet breakup, aerosol generation, particle sizing, marine cloud brightening, solar radiation modification, climate change.

INTRODUCTION

Marine cloud brightening (MCB) has received growing attention as a solar radiation modification strategy to address the ecosystem impacts of global warming. The strategy involves the generation of salt aerosols to provide additional cloud condensation nuclei (CCN) to marine clouds, with the aim to trigger the formation of cloud droplets and enhance cloud albedo. A small body of literature suggests certain criteria that define optimal CCN. Broadly, the aim is to produce submicron seawater droplets, leading to salt CCN sizes roughly between 30-500 nm (Wood, 2021; Salter, 2012), at a rate of at least 10^{15} s^{-1} (Salter, 2008; Latham *et al.*, 2008) with minimal energy expense and environmental impact.

A droplet generation method of interest is that of Rayleigh jet breakup. The method involves the breakup of liquid columns in laminar flow using natural and induced perturbations. The method has been used for applications such as inkjet printing and medical inhalers to produce highly monodisperse droplets at the micron scale. A small number of studies have investigated Rayleigh jet sprays for MCB (Cooper *et al.*, 2013; Salter *et al.*, 2014). These studies provided observational and qualitative insights using nozzles made from silicon wafers, although quantitative findings were limited due to fabrication challenges and nozzle clogging issues. The present study provides preliminary experimental results for saline Rayleigh jets using commercially available spray nozzle units with smaller pores than have been previously tested. Ultimately, this study aims to provide insights to assess the feasibility of Rayleigh jet breakup for the purpose of marine cloud brightening.

METHODS

The nozzle units, supplied by Medspray B.V., are made of silicon and consist of up to 145 pores per unit. Three nozzle units were tested corresponding to three different pore sizes: 1.6 µm, 1.9 µm, and 4 µm. Various solutions were tested, all consisting of a mixture of distilled water and 99.5% pure sodium chloride with salinities ranging from 0.9% to 7%. Using distilled water with pure salt was chosen to avoid clogging issues, however the nozzles have been shown to operate normally with pre-filtered seawater samples.

The nozzle testing apparatus consisted of a constant volume sampling tunnel into which solutions were sprayed. An isokinetic sampling probe was centrally positioned within the sampling tunnel and directed the sample through a dryer before splitting into a number of particle detectors to measure particle diameters and concentration.

CONCLUSIONS

Preliminary tests of Rayleigh jetting without any induced pressure perturbations, using the nozzle units of Medspray B.V., show promising results with respect to the design criteria for marine cloud brightening. Figure 1 shows representative distributions for the 1.6 µm pore unit. The modal size is approximately 160 nm and the geometric standard deviation ranges between 1.26-1.40. The production rate was found to be about 10^{8} s^{-1}; from this, scaling the design to achieve the desired production rate of 10^{15} s^{-1} will require an estimated power requirement of 150 kW. It is believed this power estimate can be significantly reduced through nozzle design optimization.

Further tests are required to adequately compare these results to theoretical expectations and to explore the effects of induced pressure perturbations using piezoelectric transducers fitted to the nozzles. Future work will also include: (i) developing a rigorous filtration system to allow the nozzles to work continuously with seawater, (ii) optimising the design of the nozzle pores for MCB, and (iii) testing large arrays of the nozzle units simultaneously.

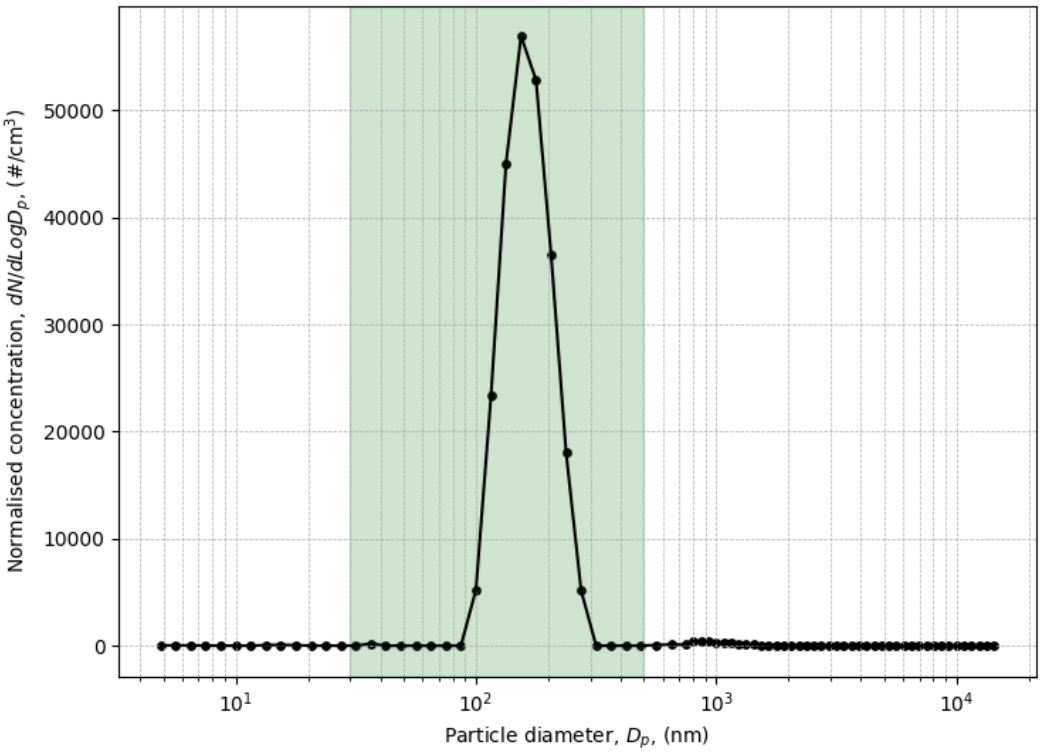


Figure 1. Normalised number distributions of salt particles generated from 100 Rayleigh jets of 3.5% saline solution from 1.6 µm pores. The green shaded region denotes the notional size range suitable for MCB (30-500 nm). The nozzle was spraying for two minutes, with each distribution recorded at 1 second intervals by an electrical mobility detector (DMS500, Cambustion) and an aerodynamic particle sizer spectrometer (APS, TSI).

ACKNOWLEDGEMENTS

We would like to thank Stefan van der Vegte, Han van Egmond, and the rest of the team at Medspray B.V. for their generosity and support in this research. This work was financially supported by the Refreeze the Arctic Foundation (RAF) and by Southern Cross University as part of the Cooling and Shading subprogram of the Reef Restoration and Adaptation Program (RRAP). The Reef Restoration and Adaptation Program is funded by the partnership between the Australian Governments Reef Trust and the Great Barrier Reef Foundation.

REFERENCES

Medspray BV (2024). *Technology*. Accessed: 2024-08-19, url: https://medspray.com/technology/.

Cooper, G., D. Johnston, J. Foster, L. Galbraith, A. Neukermans, R. Ormond, J. Rush, and Q. Wang. (2013). A Review of Some Experimental Spray Methods for Marine Cloud Brightening. *International Journal of Geosciences* vol. 4, no.1, pp. 78–97. DOI: 10.4236/ijg.2013.41009.

Wood, R. (2021). Assessing the potential efficacy of marine cloud brightening for cooling Earth using a simple heuristic model, *Atmospheric Chemistry and Physics*, vol. 21, no. 19, pp. 14507–14533. doi:10.5194/acp-21-14507-2021

Salter, S. (2012). Solar Radiation Management, cloud albedo enhancement, *Geoengineering Responses to Climate Change*, pp. 39–51. doi:10.1007/978-1-4614-5770-1_4

Latham, J., P. Rasch, C.-C. Chen, L. Kettles, A. Gadian, A. Gettelman, H. Morrison, K. Bower, and T. Choularton (2008). Global temperature stabilization via controlled albedo enhancement of low-level maritime clouds, *Phil. Trans. R. Soc. A*, vol. 366, pp. 3969–3987. doi:10.1098/rsta.2008.0137

Salter, S., G. Sortino, and J. Latham (2008). Sea-going hardware for the cloud albedo method of reversing global warming," *Phil. Trans. R. Soc. A*, vol. 366, pp. 3989–4006. doi:10.1098/rsta.2008.0136

Salter, S., T. Stevenson, T. and A. Tsiamis (2014). Engineering Ideas for Brighter Clouds. In: *Geoengineering of the Climate System*. The Royal Society of Chemistry, pp. 131-161. DOI: 10.1039/9781782621225-00131

ELECTROSPRAYING HIGHLY CONDUCTIVE SALINE SOLUTIONS FOR THE PURPOSE OF MARINE CLOUD BRIGHTENING

J. CHAPMAN[1], D. MCGRATH[1] and H. HUNT[1]

[1]*Centre for Climate Repair, Department of Engineering, University of Cambridge, United Kingdom*

Keywords: Electrospray, aerosol generation, marine cloud brightening, solar radiation modification, climate change.

INTRODUCTION

Marine cloud brightening (MCB) is a proposed solar radiation modification strategy that could be deployed on a local or global scale to protect and restore collapsing ecosystems and temporarily halt rising average global temperatures as a result of climate change. The feasibility of marine cloud brightening depends on efficient spraying of seawater to generate a monodisperse aerosol of submicron droplets and deliver large quantities of salt crystals into target clouds.

A technique of interest is the electrostatic spraying of liquids, electrospraying, due to its potential to achieve highly monodisperse sprays of submicron droplets when operated in a particular behavior mode called the cone-jet mode. Electrospraying involves forming a high electric field at the tip of a capillary filled with a charged liquid. Previous studies involving electrospraying suggest that stable operating modes with saline water cannot be achieved without the presence of electrical discharge (detrimental to power efficiency and jet stability), or else without the addition of surfactants (Jaworek, Sobczyk, *et al.*, 2014; Pongrác *et al.*, 2014; Borra, 2018; Ganan-Calvo *et al.*, 2018; Marginean, 2024; Cooper *et al.*, 2013). Therefore, the suitability of electrospraying for the purpose of marine cloud brightening is unclear where seawater, with relatively high surface tension and conductivity, would be sprayed. This study provides theoretical expectations and preliminary experimental results, and highlights the technical challenges of electrospraying solutions with properties akin to seawater. Ultimately, this study aims to provide insights that can be used to evaluate the suitability of electrospraying for marine cloud brightening.

METHODS

The experimental configuration is shown in Figure 1. Various nozzles were tested, ranging from 0.05 to 1.8 mm in diameter. A high voltage power supply (0-20 kV) was used to vary the input voltage while the spray was generated at a given flow rate (0.001-2 mL/h). Distilled water mixed with 3.5% NaCl was used as the test solution to ensure consistent liquid properties for all tests. Preliminary experiments involved varying four parameters: electrode potential difference (i.e., input voltage), solution flow rate, electrode spacing, and capillary diameter. The electrospray behavior and operating modes were recorded using a microscope camera and current sensing at the grounded electrode. Stable operating ranges with respect to the four varied parameters were identified, denoted by the onset and loss of a stable cone-jet.

CONCLUSIONS

Preliminary results are shown in Figure 2 which highlight two key findings. First, a stable cone-jet can be achieved with 3.5% saline solutions without the need for added surfactants. Second, several electrospray operating modes have been characterized using direct imaging, which show distinct liquid flow features at the capillary tip, and current sensing, which show distinct characteristic current traces for the respective modes. Future work will continue to map out stable operating modes based on the four key parameters. Results from smaller nozzle sizes are of particular interest (i.e., down to 0.05 mm), owing to the practical constraints for a large-scale MCB prototype.

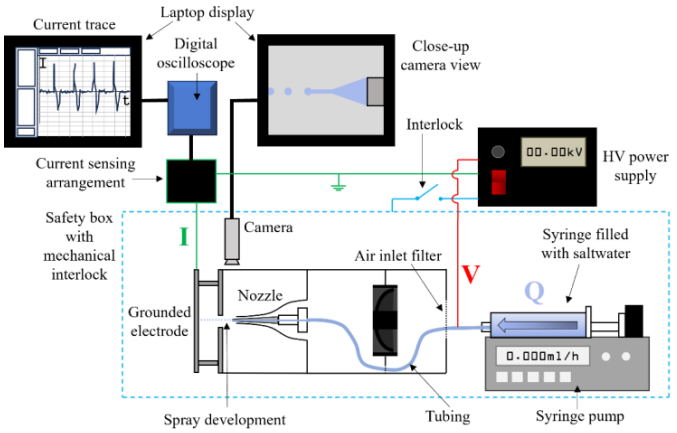


Figure 1. Experimental setup of the electrospray experimental configuration. Four parameters were varied: input voltage (V), solution flow rate (Q), nozzle diameter, and electrode separation.

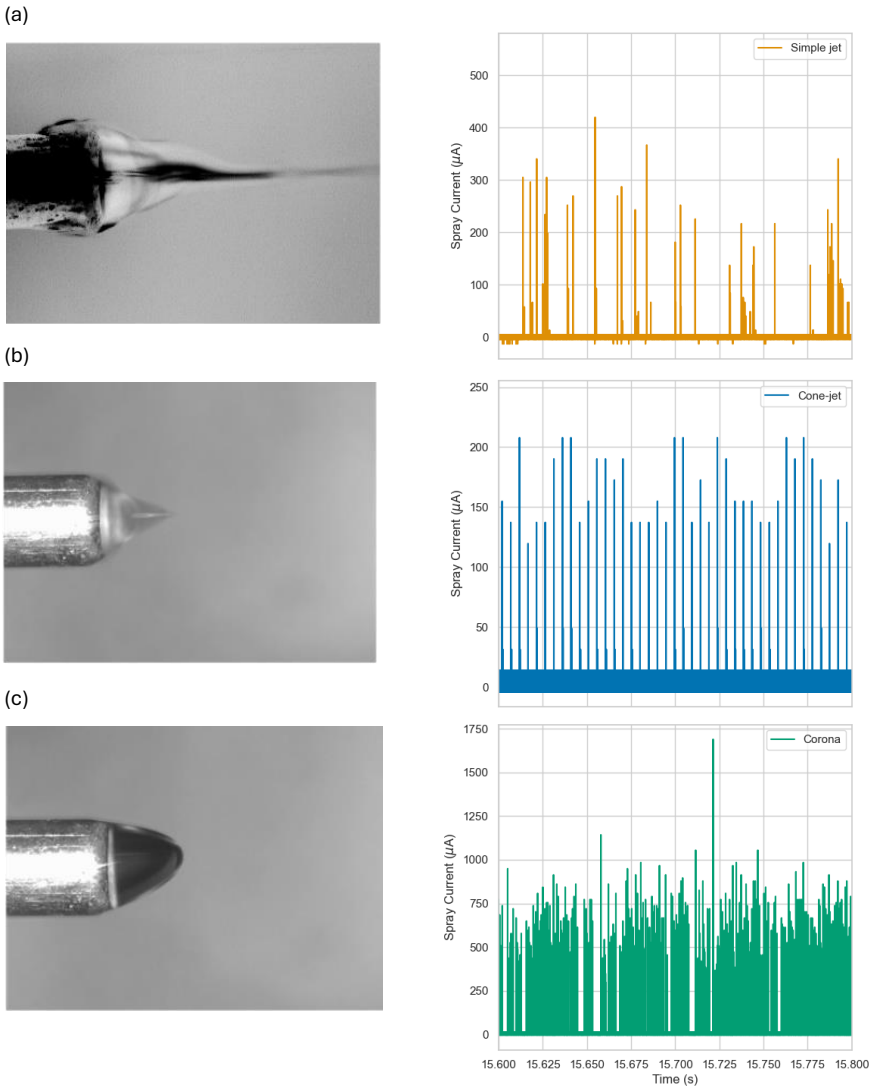


Figure 2. Images (left column) and current signatures (right column) recorded for three different modes – (a) simple jet, (b) cone-jet, and (c) corona discharge – from electrospraying 3.5% saline with a 1.8 mm diameter nozzle at an electrode separation of 30 mm.

ACKNOWLEDGEMENTS

This work was financially supported by the Refreeze the Arctic Foundation (RAF) and by Southern Cross University as part of the Cooling and Shading subprogram of the Reef Restoration and Adaptation Program (RRAP). The Reef Restoration and Adaptation Program is funded by the partnership between the Australian Governments Reef Trust and the Great Barrier Reef Foundation.

REFERENCES

Borra, J.P. (2018). Review on water electro-sprays and applications of charged drops with focus on the corona-assisted cone-jet mode for High Efficiency Air Filtration by wet electro-scrubbing of aerosols. *Journal of Aerosol Science*, vol. 125, pp. 208– 236. DOI: https://doi.org/10.1016/j.jaerosci.2018.04.005.

Cooper, G., D. Johnston, J. Foster, L. Galbraith, A. Neukermans, R. Ormond, J. Rush, and Q. Wang. (2013). A Review of Some Experimental Spray Methods for Marine Cloud Brightening. *International Journal of Geosciences*, vol. 4, no.1, pp. 78–97. DOI: 10.4236/ijg.2013.41009.

Gañán-Calvo, A. M., J.M. López-Herrera, M.A. Herrada, A. Ramos, and J.M. Montanero. (2018). "Review on the physics of electrospray: From electrokinetics to the operating conditions of single and coaxial Taylor cone-jets, and AC electrospray. *Journal of Aerosol Science*, vol. 125, pp. 32–56. DOI: https://doi.org/10.1016/j.jaerosci.2018.05.002.

Jaworek, A., A. Sobczyk, T. Czech, and A. Krupa. (2014). Corona discharge in electrospraying. *Journal of Electrostatics*, vol. 72.2, pp. 166–178. DOI: https://doi.org/10.1016/j.elstat.2014. 01.004.

Marginean, I. (2024). Classification of electrospray axial regimes as revealed by spray current measurements. *International Journal of Mass Spectrometry*, vol. 495, p. 117150. ISSN: 1387-3806. DOI: https://doi.org/10.1016/j.ijms.2023.117150.

Pongrác, B., H.H Kim, N. Negishi, et al. (2014). Influence of water conductivity on particular electrospray modes with dc corona discharge — Optical visualization approach. *The European Physical Journal D*, vol. 68, p. 224. DOI: https://doi.org/10.1140/epjd/e2014-50052-4.

ESTIMATING SHADING FROM ARTIFICIAL SEAWATER DROPLET PLUME ON THE GREAT BARRIER REEF

Z. LI[1], J. ALROE[1], L. HARRISON[2], H. SCOBLE[1], D. HARRISON[3], and Z. RISTOVSKI[1]

[1]*School of Earth and Atmospheric Sciences, Queensland University of Technology, Brisbane 4000, Australia*

[2]*School of Aerospace, Mechanical and Mechatronic Engineering, The University of Sydney, Sydney 2006, Australia*

[3]*Reefs and Oceans Research Cluster, National Marine Science Centre, Southern Cross University, Coffs Harbour 2450, Australia*

Keywords: SOLAR IRRADIATION MANAGEMENT, SEAWATER DROPLETS, SHADING.

INTRODUCTION

The warmer climate and associated rising seawater temperatures are dramatically threatening coral reef ecosystems (Hughes et al., 2018). Apart from this thermal stress, high exposure to solar irradiance (i.e., light stress) increases the likelihood of coral bleaching (Gonzalez-Espinosa and Donner, 2021). Shading coral from sunlight during periods of thermal stress has been suggested as a potential, cost-effective approach to reduce the risk of coral bleaching, especially during doldrum conditions. Recently, evidence from small-scale laboratory studies has shown that providing 30% shading up to 12 hours per day is sufficient to delay the onset of bleaching up to three degree heating weeks or more (Butcherine et al., 2023; Ellis et al., 2024). To move forward with the shading technique for future large-scale deployment, we conducted a shading trial using artificial seawater droplet plumes on the Great Barrier Reef in March 2023. Here, we will focus on the in-situ shading measurements and associated model simulations using a radiative transfer model.

METHODS

The shading trial was conducted from a spraying vessel, *R/V Bandicoot*, which was anchored upwind of the Wistari Reef or One Tree Island Reef with its engine off. A fog generator, which consists of water filters, high-pressure pumps, and an array of 1080 impact-pin nozzles with 203 μm orifices, was used to atomize the filtered seawater to generate a high number concentration of seawater droplets.

Once the seawater droplet plume was well developed, crosswind transect sampling was performed on a second sampling vessel, the *R/V* Magnetic, at multiple downwind distances of 1.5 km or less from the spraying source. We used a suite of real-time aerosol instruments installed in a temperature-controlled shipping container to measure the particle number concentration (PNC), particle number size distribution, and solar irradiance in the wavelength range of 250 – 800 nm.

Using a Gaussian plume dispersion model, we initially estimated the apparent droplet production rate from the crosswind transect PNC measurements. Based on this estimate, we simulated the plume dispersion across a 4 km² area of flat sea, with a maximum altitude of 4 km above sea level under meteorological conditions consistent with the field trial. Moreover, we computed the corresponding extinction efficiency (Q_e) for a unit mass of seawater droplets, taking into account the hygroscopic growth of the measured particles (Zieger et al., 2017). Using the htrdr radiative transfer simulator (Villefranque et al., 2019) with the spatially estimated PNC and Q_e as inputs, we calculated the downward light flux for a clear sky with and without a fully developed plume. The relative reduction in light intensity caused by the presence of seawater droplets was defined as shading.

CONCLUSIONS

Form the in-situ measurement, we observed the maximum achievable shading of up to 15% at the 5m drone pad. With increased downwind transport time, the observed shading gradually decreased due to the horizontal spread of the seawater droplet plume. With the use of the plume dispersion model, the apparent droplet rate was estimated to be in the order of 10^{14} s^{-1}. Figure 1 shows the corresponding model simulation of the shading induced by the seawater droplet plume under experimental meteorological conditions, with clear-sky solar irradiance as the reference case. Sensitivity analyses will be carried out to investigate the role of production rate and meteorological conditions on the potential achieved shading.

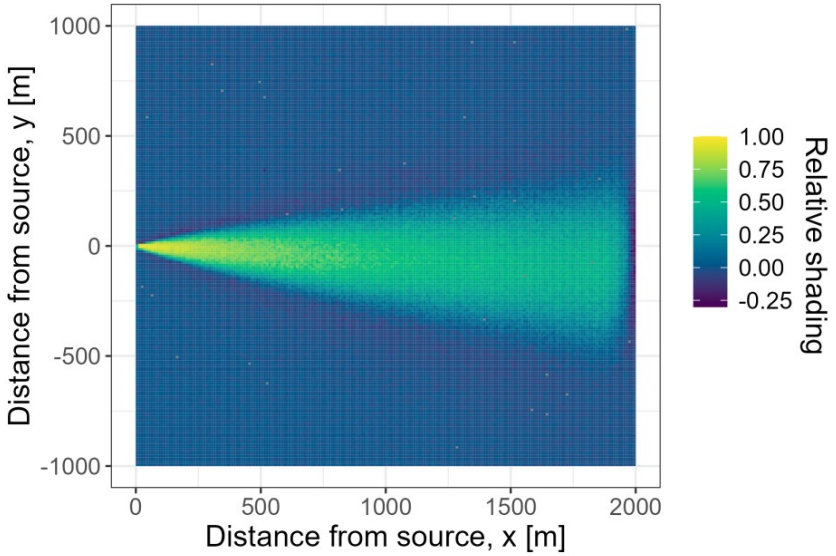


Figure 1. Simulated light intensity flux at sea level during plume production for a spraying experiment.

ACKNOWLEDGEMENTS

The work was supported by the Reef Restoration and Adaptation Program (RRAP), Cooling and Shading R&D Subprogram.

REFERENCES

Butcherine, P., Tagliafico, A., Ellis, S. L., et al., (2023), *Frontiers in Marine Science*, 10, 1162896.
Ellis, S. L., Butcherine, P., Tagliafico, A., et al., (2024), *Frontiers in Marine Science*, 11, 1333806.
Gonzalez-Espinosa, P. C. and Donner, S. D., (2021), *Glob Chang Biol*, 27, 3474-3486, 10.1111/gcb.15676.
Hughes, T. P., Anderson, K. D., Connolly, S. R., et al., (2018), *Science*, 359, 80-83.
Villefranque, N., Fournier, R., Couvreux, F., et al., (2019), *Journal of Advances in Modeling Earth Systems*, 11, 2449-2473.
Zieger, P., Vaisanen, O., Corbin, J. C., et al., (2017), *Nat Commun*, 8, 15883, 10.1038/ncomms15883.

EXPERIMENTAL INSIGHTS INTO THE DRYING OF SEAWATER DROPLETS FOR MARINE CLOUD BRIGHTENING

D. MCGRATH[1] and H. HUNT[1]

[1]*Centre for Climate Repair, Department of Engineering, University of Cambridge, Trumpington Street, Cambridge CB2 1PZ, United Kingdom.*

Keywords: Droplet evaporation, saline solutions, marine cloud brightening, solar radiation modification.

INTRODUCTION

Marine cloud brightening (MCB) is a growing topic of research within the field of solar radiation modification (SRM). MCB involves spraying microscale seawater droplets into the atmosphere to deliver nanoscale salt crystals to low-lying clouds; these crystals trigger cloud droplet formation, which can enhance cloud albedo, thereby contributing to localized cooling. Although the topic has largely been informed by computational modeling (see, e.g., Alterskjær and Kristjánsson, 2013; Latham *et al.*, 2012; Stjern *et al.*, 2018; Wood, 2021), a small number of groups are undertaking experimental work examining the generation and delivery of salt crystals conducive to cloud albedo enhancement. This engineering challenge is considered a vital 'checkpoint' informing the overall feasibility of MCB at meaningful scales (Diamond *et al.*, 2022). Droplet evaporation is a key transport mechanism to characterize the evolution of seawater droplets, underpinning model assumptions and experimental observations. In this poster, we outline a pilot parametric study providing experimental data on droplet evolution at the laboratory scale.

Below, we describe experimentation to be conducted in mid-2025. The aerosol instrumentation cited are currently undergoing calibration.

METHODS

The experiment will be undertaken in a control volume provided with filtered air and in which temperature and relative humidity are controlled. The test solution will be a mixture containing distilled water and salt (3.5% salinity). The droplets will be generated by a small selection of ultrasonic and air-blast atomizers, which are capable of generating droplets with median diameters of the order of 10^{-2} to 10^{1} μm.

The droplets will be measured at micron and submicron scale using a laser diffraction system (Spraytec, Malvern Panalytical). Measurements will be taken at a range of axial positions downstream of the atomizer outlet. Far downstream, the droplets will be sampled and fed through a diffusion dryer, whereupon the residual aerosols (including salt) will be measured using an electrical mobility system (DMS500, Cambustion). The instruments will provide estimates of the size and number concentration of the generated sprays at discrete stages of their evolution, from partially evaporated droplets to near-fully evaporated droplets.

CONCLUSIONS

The experiments will estimate droplet lifetime for a range of droplet diameters (between 10^{-2} to 10^{1} μm). Comparisons will be drawn with theoretical and empirical estimates, incorporating the Fuchs and Kelvin effects and the effects of temperature and relative humidity.

Overall, this pilot study will provide valuable insights to inform spray mechanism development and computational models. It also provides a framework by which future work may examine the transport characteristics of seawater droplets in relation to MCB. By collating data obtained from multiple measurement principles (laser diffraction and electrical mobility), the links between droplet generation and aerosol detection may be better understood. Future work will examine the role of contaminants on the evaporation rate.

ACKNOWLEDGEMENTS

This work was financially supported by the Refreeze the Arctic Foundation (RAF) and by Southern Cross University as part of the Cooling and Shading subprogram of the Reef Restoration and Adaptation Program (RRAP). The Reef Restoration and Adaptation Program is funded by the partnership between the Australian Governments Reef Trust and the Great Barrier Reef Foundation.

REFERENCES

Alterskjær, K., and J.E. Kristjánsson (2013). The sign of the radiative forcing from marine cloud brightening depends on both particle size and injection amount. *Geophysical Research Letters*, **40**(1), 210-215.

Diamond, M. S., A. Gettelman, M.D. Lebsock, A. McComiskey, L.M. Russell, R. Wood and G. Feingold (2022). To assess marine cloud brightening's technical feasibility, we need to know what to study—and when to stop. *Proceedings of the National Academy of Sciences*, **119**(4), 1–6.

Latham, J., K. Bower, T. Choularton, H. Coe, P. Connolly, G. Cooper, T. Craft, J. Foster, A. Gadian, L. Galbraith, H. Iacovides, D. Johnston, B. Launder, B. Leslie, J. Meyer, A. Neukermans, B. Ormond, B. Parkes, P. Rasch, J. Rush, S. Salter, T. Stevenson, H. Wang, Q. Wang, R. Wood. (2012). Marine cloud brightening. *Philosophical Transactions of the Royal Society A: Mathematical, Physical and Engineering Sciences*, **370**(1974), 4217–4262.

Stjern, C. W., H. Muri, L. Ahlm, O. Boucher, J.N.S. Cole, D. Ji, A. Jones, J. Haywood, B. Kravitz, A. Lenton, J.C. Moore, U. Niemeier, S.J. Phipps, H. Schmidt, S. Watanabe and J.E. Kristjánsson (2018). Response to marine cloud brightening in a multi-model ensemble. *Atmospheric Chemistry and Physics*, **18**(2), 621–634.

Wood, R. (2021). Assessing the potential efficacy of marine cloud brightening for cooling Earth using a simple heuristic model. *Atmospheric Chemistry and Physics*, **21**(19), 14507–14533.

BUBBLE-BURSTING ATOMISATION FOR MARINE CLOUD BRIGHTENING

Y. RAJ[1] and H. HUNT[1]

[1]*Centre for Climate Repair, Department of Engineering, University of Cambridge, United Kingdom*

Keywords: Aerosol generation, bubbles, marine cloud brightening, solar radiation management

INTRODUCTION

Marine cloud brightening (MCB) is a solar radiation management technique aimed at enhancing the albedo or 'brightness' of existing marine clouds using only seawater. This could reflect more incoming sunlight to create a local cooling effect and be implemented as a potential intervention for protecting vulnerable systems like the Arctic. Specifically, by spraying seawater into submicron diameter droplets, the resultant dry salt nanocrystals, upon evaporation, are delivered into the cloud layer to increase the concentration of cloud condensation nuclei and induce a 'brightening' effect. However, generating suitable particles for MCB in real life faces significant technical challenges including a narrow particle size distribution, high production rate, efficiency and resilience to environmental conditions (Latham *et al.*, 2008). To address these challenges, this research draws inspiration from the natural process of sea spray generation by waves and bubbles on the surface of the ocean.

By passing low-pressure compressed air through a semi-submerged perforated elastic tubing, bubbles are simultaneously formed and burst to generate a fine spray of submicron droplets. The inventor of this method, Mezherichter, showed that in tap water, 90–99% of droplets generated from bursting bubbles were smaller than 1 μm (Mezhericher *et al.*, 2017). This method is particularly promising as the perforated tube geometry is simple and can be easily mass-produced. Additionally, unlike other methods, no liquid filtration is required as only air is pumped, adding to the scalability. To validate this method for seawater atomisation and marine cloud brightening purposes, an experimental sampling setup was created and tested. The insights gained from this research aim to critically evaluate the viability of bubble-bursting atomisation as a suitable method for generating droplets for marine cloud brightening.

METHODS

Various tubing sections were perforated in a regular pattern to form the test geometries, varying in cross-sectional dimensions, material, and perforation pattern. These are held fixed and semi-submerged in test solutions ranging from unfiltered natural seawater to artificial seawater mixtures of distilled water and 99.5% pure sodium chloride. Connecting to a compressed air tank, the test solution is atomised and the generated droplets are extracted and mixed with HEPA filtered air in a constant volume sampling tunnel. An isokinetic sampling probe then captures and passes these droplets through a Nafion dryer which dries and splits the spray into several particle detectors which measure the particle size distribution and concentration. This also informs the energy consumption for this method.

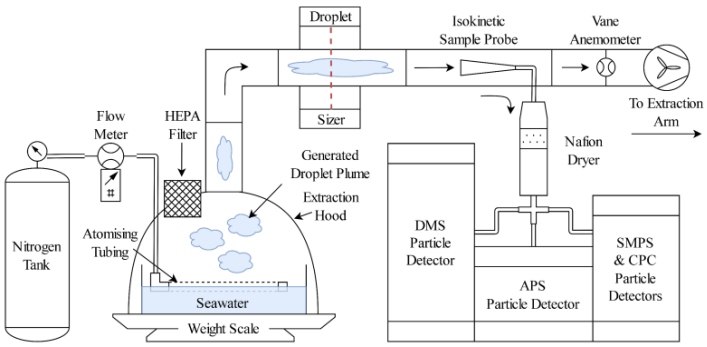


Figure 1. Schematic diagram of bubble-bursting experimental setup.

CONCLUSIONS

The initial results of this method satisfy the MCB particle size distribution requirements with 66% of generated particles falling within 30-500nm dry particle diameter (Wood, 2021). However, to reduce energy requirements for this method to a practical level requires further development including: the general optimisation of atomisation geometry, and scalability considerations like parallel tubes and the interaction of impacting bubble fronts.

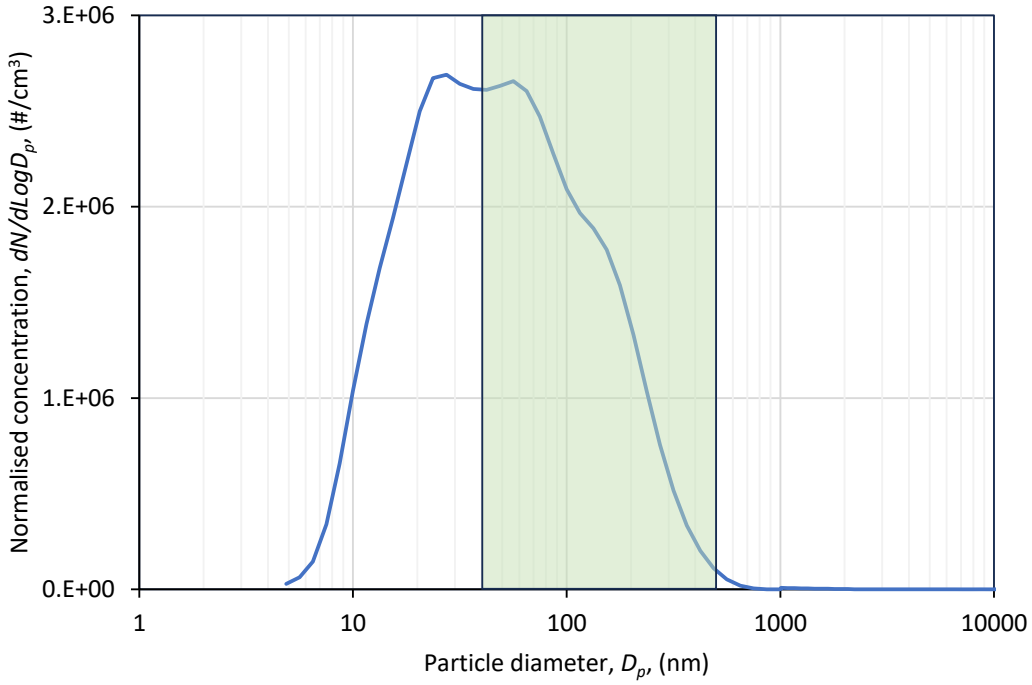


Figure 2. Normalised particle size distribution of salt particles generated using a perforated Verderprene rubber tube at 3.5 Bar and 20 LPM. The green shaded region denotes the notional size range suitable for MCB (30-500 nm). This representative distribution was measured by an electrical mobility detector (DMS500, Cambustion) and an aerodynamic particle sizer spectrometer (APS, TSI).

ACKNOWLEDGEMENTS

This work was financially supported by the Refreeze the Arctic Foundation (RAF) and the Centre for Climate Repair, University of Cambridge.

REFERENCES

Latham, J., P. Rasch, C.-C. Chen, L. Kettles, A. Gadian, A. Gettelman, H. Morrison, K. Bower, and T. Choularton (2008). Global temperature stabilization via controlled albedo enhancement of low-level maritime clouds, Phil. Trans. R. Soc. A, vol. 366, pp. 3969–3987. doi:10.1098/rsta.2008.0137

Mezrichter, M., I. Ladizhensky, and I. Etlin (2017). Atomization of liquids by disintegrating thin liquid films using gas jets, International Journal of Multiphase Flow, vol. 88, pp. 99-115, ISSN 0301-9322, doi: 10.1016/j.ijmultiphaseflow.2016.07.015

Wood, R. (2021). Assessing the potential efficacy of marine cloud brightening for cooling Earth using a simple heuristic model, Atmospheric Chemistry and Physics, vol. 21, no. 19, pp. 14507–14533. doi:10.5194/acp-21-14507-2021

ADVANCES IN SUB MICRON AEROSOL GENERATION BY SUPERHEATED ATOMISATION FOR MARINE CLOUD BRIGHTENING

E. REARDON[1]

[1]*Centre for Climate Repair, Department of Engineering, University of Cambridge, Trumpington Street, Cambridge CB2 1PZ, United Kingdom*

Keywords: Marine Cloud Brightening, sub micron particle, superheated atomization.

INTRODUCTION

No existing spray applications meet the requirements for Marine Cloud Brightening (MCB) and only a handful of groups globally are working to develop any. We are a team of engineers in Cambridge developing four different spray techniques. After researching the potential of several candidate sprayers, superheated atomisation was selected to be the focus of my work.

From literature covering superheated atomisation of any fluid, only one author has been found that demonstrates a significant proportion of submicron droplet production experimentally (Zalkind et al., 2017).

A continuous superheated sprayer and particle detection experiment was designed to efficiently generate large quantities of sub micron size distribution data, unreported elsewhere. This is recorded with pressure, temperature and flow rate data from the steady state sprayer allowing correlations to be developed and improved understanding of the atomisation processes.

METHOD

Sea water is pressurized up to 100 bar and heated to a maximum of 300°C as it flows continuously to the nozzle. At the nozzle orifice exposure to atmospheric pressure induces flash boiling. The atomised droplets are sampled, dried to salt crystals and sized using TSI's SMPS, APS and CPC. Real time sub-micron sizing is also performed using Cambustion's DMS 500 allowing observation of transient spray behavior.

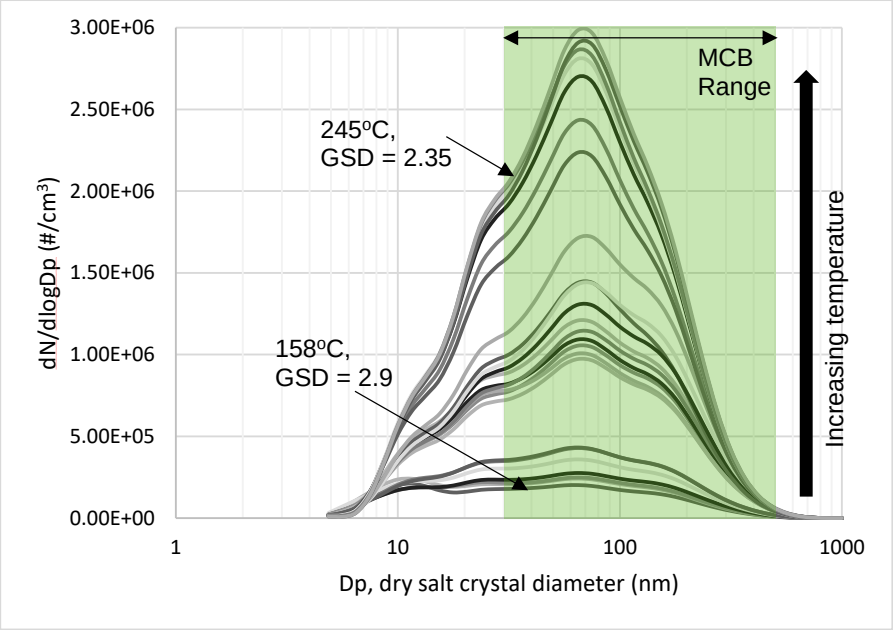


Figure 1. Number - size distributions for fluid temperatures from 158ºC to 245ºC. Shaded area is MCB range 30 to 500 nm.

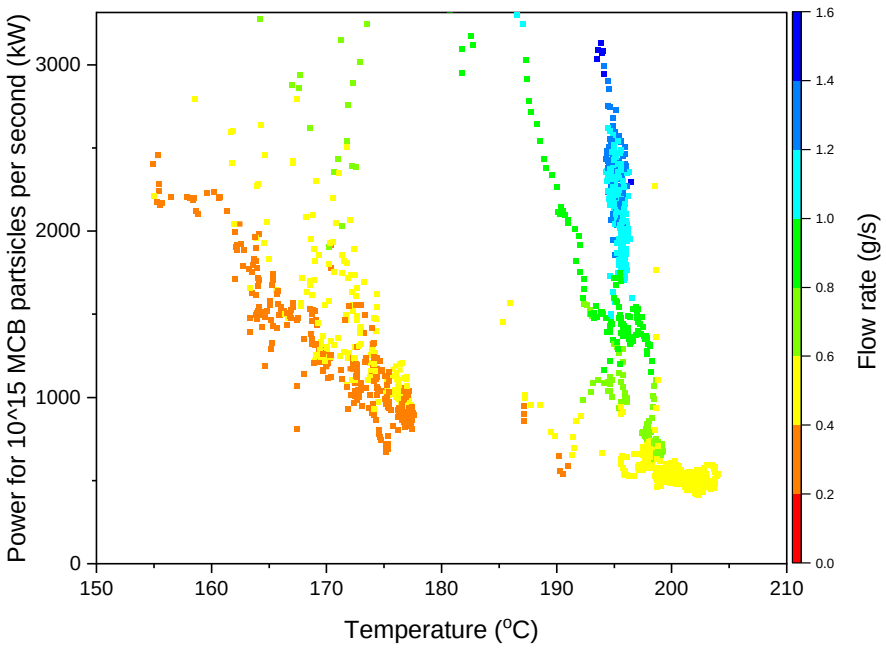


Figure 2. Fluid temperature against heating power to produce 10^{15} salt crystals per second in the range 30 to 500 nm. Colour scale is fluid flow rate through nozzle.

Size distributions are displayed with up to 77% number fraction in the MCB range, 30 to 500 nm (Figure 1). This is a suggested size range of cloud condensation nuclei that contribute to brightening, approximated from the range in Foster (2020).

Increased fluid temperature increases production rate of submicron particles and narrows the size distribution (Figure 1). The lowest power use is achieved at higher temperatures (>200ºC) and importantly, only at the lowest flow rates (Figure 2).

Producing 10^{15} salt crystals per second in the MCB range 30 to 500 nm would require 340 kW of heat energy. 10^{15} particles/s is the proposed minimum spray rate per source required to see an effect on the clouds (Latham et al., 2012). Further results from varying nozzle geometry and higher operating temperature (up to 280ºC) display similar minimum power values.

CONCLUSIONS

The potential of superheated atomisation for MCB has been demonstrated and the effects of different variables on the aerosol size distribution and energy use have been found. The objective of current tests is to develop this into a scaled up sprayer to improve on the effervescent sprayers used in current field trials.

ACKNOWLEDGEMENTS

This work was financially supported by the Refreeze the Arctic Foundation (RAF) and by Southern Cross University as part of the Cooling and Shading subprogram of the Reef Restoration and Adaptation Program (RRAP). The Reef Restoration and Adaptation Program is funded by the partnership between the Australian Governments Reef Trust and the Great Barrier Reef Foundation.

REFERENCES

Foster, J., Cooper, G., Galbrath, L., Jain, S., Ormond, R., & Neukermans, A. (2020). Continuing Results for Effervescent Aerosol Salt Water Spray Nozzles Intended for Marine Cloud Brightening. International Journal of Geosciences, 11(09), 563–589. https://doi.org/10.4236/ijg.2020.119030

Latham, J., Bower, K., Choularton, T., Coe, H., Connolly, P., Cooper, G., Craft, T., Foster, J., Gadian, A., Galbraith, L. and Iacovides, H., 2012. Marine cloud brightening. *Philosophical Transactions of the Royal Society A: Mathematical, Physical and Engineering Sciences*, *370*(1974), pp.4217-4262.

Zalkind, V. I., Zeigarnik, Yu. A., Nizovskiy, V. L., Nizovskiy, L. V., & Schigel, S. S. (2017). Superheated Water Atomization: Some New Aspects of Control and Determining Disperse Characteristics of Atomization Plume in Micron and Submicron Ranges of Droplet Size *. Journal of Physics: Conference Series, 891, 012011. https://doi.org/10.1088/1742-6596/891/1/012011

MARINE CLOUD BRIGHTENING: CONSTRAINING SMALL-SCALE UNCERTAINTY

LEVIN RUG[1], BEN ASCHER[1], JOHANNES KAINZ[1], JUNG-SUB LIM[2], FABIAN HOFFMANN[1]

[1]*Institute of Meteorology, Ludwig-Maximilians-University in Munich, Munich, Germany.*

[2]*Cooperative Institute for Research in Environmental Sciences, University of Colorado, Boulder, Colorado, USA.*

Keywords: MARINE CLOUD BRIGHTENING, CLIMATE ENGINEERING, LAGRANGIAN CLOUD MICROPHYSICS, AEROSOL-CLIMATE INTERACTIONS, AEROSOL-CLOUD INTERACTIONS.

ABSTRACT

Marine cloud brightening (MCB) is a suggested climate engineering approach to counteract some consequences of global warming on regional and global scales by increasing the amount of shortwave radiation reflected by shallow marine clouds through the seeding of sea salt aerosol particles. Assessing the potentials but also the risks of MCB requires a multiscale perspective, covering not only the intended and unintended large-scale impacts, but also critical small-scale dependencies, e.g., on the seeded aerosol size distribution or induced changes in turbulent cloud dynamics, which are usually neglected or only crudely parameterized in large-scale assessments. Therefore, a highly detailed representation of aerosol-cloud microphysics and cloud dynamics is necessary to reduce these uncertainties. In this talk, we will summarize our recent Lagrangian cloud modeling (LCM) studies that allowed us to assess (a) the implications of the seeded aerosol size distribution on the efficacy of MCB, highlighting unintended consequences of adding either too large or too many aerosol particles (Hoffmann and Feingold, 2021), (b) impacts of chemical processing on a seeded aerosol size distribution and effects on giant cloud condensation nuclei (Lim *et al.*, 2024; Rug *et al.*, 2025), and (c) implications for cloud radiative impacts (Hoffmann *et al.*, 2022).

ACKNOWLEDGEMENTS

This work was supported by the Emmy Noether program of the German Research Foundation (DFG) under grant HO 6588/1-1 and HO 6588/3-1.

REFERENCES

Hoffmann, F., and G. Feingold, 2021: Cloud Microphysical Implications for Marine Cloud Brightening: The Importance of the Seeded Particle Size Distribution. *J. Atmos. Sci.*, 78, 3247–3262, https://doi.org/10.1175/JAS-D-21-0077.1.

Lim, J.-S., Y. Noh, H. Lee, and F. Hoffmann: The Critical Number and Size of Precipitation Embryos to Accelerate Warm Rain Initiation, *EGUsphere [preprint]*, https://doi.org/10.5194/egusphere-2024-2636, 2024.

Rug, L., W. Schimmel, F. Hoffmann, and O. Knoth: The Chemical Mechanism Integrator Cminor v1.0: A Stand-Alone Fortran Environment for the Particle-Based Simulation of Chemical Multiphase Mechanisms, *Geosci. Model Dev.*, submitted, 2025.

Hoffmann, F., B. Mayer, and G. Feingold, 2022: A Parameterization of Interstitial Aerosol Extinction and Its Application to Marine Cloud Brightening. *J. Atmos. Sci.*, 79, 2849–2862, https://doi.org/10.1175/JAS-D-22-0047.1.

DIRECT OBSERVATIONS OF CORAL REEF INFLUENCE ON AEROSOL LOADING OVER THE GREAT BARRIER REEF

J. SULO[1], M. OKULJAR[1], J. ALROE[1], Z. LI[1], E. HORCHLER[1], L. CRAVIGAN[1], H. TROUNCE[1], L. HARRISON[2], D. HARRISON[2] AND Z. RISTOVSKI[1]

[1]*School of Earth and Atmospheric Sciences, Queensland University of Technology, Brisbane, QLD, Australia.*

.

[2]*National Marine Science Centre, Southern Cross University, Coffs Harbour, NSW, Australia.*

Keywords: MARINE AEROSOL, AEROSOL NUMBER CONCENTRATION, AEROSOL SIZE DISTRIBUTION, NEW PARTICLE FORMATION

INTRODUCTION

Coral reefs are among the most diverse ecosystems in the world, acting as home to roughly 25 % of all marine life while accounting for under one percent of the ocean floor. This rich ecosystem has long been thought of as a potential source of marine aerosol, but modelling studies suggest they have a negligible impact on the aerosol population (Fiddes et al., 2022; Jackson et al., 2022). In this study, we present analysis of multi-year in situ aerosol measurements over the Great Barrier Reef (GBR), showing for the first time direct observations of coral reefs contributing to aerosol loading over the reef.

METHODS

We analyzed almost 5 months of data collected across the GBR to investigate whether the coral reefs have a measurable impact into the aerosol and cloud condensation nuclei (CCN) population in the ambient atmosphere above it. The data collected spans eight years and spring and summer seasons. The aerosol size distributions were measured using Scanning Mobility Particle Sizers and an Aerodynamic Particle Sizer (APS), for diameters between 20 nm and 5 μm. CCN concentration was measured using the Cloud Condensation Nuclei counter (CCNc). The size distributions were combined with 72-hour back trajectories calculated using the HYSPLIT Lagrangian dispersion model by The National Oceanic and Atmospheric Administration (NOAA) and meteorological data from both in situ measurements and ERA5 reanalysis data. Spatial information on the GBR and locations of the reefs were taken from the Great Barrier Reef Marine Park Authority (GBRMPA) and were used to calculate the fraction of time air masses spent over coral reefs.

CONCLUSIONS

Aerosol number concentrations over the GBR are typical of a clean coastal environment (Dall'Osto et al., 2011; Peltola et al., 2022), being consistently below 1000 cm^{-3} and most commonly 200 – 500 cm^{-3}, CCN concentrations remain in the order of a few hundred cm^3 (Figure 1). The summer season exhibits overall lower aerosol and CCN loading. Aitken mode number concentrations constitute roughly half of the aerosol number concentrations over the reef. As Aitken mode particles are typically more recently formed and are more directly contributed to by local sources, we investigate Aitken mode enrichment to try and detect a contribution of local sources to aerosol loading. We split the data into deciles of Aitken mode loading defined as the fraction of Aitken mode concentration of the measured total concentration.

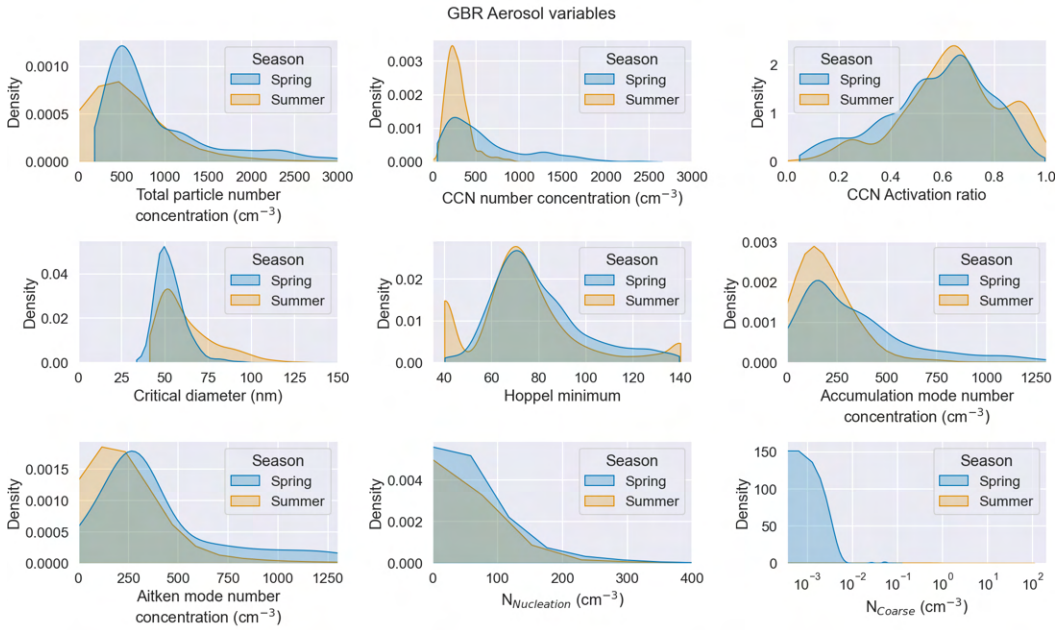


Figure 1. Kernel density estimates for in-situ aerosol-related variables collected at the GBR or calculated from in-situ measurements during spring (blue) and summer (orange). The variables shown are, total particle (a) and CCN (b) number concentration, CCN activation ratio (c), critical diameter (d), Hoppel minimum (e), accumulation (f), Aitken (g), nucleation (h), and coarse (i) mode number concentration.

Analysis of the HYSPLIT back trajectories reveals that during times of high Aitken mode aerosol loading, air masses typically spend more time over the coral reefs (Figure 2), and at lower altitudes than during lower Aitken mode aerosol loading. This Aitken mode enrichment occurs everywhere in the reef, but the overall Aitken mode loading appears to be higher in central GBR than in the southern parts of the reef.

In future work, we will investigate the reasons for spatial differences in the aerosol loading from reefs, as well as consider temporal variability in aerosol size distributions. Furthermore, spatial variability in the aerosol size distribution will be investigated, specifically in terms of different aerosol sources across the GBR.

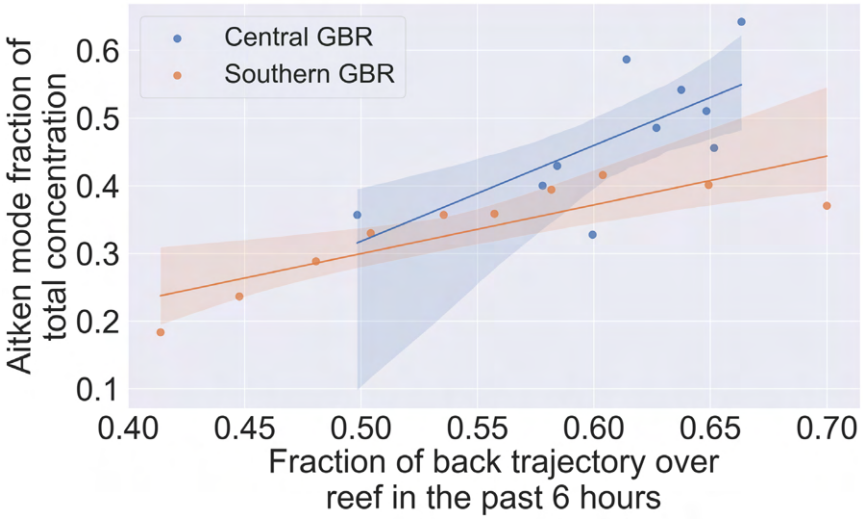


Figure 2. Fraction of the total aerosol concentration in the Aitken mode plotted against the proportion of the past six hours during which the air mass was over the reef

ACKNOWLEDGEMENTS

This research was funded by the Reef Restoration and Adaptation Program (RRAP). RRAP is funded by the partnership between the Australian Governments Reef Trust and the Great Barrier Reef Foundation.

REFERENCES

Dall'Osto, M., Monahan, C., Greaney, R., Beddows, D. C. S., Harrison, R. M., Ceburnis, D., and O'Dowd, C. D.: A statistical analysis of North East Atlantic (submicron) aerosol size distributions, Atmospheric Chem. Phys., 11, 12567–12578, https://doi.org/10.5194/acp-11-12567-2011, 2011.

Fiddes, S. L., Woodhouse, M. T., Utembe, S., Schofield, R., Alexander, S. P., Alroe, J., Chambers, S. D., Chen, Z., Cravigan, L., Dunne, E., Humphries, R. S., Johnson, G., Keywood, M. D., Lane, T. P., Miljevic, B., Omori, Y., Protat, A., Ristovski, Z., Selleck, P., Swan, H. B., Tanimoto, H., Ward, J. P., and Williams, A. G.: The contribution of coral-reef-derived dimethyl sulfide to aerosol burden over the Great Barrier Reef: a modelling study, Atmospheric Chem. Phys., 22, 2419–2445, https://doi.org/10.5194/acp-22-2419-2022, 2022.

Jackson, R.L., Woodhouse, M.T., Gabric, A.J., Cropp, R.A., Swan, H.B., Deschaseaux, E.S.M and Trounce, H.: Modelling the influence of coral-reef-derived dimethylsulfide on the atmosphere of the Great Barrier Reef, Australia, Frontiers in Marine Science, 9, doi:10.3389/fmars.2022.910423, 2022.

Peltola, M., Rose, C., Trueblood, J. V., Gray, S., Harvey, M., and Sellegri, K.: New particle formation in coastal New Zealand with a focus on open-ocean air masses, Atmospheric Chem. Phys., 22, 6231–6254, https://doi.org/10.5194/acp-22-6231-2022, 2022.

Special Session 3: Young principal investigators: shaping the research of the future

USING SINGLE PARTICLE LEVITATION TO PROBE TRANSFORMATIONS OF ATMOSPHERIC AEROSOL IN THE LABORATORY

D. DUFT[1] and T. LEISNER[1] and S.H. JONES[1,2]

[1]*Institute of Meteorology and Climate Research - Atmospheric Aerosol Research, Karlsruhe Institute of Technology, Karlsruhe, Germany.*

[2]*Department of Chemistry, York University, Toronto, Canada.*

Keywords: AEROSOL, TRANSFORMATIONS, SINGLE-PARTICLE, VISCOSITY, MORPHOLOGY

INTRODUCTION

Atmospheric aerosols impact the climate by scattering and absorbing solar radiation and through their ability to act as cloud condensation nuclei and ice nuclei (Masson-Delmotte *et al.* 2021). The chemical complexity of aerosols and their propensity to undergo various transformations during their lifetime contributes to the uncertainty associated with their impact on the Earth's radiative balance. To reduce this uncertainty, it is necessary to study aerosols in the laboratory to determine their fundamental properties and how these change as a result of transformations. Aerosol transformations occur through changes in external factors such as environmental temperature and relative humidity, and exposure to solar radiation or reactants e.g. oxidants.

In the laboratory, single particle levitation methods provide an ideal way to study aerosol in a contactless environment and can be coupled with various spectroscopic techniques to determine aerosol physical and chemical properties. In this presentation I will focus on transformations of two different societally relevant aerosols, water soluble wood smoke aerosol, and microplastic containing aerosol, studied using single particle methods. Wood smoke aerosol is a type of light absorbing organic aerosol, i.e. brown carbon (BrC), that can warm the climate (Laskin *et al.* 2015). However, the exact amount of warming it contributes remains uncertain owing to the number of transformations it can undergo during its lifetime. With the popularity of wood burning stoves and increasing number of wildfires it is important to understand the impact of transformations on the properties of BrC aerosol. Microplastics are of increasing environmental concern and have been detected around the globe (Thompson *et al.* 2024). Their incorporation into aerosol droplets e.g. during sea-spray aerosol formation and the resultant impact on aerosol properties such as reactivity and scattering and absorption of light remains to be determined. Here I will present results from a study investigating the effect of illumination on the viscosity of water-soluble wood smoke aerosol, and I will outline plans and preliminaries regarding the impact of microplastics on aerosol morphology.

METHODS

Condensate was collected from the exhaust of a wood burning stove by passing the exhaust gas through a condenser to directly sample water-soluble wood smoke aerosol which was subsequently filtered to remove any insoluble material. Particulate matter was also directly sampled on quartz filter samples from the exhaust of the stove and extracted in water. Single droplets of aqueous wood smoke material (condensate or filter extract) were levitated in an electrodynamic balance and illuminated with a Xenon lamp to simulate solar radiation. In addition to the electric field applied for levitation, an additional electric field was applied to the levitated droplet over a range of frequencies to induce shape oscillations (Singh *et al.* 2023). The resultant shape oscillations were probed using light scattering to determine the viscosity and surface tension of the wood smoke material in the dark and in the presence of illumination, as the droplets evaporated under constant relative humidity. Experiments were conducted on two different

types of wood smoke aerosol: fir logs, and beech briquette, at atmospherically relevant supercooled temperatures from 0 to -30 °C.
The influence of microplastics on the morphology of aerosol droplets will be studied by performing single droplet levitation experiments coupled with imaging and Raman spectroscopy.

RESULTS

For the wood smoke aerosol experiments conducted in the dark, a slight increase in viscosity was measured as droplets evaporated under constant relative humidity and increased in concentration. However, in the presence of illumination, a significant increase in viscosity was determined for experiments conducted at temperatures of -10 °C and below. Figure 1 shows the viscosity determined for multiple fir wood smoke droplets at – 20 °C in the absence and presence of illumination. Comparing panel a) to panel b) when the droplet has a radius of ≤ 45 μm there is a marked difference in the measured viscosity in the presence of illumination. The same trend is observed for both types of wood at temperatures of ~ -10, -20 and -30 °C. These results indicate that illumination causes an increase in viscosity of the material that may be due to photochemically induced changes in composition and/or structure of the wood smoke molecules. This is an important finding with implications for droplet reactivity, lifetime, hygroscopicity, and scattering and absorption of solar radiation in the atmosphere.

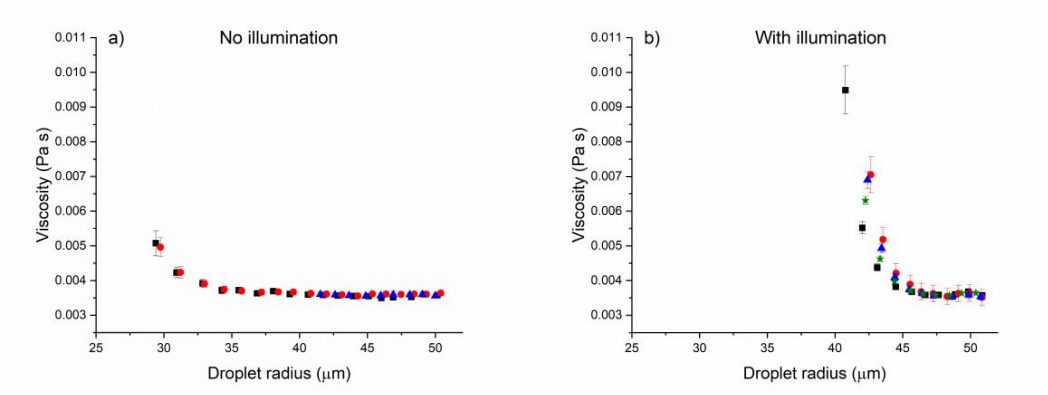


Figure 1. Impact of illumination on the measured viscosity of multiple wood smoke droplets (fir wood condensate) as they evaporate under constant humidity at ~ -20 °C. a) dark measurements without illumination for three wood smoke droplets and b) measurements in the presence of light for four wood smoke droplets. Error bars represent the uncertainty in the fit of the data.

I will also discuss planned experiments to study the impact of microplastics on droplet morphology and present preliminary findings.

CONCLUSIONS

I have presented recent results and planned experiments to study transformations of two different types of societally relevant aerosol: the effect of illumination on the viscosity of wood smoke aerosol, and the impact of microplastics on aerosol morphology. The viscosity of electrodynamically levitated water-soluble wood smoke droplets was measured in the absence and presence of illumination at supercooled temperatures. In the presence of illumination, an exponential increase in the viscosity of wood smoke droplets was determined. This finding indicates that a significant increase in viscosity can occur over short atmospherically relevant timescales (tens of minutes) which could further impact aerosol hygroscopicity, atmospheric lifetime, and optical properties. Droplet morphology resulting from the incorporation of microplastics into sea-spray aerosol is important to determine as it will impact the scattering and absorption of solar radiation as well as the ability of the aerosol to undergo ageing.

ACKNOWLEDGEMENTS

This work was supported by the DFG Eigene Stelle JO 1849/1-1. Wood smoke samples were produced at the Institute of Technical Chemistry (ITC), Karlsruhe Institute of Technology in collaboration with Sonja Mülhopt, Marko Mackert and Manuela Hauser.

REFERENCES

Masson-Delmotte, V., P. Zhai, A. Pirani, S. L. Connors, C. Péan, S. Berger, N. Caud, Y. Chen, L. Goldfarb, M. I. Gomis, M. Huang, K. Leitzell, E. Lonnoy, J. B. R. Matthews, T. K. Maycock, T. Waterfield, Ö. Yelekçi, R. Yu and B. Zhou (2021). *Climate Change 2021: The Physical Science Basis. Contribution of Working Group I to the Sixth Assessment Report of the Intergovernmental Panel on Climate Change*, (Cambridge University Press: Cambridge, United Kingdom and New York, NY, USA).
Laskin, A., J. Laskin and S. A. Nizkorodov (2015). Chemistry of Atmospheric Brown Carbon, *Chem. Rev*, 115, 10, 4335-4382.
Thompson, R. C., W. Courtene-Jones, J. Boucher, S. Pahl, K. Raubenheimer and A. A. Koelmans (2024). Twenty years of microplastic pollution research-what have we learned? *Science*, 386, 6720.
Singh, M., S.H. Jones, A. Kiselev, T. Leisner and D. Duft (2023). Determining the viscosity and surface tension of supercooled, oscillating droplets in an electrodynamic balance, *Atmos. Meas. Tech*, 16, 21, 5205-5215.

AEROSOLS IN MEGACITIES IN THE 21st CENTURY: ROLE OF SCIENCE AND SCIENTISTS

S. GANI[1,2]

[1]*Centre for Atmospheric Sciences, Indian Institute of Technology Delhi, New Delhi, India.*
[2]*Institute for Atmospheric and Earth System Research/Physics, University of Helsinki, Helsinki, Finland.*

Keywords: Megacities, Urbanization, Air Pollution, Climate Change

Megacities in the 21st century are at the forefront of global challenges, undergoing rapid transformation driven by urbanization, economic growth, and demographic shifts. Many of today's largest megacities already face severe air quality challenges, while emerging megacities—particularly in the rapidly urbanizing Global South—will bring both familiar and novel pollution concerns.

Aerosol sources are rapidly evolving, driven by shifts in energy production, waste management, and land use practices. While the energy transition, improved waste management, and agricultural changes are reducing some emissions, episodic sources, including agricultural and forest fires, are increasingly prominent. Climate change exacerbates these challenges, altering precipitation patterns and increasing the frequency and intensity of wildfires, thereby reshaping aerosol and their precursor emissions. Simultaneously, atmospheric processes governing aerosol transport and dispersion are changing, with shifts in wind patterns and boundary layer dynamics affecting ventilation efficiency and pollutant accumulation.

These transformations significantly impact aerosol concentrations (e.g., PM_{10}, $PM_{2.5}$, UFP) and composition. Reduced emissions of accumulation-mode particles may increase the fraction of ultrafine particles, driven by changes in condensation and coagulation dynamics, including enhanced new particle formation from gas-phase precursors.

Pollution exposure within megacities is starkly uneven, with marginalized communities disproportionately affected. Addressing these environmental justice concerns is critical. At the same time, unscientific interventions, such as cloud seeding and smog towers, should be critically evaluated for their inefficacy and potential to divert resources from evidence-based solutions.

Aerosol science plays a critical role in addressing these evolving challenges through advancements in monitoring, modeling, and policy guidance. Researchers can make an impact by informing policy, raising awareness, and countering misinformation. Meaningful interdisciplinary collaborations will be crucial in developing effective solutions, ensuring that policies are guided by robust scientific evidence.

ACKNOWLEDGEMENTS

This talk will contextualize these perspectives with specific examples from ongoing work by my research group and collaborators.

INVESTIGATING AEROSOL–CLOUD INTERACTIONS: THE ROLE OF BVOC-DERIVED SOA AND CLOUD WATER CHEMISTRY IN A CHANGING ATMOSPHERE

L. HEIKKINEN[1], L. FAIVRE[1], N. BEHR[1], S. BLICHNER[1], S. TALVINEN[1], C. WU[2], D. G. PARTRIDGE[3], P. ZIEGER[1], I. RIIPINEN[1], R. KREJCI[1] and C. MOHR[4]

[1]*Department of Environmental Science and Bolin Centre for Climate Research, Stockholm University, Stockholm, Sweden.*
[2]*Department of Chemistry and Molecular Biology, University of Gothenburg, Gothenburg, Sweden.*
[3]*Department of Mathematics and Statistics, Faculty of Environment, Science and Economy, University of Exeter, Exeter, United Kingdom.*
[4]*PSI Center for Energy and Environmental Sciences, Villigen PSI, Switzerland.*

Keywords: AEROSOL-CLOUD INTERACTIONS, BVOCs, SOA, CLOUD WATER CHEMISTRY.

INTRODUCTION

As we move to a warmer world, we are also entering a new chemical regime, where anthropogenic emissions reduce and an increase in the emissions of volatile organic compounds (BVOCs) is anticipated. However, our current understanding of how boreal and tropical vegetation will response to the changing climate is limited, while large amounts of uncertainty persist with the role of key anthropogenic emissions, such as SO_2 on climate through aerosol–cloud interactions. These processes, together with the uncertainties linked to cloud water chemistry and its role in shaping atmospheric composition, will limit our ability to understand or quantify feedbacks arising from biosphere responses to changing climate and declining anthropogenic emissions. Here, our planned and on-going experimental, data analysis and modeling work are outlined to eventually address the following scientific questions:

1. How does secondary organic aerosol (SOA) formation, arising from boreal BVOC emissions, influence cloud properties over the boreal forest, and how sensitive are these impacts to the build-up of SOA vs other cloud microphysical processes?
2. Is there a way to evaluate the importance of cloud water chemistry on aerosol properties using long-term field observations? What kind of impacts can these transformations have on cloud properties in the following cloud cycles?
3. How do BVOC emissions behave as function of CO_2 emissions (see e.g., Sahu et al., 2023) and under future environmental conditions? Will chemical cloud processing of aerosols remain a relevant process influencing aerosol properties, when SO_2 concentrations decline? How will these changes influence the aerosol–cloud interactions in the future?

The approaches to study these questions are diverse, and include cloud parcel modeling, field experiments and analysis of long-term observations from multiple measurement sites. Cloud parcel modeling is applied in the presented work to address how BVOC emissions and subsequent SOA formation impact cloud properties over the boreal forest and the sensitivity of this process to organic surfactants, co-condensation, updraft velocities and entrainment, in addition to the investigation of how cloud water chemistry can influence cloud properties over multiple cloud cycles. This is accompanied with an observation-based characterization of the impacts of chemical cloud processing on aerosol populations detected over the boreal forest. The planned field experiments are connected to the on-going project CLIVE (Figure 1) and in this presentation, the planned experimental setups will be introduced.

METHODS AND PLANNED FIELD WORK

The cloud parcel model is the Pseudo-Adiabatic bin-micRophySics university of Exeter Cloud parcel model with the Unified Framework for Organics (PARSEC-UFO; Heikkinen et al., 2024), which simulates the

rising, cooling and entraining air parcel with a prescribed dry aerosol size distribution and composition. It includes aerosol hygroscopic growth, cloud condensation nuclei (CCN) activation and further condensational growth of the cloud droplets. It further allows the investigation of the cloud-responses to surface-active organics (Lowe et al., 2019) and organic vapors that can co-condense with water under sub-saturated conditions (Heikkinen et al., 2024). In addition, we have recently implemented aqueous phase sulfur chemistry to the model (Behr, MSc thesis, 2025, *in prep.*).

To estimate the impacts of chemical cloud processing on aerosol properties, long time series of aerosol chemical composition and size distribution from the boreal forest of Finland are used together with NOAA's Hybrid Single-Particle Lagrangian Integrated Trajectory model (HYSPLIT) to provide an estimate for the time the sampled air masses had spent in non-precipitating clouds. This is done using a relative humidity -based proxy and filtering out trajectories that experienced precipitation, as described in Isokääntä et al. (2022).

The planned field work involves measurement campaigns in boreal (e.g., Svartberget ACTRIS station in Sweden) and tropical (ATTO station in Brazil) forests. Experiments are conducted using a field-deployable mobile chamber that allows specifically looking into the oxidation of BVOCs at the different forest environments under various environmental conditions (e.g., day vs night and dry vs wet season). The resulting SOA will hereafter pass through a supersaturated environment, resulting in the formation of cloud droplets that allows assessment of their ability to act as CCN under various supersaturations, and the potential of organic co-condensation to influence this process. Key measurements will be conducted using online chemical ionization-based mass spectrometry (Fig. 1b). Additional measurements in Panama (Gamboa Laboratories) are planned. This site is unique due experimental greenhouses that allow the investigation of BVOC emission sensitivities to CO_2 and temperature. A 'nice-to-have' additional experimental technique would be a cloud processing reactor, similar to the one described recently by Xu et al. (2024), which would allow us to study the impacts of SOA formation through aqueous phase chemistry as well as its impact on gas phase composition in situ. This would provide a valuable comparison to the recent results published by Lamkaddam et al. (2021), who reported the potential of isoprene oxidation products to form SOA in cloud water with significant mass yields.

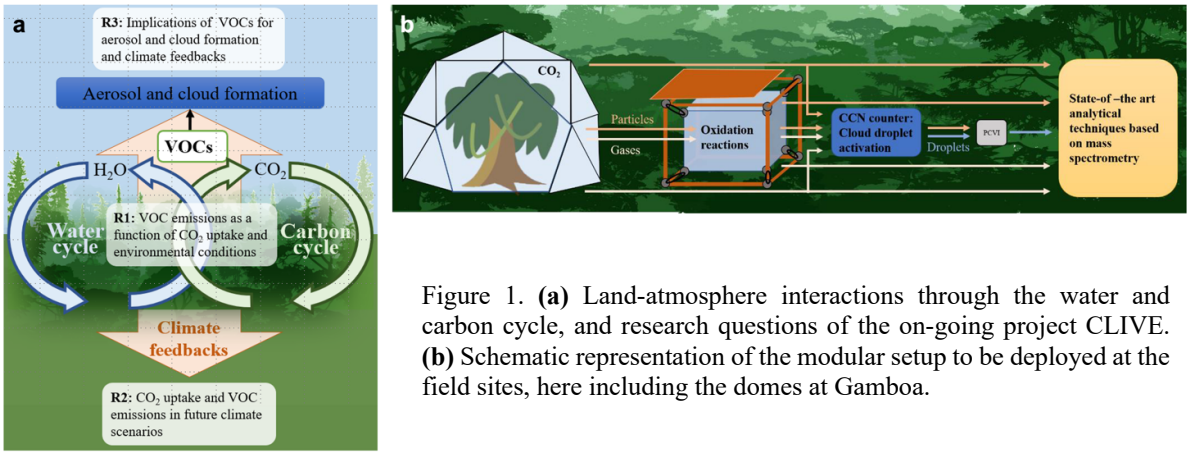


Figure 1. **(a)** Land-atmosphere interactions through the water and carbon cycle, and research questions of the on-going project CLIVE. **(b)** Schematic representation of the modular setup to be deployed at the field sites, here including the domes at Gamboa.

PRELIMINARY RESULTS

The preliminary results to be presented address questions 1–2 posed in the introduction. These results focus on the boreal environment only. While the formation of SOA over the boreal forest drastically influences the properties of aerosol particles (i.e., growth), the cloud response to this remains limited. While the number of particles able to act as CCN increases, the modeled cloud droplet number concentration (CDNC) increases less and a similar relationship is modeled between CDNC and cloud albedo (see Carslaw et al., 2013). Evaluating additional sensitivities of the modelled results to entrainment, droplet collision and coalescence, organic co-condensation and surface-active organics are in progress.

Signs of cloud water chemistry can be observed over the boreal forest, where bimodal aerosol size distribution with distinct Hoppel minima (Hoppel et al., 1986) appear after about 8 hours of cloud-processing. A simultaneous formation of sulfate and nitrate aerosol is observed, while SOA formation is suppressed with reduced photochemistry. Only a minor organic aerosol component, with chemical signatures relatable to anthropogenic emissions increases with the time the sampled air mass had spent in non-precipitating clouds. We relate this to SOA formation in cloud water, as the feature is persistent in the data, being independent of air mass origin and black carbon (BC) shows no relationship with time spent in non-precipitating clouds. Extending the analysis to other environments is underway.

Our theoretical work assessing the impact of cloud water chemistry on cloud properties in following cloud cycles shows that cloud water chemistry may reduce the number of aerosol particles acting as CCN and thereby CDNC. To capture this effect, it is critical that the sulfate mass added through cloud water chemistry is added to relevant size ranges in the model.

CONCLUSIONS

The planned field experiments, particularly those using an outdoor mobile chamber, can provide new insights into the oxidation of BVOCs under various real-world atmospheric conditions and improve the understanding of SOA formation and properties under diverse atmospheric conditions. Furthermore, the aim to quantify the sensitivity of BVOC emissions to environmental conditions, including CO_2 concentrations and temperature, will help to assess future distribution of BVOC oxidation products, their impacts on CCN budgets and SOA formation, which will further refine our understanding of biosphere–atmosphere feedbacks.

Our preliminary results highlight key non-linearities in the aerosol–cloud–climate system under present-day conditions. We find that while SOA formation significantly alters aerosol properties, its influence on cloud properties is constrained by updraft velocity and water vapor availability. This suggests that increases in biogenic emissions alone may not directly translate to stronger cloud-albedo effects, particularly under future warming scenarios, but it warrants further research. Additionally, the impacts of cloud water chemistry on boreal aerosol populations is seen mainly as an enhancement in inorganic aerosol components. Further analysis of in-cloud sulfate formation through cloud parcel modeling suggests that the formation of inorganic sulfate mass may reduce CDNC in the following cloud cycles, with implications for cloud albedo. As SO_2 emissions decline, this process may lose its significance, yet the impact and relevance of in-cloud SOA formation in such processes should be further investigated.

These findings underscore the complexity of aerosol–cloud interactions and highlight the importance of refining our understanding of biosphere-driven atmospheric chemistry in a changing climate, where CO_2 concentration continues to rise, but SO_2 declines.

ACKNOWLEDGEMENTS

Projects CLIVE and SIMPLIFY, funded by the Knut and Alice Wallenberg foundation are gratefully acknowledged.

REFERENCES

Carslaw, K. S., Lee, L. A., Reddington, C. L., Pringle, K. J., Rap, A., Forster, P. M., Mann, G. W., Spracklen, D. V., Woodhouse, M. T., Regayre, L. A., and Pierce, J. R.: Large contribution of natural aerosols to uncertainty in indirect forcing, Nature, 503, 67–71, https://doi.org/10.1038/nature12674, 2013.

Heikkinen, L., Partridge, D. G., Blichner, S., Huang, W., Ranjan, R., Bowen, P., Tovazzi, E., Petäjä, T., Mohr, C., and Riipinen, I.: Cloud response to co-condensation of water and organic vapors over the boreal forest, Atmospheric Chemistry and Physics, 24, 5117–5147, https://doi.org/10.5194/acp-24-5117-2024, 2024.

Hoppel, W. A., Frick, G. M., and Larson, R. E.: Effect of nonprecipitating clouds on the aerosol size distribution in the marine boundary layer, Geophysical Research Letters, 13, 125–128, https://doi.org/10.1029/GL013i002p00125, 1986.

Isokääntä, S., Kim, P., Mikkonen, S., Kühn, T., Kokkola, H., Yli-Juuti, T., Heikkinen, L., Luoma, K., Petäjä, T., Kipling, Z., Partridge, D., and Virtanen, A.: The effect of clouds and precipitation on the aerosol concentrations and composition in a boreal forest environment, Atmospheric Chemistry and Physics, 22, 11823–11843, https://doi.org/10.5194/acp-22-11823-2022, 2022.

Lamkaddam, H., Dommen, J., Ranjithkumar, A., Gordon, H., Wehrle, G., Krechmer, J., Majluf, F., Salionov, D., Schmale, J., Bjelić, S., Carslaw, K. S., El Haddad, I., and Baltensperger, U.: Large contribution to secondary organic aerosol from isoprene cloud chemistry, Science Advances, 7, eabe2952, https://doi.org/10.1126/sciadv.abe2952, 2021.

Lowe, S. J., Partridge, D. G., Davies, J. F., Wilson, K. R., Topping, D., and Riipinen, I.: Key drivers of cloud response to surface-active organics, Nat Commun, 10, 5214, https://doi.org/10.1038/s41467-019-12982-0, 2019.

Sahu, A., Mostofa, M. G., Weraduwage, S. M., and Sharkey, T. D.: Hydroxymethylbutenyl diphosphate accumulation reveals MEP pathway regulation for high CO2-induced suppression of isoprene emission, Proceedings of the National Academy of Sciences, 120, e2309536120, https://doi.org/10.1073/pnas.2309536120, 2023.

Xu, N., Le, C., Cocker, D. R., Chen, K., Lin, Y.-H., and Collins, D. R.: An oxidation flow reactor for simulating and accelerating secondary aerosol formation in aerosol liquid water and cloud droplets, Atmospheric Measurement Techniques, 17, 4227–4243, https://doi.org/10.5194/amt-17-4227-2024, 2024.

UNEXPECTED CRYSTALLINE SOLID PHASE STATE OF SECONDARY ORGANIC AEROSOL

F. MAHRT[1,2], S. NIKKHO[2], B. TESTA[2], G. UPPAL[2], J. ZAKS[2], A. LAM[2], L. PENG[2], Z. A. KANJI[3], M. AMMANN[4] and A. K. BERTRAM[2]

[1]*Department of Chemistry, Aarhus University, Aarhus, Denmark*

[2] *Department of Chemistry, University of British Columbia, Vancouver, Canada*

[3] *ETH Zurich, Institute for Atmospheric and Climate Science, Zurich, Switzerland*

[4] *Laboratory of Atmospheric Chemistry, Paul Scherrer Institute, Villigen, Switzerland*

Keywords: organic aerosol, aerosol phase state, atmospheric physical chemistry, cloud formation.

Atmospheric aerosols play a key role for human health and climate. Secondary organic aerosol (SOA) particles, that form from the oxidation of organic vapors followed by gas-particle conversion, constitute the largest fraction of atmospheric aerosols by mass. To accurately predict the impact of SOA on atmospheric chemistry, health and climate, it is crucial to understand their phase state, which can include liquid, amorphous semi-solid, amorphous solid, or crystalline solid phases. While atmospheric SOA is generally thought to be non-crystalline due to its complex molecular composition, comprising a multitude of different organic species, we present evidence from X-ray diffraction that SOA formed from the oxidation of catechol vapors and nitrate radicals (NO_3), an important nighttime pathway to form SOA in wildfire emissions, contains crystalline material. We show that the diffraction patterns of catechol+NO_3 SOA and those of 4-nitrocatechol (4-NC) exhibit strong similarity, indicating the presence of crystalline solid 4-NC in the catechol+NO_3 SOA. Mass spectrometry data further supports this conclusion. Our thermodynamic calculations and ambient measured 4-NC concentrations suggest that 4-NC can remain crystalline throughout most of the tropospheric temperature range. Our ice nucleation experiments further suggest that these particles can promote cloud formation. Overall, the discovery of crystalline SOA challenges traditional views assuming SOA to form non-crystalline, amorphous solids. The presence of crystalline SOA in wildfire plumes may significantly impact e.g., aerosol size distributions, heterogeneous reaction rates, and abilities to act as nuclei for clouds, with important implications for air quality and climate modelling.

From Oceans to Cities and from Clusters to Clouds: Introducing future perspectives

B. ROSATI [1,2] and D. STOLZENBURG [3]

[1]*Department of Chemistry, Aarhus University, Aarhus, Denmark*
[2]*Institute of Meteorology and Climatology, BOKU University, Vienna, Austria*
[3]*Institute of Materials Chemistry, TU Wien, Vienna, Austria*

Keywords: marine aerosols, atmospheric ageing, urban aerosols, volatile chemical products

INTRODUCTION

The largest source of natural aerosols originates from the oceans, that cover approximately 70% of the Earth's surface. These marine emissions are incredibly diverse, including primary inorganic salts, organic compounds and even living organisms such as bacteria or microalgae, as well as a wide range of volatile organic compounds (VOCs). In contrast, urban areas only cover less than 3% of the Globe, but more than half of the planet's population lives there. It is not surprising that also urban emissions are highly complex and range from traditional combustion-related primary soot particles, tire and break ware to thousands of different organic VOCs.

Both in the marine and the urban atmosphere, a decisive step for the impact of aerosols occurs after the emissions. Once these particulate and gaseous compounds are emitted into the atmosphere, they can undergo changes over time by reacting with each other or with previously present compounds. In this way, secondary particles can form, and primary particles may be transformed. For understanding this atmospheric ageing, the complexity of the mix might be decisive. From the oceans to the cities and from clusters to clouds, we have identified research on more complex mixtures of aerosols as one of the most important challenges to understand future trends in marine and urban aerosols and elucidate their impact on climate and air quality.

METHODS

To investigate the ageing processes occurring in the real (and highly complex) atmosphere it is essential to conduct ambient studies and complement them with detailed laboratory measurements addressing specific reactions.

For urban areas, the future emission scenarios predict further reductions in primary particle emissions but also a change in the VOC mix (McDonald et al., 2018). As typical combustion-related organics are declining due to updated policies on traffic and industrial emissions, other anthropogenic organic air contaminants are emerging, often classified together as volatile chemical products (VCPs). They originate from various non-combustion sources such as paints, adhesives, detergents, but also hygiene consumer products (Gkatzelis et al., 2021). However, the potential of these compounds to oxidize in the atmosphere and form products of sufficiently low volatility to contribute to new particle formation (NPF) and subsequent growth (Stolzenburg et al., 2023) has not been evaluated in-depth, while it is known that many VCPs contribute to secondary organic aerosols (SOA) (Shah et al., 2020). It has been demonstrated, that the full contribution to NPF of a given organic source can best be evaluated when the entire volatility distribution is known, also including moderately oxygenated molecules (MOM) (Stolzenburg et al., 2025). In addition, due to the complex emission patterns of many VCP emitters it is important to understand the entire oxidation chain from the volatile organic compounds (VOCs) up to the least volatile highly oxygenated organics molecules (HOMs). These challenges will be addressed with a novel combination of different instrumentation: of multi-pressure chemical ionization (Shcherbinin et al., 2024) to measure the entire oxidation chain of certain VCP sources (VOCs to MOM and HOM) with a single ultra-high resolution Orbitrap mass spectrometer, and IR-spectroscopy related tools (Dinu et al., 2022; Luhmann et al., 2023) to complement the traditional mass spectrometry based approaches in aerosol science. Together this toolset can be applied in a unique

environment in Vienna, the Seestadt, a novel district with reduced traffic but high population density. It is located at the outskirts of the Austrian capital also making it an ideal location to study city-rural interactions within longterm measurements.

Another ideal location to study interactions between urban areas and their surroundings are coastal aerosols where marine and urban emissions combine. Therefore, the optical properties of aerosol particles in different Scandinavian coastal areas were studied. By analyzing the wavelength dependence of scattering and absorption the type and source of the aerosol particles can be assessed (Cazorla et al., 2013; Cappa et al., 2016). Results were further constrained by combining these measurements with information on the particle size distributions, meteorological data and footprint analysis (Flexpart). To better understand the properties of these ambient aerosols, laboratory studies were performed to simulate potential reactions occurring in such an environment to decipher changes in their physical and chemical properties and ultimately their impact on climate. In this context, for example, the effect of the presence of α-pinene and ozone was tested on primary marine salt particles. Preliminary results revealed drastic changes in the particles' ability to scatter light or absorb water. Furthermore, a more thorough investigation of the impact of directly emitted and aged primary particles on the water uptake potential and its importance for clouds is envisaged to quantify the most significant factors in aerosol-cloud-climate interactions and improving our understanding of potential changes that may occur due to the changing climate.

ACKNOWLEDGEMENTS

B.R. was supported by a research grant from Villum Fonden (42128). D.S. acknowledges the Support of the Vienna Science and Technology Fund (WWTF) under project VRG22-003, the Austrian Science FWF under project PAT8221324.

REFERENCES

Cazorla, A., Bahadur, R., Suski, K. J., Cahill, J. F., Chand, D., Schmid, B., Ramanathan, V., and Prather, K. A. (2013): Relating aerosol absorption due to soot, organic carbon, and dust to emission sources determined from in-situ chemical measurements, Atmos. Chem. Phys., 13, 9337–9350, https://doi.org/10.5194/acp-13-9337-2013.

Cappa, C. D., Kolesar, K. R., Zhang, X., Atkinson, D. B., Pekour, M. S., Zaveri, R. A., Zelenyuk, A., and Zhang, Q. (2016): Understanding the optical properties of ambient sub- and supermicron particulate matter: results from the CARES 2010 field study in northern California, Atmos. Chem. Phys., 16, 6511–6535, https://doi.org/10.5194/acp-16-6511-2016.

Dinu, D. F., Bartl, P., Quoika, P. K., Podewitz, M., Liedl, K. R., Grothe, H., & Loerting, T. (2022). Increase of Radiative Forcing through Midinfrared Absorption by Stable CO2 Dimers? *J. Phys. Chem. A*, *126*(19), 2966–2975. https://doi.org/10.1021/acs.jpca.2c00857

Gkatzelis, G. I., Coggon, M. M., McDonald, B. C., Peischl, J., Aikin, K. C., Gilman, J. B., Trainer, M., & Warneke, C. (2021). Identifying Volatile Chemical Product Tracer Compounds in U.S. Cities. *Environ. Sci. Technol.*, *55*(1), 188–199. https://doi.org/10.1021/acs.est.0c05467

Luhmann, N., West, R. G., Lafleur, J. P., & Schmid, S. (2023). Nanoelectromechanical Infrared Spectroscopy with In Situ Separation by Thermal Desorption: NEMS-IR-TD. *ACS Sensors*, *8*(4), 1462–1470. https://doi.org/10.1021/acssensors.2c02435

McDonald, B. C., de Gouw, J. A., Gilman, J. B., Jathar, S. H., Akherati, A., Cappa, C. D., Jimenez, J. L., Lee-Taylor, J., Hayes, P. L., McKeen, S. A., Cui, Y. Y., Kim, S.-W., Gentner, D. R., Isaacman-VanWertz, G., Goldstein, A. H., Harley, R. A., Frost, G. J., Roberts, J. M., Ryerson, T. B., & Trainer, M. (2018). Volatile chemical products emerging as largest petrochemical source of urban organic emissions. *Science*, *359*(6377), 760–764.

Shah, R. U., Coggon, M. M., Gkatzelis, G. I., McDonald, B. C., Tasoglou, A., Huber, H., Gilman, J., Warneke, C., Robinson, A. L., & Presto, A. A. (2020). Urban Oxidation Flow Reactor Measurements Reveal Significant Secondary Organic Aerosol Contributions from Volatile Emissions of Emerging Importance. *Environ. Sci. Technol.*, *54*(2), 714–725. https://doi.org/10.1021/acs.est.9b06531

Shcherbinin, A., Finkenzeller, H., Mikkilä, J., Kontro, J., Vinkvist, N., Kangasluoma, J., & Rissanen, M. (2024). From Hydrocarbons to Highly Functionalized Molecules in a Single Measurement: Comprehensive Analysis of

Complex Gas Mixtures by Multi-Pressure Chemical Ionization Mass Spectrometry. *Analytical Chemistry*, *96*(50), 19926–19932. https://doi.org/10.1021/acs.analchem.4c03859

Stolzenburg, D., Cai, R., Blichner, S. M., Kontkanen, J., Zhou, P., Makkonen, R., Kerminen, V.-M., Kulmala, M., & Kangasluoma, J. (2023). Atmospheric nanoparticle growth. *Rev. Mod. Phys.*, *95*(4), 045002. https://doi.org/10.1103/RevModPhys.95.045002

Stolzenburg, D., Sarnela, N., Bianchi, F., Cai, J., Cai, R., Cheng, Y., Dada, L., Donahue, N. M., Grothe, H., Holm, S., Kerminen, V.-M., Lehtipalo, K., Petäjä, T., Sulo, J., Winkler, P. M., Yan, C., Kangasluoma, J., & Kulmala, M. (2025). Incomplete Mass Closure in Atmospheric Nanoparticle Growth. *Npj Climate and Atmospheric Sciences*, *in press*.

UPTAKE OF INDIVIDUAL MOLECULES BY BINARY WATER–NITRIC ACID CLUSTERS: NUCLEATION AT THE SUBNANOMETER SCALE

Y. YAN[1], K. FÁRNÍKOVÁ[2], K. LI[1], A. PYSANENKO[2],
E. PLUHAŘOVÁ[2], M. FÁRNÍK[2], and J. LENGYEL[1]

[1]*School of Natural Sciences, Technical University of Munich, Garching, Germany.*

[2]*Heyrovský Institute, Czech Academy of Sciences, Prague, Czech Republic.*

Keywords: new particle formation, cluster chemistry, collision dynamics, mass spectrometry.

Nearly half of the cloud seeds in the troposphere originate from atmospheric aerosol nucleation, where gaseous molecules such as acids, bases, and oxidized organics transform into subnanometer- and nanometer-sized clusters. However, current field measurements and laboratory experiments face challenges in understanding the early stages of aerosol nucleation, as they cannot reliably measure particles below 3 nm and instead rely heavily on computational data and simulation models.

A novel approach has therefore been introduced to measure the uptake of various molecules by hydrated acid clusters, enabling the direct determination of their sticking efficiency, which can be expressed as either the uptake cross section or the sticking coefficient (Pysanenko *et al.*, 2018; Lengyel *et al.*, 2020, Fárník, 2023). This approach also provides valuable information on the chemical processes involved in molecular uptake, which often lead to particle stabilization, such as proton transfer reactions (Pysanenko *et al.*, 2022). In this study, binary water-nitric acid clusters are doped with different volatile organic compounds and bases, and their interactions are examined using single-collision experiments with mass spectrometry and velocity measurements. However, the determination of relative uptake cross sections from the experimental data relies on simplifying assumptions about molecule-cluster collisions. To support these assumptions, detailed molecular dynamics simulations were performed, enabling us to identify the underlying processes in our experiment (Fárníková *et al.*, 2024).

This combined experimental and computational approach provides detailed insights into molecule-cluster interactions, such as sticking, evaporation, and scattering dynamics. Compared to atmospheric measurements, which provide large-scale trends, our method offers mechanistic details that enhance our understanding of nucleation at the molecular scale. This study focuses on the relationship between structure-related properties and sticking efficiency, particularly examining carbon chain length, O–H group position, and alkyl chain branching. The influence of different functional groups is also analyzed. Finally, the limitations of the method are highlighted, particularly in cases where uptake cross sections cannot be reliably determined.

ACKNOWLEDGEMENTS

This work was supported by the German Research Foundation (Deutsche Forschungsgemeinschaft, DFG) under grant 442679477.

REFERENCES

Fárník, M (2023). Bridging gaps between clusters in molecular-beam experiments and aerosol nanoclusters, *J. Phys. Chem. Lett.* **14**, 287.

Fárníková, K., E. Pluhařová, A. Pysanenko, M. Fárník, Y. Yan and J. Lengyel (2024). Dynamics of collisions and uptake of alcohol molecules with hydrated nitric acid clusters, *Faraday Discuss.* **251**, 296.

Lengyel, J., A. Pysanenko, K. Fárníková, E. Pluhařová and M. Fárník (2020). Oxidation enhances aerosol nucleation: Measurement of kinetic pickup probability of organic molecules on hydrated acid clusters, *J. Phys. Chem. Lett.* **11**, 2101.

Pysanenko, A., J. Lengyel and M. Fárník (2018). Uptake of methanol on mixed HNO_3/H_2O clusters: An absolute pickup cross section, *J. Chem. Phys.* **148**, 154301.

Pysanenko, A., K. Fárníková, J. Lengyel, E. Pluhařová and M. Fárník (2022). Molecular-level insight into uptake of dimethylamine on hydrated nitric acid clusters, *Environ. Sci. Atmos.*, **2**, 1292.

CLOUD DROPLET SPECTRA MEASUREMENTS: COMPARISON IN LOW STRATIFORM CLOUDS

N. ZÍKOVÁ[1], K. JULAHA[1,2], P. SEDLÁK[3], V. ŽDÍMAL[1] and D. BRUS[4]

[1]*Research Group of Aerosol Physics and Chemistry, Institute of Chemical Process Fundamentals CAS, Prague, Czech Republic.*
[2]*Department of Atmospheric Physics, Faculty of Mathematics and Physics, Charles University, Prague, Czech Republic.*
[3]*Department of Meteorology, Institute of Atmospheric Physics CAS, Prague, Czech Republic.*
[4]*Finnish Meteorological Institute, Helsinki, Finland.*

Keywords: cloud droplets, fog monitor, CDA, PVM.

INTRODUCTION

Atmospheric aerosol (AA) and its interactions with atmospheric water are of great importance (Neuberger et al. 2025); however, they are still connected to considerable uncertainties. To improve our knowledge of aerosol-cloud interactions, Seinfeld *et al.*, (2016) suggest designing large-scale in-situ field programs to provide enough data for models and also to understand how AA from different sources influences cloud micro and macrophysics.

To address such a need, a standardized measurement technique must first be established. The standard operating procedures of ACTRIS (Aerosol, Clouds, and Trace Gases Research Infrastructure) are in place for AA properties. However, the standards are being sought for cloud droplet spectra (CDS) or liquid water content (LWC) measurements.

METHODS

To provide comparison measurements for CDS and LWC, a three-month intensive in-situ campaign was conducted at Mount Milešovka in the Czech Republic (50.55 N, 13.93 E, 837 m a.s.l.). At the station, low stratus clouds, coded as fog, appear 55 % of the days during the year (Fišák et al. 2009), and during autumn and winter, up to 90 % of days with fog appearance can be expected based on the 1961-1990 data.

From 30. 10. 2024 to 22. 1. 2025, three online instruments measuring cloud water properties were installed side-by-side at the top of the station: Fog Monitor 120 (FM-120, DMT), Cloud Droplet Analyzer (CDA, Palas GmbH), and Particulate Volume Monitor (PVM, Gerber Scientific). PVM had already been running at the station, while CDA and FM-120 were located there only for this intercomparison. All three instruments were located vertically (Fig. 1), with FM-120 using the swivel inlet first but later replaced with a heated vertical inlet to prevent riming and potential instrumental clogging.



Figure 1. Measurement set-up at the Milešovka station: CDA, FM120, and PVM 100.

RESULTS

From the data, the Effective Diameter (ED), Mean Volume Diameter (MVD), and LWC were compared from all instruments. The median ED and MVD was 0.44 μm, with the highest LWC values of 0.25 g/m^3 as measured by FM-120, in good agreement with previous measurements at the station (Zíková et al. 2020).

The cloud droplet number concentration was also considered from CDA and FM-120. All the measured variables will be compared with wind speed and direction, and air mass sources will be taken into account.

ACKNOWLEDGEMENTS

This work was supported by ACTRIS, MEYS of the Czech Republic under grant ACTRIS-CZ LM2023030, by the Czech Science Foundation Grant No. 24-10768S, and by the Charles University Grant Agency, grant number 98124.

REFERENCES

Fišák, J, Tesař, M & Fottová, D. 2009. Pollutant Concentrations in the Rime and Fog Water at the Milesovka Observatory. *Water, Air, and Soil Pollution*. 196(1–4):273–285. doi.org/10.1007/s11270-008-9775-z.

Neuberger, A, Decesari, S, Aktypis, A, Andersen, H, Baumgardner, D, Bianchi, F, Busetto, M, Cai, J, et al. 2025. From Molecules to Droplets: The Fog and Aerosol Interaction Research Italy (FAIRARI) 2021/22 Campaign. *Bulletin of the American Meteorological Society*. 106(1):E23–E50. doi.org/10.1175/BAMS-D-23-0166.1.

Seinfeld, JH, Bretherton, C, Carslaw, KS, Coe, H, DeMott, PJ, Dunlea, EJ, Feingold, G, Ghan, S, et al. 2016. Improving our fundamental understanding of the role of aerosol-cloud interactions in the climate system. *Proceedings of the National Academy of Sciences of the United States of America*. 113(21):5781–5790. doi.org/10.1073/pnas.1514043113.

Zíková, N, Pokorná, P, Makeš, O, Sedlák, P, Pešice, P & Ždímal, V. 2020. Activation of atmospheric aerosols in fog and low clouds. *Atmospheric Environment*. 230(April):117490. doi.org/10.1016/j.atmosenv.2020.117490.

Special Session 4: Urban new particle formation

ATMOSPHERIC MIXING AND LOW POLLUTION ENHANCE NEW PARTICLE FORMATION IN MILAN, ITALY

M. AGRO'[1] , M. BETTINESCHI[1], S. MELINA[2] , J. SULO[1,a] , K. LEHTIPALO[1] , T. PETÄJÄ[1] , I. GRIGIONI[2], G. CIARELLI[1], J. LAMPILAHTI[1], C. COLOMBI[3] , B. BIFFI[3] , A. MARINONI[4], A. BIGI[5], C. OLIEWO[5], M. KULMALA[1] and F. BIANCHI[1]

[1]*Institute for Atmospheric and Earth System Research, University of Helsinki, Helsinki, Finland*

[2]*Department of Chemistry, University of Milan, Milan, Italy*

[3]*Regional Agency for Environmental Protection of Lombardy, Air Quality Department, Milan, Italy*

[4]*Institute of Atmospheric Sciences and Climate, National Research Council of Italy, Bologna, Italy*

[5]*Department of Engineering, University of Modena and Reggio Emilia, Modena, Italy*

[a]*now at: School of Earth and Atmospheric Sciences, Queensland University of Technology, Brisbane, Australia*

Keywords: NEW PARTICLE FORMATION, URBAN SITE, SIZE DISTRIBUTION.

INTRODUCTION

Investigating the process of New Particle Formation (NPF) is essential for safeguarding human health and tackling climate change. Ultrafine particles pose potential risks to the lungs, circulatory system, and brain. Furthermore, these particles can grow through condensation and coagulation and interact with the solar radiation either directly or by acting as cloud condensation nuclei. Despite its importance, the NPF process has not been studied yet in Milan with high resolution instruments over a prolonged period of time. This research aims to fill this gap by presenting an analysis of NPF in Milan, the most densely populated and one of the most polluted cities in the Po Valley, and a hotspot for air quality and climate-related challenges in Europe.

METHODS

We investigated NPF in Milan by analysing particle number size distributions measured by a set of advanced instruments: a nano-Condensation Nucleus Counter (1.2-3nm), a Neutral Cluster and Air Ion Spectrometer (2.5-40nm), and a Scanning Mobility Particle Sizer (10-500nm). These instruments operated for a year, between March 2023 and March 2024 at the Physics and Chemistry departments of the University of Milan, in an urban background area of the city, as ancillary measurements to the RI-URBANS project. The data was analysed using the nano-particle ranking method (Aliaga et al., 2023), alongside meteorological and pollutant concentration data provided by ARPA Lombardia. The Lagrangian particle dispersion model Flexpart, coupled with the high-resolution meteorological model WRF (Weather Research & Forecasting Model) and CAMS (Copernicus Atmosphere Monitoring Service) emissions datasets, was applied to assess the airmasses characteristics (Brioude et al., 2013).

CONCLUSIONS

Particle number size distributions exhibit a clear seasonal variation. In winter, an increase in the concentration of larger (> ca 50 nm) particles is probably due to the higher atmospheric stability, lower boundary layer height and higher residential heating emissions. Traffic-induced concentration peaks are also observed during rush hours. In spring and summer, large atmospheric mixing leads to a reduction of these

peaks and favors a frequent sub-10 nm particles' concentration increase at midday, indicating strong NPF, especially in summer. In autumn traffic-related peaks become more pronounced due to higher emissions and reduced mixing, marking a transition towards winter.
The comparison between pollutants' concentrations, meteorological conditions and ranking percentiles, representative of NPF intensity, highlight that a cleaner and more mixed atmosphere – with lower concentrations of black carbon, CO, SO_2, NO_2, PM_{10}, $PM_{2.5}$, lower condensation sink (CS) and higher atmospheric ventilation index – promote NPF (Figure 1).

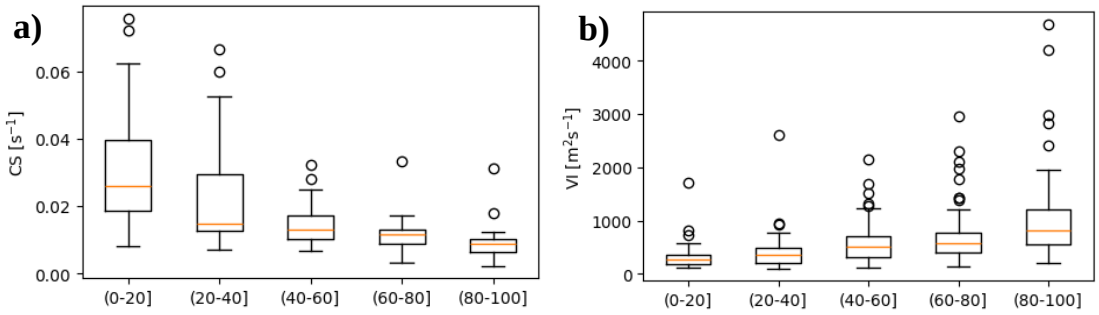


Figure 1. a) Median CS and b) daily ventilation index (VI) described through boxplots of 20-percentile of NPF rank. Specifically, going from left to right, each boxplot represents classes of stronger NPF intensity.

Our advance airmass modelling analysis supports this conclusion showing that airmasses with low residence time in the Po Valley and with low exposure to anthropogenic sources favor NPF (Figure 2). Our results indicate that NPF is most likely to occur when air masses arrive from the north, particularly northwest.

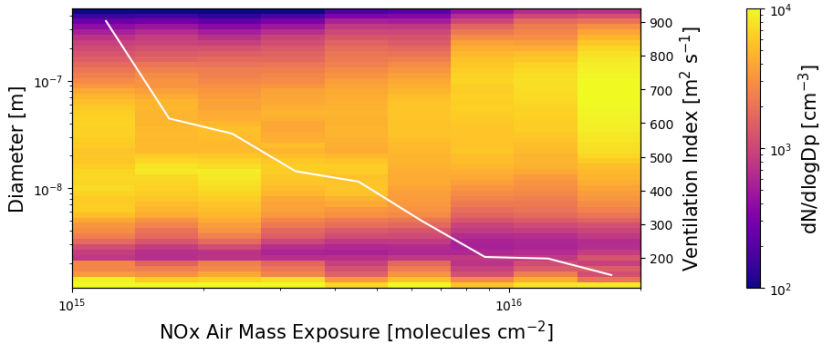


Figure 2. Relationship between airmass exposure to NO_x emissions and particle number size distribution. The white line represents the ventilation index

Formation rate analysis (J) reveals that the production of 3 nm particles (J_3) is higher during more intense NPF events. In contrast, the formation of 1.5 nm particles remains steady regardless of NPF intensity, suggesting that clustering at 1.5 nm constantly occurs, while particle growth is influenced by specific conditions.
Lastly, the analysis of the sulfuric acid proxy confirms its contribution to NPF at this site. Despite a decrease in SO_2 during strong NPF events, the precursor vapor remains available, hinting at the role of the CS reduction in promoting particle formation.
We will additionally include a comprehensive comparison with other urban sites across the world.

ACKNOWLEDGEMENTS

This project received funding from the European Union's Horizon 2020 research and innovation programme under grant agreement No 101036245 (RI-URBANS).

REFERENCES

Aliaga D., Tuovinen S., Zhang T., Lampilahti J., Li X., Ahonen L., Kokkonen T., Nieminen T., Hakala S., Paasonen P., Bianchi F., Worsnop D., Kerminen V.-M., and Kulmala M. (2023). Nanoparticle ranking analysis: determining new particle formation (NPF) event occurrence and intensity based on the concentration spectrum of formed (sub-5 nm) particles, *Aerosol Research* **1**, 81–92

Brioude J., Arnold D., Stohl A., Cassiani M., Morton D., Seibert P., Angevine W., Evan S., Dingwell A., Fast J. D., Easter R. C., Pisso I., Burkhart J., and Wotawa G (2013). The Lagrangian particle dispersion model FLEXPART-WRF version 3.1, *Geosci. Model Dev*. **6**, 1889–1904

RAPID INITIAL GROWTH OF NEW ATMOSPHERIC PARTICLES BY LARGE NANOPARTICLE CONCENTRATION GRADIENT

R. CAI[1,2], X. LI[3,4], Y. LI[4], S. BLICHNER[5], D. STOLZENBURG[2,6], L. WANG[1], D. WORSNOP[2,7], J. JIANG[4,*], M. KULMALA[2,8,9] & J. KANGASLUOMA[2]

[1]*Shanghai Key Laboratory of Atmospheric Particle Pollution and Prevention (LAP[3]), Department of Environmental Science & Engineering, Fudan University, 200438 Shanghai, China.*

[2]*Institute for Atmospheric and Earth System Research / Physics, Faculty of Science, University of Helsinki, 00014 Helsinki, Finland.*

[3]*School of Resource and Environmental Sciences, Wuhan University, 430072 Wuhan, China.*

[4]*State Key Joint Laboratory of Environment Simulation and Pollution Control, School of Environment, Tsinghua University, 100084 Beijing, China.*

[5]*Bolin Centre for Climate Research, Stockholm University, SE-106 91 Stockholm, Sweden*

[6]*Institute of Materials Chemistry, TU Wien, 1060 Vienna, Austria.*

[7]*Aerodyne Research Inc., 45 Manning Road, Billerica, 01821 Massachusetts, USA.*

[8]*Joint International Research Laboratory of Atmospheric and Earth System Research, School of Atmospheric Sciences, Nanjing University, 210023 Nanjing, China.*

[9]*Aerosol and Haze Laboratory, Beijing Advanced Innovation Center for Soft Matter Science and Engineering, Beijing University of Chemical Technology, Beijing, 100029, China.*

Keywords: INITIAL GROWTH, COAGULATION, SURVIVAL PROBABILTY, NANOPARTICLE CONCENTRATION GRADIENT

INTRODUCTION

The initial growth of freshly nucleated particles from the cluster size (~ 1 nm) to a few nanometers is the most critical stage for their survival against the coagulation scavenging of large background particles. Despite the advances in the past decade have significantly advanced the mechanistic understanding of nucleation, how new particles grow large and become relevant for climate and air quality remains uncertain. Well-controlled laboratory experiments (e.g., Tröstl *et al.*, 2016) have shown that the initial growth rate responses linearly to the concentration of condensable vapors. However, such a good consistency rarely applies to the real atmosphere, for which the measured growth rate has a rather weak dependence on the condensable vapor concentration.

Besides, the limited concentration of condensable vapors often does not explain the observed rapid initial growth rate. The concentration of gaseous sulfuric acid is typically 10^4-10^7 molecules cm^3. It can drive efficient nucleation in polluted urban atmospheres together with stabilizing bases (Yao *et al.*, 2018). Highly-oxygenated organic molecules (HOMs) with extremely low volatility have also been proposed to be a major contributor to the initial growth. However, slow initial growth and extremely low survival probability would be expected (Kulmala *et al.*, 2017) considering the limited availability of these condensable vapors in urban atmospheres, e.g., in Beijing. The puzzle for the rapid initial growth, and consequently the puzzle the frequent NPF events in polluted urban environments, remains to be solved.

METHODS

We measured and analyzed atmospheric new particle formation (NPF) at seven sites, including Beijing (BUCT station, urban), Hyytiälä (SMEAR II station, rural), Shanghai (SAES station, urban), Nanjing (SORPES station, regional background), Hong Kong (CDSS station, coastal background), and Chacaltaya (GAW station, high-altitude), and Po Valley (urban). Particles down to ~ 1 nm in urban Beijing was

measured using a diethylene glycol scanning mobility particle spectrometer (DEG-SMPS). The size distribution of sub-8 nm particles at Hyytiälä was measured in 2020 using a differential mobility analyzer-train (DMA-train), which classified particles into 6 size channels based on their electrical mobility (Stolzenburg et al. 2017). The concentration of sulfuric acid and HOMs were measured using nitrate CI-APi-TOFs at all the seven sites.

We analyzed the initial growth and survival of freshly nucleated particles during strong NPF events at Hyytiälä and Beijing. The 50% appearance time method with a correction for the influence of coagulation (Cai *et al.*, 2021) was used to retrieve the initial growth rate (GR) from the measured size distributions. The formation rate (J) was calculated using the population balance method which accounts for the high coagulation loss of new particles in polluted environments (Cai and Jiang, 2017). The survival probability (P) was retrieved using the ratio of representative parameters, i.e., J for Beijing and $dN/d\log d_p$ for Hyytiälä according to Cai *et al.* (2022). The theoretical survival probability was also theoretically predicted as a function of GR and the coagulation sink.

The initial growth rate contributed by condensable vapors was modelled from two perspectives. From a single-particle (or equivalently, monodisperse-aerosol) perspective, the growth is driven by the net condensation flux of vapors to the particle phase. The net condensation rate used determined using the measured concentration of vapors and their equilibrium concentration over the single-particle. The contributions from measured clusters to the initial growth were also accounted for. From an aerosol population perspective, the initial growth used simulated using a discrete model, which obtains the concentrations of particles with different sizes and compositions by solving a series of population balance equations. Different from the single-particle model, the discrete model accounts for the fact that the evaporation flux from larger particles after adding one more condensing molecule is lower than that from monodisperse particles due to the gradient of nanoparticle concentration as a function of their size (referred to as nanoparticle concentration gradient, NCG) (e.g., Wang *et al.*, 2013; Malina *et al.*, 2015).

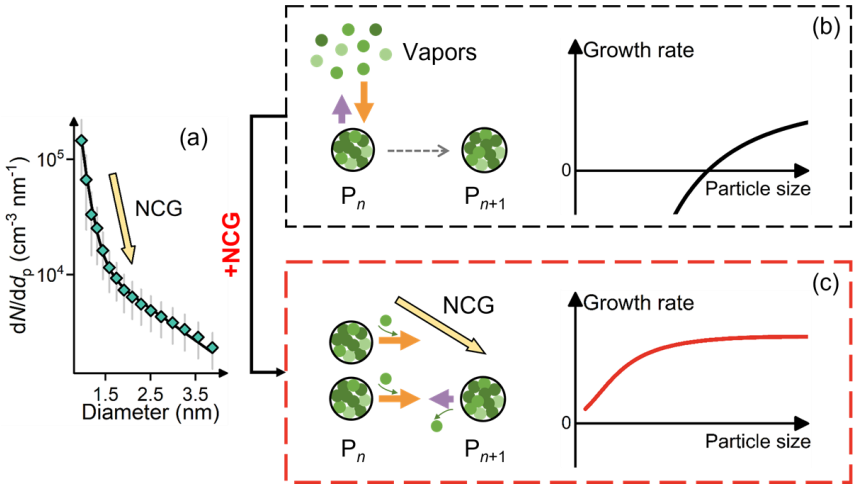


Figure 1. Illustrative schematic for the initial growth of a single particle and a population of particles. (a) average number size distribution of new atmospheric particles measured in Beijing. (b) Initial growth in a single-particle perspective. (c) The growth flux of a population of particles.

CONCLUSIONS

We find that the NCG drives more effective condensation of HOMs that previously expected from the perspective of a single particle, and the predicted sub-3 nm initial growth rate is consistent with the observed rapid initial growth. Case studies and statistically analysis of 40 strong NPF events at Beijing and Hyytiälä show that, with the overlooked NCG-enhanced OOM condensation in atmospheric

environments, the predicted growth rate can explain the observed rapid initial growth rate (sometimes exceeding 5 nm h^{-1}) of sub-3 nm particles without introducing extra undetected condensable vapors. This enhanced initial growth rate substantially elevate the survival probability of freshly nucleated particles. The elevation is most significant for NPF events in polluted urban environments with values up to several orders of magnitudes, as the survival probability is highly sensitive to GR at a high coagulation sink.

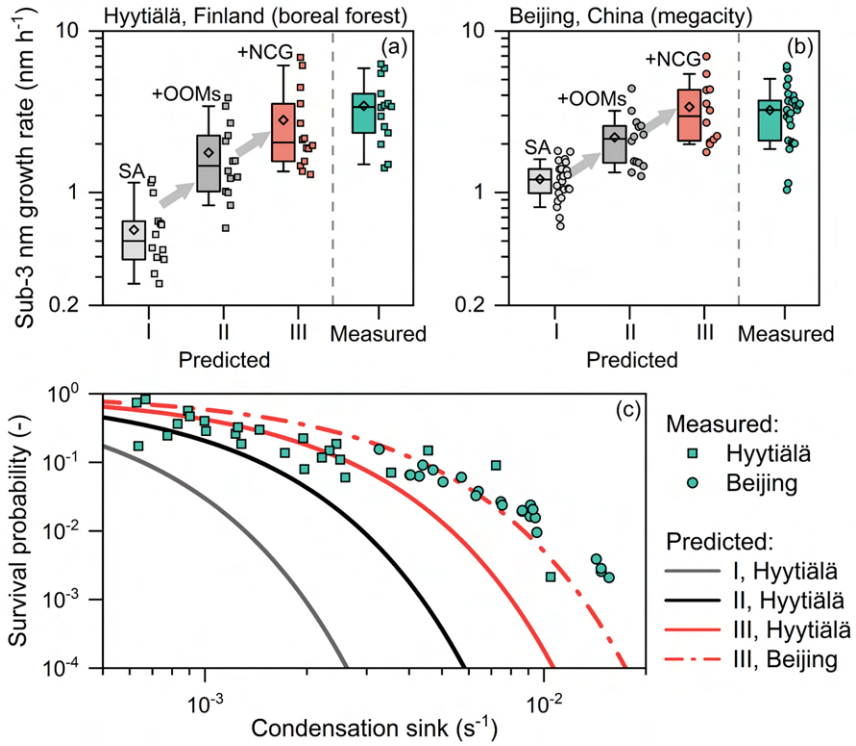


Figure 2 Growth rate and survival probability of sub-3 nm particles. (a) and (b), the measured and theoretically predicted growth rates during NPF events (c), the measured and theoretically predicted survival probabilities.

We further evaluate the initial growth and survival of new particles at seven sites across the globe. Results show that the NCG increases the initial growth rate by 45-138%, and HOMs govern the initial growth at all these sites including sulfur-rich urban sites. The enhancement in particle survival probability by the NCG is most significant for polluted megacities, and it also exceeds a factor of 2 at clean boreal forest and high-altitude sites.

Our findings address the puzzle of frequent NPF events in polluted urban environments: highly efficient clustering mechanisms drives intense nucleation, and the condensation of vapors accelerated by the NCG drives rapid sub-3 nm initial growth against high coagulation scavenging losses. The higher survival probability of freshly nucleated particles also indicates a larger fraction of cloud condensation nuclei contributed by NPF.

ACKNOWLEDGEMENTS

This work was supported by National Natural Science Foundation of China 22406024, 22376166, and 22106083, the ACCC Flagship funded by the Research Council of Finland 337549, Academy professorship funded by the Research Council of Finland 302958, Academy of Finland 332547, 325656, 311932, 334792, 316114, 325647, 325681, 333397, 328616, 357902, 345510, 347782, 346370, 364223,

325656, and 356134, Shanghai B and R Joint Laboratory Project 22230750300, Shanghai International Science and Technology Partnership Project 21230780200, Jane and Aatos Erkko Foundation "Quantifying carbon sink, CarbonSink+ and their interaction with air quality" INAR project Wihuri Foundation "Gigacity" project, European Research Council (ERC) project ATM-GTP No. 742206 and CHAPAs No. 850614, European Union Non-CO2 Forcers and their Climate, Weather, Air Quality and Health Impacts (FOCI), CRiceS (101003826), RI-URBANS (101036245), EMME-CARE (856612), FORCeS (821205), and NPF-PANDA (895875), European Commission grants INTEGRATE 867599 Swedish Research Council grant 2023-03842, the Technology Industries of Finland Centennial Foundation urbaani ilmanlaatu 2.0 -project, and Vienna Science and Technology Fund (WWTF) VRG22-003.

REFERENCES

Cai, R. and Jiang, J. (2017). A new balance formula to estimate new particle formation rate: reevaluating the effect of coagulation scavenging, *Atmospheric Chemistry Physics*, 17, 12659-12675, 10.5194/acp-17-12659-2017.

Cai, R. *et al.* (2021). Impacts of coagulation on the appearance time method for new particle growth rate evaluation and their corrections, *Atmospheric Chemistry Physics*, 21, 2287-2304, 10.5194/acp-21-2287-2021.

Cai, R. *et al.* (2022). Survival probability of new atmospheric particles: closure between theory and measurements from 1.4 to 100 nm, *Atmospheric Chemistry Physics*, 22, 14571-14587, 10.5194/acp-22-14571-2022.

Kulmala, M. et al. (2017). Atmospheric gas-to-particle conversion: why NPF events are observed in megacities?, *Faraday Discussions*, 200, 271-288, 10.1039/c6fd00257a.

Malila, J. *et al.* (2015). Communication: kinetics of scavenging of small, nucleating clusters: first nucleation theorem and sum rules, *The Journal of Chemical Physics*, 142, 011102, 10.1063/1.4905213.

Stolzenburg, D. *et al.* (2017). A DMA-train for precision measurement of sub-10 nm aerosol dynamics, *Atmospheric Measurement Techniques*, 10, 1639-1651, 10.5194/amt-10-1639-2017.

Tröstl, J. *et al.* (2016). The role of low-volatility organic compounds in initial particle growth in the atmosphere, *Nature*, 533, 527-531, 10.1038/nature18271.

Wang, J. *et al.* (2013). Growth of atmospheric nano-particles by heterogeneous nucleation of organic vapor, *Atmospheric Chemistry and Physics*, 13, 6523-6531, 10.5194/acp-13-6523-2013.

Cloud Condensation Nuclei enhancement by New Particle Formation events over a location in the Eastern Himalayan Foothills

B. DAS[1], U. BHATTACHARJEE[1], B. PATHAK[1,2], A. BORGOHAIN[3], S.S. KUNDU[3], and P. K. BHUYAN[2]

[1]*Department of Physics, Dibrugarh University, Assam, India*
[2]*Centre for Atmospheric Studies, Dibrugarh University, Assam, India*
[3]*North-East Space Application Centre, Umiam, Meghalaya, India*

Keywords: NPF, Growth rate, CCN, Enhancement

INTRODUCTION

New particle formation (NPF) has gained much attention in the world of research due to its significant effects on cloud condensation nuclei (CCN) (Gordon et al., 2017; Westervelt et al., 2013, Kulmala et al., 2007; Pierce & Adams, 2007) and plays a major role directly in cloud properties, and indirectly by modulating Earth's radiation budget (IPCC 2023; Albrecht, 1989; Twomey, 1976). According to observations (10%-60%) (Asmi et al., 2011; Kerminen et al., 2012; Kuang et al., 2009; Laakso et al., 2013; Rose et al., 2017; Sebastian et al., 2022; Yu et al., 2014; Yue et al., 2011), Field campaigns (10-143%) (Dameto de España et al. 2017; Sihto et al. 2011 etc.), and global modelling (~50%) (Spracklen et al., 2008; Westervelt et al., 2014; Yu and Luo, 2009; Gordon et al., 2017), it contributes significantly to global CCN budget. The NPF is a sporadic spatio-temporal phenomenon occurring through gas-to-particle (GTP) conversion, often in the continental boundary layer at a spatial scale of a few hundred kilometres and a timescale of 1-2 days (Kulmala et al., 2012). The enhancement of CCN during an NPF event is very complex, as nucleated atmospheric particles take hours to days to grow to CCN-active sizes, during which they are transported far from their formation sites and mix with primary-source CCN (Kerminen et al., 2012). Especially in polluted environments, nucleation events result in low CCN production efficiency due to the presence of pre-existing aerosols (Kerminen et al., 2012). Though the NPF study over the Indian region has been investigated by several researchers (Kanwade et al., 2022, reference therein), the measurements have not been integrated with CCN Counter in most of the cases. Thus, a simultaneous measurement of a Scanning Mobility Particle Sizer (SMPS) and a CCN counter (CCNc) has been conducted to understand the CCN activity in relation to the variation of aerosol number concentration.

METHODS

The present measurement is carried out at Dibrugarh (27.26°N, 94.53°E, and 111 m amsl) during the winter (3rd Jan - 4th Feb 2023). The particle number size distribution (PNSD) and CCN concentrations were measured simultaneously over Dibrugarh using an SMPS and a CCNc at a height of approximately 6 meters from the ground. Dal Maso and Kulmala (2005) established criteria for identifying NPF events, that include a distinct new mode in the nucleation range and a sign-of-growth event lasting several hours. The methodology used in the present study to understand the NPF-induced CCN was given by Kalkavouras et al. (2019). The NPF-induced CCN is usually calculated by comparing the N_{CCN} prior and after the NPF denoted as $N_{CCN_{prior,SS}}$ and $N_{CCN_{after,SS}}$ respectively. The $N_{CCN_{prior,SS}}$ is the two-hour average of N_{CCN} prior to NPF at different SS, whereas $N_{CCN_{after,SS}}$ is the average of N_{CCN} from the beginning of the NPF impacted to CCN time to the end of the NFP event. The start (t_{start}), and end (t_{end}) times were calculated from the time series of PNSD of the NPF events and the corresponding N_{CCN} at the t_{start}, ($N_{CCN_{ss,t_{start}}}$). To compute the time when NPF start impacting CCN at different supersaturation (SS) levels, the normalized $N_{CCN_{ss}}$ time series for each SS is calculated, and is denoted by R_{SS}, where $R_{SS} = \frac{N_{CCN_{SS}}}{N_{CCN_{SS,t_{start}}}}$. Initially, the R_{SS} should be equal to unity and should remain so until the new particles reach a sufficient magnitude to influence CCNs at which the R_{SS} values start to disperse over a wide range. Thus, the relative dispersion between the R_{SS} (R_D) was computed by dividing the standard deviation of

instantaneous R_{SS} values (at 0.2, 0.4%, 0.6%, 0.8%, and 1% SS) by the average value of R_{SS} at each time step of 30 min (temporal resolution). This R_D is highly sensitive; during the NPF event, when newly formed particles start impacting CCN number concentrations, considered as decoupling time (t_{dec}), the R_D exceeds the low values observed during the event's early stages. This is due to the fact that these newly formed particles are activated to become CCN at a higher SS, which corresponds to the higher dispersion in R_{SS}. The enhancement factor, denoted as E_N_{CCN}, was calculated as

$$E_N_{CCN,SS} = \frac{N_{CCN_{after,SS}}}{N_{CCN_{prior,SS}}} \quad (1)$$

where $N_{CCN_{after.SS}}$ and $N_{N_{CCN_{prior,SS}}}$ are the average CCN concentrations during t_{dec} to t_{end}, and t_{start} and t_{dec} respectively at different SS levels (Laaksonen et al., 2005; Wu et al., 2017; Zhang et al., 2019, Kalkavouras et al., 2019, and Ren et al., 2021).

CONCLUSIONS

Aerosol-CCN interaction especially during the NPF events was investigated for the first time over Dibrugarh. Four NPF events were identified from 3 January-4 February 2023 by observing their two-hourly average PNSD. The particle burst event is identified in the nucleation mode when a distinct new mode appears at the lower size ranges. The number–size spectrum typically shows peaks in the larger size regime, but during the NPF events, a "new mode" begins to appear at the lower end of the nucleation mode size ranges, which later disappears and/or shifts to a higher size range because of subsequent growth through coagulation loss or condensation sink. The contour map of PNSD on NPF days (Figure 1), suggests that NPF1 (NPF4) is of Type-I (Type-II) with stable (unstable) growth of mode diameter (D_m) with an appearance of nucleation mode in the size distribution (Dal Maso, 2005). For NPF2 and NPF3, the new mode is developed in the Aitken mode size range of the PNSD, which continued to grow in that size range and are categorized as undefined NPF types (Dal Maso, 2005).

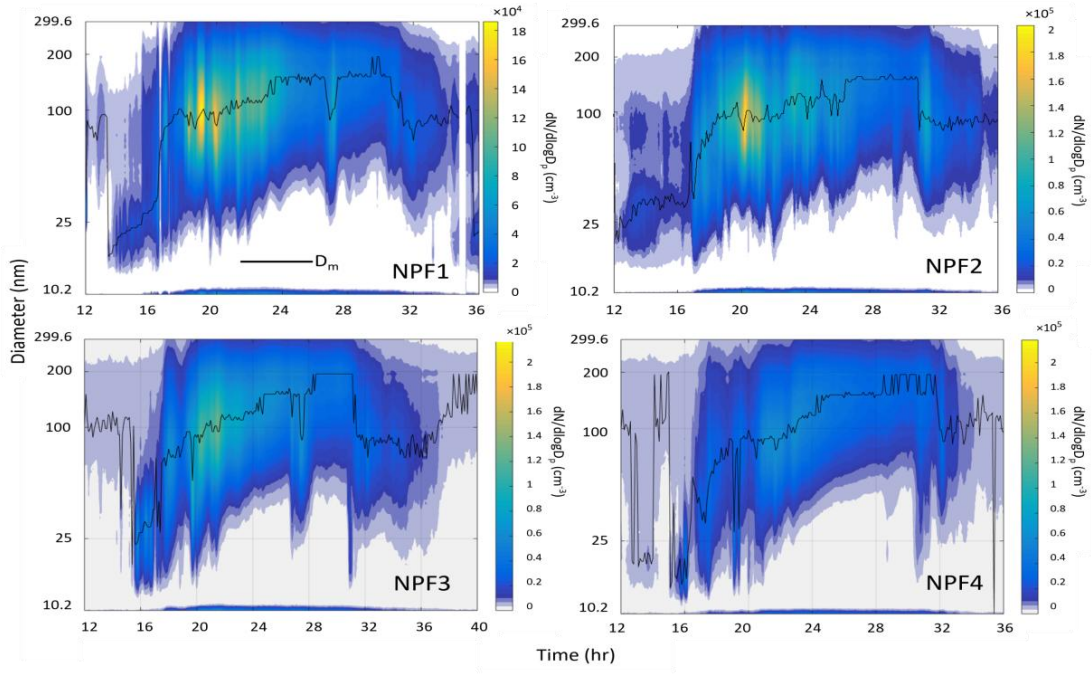


Figure 1. The evolution of PNSD with diameter during the NPF events during (a) January 5-6 (NPF1), (b) January 10-11 (NPF2), (c) January 25-26 (NPF3), and (d) February 3-4 (NPF4) of the year 2023. The solid black line represents the mode diameter (D_m).

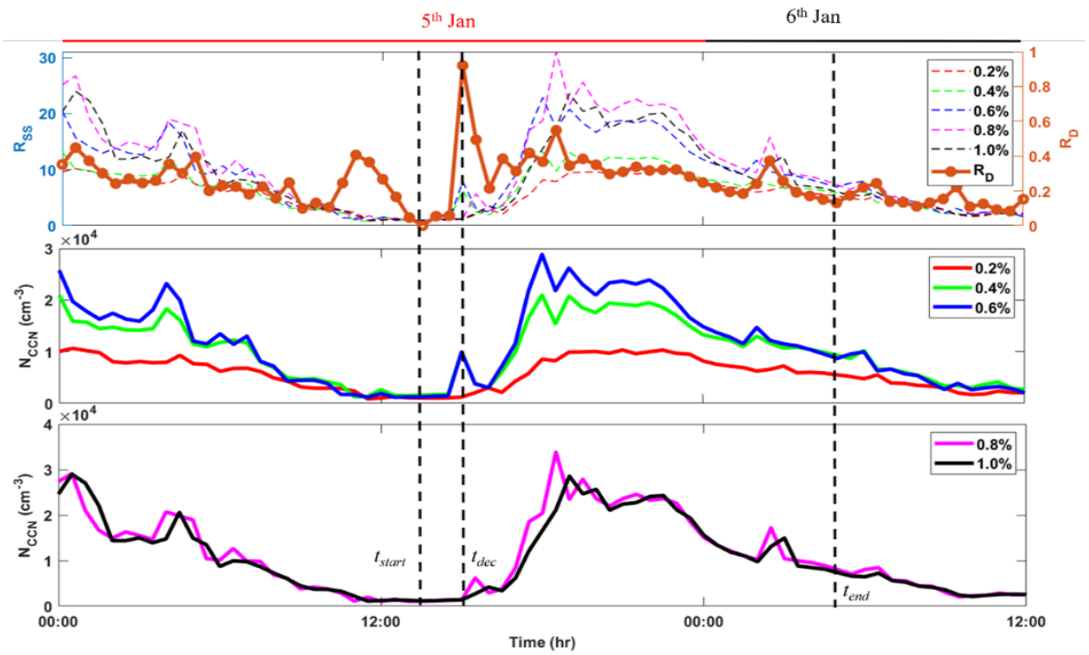


Figure 2: The time series of R_{SS}, N_{CCN} at different SS and R_D (orange) from 5th -7th January 2023. The black dotted lines are the NPF burst time (t_{start}), decoupling time (t_{dec}) and end time (t_{end}) respectively.

The time evolution of normalized N_{CCN} (denoted as R_{SS}) indicates a distinct diurnal variability, with similar values at all SS during daytime. It starts to disperse over a wide range of values (prior R_{SS} ranges from1.23±0.38 to 2.83±2.62, and after R_{SS} ranges from 7.23±2.14 to 15.20±7.06) at different SS, when the new particles are sufficient enough to influence CCNs at a given SS (Figure 2). The temporal evolution of the relative dispersion of R_{SS} among various SS can be estimated in terms of R_D which remains low during the initial stage of NPF event. Its value remains low at the initial stage of NPF and rapidly increases to a value of 0.96 at 15:00 hr on 5th January 2023, indicating a larger spread in R_{SS} resulting from supersaturation of particles formed due to NPF. This is associated with the fact that the newly formed particles are activated to become CCN at a higher SS, leading to the dispersion in R_{SS}. R_D is not only important to find $t_{dec,}$ but also fixes the t_{end} (the influence of NPF on CCN) when its value drops to initial lower values observed prior to t_{dec}, assuming that NPF impacts CCN at all SS evenly. The other R_D spikes in the spectrum can be associated with small-scale perturbation from local sources or residual particles from NPF events mixed with air masses. The average $N_{CCN_{prior,SS}}$ ($N_{CCN_{after,SS}}$) at the supersaturations 0.2, 0.4, 0.6, 0.8, 1% are found to be 1578.40, 3666.17, 3489.74, 2338.88, 2021.5 cm^{-3} (7662.48, 14351.70, 16850.50, 16702.09, 15650.16 cm^{-3}) respectively. This has resulted in an NPF-induced CCN enhancement factor of (E_N_{CCN}) 4.80, 3.91, 4.82, 7.14, 7.74 at respective supersaturations. Overall, the mean E_N_{CCN} in the present study is found to be 4.25±1.65 for all four NPFs at 0.2-1% SS. However, NPF is a phenomenon characterized by spatial and temporal heterogeneities, driven by variations in precursor gases, meteorological conditions, regional pollution levels, and the chemical composition of these particles, which further complicates the actual estimation of NPF-induced CCN. Thus, a long-term state-of-the-art measurement is required to investigate the aerosol-CCN interaction in depth.

ACKNOWLEDGEMENTS

This work falls under the project objectives of the Indian Space Research Organization's Aerosol Radiative Forcing NETwork (ARFINET) under its Geosphere-Biosphere Programme. This is a collaborative effort between Dibrugarh University and the North-Eastern Space Application Centre, Shillong to share the instruments.

REFERENCES

Albrecht, B. A. (1989). Aerosols, cloud microphysics, and fractional cloudiness. *Science*, **245**(4923). https://doi.org/10.1126/science.245.4923.1227

Asmi, E., et al. (2011). Secondary new particle formation in Northern Finland (2000–2010). *Atmos. Chem. Phys.*, **11**(24), 12959–12972. https://doi.org/10.5194/acp-11-12959-2011

Calvin, K., Dasgupta, D., Krinner, G., et al. (2023). *IPCC Climate Change 2023: Synthesis Report*. Intergovernmental Panel on Climate Change (IPCC). https://doi.org/10.59327/IPCC/AR6-9789291691647

Dal Maso, M., Kulmala, M., Riipinen, I., et al. (2005). Formation and growth of fresh atmospheric aerosols. *Boreal Environ. Res.*, **10**, 323–336.

Dameto De España, C., Wonaschütz, A., Steiner, G., et al. (2017). Long-term study of NPF as a source of CCN in Vienna. *Atmos. Environ.*, **164**, 289–298. https://doi.org/10.1016/j.atmosenv.2017.06.001

Gordon, H., Kirkby, J., Baltensperger, U., et al. (2017). Causes and importance of NPF in present-day and preindustrial atmospheres. *J. Geophys. Res. Atmos.*, **122**(16), 8739–8760. https://doi.org/10.1002/2017JD026844

Kalkavouras, P., Bougiatioti, A., Kalivitis, N., et al. (2019). Regional NPF and CCN modulation in the eastern Mediterranean. *Atmos. Chem. Phys.*, **19**(9). https://doi.org/10.5194/acp-19-6185-2019

Kanawade, V. P., Sebastian, M., Hooda, R. K., et al. (2022). NPF in India: Current understanding and gaps. *Atmos. Environ.*, **270**, 118894. https://doi.org/10.1016/j.atmosenv.2021.118894

Kerminen, V.-M., et al. (2012). Cloud condensation nuclei production associated with atmospheric nucleation: A synthesis based on existing literature and new results. *Atmospheric Chemistry and Physics*, **12**(24). https://doi.org/10.5194/acp-12-12037-2012

Kuang, C., McMurry, P. H., & McCormick, A. V. (2009). Determination of CCN production from NPF events. *Geophys. Res. Lett.*, **36**(9). https://doi.org/10.1029/2009GL037584

Kulmala, M., Petäjä, T., Nieminen, T., et al. (2012). Measurement of atmospheric nucleation. *Nat. Protoc.*, **7**(9). https://doi.org/10.1038/nprot.2012.091

Kulmala, M., Riipinen, I., Sipilä, M., et al. (2007). Toward direct measurement of atmospheric nucleation. *Science*, **318**(5847). https://doi.org/10.1126/science.1144124

Laakso, L., Merikanto, J., Vakkari, V., et al. (2013). Boundary layer nucleation as a source of CCN. *Atmos. Chem. Phys.*, **13**(4), 1957–1972. https://doi.org/10.5194/acp-13-1957-2013

Pierce, J. R., & Adams, P. J. (2009). Can cosmic rays affect CCN via NPF? *Geophys. Res. Lett.*, **36**(9). https://doi.org/10.1029/2009GL037946

Ren, J., Chen, L., Fan, T., et al. (2021). The NPF effect on CCN concentrations: A review. *Geophys. Res. Lett.*, **48**(19). https://doi.org/10.1029/2021GL095190

Sebastian, M., Kompalli, S. K., Kumar, V. A., et al. (2022). NPF observations at six Indian locations. *Atmos. Chem. Phys.*, **22**(7), 4491–4508. https://doi.org/10.5194/acp-22-4491-2022

Spracklen, D. V., Carslaw, K. S., Kulmala, M., et al. (2008). Contribution of NPF to global CCN concentrations. *Geophys. Res. Lett.*, **35**(6). https://doi.org/10.1029/2007GL033038

Twomey, S. (1977). The influence of pollution on cloud albedo. *J. Atmos. Sci.*, **34**(7), 1149–1152. https://doi.org/10.1175/1520-0469(1977)034<1149:TIOPOT>2.0.CO;2

Westervelt, D. M., Pierce, J. R., & Adams, P. J. (2014). Feedbacks between nucleation rate, survival probability, and CCN formation. *Atmos. Chem. Phys.*, **14**(11), 5577–5597. https://doi.org/10.5194/acp-14-5577-2014

Wu, Z. J., Ma, N., Größ, J., et al. (2017). Thermodynamic properties of nanoparticles during NPF in North China. *Atmos. Res.*, **188**, 55–63. https://doi.org/10.1016/j.atmosres.2017.01.007

Yu, F., & Luo, G. (2009). Simulation of particle size distribution and nucleation contribution to CCN. *Atmos. Chem. Phys.*, **9**(20). https://doi.org/10.5194/acp-9-7691-2009

Yue, D. L., Hu, M., Zhang, R. Y., et al. (2011). Potential contribution of NPF to CCN in Beijing. *Atmos. Environ.*, **45**(33), 6070–6077. https://doi.org/10.1016/j.atmosenv.2011.07.037

Zhang, F., Ren, J., Fan, T., et al. (2019). Enhanced CCN activity from nucleation-driven haze events in Beijing. *J. Geophys. Res. Atmos.*, **124**(24). https://doi.org/10.1029/2019JD031457

UNDERSTANDING THE INFLUENCE OF PARTICLE GROWTH ON AIR QUALITY AND LOCAL CLIMATE IN MEGACITY

W. DU[1,2,], Y.L. SUN[2], J. ZHAO[1], L. DADA[1,3], Y.Y. WANG[4], X.S. CHEN[2], Z.Q. LI[5], Y.J. ZHANG[6], F. Hu[2], T.V. KOKKONEN[1], V.M. KERMINEN[1], M. KULMALA[1,7,8]

[1]Institute for Atmospheric and Earth System Research / Physics, Faculty of Science, University of Helsinki, 00014, Finland.
[2]State Key Laboratory of Atmospheric Boundary Layer Physics and Atmospheric Chemistry, Institute of Atmospheric Physics, Chinese Academy of Sciences, Beijing 100029, China.
[3]Laboratory of Atmospheric Chemistry, Paul Scherrer Institute, Villigen, 5232, Switzerland.
[4]School of Atmospheric Physics, Nanjing University of Information Science and Technology, Nanjing 210044, China.
[5]Earth System Science Interdisciplinary Center and Department of Atmospheric and Oceanic Science, University of Maryland, College Park, MD, USA.
[6]School of Ecology and Nature Conservation, Beijing Forestry University, Beijing 100083, China.
[7]Joint International Research Laboratory of Atmospheric and Earth System Sciences, School of Atmospheric Sciences, Nanjing University, 210023 Nanjing, China.
[8]Aerosol and Haze Laboratory, Beijing Advanced Innovation Center for Soft Matter Science and Engineering, Beijing University of Chemical Technology, 100029 Beijing, China.

Keywords: New Particle Growth, Boundary Layer Dynamics, PM, CCN, Climate.

INTRODUCTION

New particle formation (NPF) is a process in which gaseous molecules in the atmosphere cluster together to form aerosol particles (Kulmala et al., 2013). These particles contribute significantly to the total number of aerosols in the atmosphere, further influencing air quality and climate (Kerminen et al., 2018). The environmental and climate effects of NPF largely depend on the particle growth (NPG) process; however, it remains poorly understood, especially in urban (Stolzenburg et al., 2023). In this study, we performed simultaneous measurements at the ground and at 260 m based on the 325 m meteorological tower in urban Beijing. By comparing the NPG process at the two heights, we provide new insights into the interactions between boundary layer dynamics and NPG in megacity (Du et al., 2021; Du et al., 2025).

METHODS

The sampling site is located at the tower branch of the Institute of Atmospheric Physics (IAP), Chinese Academy of Sciences (39°58′N, 116°22′E), in Beijing, China. A platform with various instruments at 260 m was built based on the Beijing 325 m meteorological tower to measure the chemical and physical characteristics of aerosol particles using Scanning Mobility Particle Sizer (SMPS, TSI) and Aerosol Chemical Speciation Monitor (ACSM, Aerodyne) above the roughness sublayer, while another set of instruments was deployed at the ground level. In addition, gaseous pollutants, including CO, SO2, and O3, were also recorded at both heights. Meteorological variables (e.g. wind speed (WS), wind direction (WD), relative humidity (RH), and temperature (T)) at 15 heights were also obtained from the meteorological tower observation system.

CONCLUSIONS

Our results show that although NPG occurred at both heights, significant differences of NPG between 260 m and the ground level were observed in megacity. When vertical diffusion is sufficient, gaseous precursors from the surface could be transported to higher altitudes. The lower temperature and higher relative humidity aloft promoted gas-to-particle conversion, leading to stronger particle growth at higher

altitudes. As a result, higher particle concentrations accompanied by stronger hygroscopicity led to >20% higher NPF-induced cloud condensation nuclei (CCN) formation aloft. However, when vertical mixing was suppressed, gaseous pollutants tended to accumulate near the surface. These pollutants then contributed to particle growth at ground level, exacerbating atmospheric haze pollution near ground. This, in turn, further reduced the boundary layer height. The valuable results provided novel information of the interactions between boundary layer dynamics and new particle growth, enhancing our understanding on the climate and environmental effects of NPF.

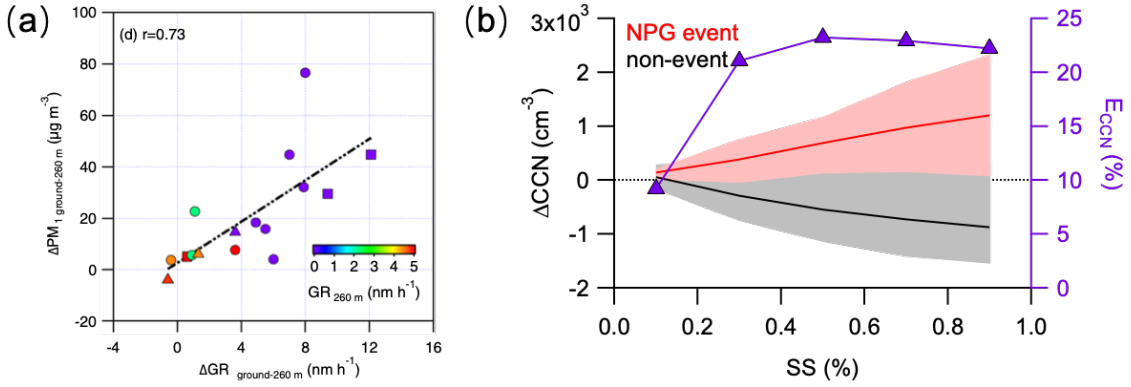


Figure 1. (a) The differences in PM1 between the ground and 260 m ($\Delta PM_{1\ ground-260\ m}$) versus the differences in GR between the two heights ($\Delta GR_{ground-260\ m}$) when vertical mixing is suppressed. (b) The differences in CCN concentrations between two heights (ΔCCN = CCN260 m – CCNground) and the changes of CCN due to enhanced NPG at 260 m (ECCN) when vertical diffusion is sufficient.

ACKNOWLEDGEMENTS

This work is supported by Wihuri Foundation, National Natural Science Foundation of China (92044301), and ACCC Flagship funded by the Academy of Finland (337549).

REFERENCES

Du Wei, Dada Lubna, Zhao Jian, Chen Xueshun, Daellenbach Kaspar R., Xie Conghui, Wang Weigang, He Yao, Cai Jing, Yao Lei, Zhang Yingjie, Wang Qingqing, Xu Weiqi, Wang Yuying, Tang Guiqian, Cheng Xueling, Kokkonen Tom V., Zhou Wei, Yan Chao, Chu Biwu, Zha Qiaozhi, Hakala Simo, Kurppa Mona, Järvi Leena, Liu Yongchun, Li Zhanqing, Ge Maofa, Fu Pingqing, Nie Wei, Bianchi Federico, Petäjä Tuukka, Paasonen Pauli, Wang Zifa, Worsnop Douglas R., Kerminen Veli-Matti, Kulmala Markku, and Sun Yele: A 3D study on the amplification of regional haze and particle growth by local emissions, npj Climate and Atmospheric Science, 4, 1-8, 10.1038/s41612-020-00156-5, 2021.

Du Wei, Zhao Jian, Dada Lubna, Xu Weiqi, Wang Yuying, Shi Yu, Chen Xueshun, Kokkonen Tom V., Cai Jing, Zhang Yingjie, Wang Qingqing, Cai Runlong, Zha Qiaozhi, Zhou Libo, Li Zhanqing, Yu Fangqun, Fu Pingqing, Hu Fei, Wang Zifa, Worsnop Douglas R., Bianchi Federico, Kerminen Veli-Matti, Kulmala Markku, and Sun Yele: Impacts of enhanced new-particle growth events above urban roughness sublayer on cloud condensation nuclei, One Earth, 8, 10.1016/j.oneear.2024.12.005, 2025.

Kerminen Veli-Matti, Chen Xuemeng, Vakkari Ville, Petäjä Tuukka, Kulmala Markku, and Bianchi Federico: Atmospheric new particle formation and growth: review of field observations, Environmental Research Letters, 13, 103003, 10.1088/1748-9326/aadf3c, 2018.

Kulmala M., Kontkanen J., Junninen H., Lehtipalo K., Manninen H. E., Nieminen T., Petaja T., Sipila M., Schobesberger S., Rantala P., Franchin A., Jokinen T., Jarvinen E., Aijala M., Kangasluoma J., Hakala J., Aalto P. P., Paasonen P., Mikkila J., Vanhanen J., Aalto J., Hakola H., Makkonen U., Ruuskanen T., Mauldin R. L., Duplissy J., Vehkamaki H., Back J., Kortelainen A., Riipinen I., Kurten T., Johnston M. V., Smith J. N., Ehn M., Mentel T. F., Lehtinen K. E. J., Laaksonen A., Kerminen V. M., and Worsnop D. R.: Direct Observations of Atmospheric Aerosol Nucleation, Science, 339, 943-946, 10.1126/science.1227385, 2013.

Stolzenburg Dominik, Cai Runlong, Blichner Sara M., Kontkanen Jenni, Zhou Putian, Makkonen Risto, Kerminen Veli-Matti, Kulmala Markku, Riipinen Ilona, and Kangasluoma Juha: Atmospheric nanoparticle growth, Reviews of Modern Physics, 95, 10.1103/RevModPhys.95.045002, 2023.

SHIP EMISSION PROFILES FROM AMBIENT MEASUREMENTS IN DUBLIN PORT AND WHAT WE ARE MISSING

K.N. FOSSUM[1], C. LIN[1,2,3], N. O'SULLIVAN[4], L. LEI[1], S. HELLEBUST[4], D. CEBURNIS[1], A. AFZAL[1,5], A. TREMPER[6], D. GREEN[6,7], S. JAIN[4], S. BYČENKIENĖ[8], C. O'DOWD[1], J. WENGER[4] and J. OVADNEVAITE[1]

[1]*School of Natural Sciences, Ryan Institute's Centre for Climate & Air Pollution Studies, University of Galway, Galway, Ireland.*

[2]*State Key Laboratory of Loess and Quaternary Geology and Key Laboratory of Aerosol Chemistry and Physics, Chinese Academy of Sciences, Xi'an, China.*

[3]*Department of Civil and Environmental Engineering, the Hong Kong Polytechnic University, Hong Kong, China.*

[4]*School of Chemistry and Environmental Research Institute, University College Cork, Cork, Ireland.*

[6]*MRC Centre for Environment and Health, Environmental Research Group, Imperial College London, UK.*

[7]*NIHR HPRU in Environmental Exposures and Health, Imperial College London, UK.*

[8]*SRI Center for Physical Sciences and Technology, Lithuania.*

Keywords: AIR QUALITY, SHIP EMISSIONS, SOURCE APPORTIONMENT, SHIP PROFILES

INTRODUCTION

Shipping traffic is set to expand worldwide, increasing pollution in port areas and potentially leading to poorer air quality. Simultaneously, the International Maritime Organization (IMO) has been radically reducing the sulfur content allowed in marine fuel (IMO 2020) in order to improve human health and reduce negative ecosystem impacts from sulfur oxide emissions from commercial shipping. Therefore, the emissions profiles of commercial ships are changing and new studies are needed to quantify and trace these ship emissions from new alternate marine fuels.

A research project, Source Apportionment of Air Pollution in the Dublin Port Area (PortAIR), was initiated to measure the aerosol physical and chemical properties in the port area and assess the impact of Dublin Port activities on air quality (see Figure 1 for site location).

METHODS

Here we present results from a 1-month period from the PortAIR project in winter, when air quality was affected both by burning of domestic solid fuels in the city and by peak port activity from goods importation. This study focuses on the analysis of aerosol chemical speciation monitor (ACSM) data using combined organic and sulfate ion positive matrix factorization (PMF). The comprehensive range of instruments deployed at the monitoring site allowed characterization of individual ship plumes and classification according to type of fuel used.

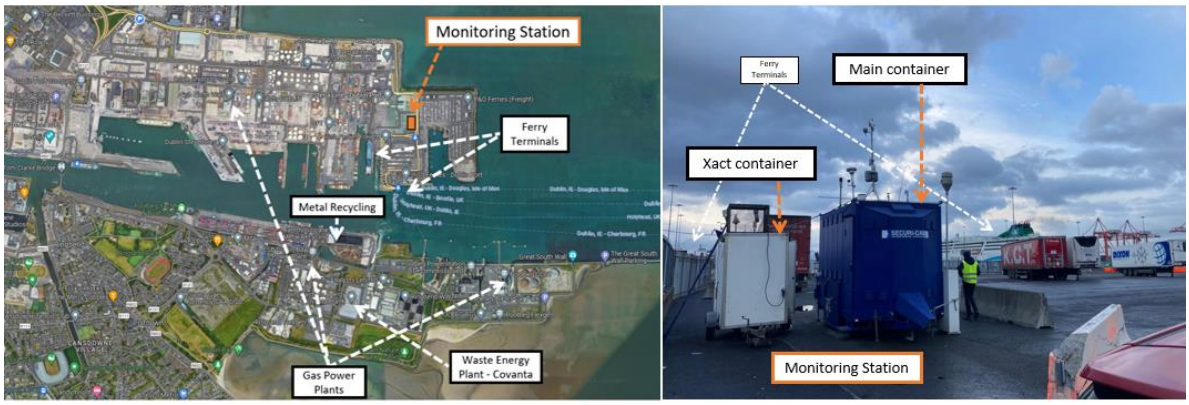


Figure 1. (left) Overview map of Dublin Port (satellite image credit: Imagery ©2024 Airbus, Landsat/Copernicus, Maxar Technologies, Map data ©2024 Google) with the Monitoring Station location (orange box). (right) an image of the main container with the Xact container in-situ (bottom).

CONCLUSIONS

Three types of ship fuel emissions were identified: sulfate-rich (S-Ship), organic-rich (O-Ship), and Marine Gas Oil (MGO). The S-Ship emissions were from heavy fuel oil use and are characterized by particles with classic V/Ni ratios from 2.7-3.9 and a large fraction of acidic sulfate aerosol. The O-Ship emissions were attributed to low-sulfur fuel types and were comprised mostly of organic aerosol (OA) with the V/Ni ratios ranging only from 0-2.3 (Table 1). MGO ship emissions were not resolved by PMF, due to sampling limitations of the ACSM, but were characterized by large numbers (e.g. 6 × 104 cm^{-3}) of particles of small sizes with diameters less than 50 nm (Figure 2).

	Plume number	Plume number $PM_1 \geq 50$	PM_1 ($\mu g/m^3$)	N ($/cm^3$)	NO_x ($\mu g/m^3$)	SO_2 ($\mu g/m^3$)	eBC ($\mu g/m^3$)	V/Ni	V ($\mu g/m^3$)	Ni ($\mu g/m^3$)
S-Ship	58	10	29 ± 22	(1.52 ± 1.55) × 10^4	117.6 ±118.0	3.5 ±3.4	1.8 ±1.4	3.41 ±0.28	0.21 ±0.15	0.060 ±0.042
			21	21.09 × 10^4	83	2.4	1.3	3.47	0.17	0.050
O-Ship	190	33	32 ± 26	(3.75 ± 2.28) × 10^4	132.3 ±108.7	3.9 ±3.2	3.0 ±1.8	0.74 ±0.35	(7 ± 6) × 10^{-3}	(8 ± 7) × 10^{-3}
			25	3.20 × 10^4	97	3.0	2.7	0.71	5 × 10^{-3}	7 × 10^{-3}

Table 1. Mean characteristics of ship plumes associated with S-Ship (58 plumes) and O-Ship (190 plumes) source apportioned factors. Median values in blue.

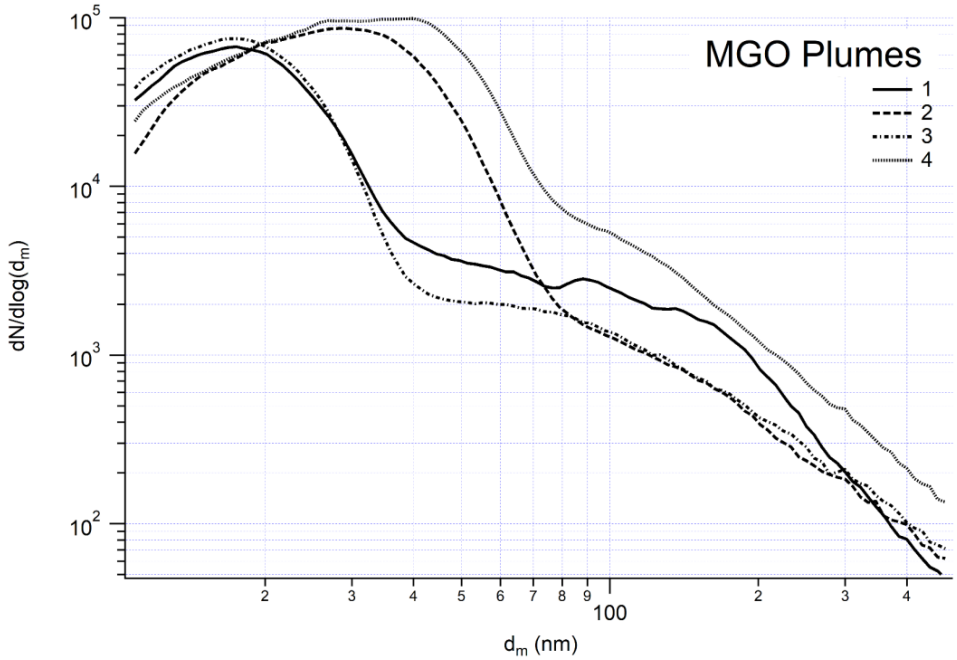


Figure 2. Averaged number-size distributions of particles observed from MGO emissions during four hoteling periods. Data is shown as the lognormal particle concentration ($dN/dlog(d_m)$) *vs* dry electrical mobility diameter (d_m) in nm.

Overall, ship plumes were observed having PM_1 concentrations from 4-252 µg m-3, with extreme concentrations usually lasting for 5-35 minutes. Despite their short duration, shipping emission plumes were frequent and contributed to at least 28%-47% of PM_1. Moreover, MGO could not be represented by the scientific and regulatory mass measurements, but ships using this type of fuel make up a significant portion of vessel traffic at Dublin Port. Therefore, future studies on air quality in will need to capture MGO emissions and other alternative fuels, as there are potentially serious implications for particle transport, toxicity, and climate forcing with emissions of large concentrations of tiny particles.

ACKNOWLEDGEMENTS

This work was funded by the Irish Environmental Protection Agency (EPA) under grant number: 2020-CCRP-LS.6, AC3/AEROSOURCE project, supported by EPA-Ireland and the Department of Environment, Climate and Communications, and Taighde Éireann – Research Ireland (22/FFP-A/10611).

SECONDARY ORGANIC AEROSOL FORMATION FROM ISOPRENE AND TOLUENE MIXTURE

Z. LI[1], S. HAN[2,4], Y. LAU[1], Y. XIAO[2,4], B. MILJEVIC[1], J. HORCHLER[1], W-P. HU[3], H. WANG[2,4], B. WANG[2,4] and Z. RISTOVSKI[1,4]

[1]*School of Earth and Atmospheric Sciences, Queensland University of Technology, Brisbane 4000, Australia*
[2]*Institute for Environmental and Climate Research, Jinan University, Guangzhou 510632, China*
[3]*Central Analytical Research Facility (CARF), Queensland University of Technology, Brisbane, QLD 4001, Australia*
[4]*JNU-QUT Joint Laboratory for Air Quality Science and Management, Jinan University, Guangzhou 510632, China*

Keywords: SECONDAR ORGANIC AEROSOL, ISOPRENE, TOLUENE, CHAMBER EXPERIMENTS.

INTRODUCTION

Anthropogenic and biogenic emission sources release a wide variety of volatile organic compounds (VOCs) into the atmosphere. They undergo a series of oxidation reactions with atmospheric oxidants (i.e., O_3, OH•, NO_3•) and form a complex matrix of products with ranges of functionalities and volatilities. Oxidation products with sufficiently low volatilities can form secondary organic aerosol (SOA) particles. During the atmospheric oxidation, oxidant products can potentially interact with each other, altering the reaction pathways and thus the formation of SOA.

Most previous experiments focused on the SOA yields from a single VOC precursor. (Kroll et al., 2006; Ng et al., 2006) Recently, increasing attention has been given to the SOA yields from binary or even ternary VOC mixtures. (Mcfiggans et al., 2019; Voliotis et al., 2022; Liu et al., 2024) Consistently, they observe complex, non-linear effects of VOC mixtures on SOA formation and the formation of cross-products. The interaction between anthropogenic and biogenic emissions can potentially impact the environment and the climate. However, knowledge regarding the formation of SOA from VOC mixtures remains unclear. In this study, we conducted a series of photooxidation experiments using two representative anthropogenic and biogenic VOCs, toluene and isoprene. Using a suite of real-time gas and particle instruments, we aim to provide insights into how SOA from isoprene and toluene oxidation products evolve during the different stages of SOA formation.

METHODS

An 8 m³ Teflon chamber was used for photooxidation experiments under low NOx conditions and 40% relative humidity. To obtain results of atmospheric relevance, we used several tens of ppb of VOCs and ~ 5,000 cm^{-3} of polydisperse ammonium sulfate (AS) or ammonium bisulfate (ABS) seed particles for each experiment. H_2O_2 was used as the source to generate OH•. Each photooxidation experiment lasted for four hours with all UV lights on. A suite of real-time instruments was used to measure gas vapours and aerosol particles simultaneously, including a chemical ionisation mass spectrometer (CIMS), an aerosol mass spectrometer (AMS), and a scanning electrical mobility spectrometer (SEMS). To resolve the complex SOA data collected by AMS, we deployed positive matrix factorisation (PMF) to deconvolute the SOA mass spectra at unit mass resolution.

CONCLUSIONS

In the mixture experiments, we observed SOA yields of approximately 10%, which falls between the yields of isoprene and toluene SOA (Figure 1). We conducted PMF to deconvolute the SOA mass spectra and identified five SOA factors, namely F-ISO-1, F-ISO-2, F-TOL-1, F-TOL-2, and F-MIX. F-ISO-1 and F-ISO-2 primarily occurred in experiments containing isoprene. The same case was applied for F-TOL-1 and F-TOL-2 when the experiments contained toluene. In addition to these four factors, a unique factor, F-MIX, was only present in experiments that contained both isoprene and toluene. A handful of gas-phase oxidised vapours showed many and even good similarities with the time series of F-MIX. This evidence indirectly suggests the presence of cross-interactions between isoprene and toluene oxidation products during SOA formation.

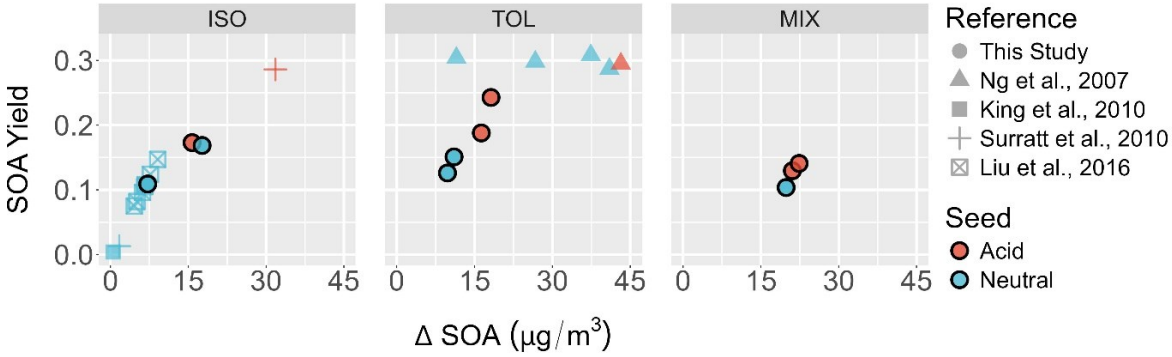


Figure 1. SOA yields as a function of SOA formation at isoprene, toluene and mixture systems in different seeds. SOA was corrected by wall loss, and the density of SOA particles is 1.4 g/cm^3.

ACKNOWLEDGEMENTS

The work was supported by the QUT Early Career Research Scheme, the National Key R&D Program of China (2023YFC3709201), the Natural Science Foundation of China (42121004, 42477100), and the Science and Technology Project of Guangdong Province of China (2024B1212040006).

REFERENCES

Kroll, J. H., Ng, N. L., Murphy, S. M., et al., (2006), *Environmental science & technology*, 40, 1869-1877.
Liu, S., Galeazzo, T., Valorso, R., et al., (2024), *Environmental Science & Technology*, 58, 13391-13401.
McFiggans, G., Mentel, T. F., Wildt, J., et al., (2019), *Nature*, 565, 587-593.
Ng, N. L., Kroll, J. H., Keywood, M. D., et al., (2006), *Environmental science & technology*, 40, 2283-2297.
Voliotis, A., Du, M., Wang, Y., et al., (2022), *Atmos Chem Phys*, 22, 14147-14175.

METEOROLOGY-INDUCED NEW PARTICLE FORMATION DURING WINTER OVER INDIA

Bala Naga Manikanta Meda[1], Chandan Sarangi[1], Vijay P. Kanawade[2,3], Mathew Sebastian[1,2], Oishi Chakraborty[2], Rakesh K. Hooda[4], Antti-P. Hyvärinen[4], Poul Cherian[1,2], and Tuija Jokinen[3]

[1]*Indian Institute of Technology Madras, Chennai, India 600036*
[2]*Centre for Earth, Ocean and Atmospheric Sciences, University of Hyderabad, India.*
[3]*Climate and Atmospheric Research Centre, Cyprus Institute, Nicosia, Cyprus*
[4]*Finnish Meteorological Institute, Helsinki, Finland.*

Keywords: New particle formation, High pressure system, Atmospheric stability, urban environments, WRF-Chem

INTRODUCTION

New Particle Formation events (NPFEs) are observed across a range of atmospheric environments but occur most frequently within the planetary boundary layer (PBL) (Andreae et al., 2022; Deot et al., 2025; Kanawade et al., 2021; Kerminen et al., 2018; Kulmala et al., 2004). Their occurrence is governed by several factors, including the availability of precursor vapors, background aerosol number concentrations, meteorological conditions, and large-scale atmospheric circulation patterns. Further, interactions of the airmass transport pathways and boundary layer dynamics, which drive the exchange of energy, moisture, precursor vapor concentration and aerosols, can modulate the occurrence of NPF events (Benson et al., 2008; Dada et al., 2022; Rose et al., 2015; Sogacheva et al., 2007). Clear-sky conditions associated with high solar radiation (high photochemical reactions) and elevated boundary layer (low condensation sink for nucleating vapors) lead to the frequent occurrence of NPF events during spring or summer. However, NPF events are generally inhibited in winter due to weaker photochemistry and shallow boundary layer height, particularly in urban areas (Boy and Kulmala, 2002). On the contrary, a recent study showed that NPFEs can occur frequently in the Hyderabad urban metropolitan during dry winter (Sebastian et al., 2022). Using ground-based particle number size distribution observations and high-resolution Weather Research and Forecasting model coupled with Chemistry (WRF-Chem) simulations, we show that NPF events over Hyderabad during winter are closely linked to cyclonic wind patterns and associated high pressure systems. Here, we provide a mechanistic understanding of NPF occurrence under the influence of high pressure system accompanied by regional scale subsidence.

METHODS

The particle number size distribution (particle diameter of 10 - 600 nm) measurements were carried out at the Earth Sciences building in the University of Hyderabad campus (17.46°N, 78.32°E, 542 m above mean sea level) during 2019-2022. The measurement site is surrounded by thin forested vegetation in a radius of 1 km, except for a few academic buildings. The three-day air mass backward trajectories starting at 500 m above the ground level starting at 11:30 a.m. local time (6 UTC) were calculated from the NOAA ARL PC-version Hybrid Single-Particle Lagrangian Integrated Trajectory (HYSPLIT) transport and dispersion model using gridded wind fields from the Global Data Assimilation System (GDAS), which has a spatial resolution of 1° × 1° longitude by latitude and a time resolution of 1 hr (Draxler & Rolph, 2010) to demonstrate the influence of long-range transported air masses at the site. Along with this, we have utilized the second Modern-Era Retrospective analysis for Research and Applications (MERRA-2) reanalysis product to investigate the dynamics of the atmosphere. To illustrate the underlying mechanistic processes, we have conducted high resolution Chemistry coupled

WRF simulations. We have used the CBMZ chemical mechanism and MOSAIC with 8 sectional aerosol bins for the simulation. Community Atmosphere Model coupled with Chemistry (CAM-Chem) global simulation output at horizontal resolution 1.9° × 1.25° and 56 vertical pressure levels at a time resolution of 6 hours are provided as initial and boundary conditions (Emmons et al., 2020). The anthropogenic emission inventory at 0.1° resolution from the Emission Database for Global Atmospheric Research for Hemispheric Transport of Air Pollution (EDGAR-HTAP v5) (Crippa et al., 2020) and biogenic emission inventory from the Model of Emissions of Gases and Aerosols from Nature (MEGAN) inventory (Guenther et al., 2012) were used.

RESULTS AND CONCLUSIONS

The observation days were classified into three classes, namely NPF events, non-events and undefined days. Despite high aerosol loading and shallow boundary layer conditions in winter, NPF occurred commonly during the dry winter season (November through February, NDJF) in Hyderabad. To address this, we first calculated the airmass backward trajectories using the HYSPLIT model. Fig. 1a shows 3-day airmass trajectories on NPFE and non-events days, indicating that the occurrence of NPF events is not airmass origin dependent. The time-altitude cross-section of air masses showed that the history of airmass as it advected through the atmosphere decides the occurrence of NPFEs (Figs. 1b and 1c). A significant fraction of air mass trajectories on NPFEs intruded from the free troposphere into the boundary layer, facilitating a vertical turbulent mixing of gases and aerosols in the vicinity of the measurement site, referred to as free tropospheric NPF events ($NPFEs_{FT}$) NPF still occurred within the boundary layer ($NPFEs_{PBL}$) although we only focus on $NFPEs_{FT}$, which constitutes about 60% of the total NPFEs during this period. A well developed high pressure system is observed during $NPFEs_{FT}$ (Fig. 1c), as indicated by the anomaly of the mean sea level pressure. Fig. 1d shows the anomaly of the mean sea level pressure during $NPFE_{PBL}$ along with quivers which show variation in wind circulation at the surface. High-pressure systems and associated subsiding air masses have been linked to enhanced NPFEs and mixing processes that can promote particle formation and growth (Pierce et al., 2014; Shen et al., 2018).

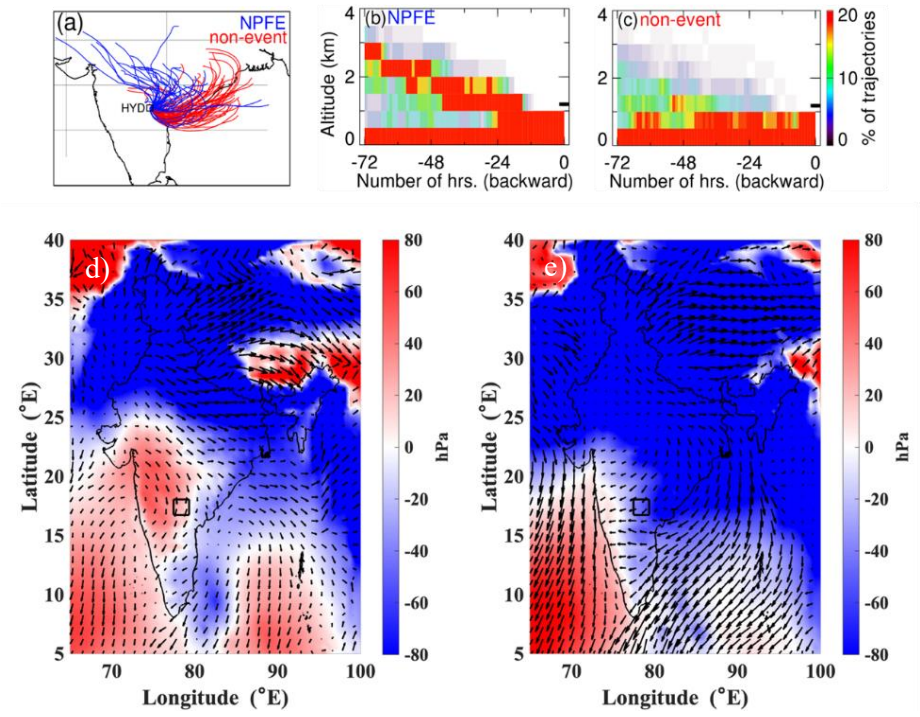


Fig 1. (a) Three-days airmass backward trajectories starting at 500 m above the ground at 11:30 am local time (6 UTC) during the dry winter season for NPFEs (blue lines) and non-events (red lines). The measurement site is shown by the open square box. Percentage occurrence of air mass trajectory altitude as a function of backward time for observed (b) NPFEs and (c) non-events. Mean sea level pressure anomaly with quiver for (d) $NPFEs_{FT}$ and (e) $NPFEs_{PBL}$

We have conducted WRF–Chem simulations over one week period (10 – 16 February 2020) during which 13 – 15 Feb represents three consecutive $NPFEs_{FT}$, to elucidate meteorological and chemical pathways during NPFE days. Simulation results reveal the anamalously high sulfur dioxide (SO_2) concentrations up to an altitude of 2-3 km along the latitude bin 16 – 19 °E and between 75 and 85 °N longitudes (Fig. 2a), while less significant variations in SO_2 concentrations were observed during non-event days (Fig. 2b). The diurnal variation of SO_2 also show high concentration through the night up to morning 10 AM during $NPFEs_{FT}$ (Fig. 2c) along with strong subsidence during the same period (Fig. 2e) compared to non-event days (Figs. 2d and 2f). This reveals that entrainment of free tropospheric air into the boundary layer not only leads to saturated vapor concentrations but also reduces the condensation sink through vertical mixing. Sensitivity experiments will be conducted to illustrate the accumulation of gas/aerosol concentrations over the high pressure region.

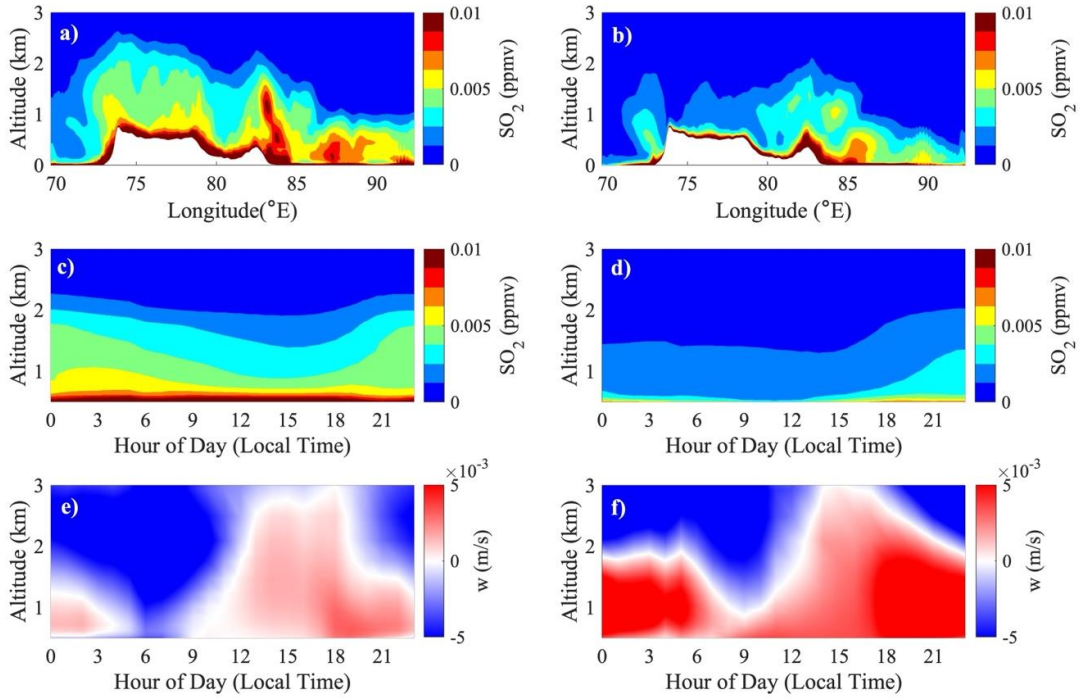


Fig. 2. Longitude-altitude cross-section of SO_2 averaged over latitude bins 16 – 19 °E for (a) $NPFEs_{FT}$ and (b) non-events. Diurnal variation of SO_2 for (c) $NPFEs_{FT}$ and (d) non-events. Diurnal variation of vertical velocity (W) for (e) $NPFEs_{FT}$ and (f) non-events.

REFERENCES

Andreae, M. O., T. W. Andreae, F. Ditas, and C. Pöhlker (2022), Frequent new particle formation at remote sites in the subboreal forest of North America, *Atmos. Chem. Phys.*, *22*(4), 2487-2505, doi:https://doi.org/10.5194/acp-22-2487-2022.

Benson, D. R., Y. Li-Hao, L. Shan-Hu, T. L. Campos, D. C. Rogers, and J. Jensen (2008), The effects of airmass history on new particle formation in the free troposphere: case studies, *Atmos. Chem. Phys.*, *8*(12), 3015-3024, doi:10.5194/acp-8-3015-2008.

Crippa, M., Solazzo, E., Huang, G., Guizzardi, D., Koffi, E., Muntean, M., et al. (2020). High-430 resolution temporal profiles in the Emissions Database for Global Atmospheric Research. 431 Scientific Data, 7(1), 121. https://doi.org/10.1038/s41597-020-0462-2

Dada, L., et al. (2022), A central arctic extreme aerosol event triggered by a warm air-mass intrusion, *Nature Communications*, *13*(1), 5290, doi:https://doi.org/10.1038/s41467-022-32872-2.

Deot, N., Kanawade, V. P., Papetta, A., Baalbaki, R., Pikridas, M., Marenco, F., Kulmala, M., Sciare, J., Lehtipalo, K., & Jokinen, T. (2025). Effect of planetary boundary layer evolution on new particle formation events over Cyprus. *Aerosol Research*, *3*(1), 139–154. https://doi.org/10.5194/ar-3-139-2025

Emmons, L. K., Schwantes, R. H., Orlando, J. J., Tyndall, G., Kinnison, D., Lamarque, J.-F., et 438 al. (2020). The Chemistry Mechanism in the Community Earth System Model Version 2 439 (CESM2). Journal of Advances in Modeling Earth Systems, 12(4), e2019MS001882. 440 https://doi.org/https://doi.org/10.1029/2019MS001882

Guenther, A. B., Jiang, X., Heald, C. L., Sakulyanontvittaya, T., Duhl, T., Emmons, L. K., & 458 Wang, X. (2012). The Model of Emissions of Gases and Aerosols from Nature version 2.1 459 (MEGAN2.1): an extended and updated framework for modeling biogenic emissions. 460 Geosci. Model Dev., 5(6), 1471–1492. https://doi.org/10.5194/gmd-5-1471-2012

Kanawade, V. P., M. Sebastian, R. K. Hooda, and A. P. Hyvärinen (2021), Atmospheric new particle formation in India: Current understanding, knowledge gaps and future directions, *Atmospheric Environment*, doi:https://doi.org/10.1016/j.atmosenv.2021.118894.

Kerminen, V. M., X. Chen, V. Vakkari, T. Petäjä, M. Kulmala, and F. Bianchi (2018), Atmospheric new particle formation and growth: review of field observations, *Environmental Research Letters*, *13*(10), 103003, doi:https://doi.org/10.1088/1748-9326/aadf3c.

Kulmala, M., et al. (2021), Is reducing new particle formation a plausible solution to mitigate particulate air pollution in Beijing and other Chinese megacities?, *Faraday Discussions*, *226*(0), 334-347, doi:10.1039/D0FD00078G.

Rose, C., et al. (2015), Frequent nucleation events at the high altitude station of Chacaltaya (5240 m a.s.l.), Bolivia, *Atmospheric Environment*, *102*, 18-29, doi:https://doi.org/10.1016/j.atmosenv.2014.11.015.

Sebastian, M., V. P. Kanawade, and J. R. Pierce (2021), Observation of sub-3nm particles and new particle formation at an urban location in India, *Atmospheric Environment*, *256*, 118460, doi:https://doi.org/10.1016/j.atmosenv.2021.118460.

Sogacheva, L., A. Hamed, M. C. Facchini, M. Kulmala, and A. Laaksonen (2007), Relation of air mass history to nucleation events in Po Valley, Italy, using back trajectories analysis, *Atmos. Chem. Phys.*, *7*(3), 839-853, doi:10.5194/acp-7-839-2007.

INVESTIGATING AIR IONS DURING SUMMER NEW PARTICLE FORMATION EVENTS IN BOLOGNA

C.A. OLIEWO[1,2], M. PAGLIONE[3], M. RINALDI[3], A. TRENTINI[4], G. GHERMANDI[1] and A. BIGI[1]

[1]*University of Modena and Reggio Emilia, Modena, Italy.*
[2]*Istituto Universitario di Studi Superiori IUSS Pavia, Pavia, Italy.*
[3]*Institute of Atmospheric Sciences and Climate, National Research Council of Italy, Bologna, Italy.*
[4]*ARPAE Emilia-Romagna, Regional Agency for Prevention, Environment and Energy, Bologna, Italy.*

Keywords: new particle formation, charged particles, summer, urban area.

INTRODUCTION

Ultrafine particles (UFP) are atmospheric aerosols with ~1-100 nm in diameter. Depending on their chemical composition, they can have adverse impact on health since they can be transported farther in the respiratory tract. Moreover, atmospheric aerosols, including UFP, affect the earth's radiative balance both directly, by scattering and absorbing light, and indirectly by aerosol-cloud interactions. Sources of UFP include direct emissions or complex gas compounds interactions (i.e. new particle formation (NPF) processes). Research has shown that NPF occurs frequently in the atmosphere and contributes majorly to the levels of UFP and cloud condensation nuclei (CCN).

Naturally charged particles (also referred to as air ions) can enhance the rate of nucleation since their electrostatic interaction with the condensing molecules reduces the free energy required to stabilize the small clusters. Additionally, nucleated condensation, which is also the primary pathway for CCN in the atmosphere, requires much lower supersaturation levels compared to homogeneous nucleation. Air ions specifically can facilitate the formation and growth of particles in the UFP range (Hinds, 1999). These mechanisms could potentially affect the occurrence and frequency of NPF events.

There have been studies to investigate the role of ions in NPF, whose results have been quite varied especially in urban environments (Rowell *et al*., 2024). We therefore aim to research this in an urban background site in Bologna, to potentially estimate the contribution of air ions to the local concentration of UFP through NPF.

METHODS

Bologna is the largest urban agglomeration in the Southern part of the Po valley. A Neutral cluster and Air Ion Spectrometer (NAIS, Airel OÜ, Estonia) was set up on a rooftop location, about 25 meters above the ground, in urban background conditions in Bologna at the premises of the Institute of Atmospheric Sciences and Climate, alongside a Scanning Mobility Particle Sizer (13-700 nm), regulatory monitors for NOx, Ozone, an Aethalometer AE33 for aerosol absorption and equivalent black carbon and a meteorological station. The solar radiation data representative of the urban area was provided by the Bologna weather monitoring station of the Regional Environmental Agency.

The measurements from the NAIS for the summer season (1st June to 31st August 2024) were applied for this analysis. Following the classification by Rowell *et al.* (2024), the positively and negatively charged ions were further divided, based on the electrical mobility diameter, into small (1.1-1.9nm), intermediate (1.9-7.8nm), and large (7.8-22.3nm).

The NPF events were identified following the outline by Dal Maso *et al.* (2005). We further analyzed the behavior of the different sizes of ions depending on the NPF occurrence. The analysis of the

meteorological variables and pollutants measured at the site were also included to try and explain the results.

RESULTS

	Small		Intermediate		Large	
	-ve	+ve	-ve	+ve	-ve	+ve
Mean	132.8	232.9	61.2	41.9	548.2	254.4
Median	112.6	231.5	32.8	21.5	212.7	176.7
Min-Max	6.9-3576.4	11.9-2134.4	3.2-12032.5	0-3993	12-40821.1	0.6-3142.8

Table I. Statistical summary of total charged particle number concentrations per cm^3.

Negative air ions had larger concentrations than positive ones for the Intermediate and Large size range. For the large range, the negative ions mean total concentration of 548 cm^{-3} was about twice that of the positive ions (254 cm^{-3}). The mean total number concentrations for the positive ions were 1.7 times higher than the negative ions only for the 'small' range (232 cm^{-3} and 132 cm^{-3} respectively). This could be attributed to the electrode effect and the factor is not so big since the measurement site is on a rooftop.

Diurnal plots of the total number concentrations had the small ions peak in the early hours of the day, reduce around midday and increase again towards the end of the day. This could be explained by their main source being radioactive gases from the ground which are diluted when the boundary layer expands after sunrise. The intermediate and large air ions on the other hand peak in the mid morning hours probably due to photochemical reactions that drive NPF and growth, and have another peak in the late afternoon.

Of the 92-day period, we identified 33 NPF event days, 22 undefined and 37 non-event days. This translated to about 35% frequency of NPF events. Figure I below highlights the total number concentrations of positive air ions and how the 3 size ranges vary for the different classifications. The negative ions also exhibited a similar trend with the large ions on the non-event days dominating the number concentrations. The intermediate and large ions record spikes after midday more pronounced and spread during the undefined and non-event days.

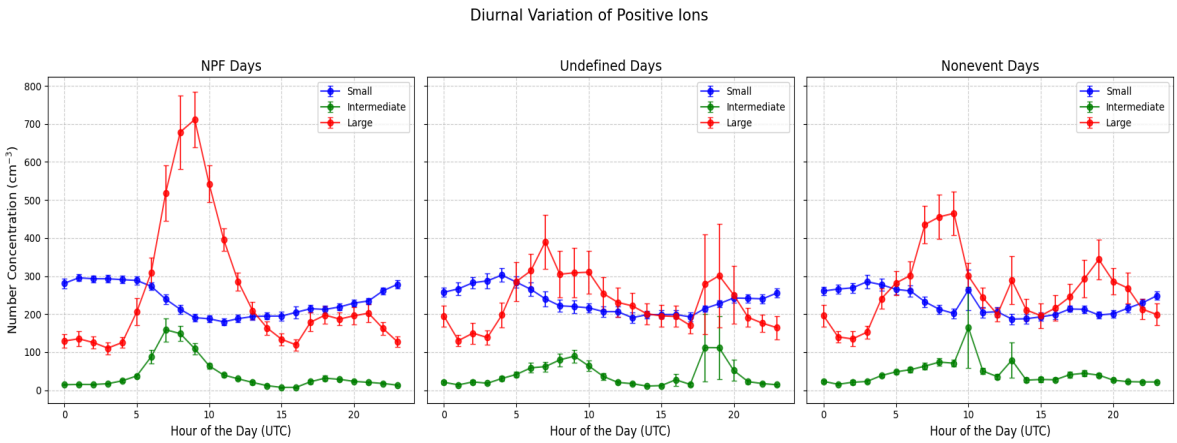


Figure I. Diurnal variation of mean total number concentrations with standard error of the mean.

During the NPF days, the steady decrease in the small ions total number concentration, which could be indicate ion-induced nucleation, coincides with the steady increase in total charged particle number concentration from around 0500 to 0700 UTC for intermediate and 0900 UTC for large air ions coincides

with the peaking time period for solar radiation (0800 to 1300 UTC) which could be due to enhanced ionization from cosmic rays and ion cluster stabilization. Additionally, the large ions on the NPF days illustrate a defined and high peak compared to the 2 other categories.

The gradual decrease after 0900 UTC, corresponding to the gradual increase in total number concentration for neutral particles of range greater than the large air ions, suggests ion induced condensation and growth or coagulation. The neutral particles' total number concentrations peaked at about 1100 UTC, followed by a gradual drop.

The diurnal variation of relative humidity (RH) followed the same pattern for all the days, with a peak in the early morning and a trough around midday. The NPF event days recorded the lowest mean RH values throughout the day. This is in line with previous studies, which found that lower RH promotes gas to particle conversion.

Interestingly, the condensation sink (CS) diurnal variation exhibited the lowest values in the early morning across the 3 categories of days, followed by an increase from 0500 UTC and a decrease again from 1000 UTC. NPF event days record a very sharp increase in CS from 0500 UTC peaking at 0900 UTC, while having the lowest values across the 3 categories till 0600 UTC. On NPF event days, no sharp increase is observed in the diurnal plots for NOx and black carbon during these hours, which could suggest that the ions produced by increased ionization as the solar radiation peaks contribute to the increase in CS.

On the other hand, the fast decrease from around 1000 UTC coincides with the growth of neutral particles recorded during the NPF event days. Furthermore, Pearson's linear correlation coefficients (Figure II) also show the relationship between CS and the total number concentration for small (both polarity) and large (both polarity) air ions is large and statistically significant.

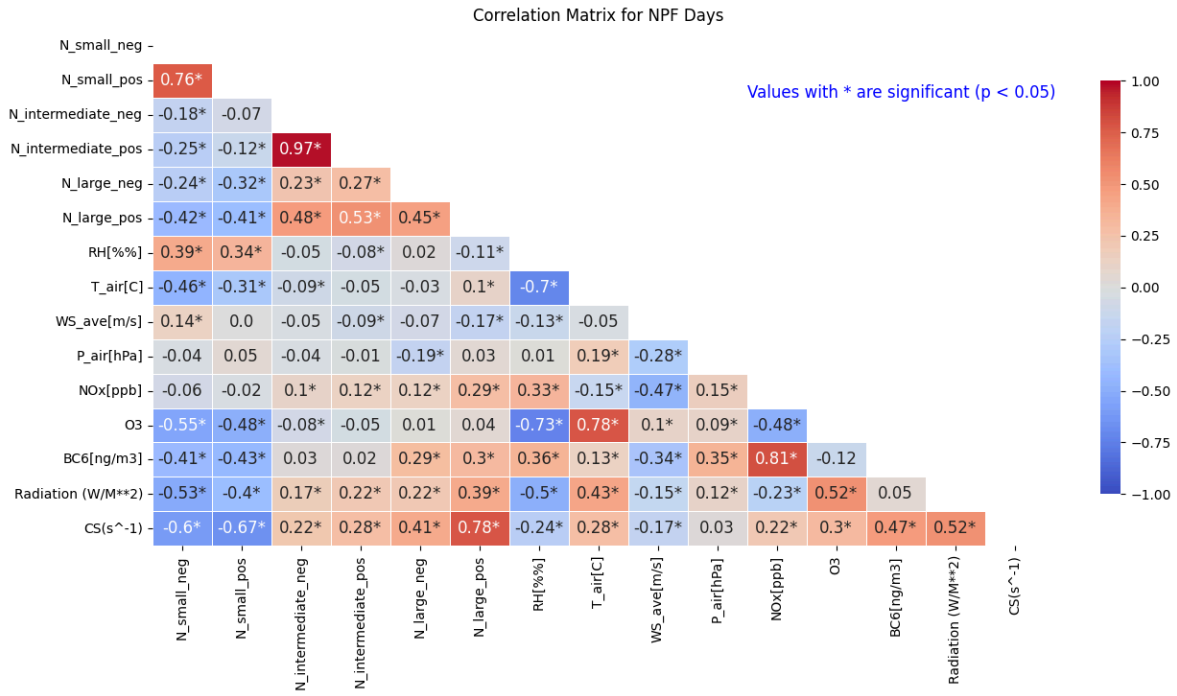


Figure II. Pearson correlation matrix between variables on the NPF event days.

It is worth noting that the small charged particles also show a strong and significant statistical inverse relationship with solar radiation, black carbon, and ozone. This could be explained by dilution due to boundary layer expansion, ion attachment, and oxidation respectively.

Overall, NOx exhibited a weak correlation with the air ions, which is also non-significant for the small range. This could be because being a gas, its effect on atmospheric particles is indirect, but a strong positive relation with BC, since their sources are similar. The diurnal variation of NOx has peaks in the mid morning and evening, that could be explained by the traffic rush hours. These peaks were most consistent with the large range of air ions on the non-event days.

CONCLUSION

The observed NPF occurrence frequency of 35% in summer at this site is comparable to other urban sites. Additionally, the diurnal variation during NPF event days suggests an occurrence between 0500 UTC and 1500 UTC (~0600 - 1600 solar time). Overall, the small charged particles (1.1 – 1.9 nm) exhibited the largest and statistically significant relation to the meteorological variables and pollutants while the intermediate range recorded the weakest correlation. The concentration of the intermediate and large ions exhibited a decline at the times coinciding with the start of NPF events suggesting they could act as nuclei. The complex relationship between the ions, meteorological variables and pollutants all contribute to the occurrence or lack thereof of NPF events.

ACKNOWLEDGEMENTS

Project funded under the National Recovery and Resilience Plan (NRRP), Mis.04 Comp.2 Inv.1.5 – NextGen.EU, RFT n. 3277, 30/12/2021. Award Nr: 0001052, 23/06/2022 (ECS_00000033_ECOSISTER).

REFERENCES

Dal Maso M et al. (2005): Formation and growth of fresh atmospheric aerosols: eight years of aerosol size distribution data from SMEAR II, Hyytiala, Finland. *Boreal Environ Res*; **10**: 323–336.
Hinds WC (1999): *Condensation and Evaporation.* Aerosol Technology Properties Behaviour Measurements Airborne Particles (2nd ed. New York, Wiley).
Rowell A et al. (2024): The behaviour of charged particles (ions) during new particle formation events in urban Leipzig, Germany. *Atmospheric Chem Phys*; **24**: 10349–10361.

Semi-empirical constraint on the rate of p-xylene autoxidation chemistry from a flow tube setup

L. PICHELSTORFER[1,2], A. KUMAR[3] , N. VINKVIST[4], S. IYER[3] and M. RISSANEN[3,4]

[1]*pi-numerics, Neumarkt am W., 5202, Austria.*

[2]*Institute for Atmospheric and Earth System Research/Physics, University of Helsinki, 00560 Helsinki, Finland.*

[3]*Aerosol Physics Laboratory, Tampere University, 33720 Tampere, Finland.*

[4]*Department of Chemistry, University of Helsinki, 00014 Helsinki, Finland.*

Keywords: autoxidation, flow tube, modelling, rate coefficient.

INTRODUCTION

The vast majority of the world's population is living under elevated particulate matter concentrations (WHO, 2022). Despite not being the dominant source of airborne mass, secondary organic aerosol (SOA) may dominate the toxicity of the inhalable aerosol (Daellenbach et al., 2020). The complexity of SOA precursor formation pathways, involving poorly quantified autoxidation chemistry, represents a severe hurdle in the aim to set counter measures. Autoxidation effectively produces condensable species of low enough saturation vapour pressure to contribute to the growth of nano-clusters and larger particles (Ehn et al., 2014). In this work, we introduce a semi-empirical method aiming to quantify autoxidation chemistry and competing reaction pathways which govern the formation of SOA precursors. The method is based on two pillars: 1) lumping of chemical pathways to overcome the overwhelming complexity of autoxidation chemistry; and 2) constraint of the lumped reaction rates based on analytical mathematics and measurement of oxygenated carbon species and their change rates considering an instrument reporting molecular specificity at high sensitivity. The method is highly automated and can be applied to any volatile organic compound (VOC). Results generated (i.e. full sets of rate coefficients) with the method represent mechanistically valid, however, non-unique solutions to the problem.

METHODS

Chemistry schemes are generated applying the autoAPRAM-fw (Pichelstorfer et al., 2024a). The framework allows to create lumped autoxidation reaction schemes for any VOC system by selecting the reaction types considered. However, it does not aim to cover the chemistry of the basic degradation of the VOC as is provided by e.g., MCM (Jenkin et al., 2003). Rate coefficients of the autoAPRAM-generated scheme represent averages for an unknown variety of isomers. Accordingly, they can't be predicted by theory (except for upper and lower limits) but require semi-empirical quantification. This can be done by relating the reaction scheme to observations (Pichelstorfer et al., 2024b):

$$\frac{\Delta C_{\mathrm{exp},i}}{\Delta t} = \frac{\sum_{j \to i} \Delta C_{chem,j}}{\Delta t} - \frac{\Delta C_{phys,i}}{\Delta t} \qquad \text{Equ. (1)}$$

where $C_{exp,i}$ is the experimentally determined concentration of all oxygenated species isomers, t is time, $C_{chem,j}$ are the isomeric species of the autoxidation scheme with similar atomic composition as $C_{exp,i}$. $\Delta C_{phys,i}$ represent the change in concentration due to physical processes (e.g., wall loss or dilution).

Equ. (1) relates changes in the observed isomer concentrations $C_{exp,i}$ to change terms of the autoAPRAM scheme and physical losses. The experimental setup to derive concentrations and their changes is depicted

by Fig. (1). VOC and oxidant are mixed in a flow tube and react while travelling through (Barua et al., 2023; Iyer et al., 2023). The flow tube serves well to observe the chemistry, as physical processes are strongly limited (i.e., no dilution, very limited wall interaction as well as mixing, due to the laminar flow within the tube). As a consequence, observed changes of the oxygenated species directly relate to chemical reactions. Probing of the species at three points in time allow to derive the concentration $C(t_2)$ as well as the change rate $\Delta C(t_2)/\Delta t \approx (C(t_3)-C(t_1))/\Delta t$. This enables to solve equ. (1).

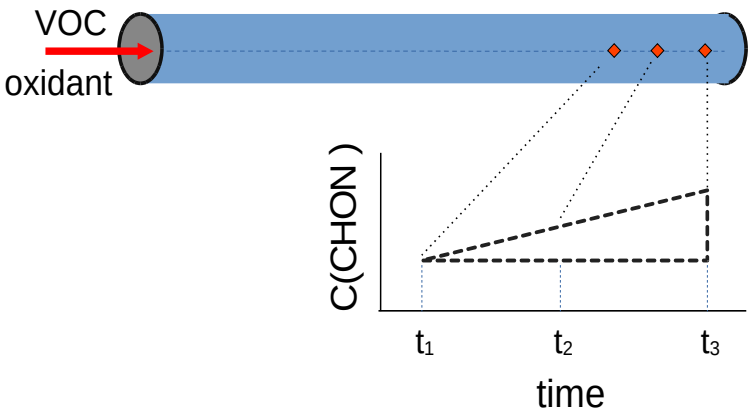


Figure 1. Setup of the flow tube experiment. VOC and oxidant are introduced and start the chemical reactions. Sampling of the oxygenated species of atomic composition C/H/O/N is done at three points at the centre-line of the tube which is equivalent to three points in time (t_1 to t_3).

CONCLUSIONS

The presented method to quantify autoxidation rate coefficients overcomes the issue of overwhelming complexity of the chemistry by lumping reaction pathways. As a result, the reaction rate coefficients require empirical quantification which is approached by considering the most detailed information on the oxygenated species experimentally available (i.e., provided by the nitrate chemical ionization mass spectrometer; Jokinen et al., 2012) as well as theoretically suggested reaction pathways and related limitations for the rate coefficients. Results are non-unique. However, due to the linear form of equ. (1), unique results may be approached by considering multiple experimental datasets. Currently, we are investigating p-xylene data from a flow tube setup a) sampled at three points within the tube using an injector and b) applying three different volume flows while sampling at a stationary point. Both approaches allow to construct the C and C pairs required by equ. (1).

ACKNOWLEDGEMENTS

This work was supported by the Research Council of Finland: 346373, 353836, 358066, 355966 and European Research Council Consolidator grant ADAPT (Grant No. 101002728).

REFERENCES

Barua, S., Iyer, S., Kumar, A., Seal, P., & Rissanen, M. (2023). An aldehyde as a rapid source of secondary aerosol precursors: theoretical and experimental study of hexanal autoxidation, *Atmos. Chem. Phys.*, **23**, 10517–10532, https://doi.org/10.5194/acp-23-10517-2023.

Daellenbach, K. R., et al. (2020). Sources of particulate-matter air pollution and its oxidative potential in Europe, *Nature*, **587**, 414–419, https://doi.org/10.1038/s41586-020-2902-8, 2020.

Ehn, M., et al. (2014). A large source of low- volatility secondary organic aerosol, *Nature*, **506**, 476–479, https://doi.org/10.1038/nature13032.

Iyer, S., Kumar, A., Savolainen, A., Barua, S., Daub, C., Pichelstorfer, L., Roldin, P., Garmash, O., Seal, P., Kurtén, T., & Rissanen, M. (2023). Molecular rearrangement of bicyclic peroxy radicals is a key route to aerosol from aromatics. *Nat. Comm.*, **14**, 4984, https://doi.org/10.1038/s41467-023-40675-2.

Jenkin, M. E., Saunders, S. M., Wagner, V., and Pilling, M. J. (2003). Protocol for the development of the Master Chemical Mechanism, MCM v3 (Part B): tropospheric degradation of aromatic volatile organic compounds, *Atmos. Chem. Phys.*, **3**, 181–193, https://doi.org/10.5194/acp-3-181-2003.

Jokinen, T., et al., (2012) Atmospheric sulphuric acid and neutral cluster measurements using CI-APi-TOF, *Atmos. Chem. Phys.*, **12**, 4117–4125, https://doi.org/10.5194/acp-12-4117-2012.

Pichelstorfer, L., et al. (2024). Towards automated inclusion of autoxidation chemistry in models: from precursors to atmospheric implications, *Environ. Sci.: Atmos.*, 10.1039.D4EA00054D, https://doi.org/10.1039/D4EA00054D.

Pichelstorfer, L., O'Meara, S. P., and McFiggans, G. B (2024) Theory informed, experiment based, constraint on the rate of autoxidation chemistry – An analytical approach, *Aerosol Research Discuss*. [preprint], https://doi.org/10.5194/ar-2024-40, in review.

WHO (https://www.who.int/news-room/fact-sheets/detail/ambient-(outdoor)-air-quality-and-health) last accessed: March, 27th , 2025.

AN OPEN TOOLKIT FOR PARTICLE SIZE DISTRIBUTION ANALYSIS

G. SRIVASTAV[1,2*], J. LAMPILAHTI[3], K. LEHTIPALO[3], S. GANI[1,3]

[1]Centre for Atmospheric Sciences, Indian Institute of Technology Delhi, New Delhi, India.
[2]*India Meteorological Department, Ministry of Earth Sciences, Government of India*
[3]*Institute for Atmospheric and Earth System Research/Physics, University of Helsinki, Helsinki, Finland.*

Keywords: Aerosol toolkit, Global aerosol analysis, Particle size distribution, Mode fitting.

Presenting author email: asz248255@iitd.ac.in

INTRODUCTION

Particle size distribution (PSD) analyses are essential for understanding atmospheric aerosol dynamics, encompassing mode fitting, calculation of particle number concentration in various size ranges, growth rates, formation rates, condensation sink, and coagulation sink (Kulmala et al., 2012). To simplify these complex analyses, we developed a user-friendly Graphical User Interface (GUI) toolkit. This toolkit enables users to visualize data, select and label areas of interest, and fit multimodal log-normal distributions to the selected data. Additionally, it allows for the saving and loading of regions of interest within the PSD time-series, making it a versatile tool for both novice and experienced researchers in the field.

METHODS

Our GUI toolkit follows standard approaches for calculating parameters such as particle number concentration in different size ranges, growth rates, formation rates, condensation sink, and coagulation sink, as described in existing literature (Kulmala et al., 2012). The GUI streamlines these calculations, making them more accessible and easier to understand. The mode fitting segment of the GUI employs a cluster-initialized least square fit algorithm, which can automatically determine the optimum number of modes using a mean square error-based elbow method. This data-driven approach is independent of location-specific assumptions, allowing it to be applied to global datasets without modification, making it a robust tool for analyzing aerosol dynamics and new particle formation (NPF) processes across diverse environments.

We evaluated our method against test cases and long-term datasets from various environments and compared it with existing mode fitting methods (e.g., Hussein et al., 2005). The GUI tool provides visual feedback on the quality of the fits, reducing the likelihood of errors. It also allows researchers to label and classify aerosol size distributions for data analysis and machine learning purposes, as well as for quality assurance by identifying regions of bad data.

CONCLUSIONS

Our GUI toolkit offers a comprehensive solution for analyzing aerosol dynamics, integrating advanced multimodal fitting algorithms with user-friendly features. The tool's ability to provide visual feedback and streamline complex calculations makes it a valuable resource for researchers. We are continuously upgrading the toolkit and in process to add other features to calculate other parameters as well. We anticipate that feedback from the aerosol community, such as that received at EAC25, will help us further enhance its capabilities and incorporate additional features to meet the evolving needs of researchers in this field

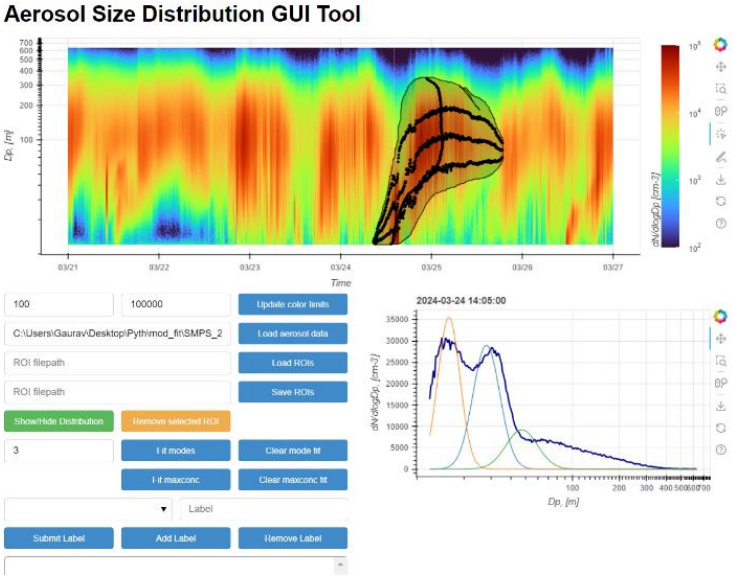


Figure I. GUI Tool Front-end.

REFERENCES

Hussein, Tareq, et al. "Evaluation of an automatic algorithm for fitting the particle number size distributions." Boreal environment research 10.5 (2005): 337.

Kulmala, Markku, et al. "Measurement of the nucleation of atmospheric aerosol particles." Nature protocols 7.9 (2012): 1651-1667.

ATMOSPHERIC IONS AND PARTICLES IN THE INDO-GANGETIC PLAIN

G. SRIVASTAV[1,2*], A. WAGAY[1], J. LAMPILAHTI[3], J. RATHORE[1], R.K. KUNCHALA[1], D. GANGULY[1], M. KULMALA[3], P. PAASONEN[3], R. THAKUR[3], S. GANI[1,3]

[1]Centre for Atmospheric Sciences, Indian Institute of Technology Delhi, New Delhi, India.
[2]India Meteorological Department, Ministry of Earth Sciences, Government of India.
[3]Institute for Atmospheric and Earth System Research/Physics, University of Helsinki, Helsinki, Finland.

Keywords: Atmospheric Ions, Particle size distribution, India, Indo-Gangetic Plain

[*]Presenting author email: asz248255@iitd.ac.in

INTRODUCTION

The Indo-Gangetic Plain (IGP) is a densely populated area that frequently experiences high pollution levels resulting in substantial reductions in life expectancy. This region has a large population, including megacity like Delhi. Recent studies have shown that the number density of sub-nanometer particles is remarkably high (Gani et al., 2020), and they may have adverse health effects on the cardiovascular system and the brain. This high vulnerability highlights the need to comprehensively investigate all potential factors affecting the local population. Despite their importance in the dynamics of sub-nm aerosol particles, new particle formation (NPF), condensation sink, coagulation sinks, and air-ion (charged particles in the atmosphere) concentration have not been well monitored and explored in the IGP area. Studies based on chemical and mass concentration perspective exist but there has been a lack of research on atmospheric aerosol physics, particularly size distribution aspects in this area. This study employs advanced instrumentation, including the Neutral cluster and Air Ion Spectrometer (NAIS) for the size range of 0.8–40 nm and the Scanning Mobility Particle Sizer (SMPS) for the size range of 10–500 nm, to investigate particle size distribution and NPF events in the IGP.

NPF is a crucial source for secondary aerosols which can increase the particle number concentration. The particles can grow further leading to climate effects, health effects and other cloud-haze related weather phenomena. This study seeks to address the existing knowledge gap in aerosol physics by analyzing NPF events and their governing factors in the polluted IGP region. Additionally, we assess the influence of meteorological conditions—such as temperature, humidity, and boundary layer height—on the atmospheric processes driving particle formation and growth. Understanding these processes is crucial for assessing their impact on air quality, climate, and human health. Furthermore, integrating studies from other regions can help contextualize these results on a global scale. This broader perspective will enhance our understanding of atmospheric processes and their implications worldwide.

METHODS

The analysis is based on year-long (Jan 2023–Feb 2024) size-segregated particle data collected at the IITD Sonipat campus situated in IGP region (upwind site of Delhi, India). Existing classification algorithms (Dal Maso et al., 2025; Dada et al., 2018; Aliaga et al., 2023) were applied, showing strong agreement for intense NPF days but discrepancies for weak or non-event days Using SMPS data coagulation sink (CS) and condensation sink (CS), have been calculated for representative days of each

event type to explore differences in sink dynamics. We have also characterized the basic parameters including growth rates and formation rates associated with NPF events (Kulmala et al., 2012).

We also investigated variability and correlations of NPF events with meteorological parameters using ERA5 data for NPF and non-NPF days. We will further incorporate on-site ceilometer and AWS data to further investigate variability and its impact.

CONCLUSIONS

This integrated approach offers preliminary insights into aerosol dynamics and atmospheric processes in the IGP, with a focus on NPF events and their key governing factors. The study reveals that NPF events were more frequent during the summer months, possibly driven by higher solar radiation, elevated temperatures, and favorable meteorological conditions. On event days, distinct peaks in ion and particle concentrations were observed, which were closely linked to low condensation sinks and the availability of precursor gases. In contrast, non-event days exhibited fluctuations in concentrations without clear peaks, suggesting less favorable conditions for particle formation.

During the study period, particles growth rate has been observed to range from 4 to 13 nm/hour with a median of 7 nm/hour which is comparable to urban locations in China, where GR values typically range from 4.1 to 12 nm/hour with a median of 6.4 nm/hour (Kerminen et al, 2018). This similarity suggests the consistent behavior of particle growth in sub-urban environments, despite regional differences in pollution sources and atmospheric conditions. Further investigations to explore this alignment may reveal more about the underlying mechanisms governing particle growth across different regions with comparable atmospheric conditions.

Using ERA5, meteorological parameters and atmospheric mixing are analysed to see the influence on particle dynamics. The increasing boundary layer height and temperature favor particle growth. However, factors such as condensation sinks and precursor gas availability also play critical role, increasing the complexity of particle formation and growth processes. Future work will build on these findings by incorporating ceilometer data to better understand the relationships between boundary layer height, wind, temperature, relative humidity, particle concentrations, and ion dynamics. This integrated approach will provide a more comprehensive understanding of aerosol behavior.

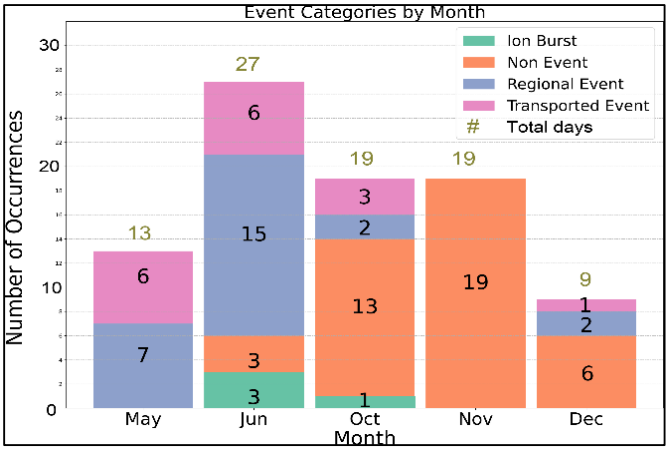


Figure I. Result of one of the NPF classification schemes (Dada et al 2018) applied on NAIS data during the total study period.

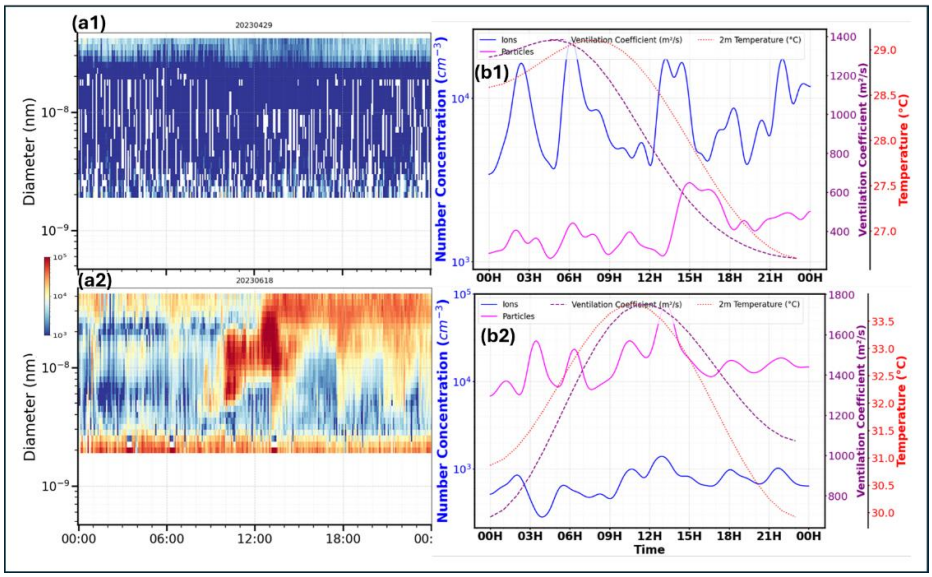


Figure II. Heatmap of particle number concentrations as a function of time and diameter (nm), for (a1) a non-event day (2023-04-29) and (a2) an event day (2023-06-18) along with the (b1), (b2) variation of ventilation coefficient (VC) = BLH * Wind and 2m temperature.

ACKNOWLEDGEMENTS

We acknowledge the importance of IIT Delhi and INAR for their support in providing the required facilities.

REFERENCES

Aliaga, Diego, et al. "Nanoparticle ranking analysis: determining new particle formation (NPF) event occurrence and intensity based on the concentration spectrum of formed (sub-5 nm) particles." Aerosol Research 1.1 (2023): 81-92.

Dal Maso, Miikka, et al. "Formation and growth of fresh atmospheric aerosols: eight years of aerosol size distribution data from SMEAR II, Hyytiälä, Finland." Boreal environment research 10.5 (2005): 323.

Dada, Lubna, et al. "Refined classification and characterization of atmospheric new-particle formation events using air ions." Atmospheric Chemistry and Physics 18.24 (2018): 17883-17893.

Gani, Shahzad, et al. "Particle number concentrations and size distribution in a polluted megacity: the Delhi Aerosol Supersite study." Atmospheric Chemistry and Physics 20.14 (2020): 8533-8549.

Kerminen, Veli-Matti, et al. "Atmospheric new particle formation and growth: review of field observations." Environmental Research Letters 13.10 (2018): 103003.

Kulmala, Markku, et al. "Measurement of the nucleation of atmospheric aerosol particles." Nature protocols 7.9 (2012): 1651-1667.

NEW PARTICLE FORMATION POTENTIAL OF EMERGING AIR POLLUTANTS PROBED BY MULTI-PRESSURE CHEMICAL IONIZATION MASS SPECTROMETRY

D. STOLZENBURG[1], M. TISCHBERGER[1], R. VERMA[1] and H. GROTHE[1]

[1]*Institute of Materials Chemistry, TU Wien, Vienna, Austria.*

Keywords: multi-pressure chemical ionization mass spectrometry, Orbitrap, Volatile Chemical Products, Volatility-Basis-Set

INTRODUCTION

New particle formation can also proceed effectively in polluted urban environments, often mediated by oxygenated organics, especially in the phase of early growth (Stolzenburg et al., 2023). The volatility distribution of the organics, often expressed within a volatility-basis-set (VBS), determines at what stage organics can start to contribute to NPF (Stolzenburg et al., 2022). However, the urban organic mix is changing (McDonald et al., 2018). As typical combustion-related organics are declining due to updated policies on traffic and industrial emissions, other anthropogenic organic air contaminants are emerging, often classified together as volatile chemical products (VCPs). They originate from various non-combustion sources such paints, adhesives, detergents, but also hygiene consumer products (Gkatzelis et al., 2021). However, the potential of these compounds to oxidize in the atmosphere and form products of sufficiently low volatility to contribute to NPF has not been evaluated in-depth, while it is known that many VCPs contribute to SOA (Shah et al., 2020).

It has been demonstrated, that the full contribution to NPF of a given organic source can best be evaluated when the entire volatility distribution is known, also including moderately oxygenated molecules (MOM) (Stolzenburg et al., 2025). In addition, due to the complex emission patterns of many VCP emitters it is important to understand the entire oxidation chain from the volatile organic compounds (VOCs) up to the least volatile highly oxygenated organics molecules (HOMs) to make adequate changes in product design which could reduce the air quality footprint of consumer products.

METHODS

Here, we therefore use the recently developed potential of multi-pressure chemical ionization (Shcherbinin et al., 2024) to measure the entire oxidation chain of certain VCP sources (VOCs to MOM and HOM) with a single ultra-high resolution Orbitrap mass spectrometer. VOCs are measured using the internal fluoranthene ($C_{16}H_{10}$) ion sources at low pressure (<1 mbar), MOMs are quantified using chemical ionization at atmospheric pressure with protonated urea ($CN_2H_5O^+$) as the reagent ion and HOMs are ionized at atmospheric pressure using the well-known negatively charged nitrate (NO_3^-).In combination with the ultra-high mass resolution and the easy polarity-switching capabilities of an Orbitrap Exploris MX mass detector, we obtain a quite complete coverage of the entire spectrum of organics. We oxidize the precursor or the volatiles originating from that precursor in a newly designed oxidation flow reactor (OFR) having an especially large cross-section to volume ratio to reduce wall interactions.

Results of a simple α-pinene ozonolysis experiment are shown in Figure 1, with three different concentrations of α-pinene introduced to the OFR. We show time series of α-pinene and its major oxidation products in the $C_{10}H_{16}O_x$ series, together with the traces of the different reagent ions indicating the switching between the ionization modes. We further show the evolution of the particle size-distribution and oxidant concentrations which are monitored at the OFR outlet simultaneously.

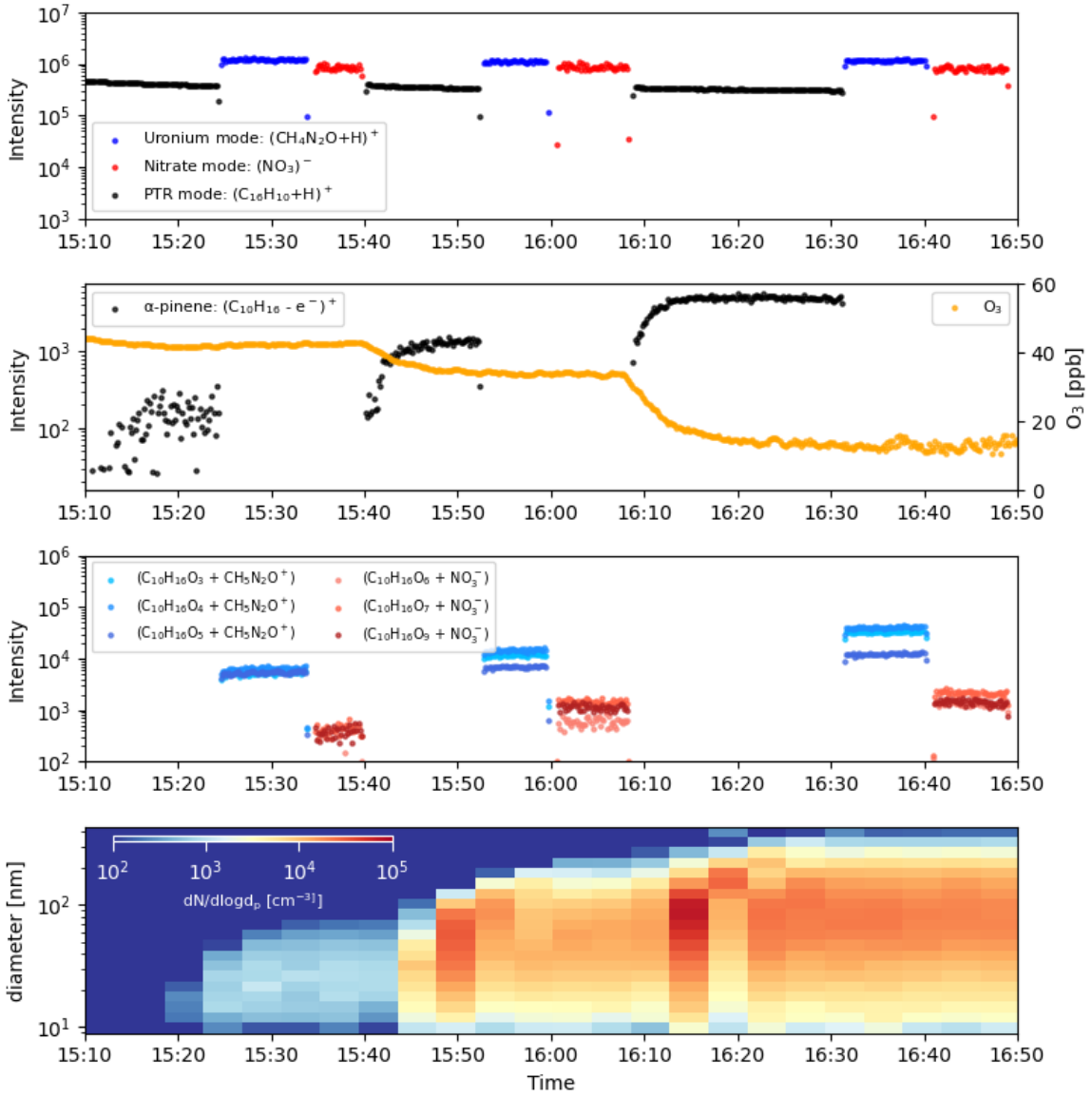


Figure 1. *Demonstration of multi-pressure chemical ionization mass spectrometry coupled with an oxidation flow reactor and supporting measurements for three intensities of α-pinene ozonolysis. The upper panel illustrates the switching between different ionization modes once steady state conditions have been reached in the flow reactor. The second panel shows the evolution of the precursors (α-pinene and ozone) and the third panel shows the evolution of the major products of the $C_{10}H_{16}O_x$ series. The lower panel shows the evolution of the particle size distribution at the OFR exit during the course of the experiments.*

RESULTS

We investigate different potential emitters of VCPs and assign a volatility of the products with an ultrahigh resolution-based sum formula identification based on earlier approaches (Stolzenburg et al., 2022, 2025). Combination of the different high-pressure ionization modes is based on the molecular ions which are identified in both modes, as done previously (Stolzenburg et al., 2018, 2025). However, as this approach implicitly assumes uniform charging probabilities within one ionization mode, which might very often not be the case, we compare the relative VBS spectra with the one obtained from α-pinene ozonolysis as a

reference. Under the assumption that charging efficiencies might be well-related to compound volatility (Riva et al., 2019) we can thereby quantify the relative NPF potential of a certain VCP emitter compared to the "gold-standard" of α-pinene, where the NPF potential of a certain VBS distribution is mapped out precisely (Stolzenburg et al., 2018). We illustrate that relative approach in Figure 2 for a potential VCP emitter. That way, we can map out the contribution of different emerging urban air pollution sources to NPF. Combined with the coverage of the originally emitted VOCs using our low-pressure ionization mode, this allows even for potential identification of the precursors to be eliminated within product design.

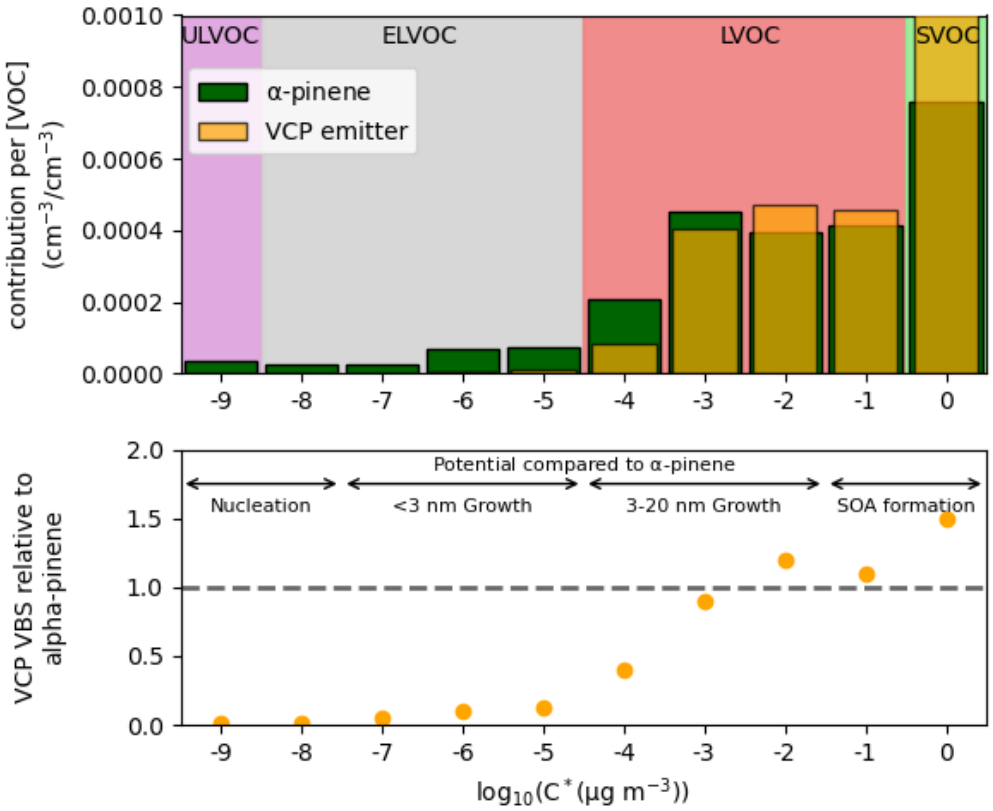


Figure 2. *VBS distribution obtained from two high-pressure chemical ionization modes of α-pinene and a potential VCP emitter together with the relative emissions indicating the NPF potential of the VCP emitter with respect to the well-understood α-pinene system.*

CONCLUSIONS

We show how multi-pressure chemical ionization can be used to map out the contribution of different VCP sources to future urban air pollution through NPF and simultaneously identify key precursor molecules which could be altered in product design. This illustrates the power of multi-pressure chemical ionization coupled with ultra-high resolution Orbitrap mass spectrometry and a state-of-the-art oxidation flow reactor as a tool to investigate NPF involving emerging urban organic sources, such as personal care products, architectural coatings and even asphalt.

ACKNOWLEDGEMENTS

This research was funded in whole or in part by the Austrian Science Fund (FWF) 10.55776/PAT8221324 and by the Vienna Science and Technology Fund (WWTF) under project VRG22-003.

REFERENCES

Gkatzelis, G. I., Coggon, M. M., McDonald, B. C., Peischl, J., Aikin, K. C., Gilman, J. B., Trainer, M., & Warneke, C. (2021). Identifying Volatile Chemical Product Tracer Compounds in U.S. Cities. *Environ. Sci. Technol.*, *55*(1), 188–199. https://doi.org/10.1021/acs.est.0c05467

McDonald, B. C., de Gouw, J. A., Gilman, J. B., Jathar, S. H., Akherati, A., Cappa, C. D., Jimenez, J. L., Lee-Taylor, J., Hayes, P. L., McKeen, S. A., Cui, Y. Y., Kim, S.-W., Gentner, D. R., Isaacman-VanWertz, G., Goldstein, A. H., Harley, R. A., Frost, G. J., Roberts, J. M., Ryerson, T. B., & Trainer, M. (2018). Volatile chemical products emerging as largest petrochemical source of urban organic emissions. *Science*, *359*(6377), 760–764.

Riva, M., Rantala, P., Krechmer, J. E., Peräkylä, O., Zhang, Y., Heikkinen, L., Garmash, O., Yan, C., Kulmala, M., Worsnop, D., & Ehn, M. (2019). Evaluating the performance of five different chemical ionization techniques for detecting gaseous oxygenated organic species. *Atmos. Meas. Tech.*, *12*(4), 2403–2421. https://doi.org/10.5194/amt-12-2403-2019

Shah, R. U., Coggon, M. M., Gkatzelis, G. I., McDonald, B. C., Tasoglou, A., Huber, H., Gilman, J., Warneke, C., Robinson, A. L., & Presto, A. A. (2020). Urban Oxidation Flow Reactor Measurements Reveal Significant Secondary Organic Aerosol Contributions from Volatile Emissions of Emerging Importance. *Environ. Sci. Technol.*, *54*(2), 714–725. https://doi.org/10.1021/acs.est.9b06531

Shcherbinin, A., Finkenzeller, H., Mikkilä, J., Kontro, J., Vinkvist, N., Kangasluoma, J., & Rissanen, M. (2024). From Hydrocarbons to Highly Functionalized Molecules in a Single Measurement: Comprehensive Analysis of Complex Gas Mixtures by Multi-Pressure Chemical Ionization Mass Spectrometry. *Analytical Chemistry*, *96*(50), 19926–19932. https://doi.org/10.1021/acs.analchem.4c03859

Stolzenburg, D., Cai, R., Blichner, S. M., Kontkanen, J., Zhou, P., Makkonen, R., Kerminen, V.-M., Kulmala, M., & Kangasluoma, J. (2023). Atmospheric nanoparticle growth. *Rev. Mod. Phys.*, *95*(4), 045002. https://doi.org/10.1103/RevModPhys.95.045002

Stolzenburg, D., Fischer, L., Vogel, A. L., Heinritzi, M., Schervish, M., Simon, M., Wagner, A. C., Dada, L., Ahonen, L. R., Amorim, A., Baccarini, A., Bauer, P. S., Baumgartner, B., Bergen, A., Bianchi, F., Breitenlechner, M., Brilke, S., Buenrostro Mazon, S., Chen, D., … Winkler, P. M. (2018). Rapid growth of organic aerosol nanoparticles over a wide tropospheric temperature range. *P. Nat. Acad. Sci. USA*, *115*(37), 9122–9127. https://doi.org/10.1073/pnas.1807604115

Stolzenburg, D., Sarnela, N., Bianchi, F., Cai, J., Cai, R., Cheng, Y., Dada, L., Donahue, N. M., Grothe, H., Holm, S., Kerminen, V.-M., Lehtipalo, K., Petäjä, T., Sulo, J., Winkler, P. M., Yan, C., Kangasluoma, J., & Kulmala, M. (2025). Incomplete Mass Closure in Atmospheric Nanoparticle Growth. *Npj Climate and Atmospheric Sciences*, *in press*.

Stolzenburg, D., Wang, M., Schervish, M., & Donahue, N. M. (2022). Tutorial: Dynamic organic growth modeling with a volatility basis set. *J. Aerosol Sci.*, *166*, 106063. https://doi.org/https://doi.org/10.1016/j.jaerosci.2022.106063

UNEXPECTED GAS-PHASE FORMATION OF GLYCOLIC ACID SULFATE IN THE ATMOSPHERE

Haowei Sun[1,2], Yuliang Liu[1,2], Wei Nie[1,2], Yuanyuan Li[1,2], Dafeng Ge[1,2], Tao Xu[1,2], Junchao Yin[1,2], Chong Liu[3], Zihao Fu[4], Ximeng Qi[1,2], Tengyu Liu[1,2], Qiaozhi Zha[1,2], Chao Yan[1,2], Xuguang Chi[1,2], and Aijun Ding[1,2]

[1]*Joint International Research Laboratory of Atmospheric and Earth System Research, School of Atmospheric Sciences, Nanjing University, Nanjing, 210023, China.*

[2]*National Observation and Research Station for Atmospheric Processes and Environmental Change in Yangtze River Delta, Nanjing, 210023, China.*

[3]*Hubei Province Academy of Eco-Environmental Sciences, Wuhan 430072, China.*

[4]*State Key Joint Laboratory of Environmental Simulation and Pollution Control, International Joint Laboratory for Regional Pollution Control, Ministry of Education (IJRC), College of Environmental Sciences and Engineering, Peking University, Beijing 100871, China.*

Keywords: OSs, GAS, ELVOC, SO_3, gas-phase.

Secondary organic aerosols (SOAs) are known to influence climate, air quality and human health. Organosulfates (OSs), which form through organic-sulfur interactions, are a significant class of compounds within SOAs (Brüggemann et al., 2020).

Glycolic acid sulfate (GAS), one of the simplest OSs containing both carboxyl and sulfate groups, is widely detected in ambient aerosols. Recent studies have hinted at the intriguing possibility of GAS existing in the gas phase. The possibility of gas-phase GAS was firstly proposed using an APi-TOF (Ehn et al., 2010). Subsequent studies using FIGAERO-I-CIMS detected signals consistent with gas-phase GAS (Le Breton et al., 2018; Wang et al., 2023). Additionally, theoretical studies have already begun exploring potential implications of gaseous GAS, such as its role in nucleation mechanisms involving sulfuric acid and dimethylamine (Zhang et al., 2024). Nevertheless, it is crucial to emphasize that the sources, formation mechanisms, and even the very existence of gas-phase OSs, including GAS, remain largely unconfirmed.

We present reliable measurements of gaseous GAS in the atmosphere using a nitrate APi-TOF over four seasons at SORPES. We also employed a FIGAERO-I-CIMS to investigate GAS gas-particle partitioning, providing evidence for its gas-phase existence and formation.

Our study provides the first systematic field evidence for the consistent presence of a gas-phase OS, GAS, in the atmosphere. We identified GAS as an ELVOC and discovered its gas-phase fraction substantially exceeded predictions based on gas-particle equilibrium, underscoring the necessity of its gas-phase formation pathway (Fig. 1). And we further identified the reaction between SO_3 and GA as a potential mechanism for gas-phase GAS formation, with a near-collision-limited rate constant ($k \approx 2.20 \times 10^{-10}$ cm^3 s^{-1}) .

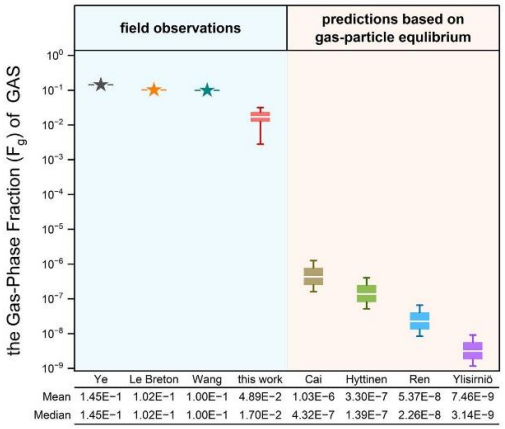


Fig. 1. Evidence for gas-phase formation of GAS: comparison between observed and predicted gas-phase fractions under equilibrium conditions.

ACKNOWLEDGEMENTS

We thank colleagues and students at the School of Atmospheric Sciences at Nanjing University for their contributions to the maintenance of the measurements. We thank the tofTools team for providing tools for mass spectrometry analysis. This work was supported by the National Natural Science Foundation of China (NSFC) project (grant nos. 42220104006 and 42305119), Natural Science

Foundation of Jiangsu Province (BK20230773), the Jiangsu Provincial Collaborative Innovation Center of Climate Change and the Fundamental Research Funds for the Central Universities.

REFERENCES

Brüggemann, M., et al., (2020). *Environ. Sci. Technol.* **54** (7): 3767-3782.
Ehn, M., et al., (2010). *Atmos. Chem. Phys.* **10**(17): 8513-8530.
Le Breton, M., et al., (2018). *Atmos. Chem. Phys.* **18**(14): 10355-10371.
Wang, Y., et al., (2023). *Sci. Total Environ* **904**: 166851.
Zhang, X., et al., (2024). *Atmos. Chem. Phys.* **24**(6): 3593-3612.

ONGOING ANTHROPOGENIC EMISSION ABATEMENT PROMOTES NEW PARTICLE GROWTH IN A CHINESE MEGACITY

LIZI TANG[1], ZEYU FENG[1], DONGJIE SHANG[1], LINHAN ZENG[1], ZHIJUN WU[1,2], HUI WANG[3], SHIYI CHEN[1], XIN LI[1,2], LIMIN ZENG[1,2], JIANLIN HU[2], MIN HU[1,2*]

[1]*State Key Laboratory of Regional Environment and Sustainability, International Joint Research Center for Atmospheric Research (IJRC), College of Environmental Sciences and Engineering, Peking University, Beijing 100871, China.*

[2] *Collaborative Innovation Center of Atmospheric Environment and Equipment Technology, Nanjing University of Information Science and Technology, Nanjing 210044, China.*

[3] *Institute of Climate and Energy systems, Troposphere, ICE-3, Forschungszentrum Jülich, 52425 Jülich, Germany.*

Keywords: NEW PARTICLE GROWTH, VOLATILE ORGANIC COMPOUNDS, NOx, OOMS

INTRODUCTION

New particle growth determines the survival probability of newly-formed particles to larger size in the presence of pre-existing aerosols in polluted urban atmosphere, with higher growth rate (GR) accelerating haze developments. Although numerous NPF observations in urban areas exist, most short-term observations cannot establish GR trends, hindering assessment of long-term environmental effects of NPF under ongoing anthropogenic emission abatement. Gaseous sulfuric acid (SA) drives nucleation and initial growth (< 3 nm), and oxygenated organic molecules (OOMs) condensation has been proposed to dominate subsequent growth to sub-micro particles. In the context of continuous AVOCs and NOx emission abatement in China, OOM formation may have undergone substantial changes, which may drive a long-term variation in GR. In this work, we conducted comprehensive measurements in Beijing, a megacity in China, to investigate the trends and mechanisms of new particle growth. We discovered the increasing trends in urban Beijing during autumn from 2017 to 2021. Based on the quantitative relationship originated from comprehensive measurements of gaseous oxygenated organic molecules (OOMs) in autumn 2021, we have identified the primary driver for annual GR variations.

METHODS

The measurements were conducted at the Peking University Urban Atmosphere Environment MonitoRing Station (PKUERS) measurement site at the campus of Peking University (39°59′21″N, 116°18′25″E) in the northwest of Beijing. The measurement of particle number size distribution (PNSD) and trace gases including NOx and SO_2 were performed in the autumn (September to November) of 2017-2021. A total of 105 NPF events in the autumn of 2017-2021 were identified. VOCs were measured in the autumn of 2017, 2018 and 2021. The measurements of OOMs and SA were conducted from 18 September to 31 October 2021, including 13 NPF events. The OOMs data were compared with a study conducted in 2018 (Qiao *et al*., 2018).

OOMs and sulfuric acid were measured with the Nitrate CI-APi-TOF (Aerodyne Research Inc., USA). The long-TOF (LTOF) detector has the m/z resolution of ~7000 Th/Th. Ambient air at a flow rate of 10 LPM and sheath air at a flow rate of 20 LPM was drawn into the ionization source. The sampling line was straight Teflon tubing with a length of 0.8 m and a diameter of 1/2 in. A mixture of 2.5 ml min-1 ultrahigh purity nitrogen flow containing nitric acid is flushed over the ionizer to generate reagent ions.

OOMs were defined as the gas-phase oxygen-containing organic molecules formed during the oxidation of VOCs, including anthropogenic VOCs (AVOCs) and biogenic VOCs (BVOCs). The OOMs sources are identified based on the molecular composition and the up-to-date knowledge of atmospheric OOM

formation chemistry (Nie *at al.*, 2022). The volatility of OOMs was parameterized with Mohr, C. *et al.*'s method (2019). we used a dynamic condensation model (Stolzenburg *et al.*, 2022) to simulate the process of particle growth driven by the condensation of the condensed vapor (OOMs and sulfuric acid). The model uses the measured VBS distribution as input to model the mass transfer from the gas- to the particle-phase.

CONCLUSIONS

The strict emission controlments significantly reduced air pollutants from 2017 to 2021 (Fig. 1a). Figure 1b reveals a significant increasing trend in size-resolved GR from 2017-2021 (Mann-Kendall test, $p < 0.05$). The averaged GR in 3-7 nm and 7-25 nm (GR3-7 and GR7-25) increased from 2.2 ± 1.2 and 2.9 ± 1.3 nm h-1 in 2017 to 3.2 ± 1.3 and 3.9 ± 1.7 nm h-1 in 2021, with the annual increasing rates of 0.15 to 0.38 nm h-1 yr-1 and 0.12 to 0.32 nm h-1 yr-1, respectively.

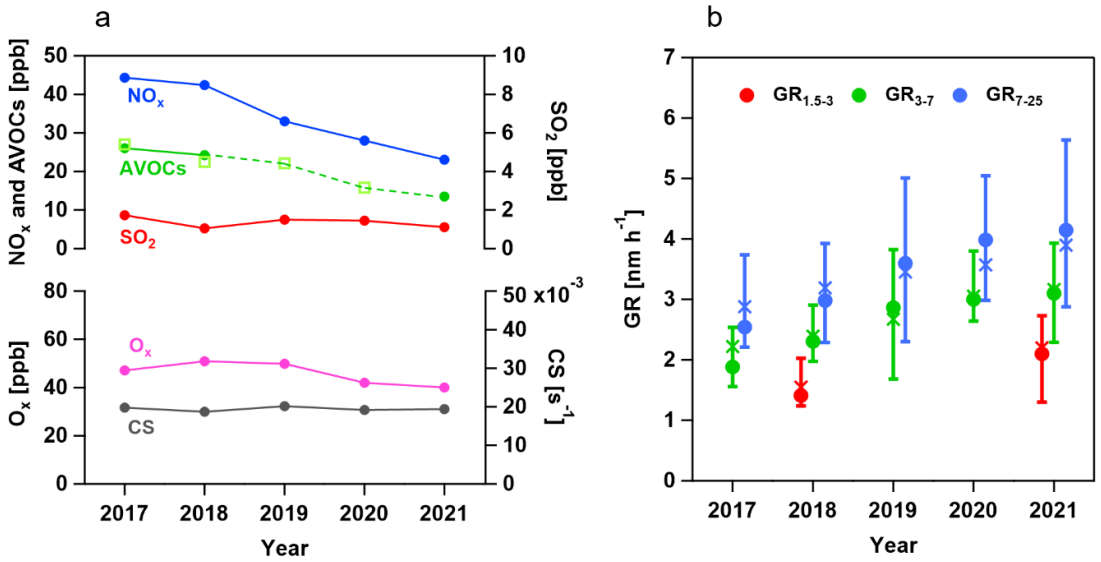


Figure 1. Variations of the growth rates (GR), gas pollutants and condensational sink (CS) in the autumn from 2017 to 2021. a Variations of NOx, anthropogenic VOCs (AVOCs), SO_2, Ox (NO_2 + O_3) and CS. The circular marks are values measured in this study, and the square marks of AVOCs are from Liu et al.43 as a supplement. b Variations of GR in the size ranges of 1.5-3 nm, 3-7 nm, 7-25 nm. The circular and cross markers represent the median and mean values, respectively. The whiskers correspond to the 25th and 75th percentiles.

OOMs dominated particle growth across all size ranges, contributing 68%, 80% and 70% in $GR_{1\text{-}3}$, $GR_{3\text{-}7}$ and $GR_{7\text{-}25}$, respectively. According to the measured OOM concentration in Beijing in 2021, $GR_{1.5\text{-}3}$, $GR_{3\text{-}7}$ and $GR_{7\text{-}25}$ were mainly contributed by OOMs with $\log_{10}(C^*) \leq -4$, $\log_{10}(C^*) \leq -3$ and $\log_{10}(C^*) \leq -2$, respectively (Fig. 2a), those are defined as condensable OOMs. The concentration of the total OOMs in 2018 (Qiao et al., 2018) was higher than that in 2021, but mainly concentrated in $\log10(C^*) > -2$. On the contrary, a higher absolute concentration of condensable OOMs was observed in 2021, especially for $\log10(C^*) \leqslant -4$ with highest CP.

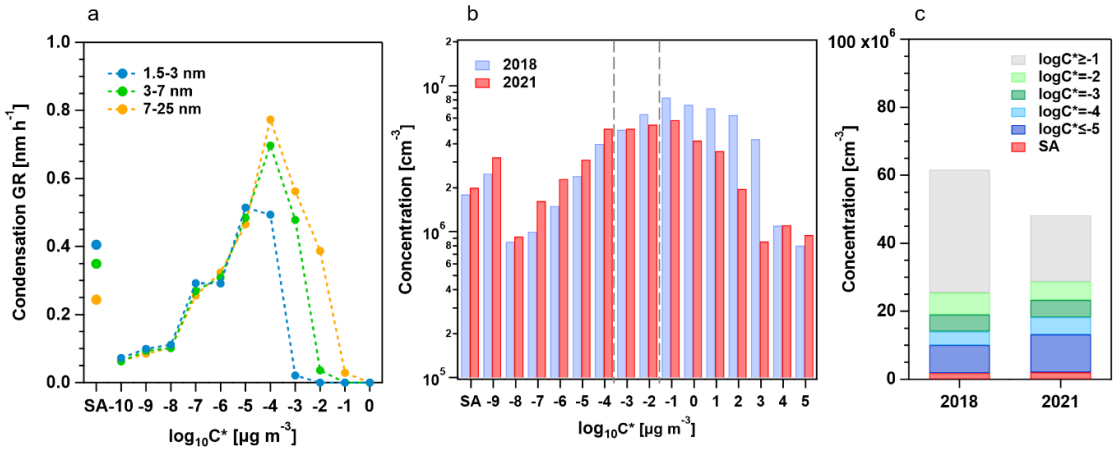


Figure 2. Characteristics of OOM volatility distribution and its link to GR. a The condensation GR contributed by OOMs with different volatilities for 1.5-25 nm particles. b Volatility distribution of SA and OOMs at measured ambient temperature in NPF days in the autumn of 2018 and 2021 in Beijing. Bars corresponding to the locations of -9 and 5 on the horizontal axis are the total concentration of OOMs with $\log_{10}C^* \leqslant -9$ and $\log_{10}C^* \geqslant 5$, respectively. c The concentration of SA and OOMs with different volatilities in 2018 and 2021. The volatility distribution of OOMs in 2018 is from Qiao et al.

The observation revealed significant positive correlations between the concentration of total OOMs and condensable OOMs with different volatilities and precursor AVOC levels (and $AVOCs_{nC \geq 4}$) (Fig. 3a). On the contrary, the fraction of OOMs with log10(C*) ⩽ -4, log10(C*) ⩽ -3 and log10(C*) ⩽ -2 decreased significantly as NOx increased (Fig. 3b). Based on the discussion above, the concurrent decline of AVOCs and NOx since 2017 has led to a reduction in total OOM concentration, and an increased proportion of condensable OOMs participating in new particle growth. To quantify these coupled effects on condensable OOM concentration and GR during 2017-2021, we developed a simplified parameterization scheme based on OOM observation in 2021. The agreement between simulations and measurements confirms that the GR increase in 2017-2021, which is primarily driven by elevated condensable OOM levels, resulted from the unbalanced emission reductions between AVOCs and NOx.

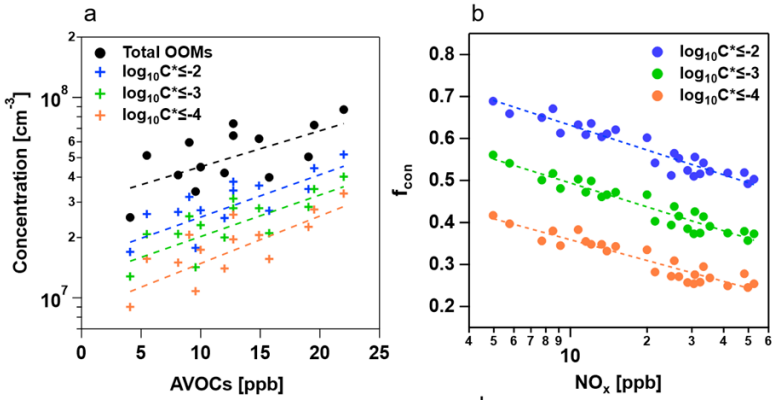


Fig. 3. Impact of AVOCs and NO_x on condensable OOM concentration. a The relationships between daily average concentration of OOMs and AVOCs at campaign-average temperature (289 K) during the observations in 2021. The dashed line represents the linear fitting line, and the fitting result is shown in Methods. (b) The relationships between daily average fraction of condensable OOMs (f_{con}) and NO_x at average temperature (289 K) during the observations in 2021. The dashed lines represent the logarithmic fitting line, and the fitting results is shown in Methods.

Our analysis reveals that prioritizing AVOCs control over NOx may more effectively suppress GR. The source-segregated OOM contribution is a vital basis for targeted AVOCs controlment.

ACKNOWLEDGEMENTS

Financial support from the National Key Research and Development Program of China (2022YFC3701000, task1), the National Natural Science Foundation of China-Creative Research Group Fund (22221004), Youth Fund of the National Natural Science Foundation of China (42305103), the National Key Research and Development Program of China (2022YFE0135000).

REFERENCES

Nie, W. *et al.* (2022) Secondary organic aerosol formed by condensing anthropogenic vapours over China's megacities. *Nature Geoscience* **15**, 255-261.

Qiao, X. *et al.* (2021) Contribution of Atmospheric Oxygenated Organic Compounds to Particle Growth in an Urban Environment. *Environmental Science & Technology* **55**, 13646-13656.

Stolzenburg, D., Wang, M., Schervish, M. & Donahue, N. M. (2022).Tutorial: Dynamic organic growth modeling with a volatility basis set. *Journal of Aerosol Science* **166**, 106063.

Mohr, C. *et al.* (2019) Molecular identification of organic vapors driving atmospheric nanoparticle growth. *Nature Communications* **10**, 4442.

COMPREHENSIVE SOURCE APPORTIONMENT OF URBAN VOCs: EVIDENCE FOR VCP-DOMINATED EMISSIONS USING HIGH-RESOLUTION MASS SPECTROMETRY AND BINPMF DURING THE ACROSS CAMPAIGN IN PARIS

RULAN VERMA[1,2], SEBASTIEN PERRIER[1], URS ROHNER[3], VINCENT MICHOUD[4], CLAUDIA DI BIAGIO[4], ALINE GRATIEN[4], LELIA HAWKINS[5], BARBARA D'ANNA[6], JULIEN KAMMER[6], ANNE MONOD[6], CHRISTOPHER CANTRELL[4], CHRISTIAN GEORGE[1], FELIPE LOPEZ HILFIKER[3], HARALD STARK[7,8], MATTHIEU RIVA[1,3]

[1]Univ. Lyon, Universite Claude Bernard Lyon1, CNRS, IRCELYON, 69626 Villeurbanne, France

[2]Institute of Materials Chemistry, TU Wien, Vienna, 1060, Austria

[3]Tofwerk AG, 3600 Thun, Switzerland

[4]Université Paris Cité and Univ Paris Est Creteil, CNRS, LISA, F-75013 Paris, France

[5]Department of Chemistry, Harvey Mudd College, 301 Platt Blvd, Claremont, California 91711, United States

[6]Aix Marseille Université, CNRS, LCE, Marseille, France

[7]Aerodyne Research Inc., Billerica, Massachusetts 01821, USA

[8]Cooperative Institute for Research in Environmental Sciences and Department of Chemistry, University of Colorado, Boulder, Colorado 80309, United States

.

Keywords: URBAN AIR QUALITY, HIGH RESOLUTION MASS SPECTROMETRY, BIN PMF, ATMOSPHERIC CHEMISTRY, VOLATILE ORGANIC COMPOUNDS, VOLATILE CHEMICAL PRODUCTS, EMISSION INVENTORY

INTRODUCTION

The growing presence of emerging pollutants in urban environments poses a significant challenge to air quality and climate. Among the key contributors to urban air quality are volatile organic compounds (VOCs), a diverse group of chemicals emitted from both anthropogenic and biogenic sources. Historically, road traffic was considered the dominant source of VOCs in cities. However, recent studies e.g., (McDonald et al., 2018) have shown that in many developed countries, emissions from Volatile Chemical Products (VCPs), such as personal care products, industrial solvents, and coatings, have overtaken vehicle emissions. Despite their growing importance, VCP emissions remain poorly characterized, and existing emission inventories often underestimate their role. The shift in pollution sources from traditional combustion-related emissions (e.g., transportation) to VCPs is largely driven by regulatory changes and evolving consumer behaviors (Coggon et al., 2021; McDonald et al., 2018; Seltzer et al., 2021).

Without effective VOC control, air pollution has shifted between chemical regimes, varying from VOC-limited in megacities to nitrogen oxides (NOx)--limited in rural areas (Ren et al., 2022). However, the hitherto lack of comprehensive ambient air observations hinders a thorough understanding of this evolving VOC landscape. This gap stems from a lack of comprehensive ambient measurements and source apportionment

studies. The ACROSS campaign aimed to close this knowledge gap by deploying advanced instrumentation to measure VOCs at high temporal and chemical resolution in the Paris metropolitan area.

METHODOLOGY

Field Campaign and Site Description

In the framework of the ACROSS project (Atmospheric ChemistRy Of the Suburban foreSt) an intensive summertime field campaign was performed to investigate the intricate chemical and physical aspects of urban air, mixed with biogenic emissions. It took place from June 14 to July 25, 2022, in Paris, France. Paris is one of the largest mid-latitude post-industrial megacities in Europe. Its population is estimated to be around 2.16 million and increases to approximately 12 million when considering the Greater Paris area (World Population Review, 2023).

The data collected at the Paris Rive Gauche (PRG) urban site (48.83°N, 2.38°E), at the top of a 7th-floor building at a height of 25 m above ground located at the Université Paris Cité are presented in this study. This site is influenced by strong anthropogenic emissions and partially from biogenic emissions from nearby green areas. According to AirParif, residents in the Île-de-France region are frequently exposed to NO_x and O_3 levels exceeding WHO thresholds, making it an ideal location to study complex VOC mixtures in a real-world urban context (AirParif, 2018, 2023).

Instrumentation

Two high-resolution chemical ionization mass spectrometers were deployed:

- Vocus PTR-TOF-MS (Proton Transfer Reaction, Time of Flight)
- Vocus-B Fast Polarity Switching TOF-MS, using NH_4^+ and I^- adduct chemistry

The instruments were connected to a 4.3 L manifold via a 15-meter Teflon sampling line, operated at 40 L/min to minimize residence time. The Vocus-B instrument employed 2-second cycles alternating between ion modes every 0.5 s, enabling comprehensive detection of a wide VOC range. Resolving power reached ~10,000 for the Vocus PTR-TOF and ~5,000 for the Vocus-B. Due to the high sensitivity and mass resolving power of the instruments, thousands of peaks were detected.

Data were post-processed using Tofware v3.3.0 (in Igor Pro 9.0). Further, source apportionment was performed on this big dataset using binPMF (binned positive matrix factorization) in SoFi. binPMF enhances PMF analysis of complex mass spectrometric datasets, simplifying data processing and improving source identification (Olin et al., 2022; Zhang et al., 2019, 2020). By integrating PMF with molecular information, it helps determine the sources and chemical processes of measured species (Zhang et al., 2019). To account for volatility differences and varying signal intensities, the high-resolution mass spectrometry data were binned into two distinct mass ranges and at multiple bin widths. This resulted in six separate datasets representing different mass domains. This dataset was analyzed with Sofi PMF which decomposed the data matrix into distinct source-related factors. After this, the top 10–25 major peaks in each factor profile were individually peak-fitted and characterized. This combined approach simplifies the complex, high-dimensional dataset and allows for the extraction of meaningful chemical signatures linked to specific emission sources. In this study, we have optimized binPMF and applied it to unravel VOC and Oxygenated VOC (OVOC) sources and their chemical evolution in the ambient environment.

RESULTS

The analysis revealed a diverse range of VOC classes, including acids, alcohols, acetates, esters, glycols, ketones, carbonyls, and siloxanes. Using binPMF, we were able to retain over 75% of the mass spectrometric dataset, identifying more than 350 key VOCs and resolving 13 distinct emission sources. Key sources included VCP-related emissions (e.g., glycols, glycol ethers, acrylates, coating solvents), cyclic volatile methyl siloxanes (cVMS) from personal care products, industrial and household solvents, road transport, and biogenic precursors with their oxidation products.

As depicted in Figure 1 anthropogenic VOCs (AVOCs) dominated the measured mass, accounting for 85% of the total, with VCP-related emissions contributing 47% and increasing to 64% when including mixed

oxidation products. Road transport sources made up only 21%, while biogenic VOCs, notably isoprene oxidation products, contributed 15%. Other biogenic compounds, such as monoterpene and sesquiterpene oxidation products, were detected at levels below 1%, reflecting their secondary role in this urban environment. The binPMF analysis revealed distinct diurnal patterns in source contributions, with clear differences between daytime and nighttime profiles. Secondary oxidation products, as well as personal care product emissions, were prominent during both periods. While traffic-related VOCs showed a typical rush-hour pattern, VCP-related signals remained relatively consistent throughout the day. These findings align with prior hypotheses, including (McDonald et al., 2018) which forecast a transition from traffic to VCP dominance in urban VOC sources.

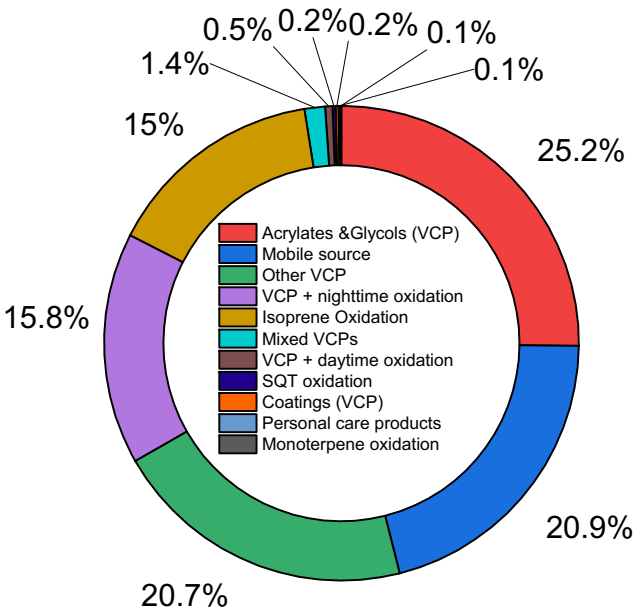


***Figure 1**. Relative contribution from different VOC sources at the measurement site*

CONCLUSIONS

We show that this shift has direct implications for air quality policy, as current European emission inventories often overestimate the contribution of road traffic while underrepresenting emissions from solvents and consumer products. Our results underscore the need to update these inventories and implement revised regulatory strategies that reflect the changing urban emission landscape. Overall, this study represents one of the most comprehensive VOC source apportionment efforts in a European megacity to date. By integrating high-resolution mass spectrometry with advanced analytical techniques, we demonstrate a clear transition in VOC emissions, with VCPs emerging as the dominant source in Paris. These insights are crucial for developing accurate emission inventories and designing targeted air pollution control strategies. In doing so, our work advances the understanding of urban atmospheric chemistry and provides policymakers with robust, real-world data to support more effective air quality management in rapidly evolving urban environments.

ACKNOWLEDGEMENTS

The authors gratefully acknowledge the French institution “Ecole Urbaine de Lyon” (EUL - Institut de Convergences) for funding the Ph.D. grant awarded to Rulan Verma, and Tofwerk for providing with the instruments. Dissemination support was provided by the Vienna Science and Technology Fund (WWTF) through project VRG22-003. The ACROSS project has received funding from the French National Research Agency (ANR) under the investment program integrated into France 2030, with the reference ANR-17-MPGA-0002, and it has been supported by the French national program LEFE (Les Enveloppes Fluides et l'Environnement) of the CNRS INSU (Centre National de la Recherche Scientifique - Institut National des Sciences de l'Univers).

REFERENCES

AirParif. (2018). Inventaire 2018 des émissions atmosphériques en Île-de-France | Airparif. https://www.airparif.asso.fr/actualite/2021/inventaire-2018-des-emissions-atmospheriques-en-ile-de-france

AirParif. (2023). Air quality is improving in Île-de-France, but the stakes are rising. https://www.airparif.asso.fr/en/understanding-pollution/sources-pollution

Coggon, M. M., Gkatzelis, G. I., McDonald, B. C., Gilman, J. B., Schwantes, R. H., Abuhassan, N., Aikin, K. C., Arend, M. F., Berkoff, T. A., Brown, S. S., Campos, T. L., Dickerson, R. R., Gronoff, G., Hurley, J. F., Isaacman-VanWertz, G., Koss, A. R., Li, M., McKeen, S. A., Moshary, F., … Warneke, C. (2021). Volatile chemical product emissions enhance ozone and modulate urban chemistry. PNAS, 118(32). https://doi.org/10.1073/pnas.2026653118

McDonald, B. C., de Gouw, J. A., Gilman, J. B., Jathar, S. H., Akherati, A., Cappa, C. D., Jimenez, J. L., Lee-Taylor, J., Hayes, P. L., McKeen, S. A., Cui, Y. Y., Kim, S.-W., Gentner, D. R., Isaacman-VanWertz, G., Goldstein, A. H., Harley, R. A., Frost, G. J., Roberts, J. M., Ryerson, T. B., & Trainer, M. (2018). Volatile chemical products emerging as largest petrochemical source of urban organic emissions. Science, 359(6377), 760–764. https://doi.org/10.1126/science.aaq0524

Olin, M., Okuljar, M., Rissanen, M. P., Kalliokoski, J., Shen, J., Dada, L., Lampimäki, M., Wu, Y., Lohila, A., Duplissy, J., Sipilä, M., Petäjä, T., Kulmala, M., & Dal Maso, M. (2022). Measurement report: Atmospheric new particle formation in a coastal agricultural site explained with binPMF analysis of nitrate CI-APi-TOF spectra. Atmospheric Chemistry and Physics, 22(12), 8097–8115. https://doi.org/10.5194/acp-22-8097-2022

Ren, J., Guo, F., & Xie, S. (2022). Diagnosing ozone–NO_x–VOC sensitivity and revealing causes of ozone increases in China based on 2013–2021 satellite retrievals. Atmospheric Chemistry and Physics, 22(22), 15035–15047. https://doi.org/10.5194/acp-22-15035-2022

Seltzer, K. M., Murphy, B. N., Pennington, E. A., Allen, C. C. R., Talgo, K., & Pye, H. O. T. (2021). Volatile Chemical Product Enhancements to Criteria Pollutants in the United States. Environmental Science & Technology. https://doi.org/10.1021/acs.est.1c04298

World Population Review. (2023). Paris Population 2023. https://worldpopulationreview.com/world-cities/paris-population

Zhang, Y., Peräkylä, O., Yan, C., Heikkinen, L., Äijälä, M., Daellenbach, K. R., Zha, Q., Riva, M., Garmash, O., Junninen, H., Paatero, P., Worsnop, D., & Ehn, M. (2019). A novel approach for simple statistical analysis of high-resolution mass spectra. Atmospheric Measurement Techniques, 12(7), 3761–3776. https://doi.org/10.5194/amt-12-3761-2019

Zhang, Y., Peräkylä, O., Yan, C., Heikkinen, L., Äijälä, M., Daellenbach, K. R., Zha, Q., Riva, M., Garmash, O., Junninen, H., Paatero, P., Worsnop, D., & Ehn, M. (2020). Insights into atmospheric oxidation processes by performing factor analyses on subranges of mass spectra. Atmospheric Chemistry and Physics, 20(10), 5945–5961. https://doi.org/10.5194/acp-20-5945-2020

The significant impact of organic transport on new particle formation and ultrafine particle concentration in Beijing

Ying. WEI[1], Xueshun CHEN[2], Zhiheng. LIAO[1], Pengkun MA[1], and Jiannong QUAN[1]

[1]*Institute of Urban Meteorology, China Meteorological Administration, Beijing, China.*

[2] *Institute of Atmospheric Physics, Chinese Academy of Sciences, Beijing, China.*

Keywords: Ultrafine particle, Organic aerosols, NPF, Vertical distribution.

INTRODUCTION

Organic compounds play a critical role in new particle formation (NPF) and $PM_{2.5}$ development in urban environments. In megacities like Beijing, extensive field campaigns and laboratory studies have shed light on the mechanisms and growth processes of NPF under varying atmospheric conditions—particularly during spring and summer when strong solar radiation and abundant volatile organic compound (VOC) emissions prevail. However, the influence of organic emissions on regional-scale NPF remains insufficiently understood, especially regarding their vertical three-dimensional characteristics, due to limited modeling studies. In this work, we apply a three-dimensional atmospheric chemistry model coupled with a detailed Aerosol Microphysics module (APM) and a volatility basis set (VBS)–based organic aerosol module, which explicitly resolves NPF and subsequent particle growth processes, capturing the dynamic evolution from nanometer-scale clusters to submicron particles. Incorporating multi-level vertical observations from the CITIC Tower (528 m) in Beijing, we systematically evaluate the contribution of organic aerosols to ultrafine particle number concentrations and size distributions during typical NPF events. The results reveal distinct vertical differences in the dominant factors affecting organic aerosol concentration. Near the surface, local primary emissions play a leading role, whereas aloft, regional transport becomes the primary driver of organic aerosol variability. This study highlights the critical role of organic aerosols in shaping the vertical structure of NPF and provides important numerical insights into the combined impacts of regional transport and local sources on urban ultrafine particle formation.

METHODS

Site	Height (m)	Observation period	Observed species
CITIC	90	2022.04.01-2022.04.30	PNSD and mass concentration of secondary inorganic aerosols (SIA) and organic matter (OM)
CITIC	520	2022.04.01-2022.04.30	PNSD and mass concentration of SIA, black carbon and OM
CNEMC	Surface	2022.04.01-2022.04.30	$PM_{2.5}$

Table 1. Information of observations.

CONCLUSIONS

The results reveal distinct vertical differences in the dominant factors affecting organic aerosol concentration. Near the surface, local primary emissions play a leading role, whereas aloft, regional transport becomes the primary driver of organic aerosol variability.

ACKNOWLEDGEMENTS

We thank the China National Environmental Monitoring Center for their support with $PM_{2.5}$ data and the support of the Technological Infrastructure project “Earth System Science Numerical Simulator Facility” (EarthLab).

REFERENCES

Chen, X., Yu, F., Yang, W., Sun, Y., Chen, H., & Du, W., et al. (2021). Global-regional nested simulation of particle number concentration by combing microphysical processes with an evolving organic aerosol module. Atmospheric Chemistry & Physics. 21, 9343–9366.

Wei Y., Chen X., Chen H., Sun Y., Yang W., & Du H., et al. (2021). Investigating the importance of sub-grid particle formation in point source plumes over eastern China using IAP-AACM v1.0 with a sub-grid parameterization, Geoscientific Model Development. 14, 4411–4428.

Wei Y., Chen X., Chen H., Li Jie, Wang Z., & Yang W., et al. (2019): IAP-AACM v1.0：Global to regional evaluation of the atmospheric chemistry model in CAS-ESM, Atmospheric Chemistry and Physics.

New Particle Formation in China's Megacities

C. YAN[1,2], W. NIE[1,2], M. KULMALA[1,2,3], and A. J. DING[1,2]

[1]*Nanjing-Helsinki Institute in Atmospheric and Earth System Sciences, Nanjing University, Suzhou, China*
[2]*School of Atmospheric Science, Nanjing University, Nanjing, China*
[3]*Department of Physics, University of Helsinki, Helsinki, 00140, Finland*

Keywords: new particle formation, urban environment, traffic emission, vertical distribution.

INTRODUCTION

Decades of research have significantly advanced our understanding of new particle formation (NPF) mechanisms through two parallel approaches: (1) Technological breakthroughs in detection methods (Vanhanen et al., 2011; Jokinen et al., 2012; Junninen et al., 2010; Stolzenburg et al., 2017), and (2) Controlled chamber experiments elucidating fundamental processes (Kirkby et al., 2011, 2016; Almeida et al., 2013; Riccobono et al., 2014; Lehtipalo et al., 2018; He et al., 2021; Shen et al., 2024). These mechanisms have been validated in environments less influenced by human activities, including forests (Rose et al., 2018; Mohr et al., 2019; Roldin et al., 2019), high-altitude sites (Bianchi et al., 2016, 2020; Zha et al., 2024), and marine/upper tropospheric regions (Sipilä et al., 2016; Wang et al., 2016; Curtius et al., 2024).

However, urban NPF under profound anthropogenic influence presents unresolved complexities: (1) The predominance of nucleation mechanisms remains contested, (2) Traffic emission contributions lack quantification, and (3) Vertical heterogeneity in boundary layer NPF is poorly characterized. Since 2018, our group has conducted systematic investigations across Chinese megacities (Beijing, Nanjing and etc.) to address these knowledge gaps.

This presentation will synthesize key findings regarding three fundamental questions:
Mechanistic dominance: What are the relative contributions of different nucleation pathways in urban environments?
Source apportionment: How significantly do traffic emissions contribute to urban NPF frequencies and intensities?
Spatial dynamics: How does NPF exhibit vertical stratification within urban boundary layers?

METHODS

NPF was investigated using both comprehensive measurement at two ground-level stations, i.e., the BUCT-AHL (Liu et al., 2020) in Beijing and SORPES (Ding et al., 2016) in Nanjing. In addition, a high-loading tethered balloon was used to study NPF at different height within the urban boundary layer. Instruments deployed at these two stations and in the tethered balloon are listed in Table 1.

Table 1 A list of key instruments at BUCT-AHL, SORPES and the tethered-balloon.

Location	Key instruments	Species measured
BUCT-AHL	Nitrate-CIMS	(highly) oxygenated organic molecules
BUCT-AHL	Iodide-CIMS	oxygenated organic molecules and halogen
BUCT-AHL	PSM	Nano-cluster concentration (<3 nm)
BUCT-AHL	DEG-SMPS+PSD	particle number size distribution (1.5 – 1000nm)

SORPES	Nitrate-CIMS	(highly) oxygenated organic molecules
SORPES	PSM	Nano-cluster concentration (<3 nm)
SORPES	DMPS	Particle number size distribution (6 – 500nm)
Balloon	Nitrate-CIMS	(highly) oxygenated organic molecules
Balloon	Nano-SMPS	Particle number size distribution (4 – 60nm)

REFERENCES

Almeida, J. et al. Molecular understanding of sulphuric acid-amine particle nucleation in the atmosphere, Nature, 502, 359-363, 10.1038/nature12663, 2013.

Bianchi, F. et al. Biogenic particles formed in the Himalaya as an important source of free tropospheric aerosols, Nature Geoscience, 14, 4-9, 2020.

Bianchi, F. et al. New particle formation in the free troposphere: A question of chemistry and timing, Science, 352, 1109-1112, , 2016.

Curtius, J. et al. Isoprene nitrates drive new particle formation in Amazon's upper troposphere, Nature, 636, 124-130, 2024.

Ding, A. et al. Long-term observation of air pollution-weather/climate interactions at the SORPES station: a review and outlook, Front Env Sci Eng, 10, 2016.

He, X. C. et al. Role of iodine oxoacids in atmospheric aerosol nucleation, Science, 371, 589-595, 2021.

Jokinen, T. et al. Atmospheric sulphuric acid and neutral cluster measurements using CI-APi-TOF, Atmospheric Chemistry and Physics, 12, 4117-4125, 2012.

Junninen, H. et al. A high-resolution mass spectrometer to measure atmospheric ion composition, Atmospheric Measurement Techniques, 3, 1039-1053, 2010.

Kirkby, J. et al. Role of sulphuric acid, ammonia and galactic cosmic rays in atmospheric aerosol nucleation, Nature, 476, 429-433, 2011.

Kirkby, J. et al. Ion-induced nucleation of pure biogenic particles, Nature, 533, 521-526, 2016.

Lehtipalo, K. et al. Multicomponent new particle formation from sulfuric acid, ammonia, and biogenic vapors, Sci Adv, 4, eaau5363, 2018.

Liu, Y. et al. Continuous and comprehensive atmospheric observations in Beijing: a station to understand the complex urban atmospheric environment, Big Earth Data, 4, 295-321, 2020.

Mohr, C. et al. Molecular identification of organic vapors driving atmospheric nanoparticle growth, Nat Commun, 10, 4442, 2019.

Riccobono, F. et al. Oxidation products of biogenic emissions contribute to nucleation of atmospheric particles, Science, 344, 717-721, 2014.

Roldin, P. et al. The role of highly oxygenated organic molecules in the Boreal aerosol-cloud-climate system, Nat Commun, 10, 4370, 2019.

Rose, C. et al. Observations of biogenic ion-induced cluster formation in the atmosphere, Sci Adv, 4, eaar5218, 2018.

Shen, J. et al. New particle formation from isoprene under upper-tropospheric conditions, Nature, 636, 115-123, 2024.

Sipilä, M. et al. Molecular scale evidence of new particle formation via sequential addition of HIO3, Nature, 532-537, 2016.

Stolzenburg, D. et al. A DMA-train for precision measurement of sub-10 nm aerosol dynamics, Atmospheric Measurement Techniques, 10, 1639-1651, 2017.

Vanhanen, J. et al. Particle Size Magnifier for Nano-CN Detection, Aerosol Science and Technology, 45, 533-542, 2011.

Wang, J. et al. Amazon boundary layer aerosol concentration sustained by vertical transport during rainfall, Nature, 539, 416-419, 2016.

Zha, Q. et al. Oxidized organic molecules in the tropical free troposphere over Amazonia, Natl Sci Rev, 11, nwad138, 2024.

New Insights into New Particle Formation from A Comparison Study Between Biogenic and Anthropogenic Emissions Dominated Environments

TINGHAN. ZHANG[1,2], WEI.DU[1,2], JANNE. LAMPILAHTI[1], XINRAN. ZHANG[1], ZEHAO. ZOU[1], TOM. KOKKONEN[1], VELI-MATTI. KERMINEN[1], AND MARKKU KULMALA[1,2]

[1]*Institute for Atmospheric and Earth System Research (INAR), University of Helsinki, Helsinki, 00560, Finland.*

[2]*Aerosol and Haze Laboratory, Beijing Advanced Innovation Center for Soft Matter Science and Engineering, Beijing University of Chemical Technology, Beijing, China.*

Keywords: NEW PARTICLE FORMATION, URBAN ENVIRONMENT, BOREAL FOREST.

INTRODUCTION

Atmospheric new particle formation (NPF) and growth involves the formation of molecular clusters and their subsequent growth to larger particles, potentially reaching sizes at which they can serve as cloud condensation nuclei (CCN) (Kulmala et al., 2012). Current studies indicate that NPF occurs ubiquitously in the global atmosphere (Kerminen et al., 2018). In this study, we employ a novel nano-ranking method (Aliaga et al., 2023) to comparatively analyze NPF events in two distinctly different environments: the megacity of Beijing in China and the boreal forest of Hyytiälä in Finland. Based on a five-year dataset from 2018 to 2020, we investigate the seasonal variations in NPF characteristics: NPF probabilities, NPF intensities, formation rates, and growth rates, in environments dominated by both biogenic and anthropogenic emissions. Furthermore, by investigating the sources, sinks, and meteorological factors influencing NPF, we aim to elucidate similarities and differences in the underlying mechanisms driving NPF in these two contrasting environments. Additionally, this study examines quiet NPF events, referring to days traditionally classified as non-NPF event days that have previously been overlooked (Kulmala et al., 2022) at both locations.

METHODS

In this work, a novel nano-ranking method is used for characterizing the intensity and frequency of NPF, which was determined by the daily peak of total particle number concentration between 2.5nm and 5nm ($N_{2.5\text{-}5}$). This method is based on the theory that daily fluctuation of the particle number concentrations within the 2.5–5 nm diameter range ($N_{2.5\text{-}5}$) is acutely sensitive to the presence of atmospheric NPF. The lower boundary of particle size is set as 2.5nm to avoid the interference from the continuous mode of molecular clusters, while the higher boundary is chosen as 5nm to minimize the influence of ultrafine particles from traffic emission sources.

CONCLUSIONS

Through a comparative analysis between Beijing and Hyytiälä, we demonstrate that the nano-ranking method effectively characterizes both the probability and intensity of NPF at each location. Our results indicate that NPF events are more frequent in spring in Hyytiälä, whereas in Beijing, the highest frequency occurs during winter. Seasonal differences in NPF characteristics at both locations are mainly governed by

variations in gaseous precursors and the condensation sink. The driving sources of NPF differ substantially between the two sites: sulfuric acid (SA) dimers play a key role in Beijing, while NPF events in Hyytiälä are primarily driven by the combined influence of SA and highly oxygenated organic molecules (HOMs). Additionally, quiet NPF occur at both sites, and we find that during these quiet NPF periods, the growth rates of particles in the size range of 6–25 nm do not significantly differ between the two locations.

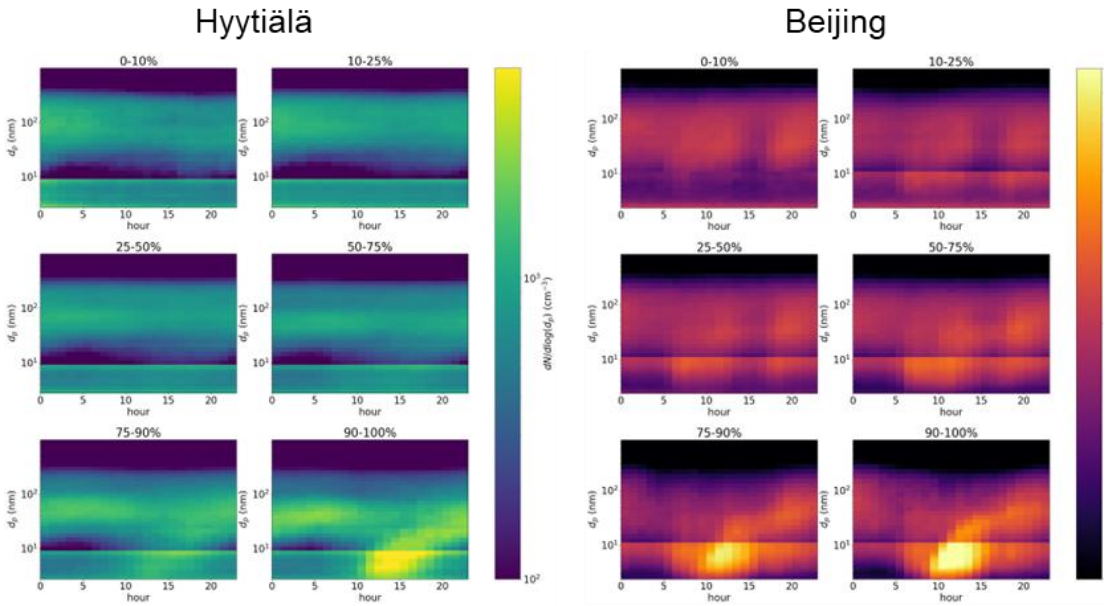


Figure 1. Daily median number particle size distributions grouped into intervals based on the nano-ranking method. The diameter limits (y axis) in the surface plots are 2.5 and 1000 nm and are used to illustrate the shape of the potential NPF events in each interval. For illustration purposes, the particle number concentrations obtained from the neutral cluster and air ion spectrometer (NAIS, 2.5–20 nm) and the differential mobility particle sizer (DMPS, 20–1000 nm) are combined.

ACKNOWLEDGEMENTS

This work was supported by the ACCC Flagship funded by the Academy of Finland (grant nos. 337549), Academy of Finland project (grant nos. 316114, 325647, 325681 and 347782), and the “Gigacity” project funded by the Jenny and Antti Wihuri Foundation.

REFERENCES

Aliaga, D., Tuovinen, S., Zhang, T., Lampilahti, J., Li, X., Ahonen, L., Kokkonen, T., Nieminen, T., Hakala, S., & Paasonen, P. (2023). Nano Ranking Analysis: determining NPF event occurrence and intensity based on the concentration spectrum of formed (sub-5 nm) particles. *Aerosol Research Discussions*, *2023*, 1-19.

Kerminen, V.-M., Chen, X., Vakkari, V., Petäjä, T., Kulmala, M., & Bianchi, F. (2018). Atmospheric new particle formation and growth: review of field observations. *Environmental Research Letters*, *13*(10), 103003.

Kulmala, M., Junninen, H., Dada, L., Salma, I., Weidinger, T., Thén, W., Vörösmarty, M., Komsaare, K., Stolzenburg, D., & Cai, R. (2022). Quiet new particle formation in the atmosphere. *Frontiers in Environmental Science*, *10*, 912385.

Kulmala, M., Petäjä, T., Nieminen, T., Sipilä, M., Manninen, H. E., Lehtipalo, K., Dal Maso, M., Aalto, P. P., Junninen, H., & Paasonen, P. (2012). Measurement of the nucleation of atmospheric aerosol particles. *Nature protocols*, *7*(9), 1651-1667.

Volatility parametrization of atmospheric organic compounds based on molecular formula

Xiao Zhang[1], Chuang Li[1], Runlong Cai[1], Lei, Yao[1], Lin Wang[1]

[1]Shanghai Key Laboratory of Atmospheric Particle Pollution and Prevention (LAP[3]), Department of Environmental Science & Engineering, Jiangwan Campus, Fudan University, Shanghai 200438, China.

ABSTRACT: Saturation vapor pressure of atmospheric organic compounds plays a crucial role in understanding their gas-particle partitioning. Yet measurements of such a property are quite incomplete, and an accurate and efficient volatility parameterization remains a challenge. In this study, we utilized a Long Time-of-Flight Chemical Ionization Mass Spectrometer (LToF-CIMS) coupled with a Filter Inlet for Gases and Aerosols (FIGAERO) to measure molecular composition and saturation vapor pressure of organic compounds in ambient aerosols. Two desorption procedures, i.e., one with a high-temperature range of 20-160°C and the other with a low-temperature range of 5-35°C, were implemented to analyze particulate samples collected from Wangdu, Dianshan Lake, and Tai Lake, China across different seasons with a wide temperature coverage. The obtained saturation vapor pressure for organic components in aerosol particles, together with results from previous studies, were converted with particle phase activity (α) to those for pure compounds by taking into account non-ideal molecular interactions. Then the Synthetic Minority Oversampling Technique (SMOTE) and Random Under-sampling (RUS) were applied to consider the imbalanced number of datapoints across different volatility ranges. As a final step, a novel volatility parameterization was developed via an 8-parameter fitting of a commonly used volatility formula. Comparison of volatilities predicted by different parameterizations and those from NCI (National Cancer Center) demonstrates improved accuracies, for both CHO and CHON compounds, by our parameterization, which helps to improve the performance for atmospheric models that use volatility as a key input.

DRCREASING SO2 LEVELS FORM COAL POWERPLANTS INFLUENCE ATMOSPHERIC PARTICLE FORMATION

X. ZHANG[1], Y. LI[1,2], Y. GU[1], L. VETTIKKAT[3], S. SCHOBESBERGER[3], M. KULMALA[1], and M. EHN[1]

[1]*Institute for Atmospheric and Earth System Research, University of Helsinki, Helsinki, Finland.*

[2]*Joint International Research Laboratory of Atmospheric and Earth System Sciences, School of Atmospheric Sciences, Nanjing University, Nanjing, China.*

[3]*Department of Technical Physics, University of Eastern Finland, Kuopio, Finland.*

Keywords: SO_2, NH_3, H_2SO_4-NH_3 CLUSTERS, NEW PARTICLE FORMATION.

INTRODUCTION

Sulfur dioxide (SO_2) plays a crucial role in new particle formation (NPF) by being oxidized in the atmosphere to produce sulfuric acid (H_2SO_4), one of the most important compounds involved in the nucleation process. SO_2 emissions, primarily from volcanic eruptions, fossil fuel combustion, and industrial activities, contribute to atmospheric sulfuric acid levels, which in turn promote the growth of clusters into larger aerosol particles.
The Northern agricultural ecosystem and agricultural activities play a crucial role in atmospheric chemistry and climate regulation. Agricultural activities release ammonia (NH_3), which can react in the atmosphere with H_2SO_4 to form $(H_2SO_4)_m(NH_3)_n$ clusters that can grow to new particles. This new particle formation can subsequently exert significant impact on the production of cloud condensation nuclei (CCN) and, thus, the regulation of atmospheric temperature.

METHODS

We performed measurements of H_2SO_4, $(H_2SO_4)_m(NH_3)_n$ clusters, and highly oxidized organic molecules (HOMs) at an agricultural field site in Viikki, Helsinki (SMEAR Agri) from April to September 2023. Species were measured using a nitrate ion (NO_3^-)-based chemical ionization atmospheric pressure interface time-of-flight mass spectrometer (CI-APi-TOF, Aerodyne Research Inc. & Tofwerk AG) (Jokinen *et al*., 2012). Concentrations of ions in the range of 0.8–42 nm and particles in the range of 2.5–40 nm were measured using a neutral cluster and air ion spectrometer (NAIS; Airel Ltd) (Mirme and Mirme, 2013; Manninen *et al*., 2016).

CONCLUSIONS

Our study highlights the significant role of $(H_2SO_4)_m(NH_3)_n$ clusters in NPF at the Viikki station, particularly during periods of elevated SO_2 concentrations. NH_3 levels were almost consistently high enough to not limit cluster formation or growth, indicating that SO_2 is a key tracer in this process. We observed clear correlations across species, from H_2SO_4 monomers and dimers to $(H_2SO_4)_m(NH_3)_n$ clusters, negative ions between 2-2.3 nm, and small particle number concentrations (3–5 nm). This progression indicates that $(H_2SO_4)_m(NH_3)_n$ clusters are crucial in connecting SO_2 emissions to the formation and growth of atmospheric particles in this region, with implications for future trends in new particle formation as global SO_2 concentrations decline.

REFERENCES

Jokinen, T. et al (2012). Atmospheric sulphuric acid and neutral cluster measurements using CI-APi-TOF. Atmospheric Chemistry and Physics 12, 4117–4125.

Mirme, S. & Mirme, A (2013). The mathematical principles and design of the NAIS – a spectrometer for the measurement of cluster ion and nanometer aerosol size distributions. Atmospheric Measurement Techniques 6, 1061–1071.

Manninen, H. E., Mirme, S., Mirme, A., Petäjä, T. & Kulmala, M (2016). How to reliably detect molecular clusters and nucleation mode particles with Neutral cluster and Air Ion Spectrometer (NAIS). Atmospheric Measurement Techniques 9, 3577–3605.

Special Session 5: Instruments, chambers, facilities

HOMOGENEOUS AND HETEROGENEOUS GENERATION OF NANOPARTICLES BY EVAPORATION-CONDENSATION WITH THE SILVER PARTICLE GENERATOR

P.S. BAUER[1], V. BERGER[1], K.M. RISBY[2], E. SORANI[1], H.J. SCHULZ[1], J. SWANSON[1,3], A. BOIES[1,4]

[1] *Catalytic Instruments GmbH & Co.KG, 83026 Rosenheim, Germany.*
[2] *University of Cambridge, Department of Engineering, Cambridge CB2 1PZ, United Kingdom.*
[3] *Minnesota State University, Mankato, MN 56001, United States.*
[4] *Stanford University, Department of Engineering, Stanford, CA 94305, United States.*

Keywords: evaporation-condensation, silver nanoparticles, heterogeneous condensation, aerosol generator.

INTRODUCTION

A stable and defined aerosol source is one key component for many nucleation and aerosol studies. The evaporation-condensation method has been established as one of the most versatile and reliable techniques to generate nanoparticles from different materials, e.g., from salts, metals or even plastics (Scheibel and Porstendörfer, 1983; Wlasits *et al.*, 2022). However, each laboratory has its own setup of this method and results from one study cannot easily be replicated and utilized for another study. The silver particle generator (SPG) from Catalytic Instruments (CI) was developed to standardize the evaporation-condensation generation method (Hammer *et al.*, 2022) and despite its name, it can be used with all different kinds of materials (Krasa *et al.*, 2025). Nevertheless, silver (Ag) nanoparticles represent one of the most used test aerosols with applications ranging from heterogeneous nucleation studies (Porstendörfer *et al.*, 1985; Winkler *et al.*, 2016), aerosol charging (Wiedensohler and Fissan, 1991) to calibration of differential mobility analyzers (DMAs) and condensation particle counters (CPCs) (EN 16976:2024; Wiedensohler *et al.*, 2018; Wlasits *et al.*, 2020). The advantages of silver is that it is solid, rather unreactive, normally insoluble and it can be formed to a thermally stable and compact sphere. Especially this last feature is essential because many fundamental aerosol characteristics are first and foremost defined for spherical particles. There are two ways to achieve spherical silver particles beyond 20 nm. One is by generating large fractal-like particles, which must be thermally treated (sintered) at temperatures in the range of 400 to 700 °C (Ku *et al.*, 2006; Zihlmann *et al.*, 2014; Tuch *et al.*, 2016; Berger *et al.*, 2024). Thereby spheres of up to 100 nm particles are feasible as low-density agglomerates shrink about 70 % in mobility size to form solid spheres (Zihlmann *et al.*, 2014; Berger *et al.*, 2024). Another way is by heterogeneous nucleation and condensation of silver vapor onto seed particles, where it has been shown that spherical particles up to 104 nm can be achieved (Zihlmann *et al.*, 2014). Here, we present the SPG as a versatile tool to generate particles of different materials but also for heterogeneous condensation studies in a tandem SPG setup.

METHODS

Switching between different materials with the evaporation-condensation method is a tedious task when a tube furnace is used because the whole generation tube must be exchanged to avoid cross contamination. The SPG has a tube-set inside, which is connected to the air supply and the outlet of the SPG and can easily be exchanged. Due to the relatively small volume of the tube-set the heat-up times are fast while the instrument design ensures a very stable aerosol production. With this it is possible to evaporate and condense plastics and organic molecules like tetracontane ($C_{40}H_{82}$) with relatively low melting points < 200 °C, different salts (NaCl, KCl, LiCl, NaI, etc.) in the medium temperature range between 300 to 700 °C or metals with melting points above 800 °C (e.g., Ag, Au) in a standardized way. Here we will present some of the concentrations and size distributions that can be achieved with different materials in the SPG. Another benefit is that if settings for one material are found in one SPG the tube-set can be transferred to another SPG and similar distribution can be generated with the same settings.
This feature was utilized in the tandem SPG setup (Fig. 1) where silver seed particles were generated with SPG 1. There the concentration and size distribution of the seed particles can be determined beforehand and set during the tandem experiment. Then either the whole size distribution of seed particles or size selected

particles (charge conditioner + DMA 1) were sent into the second SPG 2, where they are exposed to silver vapor. The silver vapor in SPG 2 can then heterogeneously nucleate and condense onto the seed particles. In a first step, we aimed to reproduce the results of Zihlmann *et al.* (2014) by using silver seed particles with a silver coating.

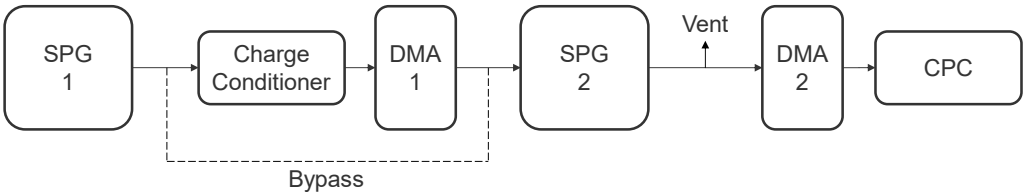


Figure 1. Experimental setup of the tandem SPG setup to produce spherical silver particles by heterogenous condensation. The seed particles are produced in SPG 1. Either the full seed particle distribution or only size selected particles are (charge conditioned + DMA 1) are sent into SPG 2, where silver vapor condenses heterogeneously onto the seed particles. DMA 2 and CPC are used as a scanning mobility particle sizer (SMPS) system.

In the second step the potential of the tandem SPG setup was examined in more detail. Because the SPG's temperature and flow rates can be adjusted quickly, the parameter space of temperature and gas flow combinations can be effectively investigated over a wide range for the two SPGs. The primary objectives were to determine the maximum particle size limit and whether heterogeneous silver deposition can produce monodisperse aerosol particles from polydisperse seeds. Furthermore, the generated particles' morphology was examined using TEM imaging.

CONCLUSIONS

The generation of nanoparticles from different materials has many different applications in aerosol and material research. With the SPG it is easy and clean to switch between different materials as the whole tube-set can be switched. With the standardization of the evaporation-condensation method the parameters for one material can be transferred from one SPG to another. This also helped with the tandem SPG setup. Here one SPG generated seed particles with predefined settings, which then were sent into another SPG for heterogeneous condensation. This combination of two SPGs generating seed particles with coating has great potential in aerosol science (large spherical particles), but also in material research when different materials are used as seed particle and coating.

ACKNOWLEDGEMENTS

This work was supported by the EPSRC Centre for Doctoral Training in Aerosol Science (EPSRC / CDT) under grant code EP/S023593/1.

REFERENCES

Berger, V., Sorani, E., Wu, A., Schulz, H. J., Boies, A., and Swanson, J. (2024) Evaluation of Monodisperse Silver Particle Sintering Using a Tandem DMA Setup. *27th ETH Nanoparticles Conference*, Zurich, Switzerland.

EN 16976:2024 (2024). Ambient air - Determination of the particle number concentration of atmospheric aerosol. *European Committee for Standardization*.

Hammer, T., Irwin, M., Swanson, J., Berger, V., Sonkamble, U., Boies, A., Schulz, H., and Vasilatou, K. (2022). Characterising the silver particle generator; a pathway towards standardising silver aerosol generation. *Journal of Aerosol Science* 163:105978.

Krasa, H., Risby, K.M., Kupper, M., Bergmann, A., and Boies, A.M. (2025). Stable Generation and Counting Efficiency Evaluation of Various Salt Aerosols With the Silver Particle Generator. *Aerosol Science and Technology* (accepted 19. Mar. 2025).

Ku, B.K. and Maynard, A.D. (2006). Generation and investigation of airborne silver nanoparticles with specific size and morphology by homogeneous nucleation, coagulation and sintering. *Journal of Aerosol Science* 37 (4):452.

Porstendörfer, J., Scheibel, H.G., Pohl, F.G., Preining, O., Reischl, G., and Wagner, P.E. (1985). Heterogeneous Nucleation of Water Vapor on Monodispersed Ag and NaCl Particles with Diameters Between 6 and 18 nm. *Aerosol Science and Technology* 4 (1):65.

Scheibel, H.G. and Porstendörfer, J. (1983). Generation of monodisperse Ag- and NaCl-aerosols with particle diameters between 2 and 300 nm. *Journal of Aerosol Science* 14 (2):113.

Tuch, T., Weinhold, K., Merkel, M., Nowak, A., Klein, T., Quincey, P., Stolzenburg, M., and Wiedensohler, A. (2016). Dependence of CPC cut-off diameter on particle morphology and other factors. *Aerosol Science and Technology* 50 (4):331.

Wiedensohler, A. and Fissan, H.J. (1991). Bipolar Charge Distributions of Aerosol Particles in High-Purity Argon and Nitrogen. *Aerosol Science and Technology* 14 (3):358.

Wiedensohler, A., Wiesner, A., Weinhold, K., Birmili, W., Hermann, M., Merkel, M., Müller, T., Pfeifer, S., Schmidt, A., Tuch, T., Velarde, F., Quincey, P., Seeger, S., and Nowak, A. (2018). Mobility particle size spectrometers: Calibration procedures and measurement uncertainties. *Aerosol Science and Technology* 52 (2):146.

Winkler, P.M., McGraw, R.L., Bauer, P.S., Rentenberger, C., and Wagner, P.E. (2016). Direct determination of three-phase contact line properties on nearly molecular scale. *Scientific Reports* 6 (1):26111.

Wlasits, P.J., Stolzenburg, D., Tauber, C., Brilke, S., Schmitt, S.H., Winkler, P.M., and Wimmer, D. (2020). Counting on chemistry: laboratory evaluation of seed-material-dependent detection efficiencies of ultrafine condensation particle counters. *Atmospheric Measurement Techniques* 13 (7):3787.

Wlasits, P.J., Stöllner, A., Lattner, G., Maggauer, K., and Winkler, P.M. (2022). Size characterization and detection of aerosolized nanoplastics originating from evaporated thermoplastics. *Aerosol Science and Technology* 56 (2):176.

Zihlmann, S., Lüönd, F., and Spiegel, J.K. (2014). Seeded growth of monodisperse and spherical silver nanoparticles. *Journal of Aerosol Science* 75:81.

A REACTIVE CONDENSATION PARTICLE COUNTER FOR MEASURING ATMOSPHERICALLY RELEVANT CONCENTRATIONS OF SULFURIC ACID

DOMINIC A. CASALNUOVO[1,2], DARREN CHENG[2,3], MICHEL FLORES-ROMERO[4], ALEJANDRO MONTESINOS-CASTELLANOS[4], COTY N. JEN[1,2]

[1]Department of Chemical Engineering, Carnegie Mellon University, Pittsburgh, 15213, USA
[2]Center for Atmospheric Particle Studies, Carnegie Mellon University, Pittsburgh, 15213, USA
[3]Department of Mechanical Engineering, Carnegie Mellon University, Pittsburgh, 15213, USA
[4]Tecnologico de Monterrey, School of Engineering and Sciences, Ave. Eugenio Garza Sada 2501 Sur, Monterrey, N.L., Mexico, 64849

Keywords: Sulfuric acid, condensation particle counter, dimethylamine.

INTRODUCTION

Atmospheric sulfuric acid is currently measured using a chemical ionization mass spectrometer (CIMS). This instrument exhibits high sensitivity, often down to $10^4 - 10^5$ molecules cm^{-3}, and can resolve sulfuric acid from other atmospheric trace compounds. However, CIMS is an expensive ($300K-$500K), heavy (50-100 kg), and power-intensive (1-2 kW) instrument. In addition, maintaining these instruments and processing the data is technically challenging. All these traits combined prevent numerous research groups and monitoring stations from obtaining and deploying CIMS for laboratory and field measurements. As such, only sparse and short-duration measurements of sulfuric acid exist for locations around the world (Cai et al., 2021; Chen et al., 2012; Hodshire et al., 2016; Myers et al., 2022). A more compact and less expensive instrument is essential to provide a comprehensive observational data set for constraining how atmospheric nucleation and aerosols influence Earth's radiative budget.

This study presents the Sulfuric Acid Dimethylamine-Reactive Condensation Particle Counter (SAD-RCPC), a new method to measure atmospheric sulfuric acid concentrations. This technique leverages the known nucleation reactions of sulfuric acid and dimethylamine to estimate gaseous sulfuric acid concentrations (Jen et al., 2014; Kürten et al., 2018). The SAD-RCPC combines a compact nucleation flow reactor that reacts gaseous sulfuric acid with dimethylamine to form 1-nm particles that are then detected by a condensation particle counter. Laboratory and field validations of the SAD-RCPC with a CIMS are presented to demonstrate the feasibility of the SAD-RCPC instrument. Ultimately, the cost, ease of use, and portability of the SAD-RCPC and its future iterations will allow it to be deployed more widely, such as for long-term measurements or on unmanned aerial vehicles. These measurements will help constrain aerosol microphysics models and provide the needed information on how nucleation occurs throughout the boundary layer.

METHODS

The Sulfuric Acid Dimethylamine-Reactive Condensation Particle Counter (SAD-RCPC) operates by reacting sulfuric acid (SA) with a stabilizing compound in a controlled manner to form detectable 1-nm particles. The stabilizing compound must react and nucleate with SA at the gas collision limit to maximize the amount of SA converted into particles. In addition, the stabilizing compound should not appreciably nucleate with itself or any other atmospherically relevant compounds on the nucleation timescales utilized in the SAD-RCPC. Dimethylamine (DMA, $(CH_3)_2N$) was chosen as it was previously shown to not nucleate with itself, water, or other atmospherically relevant acids such as formic, malonic, acetic, and oxalic acids at temperatures >273 K (Fomete et al., 2023; Johnson & Jen, 2023; Olenius et al., 2017). SA-DMA nucleation in the SAD-RCPC was modeled following the simplified acid-base nucleation reaction presented by Johnson and Jen (2022, 2023).The SA concentration was indirectly measured by the SAD-RCPC by relating the particle concentration measured by the DEG wCPC to the particle concentration

predicted from SA-DMA nucleation reaction model. pecifically, the differential cluster balance equations (Equation S1) from the model were numerically integrated to the given nucleation reaction time (e.g., 25 s) with a guess initial SA concentration and an initial DMA concentration of 1 ppbv. The resulting solution from the cluster balance equations was the modeled cluster concentrations for different cluster sizes. Modeled cluster concentrations were then multiplied by the detection efficiency of the DEG wCPC and compared to the measured particle concentration of the SAD-RCPC. The initial SA concentration was then varied until the modeled detectable particle concentration was within 0.01% of the measured particle concentration. This initial SA concentration equaled the sampled SA concentration in the SAD-RCPC.

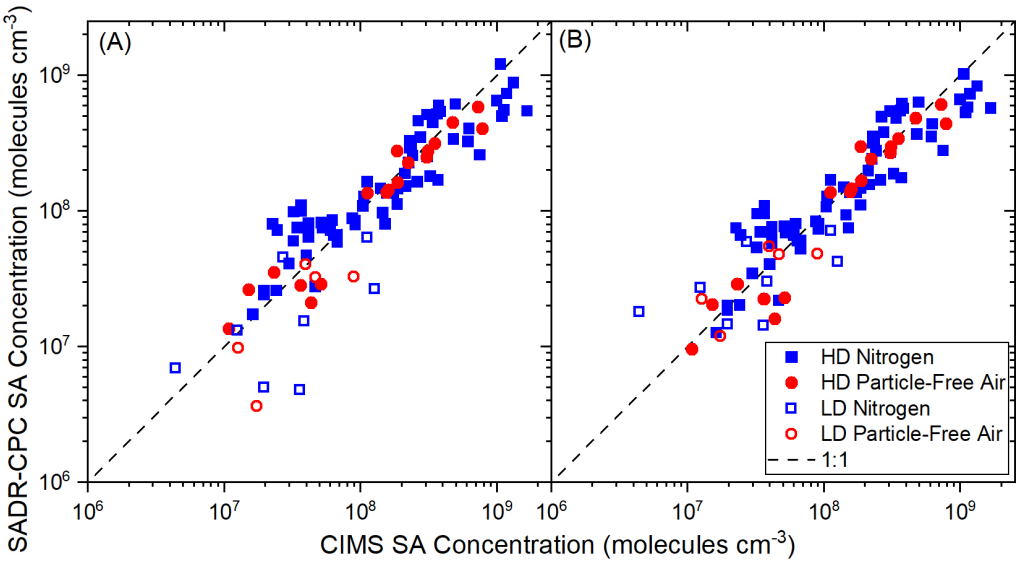


Figure **1**. Comparison of SAD-RCPC sulfuric acid (SA) to CIMS measured SA concentrations. SAD-RCPC SA concentrations were calculated using (A) the nucleation reaction model and (B) empirical fit. Measurements with nitrogen as a carrier gas are blue squares, and particle-free air are red circles. The solid points are measurements taken in the High Dilution (HD) configuration, and hollow points are measurements taken in the Low Dilution (LD) configuration. The dashed line is the 1:1 comparison.

Figure 1(A) illustrates SAD-RCPC SA concentration calculated from the reaction model compared to CIMS measurements for both high and low dilutions (HD and LD respectively) flow configurations. The HD configuration was able to detect SA concentrations ranging from 2×10^7 to 2×10^9 molecules cm^{-3}, and the LD configuration measured SA from 4×10^6 to 5×10^8 molecules cm^{-3}. The SAD-RCPC HD configuration measurements averaged 19% higher than the CIMS, with a mean absolute relative error of 45%. The LD configuration averaged 31% lower than the CIMS and had a mean relative error of 52%. There is greater uncertainty for the LD configuration due to the high dilution factor from the low SA injection flow rate into the CIMS sampling tube and SAD-RCPC.

An alternative method to the nucleation reaction model is to fit the SAD-RCPC particle concentrations to the "true" CIMS-measured SA concentrations (Figure 1B). The mean absolute error was 42% for the HD regression model, which is comparable to the 45% error from the reaction model. The LD regression model had a mean error of 73%, which was higher as there was insufficient data to properly fit the regression. A major disadvantage to the linear regression method is that a new comparison measurement between the two instruments must be performed whenever SAD-RCPC operating conditions change (e.g., flow rate, reactor dimensions, and temperature). Furthermore, in situations where operating conditions vary over short time scales, such as during field measurements, using the more robust reaction model is more straightforward to determine SA concentrations compared to needing to periodically intercompare the CIMS and SAD-RCPC.

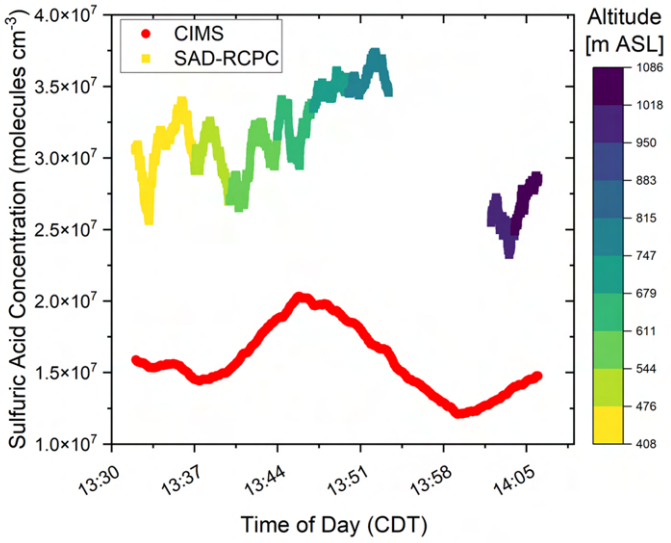


Figure 2 Sulfuric acid (SA) concentrations measured by CIMS and SAD-RCPC at ARM SGP during nucleation (6/6/2024).

The SAD-RCPC was tested at the Department of Energy Atmospheric Radiation Measurement Southern Great Plains (ARM SGP, Lamont, OK) atmospheric observatory on June 6th, 2024, during an NPF event. The SAD-RCPC was attached to a tethered balloon system, so there are limited measurements near ground level to compare to the CIMS located at ground level in a different facility from where the TBS launched. As seen in Figure 2, the SAD-RCPC SA mean concentration was 2.9×10^7, which was 1.9 times higher than the CIMS SA mean concentration of 1.5×10^7. The mean relative error of 90% is higher than laboratory measurements (45% to 52%). This could be due to the higher ambient temperatures when operating outdoors, different DEG wCPC operating temperatures, movement of the instrument on the tethered balloon system, and spatial heterogeneity of SA concentrations at ARM SGP. Additional assumptions, such as the effects of temperature on the reaction model, were made when calculating the SA concentration. With these added uncertainties, the mean relative error is a factor of two larger than the uncertainty for the CIMS (Erupe et al., 2010), indicating that the assumptions made were reasonable.

CONCLUSIONS

The Sulfuric Acid Dimethylamine Reactive Condensation Particle Counter (SAD-RCPC) is a novel method to measure gaseous concentrations of sulfuric acid ranging from ~4×10^6 to 2×10^9 molecules cm^{-3}. The SAD-RCPC operates by reacting sulfuric acid with DMA in a flow reactor to form 1-nm particles detected by a DEG wCPC. A laboratory comparison of the SAD-RCPC using the reaction model with the traditionally used CIMS showed good agreement. SAD-RCPC was also deployed into the field, where background particle concentrations were subtracted from the SAD-RCPC observations to determine the SA concentration. The background-subtracted SAD-RCPC measured atmospheric SA concentrations 90% higher than what the CIMS measured, which may be due to SAD-RCPC operating conditions or spatial heterogeneity of SA. The SADR-CPC will potentially provide a lower cost, more portable, and less power-intense alternative to measuring atmospheric sulfuric acid vapor compared to the currently used CIMS.

ACKNOWLEDGEMENTS

The DAC, DC, and CNJ acknowledge support from DOE ASR DE-SC0022224. DAC was supported by NSF GRFP (DGE2140739). MFR was supported by supported by a Ph.D. scholarship from CONACYT, a tuition waiver from Tecnologico de Monterrey, and the CITRIS-TEC Seed Fund 2020 (ID: 2020CI-0000000016).

REFERENCES

Cai, R., Yan, C., Yang, D., Yin, R., Lu, Y., Deng, C., et al. (2021). Sulfuric acid–amine nucleation in urban Beijing. *Atmospheric Chemistry and Physics*, *21*(4), 2457–2468. https://doi.org/10.5194/acp-21-2457-2021

Chen, Titcombe, M., Jiang, J., Jen, C., Kuang, C., Fischer, M. L., et al. (2012). Acid–base chemical reaction model for nucleation rates in the polluted atmospheric boundary layer. *Proceedings of the National Academy of Sciences*, *109*, 18713–18718. https://doi.org/10.1073/pnas.1210285109

Erupe, M. E., Benson, D. R., Li, J., Young, L.-H., Verheggen, B., Al-Refai, M., et al. (2010). Correlation of aerosol nucleation rate with sulfuric acid and ammonia in Kent, Ohio: An atmospheric observation. *Journal of Geophysical Research: Atmospheres*, *115*(D23). https://doi.org/10.1029/2010JD013942

Fomete, S. K. W., Kubečka, J., Elm, J., & Jen, C. N. (2023). Limited Role of Malonic Acid in Sulfuric Acid–Dimethylamine New Particle Formation. *ACS Omega*, *8*(22), 19807–19815. https://doi.org/10.1021/acsomega.3c01643

Hodshire, A. L., Lawler, M. J., Zhao, J., Ortega, J., Jen, C., Yli-Juuti, T., et al. (2016). Multiple new-particle growth pathways observed at the US DOE Southern Great Plains field site. *Atmospheric Chemistry and Physics*, *16*(14), 9321–9348. https://doi.org/10.5194/acp-16-9321-2016

Jen, C. N., McMurry, P. H., & Hanson, D. R. (2014). Stabilization of sulfuric acid dimers by ammonia, methylamine, dimethylamine, and trimethylamine. *Journal of Geophysical Research: Atmospheres*, *119*(12), 7502–7514. https://doi.org/10.1002/2014JD021592

Johnson, J. S., & Jen, C. N. (2022). A sulfuric acid nucleation potential model for the atmosphere. *Atmospheric Chemistry and Physics*, *22*(12), 8287–8297. https://doi.org/10.5194/acp-22-8287-2022

Johnson, J. S., & Jen, C. N. (2023). Sulfuric Acid Nucleation Potential Model Applied to Complex Reacting Systems in the Atmosphere. *Journal of Geophysical Research: Atmospheres*, *128*(20), e2023JD039344. https://doi.org/10.1029/2023JD039344

Kürten, A., Li, C., Bianchi, F., Curtius, J., Dias, A., Donahue, N. M., et al. (2018). New particle formation in the sulfuric acid–dimethylamine–water system: reevaluation of CLOUD chamber measurements and comparison to an aerosol nucleation and growth model. *Atmos. Chem. Phys.*, *18*(2), 845–863. https://doi.org/10.5194/acp-18-845-2018

Myers, D. C., Kim, S., Sjostedt, S., Guenther, A. B., Seco, R., Vega Bustillos, O., et al. (2022). Sulfuric acid in the Amazon basin: measurements and evaluation of existing sulfuric acid proxies. *Atmospheric Chemistry and Physics*, *22*(15), 10061–10076. https://doi.org/10.5194/acp-22-10061-2022

Olenius, T., Halonen, R., Kurtén, T., Henschel, H., Kupiainen-Määttä, O., Ortega, I. K., et al. (2017). New particle formation from sulfuric acid and amines: Comparison of monomethylamine, dimethylamine, and trimethylamine. *Journal of Geophysical Research: Atmospheres*, *122*(13), 7103–7118. https://doi.org/10.1002/2017JD026501

DETECTION EFFICIENCY OF A WATER CONDENSATION PARTICLE COUNTER USING ELECTRICALLY NEUTRAL SULFURIC ACID AND SULFURIC ACID-DIMETHYLAMINE CLUSTERS

DARREN CHENG[a,b], JOY KIGURU[b,c], and COTY N. JEN[b,c]

[a] Department of Mechanical Engineering, Carnegie Mellon University, Pittsburgh, PA, USA

[b]Center for Atmospheric Particle Studies, Carnegie Mellon University, Pittsburgh, PA, USA

[c]Department of Chemical Engineering, Carnegie Mellon University, Pittsburgh, PA, USA

Keywords: Condensation Particle Counter, nucleation, detection efficiency

INTRODUCTION

Accurately quantifying atmospheric new particle formation (NPF) rates has pushed the development of condensation particle counters (CPCs) to detect smaller and smaller particles (Kangasluoma and Attoui, 2019). Consequently, CPC observations can be used directly to derive new particle formation rates by either observing the appearance of particles over a specific time (Glasoe et al., 2015) or by using the difference in particle concentrations between CPCs with differing d_{50} (Sulo et al., 2024). However, both approaches will predict artificially high 1 nm particle formation rates if the detection efficiency of sub-1 nm particles, including a gas molecule, is incorrectly assumed to be zero. Currently, CPC detection efficiencies are determined by comparing measured concentrations of size-selected ions with an aerosol electrometer (Kangasluoma and Attoui, 2019). However, neutrally charged particles represent over 90% of particles formed during new particle formation events (Hirsikko et al., 2011) and may differ in detection efficiency compared to charged particles (Kangasluoma and Attoui, 2019). Furthermore, detection efficiency experiments typically use charger ions, ammonium sulfate, sodium chloride, or silver ion particles that each display different detection efficiencies (Wlasits et al., 2020). These compositions differ from particles formed via previously observed atmospheric nucleation of SA and dimethylamine (Lee et al., 2019).

This study presents a novel method to characterize the detection efficiency of electrically neutral sulfuric acid (SA) vapor and SA-dimethylamine (DMA) particles <1.5 nm in mobility diameter. The detection efficiency was inverted from measured water condensation particle counter (wCPC) concentrations and predicted concentrations of SA-DMA clusters at atmospherically relevant SA concentrations. Detection efficiency was determined for a custom, three-stage wCPC (Cheng et al., 2025). The wCPC was operated at seven different initiator temperatures (98, 91, 81, 71, 61, 51, and 41 °C), while the conditioner, moderator, and optics head were held constant at 1, 1, and 35 °C respectively. These conditioner-to-initiator temperature differences (ΔT) exhibited d_{50} between 1.8 to 2.6 nm, characterized by traditional ion calibration.

METHODS

SA and SA-DMA clusters were produced in a very clean and repeatable flow reactor (Fomete et al., 2021). Briefly, SA, ultra-high purity nitrogen, and humidified nitrogen gases were introduced into a 5 cm ID x 120 cm long glass flow reactor at a total flow of 6 L min^{-1}. The concentration of SA in the flow reactor ranged from [SA] = 10^6 – 10^9 molecules cm^{-3}. The temperature varied between 292 to 297 K, but no more than 1 K during any experiment. DMA was injected into the centerline of the flow reactor at 60 cm^3 min^{-1} and reacted with SA for 1.2 s until sampled by the wCPC from the centerline of the reactor. An ambient pressure chemical ionization quadrupole mass spectrometer (CIMS) was used to measure concentrations of SA and DMA (Jen et al., 2014).

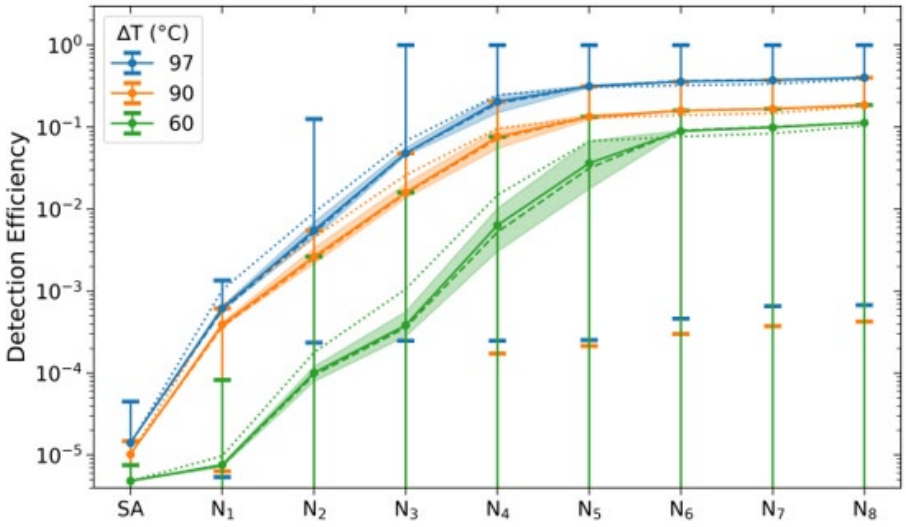


Figure 1. Detection efficiencies of SA and SA-DMA clusters for wCPC ΔT=97, 90, and 60 °C. *Ni* is a cluster with *i* number of SA and DMA molecules. The solid lines with the points indicate the inverted detection efficiency values averaged over the sub-samples (913, 884, and 676 for ΔT=97, 90, and 60 °C respectively). The shaded region indicates the range of detection efficiencies when varying the DMA dilution rate and SA-DMA nucleation reaction time by ±10%. The dashed and dotted lines indicate the detection efficiency when changing the 0 and 1 s^{-1} respectively. The error bars represent the maximum and minimum inverted values from the sub-sampled solutions.

Figure 2 shows the calculated, size-dependent detection efficiencies for ΔT=97, 90, and 60 °C. For the largest ΔT=97°C, the detection efficiency increases from $1.4x10^{-5}$ for SA to 0.40 at N_8. The inverted detection efficiency of SA is within a factor of 2 to the $7.1x10^{-6}$ detection efficiency of SA determined by a linear fit of Fig. 1a. In addition, the 40% detection efficiency of the neutral SA-DMA N_8 cluster (~1.6 nm mobility diameter (Thomas et al. 2016)) is only slightly lower than a similarly sized positively charged ammonium sulfate ion (42%). The detection efficiency also correctly plateaus with increasing cluster size because the change in diameter decreases as the cluster size increases.

CONCLUSIONS

This study demonstrates that the wCPC is capable of detecting electrically neutral SA and SA-DMA particles <1.5 nm in size at the largest ΔTs. The detection efficiencies of SA and their clusters are significant and must be considered when interpreting the formation rates of freshly nucleated particles measured using differential CPC d_{50} techniques. However, as the detection efficiency varies between CPCs, this method should be applied to other CPCs used to study NPF. If the detection efficiency of these clusters is incorrectly assumed to be zero, the formation rate of particles entering the smallest size bin of the measured size distribution will be overestimated. Thus, the detection efficiency of SA and its molecular clusters must be considered to accurately measure new particle formation rates with CPC-based size distribution instrumentation.

ACKNOWLEDGEMENTS

Support from DOE awards DE-SC0022224 and DE-SC0024842 is gratefully acknowledged.

REFERENCES

Cheng, D., Amanatidis, S., Lewis, G. S., and Jen, C. N.: Fast and sensitive measurements of sub-3 nm particles using Condensation Particle Counters For Atmospheric Rapid Measurements (CPC FARM), Atmospheric Meas. Tech., 18, 197–210, https://doi.org/10.5194/amt-18-197-2025, 2025.

Fomete, S. K. W., Johnson, J. S., Casalnuovo, D., and Jen, C. N.: A tutorial guide on new particle formation experiments using a laminar flow reactor, J. Aerosol Sci., 157, 105808, https://doi.org/10.1016/j.jaerosci.2021.105808, 2021.

Glasoe, W. A., Volz, K., Panta, B., Freshour, N., Bachman, R., Hanson, D. R., McMurry, P. H., and Jen, C.: Sulfuric acid nucleation: An experimental study of the effect of seven bases, J. Geophys. Res. Atmospheres, 120, 1933–1950, https://doi.org/10.1002/2014JD022730, 2015.

Hirsikko, A., Nieminen, T., Gagné, S., Lehtipalo, K., Manninen, H. E., Ehn, M., Hõrrak, U., Kerminen, V.-M., Laakso, L., McMurry, P. H., Mirme, A., Mirme, S., Petäjä, T., Tammet, H., Vakkari, V., Vana, M., and Kulmala, M.: Atmospheric ions and nucleation: a review of observations, Atmospheric Chem. Phys., 11, 767–798, https://doi.org/10.5194/acp-11-767-2011, 2011.

Jen, C. N., McMurry, P. H., and Hanson, D. R.: Stabilization of sulfuric acid dimers by ammonia, methylamine, dimethylamine, and trimethylamine, J. Geophys. Res. Atmospheres, 119, 7502–7514, https://doi.org/10.1002/2014JD021592, 2014.

Kangasluoma, J. and Attoui, M.: Review of sub-3 nm condensation particle counters, calibrations, and cluster generation methods, Aerosol Sci. Technol., 53, 1277–1310, https://doi.org/10.1080/02786826.2019.1654084, 2019.

Lee, S.-H., Gordon, H., Yu, H., Lehtipalo, K., Haley, R., Li, Y., and Zhang, R.: New Particle Formation in the Atmosphere: From Molecular Clusters to Global Climate, J. Geophys. Res. Atmospheres, 124, 7098–7146, https://doi.org/10.1029/2018JD029356, 2019.

Sulo, J., Enroth, J., Pajunoja, A., Vanhanen, J., Lehtipalo, K., Petäjä, T., and Kulmala, M.: Pushing nano-aerosol measurements towards a new decade – technical note on the Airmodus particle size magnifier 2.0, Aerosol Res., 2, 13–20, https://doi.org/10.5194/ar-2-13-2024, 2024.

Wlasits, P. J., Stolzenburg, D., Tauber, C., Brilke, S., Schmitt, S. H., Winkler, P. M., and Wimmer, D.: Counting on chemistry: laboratory evaluation of seed-material-dependent detection efficiencies of ultrafine condensation particle counters, Atmospheric Meas. Tech., 13, 3787–3798, https://doi.org/10.5194/amt-13-3787-2020, 2020.

FREEZING ATMOSPHERIC ORGANIC NUCLEATION: USING MATRIX ISOLATION FTIR AS A NEW METHOD

V. ENDERS[1], D.F. DINU[1], H. GROTHE[1], M. PODEWITZ[1], M. TISCHBERGER[1] and D. STOLZENBURG[1]

[1]*Institute of Materials Chemistry, TU Wien, Vienna, Austria.*

Keywords: New Particle Formation, Matrix Isolation, FTIR, Monoterpenes, Organic Aerosols.

INTRODUCTION

New particle formation (NPF) represents the predominant source of atmospheric aerosols in terms of particle number, significantly influencing global climate and human health. This process involves the stabilization of low-volatility vapors into molecular clusters, which subsequently grow through molecular condensation (Kulmala, 2003). Inorganic acids, such as sulfuric and iodic acid, are often the primary drivers of initial cluster formation (Kulmala *et al*., 2013; Sipilä *et al*., 2016). While organic molecules play a crucial role in particle growth (Stolzenburg *et al*., 2023), the precise stage at which they begin contributing to NPF remains uncertain. Specifically, the clustering mechanisms involving organic compounds or organic-inorganic mixtures are poorly understood. It is not clarified exactly which organic molecules can participate at what stages (Elm *et al*., 2017). This knowledge gap arises partly because state-of-the-art mass spectrometry techniques provide only compositional data, lacking structural insights into molecular clusters or the functionalization of growing nanoparticles. However, the ultimate properties of these clusters are determined by interactions between functional groups, highlighting the need for a deeper structural understanding (Stolzenburg *et al.*, 2023).

Here, we use matrix-isolation Fourier transform infrared spectroscopy (MI-FTIR) as a new tool to investigate the formation of organic molecular clusters. Comparing vibrational frequencies measured with MI-FTIR with quantum chemical (QC) calculations can facilitate the functionalization and the non-covalent binding of oligomers or small clusters. This potentially allows the identification of the most common clustering routes in atmospheric nucleation involving organics.

METHODS

MI-FTIR has been applied to analyze various unstable analytes, such as molecular ions and highly reactive species (Andrews & Moskovits, 1989). We have previously demonstrated that our MI-FTIR setup is a reliable tool for studying small molecular clusters such as the monomethyl ester of carbonic acid (Köck *et al.*, 2020) and the CO_2 dimer (Dinu *et al.*, 2022). Similar MI-FTIR setups were used to study compounds relevant to aerosol formation, such as the sulfuric acid-monohydrate complex (Rozenberg & Loewenschuss, 2009), the sulfuric acid-ammonia complex (Rozenberg *et al.*, 2011) and acetonitrile-sulfuric acid-water clusters (Rozenberg *et al.*, 2020).

MI-FTIR is based on freezing small quantities of an analyte in a noble gas matrix. Due to cryogenic temperatures, rotational transitions are suppressed, making the identification of the cluster constituents and the cluster's molecular structure easier than in conventional gas-phase FTIR. A schematic of the current MI-FTIR setup at TU Wien can be seen in Figure 1. The analyte and the host gas are deposited onto a gold mirror kept at 5 K and then analyzed using a conventional FTIR spectrometer. Solid analytes such as aerosol precursor substances can be moved into the apparatus through a separate inlet and mixed with the host almost *in situ* to study their initial clustering (right panel of Figure 1). To analyze larger aerosol particle composition, size-resolved particles produced in a flow reactor are collected on filters and then thermally desorbed into the host gas.

In the present work, we investigate organic precursor vapors, their oxidation products, and newly formed clusters as stabilized in inert noble-gas matrices. The current study focuses on NPF involving α-pinene, a

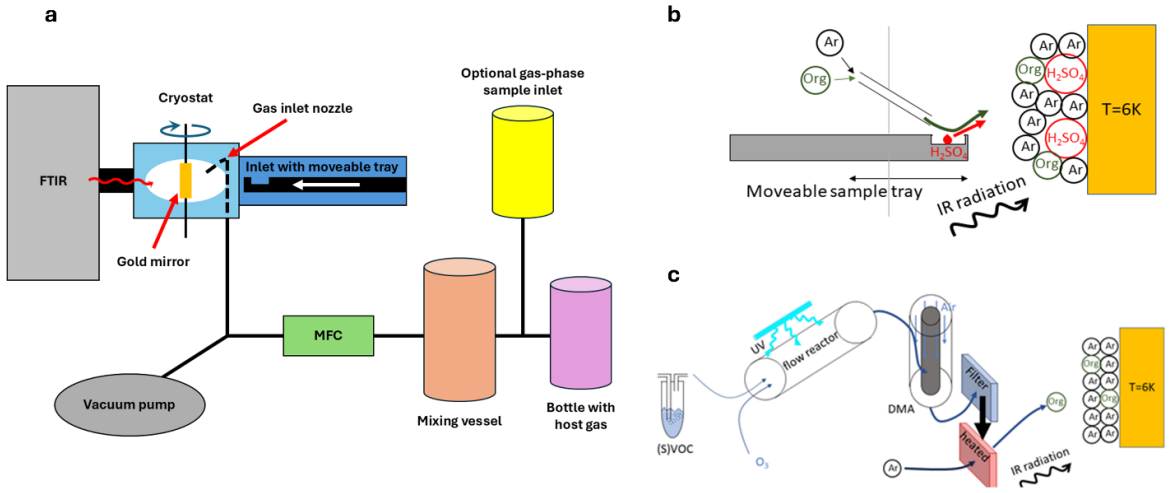


Figure 1. a: Schematic of the MI-FTIR setup at TU Wien showing the FTIR spectrometer, the cryostat, the mass flow controller (MFC), and the system for mixing host gas and analyte. b/c: Two proposed ways of transferring the analyte to the cooled gold mirror: Usage of a sample tray (b) and loading of filters with a differential mobility analyzer (DMA) and a flow reactor (c).

monoterpene that is recognized to be rapidly convertible to extremely low volatile organic compounds (ELVOC) (Ehn *et al.*, 2014). We present spectra of α-pinene and its primary oxidation products, including pinic and pinonic acid, isolated in noble gas matrices. Examples can be seen in Figure 2. Infrared absorption bands are analyzed and compared with density functional theory (DFT) calculations, as certain bands indicate the presence of oligomers within the matrix. In addition, we explore the ability of the MI-FTIR setup to analyze the bulk functionalization of aerosol particles created from α-pinene ozonolysis in the flow reactor setup and deposited onto filters that are thermally desorbed with up to 125 °C into the host gas.

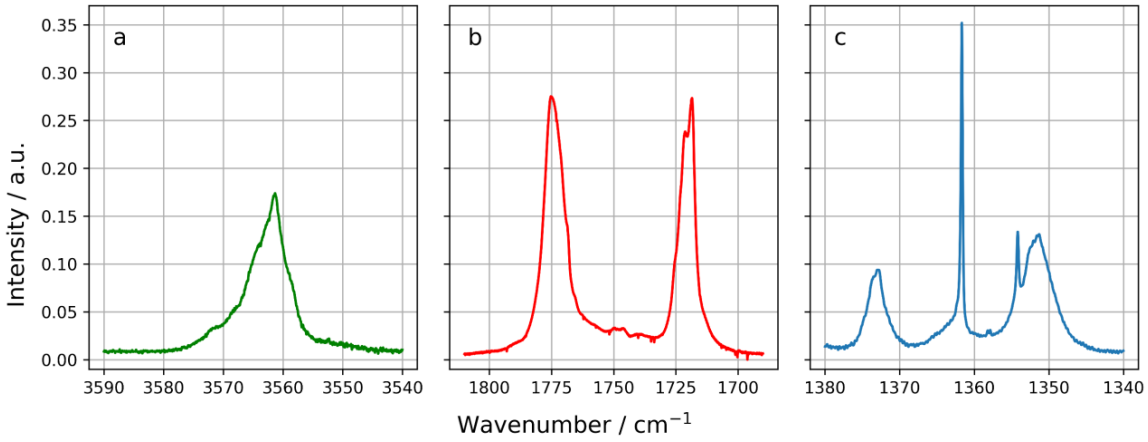


Figure 2. MI-FTIR spectrum of pinonic acid isolated in an argon matrix. a: O-H stretching vibration. b: C=O stretching vibration. c: Part of the CH_3 deformations vibration.

RESULTS

The current study focuses on clustering routes involving the most dominant monoterpene, α-pinene. As an example, extracts from the vibrational spectrum of pinonic acid, an oxidation product of α-pinene, are shown in Figure 2. Peaks corresponding to, e.g., the OH-stretching mode and the C=O stretching mode (with two peaks, one for the ketone and one for the acid) can be clearly distinguished due to the suppression of the rotational sidebands at cryogenic temperatures. Because of this, it is possible to compare the experimentally measured vibrational frequencies to harmonic frequencies calculated using density functional theory (DFT) at the wB97X-3c level, as is shown in Table 1. This comparison makes it possible to assign the experimentally observed transitions using a chemical notation and, thus, rationalizing functional groups.

Harmonic frequency (cm^{-1})	Experimental frequency (cm^{-1})	Assigned vibration
673.3	624.6	ν(COH)
1210.8	1114.4	δ(COH)
1419.8	1361.7	δ(CH)
1858.1	1718.6	ν(C=O)
1888.7	1775.1	ν(C=O)
3879.8	3561.4	ν(OH)

Table 1. Vibrational transitions of pinonic acid. Comparison between harmonic frequencies calculated using DFT (wB97X-3c) and measured frequencies based on MI-FTIR measurements made with argon as host gas. Only the most prominent vibrational peaks are listed.

The MI-FTIR spectra of the pure α-pinene oxidation products can now also be compared to those of oligomers. The vibrational frequencies of the atoms involved in the binding of the oligomers are significantly shifted. These additional vibrational frequencies appearing in the spectra can be attributed to oligomerization or bonds between the cluster constituents, giving an insight into the possible binding and clustering routes of early-stage NPF. In addition, the specific and well-separated vibrational modes of organic functional groups, which are decisive for lowering the volatility of aerosol precursors (-OH, C=O, C(=O)OH as shown in Figure 2 and Table 1), also allow for the estimation of bulk functionalization of thermally desorbed complex aerosol samples.

CONCLUSION

Here, we demonstrate the usage of MI-FTIR as a new tool to investigate potential clustering routes in NPF. Based on the comparison of measured vibrational frequencies to harmonic frequencies calculated with DFT, it is possible to assign vibrational modes and get insights into functionalization, oligomerization, and, ultimately, the structure of early-stage clusters.

ACKNOWLEDGEMENTS

This research was funded in whole or in part by the Austrian Science Fund (FWF) 10.55776/PAT8221324.

REFERENCES

Andrews, L. and M. Moskovits (1989). *Chemistry and Physics of Matrix-Isolated Species* (North Holland, Amsterdam, The Netherlands).

Dinu, D.F., P. Bartl, P.K Quoika, M. Podewitz, K.R. Liedl, H. Grothe and T. Loerting (2022). Increase of Radiative Forcing through Midinfrared Absorption by Stable CO 2 Dimers? *J. Phys. Chem. A* **126**, 2966–2975.

Ehn, M., J.A. Thornton, E. Kleist, M. Sipilä, H. Junninen, I. Pullinen, M. Springer, F. Rubach, R. Tillmann, B. Lee, F. Lopez-Hilfiker, S. Andres, I.-H. Acir, M. Rissanen, T. Jokinen, S. Schobesberger, J. Kangasluoma, J. Kontkanen, T. Nieminen, T. Kurtén, L.B. Nielsen, S. Jørgensen, H.G. Kjaergaard, M. Canagaratna, M.D. Maso, T. Berndt, T. Petäjä, A. Wahner, V.-M. Kerminen, M. Kulmala, D.R. Worsnop, J. Wildt and T.F. Mentel (2014). A significant source of low-volatility secondary organic aerosol. *Nature* **506**, 476–479.

Elm, J., J. Kubečka, V. Besel, M.J. Jääskeläinen, R. Halonen, T. Kurtén and H. Vehkamäki (2020). Modeling the formation and growth of atmospheric molecular clusters: A review. *J. Aerosol Science* **149**, 105621.

Köck, E., J. Bernard, M. Podewitz, D.F. Dinu, R.G. Huber, K.R. Liedl, H. Grothe, E. Bertel, R. Schlögl, and T. Loerting (2020). Alpha-Carbonic Acid Revisited: Carbonic Acid Monomethyl Ester as a Solid and its Conformational Isomerism in the Gas Phase. *Chemistry A European J* **26**, 285–305.

Kulmala, M. (2003). How Particles Nucleate and Grow. *Science* **302**, 1000–1001.

Kulmala, M., J. Kontkanen, H. Junninen, K. Lehtipalo, H.E. Manninen, T. Nieminen, T. Petäjä, M. Sipilä, S. Schobesberger, P. Rantala, A. Franchin, T. Jokinen, E. Järvinen, M. Äijälä, J. Kangasluoma, J. Hakala, P.P. Aalto, P. Paasonen, J. Mikkilä, J. Vanhanen, J. Aalto, H. Hakola, U. Makkonen, T. Ruuskanen, R.L. Mauldin, J. Duplissy, H. Vehkamäki, J. Bäck, A. Kortelainen, I. Riipinen, T. Kurtén, M.V. Johnston, J.N. Smith, M. Ehn, T.F. Mentel, K.E.J. Lehtinen, A. Laaksonen, V.-M. Kerminen and D.R. Worsnop (2013). Direct Observations of Atmospheric Aerosol Nucleation. *Science* **339**, 943–946.

Rozenberg, M. and A. Loewenschuss (2009). Matrix Isolation Infrared Spectrum of the Sulfuric Acid−Monohydrate Complex: New Assignments and Resolution of the “Missing H-Bonded ν(OH) Band” Issue. *J. Phys. Chem. A* **113**, 4963–4971.

Rozenberg, M., A. Loewenschuss and C.J. Nielsen (2011). Complexes of Molecular and Ionic Character in the Same Matrix Layer: Infrared Studies of the Sulfuric Acid/Ammonia System. *J. Phys. Chem. A* **115**, 5759–5766.

Rozenberg, M., A. Loewenschuss and C.J. Nielsen (2020). Acetonitrile/sulfuric acid/water clusters: A matrix isolation infrared and computational study. *Journal of Molecular Structure* **1199**, 126948.

Sipilä, M., N. Sarnela, T. Jokinen, H. Henschel, H. Junninen, J. Kontkanen, S. Richters, J. Kangasluoma, A. Franchin, O. Peräkylä, M.P. Rissanen, M. Ehn, H. Vehkamäki, T. Kurten, T. Berndt, T. Petäjä, D. Worsnop, D. Ceburnis, V.-M. Kerminen, M. Kulmala and C. O’Dowd (2016). Molecular-scale evidence of aerosol particle formation via sequential addition of HIO_3. *Nature* **537**, 532–534.

Stolzenburg, D., R. Cai, S.M. Blichner, J. Kontkanen, P. Zhou, R. Makkonen, V.-M. Kerminen, M. Kulmala, I. Riipinen and J. Kangasluoma (2023). Atmospheric nanoparticle growth. *Rev. Mod. Phys.* **95**, 045002.

Voltage scanning application of nitrate chemical ionization mass spectrometer

Yuliang Liu[1], Bisen Han[2], Chao Yan[1,2], Wei Nie[1,2], Federico Bianchi[3], Markku Kulmala[2,3], Aijun Ding[1,2]

[1]*School of Atmospheric Science, Nanjing University, Nanjing, China*
[2]*Nanjing-Helsinki Institute in Atmospheric and Earth System Sciences, Nanjing University, Nanjing, China*
[3]*Department of Physics, University of Helsinki, Helsinki, 00140, Finland*

Keywords: voltage scanning, nitrate CIMS, SOA, quantitative method

Volatile organic compounds (VOCs), important precursors of secondary organic aerosols (SOA), significantly impact radiative forcing and human health (Hallquist et al., 2009; Kroll & Seinfeld, 2008; Nel, 2005). Chemical ionization mass spectrometry (CIMS) serves as a powerful tool for studying VOC oxidation due to its high time and mass resolution (Ehn et al., 2010). The subsequent development of nitrate CI-APi-ToF (chemical ionization atmospheric pressure interface time-of-flight mass spectrometer) (Jokinen et al., 2012) enabled highly sensitive detection of gaseous sulfuric acid and oxidized organic compounds.

Lopez-Hilfiker et al. (2016) introduced a declustering voltage scanning method to assess the binding ability of target OOMs (oxygenated organic molecules) to reagent ions. The semi-dissociation voltage (dV_{50}) exhibits a linear correlation with cluster binding energy, which in turn influences instrument sensitivity (Iyer et al. 2016). By calibrating the instrument's sensitivity of a few known OOMs and obtaining their corresponding dV_{50}, a dV_{50}-sensitivity correlation curve can be established. This allows indirect sensitivity determination for unknown OOMs based on their dV_{50}, enabling quantitative analysis.

In this study, we employed a cyclic program that resets dV to 0 (Fig. 1), enabling the voltage scanning in field conditions. For further sensitivity calibration of specific OOMs, we used a shared gas line connecting both the instrument and offline sampling system to minimize interference (e.g., wall losses). Based on the characterization of OOM sensitivity in nitrate CIMS, we re-evaluate OOMs in the urban atmosphere, particularly regarding their source contribution, chemical features, as well as volatility distribution.

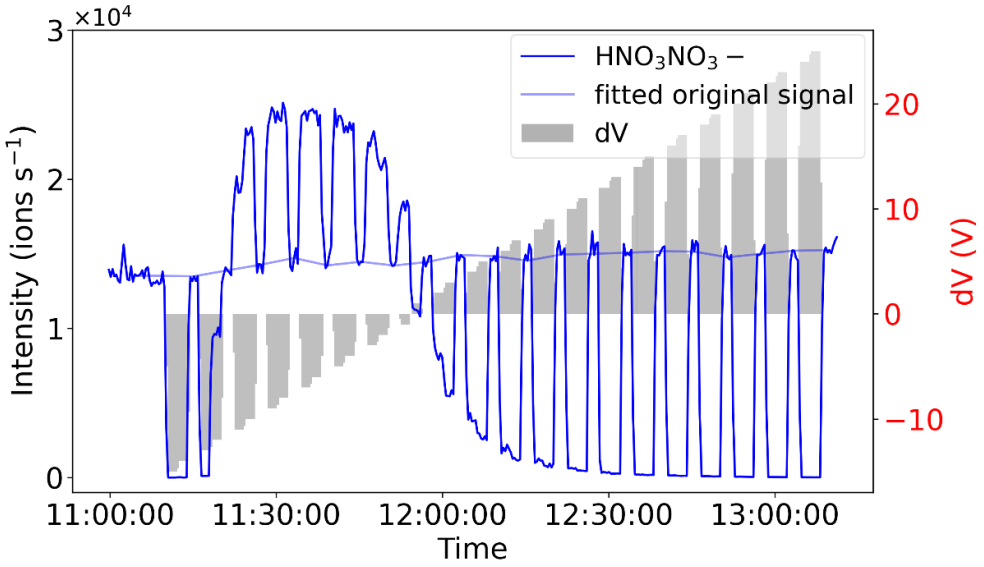


Figure 1. An example of a voltage scanning performed by nitrate CI-APi-ToF when measuring ambient air. The dark blue solid line is a change in the nitrate dimer signal during a voltage scanning. A reference line (light blue) is obtained by linear interpolation of the intermittent repeated nitrate dimer signal at dV=0.

ACKNOWLEDGEMENTS

This study is funded by the National Natural Science Foundation of China (NSFC) project 42475118.

REFERENCES

Ehn, M., Junninen, H., Petäjä, T., Kurtén, T., Kerminen, V.M., Schobesberger, S., Manninen, H.E., Ortega, I.K., Vehkamäki, H., Kulmala, M., & Worsnop, D.R. (2010). Composition and temporal behavior of ambient ions in the boreal forest. *Atmospheric Chemistry and Physics, 10*, 8513-8530

Hallquist, M., Wenger, J.C., Baltensperger, U., Rudich, Y., Simpson, D., Claeys, M., Dommen, J., Donahue, N.M., George, C., Goldstein, A.H., Hamilton, J.F., Herrmann, H., Hoffmann, T., Iinuma, Y., Jang, M., Jenkin, M.E., Jimenez, J.L., Kiendler-Scharr, A., Maenhaut, W., McFiggans, G., Mentel, T.F., Monod, A., Prévôt, A.S.H., Seinfeld, J.H., Surratt, J.D., Szmigielski, R., & Wildt, J. (2009). The formation, properties and impact of secondary organic aerosol: current and emerging issues. *Atmospheric Chemistry and Physics, 9*, 5155-5236

Iyer, S., Lopez-Hilfiker, F., Lee, B.H., Thornton, J.A., & Kurtén, T. (2016). Modeling the Detection of Organic and Inorganic Compounds Using Iodide-Based Chemical Ionization. *Journal of Physical Chemistry A, 120*, 576-587

Jokinen, T., Sipilä, M., Junninen, H., Ehn, M., Lönn, G., Hakala, J., Petäjä, T., Mauldin Iii, R.L., Kulmala, M., & Worsnop, D.R. (2012). Atmospheric sulphuric acid and neutral

cluster measurements using CI-APi-TOF. *Atmospheric Chemistry and Physics, 12*, 4117-4125

Kroll, J.H., & Seinfeld, J.H. (2008). Chemistry of secondary organic aerosol: Formation and evolution of low-volatility organics in the atmosphere. *Atmospheric Environment, 42*, 3593-3624

Kürten, A., Rondo, L., Ehrhart, S., & Curtius, J. (2012). Calibration of a Chemical Ionization Mass Spectrometer for the Measurement of Gaseous Sulfuric Acid. *The Journal of Physical Chemistry A, 116*, 6375-6386

Lopez-Hilfiker, F.D., Iyer, S., Mohr, C., Lee, B.H., D'Ambro, E.L., Kurtén, T., & Thornton, J.A. (2016). Constraining the sensitivity of iodide adduct chemical ionization mass spectrometry to multifunctional organic molecules using the collision limit and thermodynamic stability of iodide ion adducts. *Atmospheric Measurement Techniques, 9*, 1505-1512

Nel, A. (2005). Air Pollution-Related Illness: Effects of Particles. *Science, 308*, 804-806

EXPLORING IN-FLIGHT ATMOSPHERIC AEROSOL SAMPLING CHALLENGES

Z.R. MILANI[1,2], L. NICHMAN[1] and E. MATIDA[2]

[1]*Flight Research Laboratory, National Research Council of Canada, Ottawa, Canada.*

[2]*Mechanical and Aerospace Engineering Dept., Carleton University, Ottawa, Canada.*

Keywords: AEROSOL, AIRCRAFT, IN-SITU.

INTRODUCTION

Accurate in-situ measurements of atmospheric aerosols are crucial for understanding the impact aerosol–cloud interactions have on global weather patterns and forecasting in the short term, and the atmospheric radiative energy budget in the long term. While advanced spaceborne technologies such as CALIPSO (Winker et al., 2010), EarthCARE (Wehr et al., 2023), and ACDL/DQ-1 (Dai et al., 2024) have and will continue to provide invaluable data on global aerosol profiles, the suborbital calibration and validation of satellite data using airborne systems remains essential. For instance, observations over polar regions have historically been scarce and suffer from unique challenges (e.g., low satellite coverage, lack of ground infrastructure, and a generally harsh environment). This has led to gaps in knowledge about Arctic processes and how they affect global weather and climate patterns (Lucas et al., 2023) which will continue to attract research as this region warms at a rate 4× the global average (Rantanen et al., 2022). The anthropogenic aerosol contribution due to aircraft emissions and persistent contrail formation has also been in the spotlight recently, with some upcoming projects planning to sample aircraft exhaust using a tandem chase aircraft or through self-sampling methodologies (e.g., UNIC (CORDIS: 101192598, 2024)).

Careful airborne sampling is key for the collection of useful data and the derivation of unambiguous conclusions (DeMott et al., 2010). In-situ airborne aerosol sampling techniques, whether via wing mounted pods or fuselage-mounted inlets, remain challenging due to aircraft boundary layer effects across the flight envelope, inlet inefficiencies and concentration enhancement factors, sampling losses, etc. These challenges can result in artifacts that introduce bias into aerosol counts, partitioning, and activated fraction calculations that must be considered during analysis. This preliminary work explores the lessons learned from past aerosol measurements conducted by National Research Council of Canada (NRC) Convair-580 research aircraft over several flight campaigns to better inform future missions such as PONEX (Qu, 2023), UNIC (CORDIS: 101192598, 2024) and the development of new airborne platforms such as MAPLE (National Research Council Canada, 2024).

METHODS

In-situ atmospheric aerosol measurements are typically conducted using research aircraft with sizable payload capacity. One example of such a facility is the Convair-580 research aircraft owned and operated by the NRC. The benefit of having a large research payload capacity is the ability to fly several instruments that measure a variety of properties related to the mission objective. This leads to a more detailed characterization of the atmospheric environment and some level of redundancy for backup and cross-validation when multiples of the same instrument are used. For instance, the NRC Convair-580 can provide high-quality coincident in-situ measurements which cover the entire scale of atmospherically relevant particle diameters (Nguyen et al., 2022). During past flight campaigns, e.g., (Bernstein et al., 2021; Kollias et al., 2025), the NRC-Convair-580 suite of rack-mounted aerosol instruments often included the Ultra-High Sensitivity Aerosol Spectrometer (UHSAS-C), Condensation Particle Counter (CPC), Cloud Condensation Nuclei Counter-100 (CCNc-100, equipped with a constant pressure inlet), and a Single Particle Soot Photometer (SP2). All cabin mounted instruments were tapped into a main aerosol inlet mounted on the top side of the fuselage, behind the flight deck, and ~10.5 inches away from the surface to sample outside the boundary layer. The aerosol inlet was heated to protect from ice accretion and kept at near isokinetic conditions (i.e., ~100 m/s, the measurement true air speed of the NRC Convair-580). In some variations the

main aerosol line had a liquid-water trap installed inline and upstream of the aerosol instrument taps, in other variations the main line was split between residual sampling behind CVI and a clear-air isokinetic inlet sampling. In addition to the rack-mounted instruments, a wing mounted version of UHSAS-A (now decommissioned) was also installed on a pylon at the wing tip, providing a unique opportunity to compare the performance of cabin and free stream aerosol measurements during flight.

This work uses a laser-scanned model of the NRC Convair-580 to simulate the flow field around the aircraft and identify boundary layer heights in different flow regimes. Flow solutions were obtained using Ansys FENSAP-ICE and were then used as an input for the DROP3D module to estimate the aerosol concentration around the aircraft for different diameters to ensure the aerosol inlets were outside the reduction and enrichment zones caused by the aircraft nose. The aerosol sampling system layout was itemized and a model to describe sampling efficiency was assembled by compiling the empirical particle loss and enhancement factors described throughout several resources including, e.g., Brockmann, 2011; Hiranuma et al., 2013; Matida et al., 2000; Shingler et al., 2012; Von Der Weiden et al., 2009. This work corrects measured data for the effects of non-isoaxial sampling, non-isokinetic sampling, enhancement factor at the CVI inlet, turbulent diffusion, Brownian motion, sedimentation, inertial deposition in bends and contractions, and changes in pressure and temperature.

RESULTS / DISCUSSION

This work explores past NRC Convair-580 aerosol measurements in detail and provides commentary about: i) selecting probe inlet locations; ii) methodology for estimating sampling losses and a parametrization study of different loss and enhancement mechanisms based on in-flight measurements; and iii) instrument performance including the intercomparison of cabin vs wing sampling. General results are presented in the context of the specific flight campaign environments and measurement bias and uncertainty will be discussed. In particular, this work will comment on the discrepancies between cabin and wing data and the potential link to altitude observed by Ortega et al., 2019, the impact of enhancement factor calculations on nucleation measurements, the CPC altitude ceiling of 2 km, and the CCN constant pressure inlet corrections for high altitudes. Figure 1 presents preliminary simulation results for the flow field and particle environment around the fuselage of the NRC Convair-580 using Ansys FENSAP-ICE. At 2° angle of attack, 100 m/s, 75 kPa, -10°C, and for 10 µm water droplets, Figure 1 shows very low levels of droplet collection efficiency (~1%) due to the tendency for this particle diameter to follow the fluid flow lines rather than exhibiting ballistic behavior. The dark and light shading around the aircraft show reduction and enrichment zones around the fuselage, which will be studied for more flow regimes (i.e., different combinations of roll, pitch, and yaw angles) to ensure the inlets are always sampling clear air. The red and yellow ‘X’ marks the approximate locations of the isokinetic and CVI inlets, respectively. Preliminary simulations suggest these inlets will sample ambient conditions at this flow regime, however, the proximity of CVI inlet to the vortices rolling off the window should be further investigated. Based on these simulations, and if needed, it may be possible to develop correction factors when sampling aerosols in flight envelopes that do not result in unobstructed clean air sampling.

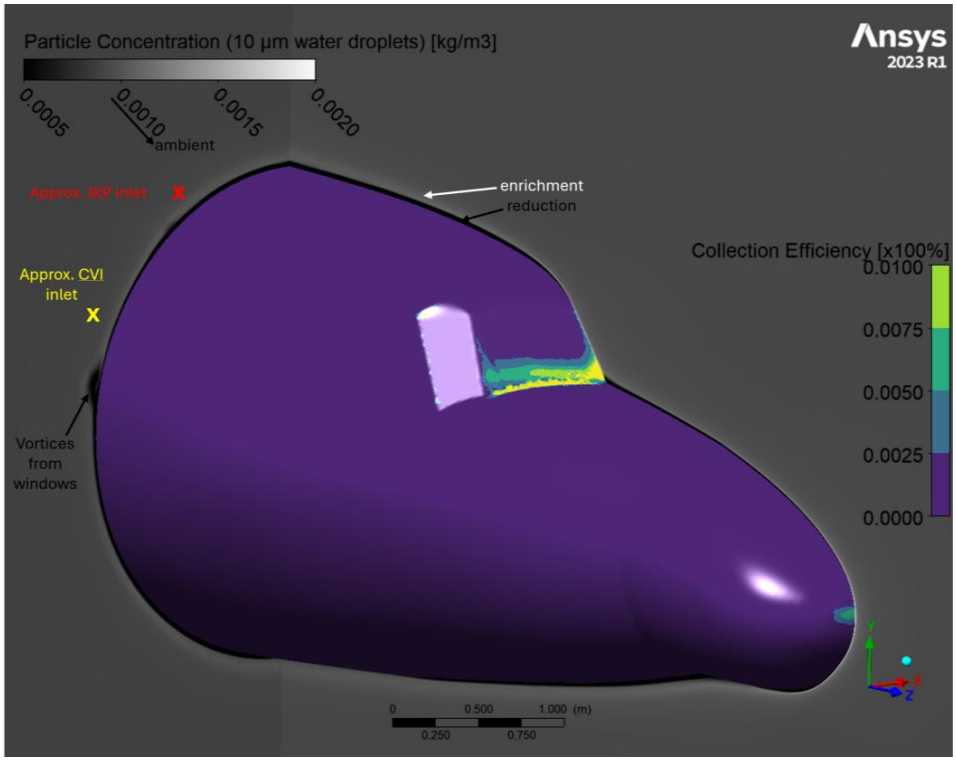


Figure 1: Flow field and particle concentration simulation results from Ansys FENSAP-ICE for 2° angle of attack, 100 m/s true air speed, 75 kPa, -10°C, and assuming particles are 10 µm water droplets with an ambient concentration of 0.001 kg/m^3.

REFERENCES

Bernstein, B., DiVito, S., Riley, J. T., Landolt, S., Haggerty, J., Thompson, G., Adriaansen, D., Serke, D., Kessinger, C., Tessendorf, S., Wolde, M., Korolev, A., Brown, A., Nichman, L., Sims, D., & Dumont, C. (2021). *The In-Cloud Icing and Large-Drop Experiment (ICICLE) Science and Operations Plans*.

Brockmann, J. E. (2011). Aerosol Transport in Sampling Lines and Inlets. In P. Kulkarni, P. A. Baron, & K. Willeke (Eds.), *Aerosol Measurement* (1st ed., pp. 68–105). Wiley. https://doi.org/10.1002/9781118001684.ch6

CORDIS: 101192598. (2024, December). *Understanding Non-CO2 Impact for deCarbonized aviation | UNIC Project | Fact Sheet | HORIZON*. CORDIS | European Commission. https://cordis.europa.eu/project/id/101192598

Dai, G., Wu, S., Long, W., Liu, J., Xie, Y., Sun, K., Meng, F., Song, X., Huang, Z., & Chen, W. (2024). Aerosol and cloud data processing and optical property retrieval algorithms for the spaceborne ACDL/DQ-1. *Atmospheric Measurement Techniques*, *17*(7), 1879–1890. https://doi.org/10.5194/amt-17-1879-2024

DeMott, P. J., Prenni, A. J., Liu, X., Kreidenweis, S. M., Petters, M. D., Twohy, C. H., Richardson, M. S., Eidhammer, T., & Rogers, D. C. (2010). Predicting global atmospheric ice nuclei distributions and their impacts on climate. *Proceedings of the National Academy of Sciences*, *107*(25), 11217–11222. https://doi.org/10.1073/pnas.0910818107

Hiranuma, N., Brooks, S. D., Moffet, R. C., Glen, A., Laskin, A., Gilles, M. K., Liu, P., Macdonald, A. M., Strapp, J. W., & McFarquhar, G. M. (2013). Chemical characterization of individual particles and residuals of cloud droplets and ice crystals collected on board research aircraft in the ISDAC 2008 study. *Journal of Geophysical Research: Atmospheres*, *118*(12), 6564–6579. https://doi.org/10.1002/jgrd.50484

Kollias, P., McFarquhar, G. M., Bruning, E., DeMott, P. J., Kumjian, M. R., Lawson, P., Lebo, Z., Logan, T., Lombardo, K., Oue, M., Roberts, G., Shaw, R. A., Van Den Heever, S. C., Wolde, M., Barry, K. R., Bodine, D., Bruintjes, R., Chandrasekar, V., Dzambo, A., … Zhu, Z. (2025). Experiment of Sea Breeze Convection, Aerosols, Precipitation, and Environment (ESCAPE). *Bulletin of the American Meteorological Society*, *106*(2), E310–E332. https://doi.org/10.1175/BAMS-D-23-0014.1

Lucas, S., Johannessen, J. A., Cancet, M., Pettersson, L. H., Esau, I., Rheinlænder, J. W., Ardhuin, F., Chapron, B., Korosov, A., Collard, F., Herlédan, S., Olason, E., Ferrari, R., Fouchet, E., & Donlon, C. (2023).

Knowledge Gaps and Impact of Future Satellite Missions to Facilitate Monitoring of Changes in the Arctic Ocean. *Remote Sensing*, *15*(11), 2852. https://doi.org/10.3390/rs15112852

Matida, E. A., Nishino, K., & Torii, K. (2000). *Statistical simulation of particle deposition on the wall from turbulent dispersed pipe ¯ow*.

National Research Council Canada. (2024, January). *NRC facilities renewal – Convair aircraft replacement*. https://nrc.canada.ca/en/research-development/nrc-facilities/nrc-facilities-renewal-convair-aircraft-replacement

Nguyen, C. M., Wolde, M., Battaglia, A., Nichman, L., Bliankinshtein, N., Haimov, S., Bala, K., & Schuettemeyer, D. (2022). Coincident in situ and triple-frequency radar airborne observations in the Arctic. *Atmospheric Measurement Techniques*, *15*(3), 775–795. https://doi.org/10.5194/amt-15-775-2022

Ortega, J., Snider, J. R., Smith, J. N., & Reeves, J. M. (2019). Comparison of aerosol measurement systems during the 2016 airborne ARISTO campaign. *Aerosol Science and Technology*, *53*(8), 871–885. https://doi.org/10.1080/02786826.2019.1610554

Qu, Z. (2023, November 13). *Arctic POlar Night EXperiment (PONEX) aircraft campaign*. ESA-JAXA Pre-Launch EarthCARE Science and Validation Workshop, Frascati (Rome), Italy. https://airdrive.eventsair.com/eventsairwesteuprod/production-nikal-public/e52075844b8d47f1b863e185a7c14c31

Rantanen, M., Karpechko, A. Y., Lipponen, A., Nordling, K., Hyvärinen, O., Ruosteenoja, K., Vihma, T., & Laaksonen, A. (2022). The Arctic has warmed nearly four times faster than the globe since 1979. *Communications Earth & Environment*, *3*(1), 1–10. https://doi.org/10.1038/s43247-022-00498-3

Shingler, T., Dey, S., Sorooshian, A., Brechtel, F. J., Wang, Z., Metcalf, A., Coggon, M., Mülmenstädt, J., Russell, L. M., Jonsson, H. H., & Seinfeld, J. H. (2012). Characterisation and airborne deployment of a new counterflow virtual impactor inlet. *Atmospheric Measurement Techniques*, *5*(6), 1259–1269. https://doi.org/10.5194/amt-5-1259-2012

Von Der Weiden, S.-L., Drewnick, F., & Borrmann, S. (2009). Particle Loss Calculator – a new software tool for the assessment of the performance of aerosol inlet systems. *Atmospheric Measurement Techniques*, *2*(2), 479–494. https://doi.org/10.5194/amt-2-479-2009

Wehr, T., Kubota, T., Tzeremes, G., Wallace, K., Nakatsuka, H., Ohno, Y., Koopman, R., Rusli, S., Kikuchi, M., Eisinger, M., Tanaka, T., Taga, M., Deghaye, P., Tomita, E., & Bernaerts, D. (2023). The EarthCARE mission – science and system overview. *Atmospheric Measurement Techniques*, *16*(15), 3581–3608. https://doi.org/10.5194/amt-16-3581-2023

Winker, D. M., Pelon, J., Jr, J. A. C., Ackerman, S. A., Charlson, R. J., Colarco, P. R., Flamant, P., Fu, Q., Hoff, R. M., Kittaka, C., Kubar, T. L., Treut, H. L., Mccormick, M. P., Mégie, G., Poole, L., Powell, K., Trepte, C., Vaughan, M. A., & Wielicki, B. A. (2010). *A Global 3D View of Aerosols and Clouds*.

CHARGER-RELATED UNCERTAINTY IN ELECTRICAL AEROSOL MEASUREMENTS

M. NISKANEN[1], A. SEPPÄNEN[1] and K. E. J. LEHTINEN[1]

[1]*Department of Technical Physics, University of Eastern Finland, Kuopio, Finland.*

Keywords: BIPOLAR CHARGE DISTRIBUTION, ELECTRICAL AEROSOL MEASUREMENT, UNCERTAINTY QUANTIFICATION.

INTRODUCTION

The charge distribution, which is required knowledge for inferring the particle size distribution (PSD) in electrical mobility -based measurements, is also the greatest source of uncertainty in such measurements (López-Yglesias and Flagan, 2013). In current inversion methods, the charge distribution produced by a bipolar charger is almost ubiquitously approximated by the model of Wiedensohler (1988), which is an empirical fit to a theory describing charge transfer from gas ions to particles. This simplified model has facilitated widespread adoption of the bipolar diffusion charging theory in electrical mobility -based measurements but doesn't consider the effect of differing environmental conditions, such as ion mobility, on the charge distribution. In this work, we show how allowing for the possibility of different charging conditions leads to uncertainty in the charge distribution. We then account for this uncertainty in the measurement process and investigate how it shows in the estimates of the PSD.

METHODS

We adopt the model of López-Yglesias and Flagan (2013) (LYF) for computing the charge distribution, and over many simulations vary the charging ion mobilities within the range of $\mu_+ \in [1.05, 1.7]$ cm^{2}V^{-1}s^{-1} and $\mu_- \in [1.1, 2.1]$ cm^{2}V^{-1}s^{-1} for the positive and negative ion mobility, respectively, with the condition $\mu_- \geq \mu_+$. These correspond to a range of measured mobilities that have been reported in literature (Tigges *et al.*, 2015). Fig. 1 shows the variation in the predicted charge distribution for charges -1, 0, and +1, as well as the prediction given by the Wiedensohler model.

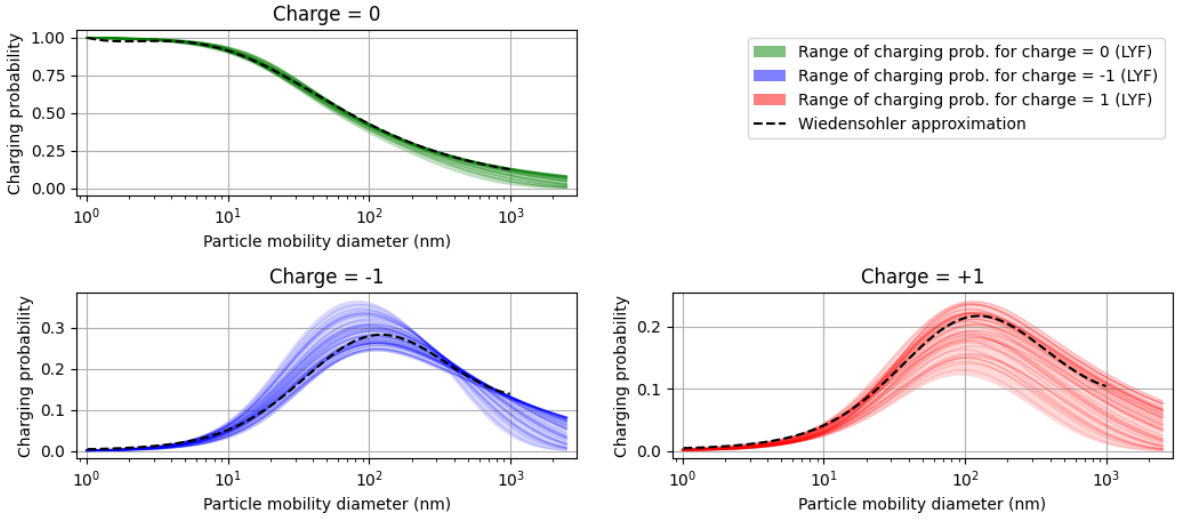


Figure 1. Charging probabilities for an aerosol particle to acquire a charge -1, 0, or +1, given by the LYF model when the ion mobilities are varied, and the Wiedensohler approximation.

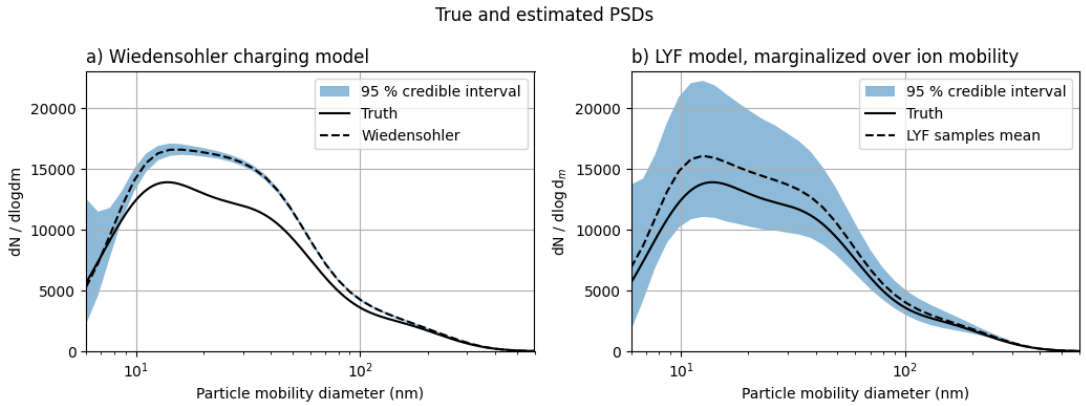


Figure 2. Estimated PSDs with uncertainty bounds when: a) The charge distribution is given by the Wiedensohler model, b) The charge distribution is given by the LYF model *and* uncertainty in the charge distribution is considered.

To investigate the effect of charging uncertainty in the PSD estimates, we simulated a differential mobility particle sizer (DMPS) measurement of a known PSD (the "truth") and conducted inversion tests. Our inversion approach is based on the Bayesian framework for inverse problems. We used the LYF charging model with an arbitrary choice of $\mu_+ = 1.4$ cm^{2}V^{-1}s^{-1} and $\mu_- = 1.9$ cm^{2}V^{-1}s^{-1} for creating measurement data and carried out inversion both with and without considering the charging uncertainty. The former was done by marginalization over the ion mobility using the LYF model and in the latter, we used the Wiedensohler model. While the result shown in Fig. 2 a) with the Wiedensohler model *seems* accurate because of the narrow credible intervals, the fact that the intervals don't contain the truth indicates an issue (which in this case is that the charging model is wrong for this data but assumed accurate). Note that this isn't a problem with the Wiedensohler model *per se*. On the other hand, when the uncertainty in the charge distribution is accounted for by marginalization, as shown in Fig. 2 b), the credible intervals get considerably wider. This is an advantage because they now more realistically reflect the uncertainty in the PSD estimate and, crucially, contain the truth.

CONCLUSIONS

The charge distribution plays an essential role in the inversion of electrical mobility -based data but is in practice unknown to some degree. Therefore, neglecting the charging-related uncertainty leads to bias and overconfidence in the results. By considering a range of realistic values for ion mobility, we showed that the uncertainty in PSDs measured with a DMPS-like instrument may be much higher than traditionally thought but can be quantified.

ACKNOWLEDGEMENTS

This research has been supported by the Research Council of Finland Center of Excellence project VILMA (grant no. 346375).

REFERENCES

López-Yglesias, X. and Flagan, R. C. (2013). Ion–Aerosol Flux Coefficients and the Steady-State Charge Distribution of Aerosols in a Bipolar Ion Environment, *Aerosol Sci. Technol.* **47**, 688–704.

Wiedensohler, A. (1988). An approximation of the bipolar charge distribution for particles in the submicron size range, *J. Aerosol Sci.* **19**, 387–389.

Tigges, L., Jain, A. and Schmid, H.-J. (2015) On the bipolar charge distribution used for mobility particle sizing: Theoretical considerations, *J. Aerosol Sci.* **88**, 119-134.

THE KOREA CLOUD PHYSICS EXPERIMENTAL CHAMBER (K-CPEC): DESIGN, CAPABILITIES, AND PRELIMINARY RESULTS FROM ICE NUCLEATION EXPERIMENTS

M. PARK[1], J.W. CHA[2], S. PARK[3], J. KIM[3], Y. KIM[2], M. BELORID[2], B.-Y. KIM[2], J. BAEK[2], S. KIM[2], K. LEE[2], P. SEO[1], C. AHN[1], J. LEE[4], S.S. YUM[1,5], J. UM[3,6,7]

[1]*Department of Atmospheric Sciences, Yonsei University, Seoul, Republic of Korea.*
[2]*Research Applications Department, National Institute of Meteorological Sciences, Jeju, Republic of Korea.*
[3]*BK21 School of Earth and Environmental System, Division of Earth Environmental Systems, Department of Atmospheric Sciences, Pusan National University, Busan, Republic of Korea.*
[4]*Department of Polymer Science and Engineering, Pusan National University, Busan, Republic of Korea.*
[5]*Climate and Environmental Research Institute, Korea Institute of Science and Technology, Seoul, Republic of Korea.*
[6]*Department of Atmospheric Sciences, Pusan National University, Busan, Republic of Korea.*
[7]*Institute of Environmental Studies, Pusan National University, Busan, Republic of Korea.*

Keywords: Cloud microphysics, Cloud chamber, Ice nucleation, Aerosol-cloud interaction.

INTRODUCTION

Clouds are a critical component of Earth's climate system, playing a significant role in regulating atmospheric processes by influencing both the hydrological cycle and the radiation budget. Despite their importance, cloud formation and microphysical processes remain among the most uncertain aspects in climate science. Aerosols can act as cloud condensation nuclei (CCN) or ice-nucleating particles (INPs), affecting cloud albedo, lifetime, and precipitation efficiency. Understanding these interactions requires controlled experiments, such as cloud chambers, which cannot be easily studied through field observations alone.

To address these challenges, the Korea Cloud Physics Experimental Chamber (K-CPEC) was constructed in 2022 by the National Institute of Meteorological Sciences (NIMS), a branch of Korea Meteorological Administration (KMA), as a state-of-the-art research facility designed to investigate cloud microphysical processes under controlled laboratory conditions (Cha et al., 2024; Park et al., submitted). The facility is located in Seogwipo, Jeju Island, South Korea. This facility allows researchers to systematically study cloud microphysics, aerosol-cloud interactions, and ice nucleation processes by simulating a wide range of atmospheric conditions, thereby oppering a controlled and reproducible platform for cloud formation studies. The chamber provides valuable insights into cloud microphysics and serves as a platform for testing weather modification techniques and investigating ice nucleation processes. This presentation introduces the design, capabilities, and applications of K-CPEC, along with preliminary experimental results obtained from the facility.

METHODS

The K-CPEC consists of a cloud chamber, an aerosol chamber, a wind tunnel, and subsidiary facilities. The cloud chamber is an expansion-type cloud chamber with a double-walled structure to reduce heat flux from outer chamber walls and provide stable experimental conditions. The inner wall temperature is dynamically controlled to match the air temperature inside the inner chamber to mimic adiabatic cooling,

which is crucial for replicating atmospheric cloud formation. The inner chamber of the cloud chamber has a volume of approximately 21 m^3. It is the largest cloud chamber among expansion-type cloud chambers with dynamically controlled walls. This large volume enables the formation of relatively large clouds and allows them to persist for extended periods, facilitating detailed observations of cloud microphysical processes. The chamber can be depressurized to 30 hPa and the inner wall temperature can be controlled from -70°C to +60°C, allowing the replication of various clouds observed in Earth's atmosphere. The K-CPEC cloud chamber has a large volume, which enables the simultaneous integration of multiple instruments for comprehensive cloud microphysics studies. The cloud chamber is equipped with advanced instruments that allow for the measurement of meteorological variables such as pressure, temperature, and humidity, as well as the characterization of aerosol and cloud particle properties. These include pressure sensors, T-type thermocouples, chilled-mirror hygrometer, a condensation particle counter (CPC), a scanning mobility particle sizer (SMPS), CO_2/H_2O analyzers, white laser aerosol spectrometer (WELAS) optical particle counters (OPCs), a cloud condensation nuclei counter (CCNC), a portable ice nucleation experiment (PINE), a cloud particle imager (CPI), a cloud, aerosol, and precipitation spectrometer with depolarization (CAPS-DPOL), and a particle image velocimetry (PIV) system. These measurements provide essential data for understanding cloud microphysical processes under controlled conditions. A fan agitator is also installed to ensure uniform mixing of the air within the inner chamber.

The aerosol chamber is designed for the controlled generation, storage, and injection of aerosol particles into the cloud chamber. The chamber is equipped with various aerosol generation systems, including an atomizer for water-soluble aerosols and a dry powder disperser for solid aerosol particles. Additionally, it is equipped with an inlet that connects to the external environment, allowing for the introduction of ambient air into the cloud chamber. This feature allows researchers to introduce a wide range of CCN and INP types under well-regulated conditions. It also has a fan agitator to ensure uniform aerosol distribution before being introduced into the cloud chamber. The ability to control aerosol type, concentration, and composition enables systematic studies on aerosol-cloud interactions and ice nucleation efficiency.

The wind tunnel is designed to generate cloud seeding materials from flares under varying airflow conditions. It can generate wind speeds of up to 100 m/s, allowing for replication of flare experiment under both ground-based and seeding aircraft conditions. Seeding materials generated by combustion flares in the wind tunnel can be transported through the aerosol chamber before being introduced into the cloud chamber. This setup allows for cloud formation experiments using seeding materials, enabling detailed investigations into their effects on cloud microphysical properties and precipitation processes.

Cloud formation within the K-CPEC begins with the preparation of initial conditions using dry, filtered air or ambient air from the external inlet. The initial air temperature inside the inner chamber is adjusted by controlling the temperature of the chamber walls. Depending on the research objective, additional water vapor or aerosols can be selectively introduced to control humidity and aerosol concentration. Once the desired initial conditions are established, cloud formation is initiated through adiabatic expansion. The chamber pressure is reduced using a vacuum pump, causing the internal air temperature to decrease via adiabatic cooling. Simultaneously, the inner wall temperature is also decreased to synchronize with the cooling rate of the air inside the inner chamber. As a result, supersaturation is achieved in the inner chamber, leading to the activation of CCN and the formation of cloud droplets. Depending on the experimental setup, the presence of INPs can also facilitate the formation of ice crystals. By precisely controlling the pressure drop rate, wall temperature, and initial humidity, a wide range of cloud types, from warm clouds to mixed-phase and ice clouds, can be reproduced. The controlled environment of the K-CPEC enables researchers to investigate fundamental cloud formation mechanisms and evaluate the effects of aerosol properties on cloud evolution.

RESULTS

This section presents one of the preliminary experimental results obtained using the K-CPEC, focusing on the formation and evolution of mixed-phase clouds under different aerosol conditions. All experiments were conducted using ambient air as the baseline condition, ensuring a realistic representation of atmospheric conditions.

To analyze the role of INPs, Arizona Test Dust (ATD) and silver iodide (AgI) were introduced separately into the chamber, and their effects on cloud microphysics were examined. The experiments aimed to observe how these aerosols influenced cloud droplet freezing, ice crystal growth, and the overall phase transition within the cloud chamber.

In the control experiment, which utilized only ambient air, most cloud droplets remained in a supercooled liquid state even at temperatures as low as -30°C. Since ambient air naturally contains a low concentration of INPs, only a limited number of ice crystals were observed (Fig. 1). In the experiments with ATD, ice crystal formation began at approximately -20°C, with ice crystals gradually growing through vapor deposition. The observed ice crystal number concentration indicated that ATD effectively facilitated heterogeneous freezing. In contrast, when AgI was introduced instead of ATD, ice nucleation occurred at much higher temperatures, leading to the formation of ice crystals at approximately -5°C. The presence of AgI resulted in a rapid phase transition from supercooled liquid droplets to ice, leading to a notable increase in ice crystal concentration. In the experiment with AgI, as time progressed, ice crystals deposited on the inner chamber walls, leading to a rapid decrease in their concentration. In the control experiment and experiments with ATD or AgI, the shapes of ice crystals formed by heterogeneous freezing at different temperatures aligned with ice crystal habit diagrams reported by previous studies (e.g., Bailey and Hallett, 2009).

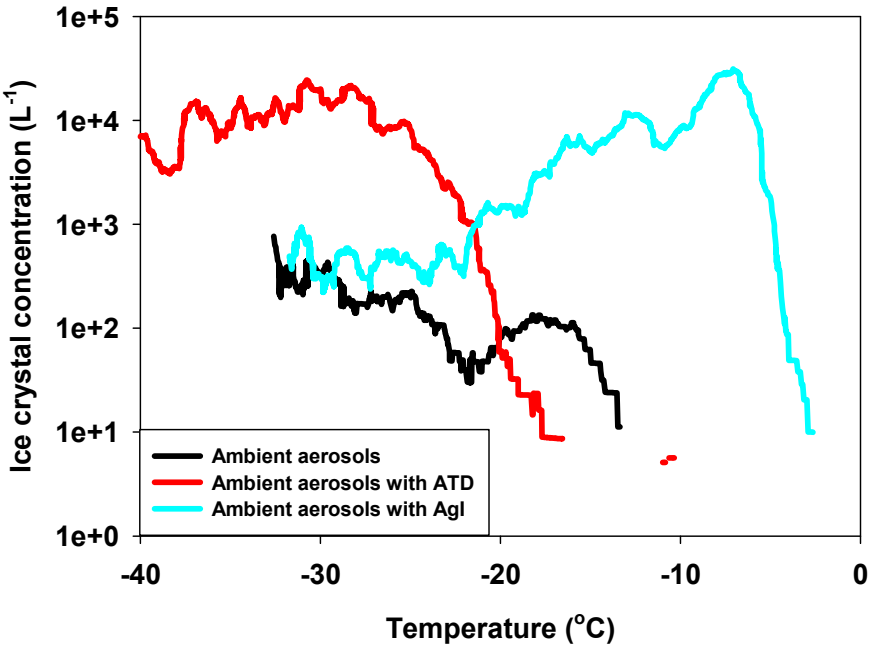


Figure 1. Ice crystal number concentration during cloud formation experiments using the K-CPEC. Black, red, and cyan colors represent ambient aerosols, ambient aerosols with ATD, and ambient aerosols with materials from an AGI flare, respectively.

CONCLUSIONS

The K-CPEC provides a controlled environment for studying cloud microphysics, including aerosol-cloud interactions and ice nucleation processes. By enabling systematic investigations into CCN and INP effects, it contributes to a better understanding of cloud evolution and precipitation processes. The ability to simulate diverse cloud conditions under well-regulated settings makes it a valuable tool for understanding cloud microphysics.

K-CPEC is also open to international collaborations, and we strongly encourage researchers worldwide to participate in joint studies to advance cloud physics research. By fostering cooperation among institutions, the facility can serve as a global hub for experimental atmospheric research, thus contributing to a deeper understanding of aerosol-cloud-precipitation interactions and their climatic implications.

As of the writing of this abstract, experiments utilizing the K-CPEC are actively being conducted, and further findings will be presented at the conference, providing additional insights into ongoing research developments.

ACKNOWLEDGEMENTS

This research has been supported by the "Research on Weather Modification and Cloud Physics" (KMA2018-00224) project of NIMS/KMA and Basic Science Research Program through the National Research Foundation of Korea (NRF) funded by the Ministry of Education (RS-2023-00246513).

REFERENCES

Bailey, M. P., and J. Hallett, (2009). A comprehensive habit diagram for atmospheric ice crystals: Confirmation from the laboratory, AIRS II, and other field studies. *J. Atmos. Sci.*, **66**, 2888–2899, https://doi.org/10.1175/2009JAS2883.1.

Cha, J.W., Y. Kim, M. Belorid, B.-Y. Kim, J. Baek, S. Kim, K. Lee, C. Cho, and S. Lee, (2024). Development of Korea's First Large Scale Advanced Cloud Physics Experimental Chamber (I): Design of the Cloud Physics Experimental Chamber System and Detailed Structural Analysis of the Cloud Chamber. *J. Environ. Sci. Int.*, **33**, 957~975, https://doi.org/10.5322/JESI.2024.33.12.957 (in Korean).

Park, M., J.W. Cha, S. Park, J. Kim, Y. Kim, M. Belorid, B.-Y. Kim, J. Baek, S. Kim, K. Lee, P. Seo, C. Ahn, J. Lee, S.S. Yum, J. Um, (submitted). Introduction to the Korea Cloud Physics Experimental Chamber (K-CPEC). *Bull. Am. Meteorol. Soc.*, (submitted).

DISTUINGISH MINERAL DUST AND BIOLOGICAL AEROSOL PARTICLES AS WELL AS WATER DROPLETS AND ICE CRYSTALS AUTOMATIC AND IN REAL-TIME WITH SWISENS POLENO JUPITER

D. Rothenfluh[1], Y. Zeder[1], E. Graf[1], A. Schwendimann[1], P. Burch[1], R. Abt[1] and E. Niederberger[1]

[1] *Swisens AG, 6032 Emmen, Switzerland*

Keywords: ice nuclei particle measurement, experimental studies, polarization, holography, automatic aerosol particle classification, automatic aerosol particle monitoring

INTRODUCTION

Field measurements by INP are important for a better understanding of ice nucleation processes. Until now, this has been very time-consuming because in many cases a complex analysis of the particles in the laboratory is necessary. The SwisensPoleno Jupiter (Poleno) offers a remedy, which can automatically monitor aerosol particles in real time and has the potential to automatically distinguish the most important INP classes such as mineral dust and primary biological aerosol particles (PBAB), but also water droplets and ice crystals, in real time.. Dies dank der verschiedenen integrierten Messmethoden wie digitale Holografie, Fluoreszenz und Polarisation. This is thanks to the various integrated measurement methods such as digital holography, fluorescence and polarisation. Swisens has validated the polarisation measurement integrated in the Jupiter and measured relevant particle classes. These results are shown below.

METHODS

The SwisensPoleno Jupiter is an airflow cytometer. It continuously draws in the aerosol particles at a rate of 40 litres/min and directs them into the measuring chamber where the individual particles are measured in flight using optical methods. Finally, the particles fly out of the measuring system again. For the polarization measurement, airborne particles are illuminated using a 405 nm laser, and the scattered light is measured at a 90° angle (Figure 1a). The intensity of the scattered light is recorded during the particle flyby using photodiodes equipped with polarization filters. This results in two time series capturing the p- and s-polarized light intensities (Figure 1b).

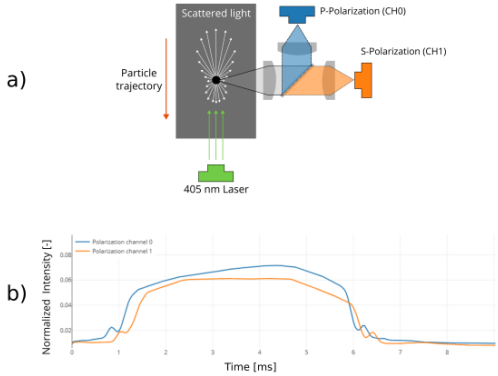


Figure 1 Polarization data collection in the SwisensPoleno Jupiter. a) Schematic representation of the measurement setup. Particles travel through the measurement chamber and are illuminated by a 405 nm laser diode. The scattered light undergoes polarization filtering before reaching two photodiodes, each measuring a different polarization component. b) Raw time series of the measured light intensity signals

for both polarization channels (channel 0: p-component, channel 1: s-component) as a particle passes by the photodiodes.

Different methods to aggregate the p- and s- component of the polarization ratio ($PR = (p-s)/(p+s)$) were evaluated. The most distinct and robust approach is based on individually integrating the mid-section of the scattering signals over time.

CONCLUSIONS

As a result, the boxplots shown in figure 2 were obtained. It is evident that the measurement results are consistent across the different Poleno instruments. Notably, water can be clearly distinguished from all other particle types as shown in Figure 3. Since the datasets are uncleaned, the boxplots are expected to improve after proper data cleaning.

Figure 3 Kaolinite mineral dust showed the lowest value compared to different types of mineral dust, pollen and water droplets. Water droplets can be clearly distinguished because of the highest values. Different mineral dust classes cannot be clearly distinguished based on this metric alone. The different types of pollen show slight differences. It is not possible to distinguish the different mineral dust classes and pollen types sufficiently based on the polarisation rate alone.

The holographic images in Figure 4 and Figure 5 show different particle classes recorded with the SwisensPoleno. These show the potential for sufficient differentiation when holography is included. Water droplets and ice crystals can be easily distinguished from each other due to their very different morphological properties compared to mineral dust. Polarisation measurement makes water drop detection even more reliable.

A possible next step could be a detailed classification of the different ice crystals based on their polarisation rate, as this depends on their shape. This could be done using a pre-classification based on morphological characteristics calculated from holographic images of the ice crystals or an AI-based classifier trained with labelled images.

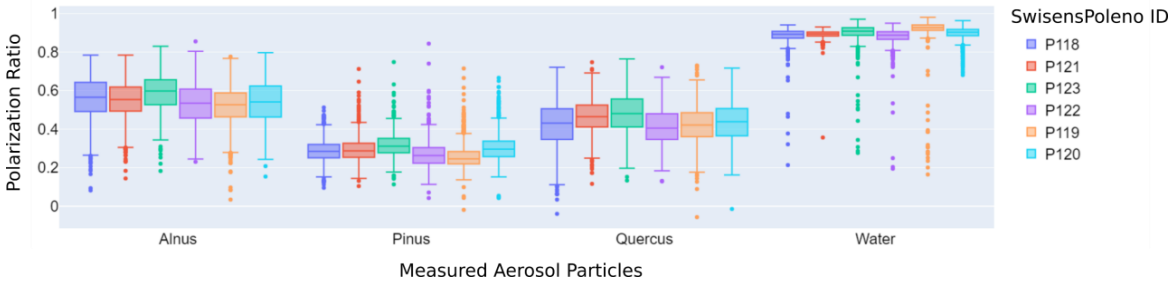


Figure 2 Comparison of PR for samples atomized in the laboratory, such as dried pollen (Alnus, Pinus, Quercus) and water droplets. For each sample at least 1'000 particles were measured with 6 SwisensPoleno Jupiter (P118, P119, P120, P121, P122, P123).

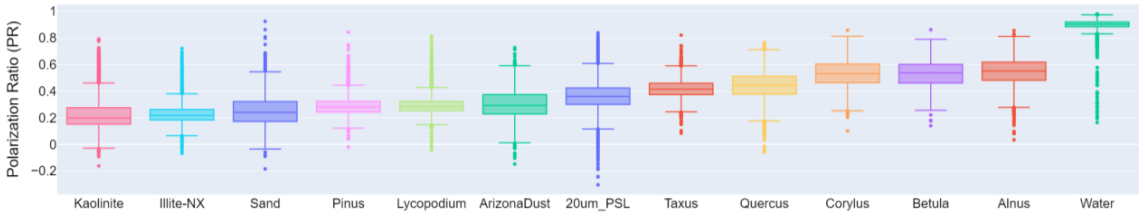


Figure 3 Boxplots of the various aerosol particles measured in the laboratory. From left to right: Kaolinite, Illite-NX, Sand, Pinus Pollen, Lycopodium, Arizona Road Dust, 20um PSL, Taxus Pollen, Quercus Pollen, Corylus Pollen, Betula Pollen, Alnus Pollen, Water droplets.

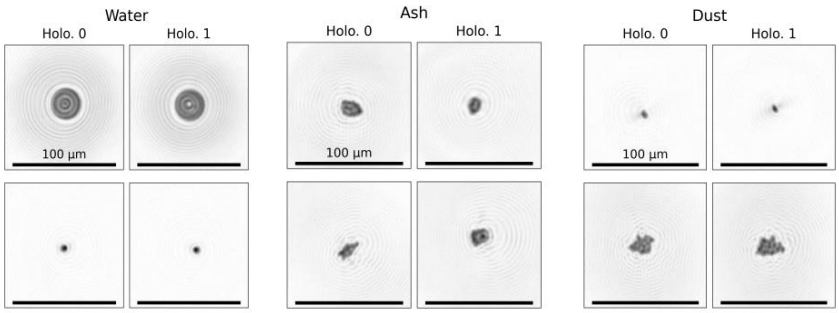


Figure 4 Holographic images obtained with SwisensPoleno. Holo. 0 and Holo. 1 show the same particle. The viewing angle of Holo. 1 is offset by 90°. Left: two examples of water droplets. Middle: two examples of volcanic ash particles from Eyjafjallajökull volcanic eruption. Right: two examples of dust particles (Beres et al 2023).

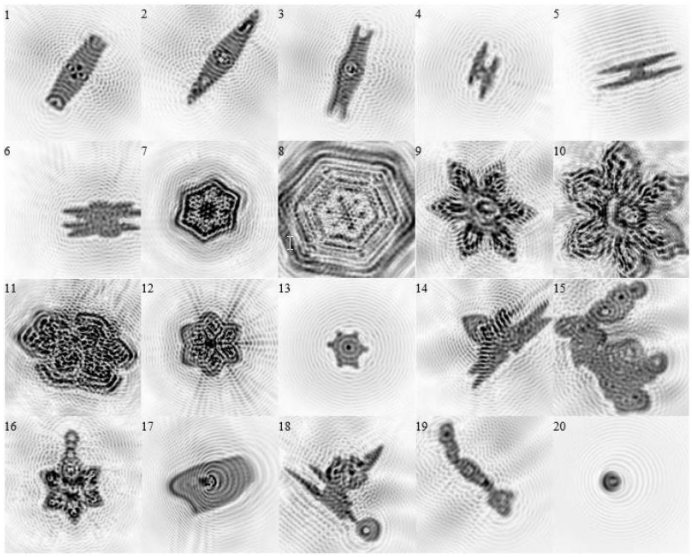


Figure 5 Ice particles in a cloud measured with SwisensPoleno on Sonnblick (Heuberger et al 2024). They were able to assign these to the classes of the Nakaya morphology diagram.

ACKNOWLEDGEMENTS

This work was part of the SYLVA project (HE-CL6-GOV-IA-2022-101086109).

REFERENCES

Beres, Nicholas et al. 2023. 'Merging Holography, Fluorescence, and Machine Learning for in Situ, Continuous Characterization and Classification of Airborne Microplastics'. EGUsphere, December, 1–31. https://doi.org/10.5194/egusphere-2023-2853

Heuberger, Anna, and Veronika Krieger. 2024. 'Crystal Clear! How Ice Crystal Nucleation and Environmental Conditions Influence the Structure of Precipitating Snow'. Poster. University Press, Cambridge, U.K.).

QUANTITATIVE ABSORPTION SPECTRUM OF HYDROCARBON AEROSOLS USING DUAL-CELL PHOTOACOUSTIC SPECTROSCOPY

JAMSHED SAEED SHAH[1] , RAHMAN ABDUL[1,] *, BALINT[1], AJTAI TIBOR[1,2], ZOLTAN BOZOKI[1,2]

[1]*Department of Optics and Quantum Electronics, University of Szeged, 9. Dóm square, Szeged, H-6720, Hungary*

[2]*HUN-REN-SZTE Research Group for Photoacoustic Monitoring of Environmental Processes, Dóm ter 9, Szeged, 6720, Hungary*

Email: Jamshedsaeed1234@gmail.com

Abstract.

We report for the first time, the development and demonstration of simplified and robust photoacoustic (PA) technology by integrating an EC-ICL with dual PA cell configuration for quantitative characterization of aerosols in the mid-IR range of 3.30 to 3.55 µm. The EC-ICL source was chosen for its stable optical output, compact design, and low power consumption. By flowing a known gas in one PA cell (reference cell), we define a wavelength-dependent transfer function (TF). The TF is used for calculating the quantitative absorption spectrum for the second PA cell, which contains analyte aerosols. The novel customized Videoton electronics is used to modulate laser and PA signal acquisition. For the proof of concept, we used a hydrocarbon mixture of propane for the reference cell and di-ethyl-hexyl-sebacate (DEHS) aerosols as analytes in the second cell to demonstrate the potential of the proposed technique.

Biography.

Jamshed Saeed Shah, PhD Student

He is studying PhD physics at the Department of Optics and Quantum Electronics, University of Szeged, Hungary, under the supervision of Professor Bozoki Zoltan and Professor Ajtai Tibor. His responsibility in this work is to study theoretically and experimentally the mid-infrared spectrum of airborne aerosols using photoacoustic spectroscopy.

ADVANCING GAS PHASE ANALYSIS IN AEROSOL RESEARCH: MPCIMS WITH URONIUM FOR COMPREHENSIVE TRACE GAS DETECTION

A. SHCHERBININ[1]; H. FINKENZELLER[1,2]; F. PARTOVI[1, 3]; N. VINKVIST[4]; J. MIKKILÄ[1]; J. KONTRO[1]; J. MIKKILÄ[1]; H.-J. JOST[1]; J. KANGASLUOMA[2]; S. IYER[3]; and M. RISSANEN[3, 4]

[1]Karsa Ltd., Helsinki, Finland;.

[2] Institute for Atmospheric and Earth System Research/ Department of Physics, Faculty of Science, University of Helsinki, Helsinki, Finland;

[3]Aerosol Physics Laboratory, Physics Unit, Faculty of Engineering and Natural Sciences, Tampere University, Tampere, Finland;

.

[4]Department of Chemistry, Faculty of Science, University of Helsinki, Helsinki, Finland

Keywords: GAS PHASE, SECONDARY ORGANIC AEROSOL FORMATION, CHEMICAL IONISATION, MASS SPECTROMETRY.

INTRODUCTION

Aerosol research requires advanced measurement techniques to analyze complex atmospheric trace gases, such as volatile organic compounds (VOCs) and oxidation products, which are important for aerosol formation. Multi-Pressure Chemical Ionization Mass Spectrometry (MPCIMS) offers a novel solution by combining high- and low-pressure ionization schemes within a single instrument. This allows for simultaneous detection of a wide range of gas-phase species, from volatile precursors to highly functionalized oxidation products. The integration of uronium as a reagent, sublimated from urea under x-ray irradiation, enhances sensitivity and reduces humidity interference, making it a promising candidate for positive mode chemical ionization.

METHODS

MPCIMS integrates both high- and low-pressure ionization schemes, enabling the measurement of a diverse range of atmospheric trace gases. Uronium is generated by sublimating solid urea under x-ray irradiation and serves as a reagent for positive mode ionization. Calibration experiments were performed under varying humidity conditions to determine ionization efficiencies for VOCs, amines, and DMSO. VOC oxidation experiments were also carried out, such as DMS and α-pinene to evaluate the performance of the MPCIMS. Preliminary results show that this system can measure trace gases at low ppqv levels, providing robust and stable analysis..

CONCLUSIONS

The integration of uronium with MPCIMS represents a significant step forward in aerosol measurement technology. This novel method enables the analysis of a comprehensive suite of atmospheric trace gases using a single instrument, combining high sensitivity, low susceptibility to humidity changes, and easy reagent handling. The simplicity and effectiveness of this approach suggest that it will become a valuable tool in aerosol and atmospheric research, allowing for detailed characterization of aerosol precursors and oxidation products.

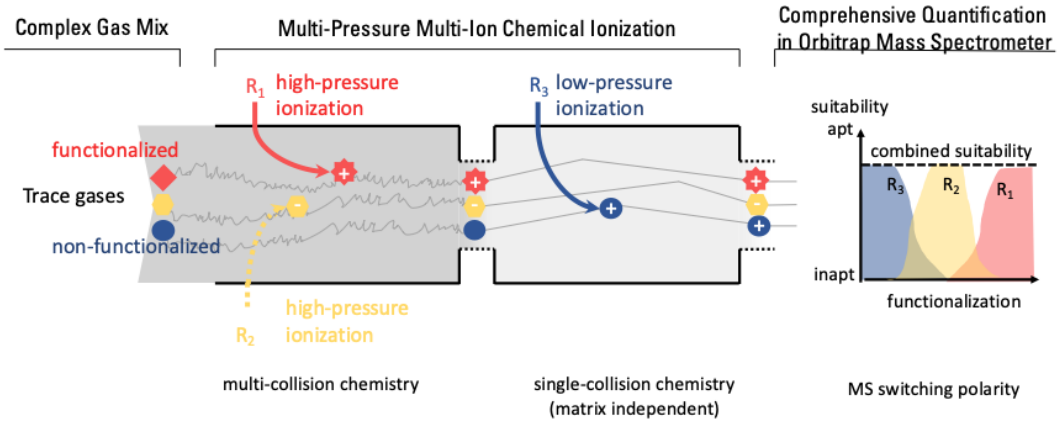


Figure 1. Conceptual diagram of the MPCIMS system demonstrating how molecules with different functionalization are analyzed using combined high- and low-pressure ionization schemes.

ACKNOWLEDGEMENTS

This study was partially funded by the Finnish Research Impact Foundation and Research Council of Finland (364223, 346370, 346373, 353836, 356134). This project has received funding from the European Research Council under the European Union's Horizon 2020 research and innovation programme under Grant No. 101002728.

REFERENCES

Shcherbinin, A., H. Finkenzeller, J. Mikkilä, J. Kontro, N. Vinkvist, J. Kangasluoma, and M. Rissanen (2024), *Analytical Chemistry* **96** (50), 19926.

.

CHARACTERIZATION OF MULTI-SCHEME BROMIDE-BASED CHEMICAL IONISATION (Br-MION2) USING TIME-OF-FLIGHT AND ORBITRAP MASS SPECTROMETERS

J. Shen[1,2*], J. Zhang[1], P. Juuti[3], J. Mikkila[3], M. Rissanen[4], A. Shcherbinin[3], M. Ehn[1], J. Kangasluoma[1], X-C. He[1]

[1]*Institute for Atmospheric and Earth System Research/ Helsinki Institute of Physics, University of Helsinki, 00014, Finland*
[2]*Helsinki Institute of Physics, University of Helsinki, Helsinki, Finland.*
[3]*Karsa Ltd., 00560 Helsinki, Finland*
[4] *Department of Chemistry, Faculty of Science, University of Helsinki, 00014 Helsinki, Finland*

Keywords: Br-MION2, APi-TOF, Orbitrap, instrument sensitivity, detection limit
*Presenting author email: jiali.shen@helsinki.fi

INTRODUCTION

The chemical ionization atmospheric pressure interface time-of-flight mass spectrometer (CI-APi-TOF) is widely used in atmospheric chemistry and aerosol formation studies due to its versatility and high sensitivity in detecting trace-level species (Eisele and Tanner, 1993; Munson and Field, 1966; Kirkby et al., 2011; Ehn et al., 2014). By utilizing different ionization reagents and techniques, CI-APi-TOF can detect a broad range of compounds, from sulfur species, halogen species to organic precursors and their oxidation products which are important players in atmospheric chemistry and aerosol formation. For example, the nitrate-APi-TOF, when equipped with an Eisele-type inlet (Eisele and Tanner, 1993), is commonly used to measure sulfuric acid (H_2SO_4) and highly oxygenated organic molecules (HOMs) due to its extremely low detection limits, reaching the parts-per-quadrillion by volume (ppqv) levels (Kirkby et al., 2011; Ehn et al., 2014). However, many other species, such as iodine and isoprene oxidation products (He at al., 2021), also contribute to particle formation but many of their oxidation products are not traceable by the nitrate-APi-TOF. Therefore, developing new ionization techniques is essential for advancing atmospheric chemistry and aerosol formation studies.

Among recent developments, the Br-MION2-APi-TOF has gained significant attention due to its high sensitivity to species with lower oxidation states, such as isoprene oxidation products ($C_5H_{12}O_6$ and $C_5H_{12}O_5$), which can contribute to new particle formation under low-temperature conditions (Shen et al., 2024). Additionally, the Br-MION2-APi-TOF can detect a range of gaseous iodine species (He at al., 2021), which helped to advance atmospheric chemistry and aerosol formation studies of iodine. It is also capable of measuring key atmospheric species such as hydroperoxyl radical, sulfur dioxide, and nitrous acid. Building on these advantages, we used Br-MION2 to evaluate instrument performance characteristics.

One of the major limitations of the APi-TOF is its mass resolving power, which determines its ability to distinguish between ions of similar mass. For example, the long time-of-flight mass spectrometer typically achieves a resolution of around 8000 for H_2SO_4, which is sufficient for reliable identification since no interfering peaks overlap with its signal. However, at higher mass-to-charge ratios (m/z), resolution becomes an issue in accurately identifying organic species, especially those containing nitrogen, sulfur and fluorine. To address this, orbitrap mass spectrometry has been adopted to measure atmospheric molecules (Riva et al., 2020). The CI-Orbitrap has a mass resolving power of 240,000 (depends on model types), which significantly improves peak identification. However, Riva et al., 2020 reported several limitations of the CI-Orbitrap, including high detection limits and non-linearity at low concentrations. Cai et al., 2022 further explored ways to improve CI-Orbitrap measurements, but issues of non-linearity and high detection limits continue to affect data interpretation. As a relatively new technique, many questions remain, espcially regarding Orbitrap optimization. It is still unclear whether non-linearity is a fundamental limitation of the instrument or if its impact depends on specific applications. In this study, we compare Br-MION2-APi-TOF and Br-MION2-Orbitrap by directly connecting them to a chamber to measure a wide range of isoprene oxidation products, assessing the performance of both instruments.

METHODS

In this study, we conducted experiments on isoprene oxidation with hydroxyl radicals (OH) in the COALA chamber. The chamber is a cuboid structure made of fluorinated ethylene propylene (FEP), with a volume of 2 m^3, and is located on the laboratory ceiling. The chamber total flow was kept constant at 55 L min^{-1} using zero air, which refers to ambient air that passed through a zero-air generator to remove water and other volatile organic compounds. We injected isoprene and tetramethylethylene (TME) from home-made gas bottles at concentrations of 547 ppm and 36 ppb, respectively. Their flows were controlled by mass flow controllers (MFCs) and delivered into the chamber through polytetrafluoroethylene (PTFE) tubing. Ozone (O_3) was generated by a 254 nm UV light, which photolyzes O_2 present in the incoming air. The O_3 concentration was adjusted by varying the light intensity and airflow. The reaction between TME and O_3 can then generate OH through ozonolysis.

Two identical Br-MION2 inlets were coupled to an APi-TOF and an Orbitrap, which were connected in parallel to the chamber via probes underneath, using ¾ inch Teflon tubes. These Teflon tubes have similar length, so we assume the losses of gas vapours going to both instruments are identical. Once the measured isoprene oxidation products stabilized, we adjusted isoprene and O_3 concentrations to vary the concentration of the isoprene oxidation products. A photometric O_3 analyzer – model 400 (Teledyne API) was used to measure O_3 concentrations in the chamber.

CONCLUSIONS

Both instruments measured the same set of compounds from the COALA chamber and shared an identical inlet design. As a result, the measured isoprene oxidation products should be consistent. Without applying calibration factors to either instrument, we compare the normalized signals of isoprene oxidation products, focusing on the species identified by Shen et al. (2024) as key drivers of particle formation. As shown in Figure 1a, all the presented species exhibit a close-to-linear correlation between Br-MION2-APi-TOF and Br-MION2-Orbitrap. The absolute difference between instruments for each species remains within a factor of three, which we attribute primarily to compound-dependent variations in transmission efficiency within the respective mass spectrometers. Notably, the concentrations of these isoprene oxidation products span four orders of magnitude - a range typical for key precursors (e.g., H_2SO_4, HOMs) in ambient measurement. This result suggests that the Br-MION2-Orbitrap maintains good linearity across the concentration range relevant for atmospheric measurements.

Zooming in on m/z = 231 (Figure 1b), with careful peak-fitting, the APi-TOF detects up to four peaks ($C_5H_{10}O_5{}^{81}Br^-$, $C_5H_{12}O_5Br^-$, $C_6H_{14}O_4{}^{81}Br^-$ and $C_{10}H_{15}O_6^-$), while the Orbitrap confidently identifies at least seven peaks. The APi-TOF misses some peaks, which could affect our understanding of the oxidation process. Additionally, the interference of $C_5H_{10}O_5{}^{81}Br^-$ and $C_6H_{14}O_4{}^{81}Br^-$ may affect the quantification of $C_5H_{12}O_5Br^-$, which is an important precursor for initiating new particle formation in the upper troposphere (Shen et al., 2024). By applying independent calibration factors, we compare the absolute concentrations between the two instruments to evaluate their quantification performance, including detection limits and sensitivity. These aspects will be discussed in this work.

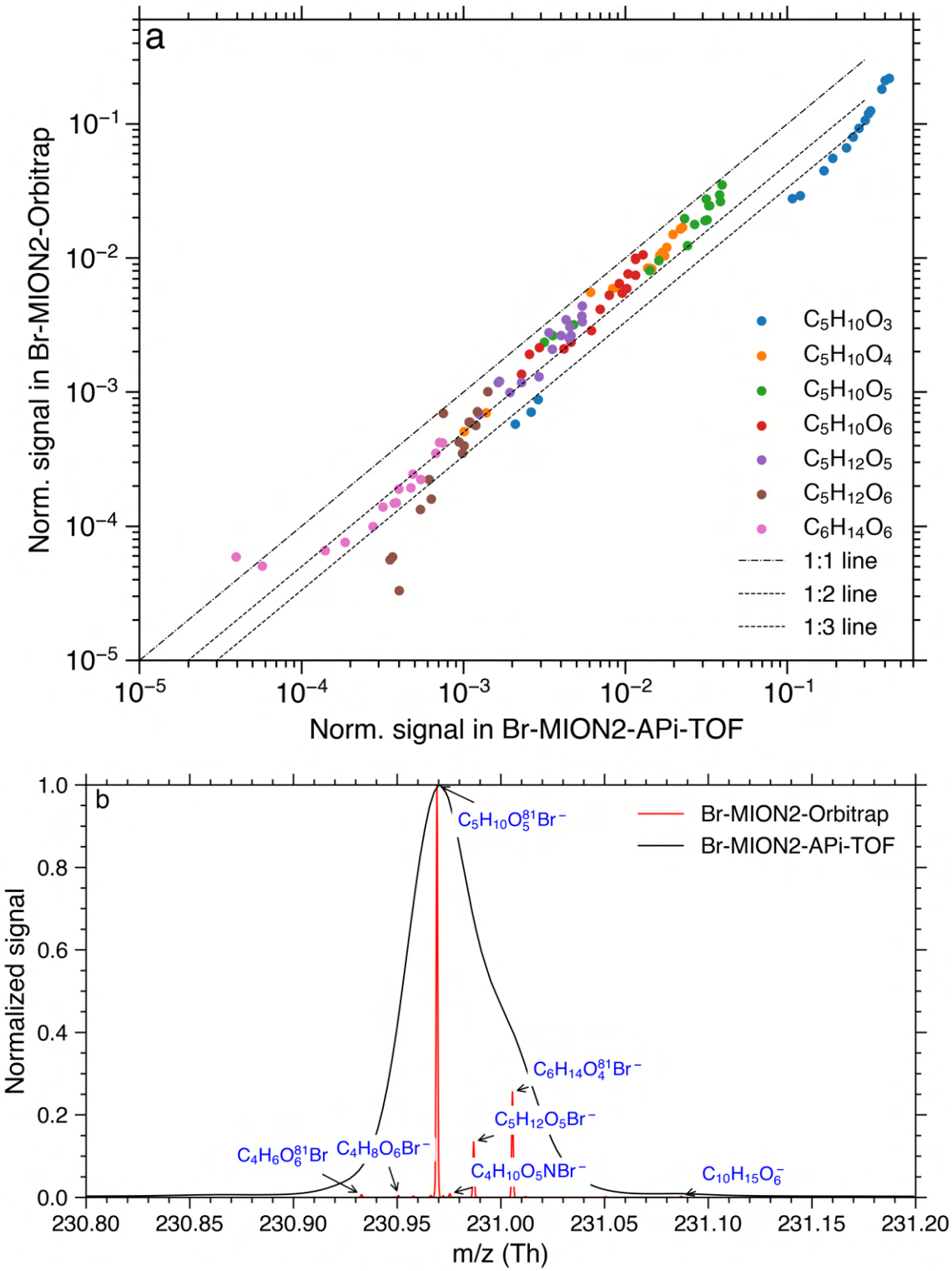


Figure 1. Measured isoprene oxidation products a) and spectrum comparison b) between Br-MION2-Orbitrap and Br-MION2-APi-TOF

ACKNOWLEDGEMENTS

This work was supported by the Helsinki Institute of Physics, the Research Council of Finland no.359331 and EU MSCA Doctoral Network CLOUD-DOC 101073026.

REFERENCES

Eisele, F.L. and Tammer, D.L. (1993). Measurement of the gas phase concentration of H_2SO_4 and methane sulfonic acid and estimates of H_2SO_4 production and loss in the atmosphere*, J of Geophysical Research: Atmospheres* **95**, 9001-9010.

Munson, M. S. B., and Field, F. H. (1966). Chemical Ionization Mass Spectrometry. I. General Introduction, J. *Am. Chem. Soc.*, **88**, 2621–2630.

Kirkby, J., and Kulmala, M. et al. (2011). Role of sulphuric acid, ammonia and galactic cosmic rays in atmospheric aerosol nucleation, *Nature*, **476**, 429–433.

Ehn, M., and Mentel, T. F. et al. (2014). A large source of low-volatility secondary organic aerosol, *Nature*, **506**, 476–479.

He, X.-C., and Sipilä, M., et al. (2011). Role of iodine oxoacids in atmospheric aerosol nucleation, *Science*, **371**, 589–595.

Shen, J., Russell, D., and He, X.-C., et al. (2024). New particle formation from isoprene under upper-tropospheric conditions, *Nature*, **636**, 115–123.

Riva, M., and Berndt, T., et al. (2020). Capability of CI-Orbitrap for Gas-Phase Analysis in Atmospheric Chemistry: A Comparison with the CI-APi-TOF Technique, *Anal. Chem.*, **92**, 8142–8150.

Cai, R., and Ehn, M., et al. (2022). Improving the Sensitivity of Fourier Transform Mass Spectrometer (Orbitrap) for Online Measurements of Atmospheric Vapors, *Anal. Chem.***, 94**, 15746–15753.

INSUFFICIENT MASS SPECTROMETRIC DETECTION OF SYNTHESIZED HYDROPEROXY ACIDS FROM ALPHA-PINENE OZONOLYSIS

M. TISCHBERGER[1], M. KAISER[2], H. GROTHE[1], M. LAIR[1], M. OPACAK[1], D. SCHACHAMAYR[2], R. VERMA[1] and D. STOLZENBURG[1]

[1]*Institute of Materials Chemistry, TU Wien, Vienna, Austria*

[2]*Institute of Applied Synthetic Chemistry, TU Wien, Vienna, Austria*

Keywords: New Particle Formation, Hydroperoxides, Chemical Ionization, Orbitrap.

INTRODUCTION

Alpha-pinene is one of the most studied precursor molecules for new particle formation (NPF). It was shown that RO_2 radicals formed by α-pinene ozonolysis can undergo autoxidation to rapidly form highly oxygenated molecules (HOMs) (Bianchi *et al*., 2019). These HOMs are hypothesized to often contain hydroperoxide (C-O-O-H) functionalization, as the RO_2 radicals undergo subsequent intramolecular H-shifts. Since the functionalization of molecules influences their vapor pressure, it is an important factor when modeling the formation and growth of new aerosol particles from different organic precursors (Stolzenburg *et al*., 2022).
Authentic standards of α-pinene derived HOMs are sparse. While some research groups have achieved the synthesis of HOM-dimers (see, e.g., Kenseth *et al*., 2023), monomeric HOM compounds with the significant hydroperoxide functionalization are still not commercially available (Mettke *et al*., 2022). There is an urgent need to investigate the detection of these compounds in the widely used chemical ionization mass spectrometers, as their charging efficiencies remain largely unknown (Alage *et al*., 2024).

METHODS AND RESULTS

In this work, we report the synthesis of two α-pinene derived molecules ($C_9H_{14}O_4$ and $C_{10}H_{16}O_4$) containing hydroperoxy-acid (C(O)-O-O-H) groups, verified by H- and C-NMR techniques. Figure 1 displays the synthetic pathway of $C_{10}H_{16}O_4$.

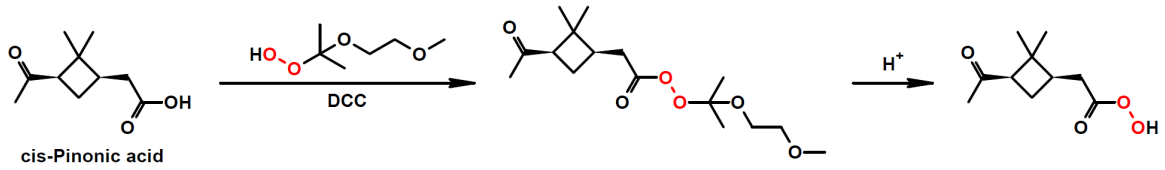


Figure 1. Synthetic pathway of $C_{10}H_{16}O_4$.

Each sample of synthesized standards contains a certain ratio of peroxy acids to their corresponding carboxylic acids. We characterized the samples using an Orbitrap mass spectrometer with heated electrospray ionization (H-ESI) and nitrate (NO_3^-) and uronium ($CH_5N_2O^+$) based chemical ionization at atmospheric pressure (MION2). Figure 2 illustrates the experimental setup. For H-ESI, samples were dissolved with a 9:1 mixture of acetonitrile and water, modified with 0.1 % v/v acetic acid, and introduced via a syringe. H-ESI achieved analyte ionization primarily via deprotonation. For MION2, samples were dissolved in deuterated chloroform and evaporated. The suspended molecules were then ionized by nitrate and uronium reagent ions in a switching sequence via both (de)protonation and cluster formation.

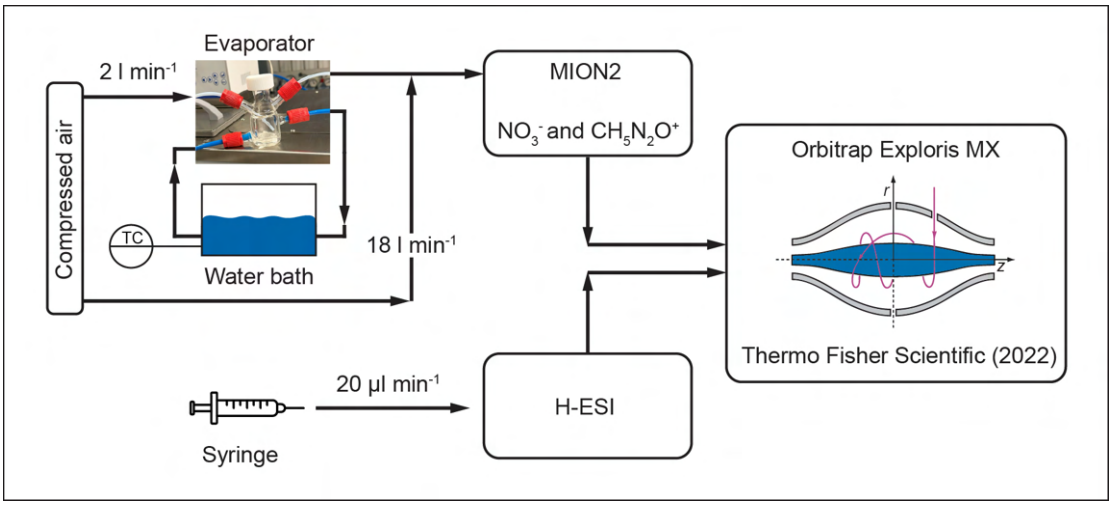


Figure 2. Experimental setup. For MION2, samples are filled into the evaporator, which is tempered by a temperature-controlled water bath. The sample air flow of 2 l min^{-1} is diluted with 18 l min^{-1} compressed air and passed on to MION2, where the analyte molecules are ionized with nitrate and uronium reagent ions in a switching sequence. In the second procedure, samples are filled into a syringe and passed on to H-ESI with a sample flow of 20 µl min^{-1}. The analyte ions are then measured with an Orbitrap Exploris MX with a mass resolution of 180000 at m/z 200.

The results for H-ESI-Orbitrap and MION2-Orbitrap with nitrate are shown in Figure 3. As displayed in Figure 3 a, both H-ESI and NO_3^- chemical ionization yielded much higher signals of the corresponding carboxylic acids. This either indicates a rapid decomposition of hydroperoxy acids into their corresponding carboxylic acids during the ionization process or a reduced ionization efficiency of hydroperoxy acids. Compared to deprotonation, the softer cluster formation ionization leads to higher signals of the peroxy acids, supporting the decomposition hypothesis. As displayed in Figure 3 b, nitrate adduct peaks are significantly less intense than the deprotonated peaks, indicating a reduced sensitivity of NO_3^- for moderately-oxygenated samples, calling for novel reagents such as uronium to achieve this coverage.

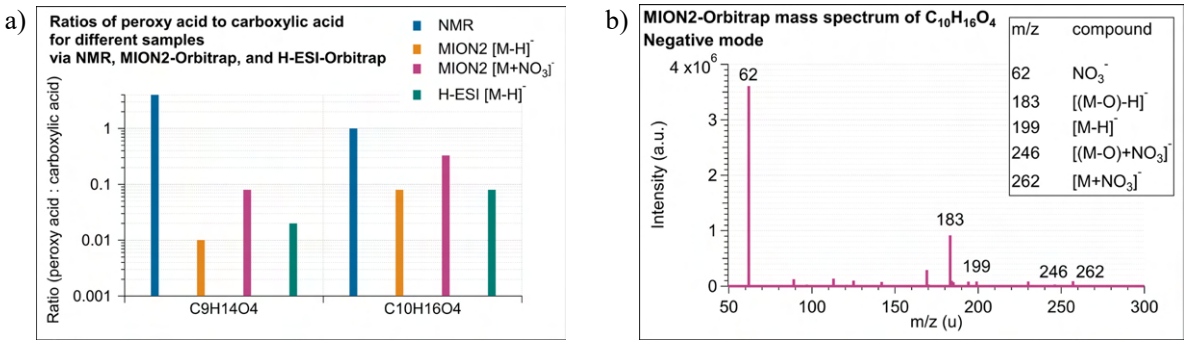


Figure 3. Results for H-ESI-Orbitrap and MION2-Orbitrap with nitrate. a) Ratios of peroxy acids to their corresponding carboxylic acids for both synthesized standards, additionally measured via NMR. b) MION2-Orbitrap nitrate mode mass spectrum of $C_{10}H_{16}O_4$ in negative ion mode.

CONCLUSIONS

Our first results imply that hydroperoxy acids formed via the autoxidation of α-pinene might often not be accurately quantified with different mass spectrometric techniques. As especially NO_3^- chemical ionization is widely used in atmospheric studies of NPF, this could result in huge discrepancies when atmospheric process rates (such as nucleation and growth rates of newly formed particles) are derived from gas-phase measurements. Novel chemical ionization reagents are needed to achieve a broad coverage of molecule oxygenation levels.

ACKNOWLEDGEMENTS

This work was supported by the Viennese Science and Technology Fund (WWTF) under the project VRG22-003 and the Austrian Science Fund (FWF) under the project PAT8221324.

REFERENCES

Alage, S., V. Michoud, S. Harb, B. Picquet-Varrault, M. Cirtog, A. Kumar, M. Rissanen and C. Cantrell (2024). A nitrate ion chemical-ionization atmospheric-pressure-interface time-of-flight mass spectrometer (NO3− ToFCIMS) sensitivity study, *Atmos. Meas. Tech*. **17**, 4709–4724.

Bianchi, F., T. Kurtén, M. Riva, C. Mohr, M. P. Rissanen, P. Roldin, T. Berndt, J. D. Crounse, P. O. Wennberg, T. F. Mentel, J. Wildt, H. Junninen, T. Jokinen, M. Kulmala, D. R. Worsnop, J. A. Thornton, N. Donahue, H. G. Kjaergaard and M. Ehn (2019). Highly Oxygenated Organic Molecules (HOM) from Gas-Phase Autoxidation Involving Peroxy Radicals: A Key Contributor to Atmospheric Aerosol, *Chemical Reviews* **119** (6), 3472-3509.

Kenseth, C. M., N. J. Hafeman, S. P. Rezgui, J. Chen, Y. Huang, N. F. Dalleska, H. G. Kjaergaard, B. M. Stoltz, J. H. Seinfeld and P. O. Wennberg (2023). Particle-phase accretion forms dimer esters in pinene secondary organic aerosol, *Science* **382**, 787-792.

Mettke, P., A. Mutzel, O. Böge and H. Herrmann (2022). Synthesis and Characterization of Atmospherically Relevant Hydroxy Hydroperoxides, *Atmosphere* **13**(4), 507.

Stolzenburg, D., M. Wang, M. Schervish and N. M. Donahue (2022). Tutorial: Dynamic organic growth modeling with a volatility basis set, *Journal of Aerosol Science* **166**, 106063.

CLOUD CONDENSATION AND ICE NUCLEATION PROCESS STUDIES BY COMBINED CLOUD SIMULATION CHAMBER AND PROCESS MODELLING ACTIVITIES

N. S. UMO[1], P. CONNOLLY[2], B. ASCHER[3], K. BI[4], S. CHEN[5], Z. DENG[6], J. ETCHETO[1], F. HOFFMANN[3], Y. HU[1], N. KIM[7], N. RIEMER[8], W. TANG[8], D. TOPPING[2], R. WAGNER[1], X. XU[8], L. XUE[5], S. S. YUM[9], B. ZHU[2], and O. MÖHLER[1]

[1]*Institute of Meteorology and Climate Research - Atmospheric Aerosol Research, Karlsruhe Institute of Technology (KIT), Germany*
[2]*Centre for Atmospheric sciences, University of Manchester, UK*
[3]*Meteorological Institute, Ludwig Maximilian University, Germany*
[4]*Beijing Weather Modification Centre, China*
[5]*Research Applications Laboratory, National Centre for Atmospheric Research, USA*
[6]*Key Laboratory of Middle Atmosphere and Global Environment Observation, Institute of Atmospheric Physics, Chinese Academy of Sciences, China*
[7]*Korea Institute of Science and Technology, South Korea*
[8]*Department of Climate, Meteorology, and Atmospheric Sciences, University of Illinois, USA*
[9]*Department of Atmospheric Sciences, Yonsei University, South Korea*

Keywords: AEROSOL, ICE NUCLEATION, CLOUD CHAMBER, CLOUD PROCESS.

INTRODUCTION

Aerosol particles in the Earth's atmosphere can impact air quality and can also play an important role in cloud formation. It has been established that aerosol particles can influence cloud formation by serving as cloud condensation nuclei (CCN) and ice-nucleating particles (INPs) (Hoose & Möhler, 2012; Kanji et al., 2017). Many studies have shown that different aerosol particles or systems have different abilities to activate cloud droplets or initiate ice formation. When different aerosol particles coexist, they can show preferential activation to cloud droplets in warm clouds. There is also a possibility of aerosol particles showing competitive behaviour either as CCN or INPs depending on the existing conditions (Simpson et al., 2018). However, the competition effects between two different aerosol particles or aerosol systems in activating cloud droplets are not clearly understood and require research efforts by both the cloud experimentalists and modellers or better still, a joint research effort. In this recent study with the key objective of **i**mproving our **S**cientific **K**nowledge of clouds, ice Cr**Y**stals, and aerosols through **LAB**oratory access to a New Dynamic Cloud Chamber (iSKYLAB), we explore the preferential activation of aerosol particles in different atmospheric conditions. This current study also provides an integrated approach to studying cloud processes and the performance of atmospheric simulation chambers such as the new Aerosol Dynamics and Interactions in the atmosphere chamber – a dynamic version (AIDAd) at the Karlsruhe Institute of Technology, Germany.

METHODS

We engaged both laboratory experiments and modelling in this study, and both methods informed each other in every phase of the study. For the laboratory, the experiments were carried out in the start-of-the-art atmospheric simulation chamber referred to as the Aerosol Dynamics and Interactions in the Atmosphere dynamic (AIDAd) chamber. This is a cylindrical chamber consisting of two concentric chambers (cloud and vacuum) of 3.8 m^3 and 15.8 m^3 respectively. AIDAd chamber provides a robust platform which cooling experiments can be conducted in the temperature range of 303 K to 218 K. The chamber is equipped with various particle generators and a battery of cutting-edge aerosol and cloud instruments for aerosol and cloud characterization. For each experiment, a prescribed number and size of

aerosol particles were injected into the cloud chamber. The particle concentration and size were measured with ultrafine condensation particle counter and scanning mobility particle sizers respectively. Afterwards, expansion experiments were performed to trigger cloud activation and ice formation in some cases.

For the modeling, we deployed the University of Manchester, ACPIM model (Fowler et al., 2020), the NCAR Lagrangian-particle-based DNS model, the LES of Ludwig-Maximillians University (Hoffmann et al., 2015), and the University of Illinois PartMC model (Riemer et al., 2019) to test whether these models are able to capture or reproduce the competition effects taking into consideration parameters such as number concentrations, aerosol composition/types, cooling rates, particle sizes, etc.

RESULTS AND CONCLUSIONS

In Figure 1, simulating a warm cloud scenario, ammonium sulfate particles of ~ 130 nm median size were activated to cloud droplets upon cooling from ~279 K at ~272 K at 0.5 K/min cooling rate. This experiment formed the baseline for the aerosol mixtures which were investigated in the work.
The results from this study showed that the relative size and the chemical compositions of the aerosol particles are very important in determining the preferential activation of such particles to cloud droplets. In addition, different updraft speeds (simulated as cooling rates in our experiments) can alter the competitive trajectory that such aerosol particles take. The results from this study shade light on the cloud processes and can inform both aerosol-cloud and climate model studies. This contribution will include a short introduction to the new dynamic cloud simulation chamber AIDAd as well as the experimental and modelling methods applied. Results on cloud condensation and ice nucleation processes with be presented and discussed.

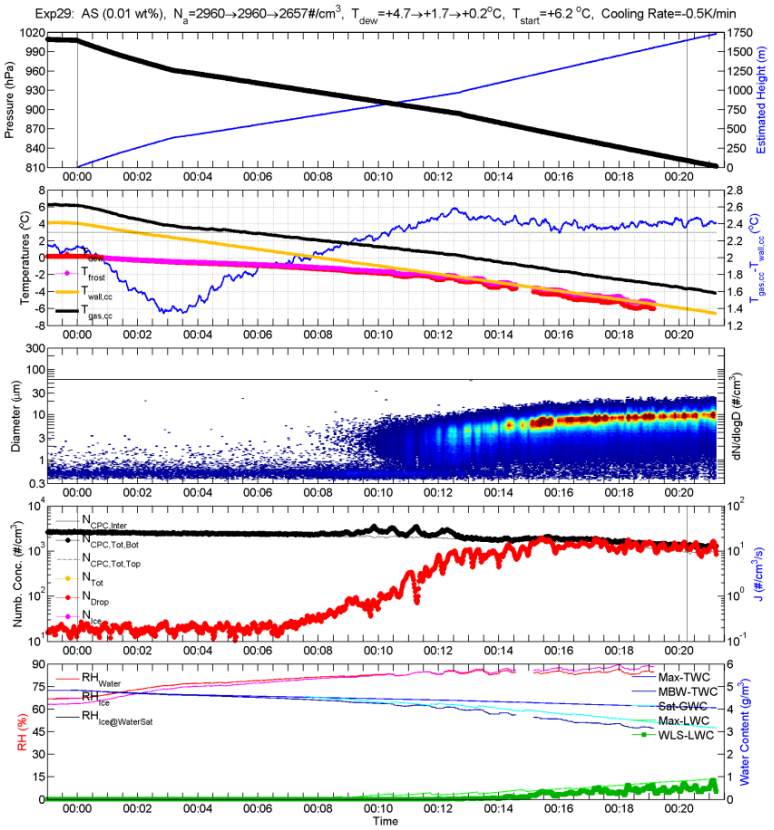


Figure 1. An example dataset obtained from the expansion experiment of ammonium sulfate ($(NH_4)_2SO_4$) at 0.5 K/min showing cloud droplet activation by $(NH_4)_2SO_4$ particles.

ACKNOWLEDGEMENTS

This work was supported by the EU ATMO-ACCESS Transnational Access (ATMO-TNA-7--0000000025) and the Helmholtz Association through the program “Changing Earth – Sustaining our Future”. We gratefully acknowledge support by the AIDA team at the Karlsruhe Institute of Technology during the AIDAd experiments.

REFERENCES

Fowler, K., Connolly, P., and Topping, D.: Modelling the effect of condensed-phase diffusion on the homogeneous nucleation of ice in ultra-viscous particles, Atmos. Chem. Phys., 20, 683–698, https://doi.org/10.5194/acp-20-683-2020, 2020.

Hoffmann F., Raascha, S., and Noh, Y.: Entrainment of aerosols and their activation in a shallow cumulus cloud studied with a coupled LCM–LES approach, Atmospheric Research 156 (2015) 43–57.

Hoose, C., and Möhler, O. (2012). Heterogeneous ice nucleation on atmospheric aerosols: a review of results from laboratory experiments. *Atmos. Chem. Phys.*, *12*(20), 9817–9854. https://doi.org/10.5194/acp-12-9817-2012.

Kanji, Z. A., Ladino, L. A., Wex, H., Boose, Y., Burkert-Kohn, M., Cziczo, D. J., and Krämer, M. (2017). Overview of Ice Nucleating Particles. *Meteorological Monographs*, *58*, 1.1-1.33. https://doi.org/10.1175/AMSMONOGRAPHS-D-16-0006.1

Riemer, N., Ault, A. P., West, M., Craig, R. L. and Curtis, J. H (2019).: Aerosol Mixing State: Measurements, Modeling, and Impacts, Reviews of Geophysics, Volume 57, Issue 2 187 - 249

Simpson, E. L., Connolly, P. J., and McFiggans, G.: Competition for water vapour results in suppression of ice formation in mixed-phase clouds, Atmos. Chem. Phys., 18, 7237–7250, https://doi.org/10.5194/acp-18-7237-2018, 2018.

Special Session 6: CLOUD

Stability of clusters of highly oxygenated organic molecules from alpha-pinene ozonolysis and sulphuric acid oxidation.

H. Junninen[1], P. Koemets[1,6], E. Sommer[2,3], R. Konrat[3], S. Mirme[1,6], K. Tamme[1], P. Winkler[3], M. Canagaratna[4], D. Worsnop[4,5] and the CLOUD collaboration

[1]*Institute of Physics, University of Tartu, Tartu 50411, Estonia*
[2]*CERN, European Organisation for Nuclear Research, 1211 Geneva, Switzerland*
[3]*Faculty of Physics, University of Vienna; Boltzmanngasse 5 1090 Vienna Austria*
[4]*Aerodyne Research Inc, Billerica, MA 01821, USA*
[5]*INAR, Faculty of Science, University of Helsinki, 00014 Helsinki, Finland*
[6]*Airel OÜ, 61602, Tõravere, Estonia*

Keywords: Atmospheric nucleation, Cluster stability, HOM, APITOF, CLOUD.

INTRODUCTION

New particle formation (NPF) contributes to more than half of all cloud condensation nuclei worldwide (Gordon et al. 2017) and plays a critical role in understanding anthropogenic climate change (IPCC, 2021). A key mechanism driving atmospheric NPF is acid-base nucleation, primarily involving anthropogenic sulfuric acid and ammonia, but also oxygenated organic molecules (HOM), produced from the oxidation of terpenes (Kirkby, 2023, Shen et al. 2024). The chemical composition of first-step oxidation products is measured and identified by elemental composition, and molecular structures are only estimated by modeling. In this paper, we estimate the structural strengths of first-step nucleating clusters by applying additional external energy in order to fragment the clusters and thus identify molecular vs. ionic clusters.

METHODS

This study focuses on measurements from the CERN CLOUD chamber, examining NPF from alpha-pinene in the presence of trace sulfuric acid concentrations ranging from 104 to 106 cm−3, levels that are commonly found in pristine regions. For calibration we used tetrabutylammonium iodite (TBAI) dimer and monomer produced by UDMA (differential mobility analyzer) and electrospray (SEADM S.L.). Clusters were detected using an atmospheric pressure interface time-of-flight mass spectrometer without any ionization sources (APiTOF, Junninen et. Al. 2010). In APiTOF the ions are transported through 3 pressure regions and guided by quadrupoles and ion lenses. We varied the instrument settings so that the overall voltage difference from the inlet to the extraction region remains the same, but we changed the pressure region where the ions are accelerated. This created conditions for collisions at different speeds and consecutive fragmentation, but with minimal effect on the transmission of the instrument. We changed one voltage (skimmer voltages) from -5 to 20V. The instrument was set up to scan the voltages in 7 steps and stay 1min at each step.

CONCLUSIONS

Figure 1 illustrates the performance of the method. UDMA was set to select TBAI dimer, and with the lowest fragmentation setting, the APITOF spectrum contained only the TBAI dimer. With the increase of energy, the dimer started to fragment, and by the last voltage setting, only the monomer was observed. All dimer had fragmented into TBAI charged monomer and neutral molecule, the neutral part is invisible for the APITOF. Transmission was not changed, and thus, the total number of detected ions remained the same. In the presentation, the results from the voltage scans during the CLOUD chamber experiment will be shown and discussed.

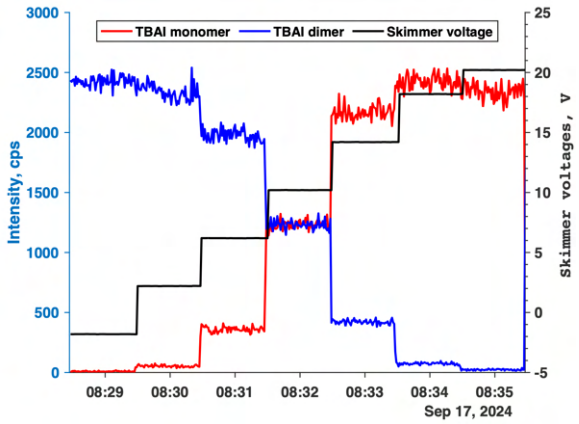


Figure 1. Fragmentation of tetrabutylammonium iodite with varying external energy (skimmer voltage).

ACKNOWLEDGEMENTS

This work was supported by the Estonian Research Council (projects PRG714, RVTT3), MSCA ITN project CLOUD-DOC (grant number 101073026)

REFERENCES

Gordon, H. et al. (2017) J. Geophys. Res. Atmos. 122, 8739-8760.
IPCC (2021) Climate Change 2021 Cambridge University Press.
Kirkby, J. et al. (2023) Nature Geoscience 16, 948-957.
Shen, J. et al. (2024) Nature 636.8041, 115-123.
Junninen et al (2010) Atmos. Meas. Tech., 3, 1039–1053

Collision rates of multiply-charged aerosol particles in the CERN CLOUD chamber

P. Rato[1,2], E. Sommer[1,3], J. Almeida[1,4], P. Koemets[5], S. Mirme[5], L. Liu[6], B. Yang[6], H. Klebach[2], J. Kirkby[1,2] and CLOUD collaboration

[1] CERN, European Organisation for Nuclear Research, 1211 Geneva, Switzerland
[2]Institute for Atmospheric and Environmental Sciences, Goethe University Frankfurt, 60438 Frankfurt, Germany
[3]Faculty of Physics, University of Vienna, 1090 Vienna, Austria
[4]Faculty of Sciences of the University of Lisbon, 1749-016 Lisbon, Portugal
[5]Institute of Physics, Faculty of Science and Technology, University of Tartu, 50411 Tartu, Estonia
[6]Paul Scherrer Institute, 5232 Villigen PSI, Switzerland

Keywords: multiple charges, collision rates, electrical mobility and CLOUD experiment

Presenting author email: pedro.rato@cern.ch

Electric charge plays a key role in ion-induced nucleation of atmospheric aerosol particles by stabilizing embryonic molecular clusters against evaporation (Kirkby *et al.,* 2011, 2016) and by enhancing their growth rates (He *et al., 2021*). However, the effect of multiply-charged particles on aerosol and cloud microphysics is relatively poorly-known experimentally, although some laboratory studies have been recently reported the effect of multiple charges on ion-ion recombination coefficients (Pfeifer *et al.,* 2023) and on aerosol-cloud droplet collision rates (Dépée *et al.* (2021).

Here we report experiments conducted at the CERN CLOUD chamber to study the interactions of unipolar small ions and multiply-charged small particles (<10 nm diameter) with large aerosol particles in the CCN size range (50-100 nm). The experiments used an electrospray generator, CHARGE2 (CHarged AeRosol GEnerator 2), for injecting multiply charged aerosol particles (~7 nm diameter), carrying up to seven positive charges) along with high concentrations of positive small ions (up to 10,000 ions/cm^3). The electrospray was operated with a sulfuric acid-water solution of either 2 wt%, which injected multiply charged particles and positive small ions together, and 0.02 wt%, which injected only positive small ions. An α-particle source (^{241}Am, 3.7 MBq) with a movable shutter, located at the exit of CHARGE2, was used to compare experiments with and without neutralisation of the electrosprayed particles.

We will report new insights into the impact of electric charge on particle-particle and particle-ion collision rates in unipolar environments.

This work was supported by MSCA ITN project CLOUD-DOC (grant number 101073026).

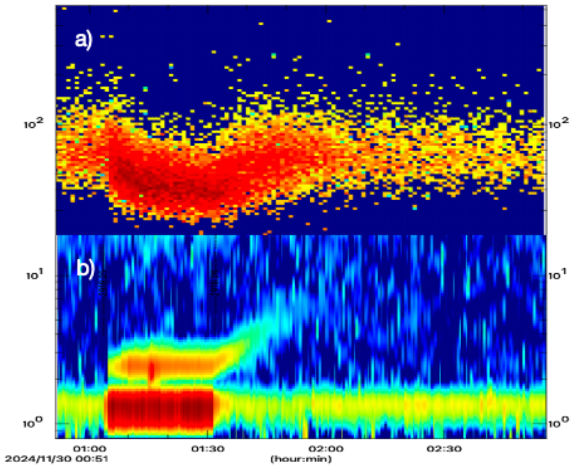


Figure 1. Apparent size spectra versus time for charged particles in CLOUD, measured by an a) lSMPS and b) AIS+. The charges on the particles are unchanged from those in the CLOUD chamber. Injection from CHARGE2 corresponds to the intense unipolar small ion band seen in panel b) near 1 nm. This multiply-charges the particles in panel a), causing an apparent shrinkage due to the increased electrical mobility. At the same time, CHARGE2 injects smaller multiply charged particles, which become progressively neutralised by cosmic ray ionisation after the injection stops, leading to apparent growth (panel b).

Dépée, A. *et al.* (2021). *Atmos. Chem. Phys.* **21**, 6963-6984.
He, X.-C. et al. (2021). *Aerosol Sci. Tech.* **55,** 231-242.
Kirkby, J. *et al.* (2011). *Nature* **476,** 429-433.
Kirkby, J. et al. (2016). *Nature* **533**, 521-526.
Pfeifer, J. et al. (2023). *Atmos. Chem. Phys.* **23**, 6703-6718.

Isoprene chemistry producing nucleator molecules under upper-tropospheric conditions

D.M. Russell[1], F. Kunkler[2], J. Shen[3], J.D. Vivo[4], CLOUD collaboration, N.M. Donahue[4], H. Harder[2], J. Kirkby[1,5], X.C. He[3] and J. Curtius[1]

[1]*Institute for Atmospheric and Environmental Sciences, Goethe University Frankfurt, 60438, Germany*
[2]*Atmospheric Chemistry Department, Max Planck Institute for Chemistry, 55128 Mainz, Germany*
[3]*Institute for Atmospheric and Earth System Research, University of Helsinki, 00014, Finland*
[4]*Department of Chemical Engineering, Carnegie Mellon University, Pittsburgh, 15213 PA, USA*
[5]*CERN, European Organisation for Nuclear Research, 1211, Geneva, Switzerland*

Keywords: Isoprene, Upper troposphere, NOx effect, Ion-induced nucleation.

INTRODUCTION

Isoprene (C_5H_8) is the most abundant non-methane hydrocarbon emitted into the atmosphere. It is produced by vegetation, especially deciduous and broad-leaved trees, and can be efficiently transported to the upper troposphere (7-15 km) via deep convective clouds (Palmer *et al.*, 2022).
The oxidation products of isoprene have recently been reported to drive rapid formation and growth of new particles in the tropical upper troposphere (Curtius, Heinritzi, *et al.*, 2024, Shen, Russell, *et al.*, 2024), revealing a large source of particles which may contribute to a band of particles at this altitude, covering 40% of the Earth's surface (Williamson *et al.*, 2019).

Isoprene is primarily oxidised by hydroxyl (OH) radicals and the resulting RO_2 are terminated by hydroperoxyl (HO_2), nitric oxide (NO) and nitrogen dioxide (NO_2) radicals, resulting in a lifetime of around 1-2 hours under daylight conditions.

High solar flux and lightning associated with deep convective clouds generate elevated concentrations of HO_x (OH + HO_2) and NO_x (NO + NO_2), with typical daytime values of OH ~ 10^6 cm^{-3}, HO_2 ~ 10^7 cm^{-3} and NO ~ 10^9 cm^{-3} (Curtius, Heinritzi, *et al.*, 2024).
Wennberg *et al.*, 2018 describes a comprehensive review of isoprene oxidation chemistry under boundary layer conditions. However, the chemical pathways involved at these low temperatures are not yet well understood. In addition, given the ion-pair production rate in the upper troposphere is a factor of 10 larger than the boundary layer, the effect of ions on this system is not well known.

METHODS

We conducted measurements at -50°C in the CERN CLOUD chamber during the CLOUD16 campaign (September – November 2023). OH radicals, generated by a combination of O_3 and H_2O_2 photolysis, were used to oxidise injected isoprene vapour under a wide range of ambient concentrations of HO_2, NO and NO_2.

Isoprene oxygenated organic molecules (IP-OOM) were measured using a combination of three mass spectrometers with different chemical ionisation (NH_4^+, Br^- and NO_3^-). An Api-TOF that could switch between positive and negative mode was used to understand the composition of the nucleating clusters. The HydrOxyl Radical measurement Unit based on fluorescence Spectroscopy (HORUS) was used to measure OH and HO_2.

In addition, a comprehensive set of instruments was used to measure other trace gases and the size and number of particles.

CONCLUSIONS

In our study, we explored the production of IP-OOM at upper tropospheric temperatures (223 and 243 K). Our measurements show that two consecutive OH oxidations are required to form IP-OOM, and therefore, contribute to particle growth, regardless of the termination reaction.
However, depending on the relative concentrations of the termination radicals (HO_2, NO, and NO_2), vastly-different IP-OOM compositions emerge, comprising a mixture of compounds containing either zero, one or two nitrogen atoms.
At the low temperatures of the upper troposphere, we measured peroxynitrates from the reaction of RO_2 + NO_2 (non-PAN), indicating a potentially important reservoir of RO_2 in the upper troposphere.
Our results agree closely with aircraft observations (Curtius, Heinritzi, *et al.*, 2024) and indicate three important regions (Amazon, Congo, Papua New Guinea) for IP-OOM formation under a nitrate dominated environment.

In addition, this presentation will discuss the volatility of key secondary oxidation products contributing to new particle formation (Curtius, Heinritzi, *et al.*, 2024, Shen, Russell, *et al.*, 2024). Moreover, it will comment on the effect of ions on nucleation for differing IP-OOM compositions.

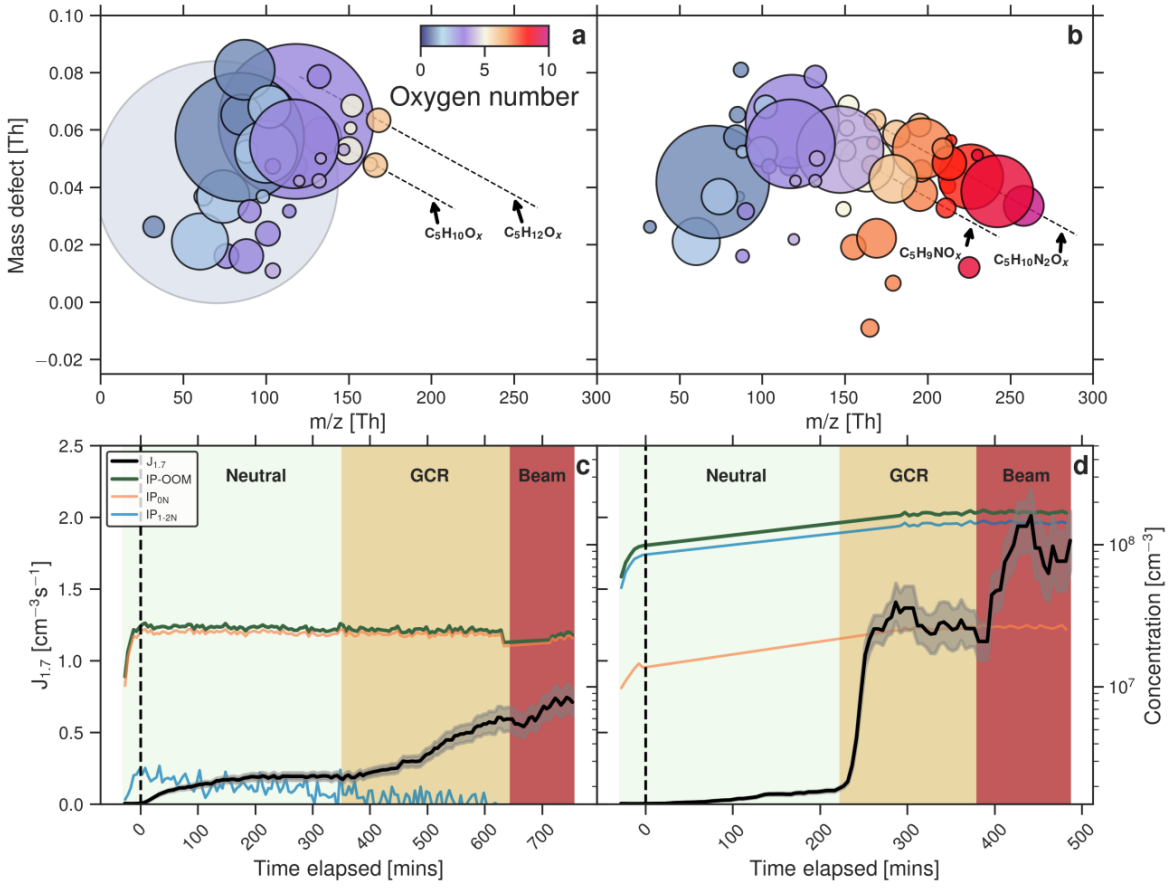


Figure 1. Two isoprene oxidation experiments at 223 K with (b,d) and without NOx (a,c). (a) and (b) exhibit the neutral molecules measured by a three mass spectrometers with different chemical ionisation (NH_4^+, Br^-, NO_3^-). (c) and (d) show the effect of different ion conditions on $J_{1.7}$ under a steady chemical system.

ACKNOWLEDGEMENTS

This work was supported by MSCA Doctoral Networks (Project 101073026 - CLOUD-DOC - HORIZON-MSCA-2021-DN-01) and the German BMBF (project “CLOUD-22” 01LK2201A)

REFERENCES

Palmer, P. I., Marvin, M. R., Siddans, R., Kerridge, B. J., and Moore, D. P.: Nocturnal survival of isoprene linked to formation of upper tropospheric organic aerosol, Science, 375, 562–566, 2022.

Curtius, J., Heinritzi, M., Beck, L. J., Pöhlker, M. L., Tripathi, N., Krumm, B. E., Holzbeck, P., Nussbaumer, C. M., Hernández Pardo, L., Klimach, T., Barmpounis, K., Andersen, S. T., Bardakov, R., Bohn, B., Cecchini, M. A., Chaboureau, J.-P., Dauhut, T., Dienhart, D., Dörich, R., Edtbauer, A., Giez, A., Hartmann, A., Holanda, B. A., Joppe, P., Kaiser, K., Keber, T., Klebach, H., Krüger, O. O., Kürten, A., Mallaun, C.,
Marno, D., Martinez, M., Monteiro, C., Nelson, C., Ort, L., Raj, S. S., Richter, S., Ringsdorf, A., Rocha, F., Simon, M., Sreekumar, S., Tsokankunku, A., Unfer, G. R., Valenti, I. D., Wang, N., Zahn, A., Zauner-Wieczorek, M., Albrecht, R. I., Andreae, M. O., Artaxo, P., Crowley, J. N., Fischer, H., Harder, H., Herdies, D. L., Machado, L. A. T., Pöhlker, C., Pöschl, U., Possner, A., Pozzer, A., Schneider, J., Williams, J., and Lelieveld, J.: Isoprene nitrates drive new particle formation in Amazon’s upper troposphere, Nature, 636, 124–130, 2024.

Shen, J., Russell, D. M., DeVivo, J., Kunkler, F., Baalbaki, R., Mentler, B., Scholz, W., Yu, W., Caudillo-Plath, L., Sommer, E., Ahongshangbam, E., Alfaouri, D., Almeida, J., Amorim, A., Beck, L. J., Beckmann, H., Berntheusel, M., Bhattacharyya, N., Canagaratna, M. R., Chassaing, A., Cruz-Simbron, R., Dada, L., Duplissy, J., Gordon, H., Granzin, M., Große Schute, L., Heinritzi, M., Iyer, S., Klebach, H., Krüger, T., Kürten, A., Lampimäki, M., Liu, L., Lopez, B., Martinez, M., Morawiec, A., Onnela, A., Peltola, M., Rato, P., Reza, M., Richter, S., Rörup, B., Sebastian, M. K., Simon, M., Surdu, M., Tamme, K., Thakur, R. C., Tomé, A., Tong, Y., Top, J., Umo, N. S., Unfer, G., Vettikkat, L., Weissbacher, J., Xenofontos, C., Yang, B., Zauner-Wieczorek, M., Zhang, J., Zheng, Z., Baltensperger, U., Christoudias, T., Flagan, R. C., El Haddad, I., Junninen, H., Möhler, O., Riipinen, I., Rohner, U., Schobesberger, S., Volkamer, R., Winkler, P. M., Hansel, A., Lehtipalo, K., Donahue, N. M., Lelieveld, J., Harder, H., Kulmala, M., Worsnop, D. R., Kirkby, J., Curtius, J., and He, X.-C.: New particle formation from isoprene under upper-tropospheric conditions, Nature, 636, 115–123, 2024.

Williamson, C. J., Kupc, A., Axisa, D., Bilsback, K. R., Bui, T., Campuzano-Jost, P., Dollner, M., Froyd, K. D., Hodshire, A. L., Jimenez, J. L., Kodros, J. K., Luo, G., Murphy, D. M., Nault, B. A., Ray, E. A., Weinzierl, B., Wilson, J. C., Yu, F., Yu, P., Pierce, J. R., and Brock, C. A.: A large source of cloud condensation nuclei from new particle formation in the tropics, Nature, 574, 399–403, 2019.

Wennberg, P. O., Bates, K. H., Crounse, J. D., Dodson, L. G., McVay, R. C., Mertens, L. A., Nguyen, T. B., Praske, E., Schwantes, R. H., Smarte, M. D., St Clair, J. M., Teng, A. P., Zhang, X., and Seinfeld, J. H.: Gas-Phase Reactions of Isoprene and Its Major Oxidation Products, Chem. Rev., 118, 3337–3390, 2018.

RO2 lifetime drives biogenic new particle formation and growth in the planetary boundary layer

B. Yang[1], L. Liu[1], A. Pignatelli[1], L. Caudillo-Plath[2], D.M. Russell[2], F. Kunkler[3], B. Judmaier[4], Z. Zheng[4], W. Scholz[4], J. DeVivo[5], E. Sommer[6], W. Yu[7], L. Dada[1], CLOUD collaboration and I.E. Haddad[1]

[1]*PSI Center for Energy and Environmental Sciences, Paul Scherrer Institute, Villigen, Switzerland.*
[2]*Institute for Atmospheric and Environmental Sciences, Goethe University Frankfurt, Frankfurt am Main, Germany*
[3]*Atmospheric Chemistry Department, Max Planck Institute for Chemistry, Mainz, Germany*
[4]*Institute for Ion Physics and Applied Physics, University of Innsbruck, Innsbruck, Austria*
[5]*Center for Atmospheric Particle Studies, Carnegie Mellon University, Pittsburgh, PA, USA*
[6]*CERN, the European Organization for Nuclear Research, Geneva, Switzerland*
[7]*Institute for Atmospheric and Earth System Research/Physics, Faculty of Science, University of Helsinki, Helsinki, Finland*

Keywords: SOA yields, RO2 lifetime.

INTRODUCTION

Biogenic new particle formation (NPF) is a major source of secondary organic aerosols (SOA) impacting both climate and human health. SOA formation involves complex atmospheric oxidation processes, making it challenging to accurately predict their yields. Current research indicates that organic oxidation initially generates peroxyl radicals (RO_2), which can undergo termination via reactions with nitric oxide (NO), hydroperoxyl radical (HO_2), or RO_2 radicals, leading to the formation of monomer or dimer products (Ehn et al., 2014). Depending on their volatility, these products contribute to particle nucleation and growth (Bianchi et al., 2019). However, the interactions among NO, HO_2, and RO_2 are governed by the HOx–ROx cycle (Cho et al., 2023; Schervish & Donahue, 2021), resulting in an intricate network of reaction pathways. This complexity makes it difficult to predict the fate of RO_2 and its contribution to SOA formation. Therefore, simplifying the parameterization of RO_2 fate across different termination regimes is crucial. To address this, we conducted a systematic experiment across NO:HO_2:RO_2 ratios relevant to the atmospheric boundary layer to investigate their influence on biogenic NPF.

METHODS

The experiment was conducted in the CLOUD chamber at CERN. A mixture of biogenic volatile organic compounds (BVOCs), specifically α-pinene (AP) and isoprene (IP), was injected into the chamber at ratios ranging from 1:2 to 1:6. The hydroxyl radical (OH) concentration was controlled between 10^6 and 10^7 molecules $\cdot$ cm^{-3} through ozone (O_3) and nitric acid (HONO) photooxidation. Two temperatures, 25°C and 5°C, were maintained to simulate summer and winter conditions, respectively. A summary of all experimental conditions is provided in Table 1.

Parameters	Conditions
Temperature	5, 25°C
AP: IP	0.6: 4ppb (~1:6), 1.4:8ppb (~1:6), 2:4ppb (1:2)
SO2	0.3 to 2 ppb
NH3	1 to 2 ppb
O3	60 ppb
OH	10^6 to 10^7 molecules $\cdot$ cm^{-3}
NO	0 to 0.8 ppb
CO	~100 ppb

Table 1. Summary of the experimental conditions.

A series of gas monitors measured SO_2, O_3, NH_3, NO and NO_2 concentration. For gas-phase organic compositions, a H_2O cluster proton transfer reaction time of flight (PTR-TOF) was used to measure the concentration of AP and IP. A nitrate-based Chemical Ionization-Atmospheric Pressure interface-Time-Of-Flight (NO_3-CI-APi-TOF) and NH_4+ mode PTR3 were used to measure the high and low oxygenated organic molecules in gas-phase. The volatilities of these molecules were confirmed by a Filter Inlet for Gases and AEROsols (FIGAERO) CIMS. For particle measurement, A combination of PSM, NAIS, nano-SMPS and long-SMPS provided the size measurement from 1 up to 550 nm. OH and HO_2 were measured by a HydrOxyl Radical measurement Unit based on fluorescence Spectroscopy (HORUS). OH concentration was cross-checked with the calculation of sulfuric acid production from SO_2. HO_2 measurement was intercompared with a Br-MION2-CIMS during campaign (Shen et al., 2024). RO_2 concentrations were determined using PTR3, HORUS, and calculations based on VOC production rate (Xiao et al., 2025). In comparison with these methods, the RO_2 levels reported here are associated with an uncertainty factor of 2.

RESULTS

This study presents a comprehensive, systematic experiment to investigate RO_2 fate. As shown in Figure 1, the variations in reaction rate ratio of NO and HO_2 (β) with RO2 lifetime (τ_{bi}), and the HO_2-to-RO_2 ratio match the modeled atmospheric RO_2 distribution (Kenagy et al., 2024). The calculated τ_{bi} (RO_2 lifetime) based on RO_2 reactions with NO and HO_2, ranges from a few seconds to approximately 100 seconds, while β spans its full possible range. The NO_2:NO ratio is minor in this study because peroxy nitrates, readily decompose back into RO_2 and NO_2 at the studied temperatures (Jenkin et al., 2019).

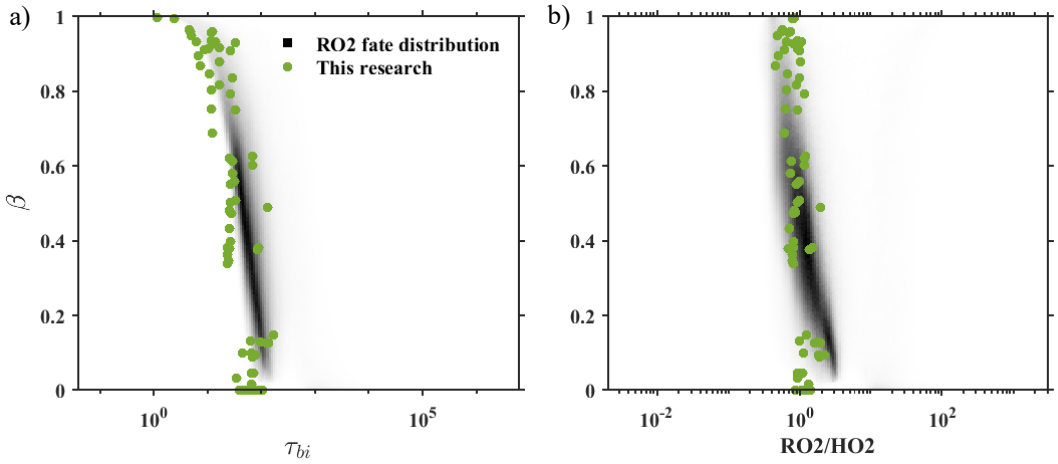


Figure 1. The fate of RO2 distribution a) β and τ_{bi}, (b) β and RO_2/HO_2, in ambient (Kenagy et al., 2024) and this study.

Previous research has highlighted the suppression of α-pinene oxidation by the RO_2-RO_2 reaction in the presence of isoprene (Heinritzi et al., 2020; McFiggans et al., 2019). However, via HOx-ROx cycle, isoprene oxidation also increases production of HO_2 (Cho et al., 2023), which consumes RO_2 as well (Baker et al., 2024). Additionally, the presence of NO further complicates the system due to its dual role — consuming RO_2 while simultaneously enhancing radical recycling (Nie et al., 2023).

To quantify the total effects of NO, HO_2 and RO_2 on RO_2 fate, τ_{total} (the RO_2 lifetime) was introduced as a unifying parameter. Unlike τ_{bi}, τ_{total} explicitly incorporates the contribution of the RO_2-RO_2 reaction, which expresses the significant influence of IP-RO_2 or AP-RO_2 itself on AP-RO_2 fate.

$$\tau_{total} = \frac{1}{k_{RO2+NO}[NO] + k_{RO2+HO2}[HO2] + k_{RO2+RO2}[RO2]}$$

The reaction rate coefficients for RO_2 with NO and HO_2 are not sensitive to RO_2 structure and are taken from the literature (Wennberg et al., 2018). In contrast, RO_2–RO_2 reaction rates vary significantly. In this

study, a rate coefficient of 2.5×10^{-11}cm^3 s^{-1} , average values for the self-reaction of AP-RO_2 and its cross-reaction with IP-RO_2 (Berndt et al., 2018), is applied for all RO_2-RO_2 reactions. Additionally, a sensitivity analysis varying $k_{RO2+RO2}$ from 1×10^{-12} to 1×10^{-10}cm^3 s^{-1} confirmed the robustness of the conclusions.

As shown in Figure 2 a), the AP C10 highly oxygenated organic molecules (HOMs) yield across three different BVOCs concentrations and varying NO levels follows a consistent trend with increasing τ_{total}. Although the BVOCs ratios differ by a factor of 3, C10 HOM yields are almost unchanged when τ_{total} is the same. This suggests that the synaptic impact of NO, HO_2, and RO_2 on AP-HOMs production is more critical than the IP-RO_2 to AP-RO_2 ratio, validating the use of τ_{total} as a unifying parameter. The correlation between $\tau_{total}$and C10 HOMs yield arises from competition between bimolecular termination and intramolecular autoxidation. Higher τ_{total} values allow more primary RO_2 radicals to undergo autoxidation, forming HOMs. The typical autoxidation rate for α-pinene at 298 K is $0.01 - 0.1 s^{-1}$ (Baker et al., 2024), consistent with this study. Furthermore, Autoxidation is highly temperature-dependent (Simon et al., 2020; Wennberg et al., 2018). Lower temperatures reduce the autoxidation rate, which explains why the 5°C slope is lower than the slope at 25°C.

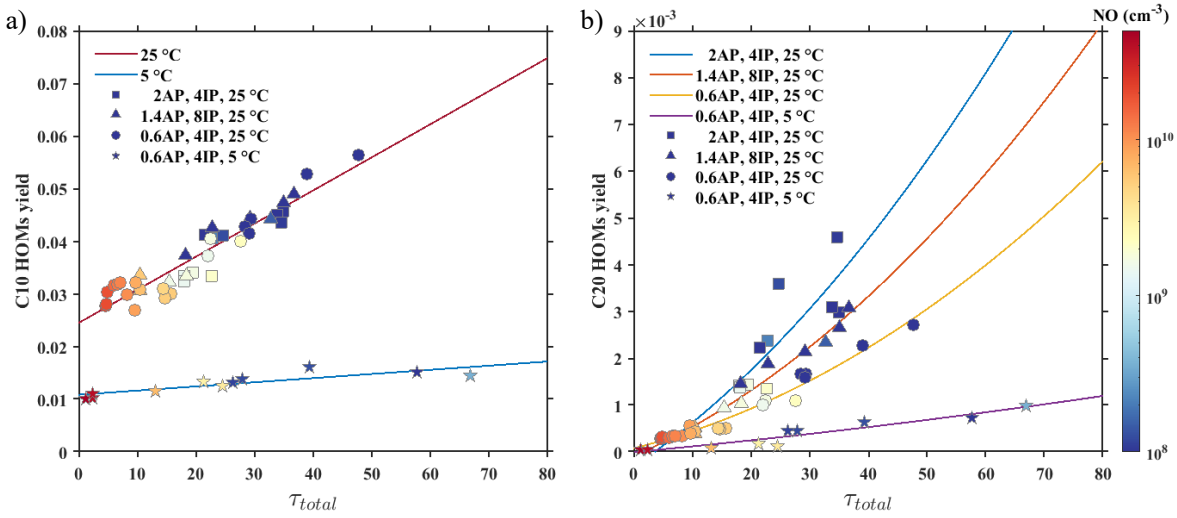


Figure 2. The correlation between τ_{total} and a) AP C10 (monomer) HOMs yield or b) AP C20 (dimer) HOMs yield.

In Figure 2 b), A similar trend is observed for dimers, where τ_{total} remains a key determinant of dimer yield. Besides, absolute AP concentration also affects dimer formation. Despite similar BVOCs ratios, the 1.4:8 ppb AP: IP condition yields more C20 HOMs than 0.6:4 ppb AP: IP. This is because dimer formation via RO_2-RO_2 reactions follows second-order kinetics. Even after normalizing by the AP production rate, C20 HOM yield remains proportional to absolute AP-RO_2 concentration. These dimers, with their extremely low volatility, play a crucial role in SOA formation. The effects of these reactions on nucleation and particle growth are also explored in this study and will be presented at the conference.

CONCLUSIONS

This study introduces τ_{total} as a unifying parameter to describe RO_2 fate by incorporating NO, HO_2 and RO_2 termination pathways. Results show that τ_{total} strongly correlates with AP HOMs formation, as higher τ_{total} favor autoxidation over bimolecular termination. Temperature influences this relationship, with lower temperatures reducing autoxidation efficiency. Dimer formation depends on τ_{total} and absolute AP concentrations, emphasizing the role of RO_2 fate in SOA formation. These findings improve our understanding of atmospheric oxidation and provide a refined framework for predicting SOA formation.

ACKNOWLEDGEMENTS

This work was supported by the EU MSCA Doctoral Network CLOUD-DOC 101073026.

REFERENCES

Baker, Y., Kang, S., Wang, H., Wu, R., Xu, J., Zanders, A., He, Q., Hohaus, T., Ziehm, T., Geretti, V., Bannan, T. J., O'Meara, S. P., Voliotis, A., Hallquist, M., McFiggans, G., Zorn, S. R., Wahner, A., & Mentel, T. F. (2024). Impact of HO2⁄RO2 ratio on highly oxygenated α-pinene photooxidation products and secondary organic aerosol formation potential. *Atmospheric Chemistry and Physics*, *24*(8), 4789-4807.

Berndt, T., Mentler, B., Scholz, W., Fischer, L., Herrmann, H., Kulmala, M., & Hansel, A. (2018). Accretion Product Formation from Ozonolysis and OH Radical Reaction of alpha-Pinene: Mechanistic Insight and the Influence of Isoprene and Ethylene. *Environ Sci Technol*, *52*(19), 11069-11077.

Bianchi, F., Kurten, T., Riva, M., Mohr, C., Rissanen, M. P., Roldin, P., Berndt, T., Crounse, J. D., Wennberg, P. O., Mentel, T. F., Wildt, J., Junninen, H., Jokinen, T., Kulmala, M., Worsnop, D. R., Thornton, J. A., Donahue, N., Kjaergaard, H. G., & Ehn, M. (2019). Highly Oxygenated Organic Molecules (HOM) from Gas-Phase Autoxidation Involving Peroxy Radicals: A Key Contributor to Atmospheric Aerosol. *Chem Rev*, *119*(6), 3472-3509.

Cho, C., Fuchs, H., Hofzumahaus, A., Holland, F., Bloss, W. J., Bohn, B., Dorn, H. P., Glowania, M., Hohaus, T., Liu, L., Monks, P. S., Niether, D., Rohrer, F., Sommariva, R., Tan, Z., Tillmann, R., Kiendler-Scharr, A., Wahner, A., & Novelli, A. (2023). Experimental chemical budgets of OH, HO2, and RO2 radicals in rural air in western Germany during the JULIAC campaign 2019. *Atmos. Chem. Phys.*, *23*(3), 2003-2033.

Ehn, M., Thornton, J. A., Kleist, E., Sipila, M., Junninen, H., Pullinen, I., Springer, M., Rubach, F., Tillmann, R., Lee, B., Lopez-Hilfiker, F., Andres, S., Acir, I. H., Rissanen, M., Jokinen, T., Schobesberger, S., Kangasluoma, J., Kontkanen, J., Nieminen, T., . . . Mentel, T. F. (2014). A large source of low-volatility secondary organic aerosol. *Nature*, *506*(7489), 476-479.

Heinritzi, M., Dada, L., Simon, M., Stolzenburg, D., Wagner, A. C., Fischer, L., Ahonen, L. R., Amanatidis, S., Baalbaki, R., Baccarini, A., Bauer, P. S., Baumgartner, B., Bianchi, F., Brilke, S., Chen, D., Chiu, R., Dias, A., Dommen, J., Duplissy, J., . . . Curtius, J. (2020). Molecular understanding of the suppression of new-particle formation by isoprene. *Atmospheric Chemistry and Physics*, *20*(20), 11809-11821.

Jenkin, M. E., Valorso, R., Aumont, B., & Rickard, A. R. (2019). Estimation of rate coefficients and branching ratios for reactions of organic peroxy radicals for use in automated mechanism construction. *Atmospheric Chemistry and Physics*, *19*(11), 7691-7717.

Kenagy, H. S., Heald, C. L., Tahsini, N., Goss, M. B., & Kroll, J. H. (2024). Can we achieve atmospheric chemical environments in the laboratory? An integrated model-measurement approach to chamber SOA studies. *Science Advances*, *10*(37), eado1482.

McFiggans, G., Mentel, T. F., Wildt, J., Pullinen, I., Kang, S., Kleist, E., Schmitt, S., Springer, M., Tillmann, R., Wu, C., Zhao, D., Hallquist, M., Faxon, C., Le Breton, M., Hallquist, A. M., Simpson, D., Bergstrom, R., Jenkin, M. E., Ehn, M., . . . Kiendler-Scharr, A. (2019). Secondary organic aerosol reduced by mixture of atmospheric vapours. *Nature*, *565*(7741), 587-593.

Nie, W., Yan, C., Yang, L., Roldin, P., Liu, Y., Vogel, A. L., Molteni, U., Stolzenburg, D., Finkenzeller, H., Amorim, A., Bianchi, F., Curtius, J., Dada, L., Draper, D. C., Duplissy, J., Hansel, A., He, X.-C., Hofbauer, V., Jokinen, T., . . . Ding, A. (2023). NO at low concentration can enhance the formation of highly oxygenated biogenic molecules in the atmosphere. *Nature Communications*, *14*(1), 3347.

Schervish, M., & Donahue, N. M. (2021). Peroxy radical kinetics and new particle formation. *Environmental Science: Atmospheres*, *1*(2), 79-92.

Shen, J., Russell, D. M., DeVivo, J., Kunkler, F., Baalbaki, R., Mentler, B., Scholz, W., Yu, W., Caudillo-Plath, L., Sommer, E., Ahongshangbam, E., Alfaouri, D., Almeida, J., Amorim, A., Beck, L. J., Beckmann, H., Berntheusel, M., Bhattacharyya, N., Canagaratna, M. R., . . . He, X.-C. (2024). New particle formation from isoprene under upper-tropospheric conditions. *Nature*, *636*(8041), 115-123.

Simon, M., Dada, L., Heinritzi, M., Scholz, W., Stolzenburg, D., Fischer, L., Wagner, A. C., Kürten, A., Rörup, B., He, X.-C., Almeida, J., Baalbaki, R., Baccarini, A., Bauer, P. S., Beck, L., Bergen, A., Bianchi, F., Bräkling, S., Brilke, S., . . . Curtius, J. (2020). Molecular understanding of new-particle formation from α-pinene between −50 and +25 ◦C. *Atmospheric Chemistry and Physics*, *20*(15), 9183-9207.

Wennberg, P. O., Bates, K. H., Crounse, J. D., Dodson, L. G., McVay, R. C., Mertens, L. A., Nguyen, T. B., Praske, E., Schwantes, R. H., Smarte, M. D., St Clair, J. M., Teng, A. P., Zhang, X., & Seinfeld, J. H. (2018). Gas-Phase Reactions of Isoprene and Its Major Oxidation Products. *Chem Rev*, *118*(7), 3337-3390.

Xiao, M., Wang, M., Mentler, B., Garmash, O., Lamkaddam, H., Molteni, U., Simon, M., Ahonen, L., Amorim, A., Baccarini, A., Bauer, P. S., Chen, D., Chiu, R., Dada, L., Duplissy, J., Finkenzeller, H., Fischer, L., He, X.-C., Heinritzi, M., . . . El Haddad, I. (2025). Anthropogenic organic aerosol in Europe produced mainly through second-generation oxidation. *Nature Geoscience*, *18*(3), 239-245.

Sponsors

Major Sponsors







Special Sponsoring: side event







Gold Sponsors















Silver Sponsors



Airel

AIRMODUS

AVL

GRIMM AEROSOL TECHNIK
DURAG GROUP

HORIBA
PALAS®

PFEIFFER
VACUUM+FAB SOLUTIONS



QUANTAQ

Bronze Sponsors



KARSA

Gustav Ignaz
Stingl
www.stingl-klavier.at

universität
wien
Vienna Doctoral School in Physics